Explorations in synthetic ion channel research: metal-ligand self-assembly and dissipative assembly

by

Andrew Krisjanis Dambenieks
Master of Science, The University of Western Ontario, 2006
Bachelor of Science, The University of Western Ontario, 2004

A Doctoral Dissertation Submitted in Partial Fulfillment
of the Requirements for the Degree of

DOCTOR OF PHILOSOPHY

in the Department of Chemistry

Supervisory Committee

Explorations in synthetic ion channel research: metal-ligand self-assembly and dissipative assembly

by

Andrew Krisjanis Dambenieks
Master of Science, The University of Western Ontario, 2006
Bachelor of Science, The University of Toronto, 2004

Supervisory Committee

Dr. Thomas Fyles, Department of Chemistry
Supervisor

Dr. Natia L. Frank, Department of Chemistry
Departmental Member

Dr. Fraser Hof, Department of Chemistry
Departmental Member

Dr. Francis E. Nano, Department of Biochemistry
Outside Member

Abstract

Supervisory Committee

Dr. Thomas Fyles, Department of Chemistry
Supervisor
Dr. Natia L. Frank, Department of Chemistry
Departmental Member
Dr. Fraser Hof, Department of Chemistry
Departmental Member
Dr. Francis E. Nano, Department of Biochemistry
Outside Member

This thesis explores fundamental design strategies in the field of synthetic ion channel research from two different perspectives. In the first part the synthesis of complex, shape persistent and thermodynamically stable structures based on metal-ligand self-assembly is explored. The second part examines transport systems with dynamic transport behavior in response to chemical inputs which more closely mimic the dissipative assembly of Natural ion channels.

In part one, two model systems, the ethylenediamine palladium(II) - 4,4'-bipyridine squares of Fujita and the trimeric bis(terpyridine) - iron(II) hexagonal macrocycles of Newkome, were targeted for structural modification towards becoming transport competent systems via improving the membrane partitioning characteristics of the final coordination compounds by increasing their lipophilicity.

Modifications of the Fujita system involved the generation of two lipophilic 4,4'-bipyridines with addition of lipophilic groups of 13 and 17 carbon long alkyl chains respectively at the 3 and 3' positions. After pursuing multiple unsuccessful synthetic routes the successful syntheses afforded the final lipophilic 4,4'-bipyridines in overall yields of 19 to 21% over two synthetic steps. Mixtures of the newly generated lipophilic 4,4'-bipyridines with a known lipophilic ethylenediamine palladium(II) "corner"

exhibited evidence of self-assembly from NMR spectroscopy experiments however attempts at further characterization by ESI-MS and X-ray crystallography were unproductive. The putative self-assembled structures were inactive in HPTS vesicle assays but showed erratic conductance activity in bilayer clamp experiments. However, the magnitude of the conductance observed was not indicative of the passage of ions through the internal pore of the square complex.

Modifications to the Newkome hexagons were aimed at generating overall neutral assemblies with external lipophilic groups. These modifications involved imparting a net -2 charge to the ligand via modifications to the terminal tridentate ligands so that upon coordination to octahedral metal centers in the +2 oxidation state the overall hexagonal complex would be neutrally charged. Two bis-polydentate ligands were generated; a dissymmetric molecule comprising one terpyridine and one dipicolinate tridentate ligand (TERPY-DPA) and a symmetrical molecule comprising two 2,2'-bipyridine-6-carboxylate tridentate ligands (BIPYA-BIPYA). The successful syntheses provided the desired trimethylsilylethyl ester protected compounds in yields of 9.2 and 7.5 % over 6 and 8 total synthetic steps for TERPY-DPA and BIPYA-BIPYA respectively. A new approach to metal-ligand complex formation by concomitant fluoride deprotection and assembly was demonstrated with a monomeric complex. Polymetallic complexes formed with a variety of transition metals based on colorimetric changes but the products were very intractable and resisted full structural or transport characterization.

Part two develops a system potentially capable of exhibiting dissipative assembly of active transporters. A library of six thioester containing compounds structurally related to known active oligoester compounds was synthesized. The successful syntheses provided the desired compounds in overall yields of 1.0 to 17.7% over 11 to 13 total synthetic steps. The intramolecular cyclization - truncation and thioester exchange reactions central to the dissipative assembly strategy were explored using a model compound. The full length compounds showed transport activity via the HPTS vesicle assay that was significantly below that of the lead compound. Bilayer clamp experiments however, revealed significant transport activity for both the full length as

well as the truncated thiol molecules. In the case of the latter the transport events had exceedingly high conductivity for such a small molecule. This unexpected activity for both the full length and truncated compounds, although different, prevented a full implementation of dissipative assembly of transport.

Table of Contents

List of Tables

List of Figures

List of Schemes

List of Abbreviations

ACN: acetonitrile

ADip: modified diphenylacetylene segment

BIPYA: 2,2'-bipyridine carboxylic acid and derivatives

But: ~C(O)$(CH_2)_3$~

DCM: dichloromethane

DHP: 3,4-dihydro-2H-pyran

DIC: *N,N*-diisopropyl carbodiimide

DiPEA: diisopropyl ethylamine

DiPhyPC: diphytanoyl phosphatidylcholine

DMF: dimethylformamide

DPA: dipicolinatic acid/dipicolinate ligand

ESI-MS: electrospray ionization mass spectrometry

Et_2O: diethylether

EtOAc: ethylacetate

g: conductance

Hex: ~C(O)$(CH_2)_5$~

HOBt: hydroxybenzotriazole

HPLC: high performance liquid chromatography

HPTS: 8-hydroxy-l,3,6-pyrene trisulfonate

MeOH: methanol

ms: milliseconds

n-BuLi: *n*-butyl lithium

NMR: nuclear magnetic resonance

Oct: ~$C(O)(CH_2)_7$~

PA: phosphatidic acidic

pA: picoAmpere

PC: phosphatidylcholine

Pent: ~$C(O)(CH_2)_4$~

PRE: prenyl

pS: picoSiemen

pTsOH: *para*-toluenesulfonic acid

sec-BuLi: *sec*-butyl lithium

TBDMS: *tert*-butyl dimethylsilane

TERPY: terpyridine

tBu: *tert*-butyl

t-BuLi: *tert*-butyl lithium

TMSE: trimethylsilyl ethanol

TMEDA: tetramethylethylenediamine

THF: tetrahydrofuran

THP: tetrahydropyran

TLC: thin-layer chromatography

TMS: trimethylsilyl

TMSOTf: trimethylsilyl triflate

List of Numbered Compounds

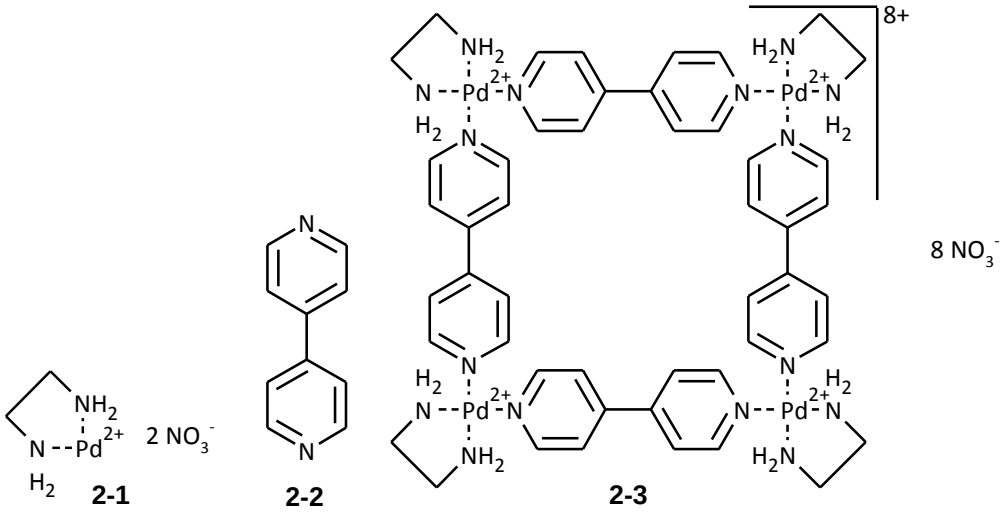

2-1 **2-2** **2-3**

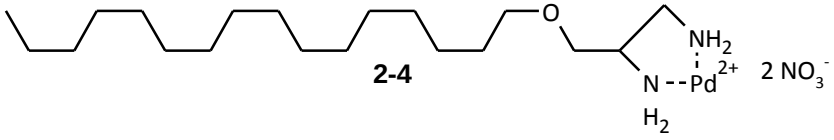

2-4

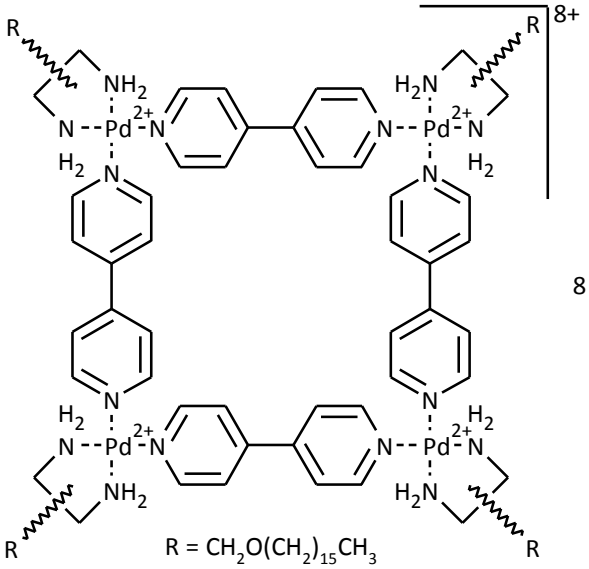

2-5

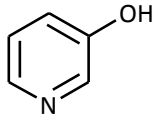

2-6

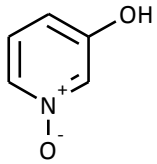

2-7

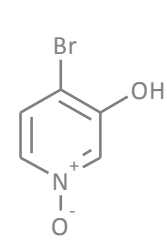

2-8

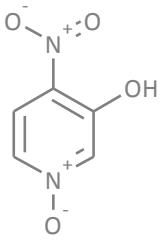

2-9

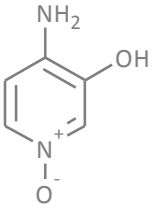

2-10

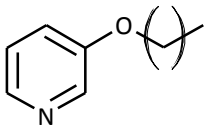

2-11

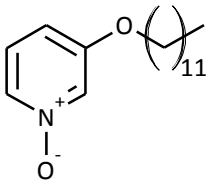

2-12

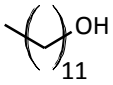

2-13

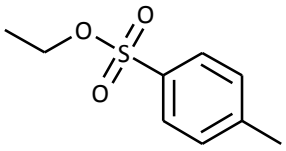

2-14

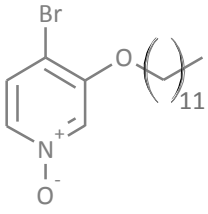

2-15

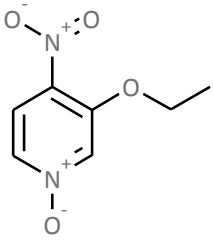

2-16

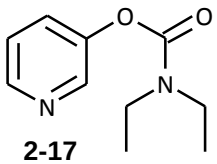

2-17

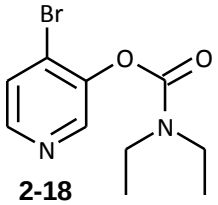

2-18

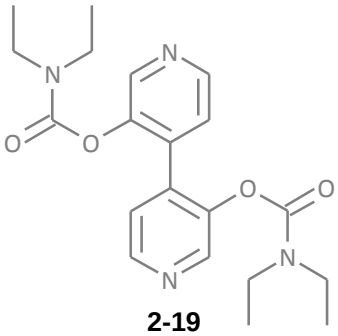

2-19

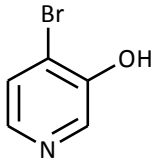

2-20

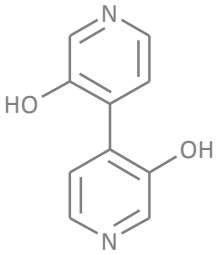

2-21

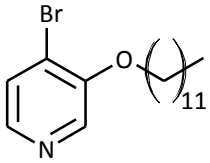

2-22

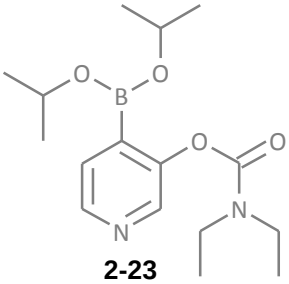

2-23

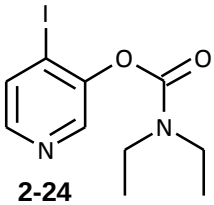

2-24

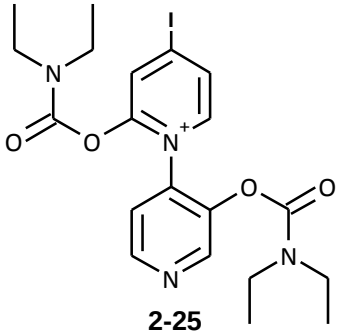

2-25

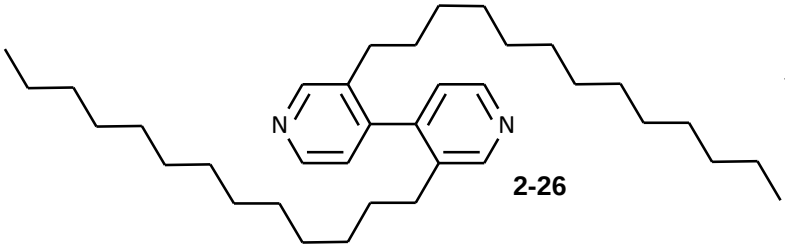

2-26

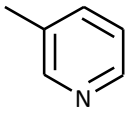

2-27

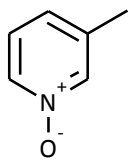

2-28

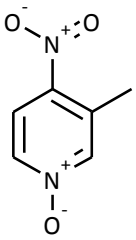

2-29

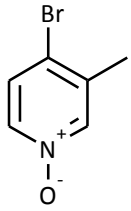

2-30

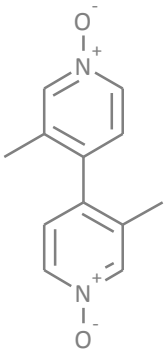

2-31

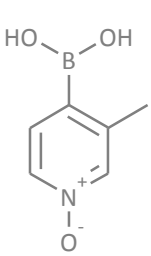

2-32

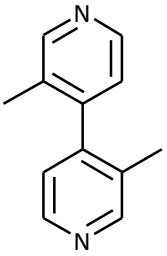

2-33

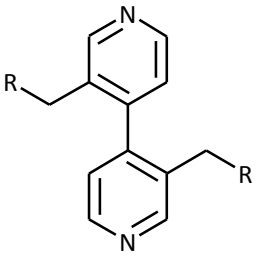

R= $C_{12}H_{25}$; **2-34**

R= $C_{16}H_{33}$; **2-35**

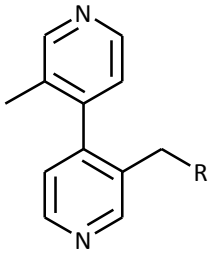

R= $C_{12}H_{25}$; **2-36**

R= $C_{16}H_{33}$; **2-37**

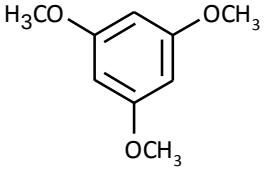

2-38

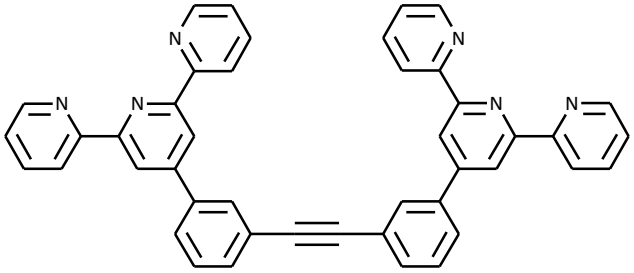

2-40

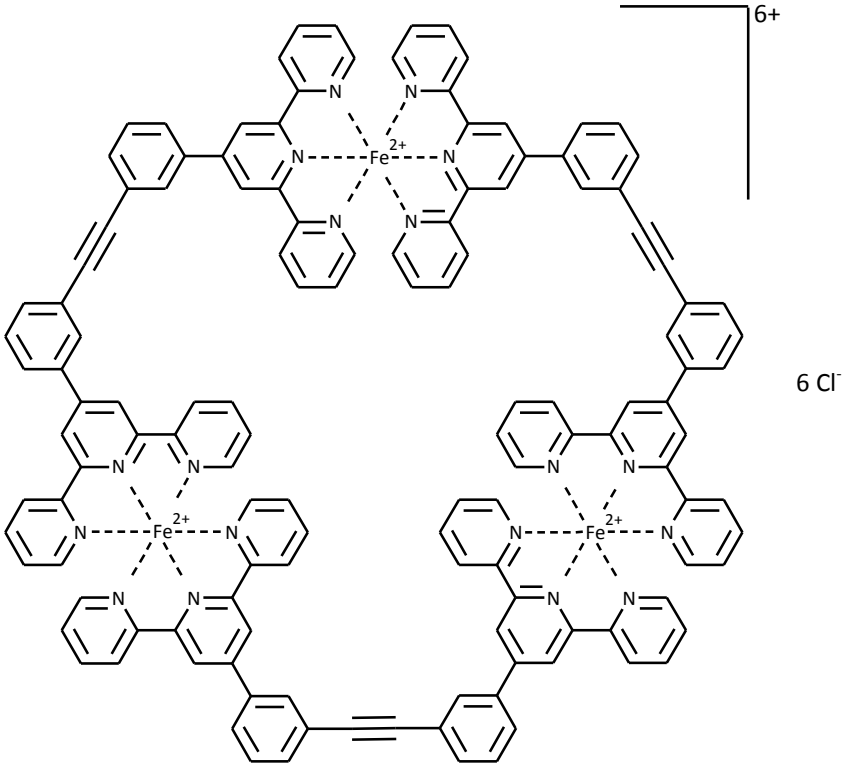

2-41

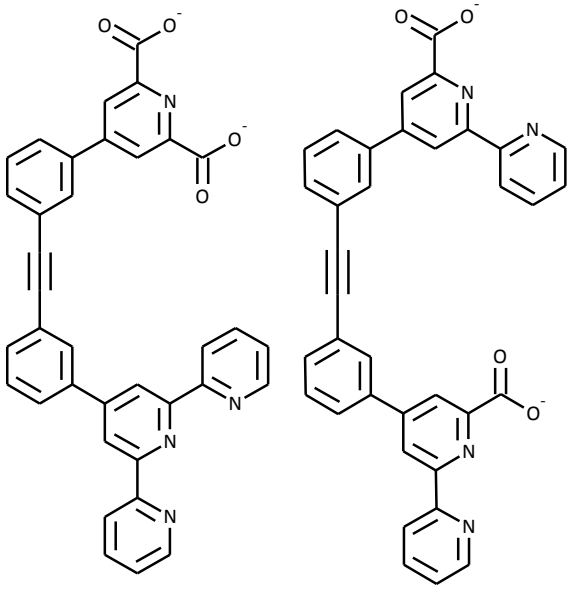

2-42

2-43

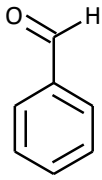

2-44

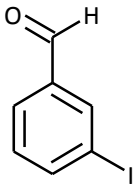

2-45

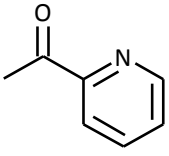

2-46

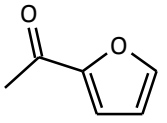

2-47

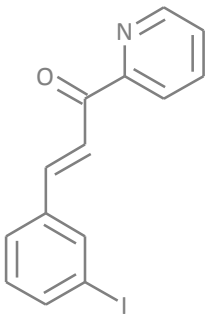

2-48

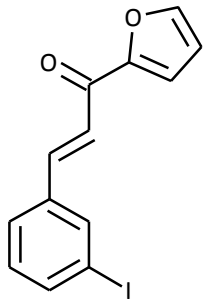

2-49

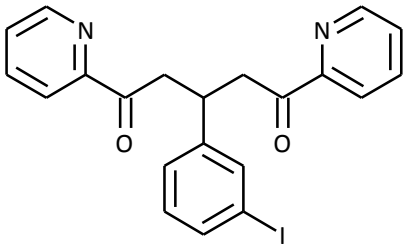

2-50

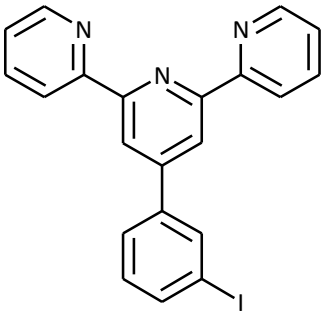

2-51

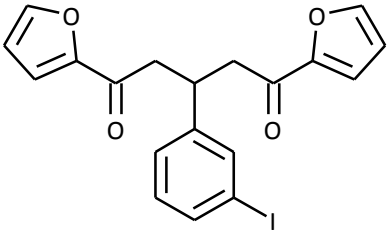

2-52

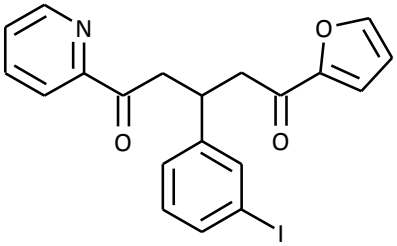

2-53

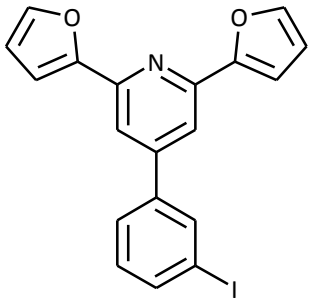

2-54

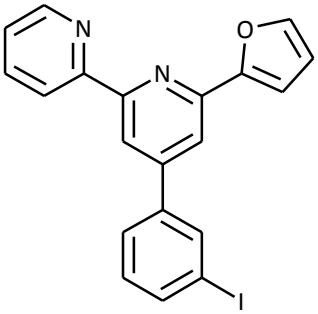

2-55

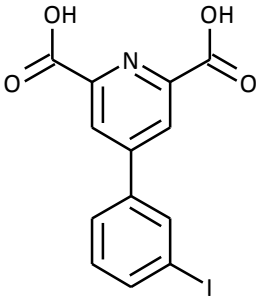

2-56

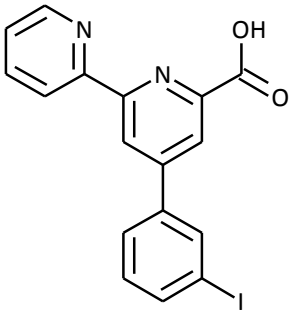

2-57

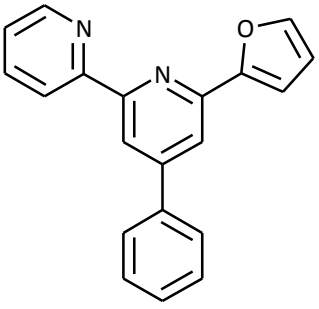

2-58

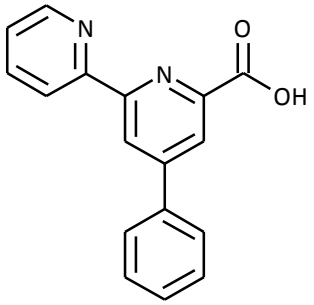

2-59

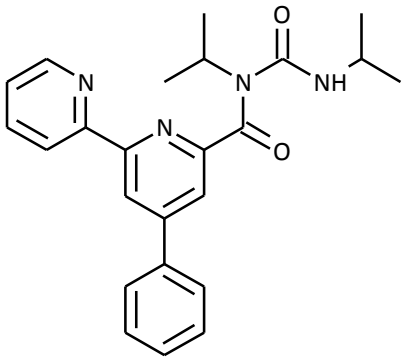

2-60

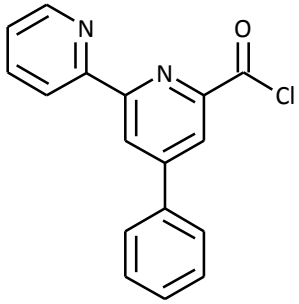

2-61

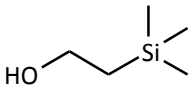

2-62

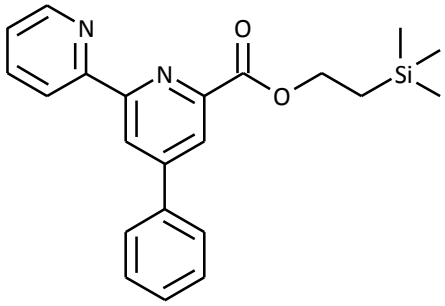

2-63

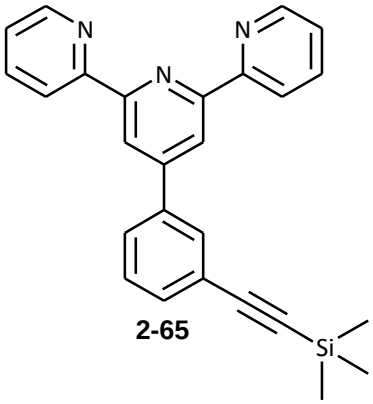

2-65

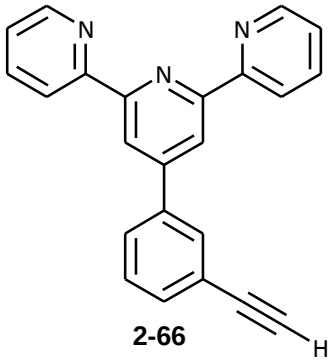

2-66

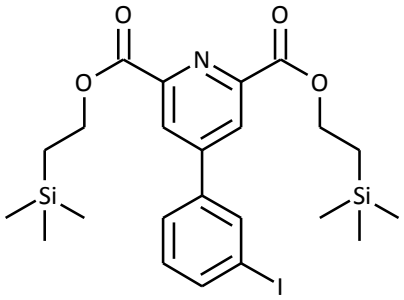

2-67

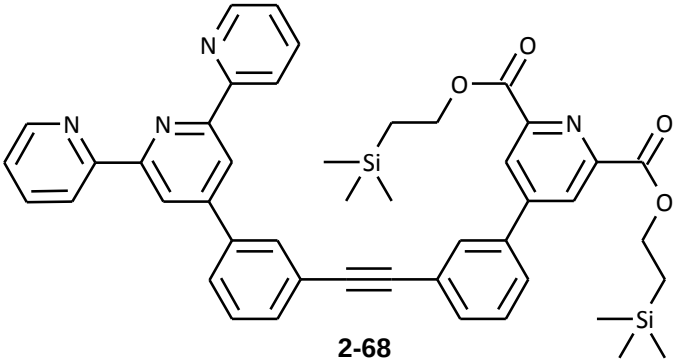

2-68

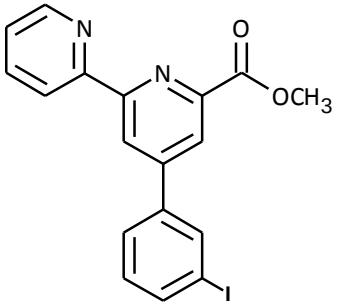

2-69

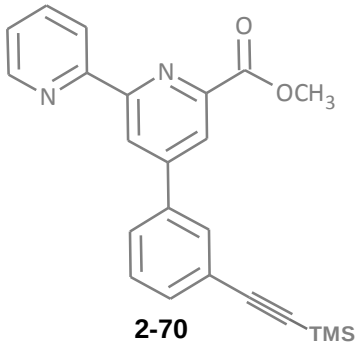

2-70

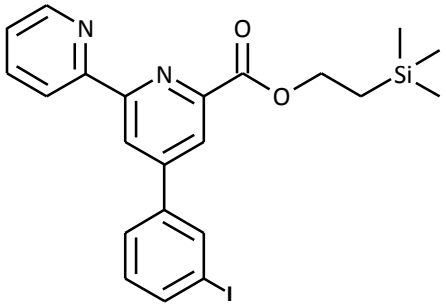

2-71

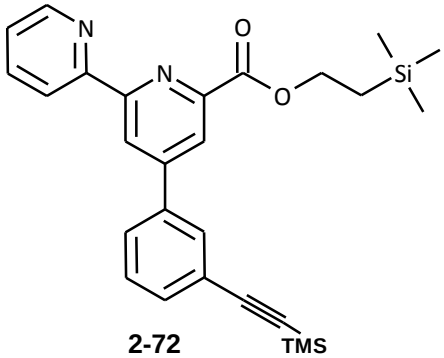

2-72

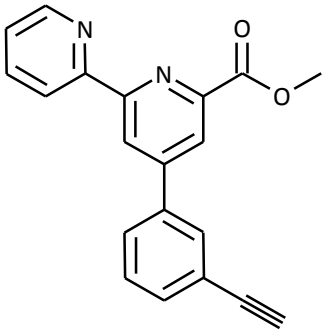

2-73

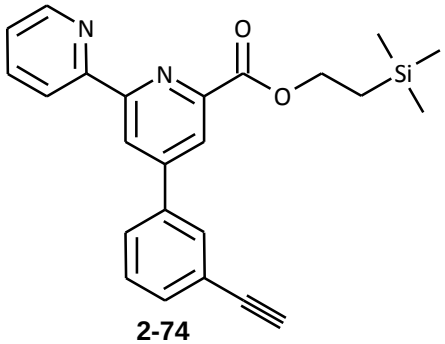

2-74

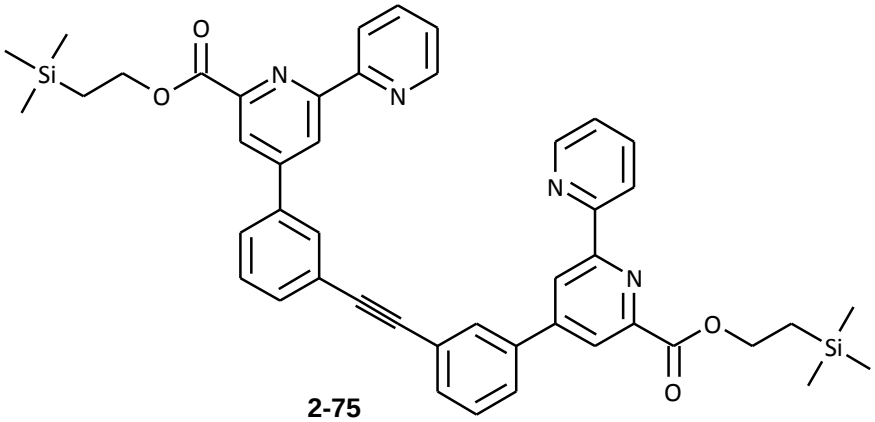

2-75

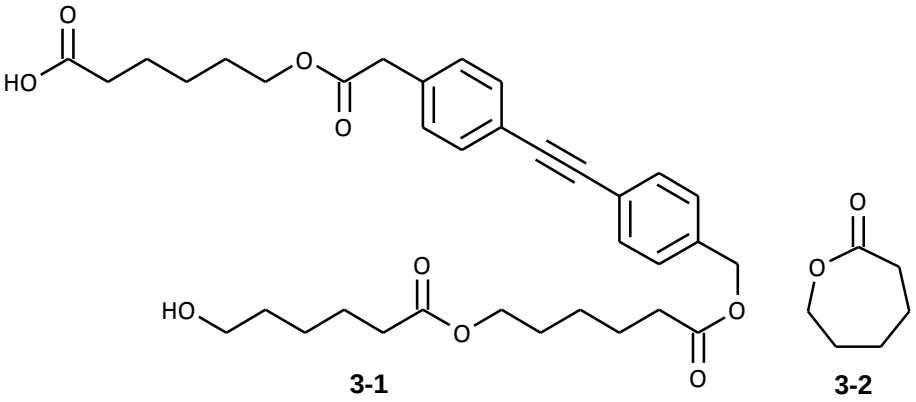

3-1

3-2

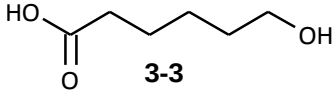

3-3

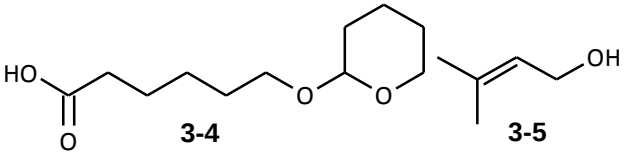

3-4

3-5

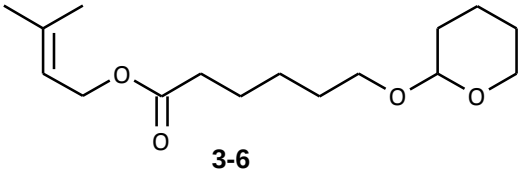

3-6

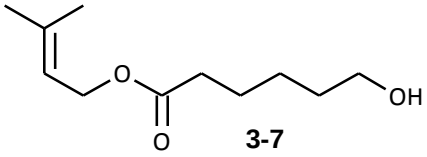

3-7

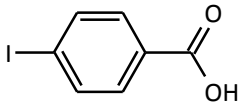

3-8

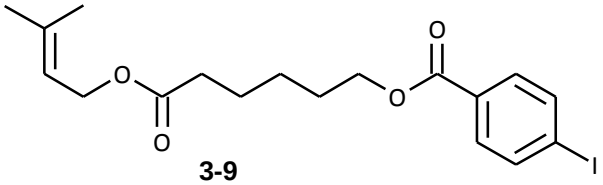

3-9

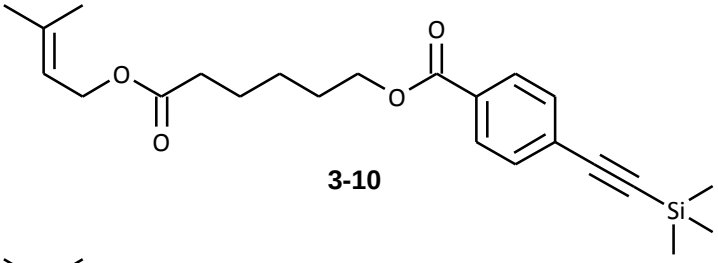

3-10

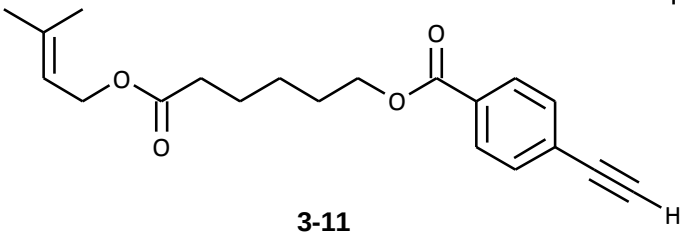

3-11

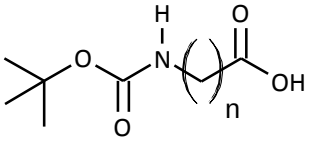

n= 3; **3-12** n= 5; **3-14**
n= 4, **3-13** n= 7; **3-15**

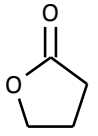

3-16

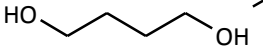

3-17

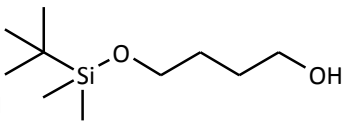

3-18

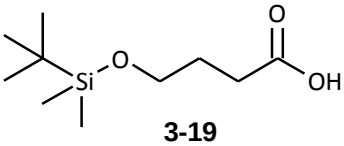

3-19

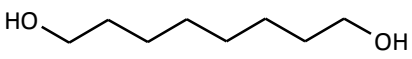

3-20

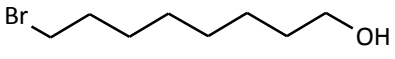

3-21

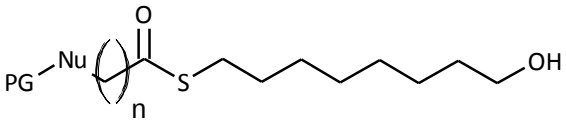

n= 3, Nu= NH, PG= tBoc; **3-23**
n= 4, Nu= NH, PG= tBoc; **3-24**
n= 5, Nu= NH, PG= tBoc; **3-25**
n= 7, Nu= NH, PG= tBoc; **3-26**
n= 3, Nu= O, PG= TBDMS; **3-27**
n= 5, Nu= O, PG= THP; **3-28**

3-22

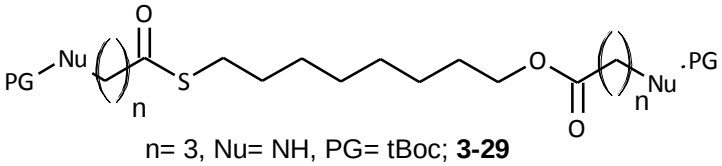

n= 3, Nu= NH, PG= tBoc; **3-29**
n= 4, Nu= NH, PG= tBoc; **3-30**
n= 5, Nu= NH, PG= tBoc; **3-31**
n= 7, Nu= NH, PG= tBoc; **3-32**
n= 3, Nu= O, PG= TBDMS; **3-33**
n= 5, Nu= O, PG= THP; **3-34**

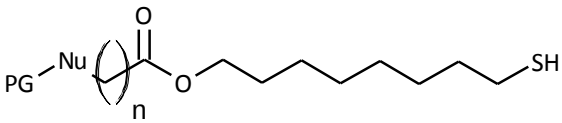

n= 3, Nu= NH, PG= tBoc; **3-35**
n= 4, Nu= NH, PG= tBoc; **3-36**
n= 5, Nu= NH, PG= tBoc; **3-37**
n= 7, Nu= NH, PG= tBoc; **3-38**
n= 3, Nu= O, PG= TBDMS; **3-39**
n= 5, Nu= O, PG= THP; **3-40**

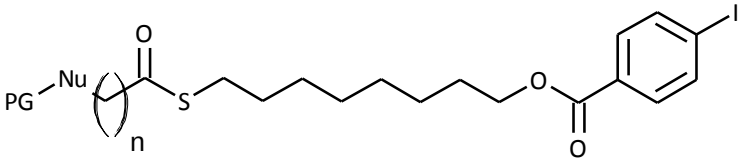

n= 3, Nu= NH, PG= tBoc; **3-41**
n= 4, Nu= NH, PG= tBoc; **3-42**
n= 5, Nu= NH, PG= tBoc; **3-43**
n= 7, Nu= NH, PG= tBoc; **3-44**
n= 3, Nu= O, PG= TBDMS; **3-45**
n= 5, Nu= O, PG= THP; **3-46**

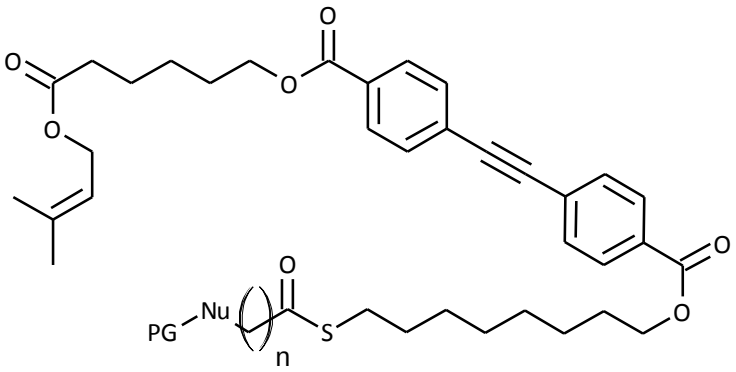

n= 3, Nu= NH, PG= tBoc; **3-47**
n= 4, Nu= NH, PG= tBoc; **3-48**
n= 5, Nu= NH, PG= tBoc; **3-49**
n= 7, Nu= NH, PG= tBoc; **3-50**
n= 3, Nu= O, PG= TBDMS; **3-51**
n= 5, Nu= O, PG= THP; **3-52**

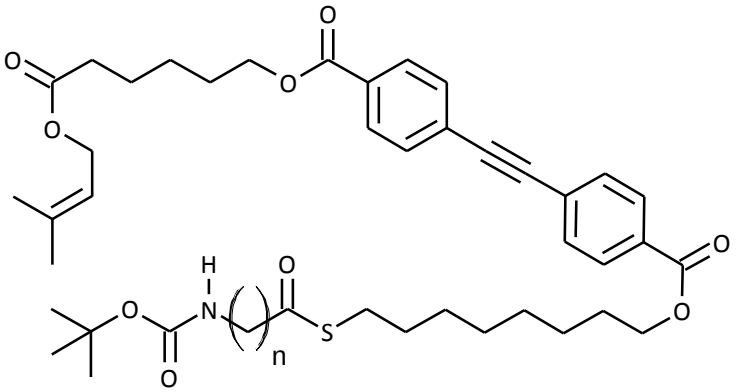

n= 3; **3-47** n= 5; **3-49**
n= 4; **3-48** n= 7; **3-50**

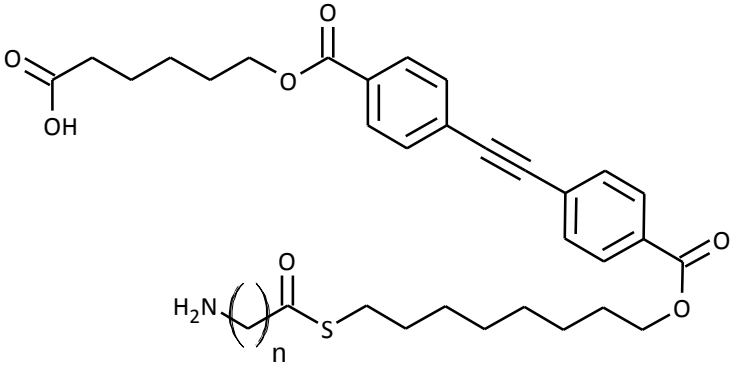

n= 3; **3-53** n= 5; **3-55**
n= 4; **3-54** n= 7; **3-56**

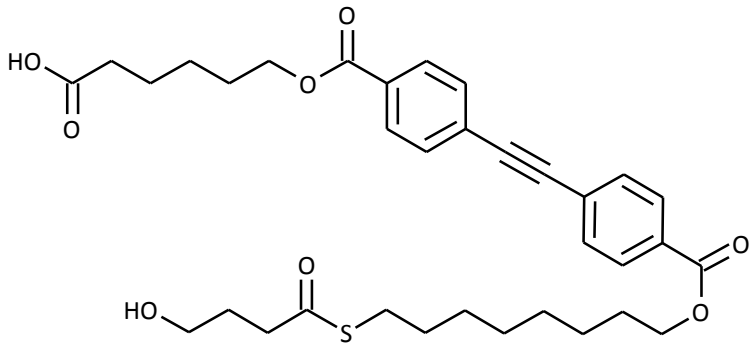

3-57

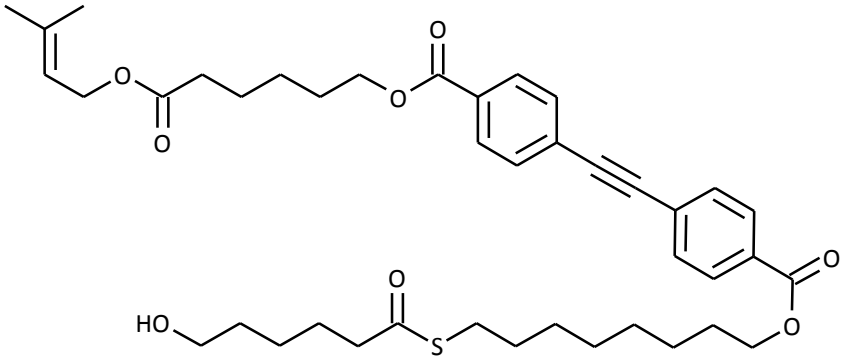

3-58

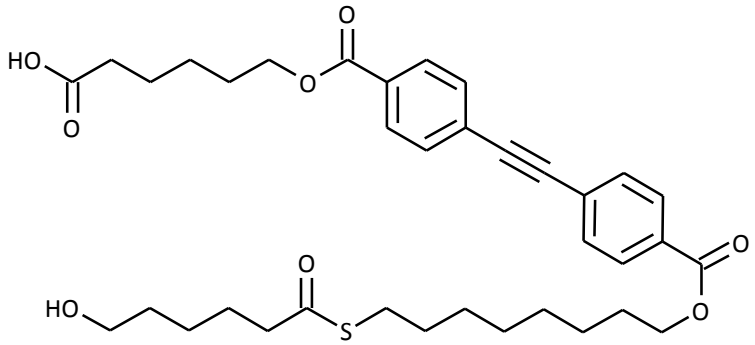

3-59

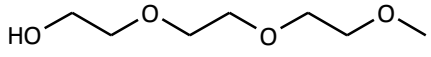

3-60

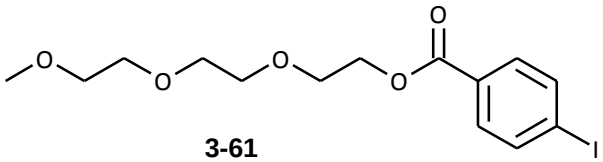

3-61

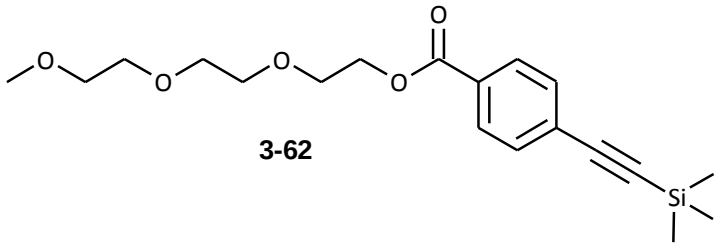

3-62

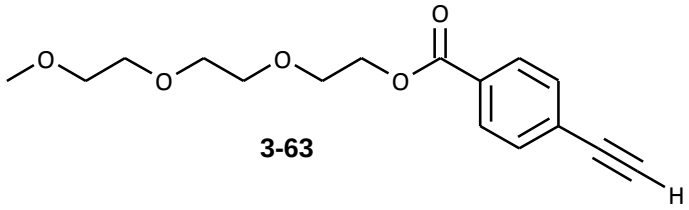

3-63

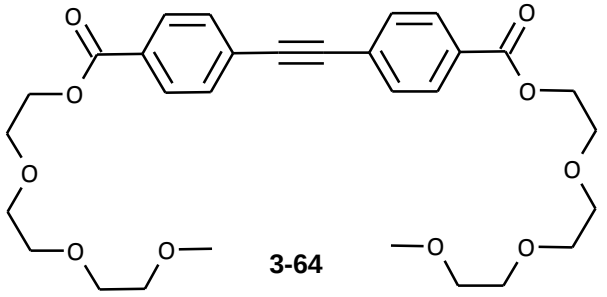

3-64

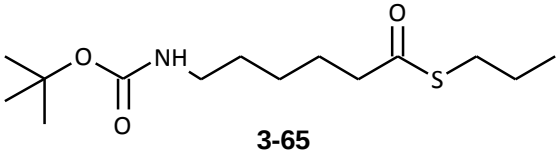

3-65

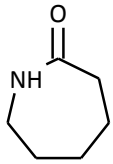

3-66

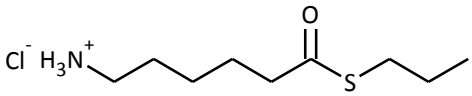

3-67

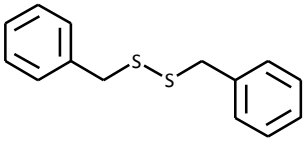

3-68

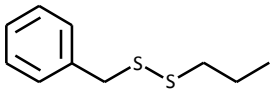

3-69

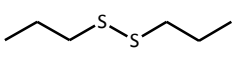

3-70

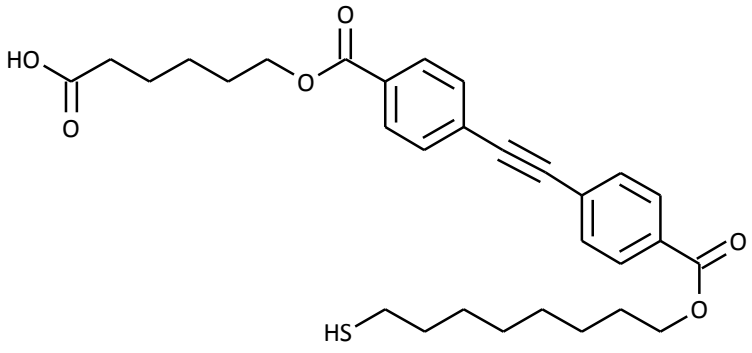

3-71

Acknowledgements

I would like to thank the faculty and support staff in the University of Victoria chemistry department whose knowledge and expertise have made this work possible, and the members of my committee in particular. Thanks also go to the University of Victoria and NSERC for providing funding for the work. Many thanks also go to all of the friends I have made during my time at UVic, and in particular fellow members of the Fyles group past and present (PP, YZ, HL, JC, KG, MT, PV) as well as the neighbors in the lab from the Burford group (SC, SL). Your companionship was invaluable to keeping my spirits up during this long and arduous process. Thanks also go to my family whose unconditional love and $upport lifted my spirits when I needed it most. Special thanks go to my supervisor Dr. Tom Fyles who is among the most intelligent, wise and amicable individuals I have had the pleasure of spending time with. I cannot envision a better supervisor and I can only aspire to one day be as great a scientific mind. Greatest thanks of all go to my lab mate and fiancée, to whom this thesis is dedicated. I cannot imagine how this work could have been realized without your patience, encouragement, insight and especially love.

1 Introduction

1.1 Summary

This work concerns the design and synthesis of artificial systems to mimic ion transport functions of naturally occurring ion channels. Although biomimetic in inspiration, the components are non-biological in origin and use traditional chemical techniques to create structures through covalent-bond synthesis. Thereafter, using the toolbox of supramolecular chemistry, the components will self-assemble using non-covalent interactions into structures that can exhibit ion transport functions. This bottom-up pathway to function is evident in Nature as well, but the emphasis is often on the structures detected by various structural methods rather than on the functions themselves. Structures are certainly required for functions, but the structures prepared in this work are designed based on the functions they are expected to perform.

1.2 Origins - The Lipid Bilayer Membrane

If there is one chemical entity that can be envisioned as serving as a progenitor for the two foci of this manuscript, synthetic ion channels and supramolecular self-assembly, it would be the lipid bilayer membrane.

Lipid bilayer membranes are integral to living organisms. They serve to define the internal from external environments of cells as well as serving critical roles in many organelles such as mitochondria, chloroplasts and the nucleus [1]. In fact it has been proposed that the very feat of compartmentalizing compounds within the internal environment of vesicles may have served as the catalyst for the origins of life as we know it [2].

Lipid bilayer membranes, as their name suggests, are composed of lipids; amphiphilic molecules consisting of a hydrophilic ionic 'head group' connected to one or two lipophilic non-polar 'tails' via ester or amide linkages [3]. The most common class of

lipids found in mammalian cells are the phospholipids for which representative structures are presented in Figure 1-1 below.

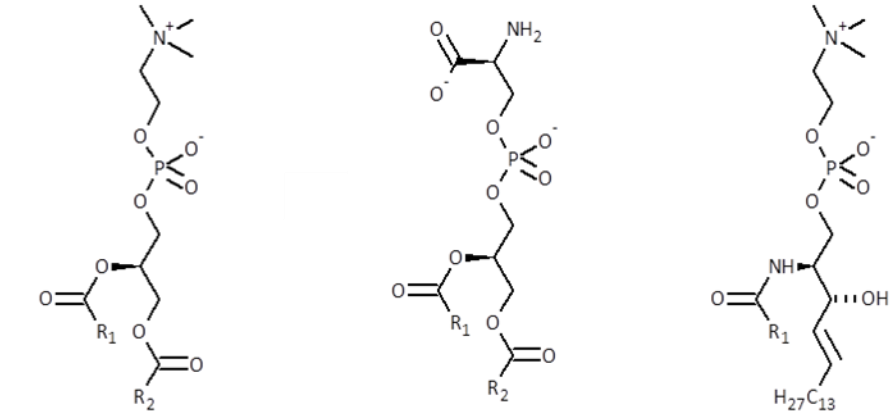

Figure 1-1: The chemical structures of some representative phospholipid molecules.

Due to their amphiphilic nature, in an aqueous environment these phospholipids self-assemble (the forces responsible for this self-assembly process will be discussed later in this introductory chapter) into a lower energy conformation in the form of a lipid bilayer membrane (Figure 1-2). In this conformation the hydrophilic ionic head groups of the molecules arrange such that they project into the aqueous environment on either side of the plane of the bilayer where they are well solvated while the hydrophobic tail portions of the molecule are situated such that they form a well packed non-polar interior environment in which water is effectively excluded. The regions linking the ionic polar head groups and the non-polar tails are of intermediate polarity and as such they form a narrow, partially solvated midpolar region between the two.

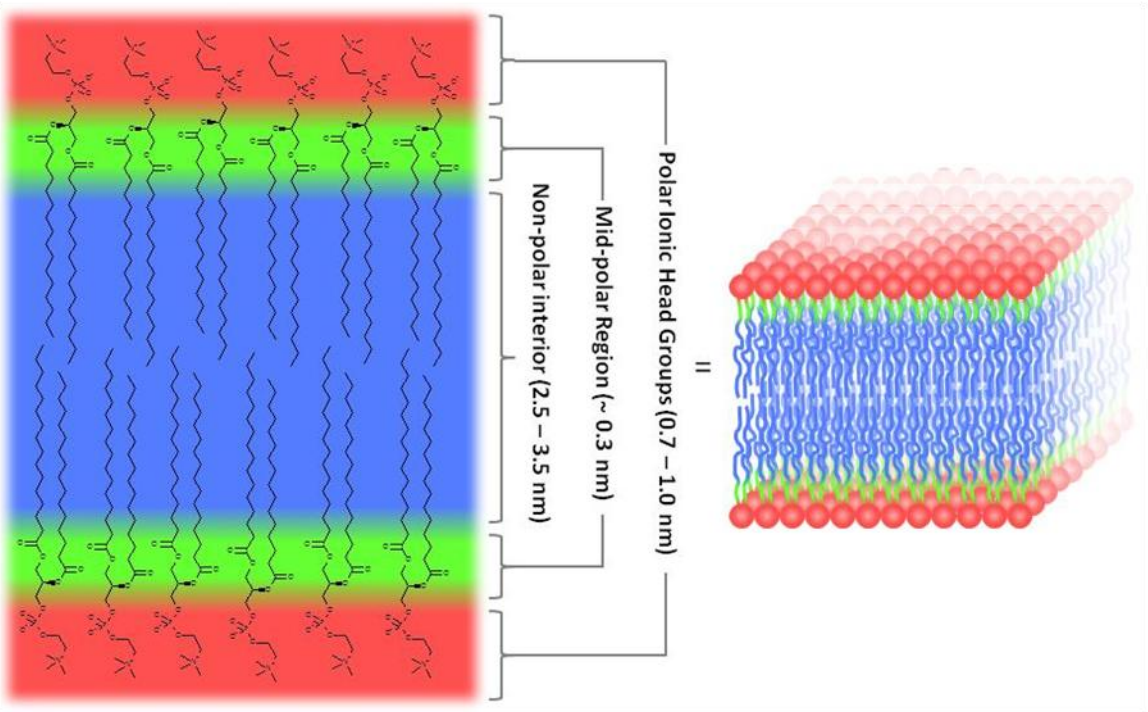

Figure 1-2: The idealized 2-D structure of a lipid bilayer membrane composed entirely of the phospholipid 1,2-dihexadecanoyl-*sn*-glycero-3-phosphocholine and a 3-D representation of a small section of a lipid bilayer membrane.

The arrangement of the individual lipid molecules as depicted in Figure 1-2 above presents an unrealistically ordered system. In reality this environment is an exceedingly chaotic with significant conformational flexibility within any particular molecule as well as spatial mobility of the molecules within and even between the bilayer leaflets [3]. Although the tendency is for the non-polar chains to be fully extended, at any one time there are also many regions within the extended structure where there is a higher degree of disorder. The disorder within these regions leads to residual free volumes within the bilayer where there can be a decreased energetic barrier to the insertion of specific compounds such as membrane bound proteins [4]. In addition the simple bilayer depicted in the figure is composed entirely of a single type of lipid molecule, 1,2-dihexadecanoyl-*sn*-glycero-3-phosphocholine. This is never the case for natural lipid bilayers which can be composed of dozens of different lipid molecules [5]. The composition of the lipid molecules in the bilayer can impart a variety of physical properties to the overall topology of the self-assembled structure as well as mediating

the function of many membrane associated compounds [3, 4, 5]. In fact the lipid composition can even vary significantly from one leaflet of a bilayer to the other resulting in changes to the conformation of the overall structure such as the curvature of a membrane [3, 4].

One of the best understood and studied physical properties of lipids is termed the shape parameter [3, 4, 6, 7]. This parameter, specific to each different lipid, can in many instances be used to qualitatively predict the preferred packing arrangement of a population of molecules when introduced to an aqueous environment. The shape parameter (S) is defined by the optimum area per molecule at the aqueous interface (a_o), the overall volume of the molecule (v) and the length of the fully extended alkyl chain (l_c) according to the following formula:

$$S = v / a_o \cdot l_c \qquad \textbf{Equation 1-1}$$

The value of S is roughly related to the ratio of cross sectional areas between the polar head group and lipophilic tail portions of a molecule and correlates to the shape of the three dimensional volume defined by its van der Waals surface as presented in Figure 1-3 below.

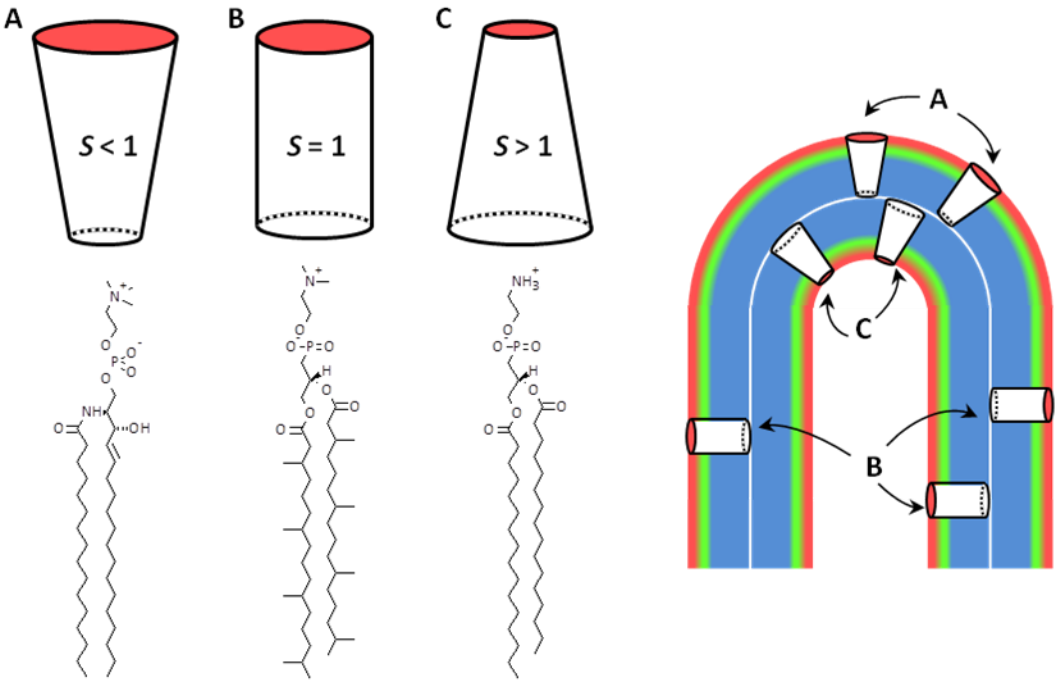

Figure 1-3: The three dimensional volumes associated with the shape parameter S, a structure of a representative for each class and their preferred arrangement within a bent bilayer structure. The pink surface of the shapes indicates the polar head group end of the molecule. A) Lipids with $S < 1$ represented by N-(hexadecanoyl)-sphing-4-enine-1-phosphocholine, B) lipids with $S = 1$ represented by 1,2-diphytanoyl-*sn*-glycero-3-phosphocholine and C) lipids with $S > 1$ represented by 1,2-dihexadecanoyl-sn-glycero-3-phosphoethanolamine.

Molecules with shape parameters close to unity are roughly cylindrical and as such the tight packing of these results in the generation of planar bilayer membrane structures which exhibit relatively low curvature over an extended area. Molecules with shape parameters slightly off of one are shaped roughly like truncated cones; those with $S < 1$ possessing larger surface area at the head group end while those with $S > 1$ having larger surface area at the end of the hydrophobic tail. The overall effect is that as the shape parameter of a molecule diverges farther and farther from $S = 1$ the tendency is for the bilayer membrane structures formed to adopt increasing degrees of curvature. In spherical bilayers, often called liposomes or vesicles, the hydrophilic surface area of the outer leaflet is larger than the area at the hydrophobic lamellar interface whereas the opposite relationship is true for the inner leaflet. Due to this fact lipids with $S < 1$ are better accommodated in the outer leaflet while the inner leaflet is more accommodating to lipids with $S > 1$; this property leads to the non-uniform distribution

of lipids with differing shape parameters between the two lamellae. At exceedingly low (<0.5) and high (>1) values of S the bilayer structure is abandoned altogether in favor of single layer micellar or inverted micellar structures which, although interesting in their own right, are of little concern to the present discussion.

Regardless of the dynamism and variety exhibited by natural lipid bilayers the generalized representation in Figure 1-2 above of the strata within the cross section going from polar ionic (red) through mid-polar (green) and finally to hydrophobic core (blue) is a satisfactory description of the bilayer environment. This simplified cartoon serves as a conceptual handle to understanding and designing compounds intended to interact with the lipid bilayer environment.

The non-polar interior (blue region) of the bilayer serves as an effective barrier to the passage of polar compounds, especially charged species such as ions or larger polar molecules such as sugars, while some smaller non-polar molecules such as carbon dioxide and even small polar molecules like water can pass somewhat freely from one side to the other [8]. Although this impermeability is critical to the role of bilayer membranes in compartmentalizing an interior environment from the external one, it also poses a dilemma. Namely, the generation of ionic concentration gradients across the lipid bilayer is a crucial form of storage of potential energy and the associated release of this potential energy via the collapse of these gradients in a controlled manner is necessary to the survival of a cell. If the non-polar interior environment of the lipid bilayer membrane presents such a large energetic barrier to the passage of these ions how can these processes occur? Fortunately Nature has evolved countless elegant molecular architectures to address this problem, often achieving high efficiency and selectivity for the necessary ionic species.

1.3 The Challenge - Ion Transport

The central problem in moving an ionic species between aqueous environments on either side of the lipid bilayer, where they are well solvated and therefore in a

relatively low energetic state, is overcoming the large energetic barrier associated with the desolvation as well as passage of an ion through the non-polar interior of the bilayer where it is not solvated and therefore in a state of relatively high energy [9, 10].

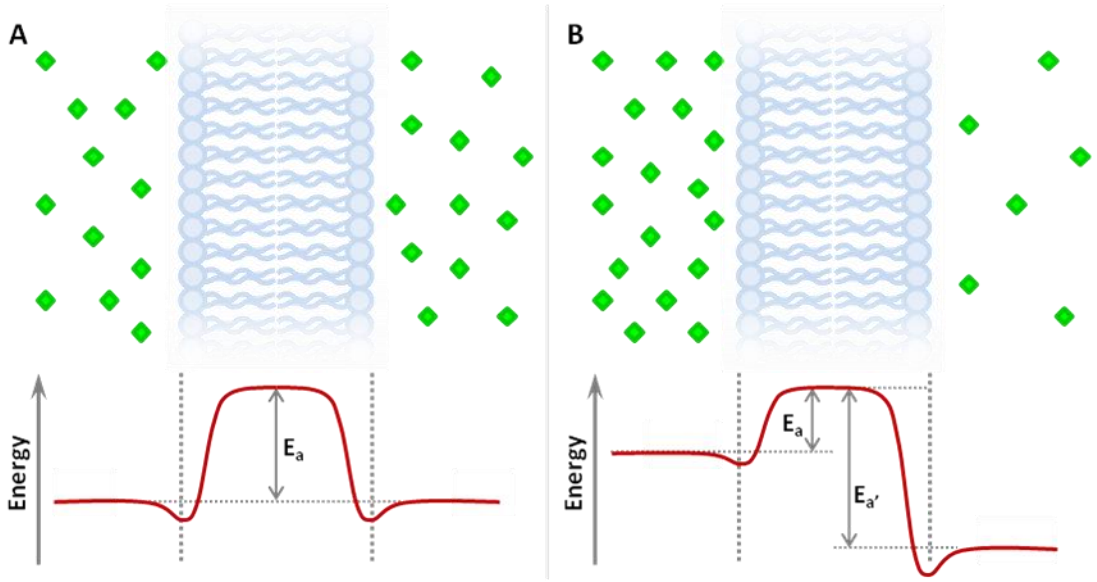

Figure 1-4: Cartoon representations of bilayer membrane environments and simplified curves of potential energy versus position associated with the passage of a membrane impermeable ionic species from one side of the lipid bilayer to the other in the case where A) equal concentrations of the species are present on either side of the bilayer and B) there is a concentration gradient from one side of the bilayer to the other.

In both cases presented in Figure 1-4 above the potential energy of an ion decreases upon approaching the ionic polar head group region relative to that in solution due to the favorable electrostatic interactions between the ionic species. This small potential energy well localized near the head group - aqueous interface causes the density of ions in this region to be slightly higher than in the bulk solvent. As an ion passes through the mid-polar region of the lipid bilayer there is a sharp increase in the potential energy associated with the loss of stabilizing interactions with the polar head groups as well as those with the polar aqueous solvent upon desolvation. The potential energy then plateaus at a maximum in the non-polar interior environment. In the system where no concentration gradient exists (Figure 1-4, A) the potential energy of the ions in solution on either side of the bilayer membrane is the same and there is no driving force to help overcome the large activation energy (E_a) necessary to move ions

through the bilayer. However, in the system where a significant concentration gradient does exist (Figure 1-4, B) the ions on the side of the lipid bilayer at higher concentration exist in a state of higher potential energy than those on the side of lower concentration. The result is that the activation energy (E_a) associated with the ions travelling from the side of high concentration to the side with low concentration is significantly smaller than for the reverse process ($E_{a'}$). Regardless, the energy barrier associated with passing an ion through the non-polar bilayer interior is still generally too large to be spontaneously overcome even when travelling along the concentration gradient

The role of an ion transporter is essentially to act as a catalyst for the transport process by lowering the 'activation' energy (E_a) associated with passing the ion through the non-polar lipid bilayer interior.

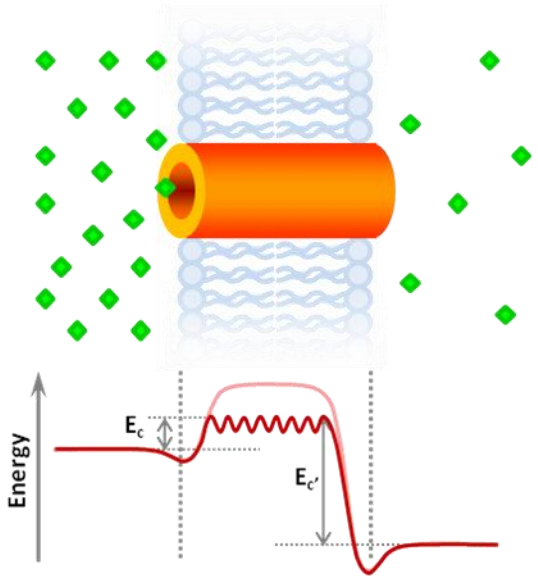

Figure 1-5: Simplified illustration of the effect of a representative ion transporter in this case depicted as a transmembrane ion channel, on the shape of the potential energy versus position profile for the movement on ions across the lipid bilayer membrane.

The illustration in Figure 1-5 above presents the general effect of an ion channel on the potential energy versus position profile for the movement of an ion across the lipid bilayer as compared to the case without the transporter (Figure 1-4, B). As can be seen, the activation energy (E_c) for transport of ions as catalyzed by an ion channel is significantly lower than that for the bare lipid bilayer membrane. In addition, the ion as

it passes through the non-polar interior environment of the lipid bilayer via the ion channel is lower in potential energy as well as experiencing several small local minima and maxima along the way. These local minima and maxima are associated with the ion forming relatively stable interactions with residues within the internal pore of the ion channel, helping to shuttle it along from one side to the other. Upon reaching the side of the bilayer with low ion concentration a relatively large and rapid drop in potential energy is observed.

There are several different structural motifs found in natural transporters but all act by isolating the ion from direct interaction with the non-polar interior environment during its journey across the lipid bilayer membrane. Conceptually there are three different motifs for transport systems of varying complexity and utility [11].

The first of these, which is of little interest in the context of this document, is transport mediated by membrane disrupting molecules. These compounds function by producing large defects in the lipid bilayer membrane through which any and all dissolved compounds can flow indiscriminately. Because of this property membrane disrupting compounds are of little use for harnessing the potential energy from concentration gradients, serving primarily as intercellular warfare agents or as self-destruct mechanisms for defective cells [12].

The second class of membrane transport motif is the carriers [13]. These compounds are of insufficient size to effectively span the distance across the lipid bilayer membrane and therefore act by forming a complex with the species to be transported at one membrane-solvent interface and then translocating through the lipid bilayer membrane to the opposite membrane-solvent interface where the transported species is released. Because these compounds are free to move within the bilayer membrane environment they can only act to move species along a concentration gradient in a process of facilitated diffusion.

The last class of membrane transport motif, and the one of greatest interest in so far as this thesis is concerned, is the transmembrane channel [14]. Channel forming

species, unlike the carriers, are sufficiently large that they can effectively span the distance from one side of the bilayer membrane to the other. Ion channels, as their name suggests, possess a roughly tubular internal pathway through which species being transported can flow. The internal diameter of this channel can vary significantly which has a significant impact on the mechanism and selectivity of species being transported. Narrower channels generally exclude most solvent molecules and therefore transport desolvated species by forming specific interactions with the species being transported [9]. Channels with larger diameters on the other hand can have significantly solvated internal volumes through which a wider variety of species can be transported. Especially large and rigid channels have interior volumes that act as columns of water through the bilayer through which many solvated species can rapidly diffuse.

Ion channels, unlike their carrier counterparts, span the bilayer and can therefore adopt a preferred orientation with respect to the internal and external environment as define by the lipid membrane. This orientation is maintained once the channel is embedded since the barrier to inversion of these large molecules within the bilayer is very high in energy. This property has a very important implication; the flow of species from high concentration to low concentration and the associated release of potential energy can be effectively harnessed to perform specific functions beyond the simple transport of ions. Harnessing this energy is critical to the most important functions of a cell such as ATP synthesis within mitochondria or carbohydrate production via photosynthesis in chloroplasts [15].

However, harnessing the potential energy from concentration gradients is predicated on there being concentration gradients to begin with. The generation of these is the task of highly specialized ion channels called ion pumps [16]. Ion pumps are modified ion channels which have the ability to move ion against the concentration gradient from areas of low concentration to an area of higher concentration. The comparison between the barriers involved in ion transport versus ion pumping can be better visualized by referring to the potential energy versus position curve depicted in

Figure 1-4. For an ion channel, the potential energy profile is followed from left to right, flowing with the concentration gradient; the energy required to catalyze the transport in this direction (E_c) is relatively low. An ion pump on the other hand works against the concentration gradient, following the potential energy profile from right to left; the energy requirement for transport catalysis in this direction ($E_{c'}$) is significantly higher. In order to affect ion transport in this direction the use of an external source of chemical energy is required.

The many different and highly complex mechanisms for the pumping of ions are beyond the scope of this document, ion channels being the primary focus. Ion pumps do however serve as inspiring examples of the types of complex functions that can potentially be achieved via extensive modification of relatively simple ion channels.

1.3.1 Natural Ion Channels

Due to the central role of ion channels in many processes vital to life, deficiencies in their function can result in very serious disease states. Cystic fibrosis for example, a condition that affects one in every 2000 - 3000 newborns of European descent, is attributed to various mutations in the gene coding for the cystic fibrosis transmembrane conductance regulator (CFTR) protein. The CFTR transmembrane protein is responsible for the regulation of the movement of chloride and sodium ions across the lipid bilayer membranes of epithelial cells. Defects in its function result in the production of excessively thick mucosal excretions resulting in depressed lung function and susceptibility to lung infections which can drastically reduce the lifespan of affected individuals [17].

In addition, the ion selective nature of many natural ion channels makes them ideal candidates for use in ion selective probes that could be used in biosensor applications among other things [18].

For these and many other reasons the study of ion channels and their functions is a worthwhile endeavor. Unfortunately, their very functions and their integral relationship with the bilayer membrane make studying natural ion channels very

difficult. Unlike many other proteins or small molecules which can be produced en masse via their over expression in genetically modified microorganisms, the over expression of ion channel molecules often results in unviable cultures due to the failure of the integrity of the bilayer membrane. The relatively large size of many ion channels also makes the laboratory synthesis of the natural structures an unmanageable exercise in all but the simplest cases.

Despite these challenges there have been some notable successes in acquiring crystal structures of some of the more ubiquitous ion channels. Some of these, such as the potassium [19] and mechanosensitive [20] channels, have provided valuable information about the nature of the relationship between structure and activity while others such as the chloride channels [21] have proven less useful. Unfortunately these successes represent only a miniscule fraction of the overall population of membrane associated proteins which are estimated to account for approximately 30% of the human genome [22].

For these reasons scientists have resorted to the synthesis of non-natural structures that behave as ion channels in order to try to obtain a greater understanding of the relations between their structures and functions.

1.3.2 Synthetic Ion Channels

The advantages of relying on synthetic ion channels as analogs of their naturally occurring relatives are many fold. As mentioned, the syntheses of these molecules are far more facile than obtaining sufficient quantities of naturally occurring channels via either genetic manipulation or synthetic methods. Chemists are also not limited by the building blocks available to natural systems, instead having the vast and constantly expanding arsenal of the synthetic chemistry toolbox at their disposal. Overall the structures that could potentially be obtained via a purely synthetic route should be as robust as the naturally occurring ion channels while being much smaller and structurally simpler. Due to their relative simplicity, it should be easier to ascribe differences in activity to particular modifications from one structure to another. In addition the

motivations of human beings towards targeting a particular function are often very different than those presented through evolution. Synthetic ion channels present the opportunity to design systems with unprecedented functions, an intriguing possibility that will be explored in this body of work.

Since the first synthetic ion channel reported by Tabushi in 1982 [23], an increasingly diverse collection of ion transporting species have been prepared by chemists. The field has been extensively and regularly reviewed [24, 25, 26, 27, 28, 29] and these fine publications should be consulted for a more comprehensive description of the progress to date than presented in this document. A small sample of synthetic ion channels from literature which illustrate some common structural properties relevant to the current work is presented in Figure 1-6 below.

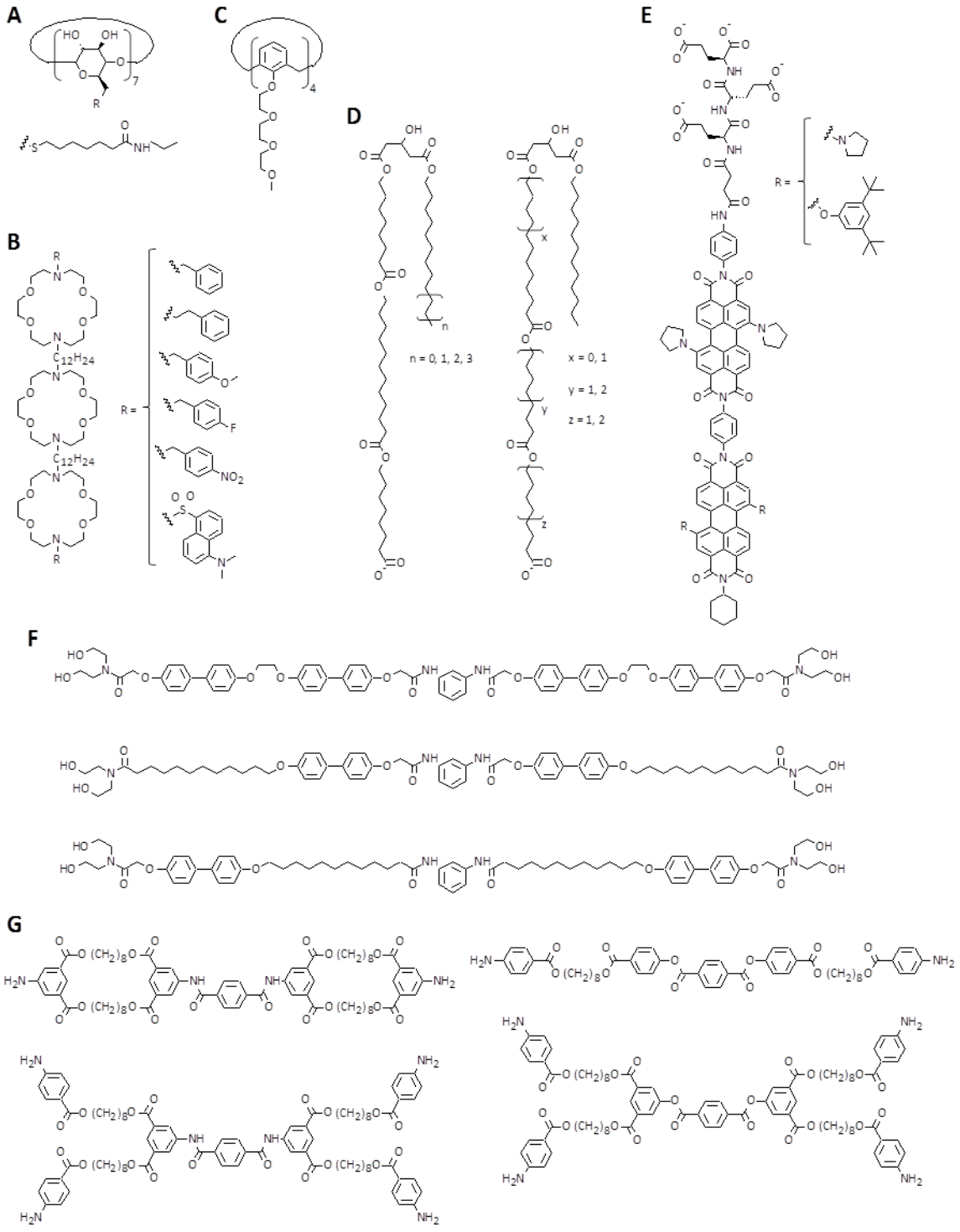

Figure 1-6: Some representative ion channels from literature; A) Tabushi's original amphiphilic β-cyclodextrin channel [23], B) Gokel's 4,13-diaza-18-crown-6 containing hydraphiles [30], C) Cragg's calixarene based channels [31], D) Fyles' oligoester amphiphiles [32], E) Matile's Pi slides [33], F) aplosspans also from Gokel [34, 35] and G) bola-amphiphiles also from Fyles [36].

As can be seen from the figure above, the variety of ion transporting structures produced to date is quite impressive.

Among the recurring motifs present in synthetic ion channel design are the incorporation of macrocyclic elements as seen in structures A, B and D, and amphiphilic structures as can be seen in structures C, E and F in Figure 1-6 above. The incorporation of these elements into synthetic transport active compounds can be seen as an attempt at mimicking the general structure of natural ion channels. The internal diameter of the macrocycles can be envisioned as serving to define the internal diameter of a transmembrane channel. The amphiphilic character is a feature common to the lipids that compose the bilayer membrane itself, this similarity in polarity characteristics means that the channels are more likely to have favorable interactions with the bilayer membrane and therefore exhibit improved partitioning from the aqueous environment.

As will be seen these two structural motifs will present themselves in the designs of the compounds synthesized for this thesis.

1.4 Studying Ion Channel Activity

The fundamental source of interest in working with ion channels is that they possess a distinct function; the transport of ions across the bilayer membrane. Without a way to study this function there is no way to draw conclusions about structure activity relationships that could exist. Fortunately, several different methods to assess the transport activity of both natural and synthetic ion channels have been developed and refined over the years and have proven to be invaluable tools in ion channel research [37, 38] These methods fall into two categories defined by the nature of the lipid mixture and by extension the topology of the membrane employed; vesicle based experiments and planar bilayer based experiments. Both of these types of methods are used extensively in the Fyles lab and specific examples pertinent to the current research are discussed below.

1.4.1 Vesicle Based Transport Activity Experiments

Many experimental methods for observing the transport activity of a purported ion channel involve the use of bilayer membranes in the form of lipid vesicles. Conceptually all vesicle based assays involve the observation of the collapse of the concentration gradient of an analyte between the internal and external environments of the lipid vesicles

A wide variety of analytes can be used in vesicle experiments depending on the property of the transporter of interest to be studied however all analytes must possess two crucial properties. Firstly, the analyte must not readily pass through the bilayer membrane without the aid of a transport catalyst such as an ion channel. Generally this means that most analytes are highly charged ionic species which have a large energetic penalty associated with being solvated in the non-polar core of the lipid bilayer membrane. Secondly there must be a method for detecting changes in the analyte concentration either within the vesicles or in the external environment. Some commonly used detection methods are ^{23}Na NMR in conjunction with a membrane impermeable paramagnetic shift reagent entrapped within the vesicle to monitor the transport of sodium ions [39], ion selective electrodes to monitor the efflux of ions from the interior of the vesicle to the external environment [40] and UV/Visible or fluorescence spectroscopy of transport induced spectral changes to concentration or ion sensitive dye molecules [41].

The dye based detection method was the one used most extensively in the Fyles' laboratory at the time of this writing, Figure 1-7 below illustrates the critical steps in the experiment as well as an example of the data produced.

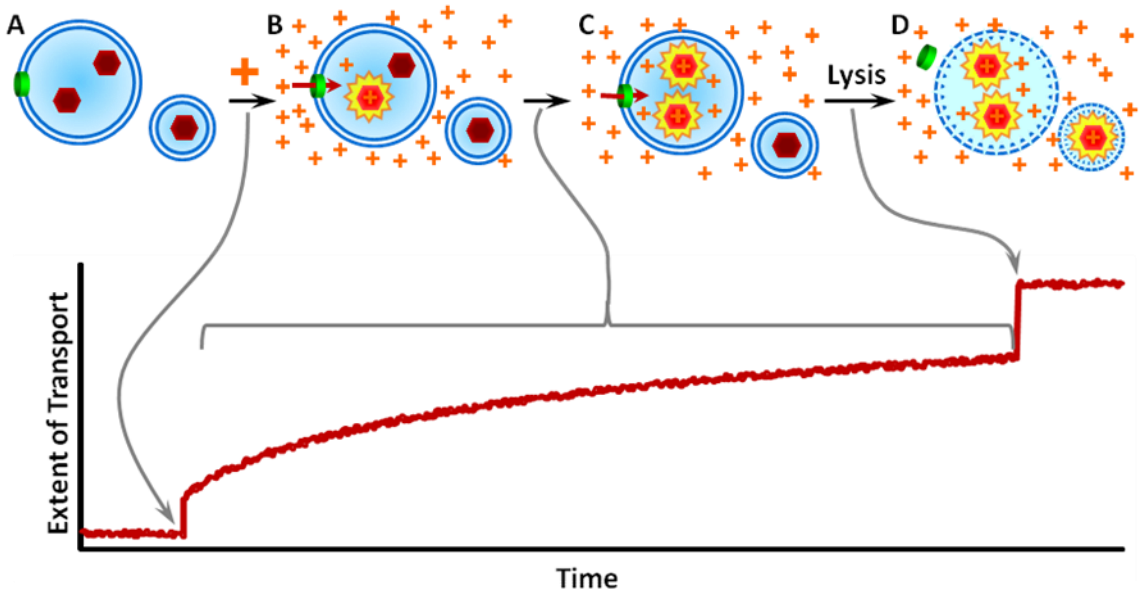

Figure 1-7: Diagram representing the series of events involved in a vesicle based assay using an entrapped ion sensitive fluorescent dye as the reporter as well as an associated graph of transport data to demonstrate observations made at each stage of the experiment.

Prior to the events depicted in Figure 1-7 above the vesicles containing the entrapped dye are incubated with the compound being studied for transport activity for a standard period of time in order to allow the partitioning of the compound into the lipid bilayer achieving the state represented at time A. At this point the time based fluorescence scan is initiated and a short period (~ 1 minute) prior to the introduction of the concentration gradient is recorded in order to obtain a baseline fluorescence intensity of the system at rest. After the establishment of this baseline the concentration gradient is induced by the injection of a concentrated solution of the species being monitored to the external solvent (A -> B). Due to osmotic stress of the rapid change in concentration this pulse often causes some short lived vesicle leakage resulting in a small instantaneous change in fluorescence intensity (B). After this initial burst in fluorescence intensity the changes in fluorescence observed during the following period (C) are due to the movement of ions into the vesicles along the concentration gradient as catalyzed by the introduced compound. After some data manipulation the slope of the line in this region of the fluorescence data provides a value for effective rate of transport of the particular species being monitored for that

compound being studied at a particular concentration. After a sufficiently long observation period (C, ~ 8 minutes) the vesicles are lysed with a detergent (D) resulting in another instantaneous change in fluorescence intensity as the destruction of the vesicles results in the collapse of the concentration gradient. This final step is performed followed by a brief period of recording (~ 1 minute) in order to obtain the final maximum fluorescence intensity so that data over different runs can be normalized.

An important feature of vesicle based assays is that they analyze the bulk behavior of a large population of channels behaving at once. The transport data obtained therefore represent an average rate constant for a compound at a particular concentration without providing any details about the exact nature of the transport active species such as stoichiometry. In addition since it is not possible to observe the specific nature of the transport mechanism using this assay, it is more difficult to isolate whether the transport behavior observed is due to a carrier, an ion channel or a membrane disruptor.

One of the most common environment sensitive dyes used for vesicle based assays of transport activity is the polyanionic membrane impermeable trisodium 8-hydroxypyrene-1,3,6-trisulfonate(HPTS) molecule depicted in Figure 1-8.

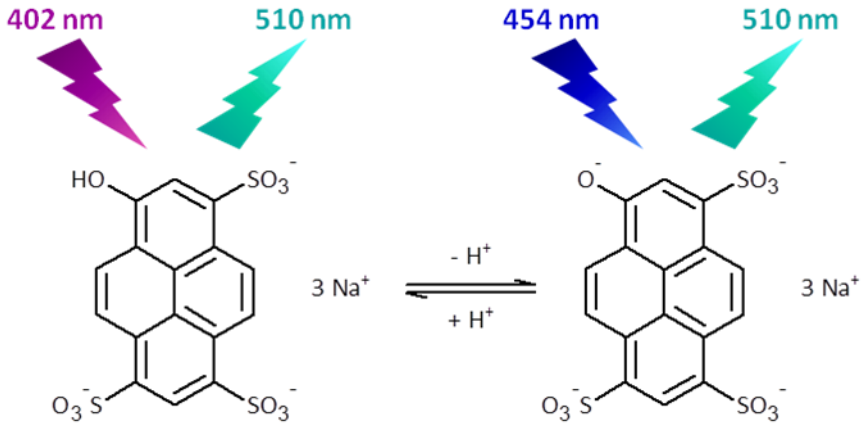

Figure 1-8: Structure of 8-hydroxypyrene-1,3,6-trisulfonate in both its protonated and deprotonated forms with associated wavelengths of maximum excitation and emission.

HPTS is a pH sensitive dye, and as such it monitors the flow of proton and hydroxyl ions in and out of lipid vesicles. The HPTS dye exhibits two different wavelengths of maximum excitation dependent on the protonation state of the hydroxyl group, 402 nm when protonated and 454 nm when deprotonated, but only a single wavelength of maximum emission at 510 nm. The pKa of the hydroxyl group is 6.4 and therefore shows the highest sensitivity to changes in protonation state in mildly acidic solutions. In addition, since the two different protonation states exhibit two different excitation maxima by simultaneously monitoring the fluorescence emission from excitation at these two wavelengths a ratiometric analysis can be used to determine the relative concentrations of the two states [42].

1.4.2 Planar Lipid Bilayer Based Transport Activity Experiments

The other commonly employed experimental technique used to study ion channel transport activity is the bilayer clamp assay [37, 38] which involves the use of planar lipid bilayers rather than spherical vesicles. The experimental set up, illustrated in Figure 1-9, involves two electrolyte filled chambers connected via a small aperture generally 150 - 250 microns in diameter. Electrodes are positioned in the two chambers such that a potential can be applied across the aperture.

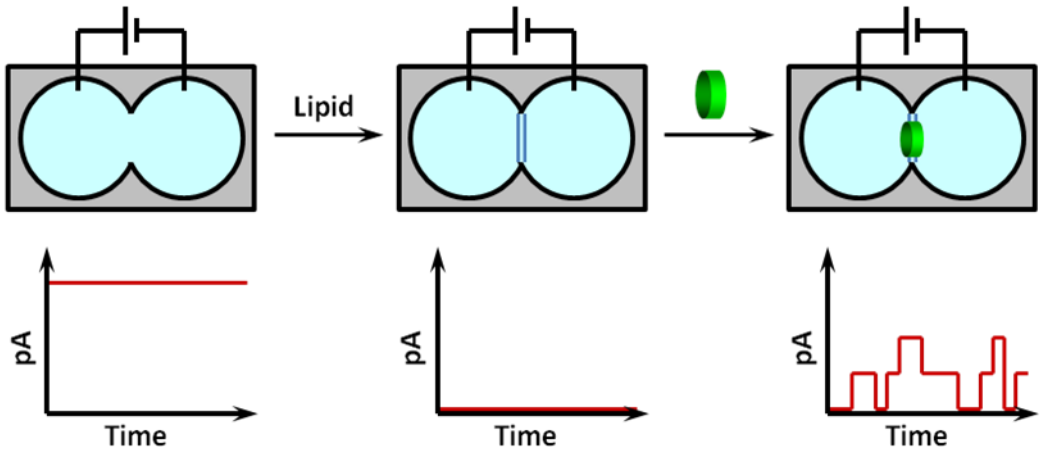

Figure 1-9: Simplified diagram of the experimental set up of the bilayer clamp experiment as well as corresponding current versus time recordings associated with applied potentials at each of the stages of the set-up.

As presented in the current versus time plots in Figure 1-9 in this initial state current is free to flow between the two chambers under an applied potential. However, a lipid bilayer when painted across the aperture acts as an insulator preventing the flow of current under an applied potential. The apparatus in this state is essentially a capacitor and in fact a common method for assessing the quality of the bilayer membrane is by taking a measurement of its capacitance. Once a properly formed bilayer has been established the purported ion transporter is added into either one or both of the chambers with gentle stirring in order to facilitate its incorporation into the bilayer membrane. Should the compound have poor aqueous solubility it can be pre-incorporated into the initial lipid solution however this method is disfavored as it makes it impossible to establish if a proper bilayer has formed. If the introduced compound is an active ion transporter a flow of current will be observed associated with the transport of charge carrying ions through the bilayer.

The bilayer clamp transport assay is a single species detection method that can be used to effectively observe individual transport events that are not possible using the vesicle based assays. The electrical properties of the bilayer are monitored over time with increases in the observed current indicating the transport of ions via one or more transport active species. This allows very detailed information about the nature of the transport activity of the compound to be acquired and from these details properties of the compound, such as the diameter or relative stability of an ion channel formed, can be estimated. Unfortunately, the observation of single transport active species leads to several potential difficulties. Firstly, because the assay detects single events it is possible that the activity observed at any one time is due, not the compound being studied, but rather a minor residual impurity leading to inaccurate inferences about activity. For this reason compounds studied using the bilayer clamp experiment must be exceedingly pure in order to obtain reliable data. In addition, due to the chaotic nature of the bilayer environment, the individual transport events observed for even the most well behaved channels exhibit a range of properties. As such, many repeated experiments must be carried out to obtain a statistically significant set of data in order

to verify that a particular activity is reproducible enough to be confident that it is not due to some artifact of any particular experiment. By the same token many experiments must be conducted in order to eliminate false positive results as well. This need for many repeated experiments means that the bilayer clamp assay can be quite labor and time intensive. Finally, it is not possible to obtain concentration dependent rate constants for the rate of transport for a compound as can be obtained from vesicle based experiments.

There are many distinct types of transport behaviors that can be observed for active compounds; however in the past the majority of the more irregular of these were either discounted outright or only mentioned in passing in favor of analyzing those more easily understood. Recent efforts have been made in the Fyles group to develop a robust method of cataloging and categorizing all potential observable behaviors in a statistically meaningful way [43]. After a comprehensive analysis of all available bilayer clamp data it was determined that three criteria were most important in defining ion channel transport behaviors; two quantitative properties in the conductance and the duration of an event and one qualitative property defining the general shape of the behavior observed. The conductance parameter, which loosely corresponds to the inner diameter of a channel, was found to vary greatly over several orders of magnitude from essentially zero to ten-thousand pS. Similarly the durations of events, related to the kinetic stability of the open channel, were also found to span several orders of magnitude from the instrument specific lower limits of detection of around 1 ms to several minutes. Finally the qualitative appearance of events was divided into five distinct categories; square top, multi-level, flicker, spike and erratic.

In order to combine these disparate types of data into one cohesive and easily referenced representation the possible values of the two quantitative parameters were subdivided, log divisions for the duration parameter and half log divisions for the conductance parameter, and plotted on the horizontal and vertical axes respectively to produce an activity grid; see Figure 1-10. The qualitative behaviors were then each

assigned a colour; green for square tops, blue for multi-level, orange for flicker, red for spike, purple for erratic and an additional grey colour as an accounting indicator for parameters outside the detection limits of a particular instrument.

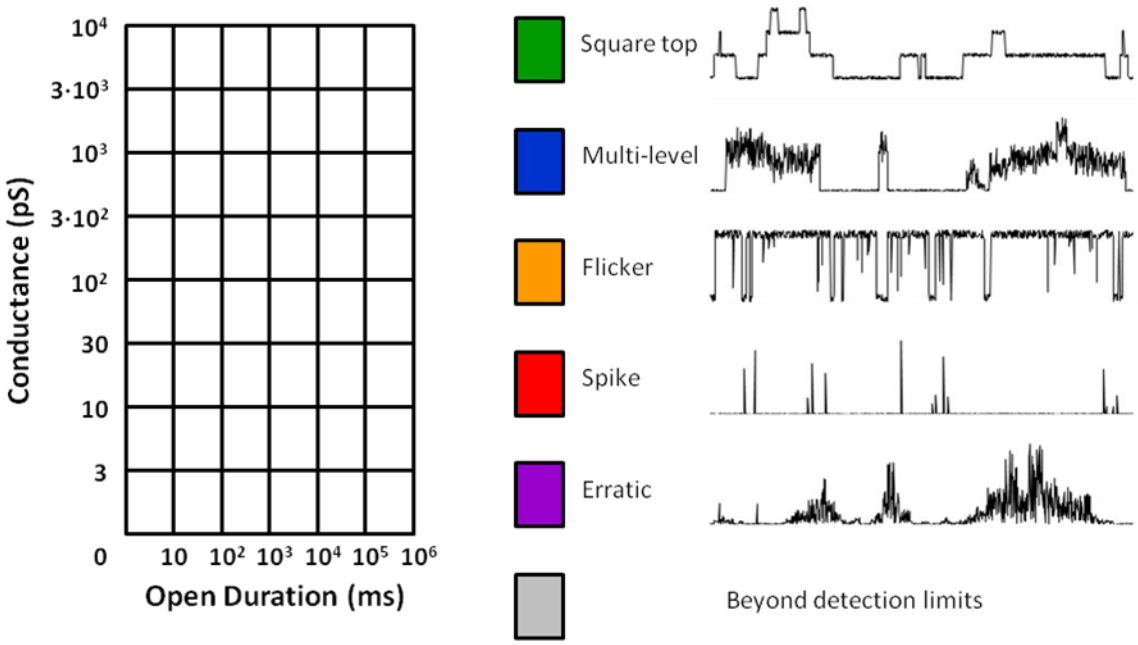

Figure 1-10: The open duration versus conductance activity grid and representative ion transport behaviors with associated colour code as developed by Fyles *et al*. for the cataloging ion transport activities as obtained from bilayer clamp experiments [43].

For a particular transport active compound each distinct event is first classified according to the type of activity observed, the open duration and the maximum conductance. The appropriate segment of the activity grid based on the open duration and maximum conductance is then filled in with the colour indicative of the type of activity observed. In this fashion an aggregate of all observed events for a channel under identical conditions can be summarized on a single activity grid. An additional level of detail can be added by varying the intensity of the colour of the various segments according to the relative frequency of the observed events. The final output of a sample activity analysis using this method is presented in Figure 1-11.

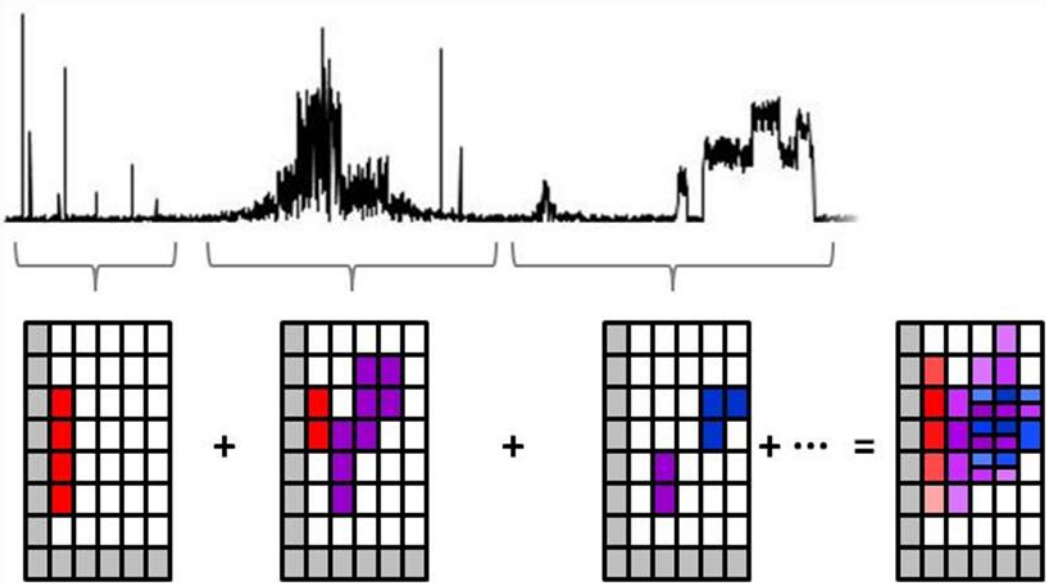

Figure 1-11: Sample activity grid analysis of a bilayer trace. By breaking down a trace into smaller segments along the time axis individual or small collections of signals can be systematically processed manually or using a computer program to generate activity grids for each segment. The number of different events for the entire trace can then be tallied and each square of the summary activity grid can be coloured the appropriate colour and intensity to reflect the types and frequencies of observed activity.

The overall result, an example of which is shown in Figure 1-11 is that the summary activity grids provide a rapid visual representation of a large number of events for a particular active compound under specific conditions. This allows for the rapid comparison of the activity for different channels or the same channel under different conditions.

When reproducible behaviors can be attributed to a compound being studied, in particular the observation of square top (green) events, it is possible to infer more specific properties of the ion channel formed. For example, from the observed current at a particular applied potential the conductance of a channel can be calculated according to the equation:

$$g = \mathrm{I}/\mathrm{V} \qquad \textbf{Equation 1-2}$$

Where g is the conductance in Siemens, I is the observed current of a single channel opening in amperes and V is the applied potential in volts. From this calculated conductance the approximate internal diameter of an ion channel can then be

determined using the Hille equation [44] which approximates the ion channel as an electrolyte filled cylinder:

$$1/g = l\rho[\pi(d/2)^2] + \rho/d \qquad \textbf{Equation 1-3}$$

Where g is the conductance, l is the length of the channel (often assumed to correspond to the thickness of the bilayer), d is the inner diameter of the channel and ρ is the resistivity of the electrolyte solution. It should be noted however that although approximations of internal diameters made using the Hille equation are relatively faithful for larger channels, for smaller channels in which specific interactions between the channel interior and the ions being transported are important the model based on an electrolyte filled cylinder is inaccurate. As such the Hille equation tends to significantly underestimate the diameters of smaller channels; caution must be exercised since conductances observed for some channels provide physically unrealistic values for the channel radius.

1.5 New Challenges of Synthetic Ion Channel Research

As eloquently summarized by a pioneer in the field of synthetic ion channel research, future progress must focus beyond developing new channel structures using existing methods.

> "It is safe to say that the simple punching of holes in membranes does not pose significant problems anymore. Fundamental studies on structure-activity relationships fully confirm this conclusion and, although highly valuable and important, have to pay attention not to become repetitive. The same holds for the introduction of new architectures that do not go beyond simple transport. What arguably matters most is conceptual innovation."
>
> - Stefan Matile (*Chem. Soc. Rev.*, 2011, **40**, 2453-2474)

Although much of the work carried out in this thesis predates the publication of this quote, the sentiment associated with it can be seen as the guiding principle for the research contained in this thesis. The challenge put forth to scientists in the field of

synthetic ion channel research by Matile can be interpreted from two different conceptual perspectives. On one hand it can be viewed from the standpoint of synthetic innovation; in order to progress towards the realization of practical uses for synthetic ion channels new methods for the rapid synthesis of these complex structures is necessary. On the other hand it is a push towards novel functions; with the ability to generate a wide array of compounds that exhibit transport activity already well documented the next logical step is towards synthetic channels that more closely mimic the dynamic behaviors of Natural ion channels. Fortunately there exists a logical common approach to both of these challenges: supramolecular self-assembly.

Supramolecular chemistry involves the study of the directed control of reversible interactions between molecules or regions of molecules in order to produce more complex superstructures via molecular self-assembly [45]. Examples of molecular systems exhibiting supramolecular interactions are myriad both in Nature as well as those devised by chemists [46]. In fact supramolecular self-assembly is fundamental to many of the topics already discussed; it organizes assemblies of lipids into bilayer structures, helps to drive membrane bound proteins into these bilayers as well as assembling subunits of pore forming molecules into transport active constructs. For many of these examples the weak interactions between molecules allows for the generation of ranges of structures that would be practically impossible to achieve by using only covalent chemistry. In addition the labile nature of these interactions is critical to the very function of many of these systems.

The first goal of the current research was to expand the field of ion channel research via synthetic innovation. As can be seen from the many examples of synthetic ion channels that have been presented so far (Figure 1-6), all share the common feature of being relatively static structures that often involve laborious syntheses. As such the generation of novel transport active structures can be an intensive and sometimes unfruitful process; successful synthesis of exceedingly complex and beautiful structures without the guarantee of realizing commensurate transport functions is a daunting

prospect. As will be seen throughout this introductory chapter exploring the field of supramolecular chemistry should be particularly suited to tackling the challenge of developing novel synthetic strategies to allow for the rapid generation of libraries of complex molecular systems.

The second and arguably more ambitious, goal of the current research was to explore the problem of introducing novel functions to the field of synthetic ion channel research. As previously stated, one of the perceived advantages of synthetic systems over Natural ones was that scientists were not bound by the evolutionary process of natural selection in guiding the development of new functions. Since function is inexorably linked to structure the logical extension of this is that in order to realize dynamism of function you must have dynamism of structure. It may very well be that the existing approach to achieving functional synthetic transport systems may be hindered by the focus on thermodynamically stable products. Although these compounds are likely easier to characterize due to their static structure, Nature has overcome the challenge of transporting charged species across the lipid bilayer involving mechanisms about as far from equilibrium as possible. To this end the field of supramolecular chemistry should also provide the tools necessary to take the first steps towards realizing the development of novel functions within the context of purely synthetic ion channels.

1.5.1 Supramolecular Chemistry and Non-Covalent Interactions

While traditional molecular chemistry deals with covalent bonds, which generally range in strength from ~150 - 950 kJ mol^{-1}, supramolecular chemistry deals with productively harnessing non-covalent interactions between molecules [47]. Through natural selection in Nature or careful design in the laboratory it is possible to harness many of these non-covalent forces synergistically in order to produce supramolecular structures which are held together with comparable stability to structures exclusively via covalent bonds. The table below summarizes the types and bonding strengths of these weak interactions along with schematic representations of each.

Table 1-1: Non-covalent interactions prevalent in supramolecular chemistry with associated bonding strengths and schematic examples of each where appropriate.

Interaction	Strength (kJ mol^{-1})	Example
Ion - Ion	100 – 350	
Ion - Dipole	50 – 200	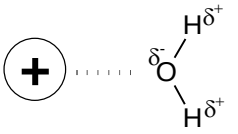
Dipole - Dipole	5 – 50	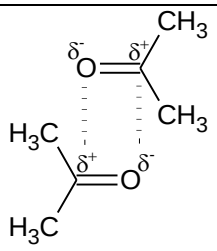
Hydrogen Bonding	4 -120	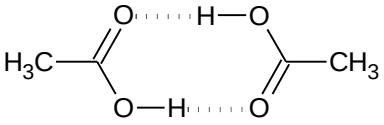
Cation - π	5 – 80	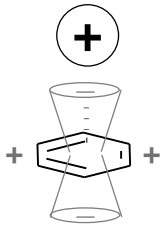
π -π	0 – 50	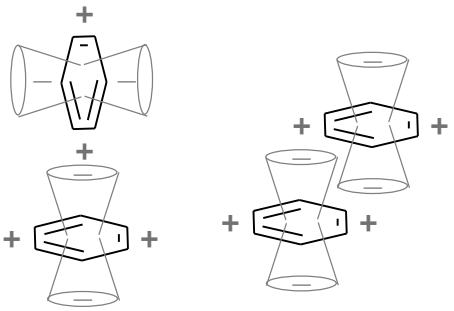 Edge to Face Staggered
London Dispersion Forces	< 5	

It is clear from Table 1-1 above that not all non-covalent interactions are created equal; they differ in both the strength of the interactions as well as the overall geometry adopted between interacting species. As will be discussed later in Section 1.7 these differences have a profound impact on the roles of the various interactions in supramolecular self-assemblies.

An important feature of all of the interactions listed in Table 1-1 above is that they are at least partially electrostatic in nature, involving the attractive interactions between species possessing oppositely charged or partially charged species. Their electrostatic foundation means that in general interactions involving ions which possess formal charges (ion - ion, ion - dipole and cation - π) are stronger than those between species only exhibiting the partial charges of fixed dipoles (hydrogen bonding and dipole - dipole) which are themselves stronger than interactions involving quadrupoles (π - π) and induced dipoles (London dispersion forces). Other factors affecting the overall strengths of these interactions due to their electrostatic nature are the distance between the two interacting species through space and the competition for interactions with other polar species, namely solvent, present in the environment.

In polar solvents, water being the canonical example, interactions between charged species and the polar solvent are favored over interactions between the charged species themselves due to the ability of the high dielectric of water to screen charges. This effect is only exacerbated by the enormous relative excess of solvent molecules to the molecular components of the self-assembly. The result is that in polar media the effective association energies between species attracted to each other via electrostatic forces is greatly reduced. In non-polar media however, which have very low dielectric properties, shielding by and interactions with the solvent are minimized and the effective association energies between species are not significantly diminished. However, since the ultimate goal is often to realize self-assembly in aqueous solvent, the designs of such systems must take into account the competition from the aqueous solvent.

An additional attribute of these non-covalent interactions is their inherent degree of directionality. In general as the directionality of an interaction increases the range of possible orientations available to two interacting species diminishes. The effect is that interacting species with fewer interactions of high directionality have more conformational freedom and tend to adopt less rigidly defined supramolecular assemblies as compared to those with more such interactions. Although for certain systems conformational polymorphism is tolerated or even desirable, for the design of systems that adopt predictable geometries, such as ion channels spatial control of the individual components is crucial.

Both of these effects factor heavily into the design of self-assembling systems that employ exclusively the non-covalent electrostatic interactions presented in Table 1-1.

1.5.2 The Hydrophobic Effect

A special class of non-covalent interaction that does not fit tidily into the discussion of those presented in Section 1.5.1 above is the hydrophobic effect [48]. Unlike the non-covalent interactions discussed already, which are defined by the electrostatic interactions between two charged species, the hydrophobic effect involves the interaction of compounds with water. As a solvent the molecular structure of water is unique in that all atoms involved have the ability to act as either hydrogen bond acceptors or donors and in addition, unlike ammonia, the number of potential donors and acceptors is equal ensuring the maximum number of hydrogen bonds is possible. Due to this structure water has the ability to form very dense networks of intermolecular hydrogen bonds which result in an enthalpic stabilization for the assembly of these molecules. In addition, because of their small size, the relative conformational freedom of the molecules within the assembly provides an additional entropic stabilization as individual molecules have the ability to move about relatively freely while continuously dissociating and reforming hydrogen bonds to adjacent water

molecules. These stabilizing forces manifest themselves in water having an exceedingly high boiling point for such a small molecule.

The strong tendency of water to self-associate is the driving force for the hydrophobic effect. This effect manifests itself upon the introduction of molecules with relatively low polarity into the aqueous environment. This is an energetically unfavorable process as it involves both the disruption of hydrogen bonding between water molecules as well as limiting the spatial and conformational freedom of the molecules closest to the introduced compound. As such the hydrophobic effect involves both enthalpic as well as entropic driving forces, the proportions of which can vary significantly from system to system. In order to counteract this loss of stabilizing energy the tendency is for non-polar hydrophobic compounds or regions of compounds to aggregate in such a way as to minimize the interfacial surface area between non-polar regions and water in order to minimize the disruption to the intermolecular interactions between water molecules. The hydrophobic effect is partially responsible for the energetic gain in π - π interactions (Table 1-1), especially those of the staggered variety where the interfacial surface area between the non-polar aromatic rings and water has been more effectively minimized. In extreme cases the hydrophobic effect involves complete phase separation of non-polar molecules from the aqueous environment such as seen in attempting to mix oil with water. The strength of the hydrophobic effect is dependent on the polarity difference between the introduced compound and water and since it implies no specific interactions does not have any inherent directionality.

The self-assembly of lipids into the bilayer membrane is a prime example of the hydrophobic effect at work. The ionic polar head groups of the lipid molecules are relatively well tolerated in the aqueous environment and as such are exposed to the aqueous phase. The non-polar tail sections would significantly disrupt the intermolecular interactions between water molecules so they are buried within the interior space at the interface between the lipid bilayer lamellae. In this conformation

the hydrophobic tails are also afforded relatively high conformational flexibility leading to an additional entropic gain. Because of this relative disorder of the bilayer membrane it is sometimes referred to as a phase separation process rather than a self-assembly which has the connotation of involving more specific non-covalent interactions. The gain in energy associated with the shielding of the non-polar regions of the lipids from the aqueous environment is more than sufficient to overcome the penalty induced by forcing the identically charged head groups into close proximity [49]. The overall result of these different driving forces in the interaction of lipids and water is the formation of the bilayer membrane.

1.5.3 Metal - Ligand Interactions

Yet another class of interaction that is not simply defined by the interaction of charged species via electrostatic interactions are those falling into the category of metal - ligand interactions to form coordination compounds [50,51, 52]. There are many possible bonding motifs available between ligands and metals depending on the exact electronic properties of the participants but in general they involve the donation of a pair of electrons from a neutral or anionic ligand which acts as a Lewis base to a neutral of cationic electron deficient metal centre which acts as a Lewis acid. This situation differs from covalent bond formation in that both electrons in the bonding interaction come from the donor atom of the ligand. Due to the formal sharing of electrons between ligand and metal the resulting interactions can involve binding energies significantly higher than the primarily electrostatic non-covalent bonds, approaching those of weaker covalent bonds of approximately 50 to 250 kJ mol^{-1} [53].

Although the competition between ligands and water for the binding to the metal centers still exists due to the ability of water to act as a Lewis base, the binding affinity of water for most transition metals is quite low. Qualitatively the reason for this can be understood by invoking hard and soft Lewis acid and base theory (HSAB) [54]. This theory attempts to arrange metals and ligands along a spectrum from ‘hard’ to ‘soft’ based on empirical evidence of metal-ligand interactions. In general the trend assigns

small, highly charged or polar and weakly polarizable species at the hard end of the spectrum while larger, neutral or charge diffuse and polarizable ones at the soft end of the spectrum. A representative collection of ligands ranked from soft to hard is presented below.

$$\textit{SOFT} \text{ -- } CN^- < S^{2-} < RS^- < I^- < Br^- < Cl^- < NH_3 < HO^- < H_2O < F^- \text{ -- } \textit{HARD}$$

The metals can also be ranked along a similar the general trends being that the hardest metal cations are those early transition metals of the first row in high oxidation states while the softest are those late transition metals of lower rows in lower oxidation states. HSAB theory states that the most stable coordination compounds are those formed between ligands and metals that have qualitatively similar hardness /softness. As can be seen from the small series of ligands presented above, water is considered to be quite hard as compared to many of the commonly used ligands such as amines. Since many of the transition metals, especially those later in the periodic table are considered to be relatively soft, there is a significantly greater mismatch between the hardness of these and water relative to many of the donor atoms present in the most common ligands. The overall result is that given the choice of coordinating to either water or to some other ligand, the latter option is generally preferable.

In addition to the relatively strong nature of these interactions they also possess a high degree of directionality associated with the coordination sphere of the transition metal. The most commonly observed arrangements of ligands around a transition metal are the square planar and octahedral geometries which involve the coordination of four and six donor atoms respectively. These geometries allow ligands to be held at right angles to each other which is a much more difficult conformation to achieve with standard covalent bond chemistry. In addition the coordinating ligand molecules are not limited to forming only one bond to the metal centre. The number of coordinating sites, termed the denticity of the ligand, can also be increased in order to achieve stronger overall binding between the ligand and metal centre due to the additive effects of the having multiple interactions as well as the energetic bonus obtained from

preorganization (discussed further in Section 1.6). Due to the strong binding that can be achieved between ligands and transition metal centres, the high degree of directionality that can be achieved as well as their relative stability in an aqueous environment these interactions are among the most useful for constructing well defined supramolecular self-assemblies.

1.5.4 Reversible Covalent Bonds

More recently the scope of interactions employed in self-assembling structures has extended to those using reversible covalent bonds [55, 56, 57, 55, 58, 59, 60]. Reversible covalent bonds, as their name suggests, are formally covalent bonds that are sufficiently weak or reactive that the equilibrium between bond formation and cleavage can be easily shifted under relatively mild reaction conditions. Since they involve covalent bonds as opposed to non-covalent interactions, structures incorporating reversible covalent bonds tend to be somewhat more robust.

The library of reversible covalent bonds that have been incorporated into dynamically assembling systems is continuously growing. A representative sample of these is presented in Figure 1-12 below.

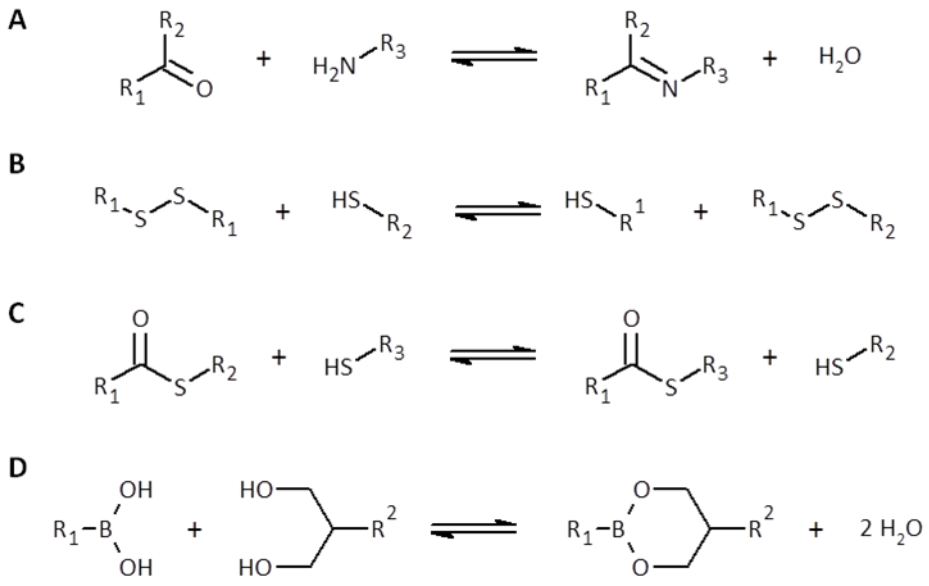

Figure 1-12: Some representative reversible covalent bonds; A) imine bond formation, B) thiol-disulfide exchange, C) thiol-thioester exchange and D) boronic ester formation.

A further advantage to using reversible covalent bonds in a self-assembly strategy is that the reactions are often highly sensitive to the environmental conditions. This can allow for the in situ exchange of different reactive components to form new structures which may lead to entirely different functions depending on the system. In addition, by changing the environmental conditions it is also possible to speed up or slow down the reactions as necessary in order to control the stoichiometry of the products formed and by extension the types of functions observed. Focus in this field to date has centered primarily on using reversible covalent chemistry towards the development of dynamic combinatorial libraries in drug design [61] and the synthesis of dynamers, environment sensitive polymers [62, 63]. The control of function via the introduction of external stimuli (reagents) is a particularly appealing aspect of reversible covalent bonds as it represents a move towards systems which exhibit properties of Natural supramolecular systems.

1.6 Molecular Recognition Strategies

As discussed previously, while any particular interaction in isolation is generally too weak to stabilize a supramolecular assembly to any appreciable extent, the additive effects of many of these interactions operating in concert can generate very robust architectures. Just as important to the design of a self-assembling supramolecular system as the use of multiple weak non-covalent interactions is the productive arrangement of these interactions to generate the desired structures. To this end there are also several important related concepts; complementarity, preorganization and the chelate and macrocyclic effects.

1.6.1 Complementarity

The concept of molecular complementarity was first introduced by Emil Fischer over a century ago in the form of his lock and key model towards the understanding of enzyme - substrate interactions. Contemporary supramolecular chemistry is of course not restricted to the study of enzymes and their substrates so in order to generalize these fundamental concepts the terms host and guest are generally used. By

convention the host is the member of an interacting pair possessing convergent interaction sites while the guest possesses divergent sites for interaction [64]. Generally the host is larger than the guest although exceptions do exist. Figure 1-13 is provided below to help illustrate the concept of complementarity.

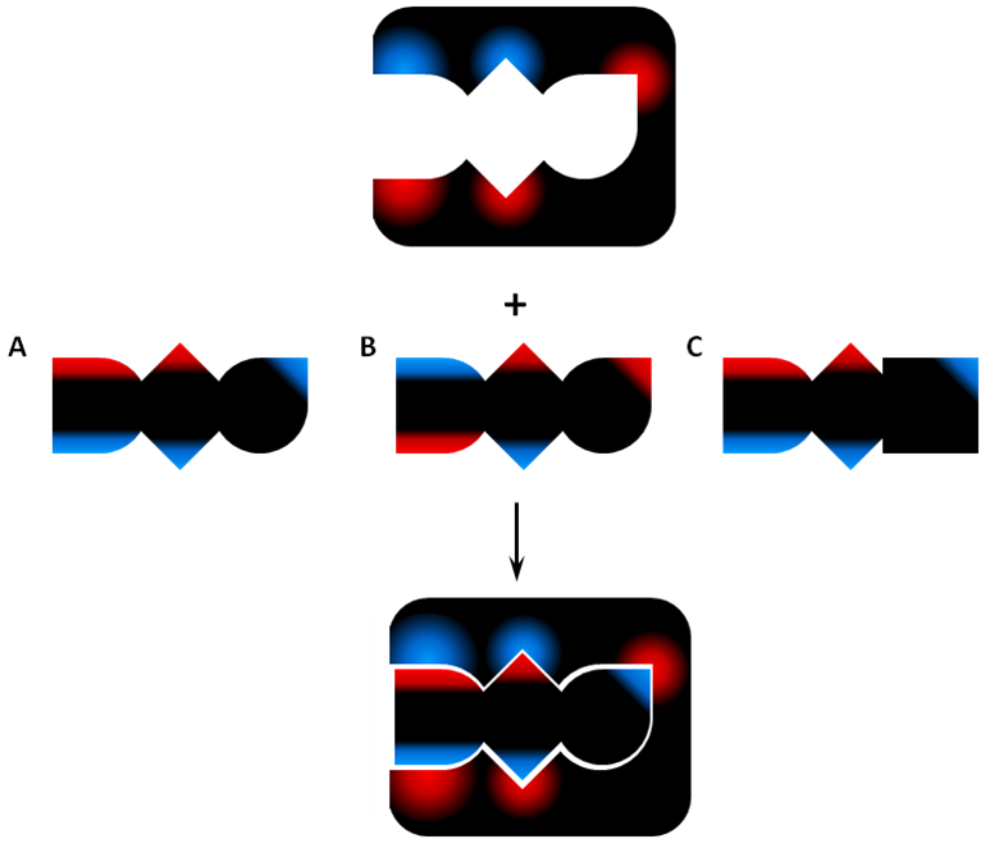

Figure 1-13: Simple representation of the concept of complementarity. Red and Blue regions of the various shapes can be envisioned as representing regions of high and low electron density respectively. Of the three guests only **A** has complementarity of both electrostatic interactions as well as shape, **B** is of the correct shape but lacks the complementary interactions whereas **C** has complementary interactions but is of a shape not accommodated by the host. According to the lock and key model, guest **A** will have the highest binding affinity.

The lock and key model states that the more complementarity that exists between the host and guest both in terms of specific non-covalent interactions as well as in terms of shape the lower the energy of interaction and therefore the more stable the complex formed. In the context of a discussion of supramolecular chemistry in general shape complementarity is better defined as belonging to the London dispersion

forces class of non-covalent interaction. Fundamentally complementarity is the driving force towards achieving greater enthalpy of formation between two interacting species.

One of the most studied and best understood examples of complementarity found in Nature is the example of nucleobase pairs found in deoxyribonucleic acid (DNA) and ribonucleic acid (RNA) polymers [65, 66]. Because of the importance of the reliable transfer of genetic information from one generation to the next for the successful continuation of a species, life on earth has evolved an elegant system for this task. Although many different non-covalent interactions are required for the successful self-assembly of single stranded DNA and RNA polymers into fully assembled double stranded DNA and RNA helices the main contributor to the selectivity of complementary strands for each other is the hydrogen bonding which occurs between the nucleobases. Naturally occurring DNA and RNA polymers each possess four possible nucleobases, illustrated in Figure 1-14; the purines adenine (A) and guanine (G) and the pyrimidines cytosine (C) and thymine (T) in DNA or uracil (U) in RNA.

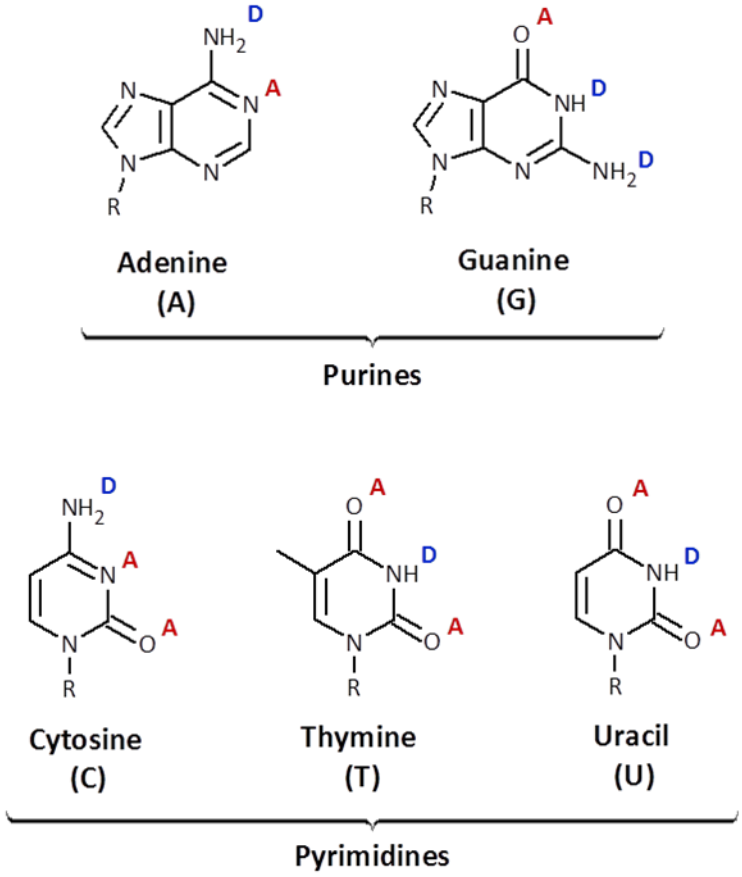

Figure 1-14: The DNA and RNA nucleobases. The R groups denote the attachment point to the phosphate sugar backbone of the polymer. The red A's and blue D's accompanying each structure denote sites on the hydrogen bonding face of these molecules which are hydrogen bond acceptors and hydrogen bond donors respectively.

As can be seen in Figure 1-15 below the hydrogen bonding motifs present on the various nucleobases shown in Figure 1-14 are such that complementarity exists only between specific pairs comprising one purine and one pyrimidine.

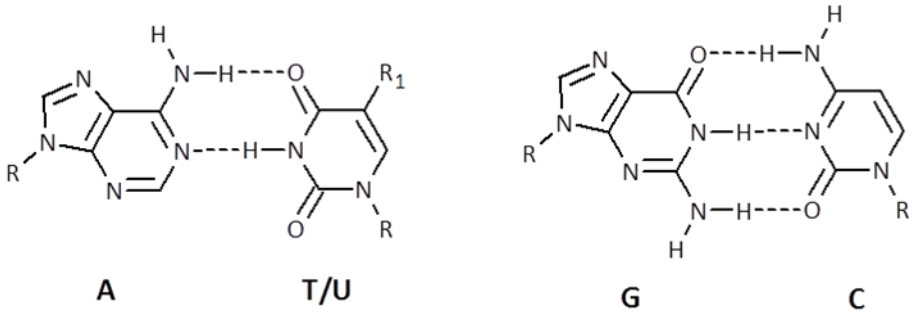

Figure 1-15: Hydrogen bonding between complimentary base pairs. The R groups denote the attachment point to the phosphate sugar backbone, the R_1 group is a methyl (CH_3) group for Thymine in DNA and a proton (H) for Uracil in RNA.

Because the most productive hydrogen bonding pairs, depicted in Figure 1-15, involve both one purine and one pyrimidine there is an additional element of size complementarity for complimentary DNA or RNA strands. If a mismatch occurs such that two purines are opposite each other there is a significant degree of additional steric strain between the strands further destabilizing the double stranded complex. Conversely, if two pyrimidines are involved in a mismatch, the two nucleobases would be held too far from each other to form hydrogen bonds to any extent if at all possible.

The overall effect is that strands of higher complementarity form more stable duplexes than those with mismatched base pairs resulting in strands exhibiting selectivity for more closely related partners. This sequence selectivity is critical to the high fidelity observed during the replication process.

The relative base pair composition of the complementary strands also has an effect on the overall association energy of the duplex with sequences rich in C and G pairs being more stable than those which are relatively deficient due to the extra hydrogen bond formed between this pairing as compared to the A and T/U pairs.

Although the complementarity between DNA and RNA polymers is the factor driving the formation of double stranded compounds it is not directly responsible for the final condensed helical structure formed. The driving force for the nucleobase

stacking and the helical pitch observed along the duplex is due both to π - π stacking interactions between adjacent nucleobases, a component of which is the hydrophobic effect acting to exclude water from the hydrophobic faces of the ring systems, and the repulsive interaction between phosphate groups along the backbone which is itself modulated by the environment in which the duplex is found. This example illustrates how the initial assembly of two or more components via strong primary non-covalent interactions (hydrogen bonding between base pairs) can be further modulated and stabilized by the action of additional weaker secondary non-covalent interactions (π - π stacking, hydrophobic effect, ion - ion interactions) into an energetically more stable final conformation. This illustrates the overall additive effects of many weak non-covalent interactions towards an exceedingly stable supramolecular self-assembly.

1.6.2 Preorganization

Preorganization is another concept of great importance to many successful supramolecular self-assemblies. Unlike complementarity which deals mainly with maximizing enthalpic contributions to improve association energies, the principle of preorganization aims to minimize entropic factors that would normally be detrimental to complex formation. Preorganization is best understood as the drive to organize host molecules such that minimal rearrangement of the structure via molecular motions such as bond rotation is required in order for productive non-covalent interactions with the guest molecule [67]. A slightly modified version of the schematic used in the discussion of complementarity is provided in Figure 1-16 below to help illustrate the concept of preorganization.

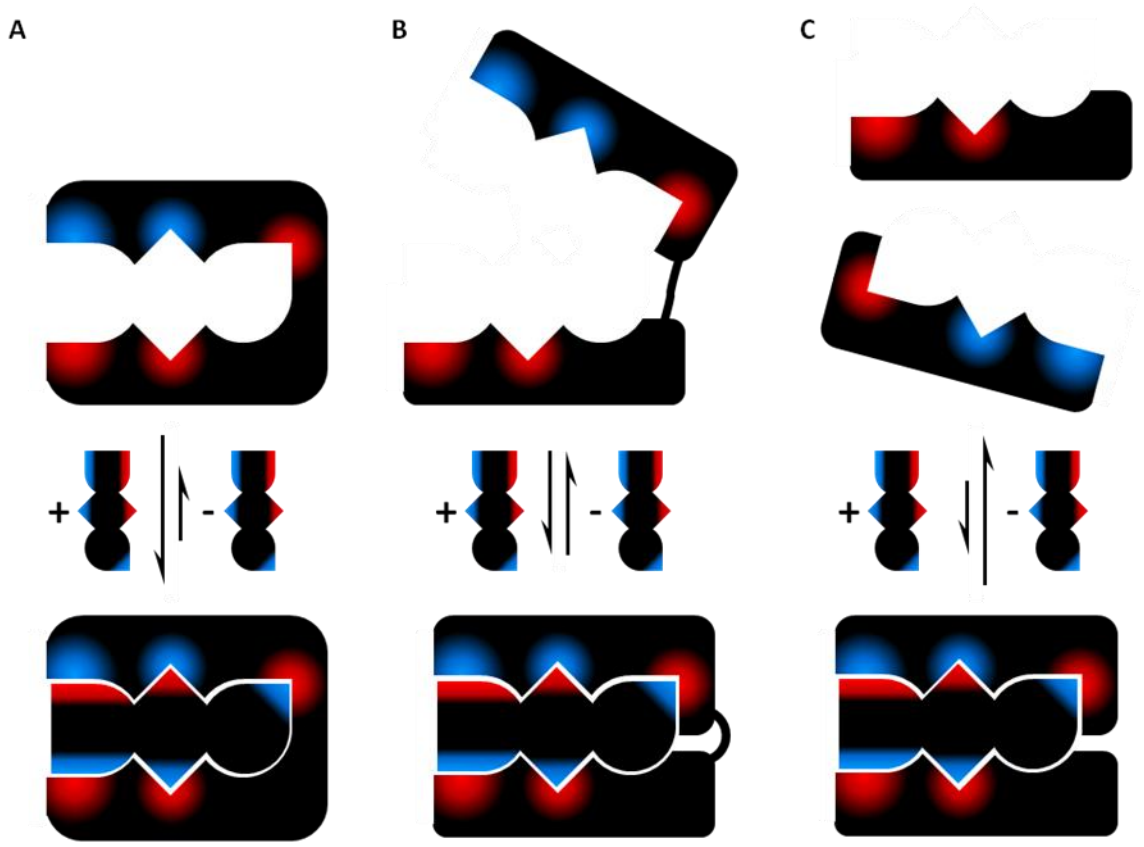

Figure 1-16: Simple representation of the concept of preorganization. The three systems pictured above are presented in decreasing order of preorganization from left to right. A) the host compound is rigidly held in a conformation that closely matches the guest molecule resulting in relatively tight binding. B) a similar system with a flexible linker between the two halves of the host allowing for some conformational freedom resulting in less stable binding of the guest. Note however that the binding of the guest into one half of the host still brings the guest relatively close to the other half resulting in some preorganization resulting in improved binding properties for the second half. C) a system where the 'host' exists as two completely independent components resulting in a large degree of conformational freedom. Unlike for case B the binding of the guest into one half of the host will have no effect on the binding of the second half as these two processes are entirely independent.

In Figure 1-16 above, three different potential host systems are presented from highest to lowest degree of preorganization. All three possess complementarity of shape and non-covalent interaction sites to the target guest molecule however they are expected to have association energies that differ greatly. The first host, which has the least conformational flexibility due to its rigid structure, experiences the smallest decrease in entropy upon binding the host. The second host, possessing some conformational flexibility due to the flexible linker joining the two halves of the molecule, must lose a larger amount of entropy than the fully rigid structure to adopt a

conformation which effectively binds the target guest. Finally, the third host, composed of two separate components, suffers the greatest entropic penalty upon binding of the guest molecule due to the loss of much more conformational flexibility. With each additional degree of conformational freedom of the system the smaller and smaller the energy gain associated with complex formation. In essence, by minimizing the entropy of the system the overall gain in energy upon complex formation can be maximized resulting in a much more tightly bound supramolecular self-assembly. It should be noted however that an excessively rigid host with a perfectly matched binding site may fail to bind the desired guest molecule if there are immovable steric barriers to the guest entering the binding site. Therefore a certain degree of conformational flexibility within the host molecule is often necessary to allow for the guest to reach the binding site.

Two common strategies for reducing the entropy of a system via preorganization often seen in Nature as well as employed by synthetic chemists involve the chelate and macrocyclic effects [68]. The chelate effect involves the gain in association energy in a host guest system with the decrease in entropy upon reducing the number of independent species involved in the final complex. As insinuated in Figure 1-16 above, the most common way to achieve the chelate effect is by using a semi-flexible linker to join several separate binding elements into one contiguous structure. In this way the total number of species in the self-assembly can be drastically reduced, thereby reducing the overall entropy of the system.

However, care must be taken in making sure that the system retains the proper complementarity of interactions as well as shape when designing preorganization into a system. If preorganization is taken to extremes such that the system is excessively rigid, even small deviations from complementarity will be poorly tolerated as the system will lack the flexibility to make small conformational adjustments to better accommodate a less than perfect match. This is especially true for the interaction of chelating ligands with metal centers. Since different metals have both well-defined sizes and preferred

coordination geometries they are themselves very rigid by nature so a ligand designed to coordinate to a target metal must be well matched in both size and the orientation of the donor atoms. For example, when trying to bind to a transition metal with square planar geometry where the orientation of coordinating sites are at a 90^{o} disposition relative to each other the bite angle of any two adjacent donor atoms in a chelating ligand should converge at as close to a right angle as possible while still providing sufficient space to accommodate the metal.

The macrocyclic effect is an extension of the chelate effect whereby a further energetic gain can be achieved by closing a linear host into a macrocycle that has the correct size to accommodate the guest. By closing a linear molecule into a macrocyclic one the degrees of freedom of the host are significantly decreased and therefore the entropy of the system is further reduced. Therefore the unfavourable decrease in entropy upon binding of the guest is significantly less for the macrocyclic species relative to the linear one.

Natural systems that exemplify the effective implementation of preorganization via the chelate and macrocyclic effects are those containing porphyrin or porphyrin like moieties such as the heme cofactor of hemoglobin and the various chlorophylls required for photosynthesis [69].

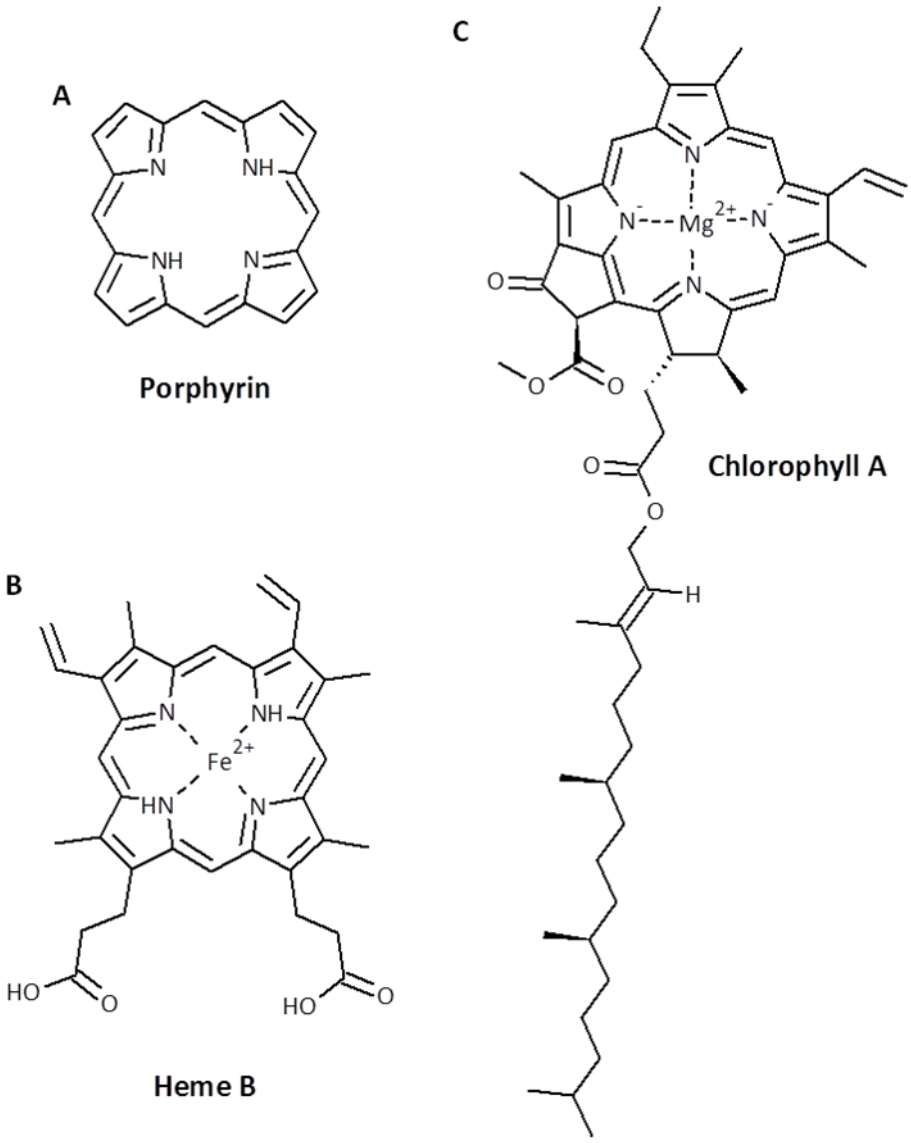

Figure 1-17: Structures of A) the porphyrin skeleton, B) heme B cofactor found in human hemoglobin, and C) chlorophyll A, the most common pigment molecule found in plants and algae.

As can be seen from the structures in Figure 1-17 above the porphyrin scaffold takes advantage of both the chelate effect, by holding multiple specific binding sites (the lone pairs of the nitrogens) together in close proximity in a single molecule, as well as the macrocyclic effect, by having the binding sites held in a semi-rigid ring such that they all face inward towards the site for metal coordination. The overall result is that these molecules form exceedingly stable complexes with transition metals, a property critical to their roles as protein cofactors necessary for two of the most critical cellular functions of life as we know it. Although examples exist of proteins which can form the

necessary specific interactions to bind transition metals, the additional entropy associated with relative flexibility of the polypeptide backbone makes it difficult to achieve the high association energies possible with porphyrin containing systems.

1.7 Designing Synthetic Self-Assembled Supramolecular Systems in Water

Having explored the types of non-covalent interactions as well as some examples from Nature illustrating useful molecular recognition strategies available in the supramolecular toolkit, the next step was the application of this knowledge towards the goals set out for the research contained in this body of work.

Recall that the first goal was the incorporation of supramolecular self-assembly strategies into the development of a novel system for generating complex transport active ion channels from relatively simple synthetic precursors. Since the formation of the lipid bilayer membrane is only possible in an aqueous environment by extension any ion channel formed via a self-assembly strategy must also be realized in the presence of water as well as the dynamic environment of the bilayer membrane. As discussed previously, the strength of the electrostatic attraction critical to many of the non-covalent interactions is severely diminished in aqueous solvent due to the competition with polar water molecules. In addition, it is desirable to produce ion channels with well-defined structure, particularly the shape and size of the pore, as this would allow for the prediction of the channel conductance in a given electrolyte under a particular applied potential using the Hille equation. If bilayer clamp experiments carried out on the system provided measurable conductances in close agreement to predictions this piece of information would go a long way towards confirming the nature of the ion transporting species. In order to produce channels with defined structure interactions with high directionality are preferred in addition to the criteria of providing strong interactions in an aqueous environment. As such many of these interactions are impractical for the establishment of primary interactions in a supramolecular ion channel with defined structure, although they may have some utility as secondary interactions to help stabilize a complex. Of the non-covalent interactions available the

ones that seem particularly suited to the task are the ligand-metal interactions. These are both exceedingly strong for non-covalent interactions in addition to providing a high degree of directionality via the coordination geometry about the metal centre.

The second goal of the research was the investigation of potential mechanisms for the generation of ion channels which mimic the ability of Natural ion channels to modulate their function in response to external stimuli. Unlike the investigations into the development of novel synthetic methodologies to generate self-assembling ion channels which are thermodynamically stable, the challenge of designing systems with dynamic function must involve working with conditions away from the state of equilibrium. As such, focus in this vein of research will be on incorporating reversible covalent bonds into ion channel design.

1.7.1 Existing Synthetic Ion Channels Incorporating Metal-Ligand Self-Assembly

The incorporation of self-assembly strategies towards the synthesis of synthetic ion channels based on metal-ligand interactions has already been implemented by several groups in the field. Systems so far realized are presented in Figure 1-18 below although the examples are limited due to the relative infancy of the research.

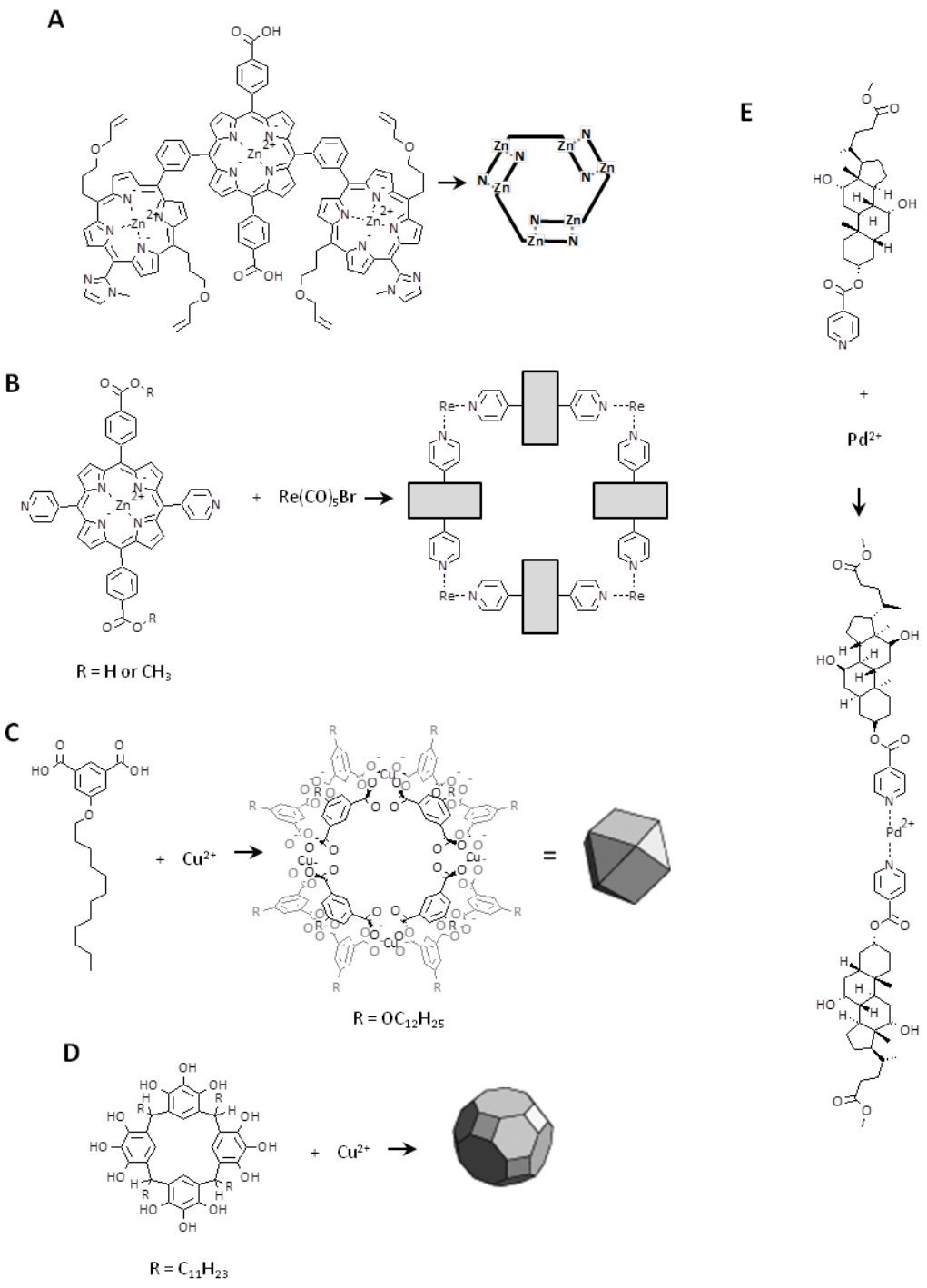

Figure 1-18: Synthetic ion channels incorporating metal-ligand self-assembly into their designs.

The first example (Figure 1-18, A) by Kobuke [70], involving the use of the previously discussed porphyrin system, relies on the coordination of the terminal imidazole ligands to the free axial position of the porphyrin bound zinc metal centers to

generate an ion channel comprising three molecules bound to form a roughly hexagonal pore with a depth corresponding to approximately half of the thickness of the bilayer membrane. A large pore diameter was inferred for this channel based on the observed ability to transport both lithium and calcium cations which, due to the large energetic penalty associated with their dehydration, are likely to pass through the channel as hydrated cations. It was also observed that the analogous compound in which the carboxylate groups were converted to methyl esters showed no transport activity. This observation was supportive of the hypothesis that the active channel molecule involved the formation of intermolecular hydrogen bonds between two supramolecular assemblies localized in each leaflet of the bilayer. In addition it was found that the transport activity could be effectively attenuated by the introduction of a polycationic dendrimer.

The second example (Figure 1-18, B) involves the self-assembly of the linear pyridine terminated porphyrin containing bis-ligand in the presence of a rhenium salt resulting in the generation of shape persistent square complex [71]. These were shown to effect the collapse of the pH gradient in the HPTS vesicle assay. A large pore diameter was also inferred for these channels based on the lack of ion selectivity for Group I cations or inorganic anions. In addition these channels, as with those of the Kobuke system (Figure 1-18, A), were found to rapidly lose the ability to transport ions by the addition of a sufficiently large polycationic dendrimer. Smaller and less highly charged dendrimers were shown to have significantly smaller effect on the transport efficiency, another indication of a large pore size.

The third example (Figure 1-18, C) involves the use of the metal organic polyhedron (MOP) created via the self-assembly of 5-dodecoxybenzene-1,3-dicarboxylic acid units via coordination to Cu^{2+} ions investigated by the Kim group [72]. This system takes advantage of the recent developments in the understanding of one of these previously reported cages, MOP-18 [73], which possesses both lipophilic modification and a diameter roughly corresponding to the thickness of the lipid bilayer. Upon

introduction of this compound to the lipid bilayer, transmembrane conductivity of transport events were observed that roughly corresponded to the sizes of the pores on both the triangular as well as square faces of the MOP. In addition the compound was found to exhibit a preference for the transport of lithium anions, a behavior rarely seen due to the high energetic penalty involved in desolvating this densely charged cation.

The fourth example (Figure 1-18, D), which shares some topological similarity to the MOP-18 channels in that the final structure takes the form of a large polyhedral capsule, is Gokel's pyrogallarene based capsule which self assembles into coordination dimers, also in the presence of Cu^{2+} cations [74]. Although the structures formed possess diameters insufficient to span the bilayer membrane the transport of ions was nonetheless observed suggesting either significant disruption of the lipid bilayer structure by a single capsule or the cooperative action of two capsules in an end to end fashion in order to bridge the distance. The compounds also showed some selectivity for the transport of the smaller cations with the relative order $Na^+ > K^+ > Cs^+$.

The final example (Figure 1-18, E) developed in the Webb laboratory [75] involves a cholate moiety modified with a terminal pyridine monodentate ligand. This compound, which in its free state only spans approximately one half of the bilayer, was designed such that upon coordination of one molecule localized in each leaflet of the bilayer membrane to a palladium metal centre a supramolecular compound which spanned the full distance would be formed. The cholate group was chosen based on previous research by Kobuke [76] which showed that a molecule consisting of two covalently linked cholate moieties exhibited excellent ion transport behavior. The palladium coordination complex effectively acts as a stand in for the covalent linkage. When the compound was introduced to the bilayer environment in the absence of metal centre no activity was observed however activity was effectively turned on upon the addition of a source of soluble palladium. In addition it was found that by adding hexathia-18-crown-6, which forms strong supramolecular complexes with palladium effectively removing it from the active complex, the transport activity could once again be turned off. This system is

particularly interesting in the context of this thesis as it represents an example of the realization of the second goal of the current research; a system exhibiting dynamic function in response to an applied chemical stimulus.

These examples, although limited in number, point towards the viability of both the metal-ligand self-assembly strategy for the generation of structures with well defined structures and associated ion transport as well as the development of systems exhibiting responsiveness to external stimuli resulting in dynamic transport activity.

1.8 Outline of the Thesis

The goals of this thesis were therefore two fold.

Firstly the investigation and implementation of a new strategy for the synthesis of ion channels using metal-ligand coordination as a mechanism for self-assembly, in particular the generation of supramolecular shape persistent macrocycles (Chapter 2). To this end two existing metal-ligand supramolecular systems, the ethylenediamine palladium(II) - 4,4'-bipyridine squares of Fujita [77] and the L_3M_3 bis-terpyridine base hexagons of Newkome [78], were selected for structural modifications towards the realization of structures with ion transport activity. In particular, modifications sought to address properties of aqueous-membrane partitioning and lipid solubility that the lead compounds do not inherently possess. The work on the Fujita system was an extension of previous research carried out in the Fyles' laboratory [79, 80] while the Newkome scaffold was chosen in response to perceived shortcomings inherent to the Fujita system.

Chapter 3 explores the other goal set out in this introduction; the development of environment sensitive ion channels that more closely mimic the behaviors seen in Natural systems. To this end the focus of the research shifts away from the use of metal-ligand interactions to generate static self-assemblies that exist at thermodynamic equilibrium, towards the exploration of the chemistry of reversible covalent bonds as a methodology for realizing systems which exhibit dynamic function in response to

externally applied stimuli. In particular reactions involving sulfur in a central role in the form of thioester - thiol and disulfide - thiol exchange reactions were investigated.

2 Thermodynamic Metal - Ligand Self-Assembly of Semi-Rigid Macrocycles

2.1 Conceptual Ion Channel Motifs

An ion channel is, in its simplest conception, a tubular structure which effectively spans the bilayer membrane. This description is of course far too simple as there are myriad other components which impart the specific properties which make each ion channel unique. Regardless, even by the minimal constraints imposed by this simple conceptual model one can in fact envision many different ways with increasing dependence on self-assembly in which to form a membrane spanning tube as outlined schematically in Figure 2-1 below [26].

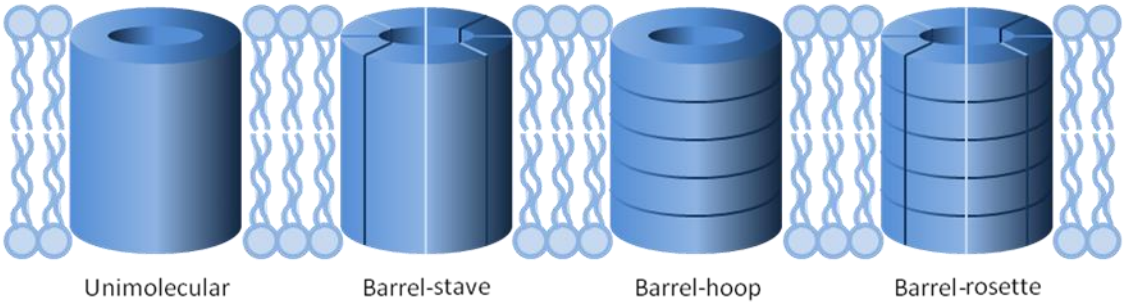

Figure 2-1: Simplified representation of the conceptually possible ion-channel motifs.

Although the unimolecular channel is appealing in that it allows for precise control over the internal diameter of the transmembrane channel the synthetic investment involved in producing a molecule large enough to retain a rigid internal channel as well as spanning the ~4 nm distance [81] from one side of the membrane to the other is quite daunting, even more so when one considers that there is no guarantee that the time and labor invested will generate an active channel at all.

Conversely the rosette model which requires the smallest individual subunits is appealing in that it initially seems to require the least synthetic investment. However one must also take into account the increasing entropic penalty involved in bringing larger and larger assemblies of the subunits together into a coherent and stable

structure. In addition the stability of the assembled structure also depends on available pathways to decomposition, in the complex and chaotic environment of the lipid bilayer membrane viable routes may become more plentiful to poorly organized systems. The design of the subunits is therefore very involved as any small perturbation from an ideal arrangement of intermolecular interactions is very likely to result in a failure to self-assemble. This entropic penalty can be overcome by ensuring that the enthalpy of each individual interaction is strong, but achieving this is likely to involve the synthesis of what could amount to quite complex molecules leading again to a relatively intensive investment of labor.

This leaves both the barrel stave and barrel hoop models as potential routes to active channel molecules. These sit comfortably in between the robust but labor intensive large tube model and the synthetically simple but entropically disfavored rosette model. At first glance the stave and hoop models may appear more or less interchangeable from a synthetic complexity argument but one must also consider the benefits and drawbacks of each system.

The barrel stave conformation's strength lies in that, if properly designed, the construct is more or less guaranteed to span the bilayer. The penalty is of course that as the number of staves increases the relative difference in energy of adding in an additional stave to the system decreases and therefore there is less control over the pore diameter and in all likelihood several pore diameters could be of similar stability. Indeed the channels themselves may dynamically 'breathe' as staves enter and leave the architecture as seen in the Natural alamethicin ion channels [82].

The barrel hoop model has the opposite advantages and disadvantages to the barrel stave model. The macrocyclic hoops, if semi-rigid, impart an inherent diameter to the architecture but in order to span the bilayer membrane several molecules must self-assemble into a tubular structure. Synthetically it is also generally more difficult to generate sufficiently large macrocyclic structures than linear ones so there is likely a slightly larger involvement of labor in the production of hoops rather than staves.

In the context of this project however there is a preference to have greater control over the diameter of the pores even at cost of increased synthetic complexity. By generating a structure with a semi-rigid pore like structure it should be possible to unambiguously recognize the structure of the channels formed based on the transport activity observed. Based on the internal diameter of a rigid channel predictions of the expected conductance in a given electrolyte can be made using the Hille equation (Section 1.4.2). If observed conductances match relatively well to these predictions it is very likely that the observed activity is in fact due to ions passing through the internal diameter of the shape persistent macrocycle.

2.2 Macrocycles and Supramolecular Self-Assembly

In order to tackle the increased synthetic complexity of generating structures containing rigid or semi-rigid macrocycles a possible approach is to employ a self-assembly strategy whereby smaller individual components are synthesized such that they are pre-programmed to come together in an ordered fashion. As discussed previously, many of the non-covalent interactions available to chemists either lack sufficient directionality or are too weak to drive self-assembly to a discrete structure, especially in the polar aqueous environment, to be useful for generating self-assembling macrocyclic constructs. One class of interactions does stand out as having the necessary strength and directionality for the task: metal - ligand interactions.

Upon first inspection it may seem that using metal - ligand interactions as the basis for constructing the individual macrocyclic elements of a barrel hoop channel forming suprastructure would be better described as being a barrel rosette motif. However, considering that the strength of metal - ligand interactions is on par with that of covalent bonds, as well as the relatively low reversibility of these interactions as compared to all other non-covalent interactions discussed, the barrel hoop description is more apt for this type of system.

2.3 The Fujita Square

With the goal of generating shape persistent macrocycles via self-assembly using metal-ligand interactions which would in turn self-assemble themselves into a barrel hoop ion transporting structure, previous efforts in the group focused on modifying existing metal - ligand assemblies. The particular lead system chosen was the Fujita square [77] (**2-3**) depicted in Scheme 2-1.

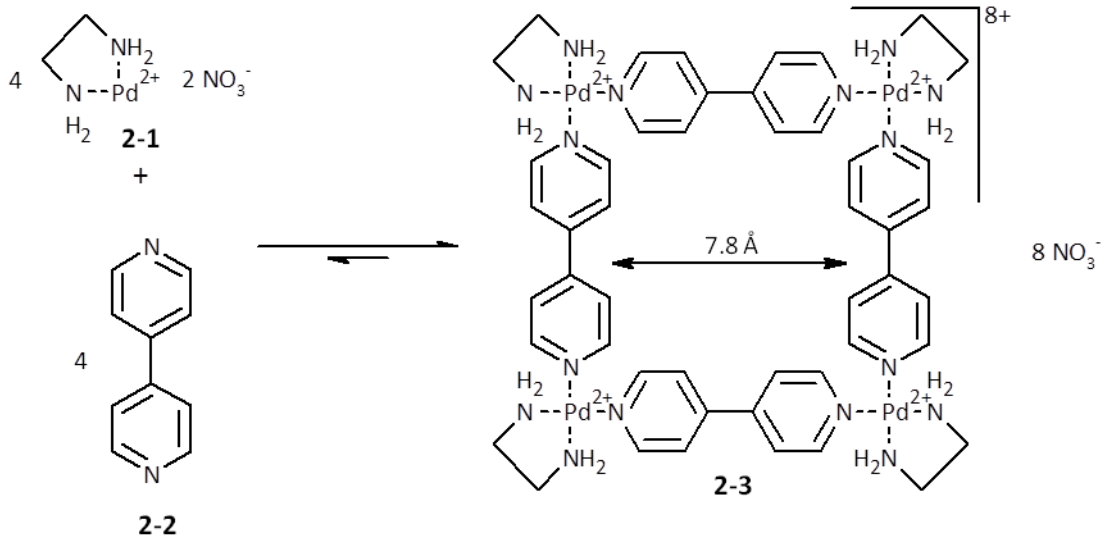

Scheme 2-1: Schematic illustrating how the component parts, ethylenediamine palladium(II) (**2-1**) and the 4,4'-bipyridine(**2-2**), self-assemble to form the Fujita square (**2-3**).

The Fujita square (**2-3**) is a well-studied metal - ligand supramolecular architecture formed from the self-assembly of four 4,4'-bipyridine molecules (**2-2**) with four ethylenediamine palladium(II) (**2-1**) moieties to form a semi-rigid square structure with an internal diameter of ~7.8 Å. If one envisions the internal diameter of this square being extended to a channel like molecule the internal diameter is more than sufficient for the transport of solvated cations all of which have hydrodynamic radii less than 2Å.

2.4 Previous Work - First Generation Modified Fujita Squares

Previous work in the group [79] involved the modification of the ethylenediamine ligand moiety (**2-1**) of the assembly with long chain hydrocarbons attached via ether bonds to generate compounds such a **2-4** shown in Figure 2-2. The hypothesis was that

if the overall architecture could be made more hydrophobic that it would preferentially partition into the non-polar bilayer membrane interior where the semi-rigid macrocycle could serve as an effective channel structure for the passage of ions as illustrated in Figure 2-2.

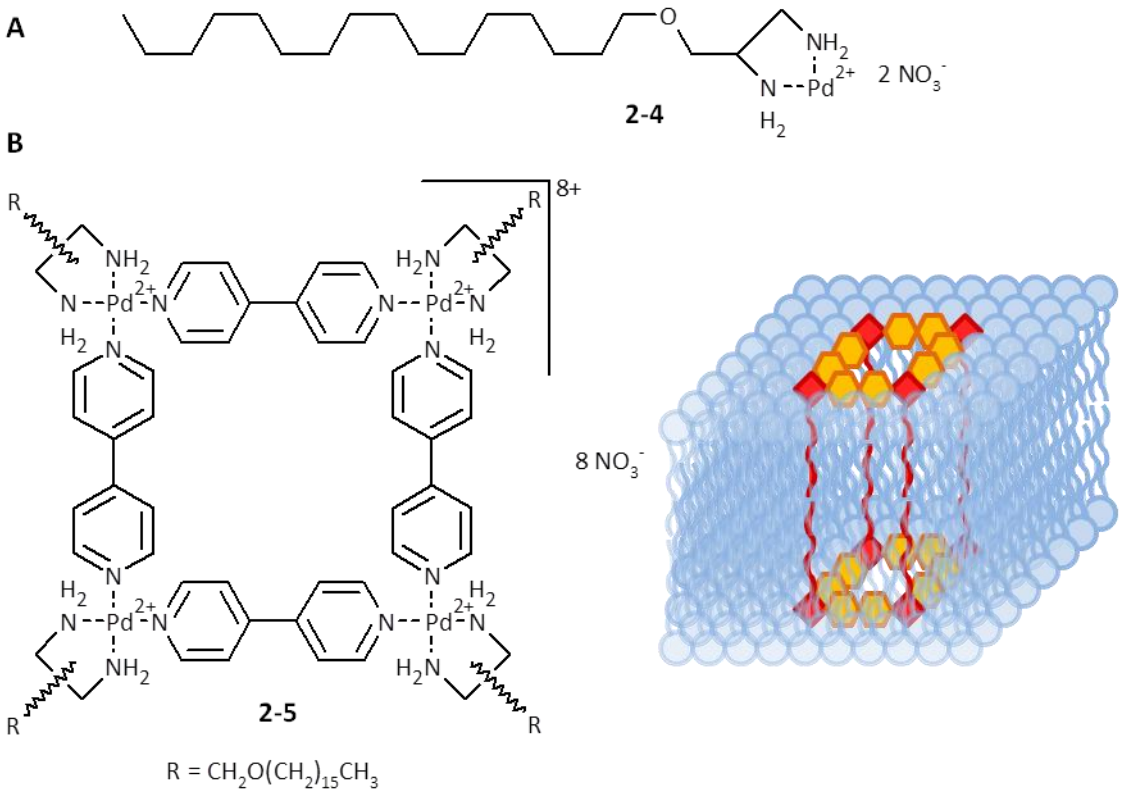

Figure 2-2: A) Structure of the first generation modified lipophilic ethylenediamine palladium(II) corner (**2-4**) and B) structure of the first generation modified Fujita square (**2-5**) and a stylized representation illustrating an idealized arrangement of two such squares in the bilayer membrane to form a channel like structure.

The modified Fujita square (**2-5**) did indeed show ion channel activity in the bilayer clamp assay; high conductance events with very long lifetimes were observed [79]. The very long duration of the openings indicated very stable channel structures however the size of the openings, as obtained from the observed conductance via the Hille equation, were too large to be attributed to the passage of ions through the 7.8 Å internal diameter of the macrocycle. In addition it was discovered that identical activity could be observed in the absence of the 4,4'-bipyridine moiety (**2-2**) suggesting that the

active structure was formed from the lipophilic ethylenediamine palladium(II) corners (**2-4**) alone.

Although disappointing, these observed behaviors supported the fundamental hypothesis that increasingly lipophilic structures could partition into the bilayer and elicit ion transport activity. The main failure of the model appeared to be the lack of effective partitioning of the 4,4'-bipyridine (**2-2**) into the bilayer along with the lipophilic ethylenediamine palladium(II) moiety (**2-4**). If the 4,4'-bipyridine moiety could not partition effectively into the bilayer then logically it is less likely that the modified square structure (**2-5**) could effectively form there either. To this end the first new synthetic targets for this body of work were 4,4'-bipyridine molecules modified to be more lipophilic and therefore have more favorable partitioning into the bilayer.

2.5 Design Considerations for Second Generation Modified Fujita Squares

Several considerations had to be taken into account when determining the desired nature of the modifications to the 4,4'-bipyridine scaffold. In order to increase the hydrophobicity of the molecule some form of appended alkyl substituent was the most logical direction as this type of modification was seen to increase partitioning of the ethylenediamine palladium(II) moiety in the first generation of modified Fujita squares (**2-5**). The geometry and nature of the bond to be formed between the alkyl substituent and the 4,4'-bipyridine scaffold required more evaluation. Due to the high degree of symmetry and the rotational freedom of the 4,4'-bipyridine molecule within the square superstructure there are essentially only two potential sites for modification; those *ortho* and *meta* to the ring nitrogen of each pyridine. Substitution at either position would lead to different steric restrictions (Figure 2-3). Modifications at the *ortho* position to the ring nitrogen would introduce steric repulsion with the ethylenediamine palladium(II) unit upon coordination [83] while modification at the *meta* position would induce steric repulsion resulting in a higher barrier to rotation between the two pyridine rings [84]. Clearly the loss of rotational freedom is preferable to potentially destabilizing the metal ligand interaction which could result in a weaker

supramolecular complex or even a failure of the square complex to form at all. In order to minimize the effect that substituents at the *meta* position would have on the rotational freedom of the molecule the functional group used to attach the alkyl chain should be carefully chosen such that it possesses the minimum steric bulk. Among these the most promising functional groups that have sufficient stability to stand up to the chemistry required in further synthetic steps are the methylene, the secondary amine or the ether linkage. Of these three the ether linkage stands out as being the least sterically bulky as two of the substituents on the oxygen are simply electron pairs whereas the secondary amine possesses one additional hydrogen atom and the methylene possesses two. Conceptually these relative barriers of rotation in the substituted 4,4'-bipyridines can be related to the *B*-values associated with the barriers to internal rotation of the structurally related substituted biphenyls [84].

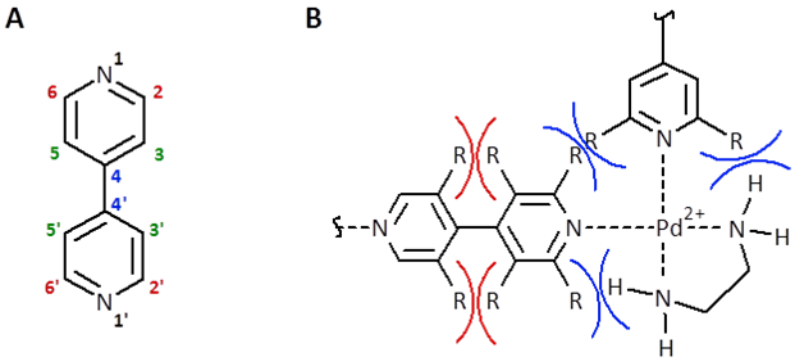

Figure 2-3: A) 4,4'-bipyridine structure with ring positions numbered and colour coded; red = ortho, green = meta, blue = para relative to ring nitrogen. B) Illustration of the different possible steric interactions induced by modifications to the 4,4'-bipyridine molecule. Interactions affecting free rotation between the two pyridine rings in red and interactions inhibiting self-assembly of the 4,4'-bipyridine and ethylenediamine palladium(II) molecules in blue.

In addition one must consider the degree of substitution, that is the number of substituents on each 4,4'-bipyridine. Having decided on limiting substitution to the positions *meta* to the ring nitrogens this means anywhere from one to four substituents. Given that the most likely synthetic route involves aryl-aryl coupling of the positions *para* to the ring nitrogen of substituted pyridines it is preferable for the molecule to possess symmetry across the single bond joining the two pyridine units in order to

simplify the synthesis. This structural arrangement also has the effect of minimizing the number of possible stereochemical configurations in the final square complex, and therefore the number of different possible square structures, possibly leading to easier characterization. This requirement eliminates the mono and tri substituted molecules as targets as well as the disubstituted molecule with both substitutions on one pyridine ring. Of the remaining two options the disubstituted molecule with one substituent on each pyridine ring is preferable to the tetrasubstituted molecule as the rotational freedom of the less substituted molecule is significantly greater.

2.6 Target Molecules and Retrosynthetic Analysis

With all of these criteria in mind the initial synthetic target for the lipophilic 4,4'-bipyridine was 3,3'-dodecyloxy-4,4'-bipyridine (A) illustrated in Scheme 2-2 below with the preliminary retrosynthetic analysis.

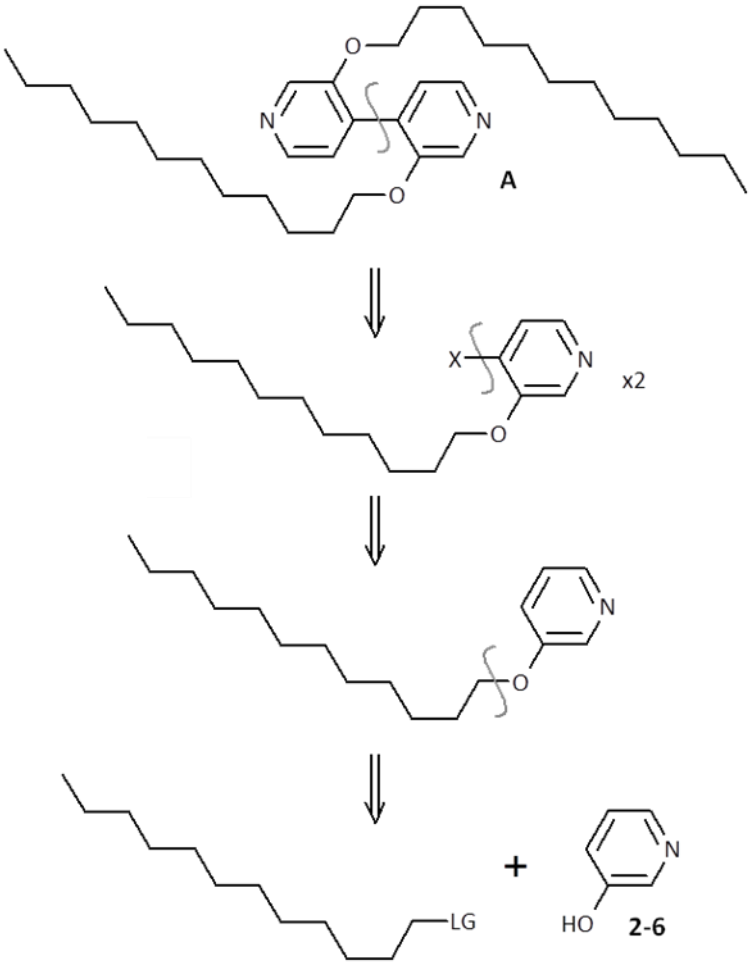

Scheme 2-2: Retrosynthetic analysis of the target 3,3'-didodecyloxy-4,4'-bipyridine (A) molecule with key disconnections shown.

The initial retrosynthetic analysis of the product was quite straight forward. The initial synthetic step was to involve the formation of an ether bond between 3-hydroxypyridine and the alkyl chain with an appropriate leaving group. This was to be followed by the installation of a halide or boronic acid at the position *para* to the ring nitrogen which would serve as the reactive components needed for the metal catalyzed carbon-carbon bond forming Suzuki reaction [85] to afford the final lipophilic 4,4'-bipyridine molecule.

2.7 Synthesis

Unlike benzene ring systems, due to the electron deficient nature of the pyridine ring structure, electrophilic aromatic substitution is not the preferred pathway to

obtaining substituted pyridines. Pyridines instead prefer to undergo substitution via nucleophilic aromatic substitution with preference for substitutions at the positions *ortho* and *para* to the ring nitrogen due to resonance delocalization of electrons to the nitrogen atom. However, nucleophilic aromatic substitutions of this nature are generally only successful for 2 or 4-halopyridines rather than unsubstituted pyridine [86]. This is due to the fact that the halides are much better leaving groups than the hydride which would need to be displaced in the case of unsubstituted pyridine. In order to counteract these preferences in the reactivity of pyridines, a common strategy is to oxidize them to the corresponding pyridine-N-oxides [87]. Due to the increased electron density of the pyridine-N-oxide ring system, especially at the sites *ortho* and *para* to the ring nitrogen through resonance delocalization, these molecules are markedly more reactive towards electrophilic aromatic substitution; see Figure 2-4.

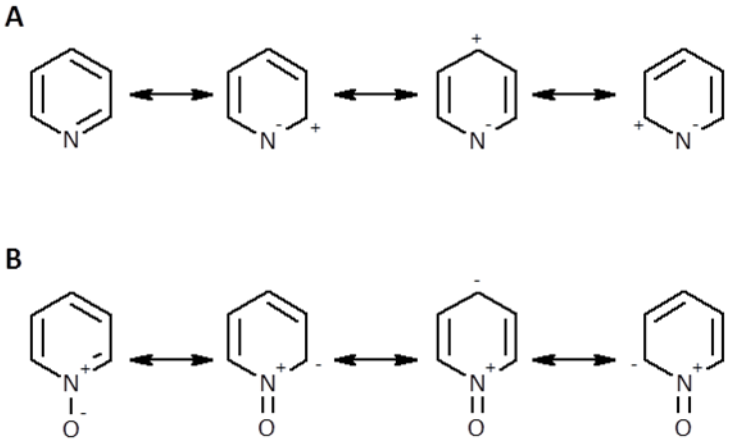

Figure 2-4: Resonance delocalization of electrons within the A) pyridine ring system and B) the pyridine N-oxide ring system to illustrate the origins of the differential reactivity between the two ring systems.

Due to these improved reactivity properties pyridine-N-oxides played an integral role in the initial attempted syntheses as described in Scheme 2-3 below.

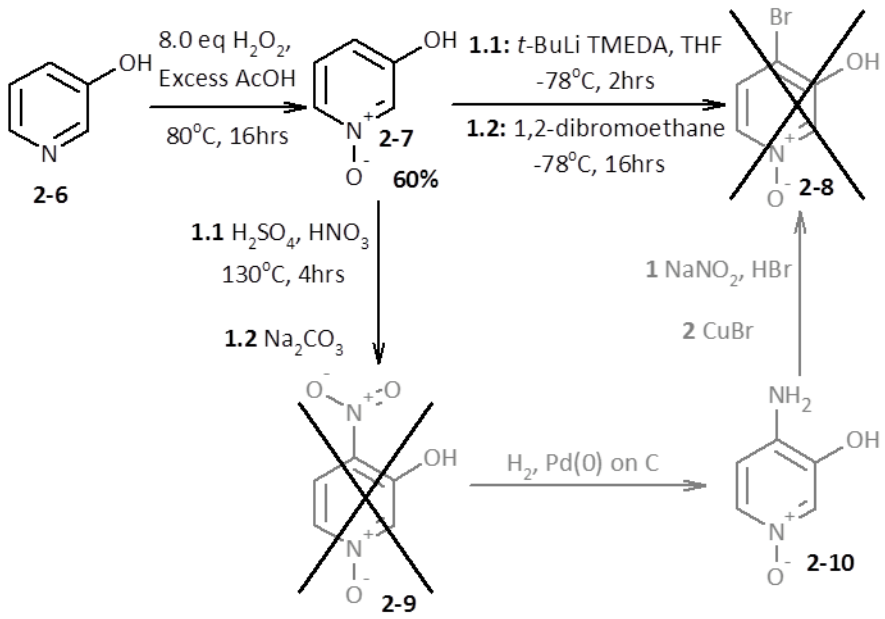

Scheme 2-3: Scheme of the initial attempt of the synthesis of 3,3'-disubstituted-4,4'-bipyridines starting with the oxidation of 3-hydroxypyridine (**2-6**) to the corresponding 3-hydroxypyridine-N-oxide (**2-7**).

As shown in Scheme 2-3, the first step in the initial attempt at the synthesis of 3,3'-dodecyloxy-4,4'-bipyridine (A) involved the oxidation of 3-hydroxypyridine (**2-6**) to 3-hydroxypyridine-N-oxide (**2-7**) using hydrogen peroxide in acetic acid [88]. The success of the reaction was confirmed by comparison of the NMR spectra to literature spectra. The next step in the synthesis was the attempted bromination of the 3-hydroxypyridine-N-oxide (**2-7**) to 4-bromo-3-hydroxypyridine-N-oxide (**2-8**) using *t*-butyllithium, tetramethylethylenediamine (TMEDA) and 1,2-dibromoethane as the bromine source. Unfortunately these conditions failed to elicit any reaction. As an alternative pathway to the brominated compound a more circuitous route was proposed involving first the nitration of the 3-hydroxypyridine-N-oxide (**2-7**) to 3-hydroxy-4-nitropyridine-N-oxide (**2-9**), followed by reduction of the newly installed nitro group to the amine to yield 4-amino-3-hydroxypyridine-N-oxide (**2-10**) and finally conversion of the amine group to the desired bromide using the Sandmeyer reaction to afford the desired 4-bromo-3-hydroxypyridine-N-oxide (**2-8**). Unfortunately attempts at nitrating the 3-hydroxypyridine-N-oxide (**2-7**) resulted in the generation of sparks and the evolution of

copious amounts of dark brown nitrogen dioxide gas as well as the decomposition of the starting material to an intractable black sludge.

At this point it was suspected that perhaps the free hydroxyl group of the 3-hydroxypyridine-N-oxide was responsible for the unwanted side reactions resulting in the decomposition of the reacting materials. It was hypothesized that in order to circumvent this unwanted reactivity the hydroxyl group could be first converted to the desired lipophilic ether in order to mitigate its reactivity. The newly conceived pathway, shown in Scheme 2-4, would start with converting the hydroxyl group of 3-hydroxypyridine (**2-6**) to 3-dodecyloxypyridine (**2-11**) followed by oxidation of this molecule to 3-dodecyloxypyridine-N-oxide (**2-12**). Performing these steps in the reverse order, that is trying to form the ether of the pyridine-N-oxide, was ruled out due to the possibility of alkylating the oxygen of the ring nitrogen.

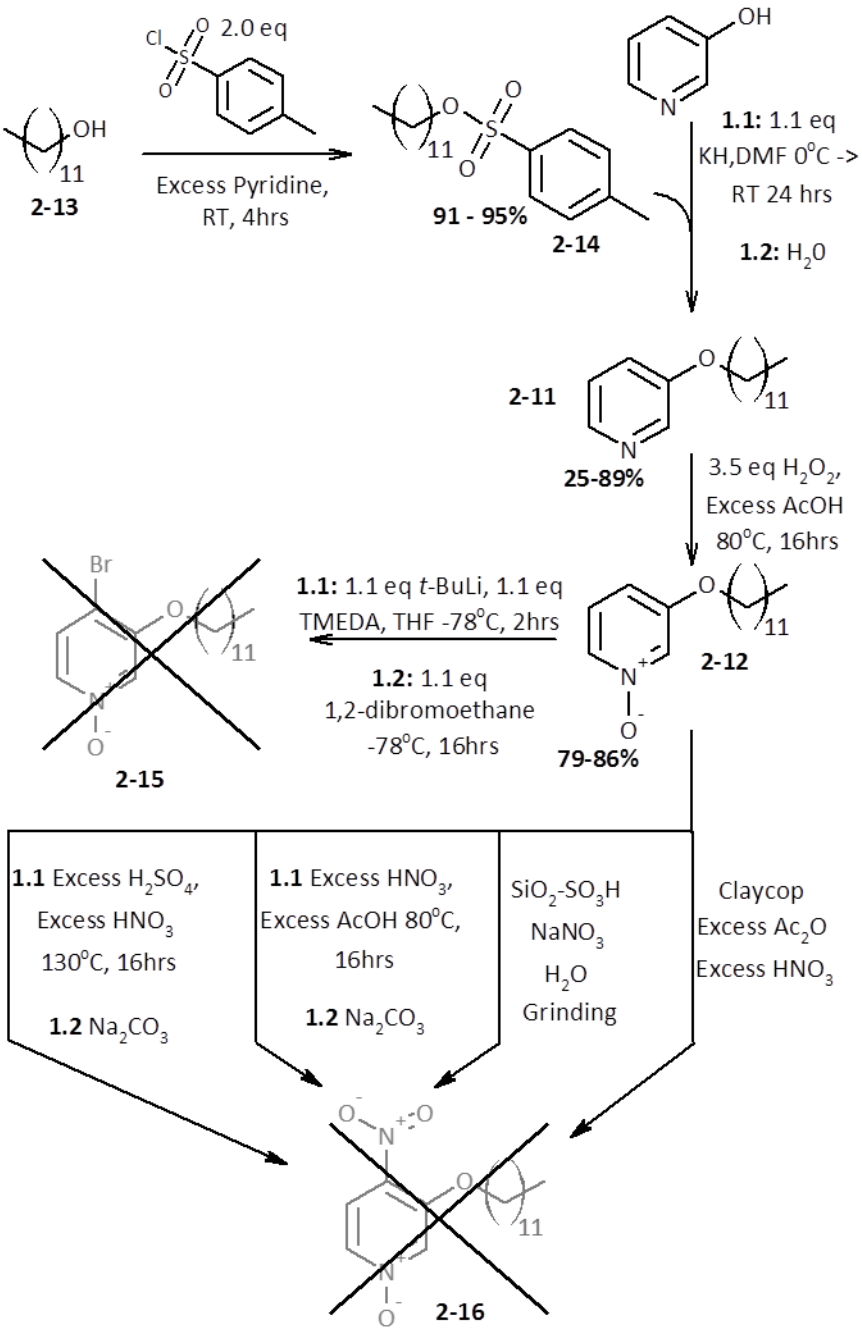

Scheme 2-4: Attempted syntheses of 4-bromo-3-dodecyloxypyridine-N-oxide (**2-15**) and 3-dodecyloxy-4-nitropyridine-N-oxide (**2-16**).

The first step in this pathway involved converting *n*-dodecanol (**2-13**) to a molecule with an appropriate leaving group for the attack from the hydroxylate of 3-hydroxypyridine (**2-6**). The chosen leaving group was the *p*-toluenesulfonyl group. This group was chosen over the similarly reactive mesylate or triflate groups primarily in

order to provide easy UV visualization of the product on thin layer chromatography. The primary alcohol of *n*-dodecanol (**2-13**) was converted to the *n*-dodecyl *p*-toluenesulfonate (**2-14**) via the reaction with *p*-toluenesulfonylchloride in pyridine as the solvent as per literature procedure [89]. The product was confirmed by comparison of NMR spectra to those from literature. Yields from this reaction were generally quite respectable so long as appropriate care was taken to ensure that the alcohol and pyridine were free of moisture.

The next step in the synthesis involved the coupling of the electrophilic *n*-dodecyl *p*-toluenesulfonate (**2-14**) with 3-hydroxypyridine (**2-6**) to yield 3-dodecyloxypyridine (**2-11**). The reaction was carried out by first deprotonating the hydroxyl group of 3-hydroxypyridine (**2-6**) using potassium hydride in an ice bath followed by the addition of the *n*-dodecyl *p*-toluenesulfonate (**2-14**) and allowing the mixture to come to room temperature. Again the reaction proved high yielding so long as care was taken to ensure that moisture was eliminated from the reaction. The NMR revealed a new triplet signal at 3.86 ppm corresponding to the methylene adjacent to the oxygen of the ether bond. Initial attempts at the reaction using the less reactive but easier to handle sodium hydride failed to produce the desired product with sufficiently high yield.

Oxidation of the resulting 3-dodecyloxypyridine (**2-11**) carried out under identical conditions to those used for the 3-hydroxypyridine (**2-6**) also provided good yields of the product, upfield shifts of the aromatic signals in the proton NMR provided evidence of the successful reaction. With the 3-dodecyloxypyridine-N-oxide (**2-12**) in hand attempts were made at carrying out the bromination reaction to yield the 4-bromo-3-dodecyloxypyridine-N-oxide (**2-15**) using the same conditions attempted with the 3-hydroxypyridine-N-oxide (**2-7**, Scheme 2-3) with similarly disappointing results. Changing focus to the more synthetically involved pathway to the brominated product as previously discussed for 3-hydroxypyridine-N-oxide (**2-7**), several attempts were made at nitrating 3-dodecyloxypyridine-N-oxide (**2-12**) to 3-dodecyloxy-4-nitropyridine-

N-oxide (**2-16**) using various nitrating reaction conditions. Unlike the attempts at nitrating the 3-hydroxypyridine-N-oxide (**2-7**) however, none of these reactions resulted in the decomposition of the starting material; rather they resulted in no significant reaction whatsoever.

Battling through these synthetic setbacks another approach was conceived whereby the hydroxyl group of the 3-hydroxypyridine (**2-6**) would first be converted to the corresponding N,N-diethylcarbamate; see Scheme 2-5. This modification was selected because it is known to induce directed *ortho* metalation allowing the addition of an electrophile *ortho* to the carbamate directing group [90].

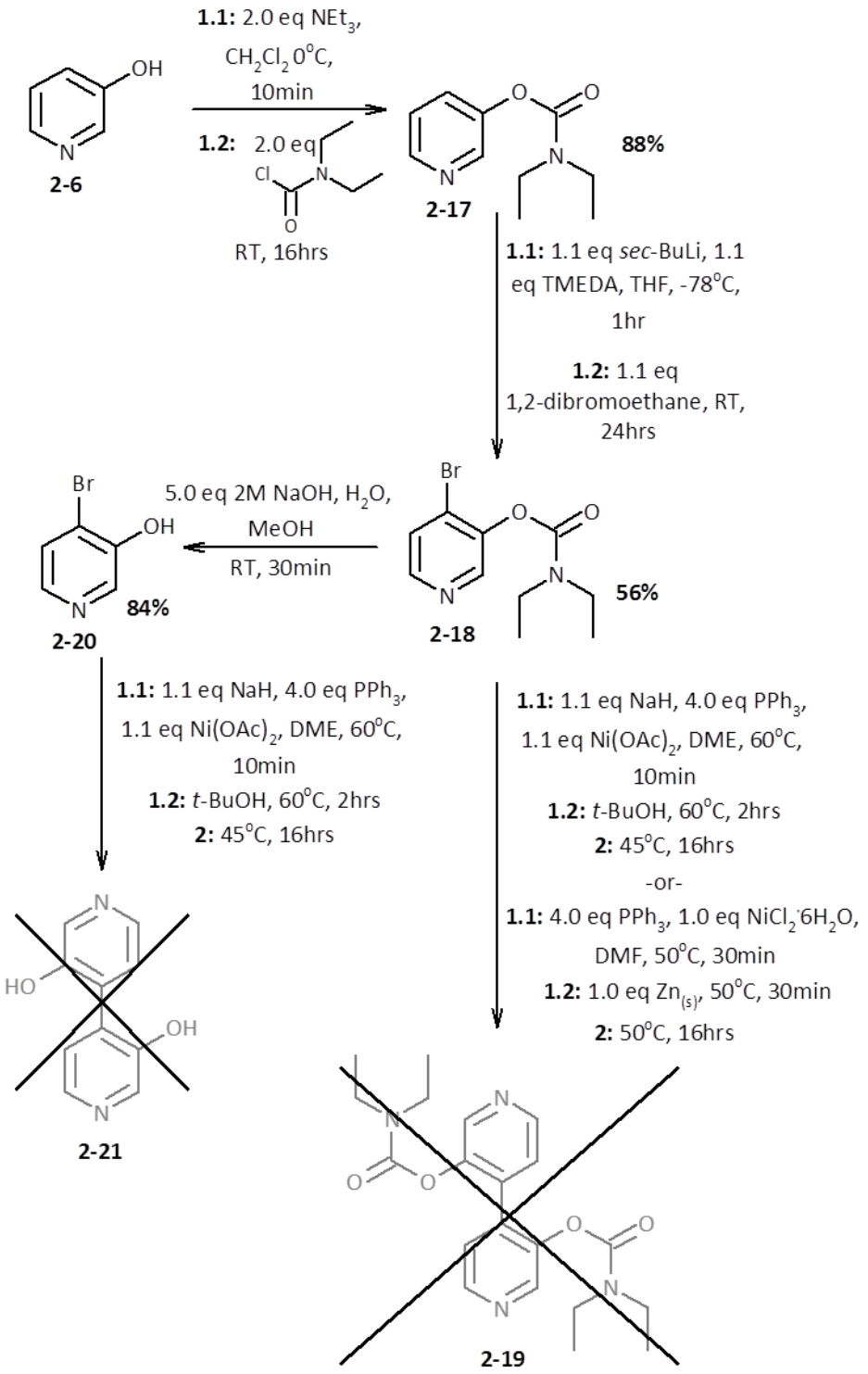

Scheme 2-5: Attempted syntheses towards 2,2'-disubstituted-4,4'-bipyridines.

The conversion of 3-hydroxypyridine (**2-6**) to the N,N-diethylcarbamate molecule (**2-17**) occurred readily and in high yields using diethylcarbamoyl chloride and triethylamine as the base using literature procedures [91]. Subsequently the carbamate protected pyridine (**2-17**) was successfully brominated at the position *para* to the ring nitrogen by first lithiating the compound using *sec*-butyllithium and tetramethylehtylenediamine (TMEDA) as catalyst at -78°C followed by the addition of 1,2-dibromoethane as the source of bromine. This procedure was also carried out according to literature with the product exhibiting identical NMR spectra [92]. From this brominated product (**2-18**), attempts were made at the direct aryl-aryl coupling using two different nickel catalyzed coupling procedures [93, 94]. Unfortunately both conditions failed to afford the desired carbamate protected bipyridine molecule (**2-19**). It was hypothesized that perhaps the N,N-diethylcarbamate group, due to it steric bulk, was preventing the proper reactive collision geometry of the aryl rings. Guided by this hypothesis the carbamate group was cleaved from the brominated pyridine molecule using a simple sodium hydroxide treatment to form compound (**2-20**) in preparation for a subsequent attempt at coupling the newly synthesized 4-bromo-3-hydroxypyridine molecule using one of the conditions attempted for the carbamate protected molecule (**2-18**). Once again these conditions proved ineffectual in yielding the desired 4,4'-bipyridine molecule (**2-21**) and much of the 4-bromo-3-hydroxypyridine (**2-20**) was recovered from the reaction.

With the hypothesis that the free hydroxyl group on the molecule may have somehow adversely affected the coupling reaction it was hypothesized that perhaps converting the free hydroxyl to the dodecyloxy group at this stage of the synthesis may allow the desired aryl-aryl cross-coupling to occur as per Scheme 2-6.

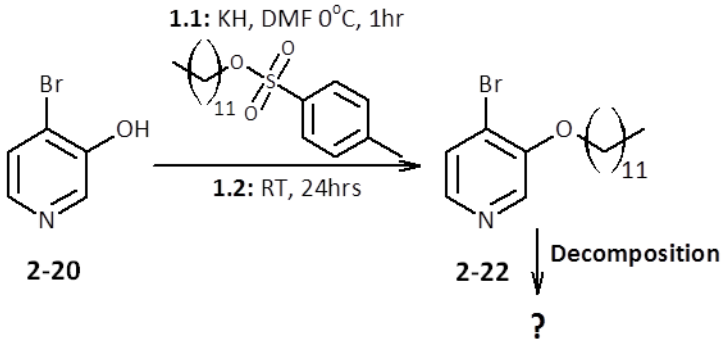

Scheme 2-6: Attempted synthesis of 4-bromo-3-(dodecyloxy)pyridine (**2-22**) from 4-bromo-3-hydroxypyridine (**2-20**).

To this end the ether substituted molecule was synthesized from the tosylated dodecanol using the same procedure as used for the non-brominated pyridine (**2-6**) as described earlier (Scheme 2-4). Initially this procedure seemed to be quite successful in producing the desired 4-bromo-3-(dodecyloxy)pyridine (**2-22**) based on TLC analysis of the reaction mixture however, over the span of a few hours the initially pale orange oil slowly turned into a dark brown intractable solid indicating that the product had decomposed.

Given the instability of this product and the overall failure of the direct aryl-aryl coupling of the 4-bromopyridines it was decided to abandon this type of coupling in favor of a Suzuki coupling procedure using one of the existing 4-bromopyridine molecules. The other component necessary to obtain the desired 4,4'-bipyridine molecule via the Suzuki cross-coupling reaction is a pyridine with a boronic acid substituent at the position *para* to the ring nitrogen.

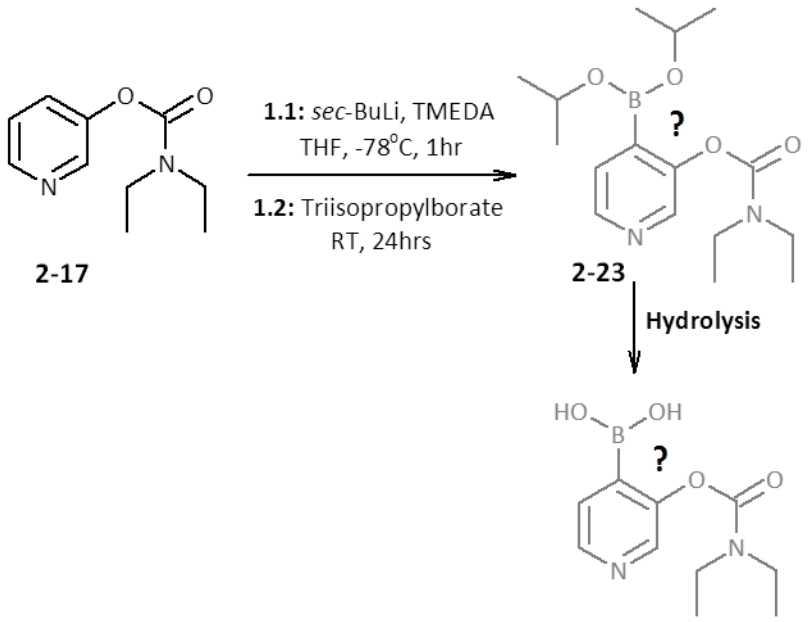

Scheme 2-7: Attempted boronation of pyridine-3-yl diethylcarbamate (**2-17**) and the subsequent hydrolysis of the resulting product mixture.

In order to synthesize such a molecule the previously synthesized carbamate protected pyridine (**2-17**) served as a good starting point; as discussed previously the carbamate moiety was shown to act as an effective *ortho* director for electrophilic aromatic substitution in the reaction to afford the 4-bromoyridine molecule (**2-18**). As shown in Scheme 2-7 a reaction was carried out according to a literature procedure [95] analogous to that for the *ortho* directed bromination except for the use of triisopropyl borate as the electrophilic component. The reaction appeared to proceed relatively well as indicated by the reduction in the intensity of the spot due to the carbamate on TLC and the appearance of a new UV active spot. However, using a variety different TLC conditions revealed that the newly observed spot was actually several spots with near identical mobilities. In an attempt to improve the resolution of these products for purification the product mixture was given a mild acid treatment to hydrolyze any potential boronic esters followed by a neutralization step with sodium bicarbonate to deprotonate the pyridine nitrogen. TLC analysis of the products of this treatment revealed no improvement in the resolution of the various products and attempts to purify either the remaining suspected boronic ester or the hydrolyzed mixture failed to afford any desired product. The observation of poorly resolved product mixtures is

likely due to the formation of various complexes between the pyridine, a Lewis base, and boronic acid, a Lewis acid.

Undeterred by the various dead-ends encountered in the synthesis to this point it was hypothesized that perhaps the pyridines with the more reactive iodine substituent at the position *para* to the ring nitrogen could serve as better starting materials for the direct aryl-aryl cross-coupling reactions.

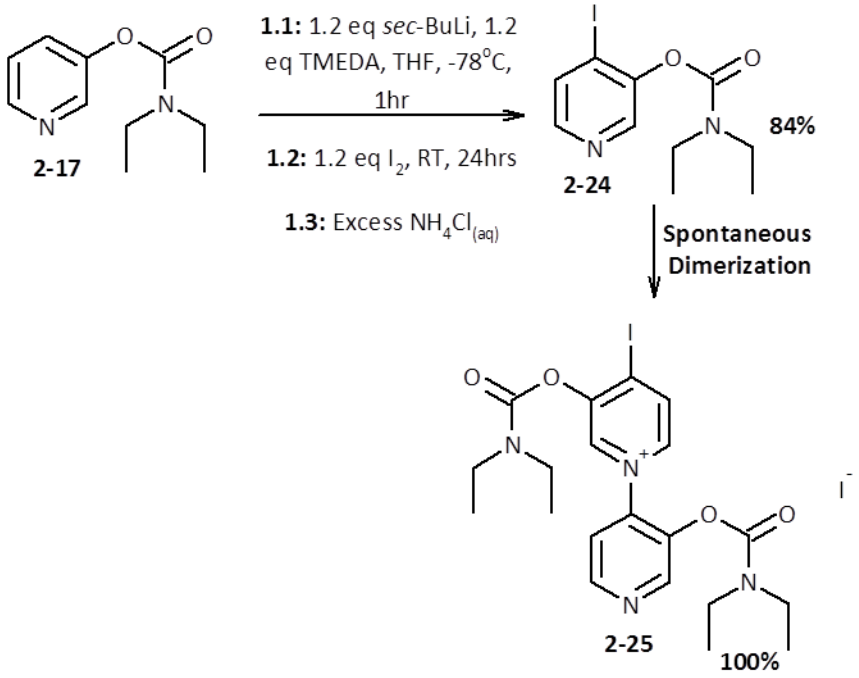

Scheme 2-8: Attempted synthesis of 4-iodopyridin-3-yl diethylcarbamate (**2-24**) from pyridine-3-yl diethylcarbamate (**2-17**) resulting in the dimerized pyridinium iodide salt product (**2-25)** instead.

With this impetus the synthesis returned once again to the pyridine-3-yl diethylcarbamate (**2-17**) for the directed ortho metallation reaction using molecular iodine as the halogen source to generate 4-iodopyridin-3-yl diethylcarbamate (**2-24**) as per a literature procedure [96]. The reaction and purification went smoothly and initial NMR analysis of the product showed only the desired product contaminated with a small amount of ethyl acetate solvent from the chromatographic purification. In an attempt to remove the residual solvent from the product, a clear colourless oil, it was put under high vacuum. Over the course of a few hours however, the product turned to

a deep brick red glasslike solid. TLC analysis of this solid revealed complete and clean conversion of the 4-iodopyridin-3-yl diethylcarbamate (**2-24**) into a new product with lower mobility. NMR spectra of this new product revealed that the initial compound had dimerized to form the pyridinium iodide salt of the desired product (**2-25**). At this point in the chemistry it became clear that an entirely new path to 3,3'-disubstituted-4,4'-bipyridines was in order.

The new strategy involved abandoning the ether linkage between the pyridine and the alkyl components altogether in favor of a methylene linkage. Even though the methylene group is more sterically demanding than the ether it also has a much smaller effect on the electron density of the various positions of the pyridine ring relative to the electron donating ability of the ether or hydroxyl substituent. This would lead to reactivity of the modified pyridine ring that was more in line with what is observed for unmodified pyridine.

The retrosynthetic analysis for the target 3,3'-disubstituted-4,4'-bipyridines with the methylene linkage rather than the ether linkage is quite similar to that for the targets containing the ether linkage, with disconnections occurring in a slightly different order as depicted in Scheme 2-9.

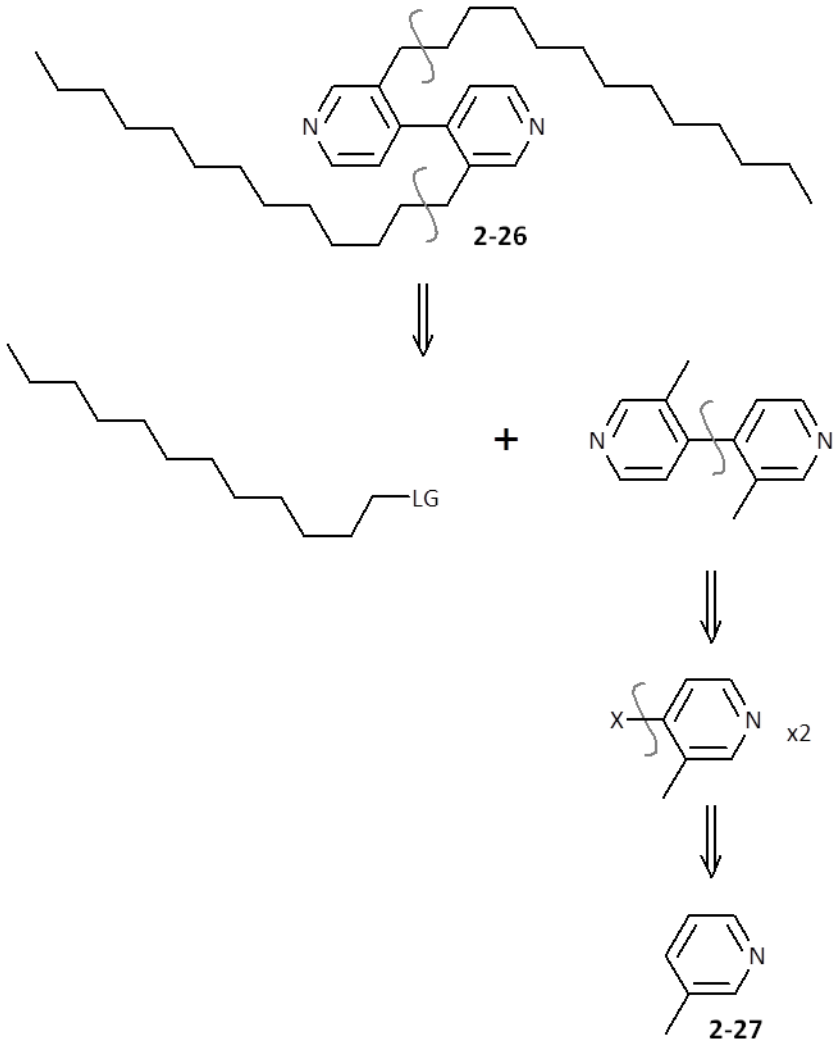

Scheme 2-9: Retrosynthetic analysis of the target 3,3'-ditridecyl-4,4'-bipyridine (**2-26**) molecule with key disconnections shown.

The major difference in the retrosynthetic analysis was that the initial starting material for the synthesis was β-picoline (**2-27**) rather than 3-hydroxypyridine (**2-6**) which precipitated the changes to the order of the disconnections.

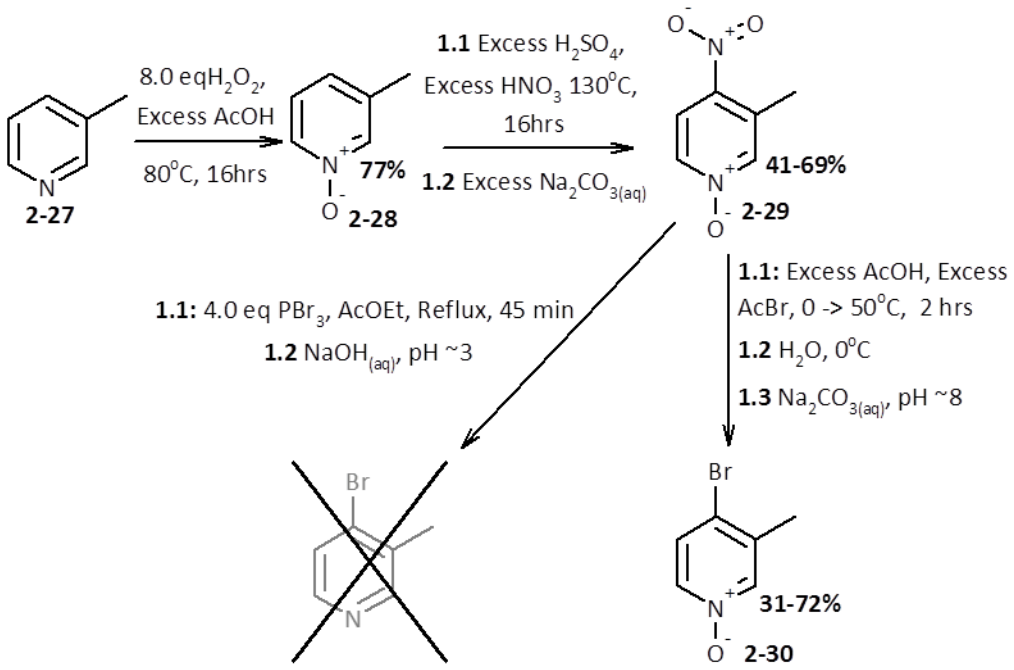

Scheme 2-10: Synthesis of 4-bromo-3-methylpyridine-N-oxide (**2-30**).

The first step attempted in the synthesis was the oxidation of β-picoline (**2-27**) to the corresponding 3-methylpyridine-N-oxide (**2-28**) employing the same literature conditions used for previous pyridine oxidations; see Scheme 2-10. The successful oxidation was determined by comparison of the NMR spectra to literature spectra. The next step was to nitrate compound (**2-28**) at the position *para* to the ring nitrogen using a mixture of sulfuric and nitric acid at elevated temperatures as per a literature procedure [97] which proved to be quite effective for this starting material unlike for the 3-hydroxypyridine-N-oxide (**2-7**) and 3-dodecyloxypyridine-N-oxide (**2-12**) starting materials. This provided further evidence to support that the oxygen bonded to the pyridine ring at the position *meta* to the ring nitrogen had an adverse effect on the reactivity of these molecules towards nitration. The next step involved the attempted conversion of the nitro group of the 3-methyl-4-nitropyridine-N-oxide (**2-29**) to a bromine atom. The first procedure carried out using phosphorous tribromide at elevated temperatures was shown in literature [97] to effect both the bromination and reduction of the pyridine-N-oxide (**2-29**) to the corresponding pyridine in the same reaction; however attempts to reproduce these results failed to afford the desired

product after several attempts. An alternative approach from literature [98] using refluxing acetyl bromide in acetic acid proved to be much more effective in obtaining the desired 4-bromo-3-methylpyridine-N-oxide (**2-30**).

With this compound in hand attempts were made at the direct Nickel catalyzed aryl-aryl cross-coupling [93] as attempted previously with 4-bromopyridin-3-yl diethylcarbamate (**2-18**) and 4-bromo-3-hydroxypyridine (**2-20**); unfortunately as with those attempts no reaction was observed; Scheme 2-11.

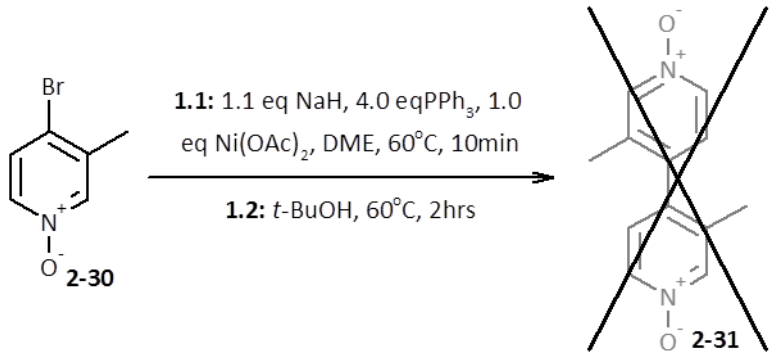

Scheme 2-11: Attempted aryl-aryl homo coupling of 4-bromo-3-methylpyridine-N-oxide (**2-31**).

With this failure, the next reaction attempted was the conversion of the bromine group of the 4-bromo-3-methylpyridine-N-oxide (**2-30**) to the boronic acid in order to provide the necessary components for a Suzuki cross-coupling reaction. A reaction was carried out using *sec*-butyllithium and triisopropyl borate however much like the attempt at a similar reaction with pyridine-3-yl diethylcarbamate (**2-17**) the reaction resulted in the formation of many products that were not chromatographically resolvable; see Scheme 2-12.

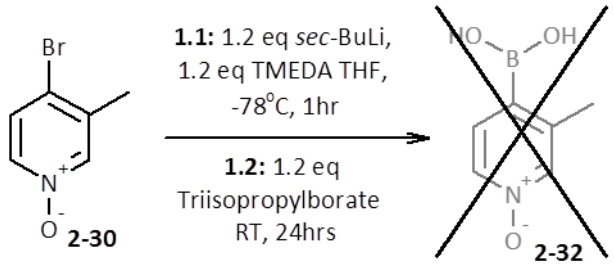

Scheme 2-12: Attempted synthesis of 3-methyl-4-pyridylboronic acid (**2-32**) from 4-bromo-3-methylpyridine-N-oxide (**2-30**).

With this most recent setback in the synthesis of 3,3'-disubstituted pyridines a literature search going back further in the past came up with an interesting procedure for the homo-coupling of two β-picoline (**2-27**) molecules to form 3,3'-dimethyl-4,4'-bipyridine (**2-33**) presented in Scheme 2-13.

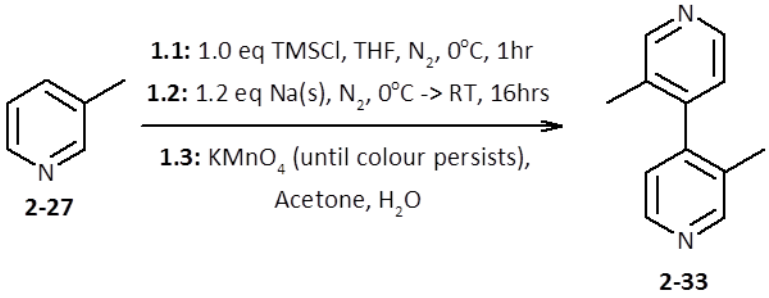

Scheme 2-13: Synthesis of 3,3'-dimethyl-4,4'-bipyridine (**2-33**).

This aryl-aryl cross-coupling, involving the reaction of β-picoline (**2-27**) with trimethylsilyl chloride (TMSCl) and solid sodium metal in dry THF under an inert nitrogen atmosphere [99], was carried out to afford a modest but encouraging yield of the desired 3,3'-dimethyl-4,4'-bipyridine (**2-33**). Further refinement of the reaction conditions such as using more finely divided sodium resulted in some improvement in yield. The structure of the final product was confirmed by comparison with literature NMR spectra. With the 3,3'-dimethyl-4,4'-bipyridine (**2-33**) finally in hand the next task was to extend the methyl groups to longer alkyl chains in order to increase the lipophilicity of the molecule as per Scheme 2-14.

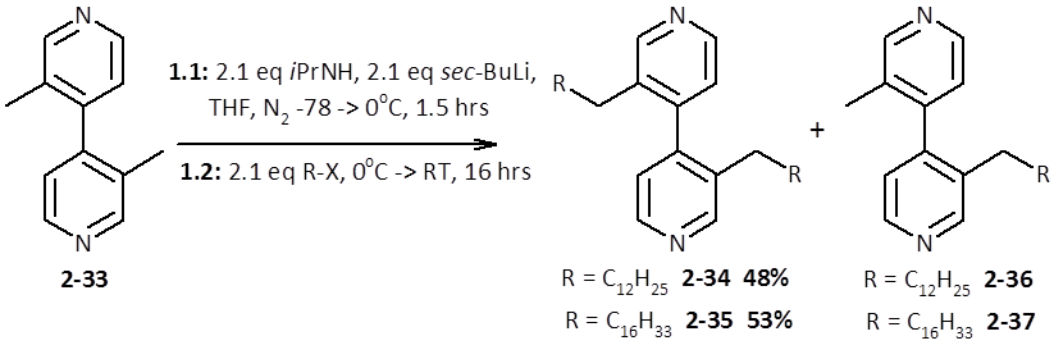

Scheme 2-14: Synthesis of 3,3'-ditridecyl-4,4'-bipyridine (**2-34**) and 3,3'-diheptadecyl-4,4'-bipyridine (**2-35**) which also produced small quantities of the side products 3-tridecyl-4,4'-bipyridine (**2-36**) and 3-heptadecyl-4,4'-bipyridine (**2-37**).

In order to accomplish this, two analogous reactions adapted from literature [100] were carried out under conditions differing only in the length of alkyl halide used; either 1-iododecane or 1-bromohexadecane. The reaction involved the in-situ generation of the strong, non-nucleophilic base lithium diisopropylamide via reaction of diisopropylamine and *sec*-butyllithium in THF at -78°C, to which was added the 3,3'-dimethyl-4,4'-bipyridine (**2-33**). This reaction mixture was then treated with the respective alkyl halides and allowed to warm to room temperature. The reactions resulted primarily in the formation of the desired 3,3'-ditridecyl-4,4'-bipyridine (**2-34**) and 3,3'-diheptadecyl-4,4'-bipyridine (**2-35**) targets as well as smaller quantities of the monosubstituted molecules **2-36** and **2-37**.

With these compounds in hand the synthesis of the lipophilic ethylenediamine palladium(II) molecule was carried out as previously reported [79].

2.8 NMR Studies of the Self-Assembly of Second Generation Lipophilic Fujita Squares

With the two target compounds with lipophilic modifications (**2-34** and **2-35**) in hand as well as the lipophilic ethylenediamine palladium(II) corner (**2-4**, Figure 2-2) focus could turn to studying the self-assembly of these components and investigating the ion-channel activity of the resulting supramolecular assembly.

The technique of choice to study the self-assembly process was nuclear magnetic resonance spectroscopy. Using this technique it should be possible to detect changes in the chemical shift of the protons of the bipyridine ring system upon coordination of the bipyridine nitrogens to the palladium metal centers; Figure 2-5.

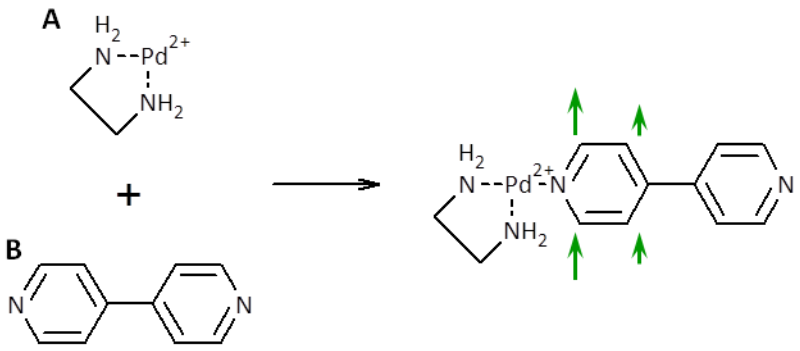

Figure 2-5: Relative changes to chemical shifts expected upon complex formation between 4,4'-bipyridine (B) and ethylenediamine palladium(II) (A), green arrows indicate which ^{1}H signals are expected to experience downfield shifts with the relative sizes of the arrows indicative of the relative magnitudes of these shifts.

The expected changes in the ^{1}H NMR spectra should be downfield shifts of the pyridine ring nitrogens as coordination to the relatively electrophilic palladium(II) centres should result in electron density being pulled out of the pyridine ring system resulting in a net deshielding of the ring protons illustrated in Figure 2-5. Before these observations could be made the important task of determining an appropriate NMR solvent had to be addressed. This seemingly simple task actually proved to be quite difficult as the lipophilic ethylenediamine palladium(II) corner (**2-4**) and the lipophilic bipyridines (**2-34** and **2-35**) had incompatible solubilities. The palladium containing compound (**2-4**) was soluble in deuterated acetonitrile (d_3-MeCN) whereas the lipophilic 4,4'-bipyridines were not; the converse situation was true in deuterated tetrahydrofuran (d_4-THF). Upon mixing the two deuterated solvent solutions of the two components a gummy white precipitate was quickly formed. This observation could indicate one of several events. One possibility was that either one or both of the components had precipitated out of the mixed solvent solution before any self-assembly of components had occurred, clearly this would be a highly undesirable

outcome. Another possibility was that the self-assembly of the two components had occurred to generate species of higher stoichiometry at which point these higher species became insoluble and at this point precipitated from the mixed solvent. A final, and most desirable, possibility could be that the precipitate was itself the desired final square complex. Attempts were made at filtering the mixture to remove the precipitate in hopes of analyzing it but these resulted in either the passage of the solids through the filter into the filtrate or rapid clogging of the filter with the gummy semi-solid produced resulting in no filtrate being collected. NMR spectra of this mixture were unsurprisingly of very poor quality and of no analytical value due to the presence of solids.

Fortunately with heating small amounts of the lipophilic ethylenediamine palladium (II) corner (**2-4**) could be dissolved into d_4-THF but the fear was that the high temperatures and the relatively good coordinating properties of THF could cause the initial palladium(II) coordination complex (**2-4**) to dissociate. If this occurred it would then be possible, upon the solution cooling, for a variety of different palladium coordination complexes to form with varying stoichiometries of 3-(hexadecyloxy)propane-1,2-diamine and d_4-THF.

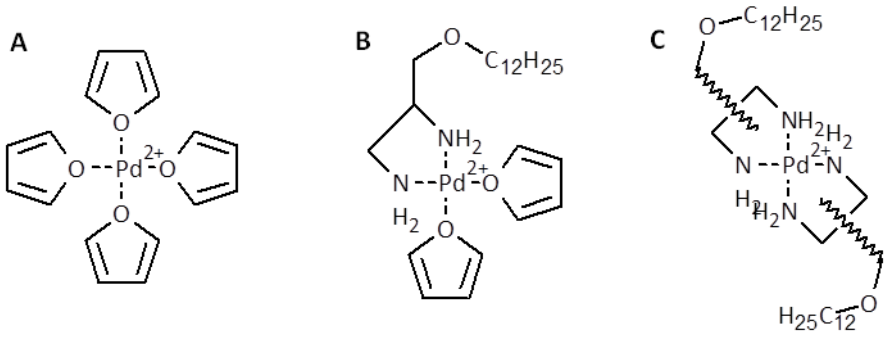

Figure 2-6: Possible palladium(II) coordination complexes formed with varying stoichiometries of lipophilic ethylene diamine and d_4-THF.

Of the possible structures, the worst case would be the bis-3-(hexadecyloxy)propane-1,2-diamine palladium(II) (C, Figure 2-6) as this compound is likely to be relatively stable and no longer able to coordinate to the nitrogens of the lipophilic bipyridine molecule to form the desired square complex since all coordination

sites are already occupied. Regardless of these potential drawbacks a solution of the lipophilic palladium corner (**2-4)** was made in d_4-THF and mixed with an equimolar solution of the 3,3'-diheptadecyl-4,4'-bipyridine (**2-35**) in the same solvent. The resulting solution was then analyzed by ^{1}H NMR to observe if there were any significant changes to the chemical shifts of the bipyridine ring nitrogens.

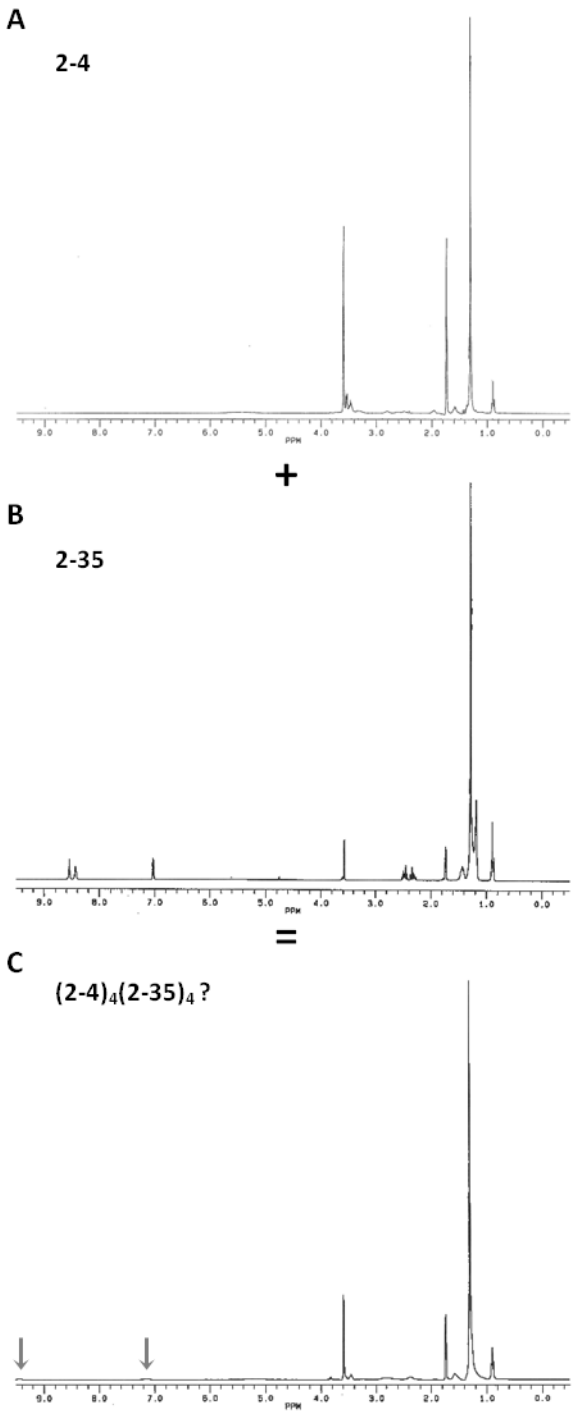

Figure 2-7: ^{1}H NMRs in d4-THF of A) the lipophilic ethylenediamine palladium(II) corner (**2-4**), B) 3,3'-diheptadecyl-4,4'-bipyridine (**2-35**) and C) a 1:1 mixture of the two compounds.

As can be seen from the NMR spectra of the mixture of the two compounds (C, Figure 2-7) as compared to the neat lipophilic bipyridine (B, Figure 2-7) spectra there are some changes to the chemical shifts of the pyridine ring protons. Although the signals

of interest found in the aromatic region are quite weak, each one represents only two protons whereas the alkyl signal at approximately 1.3ppm is due to the 89 methylene protons from the aliphatic tails of the palladium corner (**2-4**) and the 3,3'-diheptadecyl-4,4'-bipyridine (**2-35**), there does appear to be some very small signals downfield of those for the lipophilic 4,4'-bipyridine (**2-35**) on its own. Qualitatively the spectra of the mixture has some of the characteristics expected for the square complex but due to the poor resolution of the aromatic proton signals relative to the rest of the protons a definitive assessment of the success of the self-assembly of the square complex remained elusive.

While trying to determine an appropriate solvent to carry out these self-assembly studies it was discovered that the precursor to the final lipophilic 4,4'-bipyridines, 3,3'-dimethyl-4,4'-bipyridine(**2-33**,Scheme 2-13), was soluble in d_4-THF much like the lipophilic ethylenediamine palladium(II) corner (**2-4**). As an analog for the study of the effect of substitution of the 4,4'-bipyridine at the 3 and 3' positions on the self-assembly of the more lipophilic Fujita square, using the 3,3'-dimethyl-4,4'-bipyridine (**2-33**) is reasonable. Even though the methyl substituent is much smaller than the longer alkyl chains as reflected by the B values (7.4 and 8.7 kcal/mol respectively [84]), the main source of steric clash preventing free rotation about the single bond joining the two pyridine rings in the 4,4'bipyridines comes from the substituent directly attached to the ring. Substituents at increasing distances from the methylene directly attached to the ring have increasing freedom to move in order to minimize unfavourable steric interactions. Based on this information an equimolar solution of the lipophilic ethylenediamine palladium(II) corner (**2-4**) and 3,3'-dimethyl-4,4'-bipyrdine (**2-33**) was prepared in deuterated acetonitrile. NMR spectroscopy was run on this solution and the chemical shifts were compared with solutions of the individual components also in deuterated acetonitrile; see Figure 2-8.

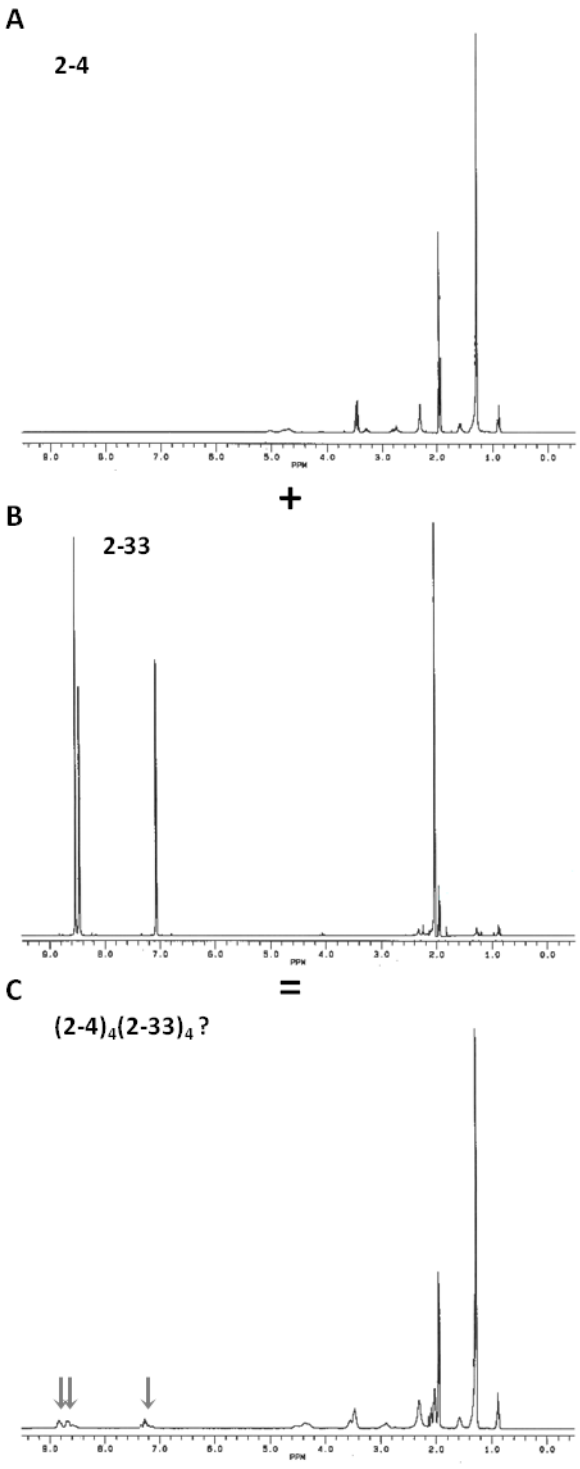

Figure 2-8: ^{1}H NMR spectra of A) 3-(hexadecyloxy)propane-1,2-diamine palladium(II) (**2-4**), B) 3,3'-dimethyl-4,4'-bipyridine (**2-33**) and C) 1:1 mixture of the two compounds all in d3-acetonitrile. Note the shifts downfield for the signals associated with the aromatic protons of the pyridine ring.

From these spectra it is clear that the signals from the pyridine ring protons have shifted significantly downfield, from 8.56, 8.37 and 7.04 ppm to 8.82, 8.70 and 7.26 ppm, as would be expected for the coordination of the 3,3'-dimethyl-4,4'-bipyridine (**2-33**) molecule to the lipophilic palladium(II) corner (**2-4**). Although this observation is supportive of the coordination of the bipyridine molecule to the palladium metal centre it does not suggest whether the major species is in fact the desired square complex. It could conceivably be some other unforeseen architecture such as a triangular one which has also been observed for similar systems [101]. However one can be confident that the complex is a small and well defined structure and not a larger coordination polymer as the proton signals observed in the NMR spectra of the complex are quite sharp whereas large polymeric molecules tend to exhibit broadened signals due to slow tumbling.

In the case of the original Fujita system, it was found that the square complex could act as a host for several different guest molecules and that upon mixing with the square complex changes to the chemical shifts of the guest molecules could be detected. One such guest, 1,3,5-trimethoxybenzene, showed shifts in the signals of 1.56 and 0.59 ppm for the aromatic and methyl protons respectively [102]. If the synthesized modified Fujita system showed similar shifts for this guest molecule upon mixing, this would serve as excellent evidence for the formation of the desired square complex.

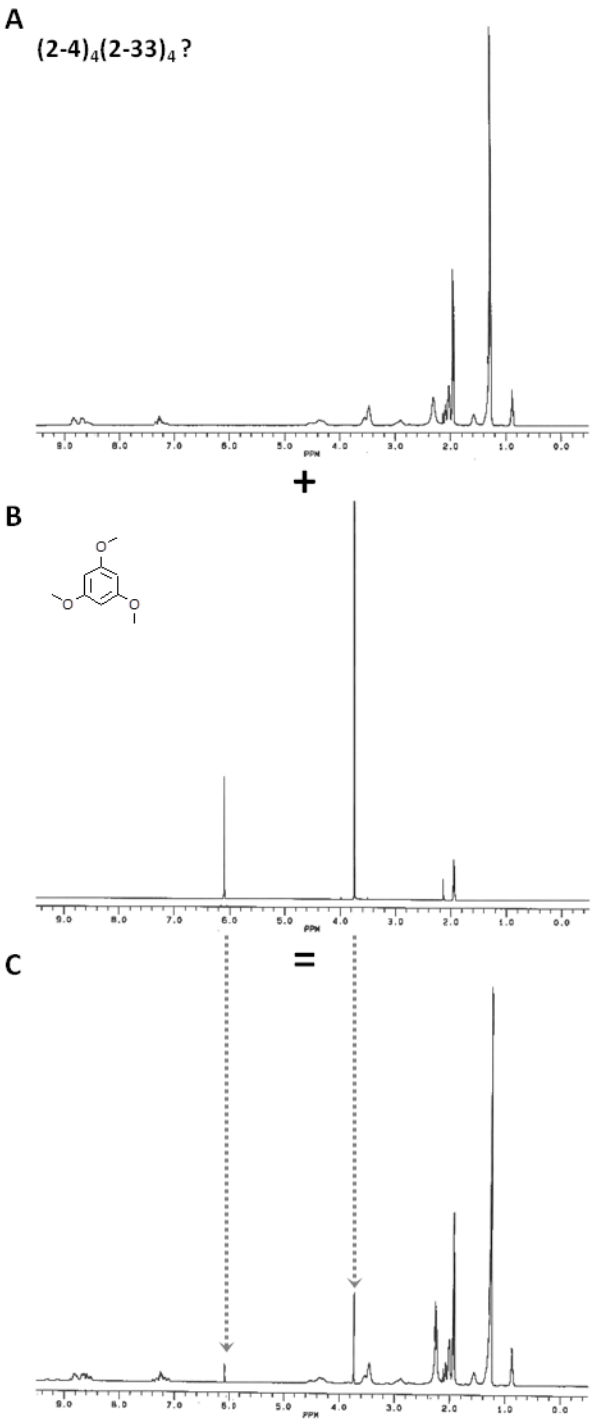

Figure 2-9: ^{1}H NMR spectra of A) the suspected square complex formed between 3-(hexadecyloxy)propane-1,2-diamine palladium(II) (**2-4**) and 3,3'-dimethyl-4,4'-bipyridine (**2-33**) B) 1,3,5-trimethoxybenzene, C) 1:0.5 mixture of A and B.

To this end the NMR sample of the suspected square complex was treated with 0.5 equivalents of 1,3,5-trimethoxybenzene to see if related changes in chemical shifts

could be observed. Unfortunately, comparison of the spectra between neat guest and the guest-potential host mixture showed no changes in the chemical shifts of guest molecule indicating that no complex had formed between the two; see Figure 2-9. There are several possible explanations for this observed behavior. One possible explanation is that no square complex formed whatsoever, however based on the observed shifts in the bipyridine ring protons upon addition of the palladium containing compound this seems the least likely possibility. Presuming therefore that the square complex had successfully formed there remained two likely explanations for the lack of binding between host and guest; one argument was based on steric interactions and the other based on the hydrophobic effect. The steric argument is based on the additional steric bulk introduced by the addition of the methyl groups *meta* to the pyridine nitrogens which will effectively decrease the size of the central pore potentially inhibiting the binding of the guest. The argument based on the hydrophobic effect stems from the necessity of using acetonitrile as the solvent to dissolve the synthesized compounds. The literature host-guest binding study was performed in water and based on the structures of the host and guests the hydrophobic effect is likely to be significant in stabilizing the complex. Changing the solvent used from water to acetonitrile eliminates any stabilization energy for the complex from the hydrophobic effect the result of which could be to destabilize the complex sufficiently so as to prevent its formation to any appreciable extent.

2.9 Vesicle Based Studies on the Self-Assembly and Ion Transport Properties of Second Generation Lipophilic Fujita Squares

Given that the overall goal of this project was the synthesis of a novel class of channel forming molecules via a self-assembly strategy the next logical step in analyzing the products was to characterize their ion transport behavior.

The first such study to be carried out was the HPTS vesicle assay. As mentioned in the introductory chapter, this assay is used to assess the bulk transport properties of a population of channels as they collapse an induced proton gradient between the

exterior and interior environment of lipid vesicles. The HPTS assay was carried out using the standard procedure developed in the group with variations on the methods of introducing the different components to the vesicles. The different methods used were: injection of solutions of the individual compounds to a vesicle solution followed by incubation, injection of a premixed solution containing suspected square complexes to the vesicle solution followed by incubation and pre-loading of one or both of the components into the lipid mixture at the onset of vesicle preparation followed by injection of the missing component, if any, followed by an incubation period. Unfortunately regardless of the method of introducing the compounds to the vesicles no transport activity was observed. A possible reason for this lack of activity is that the HPTS assay must be carried out in a narrow pH range centered about 7.3 which corresponds to the range in which the maximal difference in fluorescence emission between the acid and base forms can be observed for the fluorophore. Unfortunately this pH range is not in the optimal pH range for the self-assembly of the Fujita square as determined previously in the Fyles group [80]. The representative plots for the previously reported speciation simulations are presented in Figure 2-10 below for the system at concentrations of 10 μM (A) and 5 mM (B) in ethylenediamine palladium(II) to illustrate the pH dependence of the system. From these simulations the species of greatest interest is the one labeled 440 which represents the square species [ethylenediamine palladium(II)]$_4$(4,4'-bipyridine)$_4$.

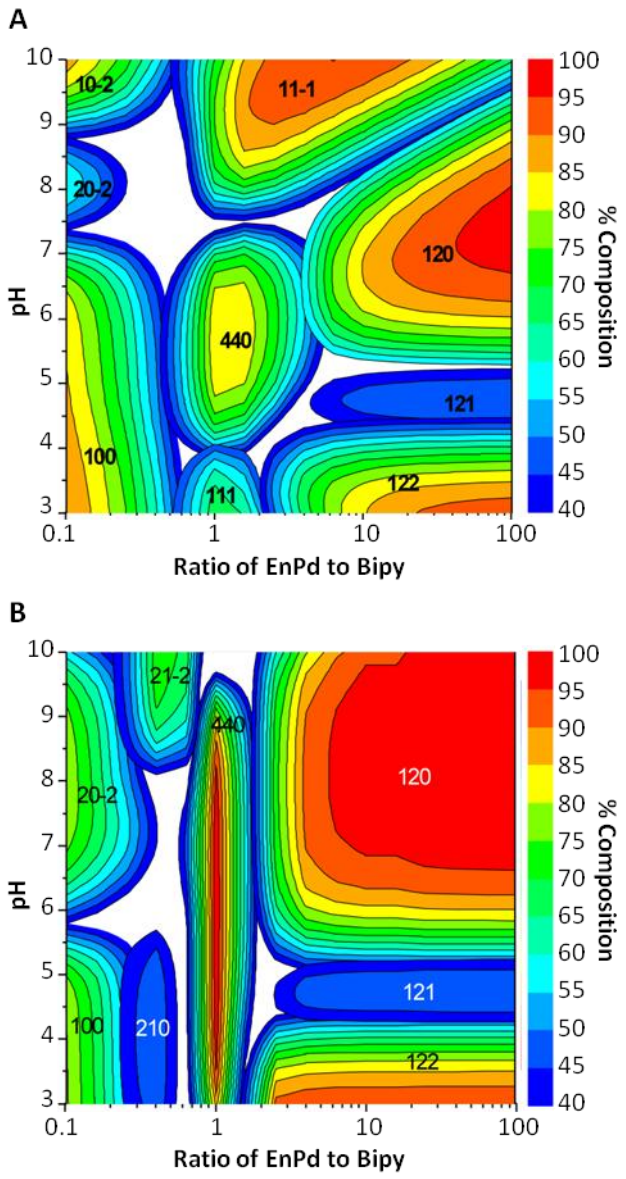

Figure 2-10: Ethylenediamine palladium(II) + 4,4'-bipyridine speciation simulation as adapted from Fyles [80]. Simulations carried out at concentrations of A) 10 µM and B) 5 mM in EnPd with varying pH and molar ratio of Bipy.

As can be seen from Figure 2-10 the simulation carried out at 10 µM (A), the ideal pH for formation of the square species at this relatively low concentration is approximately 5.6 while the pH of the HPTS assay at 7.3 is non-optimal for square formation. Because of this incompatibility between the pH of the HPTS assay and the productive self-assembly of the desired modified Fujita square it may very well be that the lack of detected activity could be due to failure of the complex to form at lower

concentrations. Although the simulation at the higher concentration of 5 mM revealed tolerance for a wider range of pH, the system also exhibited much greater sensitivity to the ratio of the two components as indicated by the very narrow distribution of the desired species along the ratio axis. In addition, concentrations of transport active species at this level could lead to excessive vesicle permeation resulting in the near instantaneous collapse of the proton concentration gradient from which valuable rate information cannot be obtained.

Based on these shortcomings in the HPTS assay for this system it was worth the effort to try to develop a novel vesicle based assay that could operate in the pH ranges for which self-assembly is expected. With this goal in mind the first task was in finding a replacement for HPTS which was water soluble, sensitive to some easily controlled change in its environment that also functions in the ideal pH range for square complex formation. Searching available and affordable environment sensitive chromophores came up with the particularly interesting candidate; 2-{[2-(2-{5-[bis(carboxymethyl)amino]-2-methylphenoxy}ethoxy)-4-(2,7-difluoro-6-hydroxy-3-oxo-3*H*-xanthen-9-yl)phenyl](carboxymethyl)amino}acetic acid, mercifully abbreviated to Fluo-4. Fluo-4 is a water soluble molecule which exhibits a greater than 100 fold increase in fluorescence emission at 516 nm upon binding Ca^{2+} ions when excited with 494 nm light, has a binding affinity of 345 nM and is highly tolerant of a wide range of pH [103] (Figure 2-11, A). The modified assay would therefore measure the rate of transport of hydrated calcium ions which, with a hydrodynamic radius of 3.1 Å, should be easily transported through the centre of the modified Fujita square as envisioned for the system.

An assay was designed to use this Fluo-4 calcium sensitive dye at a pH of approximately 5.6 in order to maximize the formation of the self-assembled square by changing the buffer used in the assay to 10 mM sodium acetate buffer with 10.8 µM Fluo-4 added to the interior of the vesicles while maintaining the same lipid mixture (8:1:1 phosphatidylcholine : phosphatidic acid : cholesterol) used for vesicle formation.

For the modified assay, in place of adding a base pulse to induce the concentration gradient a pulse of calcium chloride was used instead. In order to obtain valuable information about the relative transport activity of a compound the first task is generally to obtain a baseline transport activity in the absence of any potential channel forming compound. The establishment of this baseline activity is necessary since the vesicles often show some leakage when put under osmotic stress associated with the rapid change in ion concentration upon injection of the solution to establish a concentration gradient. Some interesting and unforeseen behavior was observed when trying to establish this baseline activity. Firstly, contrary to the expected low but measurable baseline activity, upon injection of the calcium pulse in the absence of any ion channel a rapid increase in fluorescence emission to some saturation point was observed as shown in Figure 2-11 below.

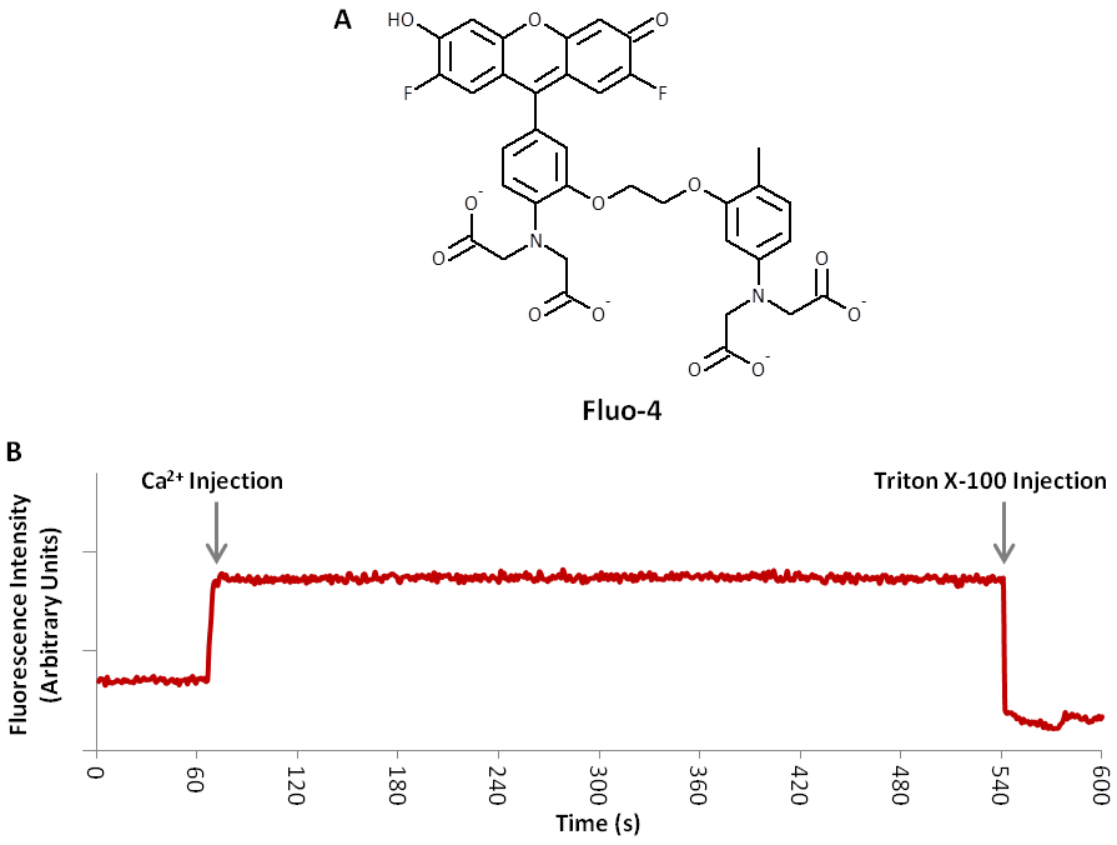

Figure 2-11: A) the chemical structure of the Ca^{2+} sensitive dye Fluo-4 and B) time based fluorescence results obtained from a trial experiment to develop a vesicle assay of Ca^{2+} transport.

At first this observation was somewhat perplexing but a search through the literature revealed that it had previously been discovered that the phosphatidic acid component of the vesicle mixture could facilitate the diffusion of calcium(II) ions across a bilayer membrane by acting as an ionophoric ion carrier [104]. This seemed a likely cause for the observed behavior of the vesicles. In addition, upon lysis of the vesicles with Triton X-100 in order to obtain the final maximal fluorescence, a decrease in the fluorescence intensity was observed instead. This was contradictory to expectations since the lysis of the vesicles should have exposed the Fluo-4 to a higher concentration of Ca^{2+} if the concentration gradient was even partially maintained resulting in greater fluorescence intensity. Even in the case where the concentration gradient had collapsed completely the small volume of detergent added should have had only resulted in a minimal decrease in fluorescence associated with the dilution of the vesicle solution. Attempts using several other chemical detergents for the lysis step, under the assumption that the Triton X-100 was interacting adversely with either the dye or Ca^{2+} ions, also yielded identical results. Unfortunately this meant that the assay as it was conceived was doomed to failure. The option existed to try to find a different lipid composition for the vesicle formulation that did not include phosphatidic acid to avoid the complication of lipid assisted transport but it was decided that efforts would best be put towards first determining if any reliable transport activity could be observed using the bilayer clamp assay.

2.10 Bilayer Clamp Studies on the Self-Assembly and Ion Transport Properties of Second Generation Lipophilic Fujita Squares

With the failure to detect transport activity for the various lipophilic Fujita squares using vesicle based assays the next logical step was to try to detect activity using bilayer clamp studies. It is not uncommon for compounds to show activity in one assay but not the other [105, 106] as the conditions of the two assays, such as bilayer membrane geometry and thickness, are necessarily different between the two. Studies using the bilayer clamp assay also have the advantage that they can monitor the activity

of single channels. If single channel events were observed with conductances on the order expected for a channel with the internal diameter of the Fujita square this would provide strong evidence of the self-assembly of the individual components.

Bilayer clamp assays of the various mixtures of synthesized compounds unfortunately failed to show well behaved 'square top' activity that could be definitively ascribed to square channels of diameters on the order those of the modified Fujita channels, instead showing very erratic behavior that could be more easily envisioned as being due to membrane disruption than discrete channels. An example of this type of activity is shown in Figure 2-12 below.

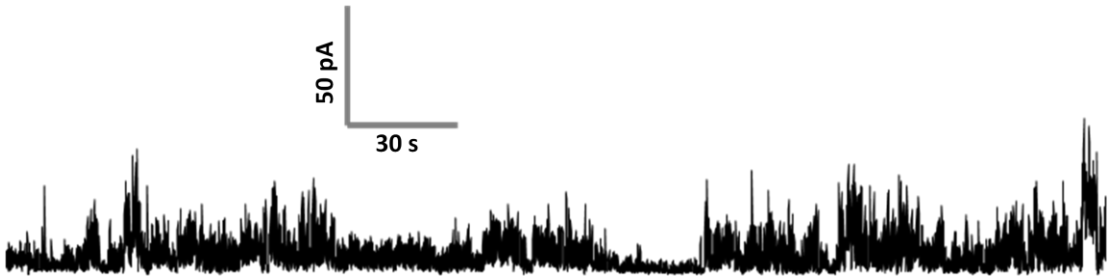

Figure 2-12: Representative bilayer clamp activity seen for second generation modified Fujita squares showing activity best fitting with the purple or erratic type activity. Conditions; 0.5M Cs_2SO_4 electrolyte, Ag/AgCl electrode, 1M KCl bridging solution, KNO_3 salt bridges, applied potential of +50 mV, 1μM final concentration of (**2-34**)$_4$(**2-4**)$_4$ 'squares' injected into each chamber.

This behavior is somewhat reminiscent of that observed to occur early on in the bilayer clamp experiment conducted on the first generation modified Fujita square (**2-5**), however this activity never developed into the long lived and stable conducting states [79]. On the other hand, the long lived channels with stable conductances that were seen for the lipophilic ethylenediamine palladium(II) molecules (**2-4**) on their own or with added 4,4'-bipyridine in studies prior to this work were never observed for any of the various mixtures with the newly synthesized lipophilic 4,4'-bipyridine molecules. The lack of this sort of activity could indicate that the lipophilic ethylenediamine palladium(II) metal centers were effectively coordinating to the 4,4'-bipyridine molecules and were therefore unable to form the channels responsible for this behavior. Unfortunately due to the single channel nature of the observations made

using the bilayer clamp the absence of evidence is not the same as the evidence of absence.

2.11 Interpretations and Hypotheses on the Failure of the Modified Fujita System

Over the course of studying the second generation modified Fujita square system in hopes of detecting regular transport activity that could be definitively associated with the passage of ions through the central pore it became increasingly obvious that the effort involved was not providing commensurate returns. It became clear that there were several potential problems with the design of the system that could explain the lack of transport activity. Of particular concern were the effect of the overall charge of the assembled complex on membrane partitioning, the number of possible stereochemical isomers and the effect of modifications near the pore on the passage of ions.

Upon square formation the modified Fujita complex would possess an overall charge of 8+; a sufficiently high charge density could disfavor the partitioning of the self-assembled supramolecule into the non-polar bilayer environment. Obviously if the complex doesn't effectively partition into the membrane then there is little chance of a transport active species being formed.

A further complication inherent to this system is the large number of possible stereochemical isomers of the completed square complex due to the chirality of the lipophilic ethylenediamine palladium(II) corner. Each corner of a square complex can adopt two arrangements for each of the two enantiomeric forms for a total of four possible stereochemistries at each corner. Taking into account equivalent geometries this results in a total of 41 isomers for the completed square complex [79]. This number is based on the assumption that the lipophilic bipyridine moieties retain relatively free rotation about the single bond joining the two pyridine units. If the rotation is restricted then upon closure of the square each lipophilic bipyridine will be constrained in one of two enantiomeric arrangements resulting in an even larger number of possible

stereochemical isomers. With so many potential isomers characterization of the final self-assembled square complex could potentially become more complicated than if only one isomer was produced.

As discussed earlier, the positions *meta* to the ring nitrogens of the pyridine rings in the 4,4'-bipyridine molecule were chosen in order to minimize any possible steric repulsion between the bipyridine and ethylenediamine palladium(II) moieties that could potentially destabilize the formation of the square complex. Unfortunately substituents at this position may rotate freely such that they could potentially block the centre to the square complex which is especially likely as aggregating into the relatively non-polar pore of the square would result in a lower energy conformation due to the hydrophobic effect. If the centre of the pore became sufficiently blocked by the substituents designed to impart lipophilicity then it is also unlikely that it could effectively transport ions. This behavior could also account for the failure to observe activity for the second generation modified Fujita square. In addition the structure of 4,4'-bipyridine does not provide for any other alternative locations for modification so the system is inherently limited.

Based on these perceived shortcomings of the Fujita square complex as a lead compound for generating a self-assembling ion transport system, a new scaffold for the design was required.

2.12 New Scaffold for Generation of Self-Assembling Ion Channels

In exploring alternative self-assembling metal-ligand constructs as potential candidate scaffolds for self-assembling ion channels, several key features were required based on the hypothesized problems with the Fujita system. Firstly, like the Fujita square the new complex should also possess a semi-rigid pore structure that is sufficiently large to allow the passage of hydrated ions or small molecules. The complex should also have a low net charge, preferably no charge, or be amenable to modifications which could limit the net charge in order to facilitate the partitioning of

the structure into the non-polar bilayer membrane. As well the new complex should have positions which can be easily modified, if necessary, in order to impart such characteristics as lipophilicity and these modifications should be in an orientation such that there is little chance of occluding the pore.

Based on these criteria the model system that was chosen, presented in Scheme 2-15, was the bis-terpyridine molecule first reported by Newkome et al. to self assemble into hexagonal architectures in the presence of iron(II) cations [78].

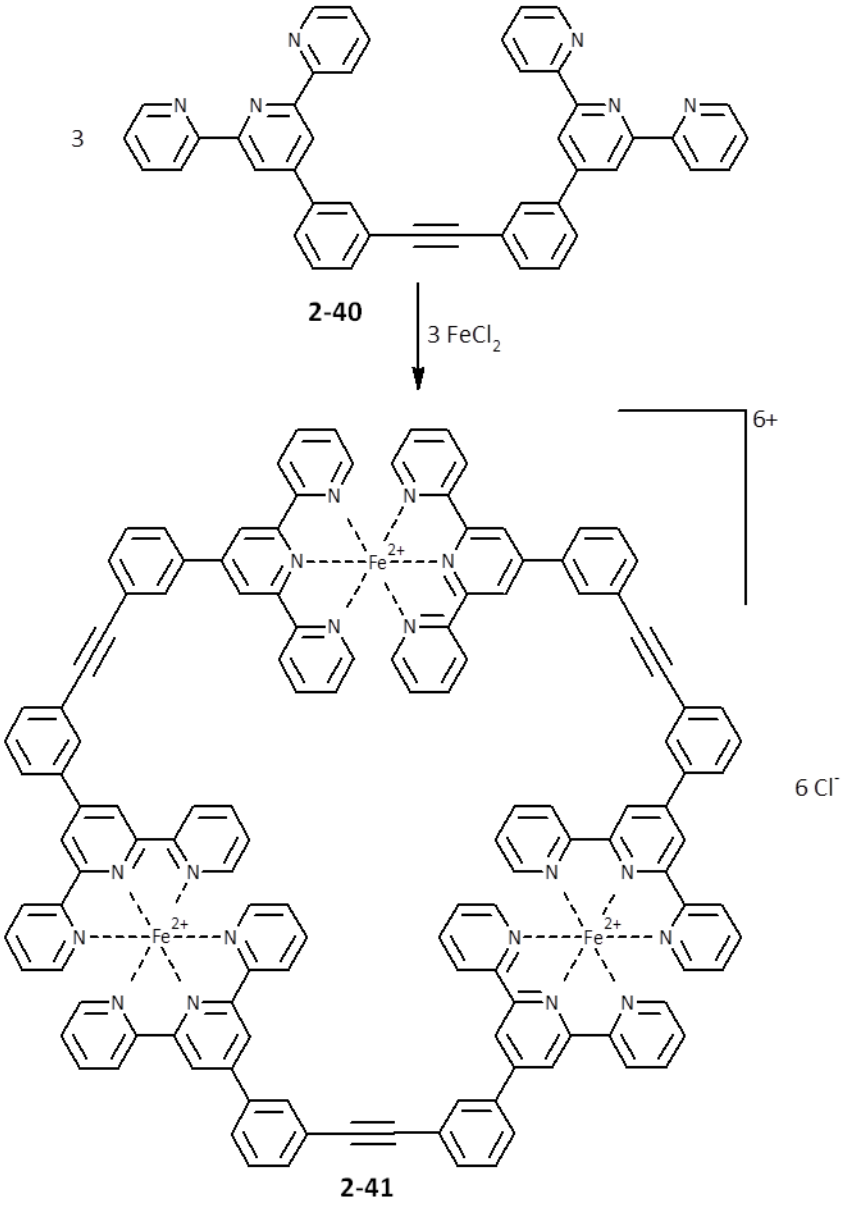

Scheme 2-15: The Newkome bis-terpyridine ligand (**2-40**) and its self-assembly into a macrocyclic hexagon (**2-41**) in the presence of iron(II) cations.

As can be seen from the schematic above, the Newkome system possesses many of the desired properties sought in a potential channel forming system. The assembled architecture results in the formation of a large shape persistent semi-rigid pore with a diameter of approximately 7 Å. In addition there are several good sites for potential modification if needed, primarily the sites on the central diphenylacetylene portion of the molecule which point away from the central pore. These sites are also far enough

away from the metal coordinating terpyridine portion of the molecule as to not interfere with metal coordination. Therefore modifications to these sites should have little to no impact on either the freedom of the pore to allow the transit of ions through it or on the ability of the complex to self-assemble via coordination to a metal centre. There are also several other potential advantages in using the Newkome hexagon as a lead system. For example, unlike for the Fujita system which required two different ligands, 4,4'-bipyridine and the pre-coordinated ethylenediamine, the Newkome system involves only one ligand possessing two coordination sites. This may simplify the self-assembly process since differential partitioning of the components should not be as troublesome. Also in moving away from square planar metal coordination center, for which there are a limited number of available metals, to the more diverse octahedral center allows for the screening of several different metals in order to find the one which imparts the best characteristics. Another potentially advantageous characteristic is that the terpyridine ligand in the Newkome system is tridentate versus the monodenate 4,4'-bipyridine ligand of the Fujita system. The extra coordination per ligand as well as the chelate effect should result in a much more stable complex overall which could potentially be studied under a wider range of conditions than the Fujita system.

Obviously the overall charge of the assembled complex, 6+, was still undesirably high and had to be addressed in the design of the modified Newkome hexagon.

2.13 Design Considerations for a Modified Newkome L_3M_3 Hexagon

Before dealing with the issue of neutralizing the overall charge of the complex, the magnitude of the charge to be neutralized first had to be addressed. Since the overall positive charge of the complex originates from the sum of the charges of the metal cations used, it is the selection of these that is the determining factor. Having already decided on using metals with octahedral coordination geometry the logical place to start is with the transition metals, especially those in the first row. The most common and second most common stable oxidation states for these elements are +2 and +3. The +2 oxidation state is especially stable because it results from the loss of the two

electrons from the 4s orbital which is higher in energy than the 3d orbitals in the first row transition metals. Using metals in the +2 and +3 oxidation states would result in hexagons with six and nine overall positive charges to neutralize respectively. The most practical and elegant solution is for all three ligand molecules in the L_3M_3 complex to be as symmetrical as possible. In the case of using metals in the +3 oxidation state this would require each ligand molecule to have a charge of -3. There is no intuitive and synthetically efficient way to modify the Newkome ligand which would impart this charge as well as maintaining the overall symmetry of the molecule. Fortunately for the alternative design using metals in the +2 oxidation state, requiring each ligand to possess a charge of -2, many more possibilities exist.

The new system therefore involved the design of a modified Newkome bis-ligand with an overall charge of -2. When considering the required modification in the context of the whole supramolecular self-assembly the very real possibility that the anionic group, being electron rich, could act as ligand itself must be addressed. A choice had to be made whether to employ this characteristic into the design of the coordination site or to try to work around it by preventing the possibility of binding between the metal and the anionic group via some mechanism such as steric crowding. Integrating the anionic portion into the coordination sphere was the more elegant and also likely the less synthetically involved option and therefore it was chosen over the alternative. The anionic functional group of choice for such a purpose is the carboxylate as there are countless examples of coordination complexes of transition metals featuring this moiety. In addition since the ion channel studies both occur in aqueous solvents at around neutral pH the carboxylic acid group will be in the carboxylate form.

Conceptually, the introduction of the carboxylate group into the coordination site of the modified Newkome system involves the replacement of one or more pyridine groups of the terpyridine moiety. In order to achieve the desired -2 charge into the modified bis-tridentate ligand, the inclusion of two carboxylate groups was required. As shown in Figure 2-13, two possible structures with these characteristics can be

envisioned; one in which one pyridine has been replaced on each of the terpyridine units of the bis-tridentate ligand to yield a molecule with symmetry about the alkyne bond (BIPYA-BIPYA, **2-43**) and the other where two pyridines of the same terpyridine unit have been replaced leaving the other terpyridine ligand of the bis-tridentate ligand unchanged generating a molecule with two distinct sides (TERPY-DPA, **2-42**).

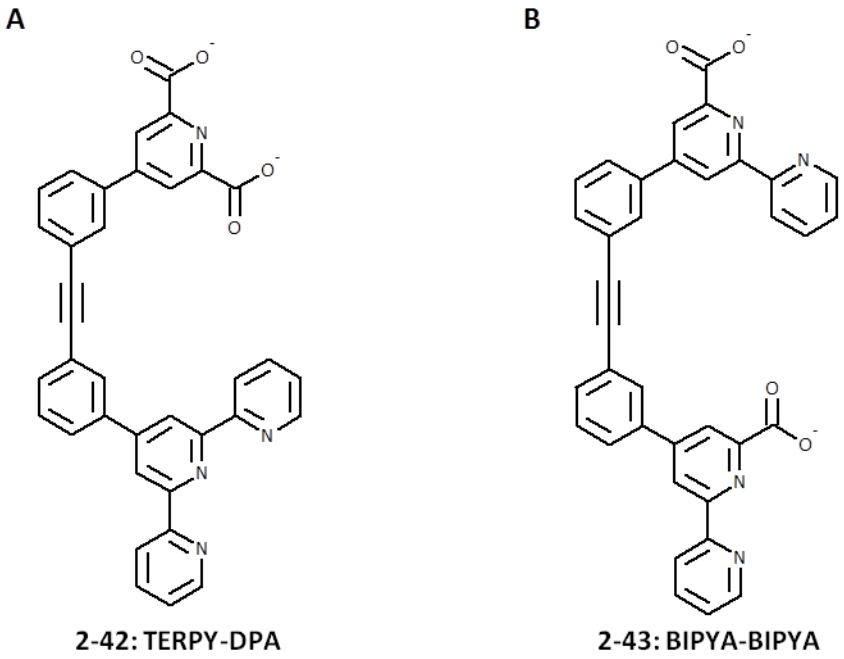

Figure 2-13: Figure of the two modified systems: A) the dissymmetric bis-tridentate ligand (**2-42**) possessing one terpyridine (TERPY) and one dipicolinate (DPA) ligand, abbreviated TERPY-DPA and B) the symmetric bis-tridentate ligand (**2-43**) possessing two 2,2'-bipyridine-6-carboxylate ligands (BIPYA), abbreviated BIPYA-BIPYA.

As can be seen from the structures of the target bis-tridentate ligands (Figure 2-13, **2-42** and **2-43**) the option exists for further modification of the system with lipophilic groups, however as an initial proof of concept for the new ligand system and its coordination to transition metals in the +2 oxidation state the first synthetic targets were simply the ligands possessing the overall -2 charge. The hypothesis being that upon self-assembly the charge neutral hexagon would have a sufficiently high preference for partitioning into the non-polar bilayer membrane that further modification would be unnecessary.

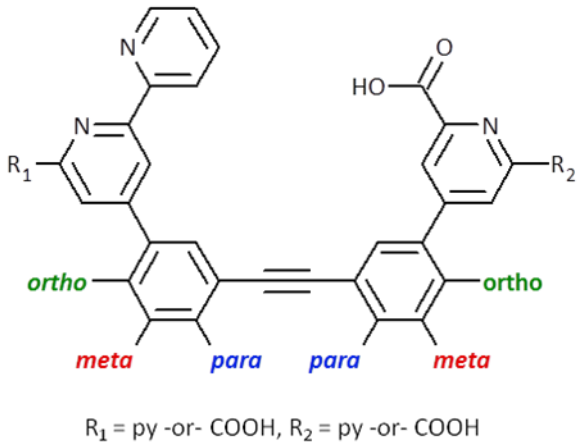

Figure 2-14: Possible sites for further substitution of the modified Newkome bis-tridentate ligands highlighted with coloured labels with reference to their disposition relative to the nearest tridentate ligand moiety.

As illustrated in Figure 2-14, all three of these sites of modification should have relatively little impact on the rotational freedom about any of the adjacent single bonds although if one had to be chosen over the others modifications to the *meta* position are likely to have the least impact on the self-assembly of the system into the L_3M_3 hexagons.

2.14 Considerations for Hexagonal Complexes from the Modified Newkome Ligands

Although both of these target molecules possess -2 charges and their self-assembly with transition metals in the +2 oxidation state should yield hexagonal complexes with no net charge, the nature and number of potential geometries of the complex differ due to the geometry of the coordination sites.

In the case of the symmetrical ligand (BIPYA-BIPYA, **2-43**), independently each metal centre can only be coordinated to two identical tridentate ligands for which there is only one possible geometry however, upon closure of the hexagon the orientation of the planes of the coordinating ligands relative to each other become locked into one of two enantiomeric conformations. The result is that the overall hexagonal complex possesses three stereocenters which translates to four different possible stereochemical

species depicted in Figure 2-15; R-R-R, R-R-S, R-S-S and S-S-S that are all likely to be of very similar energies and therefore equally prevalent in solution.

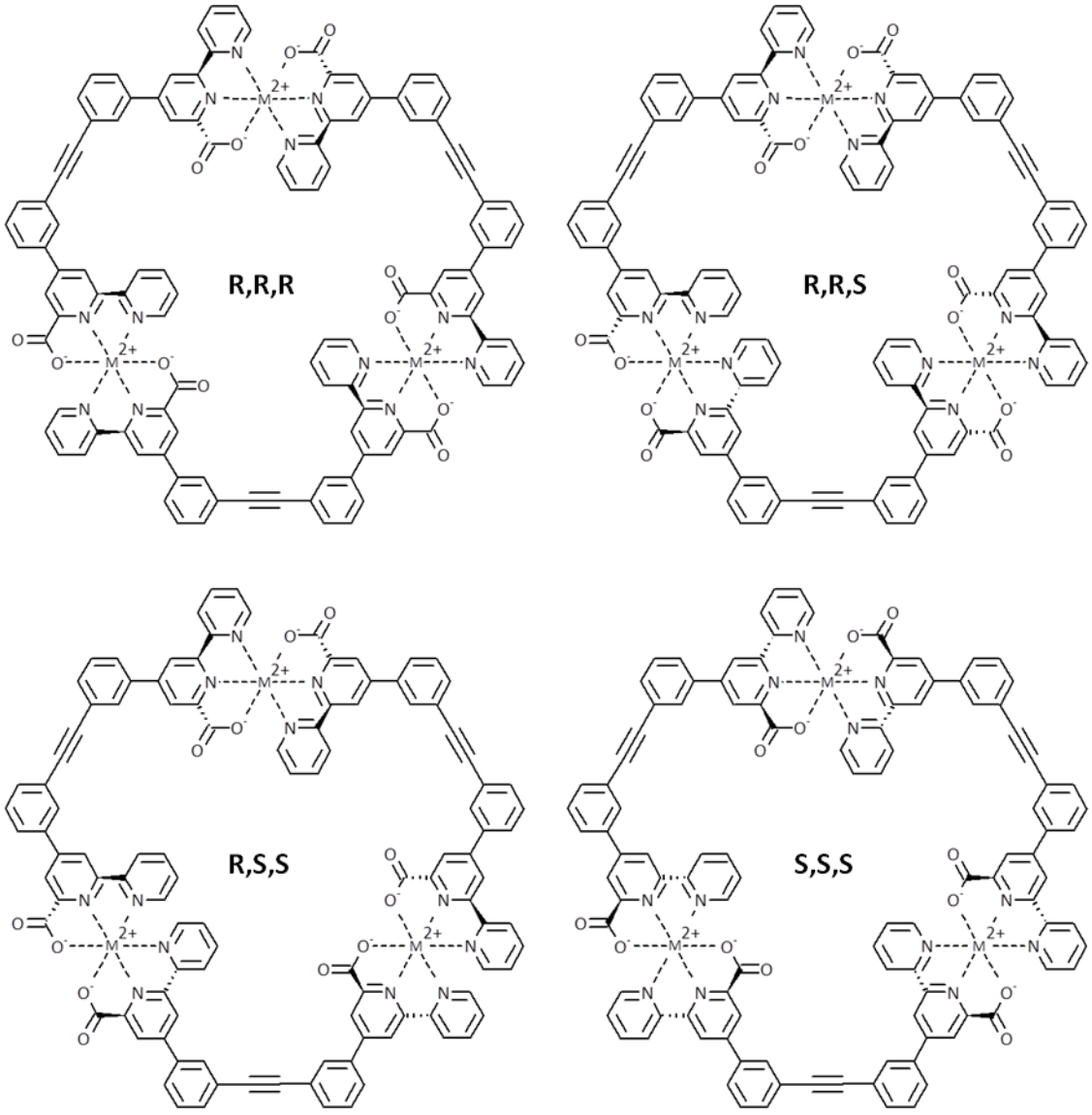

Figure 2-15: Possible geometries for the hexagonal complex formed from the symmetrical bis-tridentate ligand molecule BIPYA-BIPYA (**2-43**) coordinating to transition metals in the +2 oxidation state.

For the dissymmetric bis-ligand system the different species possible arise not from the stereochemistry of the coordination sites, since each tridentate ligand is symmetric about the central pyridine nitrogen, but from the possibility of each coordination centre to coordinate the same or different ligands. Each metal centre can coordinate one terpyridine and one dipicolinate ligand, two terpyridine ligands or two

dipicolinate ligands. The overall result on the system is that there are two possible conformations for the hexagonal complex; one in which all three coordination centres are of the terpyridine-dipicolinate variety and the other where there is one of each of terpyridine-dipicolinate, terpyridine-terpyridine and dipicolinate-dipicolinate coordination centers, see Figure 2-16.

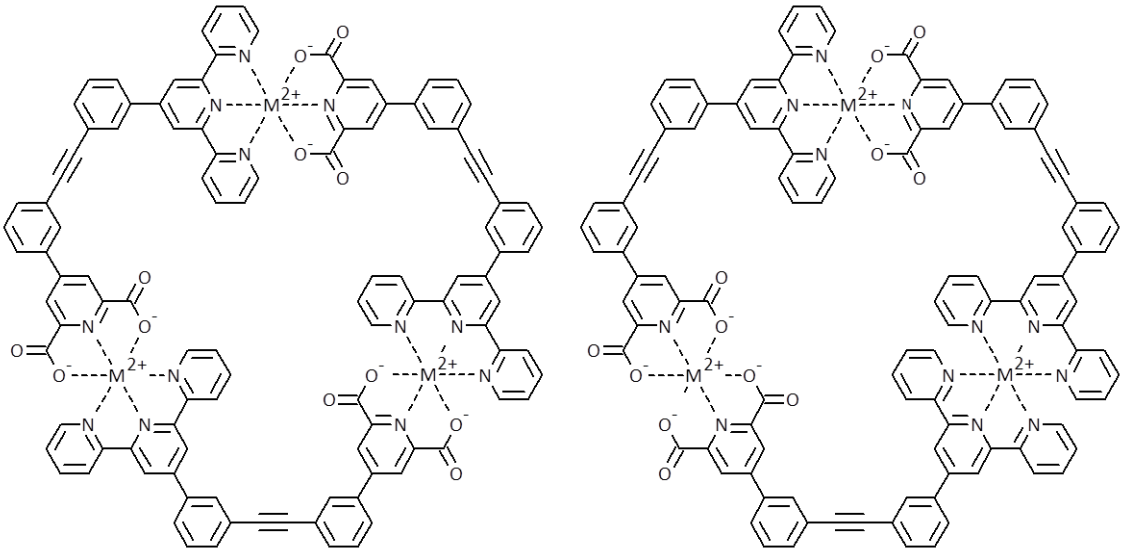

Figure 2-16: Possible geometries for the hexagonal complex formed from the dissymmetric bis-tridentate ligand molecule TERPY-DPA (**2-42**) coordinating to transition metals in the +2 oxidation sate.

2.15 Speciation Simulation for the Terpyridine-Dipicolinate Ligand System

If possible, a worthwhile exercise to undertake before synthesizing any target compounds for a self-assembling system, such as those for the modified Newkome hexagon, is to perform a rudimentary speciation simulation. Such a simulation can give insights into the thermodynamic viability of the system to self-assemble as desired and more specifically the concentration and pH ranges over which the desired assembly is most likely to form. Although a valuable tool it is important to note that it provides no information on the kinetics of the self-assembly process. As such it is entirely possible for the analysis to find the desired compound to be the thermodynamically preferred product for a system that will never form due to the kinetic barriers inherent to the process.

In order to perform such a simulation two types of information are required; a comprehensive analysis of all possible intermediates and final self-assembled structures on the path towards the fully assembled structure and the association constants for each of the possible step-wise interactions. Together these two sets of information serve as a kind of road map for the self-assembly process; the individual species indicating way-points along the path towards the final structures and the association constants plotting the course between these points. The analysis of all possible intermediates is a relatively straight forward mental exercise that can be carried out for both of the target modified Newkome systems. The association constants on the other hand have to come from experimental observations. Fortunately a search through the literature provided the necessary information for the TERPY-DPA (**2-42**) system binding to copper(II) ions [107] as both the TERPY and DPA ligands are well represented in the field of coordination chemistry [108, 109, 110, 111]. Unfortunately, due to the limited instances in current literature [112], a similar search for equivalent data on the BIPYA ligand failed to afford the required association constants. Although determining the association constants for the BIPYA ligand would allow for the simulation of the BIPYA-BIPYA bis-ligand (**2-43**) self-assembly, it was hypothesized that this system was unlikely to deviate significantly from the simulation of the TERPY-DPA (**2-42**) system for which data was readily available. Therefore for expediency's sake it was decided that this exercise was not necessary.

A few assumptions about the self-assembly process of the TERPY-DPA bis ligand were made in order to simplify the comprehensive analysis of the possible species en route to the final hexagonal construct. Firstly, although there is significant rotational freedom within the TERPY-DPA molecule and therefore many possible conformations for any particular intermediate, no energy penalty is assigned to any of these. The compound is effectively considered to have two binding sites held *ortho* (120°) to each other. In addition it was assumed that species with stoichiometries greater than three bis ligands to three metal centers were likely to occur only in relatively low concentrations and were therefore ignored in the analysis. The completed analysis of all

potential intermediate assemblies towards the final hexagons is presented in Figure 2-17 below. A shorthand notation of the individual species based on the coordination motif is provided using the metal centers as reference. For example a metal coordinated to only one TERPY-DPA molecule (**2-42**) via the DPA binding site is denoted as (DPA), a metal coordinated to two ligands is denoted as either (DPA/DPA), (DPA/TERPY) or (TERPY/TERPY) depending on whether it is coordinated to two DPA ligands, one DPA and one TERPY ligand or two TERPY ligands respectively. If a species contains more than one metal center, the braces indicate which interactions are associated with which metal center, so in the case where one TERPY-DPA bisligand (**2-42**) is binding to two metal centers the notation would be (DPA)(TERPY). A statistical factor is also provided for the species which have multiple different but equivalent approaches of a metal to a ligand.

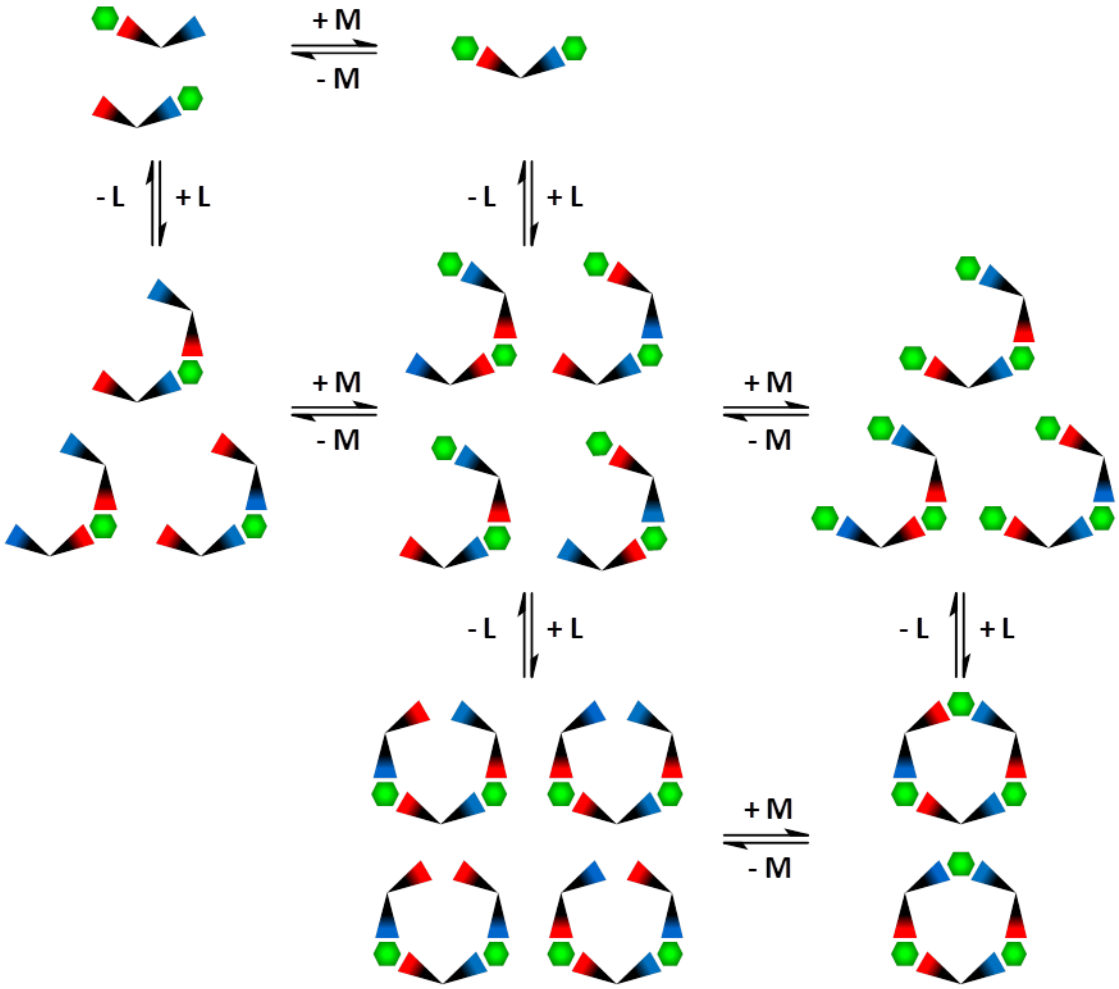

Figure 2-17: Comprehensive analysis of all potential species of given stoichiometries en route to the final M_3L_3 hexagons for the DPA-TERPY bis ligand molecule (**2-42**). The TERPY-DPA ligand is represented by the black 'V' shape with red and blue termini indicating the DPA and TERPY binding sites respectively and the transition metal centre is represented by the green hexagons.

Before delving into the specific thermodynamic parameters of the self-assembly process it is worth noting that there are no unproductive species along the pathway to either of the hexagonal complexes (DPA/TERPY)(DPA/TERPY)(DPA/TERPY) or (DPA/DPA)(TERPY/TERPY)(DPA/TERPY). The implication from this observation is that the 'error checking' process often cited as being required for self-assembling systems is not absolutely necessary. A system that forms via very stable complexation interactions to can be relied upon to eventually fall into a potential energy well for an especially stable hexagonal L_3M_3 state.

From Figure 2-17 illustrating the various possible intermediates towards the self-assembly of the final hexagonal molecule it should be noted that each of the states can be reached from any other state via a series of stepwise association/dissociation equilibria. The equilibrium constant between any two states can therefore be determined by the product of the stepwise association/dissociation constants along any particular path between the two states. The principle of microscopic reversibility states that it matters not which path is chosen so long as the path chosen is real and includes each species in the overall cumulative formation constant. In order to determine the various cumulative formation constants the association constants for the possible stepwise processes were needed. The assumption was made that due to the distance between the two binding sites of the TERPY-DPA bis ligand that binding of a metal to one of the binding sites would have no effect on the binding affinity of the other site for a second metal center. A summary of the required step wise association processes and logK values for the association with copper(II) ions are provided in Table 2-1 below.

Table 2-1: Summary of the required stepwise association processes, their notation and literature logK values for their association with copper(II) ions. In the graphical representation to the processes the DPA and TERPY binding sites of the TERPY-DPA ligand are represented by the red and blue termini respectively.

Process*	Notation	logK (Cu2+)
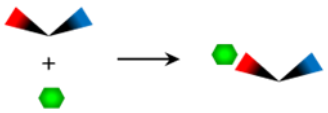	K_{DPA}	9.2
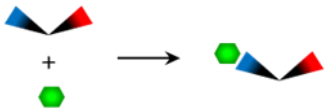	K_{TERPY}	12.3
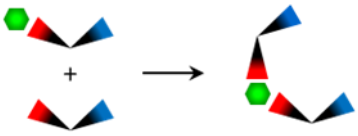	$K_{DPA\text{-}DPA}$	7.2
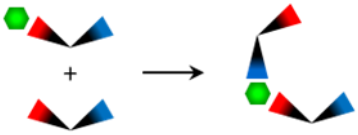	$K_{DPA\text{-}TERPY}$	8.9
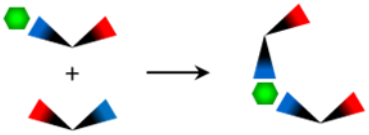	$K_{TERPY\text{-}TERPY}$	6.8

*Note that due to the principle of microscopic reversibility the process of having a TERPY bound metal becoming associated with the DPA binding site of a second ligand ($K_{TERPY\text{-}DPA}$) is not explicitly required since its place along any particular pathway can be represented by the related DPA bound metal becoming associated with the TERPY binding site of a second ligand ($K_{DPA\text{-}TERPY}$). The choice of one association process over the other was entirely arbitrary.

With these stepwise association constants the cumulative formation constants for each of the species can be determined by the product of the individual stepwise association constants. The sum of the cumulative formation constants for any set of species with identical stoichiometries will also provide the cumulative formation constant for species with that particular stoichiometry; note that one of the isomers

usually dominates. Table 2-2 below summarizes the derivation and values of various cumulative formation constants.

Table 2-2: Naming convention, derivation and values of equilibrium constants for individual species as well as for species with the same stoichiometry used for the speciation study of TERPY-DPA (**2-42**) self assembly in the presence of Cu^{2+} cations.

Species	K Notation, Derivation and logK Value	Stoichiometry	β Notation, Derivation and logβ Value
(DPA)	$K_{(DPA)}$, log $K_{(DPA)}$ = 9.2	LM	$\beta_{LM} = \beta_{(DPA)} + \beta_{(TERPY)}$ log B_{LM} = 12.3
(TERPY)	$K_{(TERPY)}$, log $K_{(TERPY)}$ = 12.3		
(DPA)(TERPY)	$\beta_{(DPA)(TERPY)} = K_{(DPA)}K_{(TERPY)}$, log$\beta_{(DPA)(TERPY)}$ = 21.5	LM_2	β_{LM2}, log β_{LM2} = 21.5
(DPA/DPA)	$\beta_{(DPA/DPA)} = K_{(DPA)}K_{(DPA-DPA)}$, log$\beta_{(DPA/DPA)}$ = 16.4	L_2M	$\beta_{L2M} = \beta_{(DPA/DPA)} + \beta_{(DPA/TERPY)} + \beta_{(TERPY/TERPY)}$, log$\beta_{L2M}$ = 19.1
(DPA/TERPY)	$\beta_{(DPA/TERPY)} = K_{(DPA)}K_{(DPA-TERPY)}$, log$\beta_{(DPA/TERPY)}$ = 18.1		
(TERPY/TERPY)	$\beta_{(TERPY/TERPY)} = K_{(TERPY)}K_{(TERPY-TERPY)}$, log$\beta_{(TERPY/TERPY}$ = 19.1		

Species	K Notation, Derivation and logK Value	Stoichiometry	β Notation, Derivation and logβ Value
(DPA/DPA)(TERPY)	$\beta_{(DPA/DPA)(TERPY)} = K_{(DPA)}K_{(DPA\text{-}DPA)}K_{(TERPY)}$, $\log\beta_{(DPA/DPA)(TERPY)} =$ 28.7 (x2)	L_2M_2	$\beta_{L_2M_2} = 2\beta_{(DPA/DPA)(TERPY)} + \beta_{(DPA/TERPY)(DPA)} + \beta_{(DPA/TERPY)(TERPY)} + 2\beta_{(TERPY/TERPY)(DPA)}$, $\log\beta_{L_2M_2} = 30.4$
(DPA/TERPY)(DPA)	$\beta_{(DPA/TERPY)(DPA)} = K_{(DPA)}^2K_{(DPA\text{-}TERPY)}$, $\log\beta_{(DPA/TERPY)(DPA)} =$ 27.3		
(DPA/TERPY)(TERPY)	$\beta_{(DPA/TERPY)(TERPY)} = K_{(DPA)}K_{(DPA\text{-}TERPY)}K_{(TERPY)}$, $\log\beta_{(DPA/TERPY)(TERPY)} =$ 30.4		
(TERPY/TERPY)(DPA)	$\beta_{(TERPY/TERPY)(DPA)} = K_{(TERPY)}K_{(TERPY\text{-}TERPY)}K_{(DPA)}$, $\log\beta_{(TERPY/TERPY)(DPA)} =$ 28.3 (x2)		
(DPA/DPA)(TERPY)(TERPY)	$\beta_{(DPA/DPA)(TERPY)(TERPY)} = K_{(DPA)}K_{(DPA\text{-}DPA)}K_{(TERPY)}^2$, $\log\beta_{(DPA/DPA)(TERPY)(TERPY)} =$ 41.0	L_2M_3	$\beta_{L_2M_3} = \beta_{(DPA/DPA)(TERPY)(TERPY)} + \beta_{(DPA/TERPY)(DPA)(TERPY)} + \beta_{(TERPY/TERPY)(DPA)(DPA)}$, $\log\beta_{L_2M_2} = 41.0$
(DPA/TERPY)(DPA)(TERPY)	$\beta_{(DPA/TERPY)(DPA)(TERPY)} = K_{(DPA)}^2K_{(DPA\text{-}TERPY)}K_{(TERPY)}$, $\log\beta_{(DPA/TERPY)(DPA)(TERPY)} =$ 39.6		
(TERPY/TERPY)(DPA)(DPA)	$\beta_{(TERPY/TERPY)(DPA)(DPA)} = K_{(TERPY)}K_{(TERPY\text{-}TERPY)}K_{(DPA)}^2$, $\log\beta_{(TERPY/TERPY)(DPA)(DPA)} =$ 37.5		

Species	K Notation, Derivation and logK Value	Stoichiometry	β Notation, Derivation and logβ Value
(DPA/DPA)(DPA/TERPY)	$\beta_{(DPA/DPA)(DPA/TERPY)} = K_{(DPA)}^{2}K_{(DPA\text{-}DPA)}K_{(DPA\text{-}TERPY)}$, $\log\beta_{(DPA/DPA)(DPA/TERPY)} = 34.5$	L_3M_2	$\beta_{L^3M^2} = \beta_{(DPA/DPA)(DPA/TERPY)} + \beta_{(DPA/DPA)(TERPY/TERPY)} + \beta_{(DPA/TERPY)(DPA/TERPY)} + \beta_{(DPA/TERPY)(TERPY/TERPY)}$, $\log\beta_{L^3M^2} = 37.3$
(DPA/DPA)(TERPY/TERPY)	$\beta_{(DPA/DPA)(TERPY/TERPY)} = K_{(DPA)}K_{(DPA\text{-}DPA)}K_{(TERPY)}K_{(TERPY\text{-}TERPY)}$, $\log\beta_{(DPA/DPA)(TERPY/TERPY)} = 35.5$		
(DPA/TERPY)(DPA/TERPY)	$\beta_{(DPA/TERPY)(DPA/TERPY)} = K_{(DPA)}^{2}K_{(DPA\text{-}TERPY)}^{2}$, $\log\beta_{(DPA/TERPY)(DPA/TERPY)} = 36.2$		
(DPA/TERPY)(TERPY/TERPY)	$\beta_{(DPA/TERPY)(TERPY/TERPY)} = K_{(DPA)}K_{(DPA\text{-}TERPY)}K_{(TERPY)}K_{(TERPY\text{-}TERPY)}$, $\log\beta_{(DPA/TERPY)(TERPY/TERPY)} = 37.2$		

Species	K Notation, Derivation and logK Value	Stoichiometry	β Notation, Derivation and logβ Value
(DPA/DPA)(DPA/TERPY)(TERPY/TERPY)	$\beta_{(DPA/DPA)(DPA/TERPY)(TERPY/TERPY)} = K_{(DPA)}^{2}K_{(DPA-DPA)}K_{(DPA-TERPY)}K_{(TERPY)}K_{(TERPY-TERPY)}$, $\log\beta_{(DPA/DPA)(DPA/TERPY)(TERPY/TERPY)} = 53.6$	L_3M_3	$\beta_{L^3M^3} = \beta_{(DPA/DPA)(DPA/TERPY)(TERPY/TERPY)} + \beta_{(DPA/TERPY)(DPA/TERPY)(DPA/TERPY)}$, $\log\beta_{L^3M^3} = 54.4$
(DPA/TERPY)(DPA/TERPY)(DPA/TERPY)	$\beta_{(DPA/TERPY)(DPA/TERPY)(DPA/TERPY)} = K_{(DPA)}^{3}K_{(DPA-TERPY)}^{3}$, $\log\beta_{(DPA/TERPY)(DPA/TERPY)(DPA/TERPY)} = 54.3$		

With the stoichiometric cumulative formation constants calculated, these values were then inputted into a HySS [113] speciation simulation along with the literature values for the various copper(II) hydroxo species. Using this software it was possible to generate 2D speciation plots and 3D speciation maps for the self-assembly of the TERPY-DPA bis ligand (**2-42**) with copper(II) ions to generate the hexagonal macrocycles at varying pH, compound concentration and ratios between the TERPY-DPA molecule (**2-42**) and copper(II) ions. Some representative simulated data for TERPY-DPA concentrations of 1, 10 and 100 nM are presented below in Figure 2-18, Figure 2-19 and Figure 2-20 respectively.

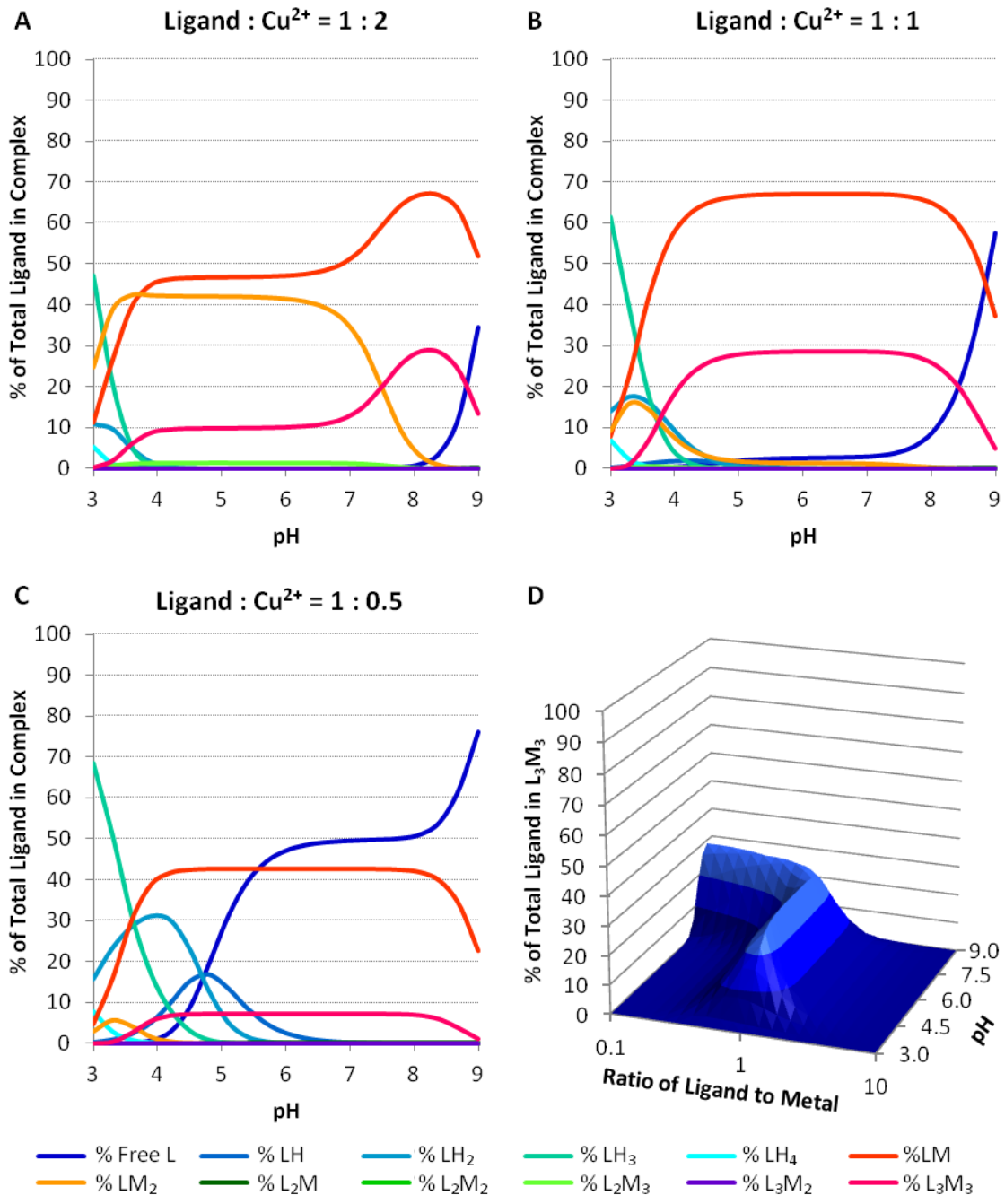

Figure 2-18: Speciation analysis carried out for a TERPY-DPA concentration of 1 nM.

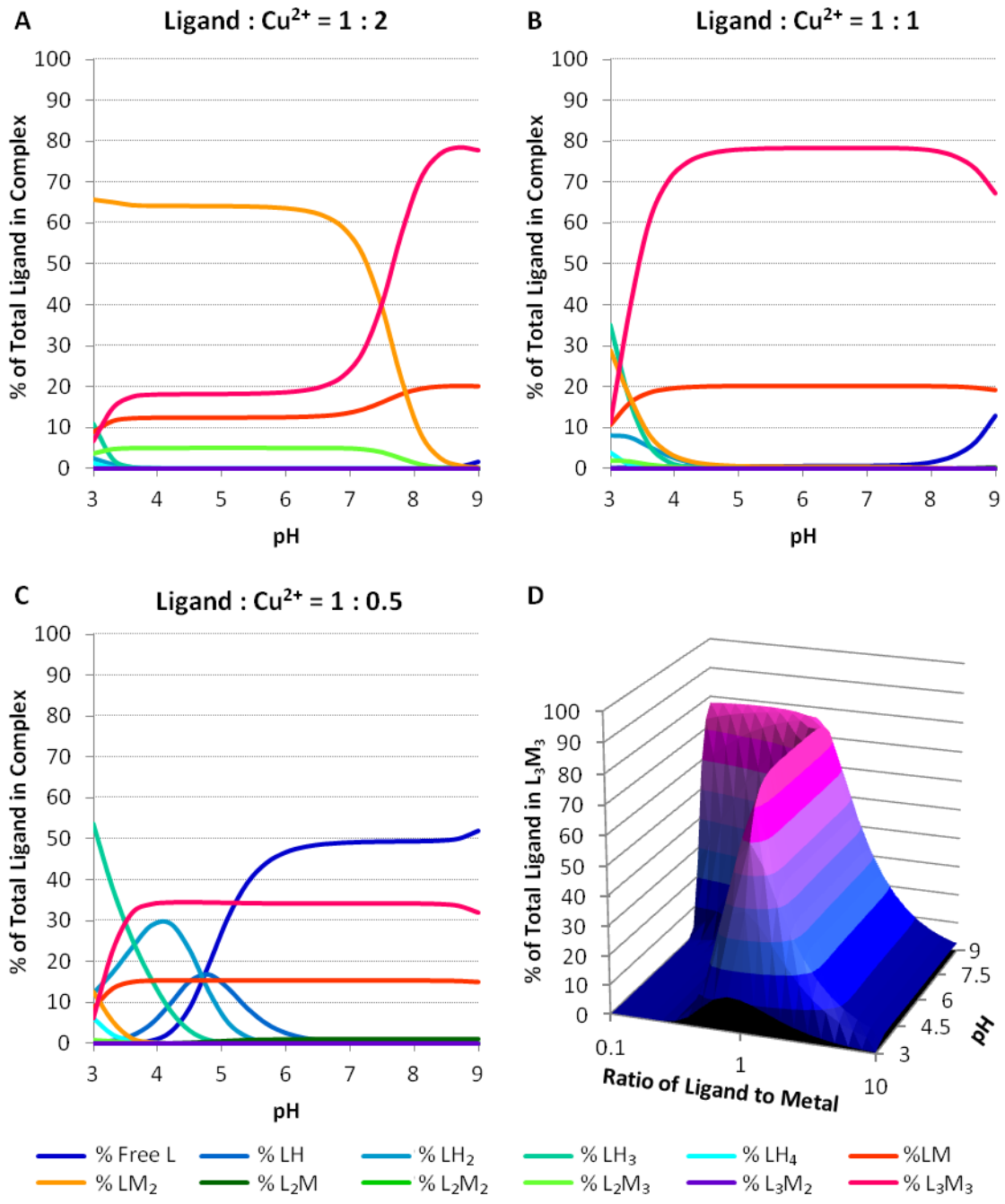

Figure 2-19: Speciation analysis carried out for a TERPY-DPA concentration of 10 nM.

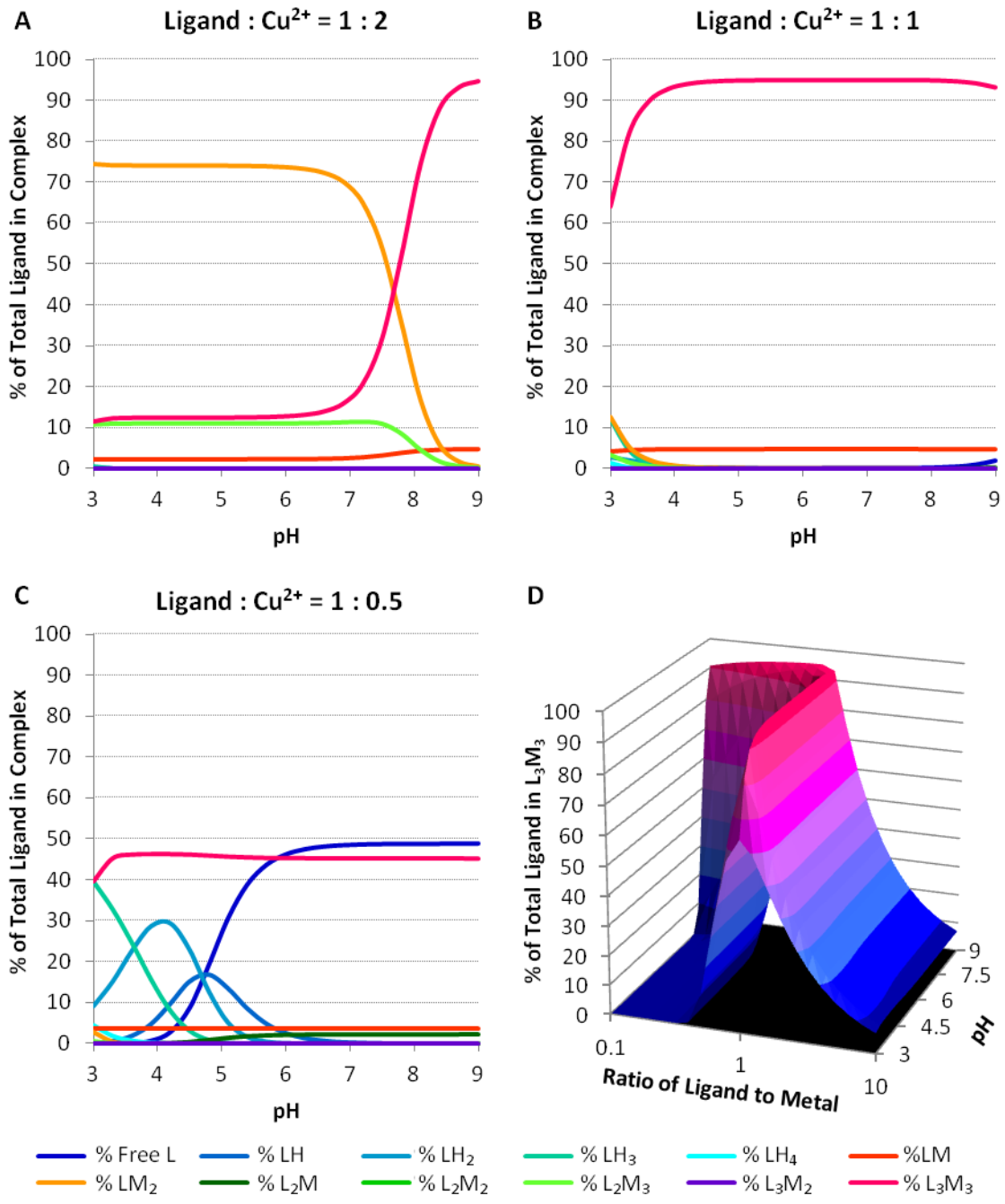

Figure 2-20: Speciation analysis carried out for a TERPY-DPA concentration of 100 nM.

Several experimentally important properties of the self-assembly of the TERPY-DPA system can be interpreted from these simulated data. Firstly, the simulation reveals that the assembly of the compound into the L_3M_3 hexagons occurs over a relatively narrow range of ratios between TERPY-DPA and copper(II) ions. This is quite

different to the behavior of the Fujita system, Illustrated in Figure 2-10, which was relatively insensitive to the stoichiometry between the ethylenediamine palladium(II) and 4,4'-bipyridine moieties at reasonable low concentrations. The implication of this property was that the relative stoichiometry of the ligand to metal should be maintained as close to unity as possible. This necessitated samples of both the bis-ligand and any metals in the 2+ oxidation state to be of high purity so that deviations from this ideal stoichiometry were minimized. Another feature of the system is that, provided the stoichiometry between the TERPY-DPA and copper(II) is near one to one, the major species formed is the desired L_3M_3 hexagons at concentrations as low as 3 nM. Again this behavior is quite different from the Fujita system which only showed a preponderance of square formation at concentrations greater than 10 μM. The low concentrations required for effective self-assembly of the L_3M_3 hexagons in this simulation were encouraging as they should translate to lower concentrations required for the observation of ion transport activity.

It is important to recall that although the speciation study for the L_3M_3 complex shows favorable thermodynamic properties, the simulation provides no information about the kinetics of the self-assembly process. If the process is too sluggish then the realization of hexagonal species may take a prohibitively long time. Conversely, if the kinetics of individual coordination events are too quick the system may skip the ring closure step entirely, instead rapidly forming species with stoichiometries greater than L_3M_3. With the speciation simulations showing some promising self-assembly characteristics for the TERPY-DPA bis-ligand system focus now turned towards the task of synthesizing the target molecules.

2.16 Synthesis of modified Newkome bis-tridentate ligands

The retrosynthetic analyses of the target molecules are summarized in Scheme 2-16 and Scheme 2-17 below.

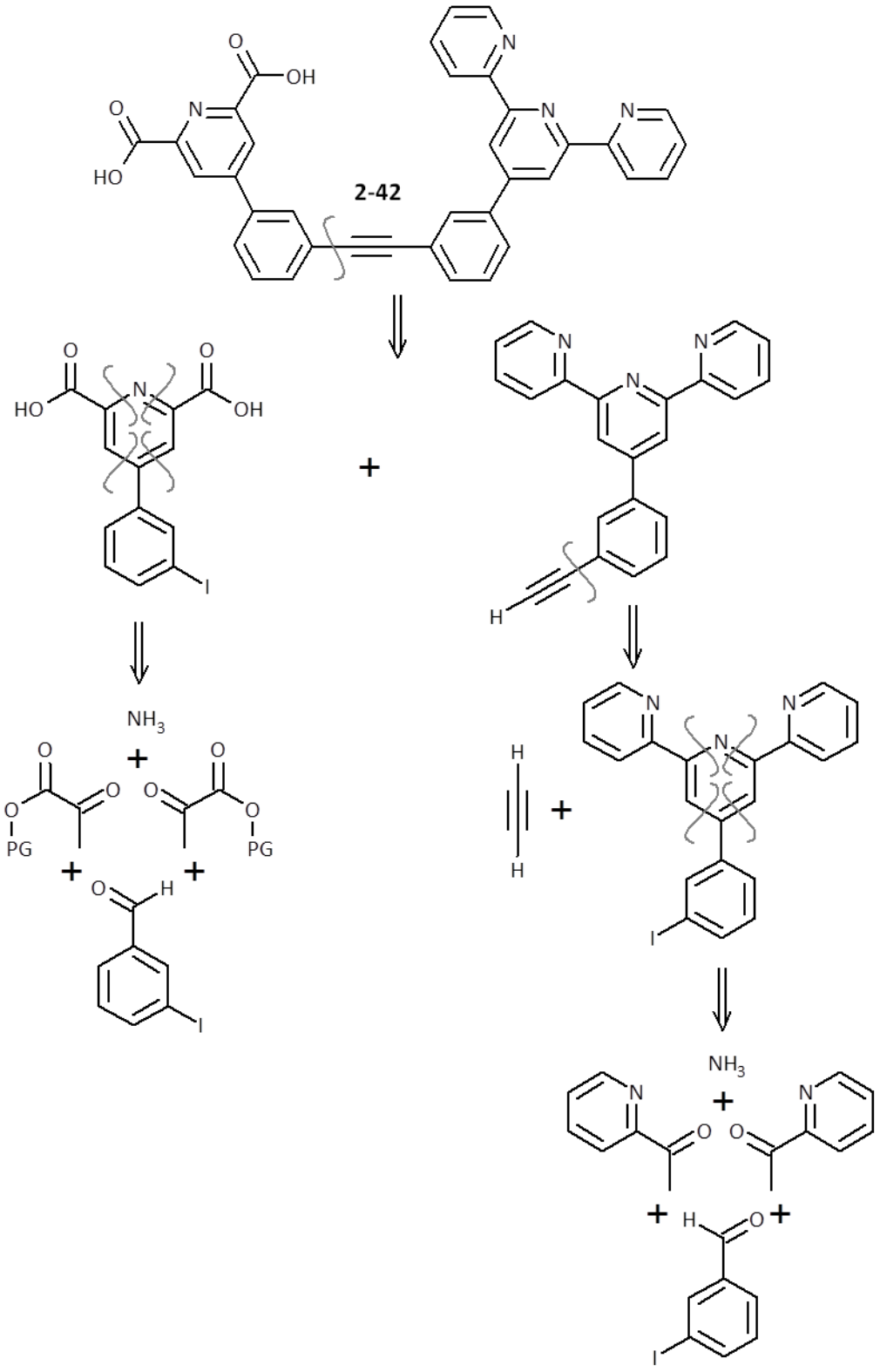

Scheme 2-16: Retrosynthetic analysis of the TERPY-DPA bis-ligand (**2-42**).

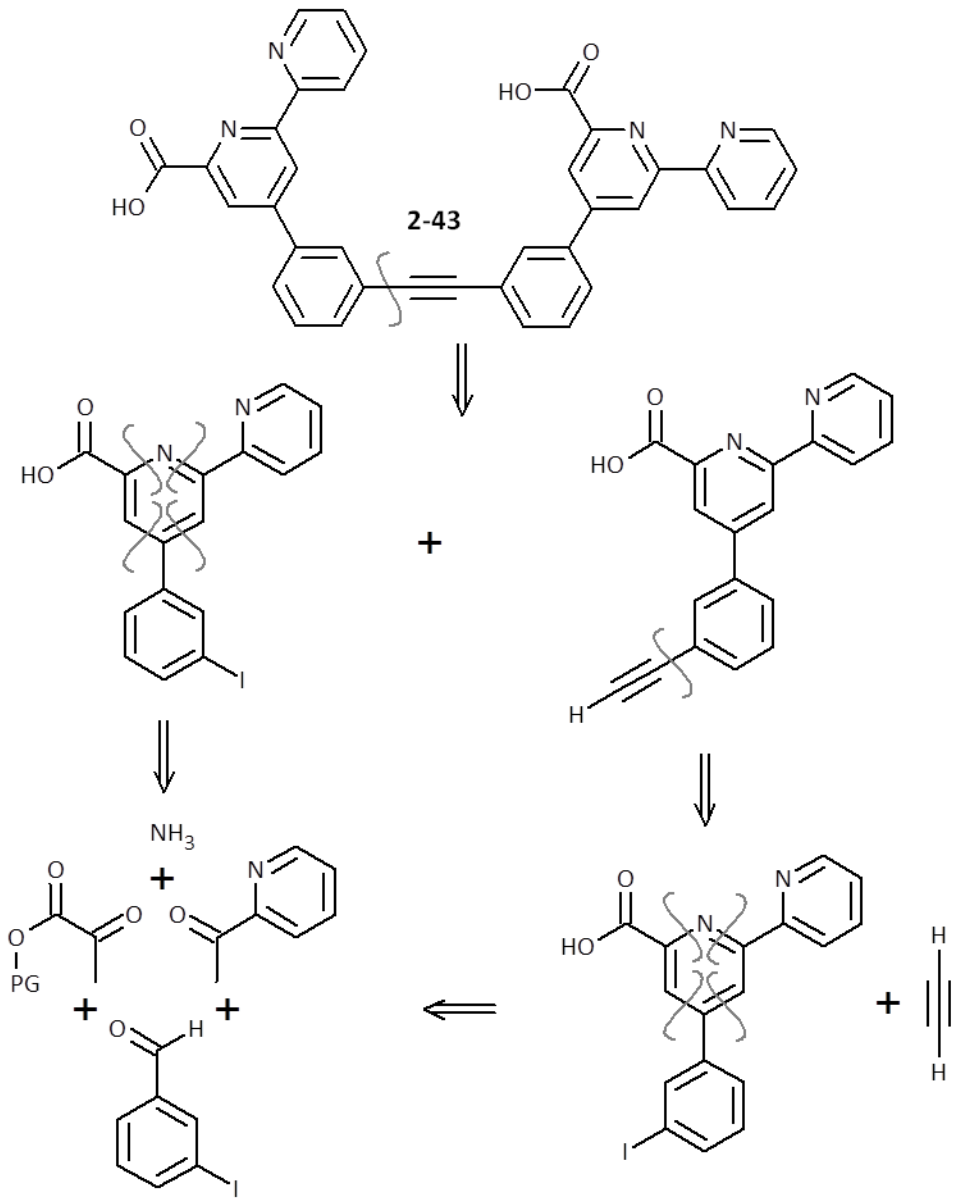

Scheme 2-17: Retrosynthetic analysis of the BIPYA-BIPYA bis-ligand (**2-43**).

As can be seen from the retrosynthetic analyses of the TERPY-DPA (**2-42**) and BIPYA-BIPYA (**2-43**) the disconnections involved in the two syntheses mirror each other quite closely so much of the chemistry involved for one compound is expected to be applicable to the other.

The synthesis of both target molecules began along identical reaction pathways as shown in Scheme 2-18. The first step in the syntheses involved the literature preparation of 3-iodobenzaldehyde (**2-45**) from the acid catalyzed reaction of

benzaldehyde (**2-44**) with sodium periodate and iodine [114]. It is worth noting that it was initially believed that this reaction was unsuccessful based on TLC analysis due to the near identical mobilities of the starting material and products. The two were only successfully differentiated by staining the TLC plate with vanillin which stained the benzaldehyde yellow while the 3-iodobenzaldehyde was stained orange. The *m*-iodobenzaldehyde product (**2-45**)was reacted under two analogous base catalyzed aldol reactions with one equivalent of either 2-acetylfuran (**2-47**) or 2-acetylpyridine (**2-46**) in an attempt to obtain the corresponding ene-ones, (2E)-1-(furan-2-yl)-3-(3-iodophenyl)prop-2-en-1-one (**2-49**) or (2E)-3-(3-iodophenyl)-1-(pyridine-2-yl)prop-2-en-1-one (**2-48**) respectively according to literature procedure [115] for structurally related compounds. The furan moiety was used as a precursor to the carboxylic acid functional group [116]. The strongly basic conditions used in the aldol reaction were not conducive to using either an unprotected carboxylic acid or one protected as the commonly used esters. Compound **2-49**, the desired product from the reaction with the 2-acetylfuran was isolated in reasonable yields as confirmed by the presence of two new trans alkene signals in the proton NMR among others, however the identical reaction with 2-acetylpyridine resulted in the generation of only a complex mixture of products from which it was impossible to purify the desired pyridine containing ene-one (**2-48**). Based on these observations the route to the dissymmetric ligand using 2-acetylpyridine was abandoned while the furan containing ene-one (**2-49**) served as the precursor to both the DPA and BIPYA tridentate ligand containing molecules.

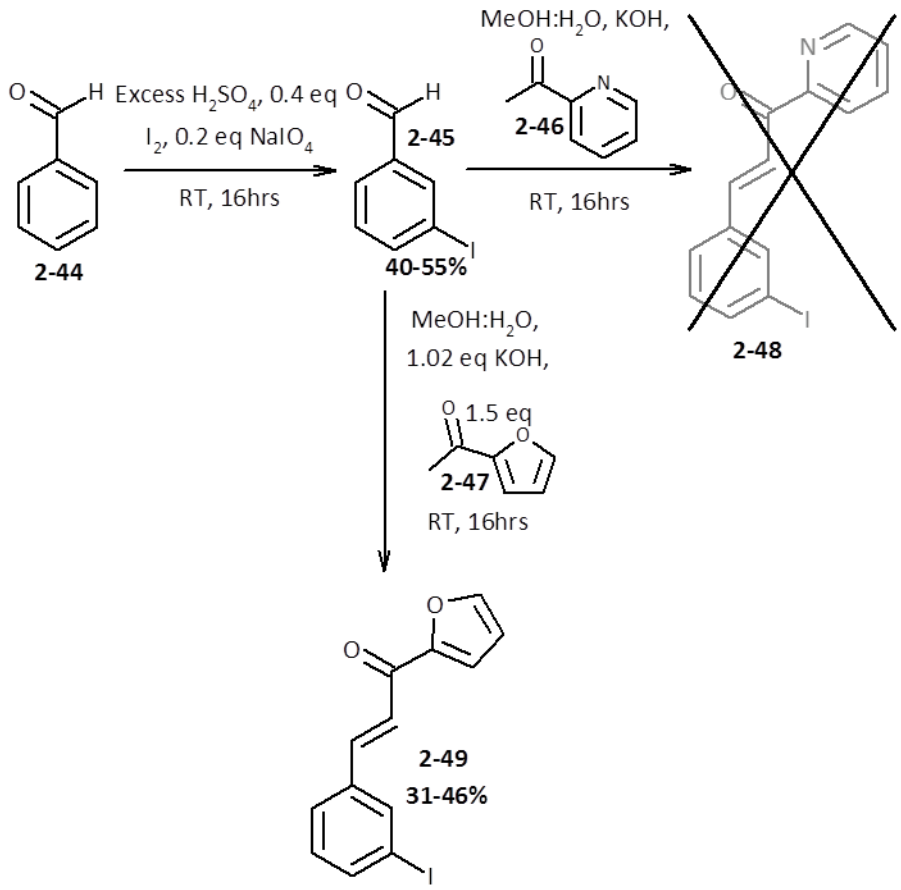

Scheme 2-18: Successful synthetic pathway to (2E)-1-(furan-2-yl)-3-(3-iodophenyl)prop-2-en-1-one (**2-49**) and unsuccessful pathway to (2E)-3-(3-iodophenyl)-1-(pyridine-2-yl)prop-2-en-1-one (**2-48**).

There was however still the need for a synthetic route to obtaining the terpyridine containing molecule. In order to obtain this product a similar reaction to the failed aldol condensation between equimolar quantities of *m*-iodobenzaldehyde (**2-45**) and 2-acetylpyridine (**2-46**) was carried out only this time using two equivalents of 2-acetylpyridine as per a literature procedure [78]; see Scheme 2-19. Based on TLC analysis of the reaction mixture it was clear that isolation of the dione product (**2-50**) would prove a greater challenge than reasonable so the crude reaction mixture was instead carried through as it was to the next step in the reaction pathway; the formation of the central pyridine ring of the terpyridine ligand. In order to effect this transformation the crude mixture was subjected to a treatment with ammonium acetate in refluxing glacial acetic acid under a stream of nitrogen according to a literature procedure [78]. Under

these conditions the central pyridine ring was successfully formed to yield the final terpyridine containing molecule 4'-(3-iodophenyl)-2,2':6',2''-terpyridine (**2-51**) as confirmed by comparison of the NMR spectra of the product to those from literature.

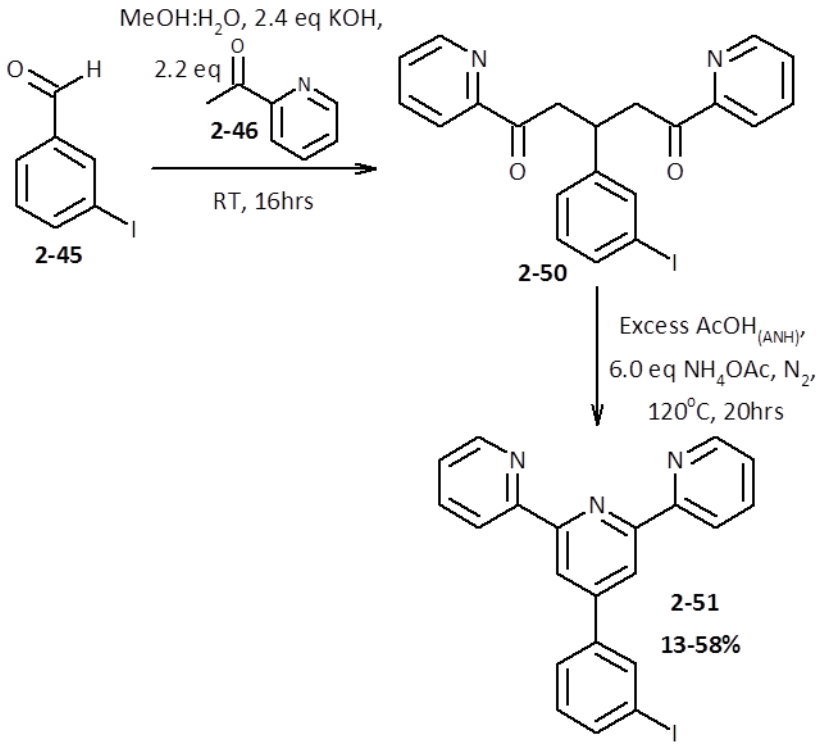

Scheme 2-19: Synthetic pathway to 4'-(3-iodophenyl)-2,2':6',2''-terpyridine (**2-51**).

The furan containing ene-one molecule (**2-49**) served as the starting material for both the DPA ligand as well as the BIPYA ligand. In order to obtain the desired compounds this molecule was subjected to another potassium hydroxide catalyzed aldol reaction with either 2-acetylfuran or 2-acetylpyridine as shown in Scheme 2-20. As with the terpyridine (**2-51**) synthesis, rather than isolating the resulting acyclic dione products (**2-52** and **2-53**) the crude mixtures from the reactions were subjected to a reflux in glacial acetic acid in the presence of ammonium acetate in order to effect the pyridine ring closures to form 2,6-di(furan-2-yl)-4-(3-iodophenyl)pyridine (**2-54**) and 6-(furan-2-yl)-4-(3-iodophenyl)-2,2'-bipyridine (**2-55**). The closure of the pyridine ring to form the desired products was confirmed by the proton and carbon NMR spectra possessing only aromatic signals.

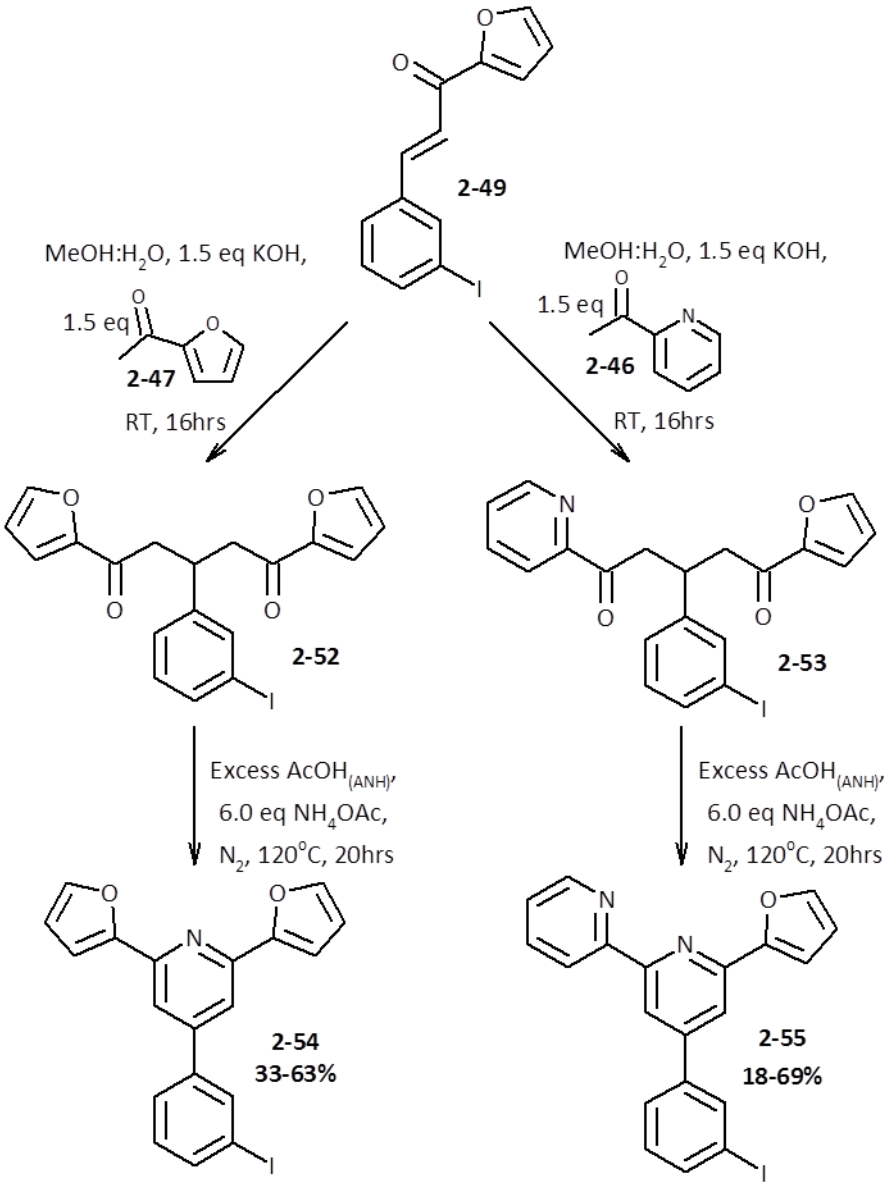

Scheme 2-20: Synthesis of 2,6-di(furan-2-yl)-4-(3-iodophenyl)pyridine (**2-54**) and 6-(furan-2-yl)-4-(3-iodophenyl)-2,2'-bipyridine (**2-55**).

As an alternative and more direct route to obtaining all three precursors to the required DPA, TERPY and BIPYA ligands (**2-54**, **2-51** and **2-55** respectively) the simultaneous reaction of 3-iodobenzaldehyde (**2-45**) with both 2-acetylfuran and 2-acetylpyridine was attempted under various conditions, the most productive of which is presented in Scheme 2-21. An initial concern was that the three molecules would be unresolvable chromatographically; however by performing TLC studies of the genuine

samples of the molecules prepared already appropriate conditions were found. Under all aldol reaction conditions carried out no attempt was made at purification of the crude mixture of diones which was instead extracted into organic solvent, dried and then subjected to the pyridine ring closing conditions found previously. It was only at this stage, with the central pyridine ring of all three precursors formed that careful chromatographic separation was carried out.

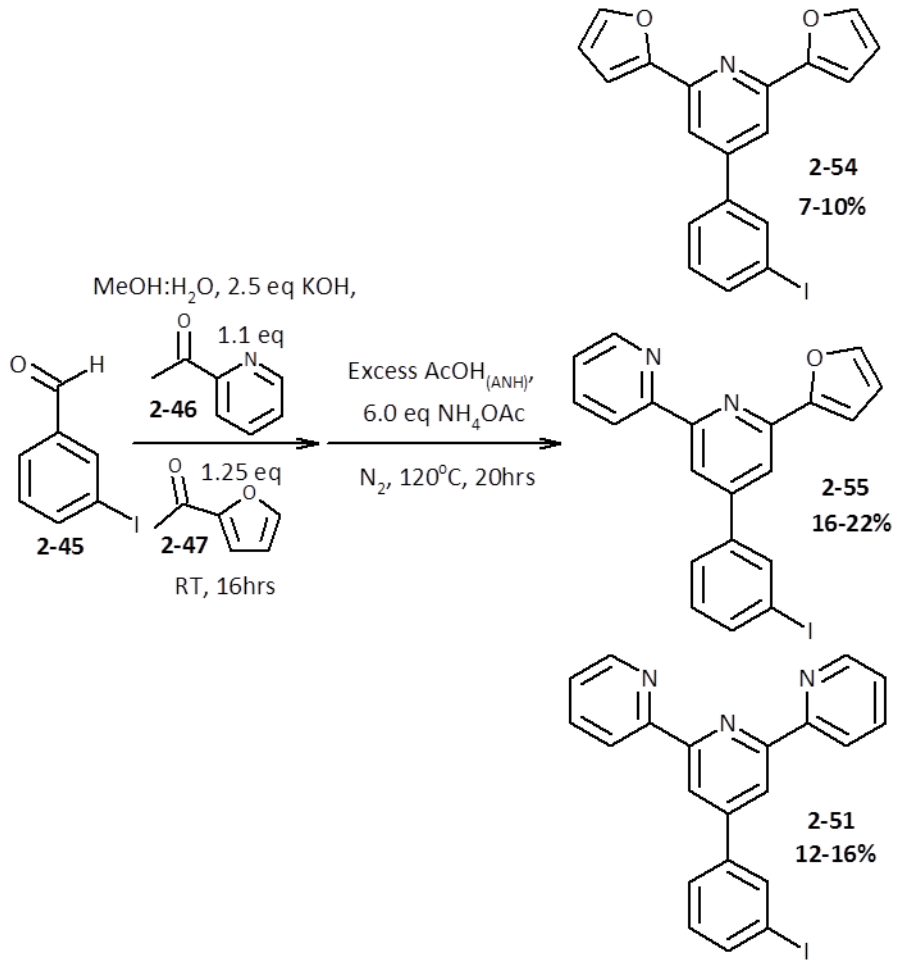

Scheme 2-21: One pot synthesis of the three tridentate ligand pre-cursors **2-54**, **2-55** and **2-51**.

In order to obtain the corresponding carboxylic acid containing molecules (**2-56** and **2-57**, Scheme 2-22) from the starting furan containing ones the appropriate starting materials, **2-54** and **2-55** respectively, were subjected to strong oxidizing conditions using potassium permanganate in a mixture of *t*-butanol and water [116]. Under these

strong oxidizing conditions furan rings substituted in the 2 position undergo oxidative degradation to yield substituted carboxylic acids. The resulting carboxylic acid containing molecules **2-56** and **2-57** were unfortunately exceedingly difficult to isolate and attempts to analyze the products by NMR were complicated by the zwitterionic nature of the compounds causing significant broadening of signals.

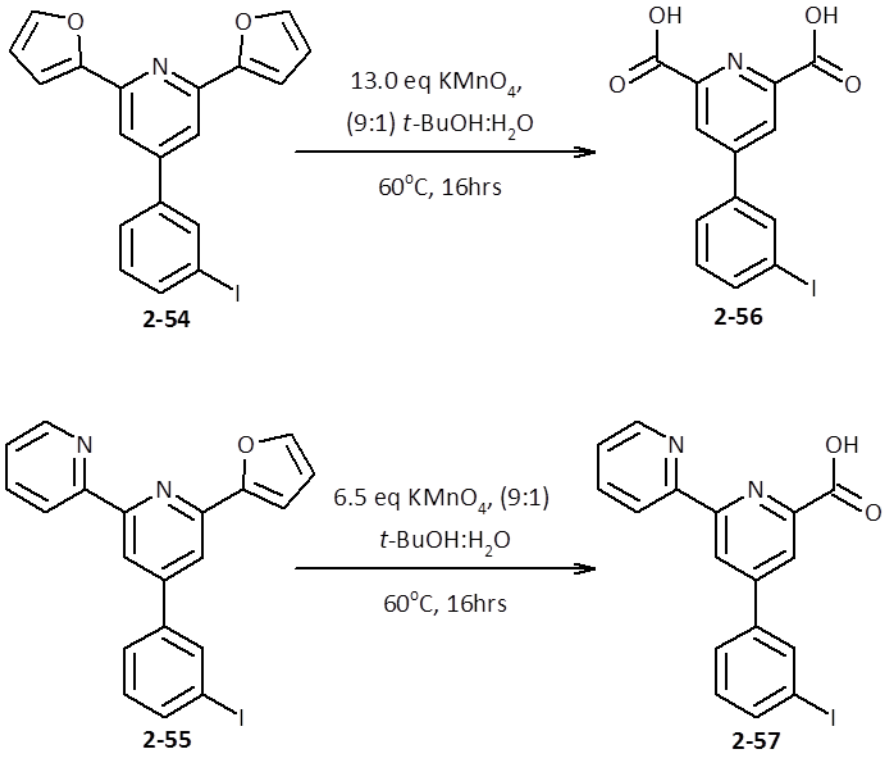

Scheme 2-22: Oxidation reactions of furan containing tridentate ligand precursors used to yield corresponding carboxylic acids.

Due to the difficulties in handling these materials it was decided that it was best to protect the carboxylic acid moieties as esters and characterize these products instead. In addition the carboxylic acids should remain protected for as long as possible in order to facilitate purification, and characterization of the products of future reactions. The first protection attempted was as the *t*-butyl ester group; however under all conditions attempted the reaction failed; see Scheme 2-23. It was hypothesized that the reason for this failure was due to the large steric bulk of the *t*-butyl group

interacting unfavorably with the relatively bulky substituents attached to the carboxylic acid groups to be protected.

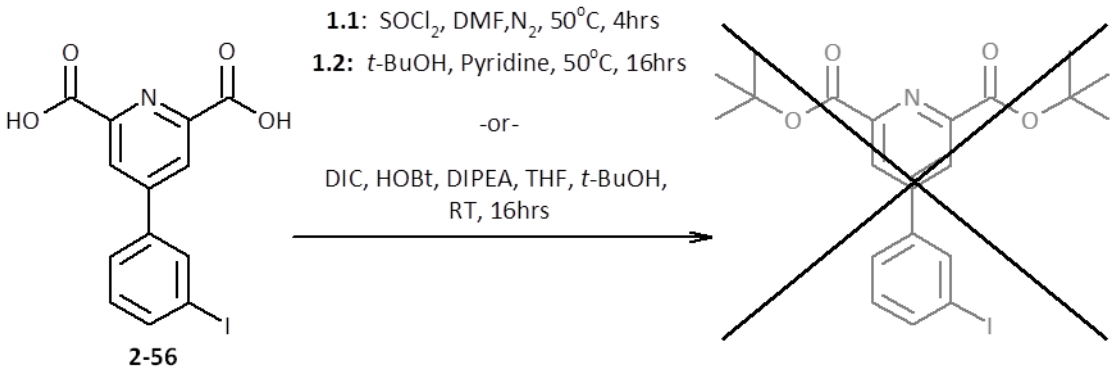

2-56

Scheme 2-23: Reaction conditions attempted for the protection the carboxylic acid groups of 4-(3-iodophenyl)pyridine-2,6-dicarboxylic acid (**2-56**).

As an alternative protecting group, the trimethylsilylethyl (TMSE) ester group was proposed as a potentially elegant solution to the problem. The trimethylsilylethyl ester group is significantly less bulky that the *t*-butyl group at the position α to the oxygen of the ester so it was expected to be easier to install. In addition this protecting group can be effectively removed using a source of fluoride ions [117]. The expectation was that by using an appropriate metal fluoride salt in the presence of the protected bis-tridentate ligand molecule a simultaneous deprotection/complex formation process could occur. This would have the great advantage of eliminating the need to handle any molecules with free carboxylates, as it was found previously that these were difficult to isolate and characterize.

In order to test this hypothesis, develop conditions for the TMSE protection of the carboxylic acids as well as to confirm the ability of the BIPYA tridentate ligand to form octahedral complexes with first row transition metals in the +2 oxidation state a simplified analog of the BIPYA-BIPYA bis ligand (**2-59**) was synthesized a shown in Scheme 2-24.

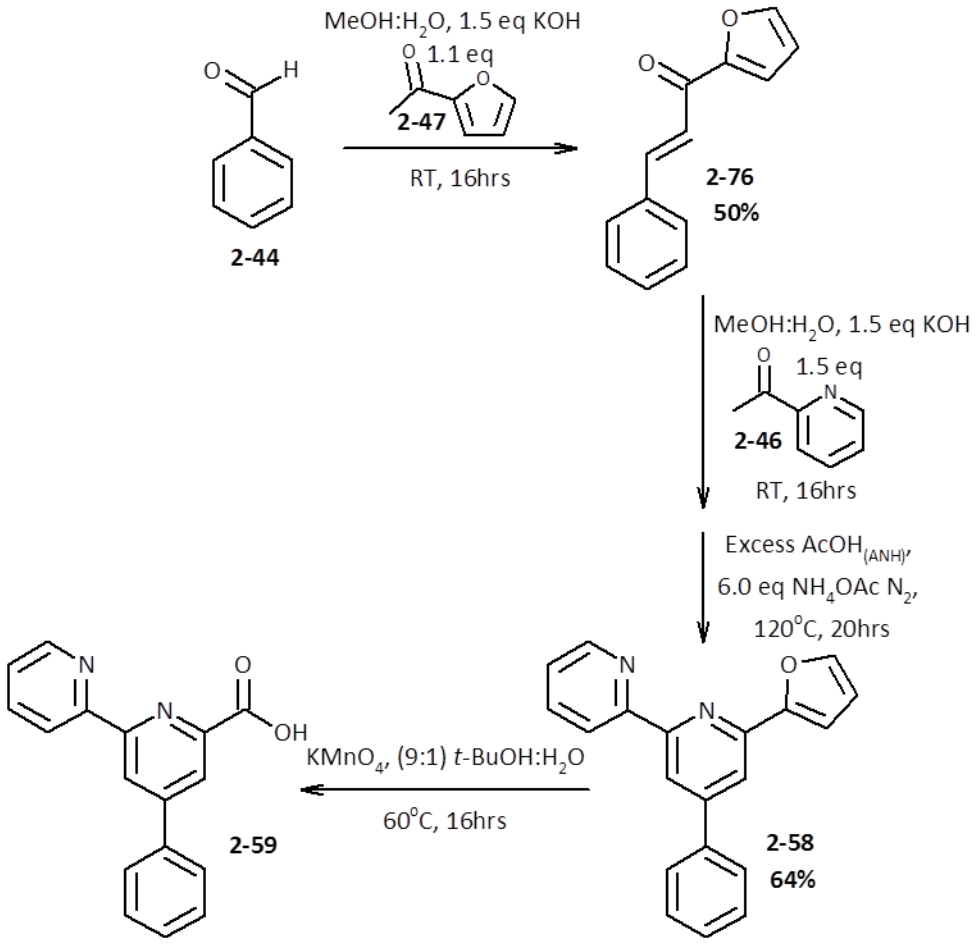

Scheme 2-24: Synthetic scheme for the synthesis of 4-phenyl-2,2'-bipyridine-6-carboxylate (**2-59**).

The reactions involved up until and including the oxidative cleavage of the furan ring to generate 4-phenyl-2,2'-bipyridine carboxylic acid (**2-59**) were analogous to those already discussed for the aryliodide containing molecules except that the synthesis began with benzaldehyde (**2-44**) rather than *m*-iodobenzaldehyde (**2-45**). The synthesis of the enone **2-76** was carried out according to and confirmed by comparison of NMR spectra from literature. The success of the synthesis of **2-58** was confirmed by the presence of only aromatic signals in both the proton and carbon NMR spectra. With the crude carboxylic acid (**2-59**) in hand several methods were attempted to install the trimethylsilylethyl ester protecting group. Among the methods attempted was the use of N,N-disopropylcarbodiimide (DIC) with 1-hydroxybenzotriazole (HOBt) in order to obtain the activated HOBt ester with which trimethylsilylethanol could react.

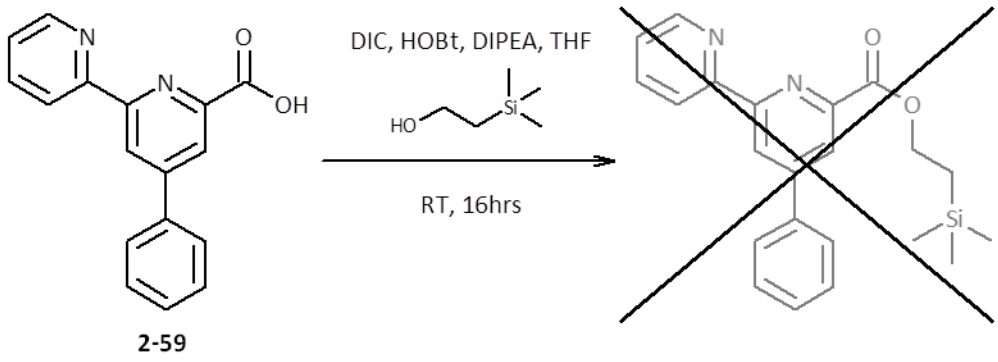

2-59

Scheme 2-25: Attempted ester coupling reaction between 4-phenyl-2,2'-bipyridine carboxylic acid (**2-59**) and trimethylsilylethanol using activated ester chemistry.

This reaction, shown in Scheme 2-25, proved to be a failure; instead of providing the desired trimethylsilylethanol protected compound it resulted instead in the relatively clean conversion of the starting material to the corresponding stable N-acylurea molecule (**5-60**, Figure 2-21). This undesirable side reaction was likely catalyzed by proton transfer with the pyridine rings adjacent to the O-acylisourea intermediate as depicted in the Figure 2-21 below, the preorganization of the 'catalytic site' causing the rearrangement to occur faster than the exchange with HOBt.

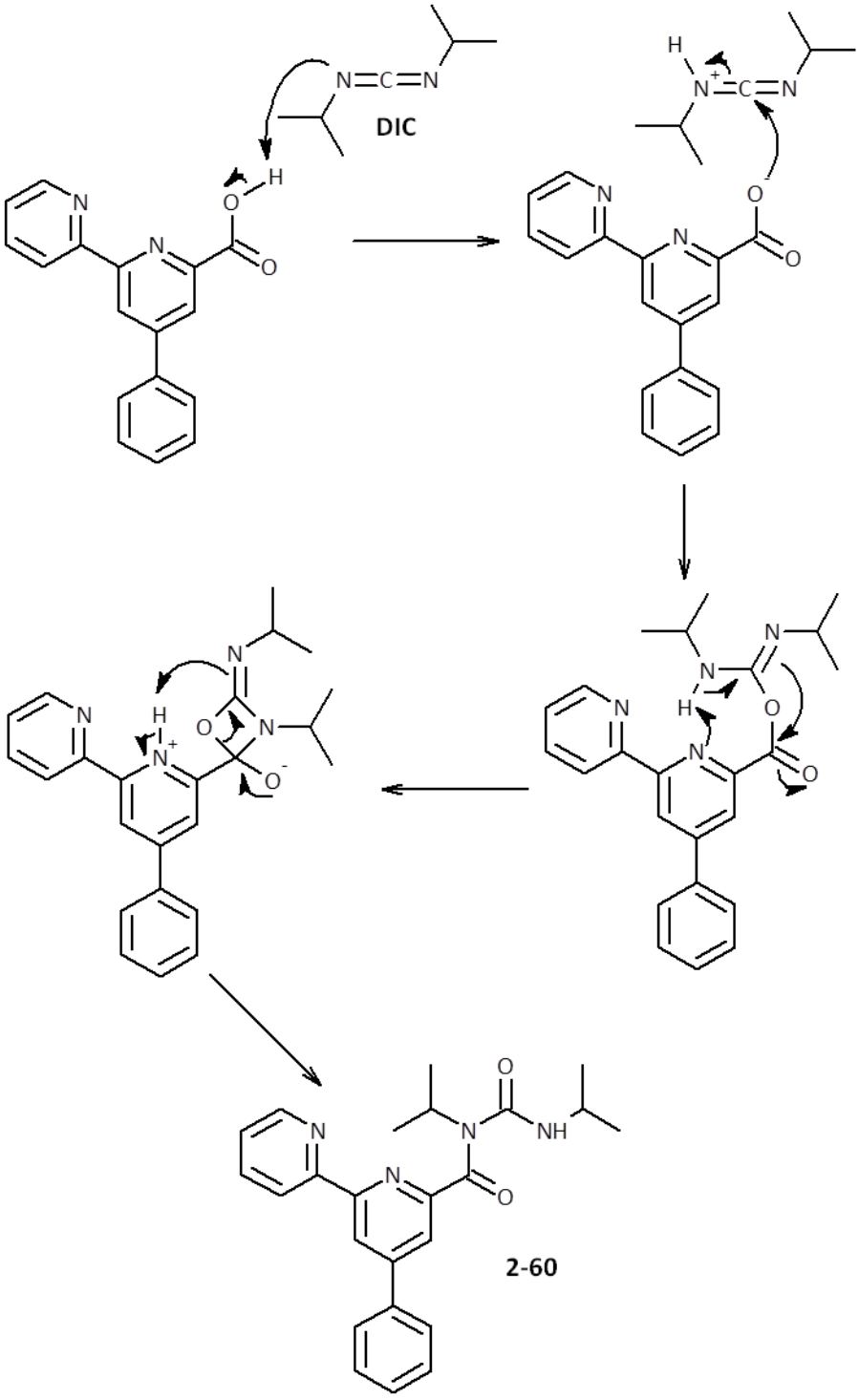

Figure 2-21: Proposed mechanism for the formation and rearrangement of the O-acylisourea intermediate to the stable N-acylurea catalyzed by proton transfer to the adjacent pyridine units.

A far more successful alternative involved a two-step procedure shown in Scheme 2-26. First the starting carboxylic acid was converted to the corresponding acyl

chloride using thionyl chloride at elevated temperatures with dimethylformamide as catalyst followed by careful removal of excess chlorinating agent under a stream of nitrogen to provide crude acyl chloride as a waxy pale yellow solid. Without any purification of this material the next step in the procedure, still under an inert nitrogen atmosphere, involved the addition of trimethylsilylethanol and a drop of dry pyridine to the crude acyl chloride mixture followed by heating to reflux to yield the final trimethylsilylethyl ester product (**2-63**).

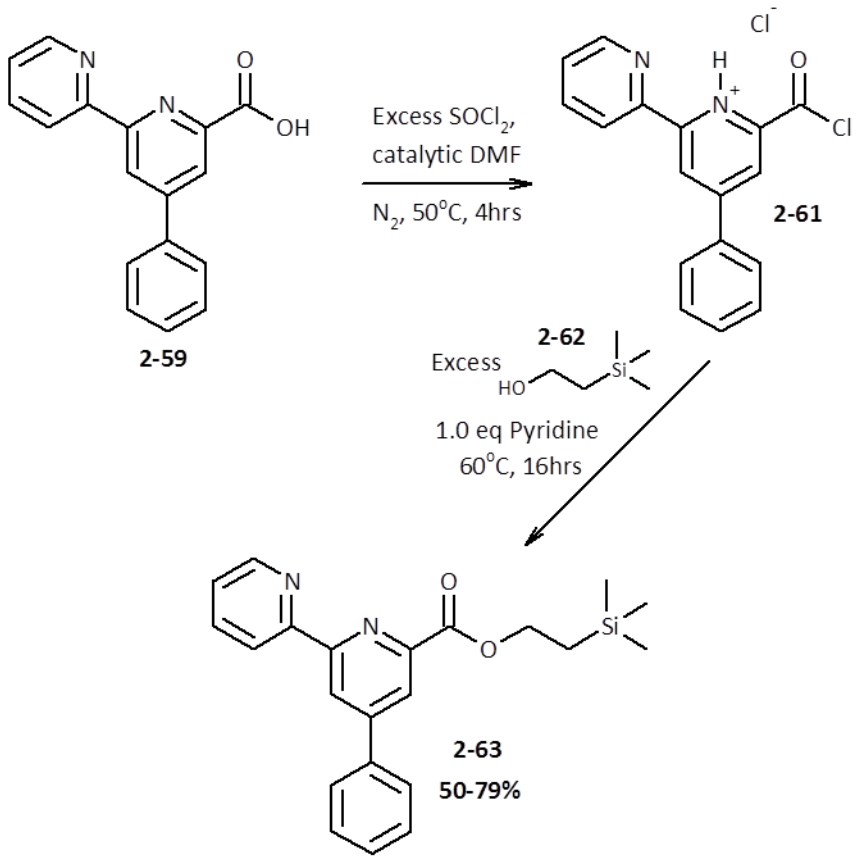

Scheme 2-26: Synthesis of trimethylsilylethyl 4-phenyl-2,2'-bipyridine carboxylate (**2-63**).

With this product in hand the next step was to react it with various transition metal fluoride salts to see if the simultaneous deprotection of the TMSE ester and metal complexation strategy could be effective. Unfortunately the number of reasonably soluble metal fluoride salts of first row transition metals in the +2 oxidation is relatively limited with only those of cobalt, nickel and zinc having appreciable solubility in

aqueous solution. Solutions of these salts were prepared and mixed with a dimethylformamide solution of the TMSE ester protected trial ligand (**2-63**) at elevated temperatures in a one to two stoichiometric ratio. Upon mixing immediate but subtle colour changes were observed followed by formation of finely divided precipitates suggesting successful reaction between the ligand molecules and the transition metal ions. Due to the steric bulk imparted to the tridentate binding site by the trimethylsilyl ester protecting group it was unlikely that the complexes could have formed without first being successfully deprotected. ESI mass spectrometry was used to analyze the resulting precipitates and, although the compounds were reluctant to ionize effectively, signals of mass to charge 609.1, 608.1 and 614.1 and appropriate isotopic patterns corresponding to M^+ for the ML_2 coordination complexes with cobalt, nickel and zinc were observed. The difficulty in obtaining mass spectra for these compounds was likely due to the necessity to ionize the metal centers because of the lack of readily ionizable sites on the complexed ligand. As further support for complex formation attempts were made at crystallizing the resulting precipitates for x-ray crystallographic analysis. Fortunately the sample from the reaction of the trial BIPYA ligand (**2-63**) with cobalt fluoride provided crystals of sufficiently high quality to provide crystallographic evidence of complex formation.

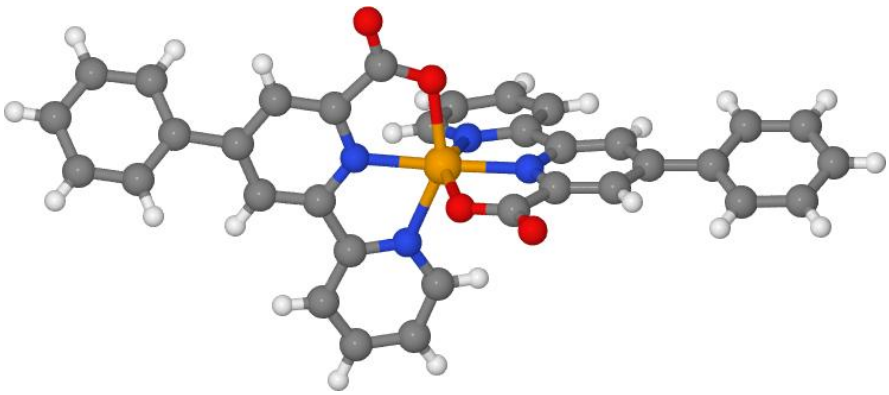

Figure 2-22: Crystal structure of the 2:1 complex of the trial BIPYA ligand with cobalt(II) ion. The compound co-crystallized with two water and one dimethylformamide molecules which were omitted from this figure for clarity. Atom legend; white = hydrogen, grey = carbon, blue = nitrogen, red = oxygen, orange = cobalt.

This crystal structure provided the best confirmation that the deprotection/ complex formation strategy was a viable route to the desired hexagonal complexes. The structure of the trial BIPYA complex with a Co^{2+} ion is in a somewhat distorted octahedral geometry with the planes formed by the pyridine rings to the two tridentate ligands arranged approximately perpendicular to each other. The distortion from the idealized octahedral geometry suggests that the cobalt is too large to be effectively accommodated by two of the tridentate ligands without some deformation. As discussed in Section 1.6.2 of the introductory chapter this poor size complementarity likely leads to the formation of a weaker complex than if all of the coordinating atoms were arranged perfectly in an octahedral arrangement around the central metal. Fortunately there was sufficient conformational flexibility in the binding site of the ligand to allow for stable complex formation.

Further complexation studies were carried out with other non fluoride transition metal salts. These studies involved first deprotecting the trimethylsilylethyl ester protected BIPYA trial ligand with cesium fluoride and then using this solution as was with various transition metal salt solutions. Generally all salts tested in these trials behaved much as those for the three fluoride salts with the protected trial BIPYA ligand; producing colourful precipitated as shown in Figure 2-23. The only exception was the reaction with ferric chloride which resulted in a very dramatic colour change of the solution from a very pale green to dark purple as well as the production of a small quantity of greyish brown precipitate. The precipitate was suggestive of the disproportionation of the iron(II) into iron(III) and solid iron(0) while the deep purple colour was indicative of the formation of a charge transfer complex, likely between the metal centre and the bipyridine moiety of the ligand [118].

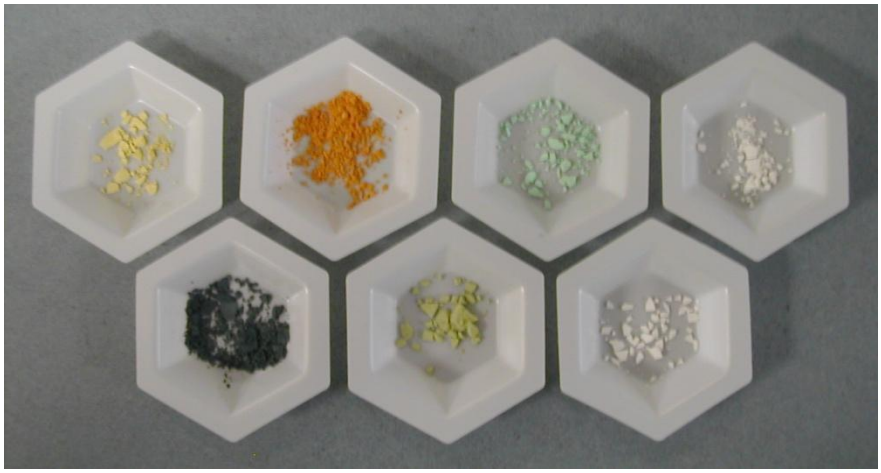

Figure 2-23: Photograph of the dried solids recovered from complexation of various transition metals in the 2+ oxidation state with the trial BIPYA ligand **2-63** to illustrate the differences in colour. The coordinated metals were clockwise from top left; manganese, cobalt, copper, zinc, cadmium, nickel and iron.

Given the successful demonstration of the deprotection/complex formation strategy with the trial ligand it was decided that the synthesis of the two different bis-tridentate ligand molecules should proceed using the trimethylsilylethyl ester protecting group for the protection of the carboxylic acid functional groups.

The final steps in the synthesis of the TERPY-DPA bis-tridentate ligand molecule (**2-42**) involved the preparation for and final Sonogashira cross-coupling between an aryl iodide and a terminal alkyne. For this dissymmetric bis-tridentate ligand system the choice existed whether to install the terminal alkyne functional group onto the DPA or the TERPY bearing molecule. Several key considerations of the reactions involved in this transformation were influential in making the decision to convert the TERPY bearing molecule to the terminal alkyne over the DPA bearing one. The first was the requirement that the DPA molecule have its carboxylic acid groups protected as trimethylsilylethyl ester groups in order to properly purify the compound. As mentioned previously this protecting group is removed with a source of fluoride ions. The other key factor was that the installation of the terminal alkyne group involves the use of the protected alkyne trimethylsilylacetylene which must then be deprotected, also using a fluoride source, in order to provide the desired terminal alkyne. Since

deprotection of both the TMSE ester and TMS alkyne protecting groups occur under the same conditions and the desire is to have the carboxylic acids protected in the final molecule it made little sense to attach the TMS-acetylene to the protected DPA molecule only to have both protecting groups removed at the same time yielding the undesired free carboxylic acids.

Conversion of the aryl iodide 4'-(3-iodophenyl)-2,2':6',2''-terpyridine (**2-51**) to the terminal alkyne 4'-(3-ethynylphenyl)-2,2':6',2''-terpyridine (**2-66**) involved first the palladium catalyzed cross-coupling to trimethylsilylacetylene using Sonogashira coupling conditions; see Scheme 2-27. The resulting trimethylsilyl protected alkyne (**2-65**) was then efficiently deprotected to the terminal alkyne (**2-66**) using tetrabutylammonium fluoride (TBAF).

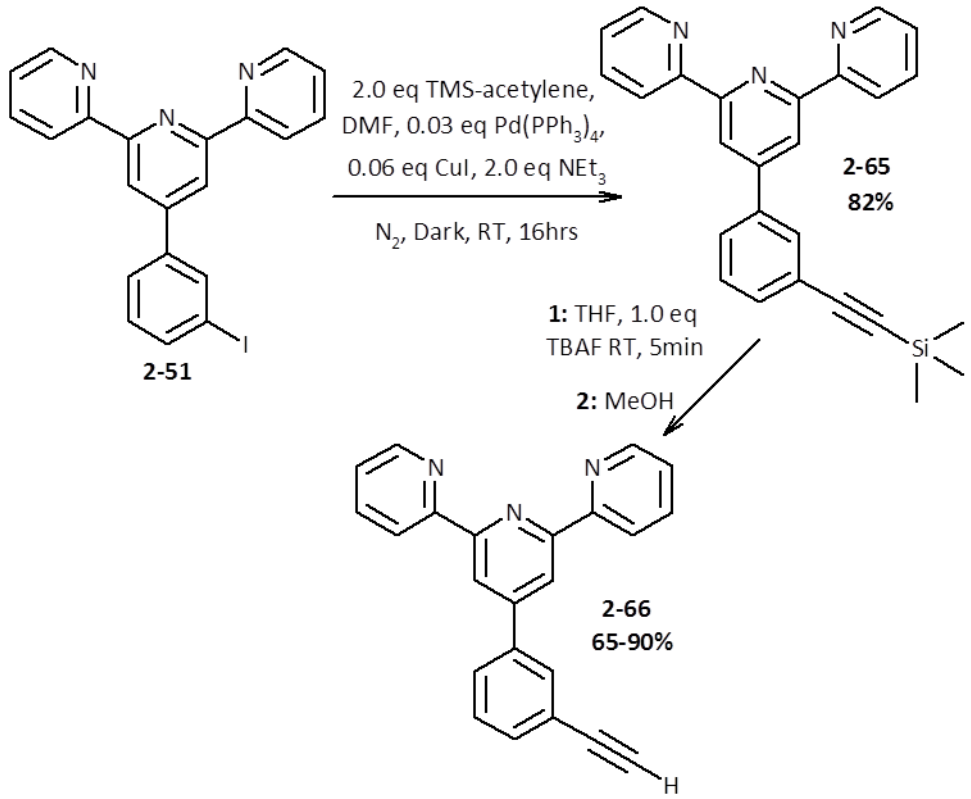

Scheme 2-27: Synthesis of 4'-(3-ethynylphenyl)-2,2':6',2''-terpyridine (**2-66**).

Preparation of the DPA bearing half of the molecule for the final cross-coupling reaction required the previously discussed protection of the carboxylic acids of

compound **2-56** as the corresponding trimethylsilylethyl esters via conversion to the acyl chloride as performed for the trial BIPYA ligand; see Scheme 2-28.

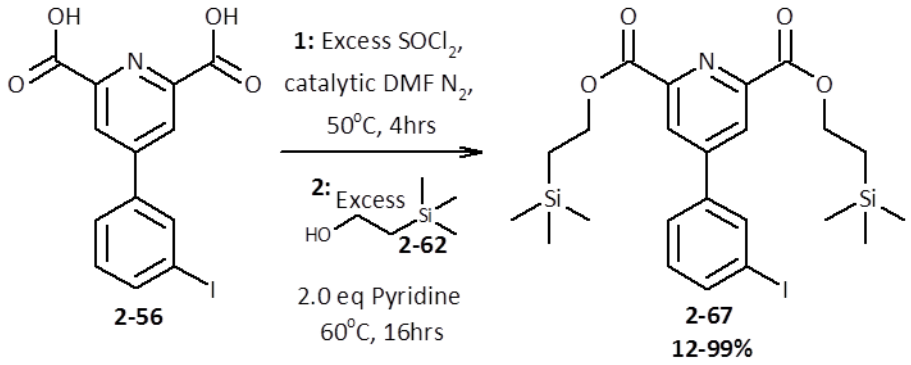

Scheme 2-28: Synthesis of di-trimethylsilylethyl 4-(3-iodophenyl)pyridine-2,6-dicarboxylate (**2-67**).

With the aryl iodide **2-67** and terminal alkyne **2-66** halves prepared the final coupling of the two to obtain the final di-TMSE ester protected DPA-TERPY bis-tridentate ligand molecule (**2-68**) was accomplished using Sonogashira cross-coupling chemistry once more as per Scheme 2-29 below. Starting from benzaldehyde the overall synthesis of the compound **2-68** provided a yield of 9.2% over six synthetic steps.

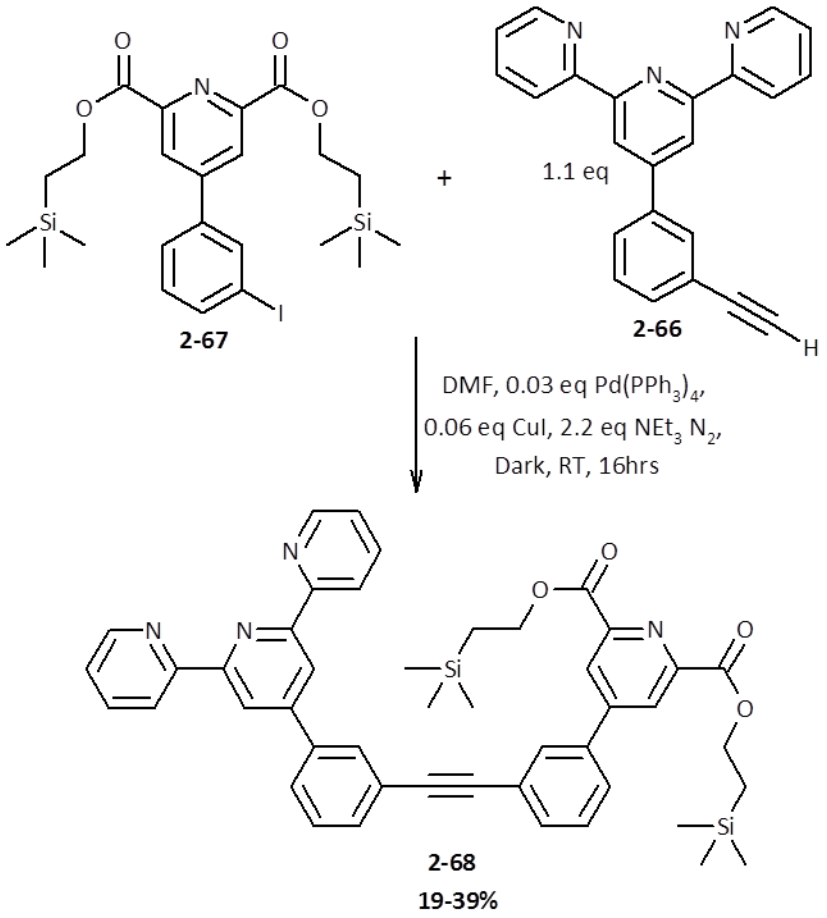

Scheme 2-29: Synthesis of the di-TMSE ester protected DPA-TERPY bis-tridentate ligand (**2-68**).

The BIPYA-BIPYA bis-tridentate ligand (**2-43**), although it appears to present a more simple synthesis due to the symmetry of the molecule, actually posed some unique challenges compared to the DPA-TERPY molecule (**2-42**). Firstly, unlike for the dissymmetric bis-tridentate ligand, there was no choice but to install the terminal alkyne functional group onto a molecule bearing a protected carboxylic acid. In order to address this issue an alternative protecting group that would not be deprotected in the same step as the deprotection of the trimethylsilyl group of the alkyne was needed. Since previous attempts at protecting the carboxylic acid as bulky *t*-butyl esters failed, the chosen alternative was to use the much smaller methyl ester protecting group. Although the direct removal of this protecting group requires relatively extreme pH, conditions which eliminate the possibility of the concerted deprotection/complex

formation strategy being employed, an additional transesterification step was envisioned whereby the methyl ester could be exchanged with the desired TMSE ester under mildly basic conditions.

To this end the methyl ester protected molecule, methyl 4-(3-iodophenyl)-2,2'-bipyridine-6-carboxylate (**2-69**), was synthesized via the acyl chloride derivative of 4-(3-iodophenyl)-2,2'-bipyridine-6-carboxylic acid (**2-57**) using conditions similar to those used for the TMSE ester protection of the trial BIPYA ligand (**2-63**, Scheme 2-26) differing only in the use of dry methanol instead of trimethylsilylethanol; see Scheme 2-30. Attempts were then made at the palladium catalyzed cross-coupling of the methyl ester protected aryl iodide (**2-69**) with TMS-acetylene, however using similar conditions to those used for the coupling between the TERPY bearing molecule (**2-51**) with the identical alkyne failed to yield the desired compound (**2-70**). It was observed while setting up the reaction that upon addition of the protected BIPYA bearing aryl iodide (**2-69**) to the DMF solution of the palladium catalyst the solution went from a pale yellow to a deep orange colour. A similar colour change was not observed for the analogous reaction using the TERPY bearing aryl iodide.

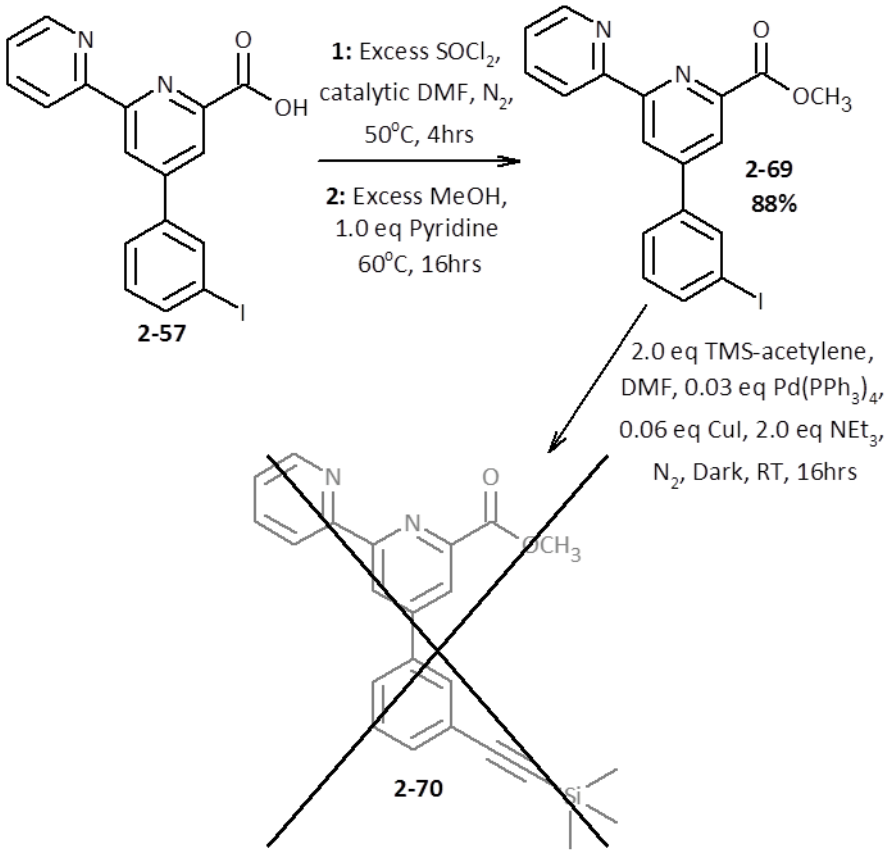

Scheme 2-30: Synthesis of methyl 4-(3-iodophenyl)-2,2'-bipyridine-6-carboxylate (**2-69**) and the subsequent attempt at the Sonogashira cross-coupling with TMS-acetylene.

With this setback focus shifted to the other required component for the final palladium catalyzed cross-coupling to yield the desired protected BIPYA-BIPYA bis-tridentate ligand; trimethylsilylethyl 4-(3-iodophenyl)-2,2'-bipyridine-6-carboxylate (**2-71**). The molecule was synthesized from compound **2-57** as per previous methodology used to install the TMSE ester protecting group. Despite being aware that cross-coupling of the trimethylsilylacetylene with this product would likely result in the deprotection of both the trimethylsilyl group from the alkyne as well as the trimethylsilylethyl ester group from the carboxylic acid in a future step, the failure of this cross-coupling with the methyl ester protected compound meant that the attempt was warranted. To this end the Sonogashira coupling reaction was carried out on the TMSE ester protected product (**2-71**) with TMS-acetylene. Somewhat surprisingly, in contrast to the reaction with the methyl ester protected product, this reaction worked

quite well providing the desired product (**2-72**) in decent yields, as shown in Scheme 2-31.

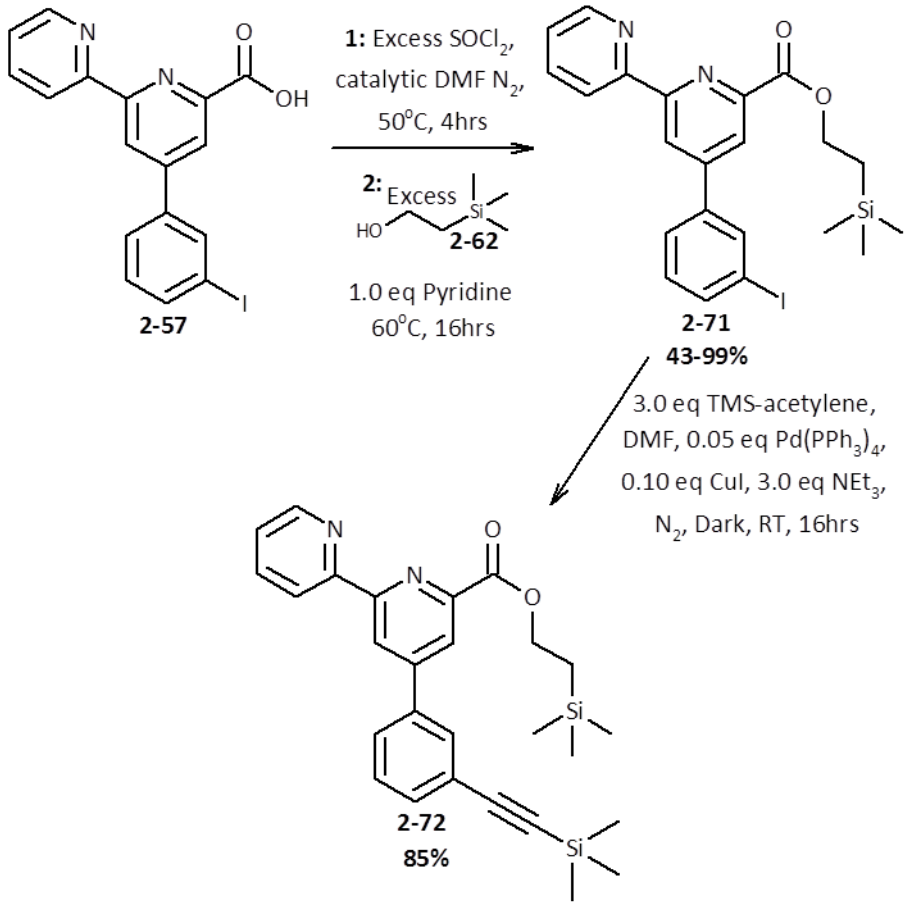

Scheme 2-31: Synthesis of the TMS and TMSE ester protected BIPYA precursor **2-72**.

Based on these differences in reactivity in conjunction with the observed colour change that occurred only when adding the methyl ester protected molecule **2-69** to the solution containing the palladium(0) catalyst it was hypothesized that the methyl ester protected BIPYA molecule (**2-69**), being less sterically constrained about the bipyridyl moiety could in fact form a coordination complex with the palladium(0) from the catalyst, poisoning it, whereas the more sterically bulky TERPY and trimethylsilylethyl ester protected BIPYA ligands (**2-71** and **2-51**) may not be able to approach close enough to effectively displace the bulky triphenylphosphine ligands and were therefore unable to poison the catalyst.

With the product of the successful Sonogashira cross-coupling (**2-72**) in hand, the next step was the deprotection of the TMS group from the alkyne, see Scheme 2-32.

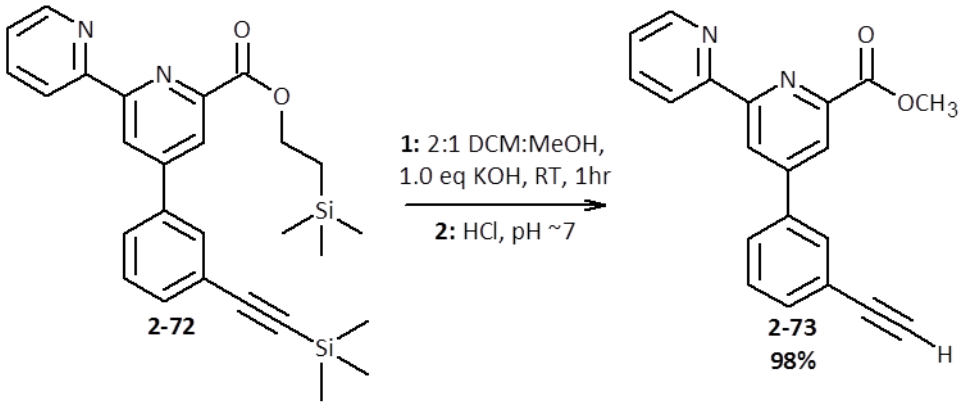

Scheme 2-32: Deprotection of the TMSE and TMS groups from **2-72** and concomitant methyl esterification to afford **2-73**.

An alternative, fluoride free, deprotection condition using potassium hydroxide in a methanol /dichloromethane mixed solvent was used to afford the terminal alkyne (**2-73**). Somewhat fortuitously, but in hindsight unsurprisingly, these conditions provided the methyl ester product rather than the free carboxylic acid. This result was encouraging as it both simplified the purification of the product as well as illustrating that the transesterification reaction was possible for this compound. The final step in the synthesis of the terminal alkyne molecule before the final cross-coupling to the aryl iodide half was just such a transesterification only this time in reverse; see Scheme 2-33.

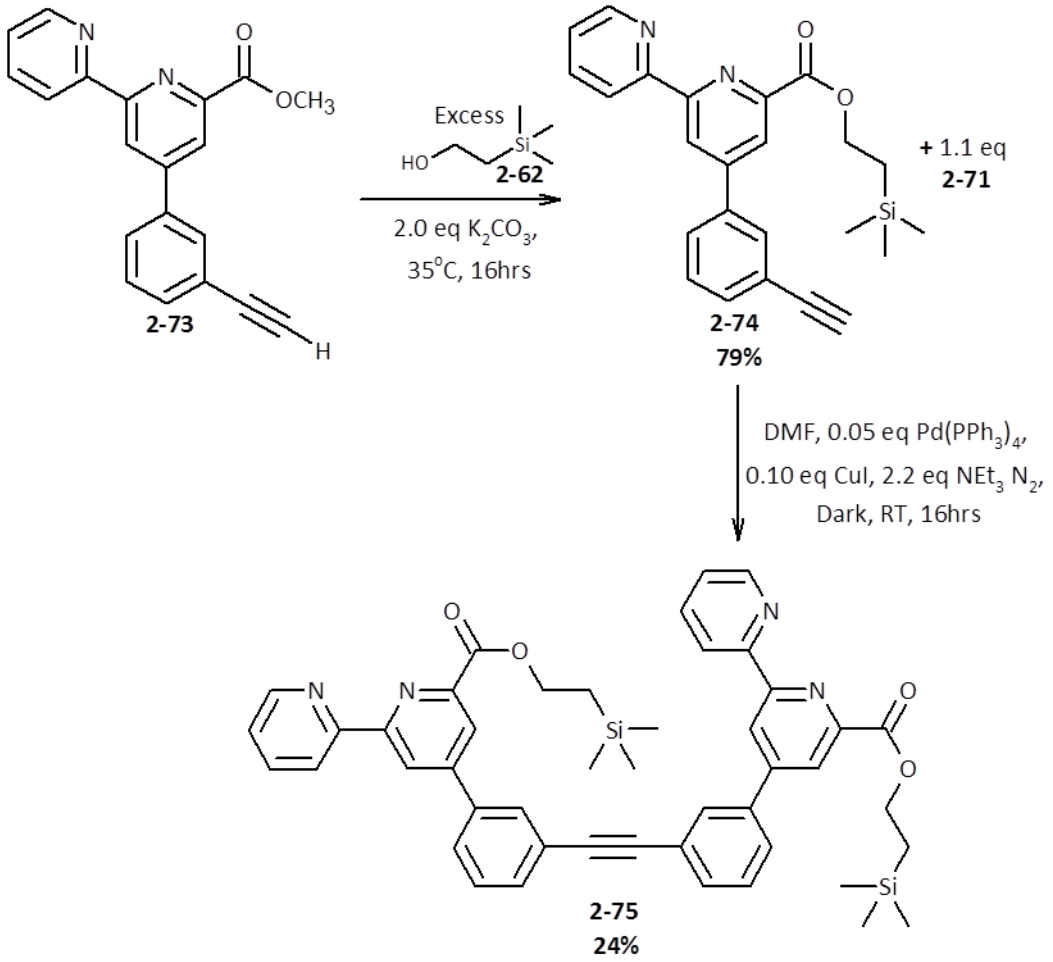

Scheme 2-33: Transesterification to afford the TMSE ester protected alkyne terminated compound **2-74** and subsequent Sonogashira cross-coupling with **2-71** to afford the final di-TMSE protected BIPYA-BIPYA bis ligand **2-75**.

The methyl ester product (**2-73**) was treated with trimethylsilylethanol and potassium carbonate as the base to yield the trimethylsilylethyl ester protected BIPYA ligand bearing the terminal alkyne. The final step in the synthesis of the symmetrical trimethylsilylethyl ester protected BIPYA-BIPYA bis-tridentate ligand (**2-75**) involved the Sonogashira coupling of the aryl iodide (**2-71**) and the terminal alkyne (**2-74**) compounds which was carried out under identical conditions to those for the trimethylsilylethyl ester protected DPA-TERPY (**2-68**) molecule.

The overall syntheses of the final appropriately protected compounds **2-68** and **2-75** involved 6 and 8 steps respectively with overall yields of 9.2 and 7.5% affording 154 and 92 mg of products for analysis.

2.17 Complexation of Bis-Tridentate ligands with Transition Metals

With the two target trimethylsilylethyl ester protected bis-tridentate ligand molecules in hand the next step was to study the simultaneous deprotection/complex formation in order to yield the final self-assembled L_3M_3 hexagons. The studies were carried out in an analogous manner to those carried out for the trial trimethsilylethyl ester protected BIPYA ligand only using equimolar quantities of ligand to metal salt rather than in a two to one ratio. Initial studies focused on the use of the soluble metal fluoride salts CoF_2, NiF_2 and ZnF_2 in order to further investigate the potential scope of the simultaneous deprotection - complex formation strategy for the trimethylsilylethyl ester protected DPA-TERPY molecule (**2-68**) and the trimethylsilylethyl ester protected BIPYA-BIPYA molecule (**2-75**). Upon mixing solutions of any of the metal fluoride salts with solutions of either the TERPY-DPA or BIPYA-BIPYA bis ligand molecules resulted in the rapid generation of variously coloured precipitates depending on the metal used as seen with the BIPYA trial ligand (**2-63**, Figure 2-23)

The isolated solids were then analyzed using ESI-MS to determine if any hexagonal species had been formed. Unfortunately, analysis of these products failed to indicate the formation of any of the hexagonal species or the presence of any uncomplexed protected or deprotected ligand molecules. The lack of evidence for the uncoordinated ligand as well as the observed colour changes were indicative of the successful complex formation although the exact nature of the complexes formed was unknown. It was hypothesized that a possible reason for the lack of observed hexagonal species could be due to the poor ionization of the self-assembled structure rather than the lack of formed hexagons. This hypothesis was based on the difficulties in obtaining mass spectra for the trial BIPYA ligand complexes, which have a net charge of zero much like the modified hexagons formed using transition metals in the +2 oxidation state. Recall

that it was hypothesized that the difficulties in obtaining mass spectra for the L_2M complexes of the trial BIPYA ligand were due to the requirement for the ionization of the metal center to obtain a charged complex. Based on this hypothesis it was decided to try to generate a modified hexagon using a transition metal in the +3 oxidation state in order to generate an architecture with a native net charge of +3. Such a charged complex should be much easier to observe using mass spectrometry as no ionization step is required. In order to achieve this however required the deprotection of the TMSE groups of the TERPY-DPA (**2-68**) and BIPYA-BIPYA (**2-75**) bis ligands as no sufficiently soluble fluoride salts were available. To obtain the deprotected compounds solutions of the protected bis-ligands in DMF of known concentration were treated with two equivalents of TBAF in THF. Upon deprotection the solutions went from clear and very pale yellow to clear and slightly pink. These solutions of known concentration were used directly for the self-assembly into the hexagons with net charge of +3. The metal salts chosen for this experiment were cobalt(III) chloride and iron(III) chloride. The solutions of the bis-ligands and the metal salts were mixed at which point deeply coloured precipitates formed rapidly. Unfortunately ESI-MS analysis of these newly formed complexes also failed to provide any indication that the desired hexagonal species had formed.

A few possible reasons for the failure to observe the desired hexagonal species were considered. One possibility is that the kinetics of the self-assembly are too rapid and that the association energy is too strong. A possible result of this would be that the addition of either bis-ligand or metal centers to the uncyclized L_3M_3 species to form insoluble complexes of higher stoichiometry would occur more quickly than it takes for the complex to rearrange in order to properly cyclize. If the association energy were relatively weak a self-correction mechanism for the complex via the dissociation of metal - ligand coordination centres of higher stoichiometry species could allow for the eventual generation of hexagons as the thermodynamic product. If on the other hand the association energy was particularly strong and the dissociation of the metal centres was a very rare occurrence an effective self-correction process would not be available.

In conjunction with the rapid formation of coordination polymers to the size at which they became insoluble, and therefore effectively conformationally frozen, the lack of self-correction would prevent the hexagonal species from forming in substantial quantities in a reasonable time frame. As discussed previously, it was hypothesized that the correction process would not be required for the bis-tridentate ligand system provided that the formation of species of stoichiometry greater than L_3M_3 was negligible. Unfortunately this prediction may have proven to be inaccurate, and it was hypothesized that the formation of coordination polymers with higher stoichiometries may be a possible reason for the failure to observe the desired hexagonal species. The presence of a collection of coordination polymers of low solubility and neutral charge would help to explain the lack of signals from ESI-MS since these species are unlikely to ionize effectively given the difficulties experienced previously with coordination compounds of the trial BIPYA ligand (**2-63**).

An alternative hypothesis is that the insoluble precipitates observed are in actuality one or more of the precursors of lower stoichiometry on the path to the final hexagonal assembly. If the self-assembly process was sufficiently slow that a significant concentration of these smaller species formed and that these lower stoichiometry species are of sufficiently low solubility in the solvents used then it is possible that they would precipitate from solution. Evidently once precipitated from solution these smaller complexes would no longer be capable of proceeding towards the desired hexagonal complex.

Unfortunately the relatively small supply of bis-tridentate ligands had been exhausted in the previous studies so it was not possible to carry out the self-assembly studies under conditions which would slow down the kinetics, such as lower temperatures and concentrations or the use of a competing ligand. In order to test this new hypothesis time consuming synthesis of more material was required so it was decided instead to focus on studying the transport activity of the already prepared ligand metal mixtures.

2.18 Trial Transport Assays - TERPY-DPA + Co^{2+} Mixture

Although no confirmation of hexagonal structures had been obtained from any of the prepared bis-tridentate ligand - transition metal mixtures, it was decided to perform some transport activity assays on one of these mixtures to see if any activity that could be attributed to the assembled hexagons could be detected. It was decided to use the TERPY-DPA (**2-68**) and Co^{2+} mixture in DMF as it was available in the greatest quantity. The mixture was heated until all solids were dissolved to afford an orange solution and a portion of this was diluted with DMF until no precipitates formed upon cooling to room temperature.

Vesicles were prepared in order to perform the HPTS assay on the diluted mixture however when attempting to obtain a baseline reading using an injection of DMF it was found that the injection of this solvent, although less than one percent of the total volume in the fluorescence cell, resulted in exceedingly leaky vesicles that were unsuitable for determining a rate of transport. The DMF solution of the TERPY-DPA and Co^{2+} mixture was evaporated very slowly under vacuum to leave behind a dark orange amorphous solid. Attempts to dissolve this solid in a variety of solvents miscible in water showed that only DMSO and DMF were suitable. Unfortunately DMSO, much like DMF resulted in leaky vesicles unsuitable for an effective experiment.

With this development focus turned away from vesicle based assays towards bilayer clamp studies. Generally bilayer clamp studies require the injection of significantly less compound than vesicle assays so it was hypothesized that perhaps the lipid bilayer formed would be unaffected by the DMF or DMSO solvents. Multiple studies were carried out with the ligand-metal mixture in both solvents, however several problems were encountered. Firstly, it was observed that upon injection of small volumes of either solution into the aqueous buffer used in the experiment the formation of a fine precipitate occurred. Clearly the formation of a precipitate meant that a significant proportion if not all of the added compound was unavailable to interact with the lipid bilayer membrane and therefore the likelihood of possible

channels forming would be quite low. Injecting more of the solution in an attempt to increase the concentration of compound in the aqueous solvent resulted in excessive destabilization of the bilayer membrane and therefore the ability to observe any transport activity was lost. As an alternative approach the lipid solution used for the formation of the bilayer was pre-mixed with a small volume of the solutions and then dried as much as possible under both vacuum and a stream of nitrogen. When this lipid solution was resuspended in decane, as per standard procedure, there was an evident increase in the turbidity of the resultant solution suggesting that there were some species which were poorly solubilized. All attempts to form stable bilayers with these pre-mixed lipid solutions resulted in failure. As control experiments involving the pre-mixing of only either the DMF or DMSO solvent with the lipid solution followed by drying under vacuum and nitrogen and resuspension in decane also resulted in turbid solutions which were not competent for forming stable bilayers. This observation suggested that once again the solvents available for the dissolution of the TERPY-DPA and Co^{2+} mixture were incompatible for studying transport activity.

At this juncture the appropriate course of action was to step back and analyze the data available on the two metal ligand systems synthesized, the modified Fujita squares and Newkome hexagons, in an attempt to separate out the positive features from the not so positive ones.

2.19 Lessons Learned and Potential Future Directions

Despite the many disappointments in so far as obtaining ion transport active self-assembling architectures based on metal-ligand interactions several important interpretations can be made by comparing the features that differ between the modified Fujita and Newkome systems.

Firstly, the denticity of the ligands used varied significantly; monodentate in the case of the 4,4’-bipyridines of the Fujita system and tridentate for all three of the TERPY, DPA and BIPYA moieties used in the Newkome system. The initial impetus for moving

from the monodentate to tridentate system was the hypothesis that perhaps the lipid bilayer membrane was too chaotic for the formation of stable self-assemblies comprising only one metal ligand interaction. In retrospect the change in design from monodentate to tridentate was likely too drastic; even though the tridentate ligands likely formed exceedingly strong interactions with added transition metal centres this may have also resulted in the loss of the ability for the self-assemblies to effectively self-correct to the desired hexagonal structures via dissociation of the metal-ligand complexes. Without this self-correction the species formed in the case of the modified Newkome system may very well have been extensive coordination polymers which would account for the poor solubilities of the metal-ligand products as well as the difficulties in obtaining meaningful results from the mass spectrometry experiments. Alternatively the system may have indeed formed the desired hexagonal species when the solutions were of low concentration and at elevated temperatures. It may have been the requirement for cooling and concentration of these solutions in order to carry out experimental analyses that led to the generation of species of higher stoichiometry. This interpretation rests on there being sufficient lability of the metal ligand interactions so that the hexagonal species could dissociate and incorporate more subunits to lead to these larger constructs. Regardless, based on these observations abandoning the monodentate ligand binding motif may have been hasty and any future designs of ion channels using metal-ligand interactions for self-assembly should return to monodentate interactions initially followed by bidentate motifs if these prove insufficient.

Another hypothesis made in transitioning from the Fujita to the Newkome based systems was that the high charge density of the Fujita square was detrimental to the effective partitioning of the self-assembled species into the non-polar bilayer membrane. The modified Newkome system attempted to address this by designing ligand - metal coordination centres that possessed no net charge. In retrospect this was also likely too drastic of a modification as the exceedingly poor solubility of all of the modified Newkome ligand - metal mixtures in aqueous solvents meant that they simply

precipitated from solution without having a chance to partition into any available bilayers. Low aqueous solubility has been previously implicated for the poor transport activity observed for oligoester molecules synthesized in the Fyles lab [32]. Although the exact solubility properties of the target modified Newkome hexagons could not be predicted prior to synthesizing the compounds it should not have come as a surprise that they would have low aqueous solubility due to their lack of charge. Future designs for systems using metal-ligand interactions for the self-assembly of ion channels should therefore generate amphiphilic assemblies. Many of the most successful synthetic ion channel forming compounds are amphiphilic in nature and returning to this tried and true design principle would hopefully result in compounds which have the proper balance between aqueous solubility and membrane partitioning. For example a design incorporating metal - ligand interactions that more closely mimicked the overall structure of the cyclodextrin based ion channels discussed in the introduction comprising a rigid macrocycle with polar groups projecting from one face and non-polar groups projecting from the other may provide a promising starting point.

There are however some design modifications that were made in going from the Fujita to Newkome systems that should be retained. For example, attempting to minimize steric obstruction of the pore, which was likely to be a problem in the modified Fujita square, should still be integral to any design.

In short, although the goal of obtaining discrete ion channels via metal - ligand self-assembly strategies proved elusive, many important lessons were learned that can be applied to future designs. The development of synthetic ion channels via novel strategies such as metal - ligand self-assembly is still a worthwhile and potentially very rewarding pursuit for the clever and determined chemist.

3 Dissipative Assembly of Transport Active Systems

3.1 Thermodynamic vs. Dissipative Assembly

Another interesting avenue of exploration under the more general sphere of self-assembly is in studying more dynamic or non-equilibrium assembly processes. They are interesting not only with respect to membrane transport activity, for which the focus in the field thus far has been on systems which thermodynamically self-assemble, but also from the more encompassing view of mimicking natural systems. In Nature few processes necessary for life remain at thermodynamic equilibrium for long. Survival of even the simplest organism requires constant intake of fuels from, and excretion of metabolites to, the environment and therefore predicates a system which is in a constant state of flux.

Conceptually the difference between thermodynamic and dissipative assembly breaks down to where along the potential energy surface the transport active species resides. A graphical representation of these processes is presented in Figure 3-1 below.

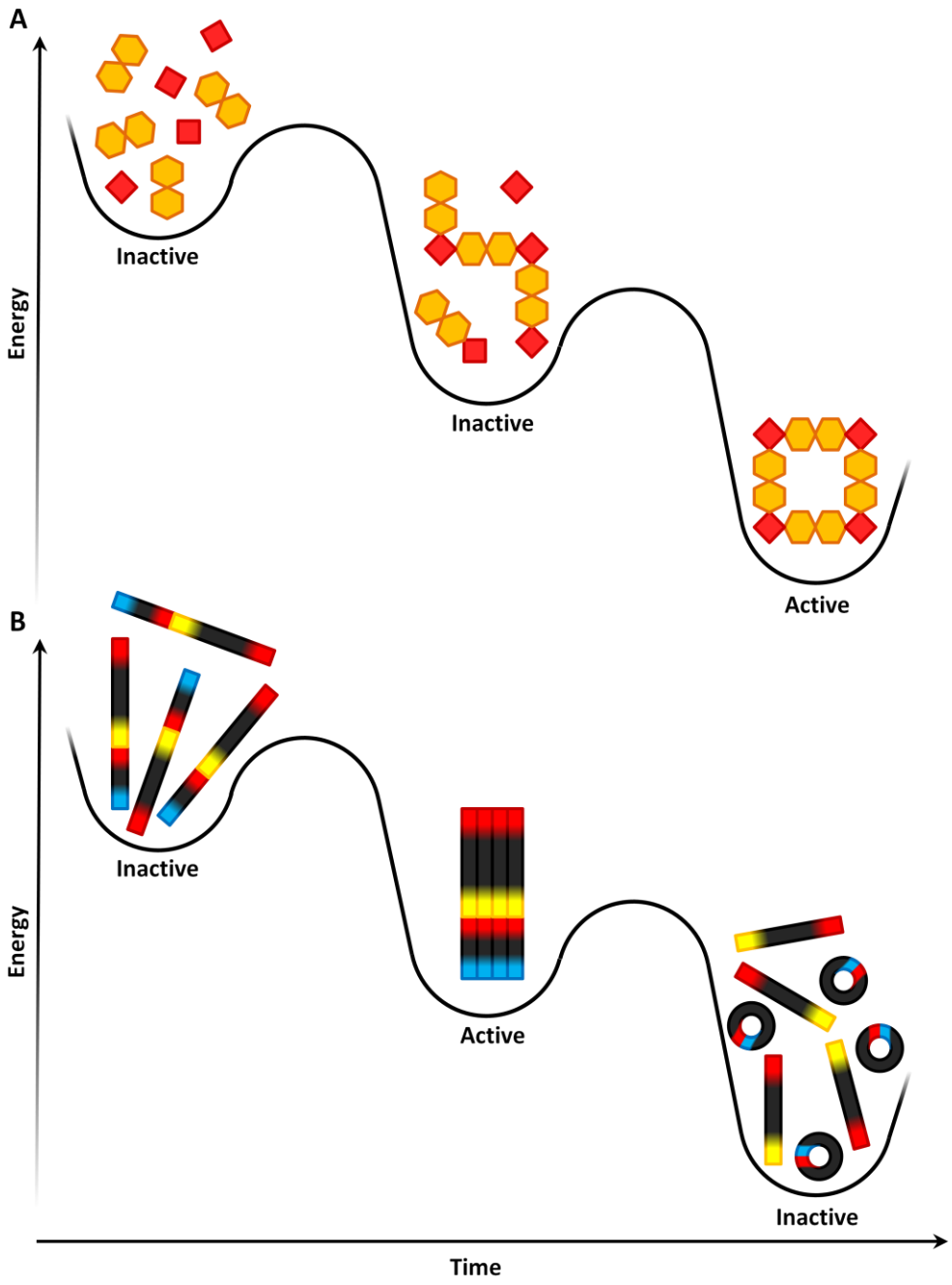

Figure 3-1: Simplified diagram illustrating the conceptual differences in potential energy surfaces between; A) a thermodynamic self-assembling system and B) a dissipative assembling system.

In both assembly processes the transport active species is formed from several higher energy components. In the conceptually simplest case of thermodynamic assembly (Figure 3-1, A) the components self-assemble through a series of discrete steps of sequentially lower and lower potential energy eventually reaching a fully

assembled structure at the global minimum on the potential energy surface. It is this highly stable species which acts as the transport active species.

In the case of a dissipative system the assembly of the higher energy components proceeds to a lower energy active species which exists at only a local minimum on the potential energy surface. From this local minimum the transport active species then decomposes to an inactive form at the global minimum on the potential energy surface via some spontaneous mechanism (Figure 3-1, B). Ideally it would also be possible to re-activate the system via the introduction of an external fuel source. Such a system would take an additional step towards achieving truly Natural like behavior, although lacking the complex peripheral mechanisms for obtaining its own fuel.

In the thermodynamic system (Figure 3-1, A) it is expected that once the desired self-assembly is generated, ion transport activity should be observed for the entire duration of the study and that the range of activity would be relatively static over the course of time. In contrast, an ion transport system that undergoes dissipative assembly is expected to show transport activity that is not constant during the time course of the studies with these changes occurring on a similar time scale to the degradation of the active species to the more thermodynamically favorable final inactive one.

3.2 Design Considerations for a Channel Exhibiting Dissipative Assembly

In order to develop a successful ion channel system within the framework of a dissipative assembly strategy several crucial design components had to be taken into account. The first consideration was that the main goal was to provide the proof of concept of the dissipative assembly strategy rather than finding a new class of ion transporting molecules. Therefore, in order to maximize the chances of observing ion transport activity, it was decided to use a preexisting channel forming molecule developed in the Fyles lab with well studied properties as the lead compound rather than trying to build a new system from the ground up.

Other important aspects to consider were the mechanism by which the system was to become deactivated and the nature of the final inactive species. However, there was no inherent preference as to whether the mechanism of deactivation was passive, that is an intramolecular process that occurs spontaneously for the active species, or induced by the addition of some other reactive component via an intermolecular process. That being said, it was necessary that if the deactivation was to involve the addition of a second reactive species that the added compound must not react or affect the integrity of the bilayer membrane in any appreciable way.

Of greater importance was that the reaction occurred on a time scale similar to that of either the vesicle based HPTS or the bilayer clamp transport activity assays. This would ensure that the evolution of the transport activity could be easily monitored with respect to time.

The HPTS assay was the experiment of choice since it is used to monitor the bulk transport activity of a population of transport active species therefore the overall activity of the system would show a rise or fall in the activity of the system as it assembles or dissipates respectively. Observation of the entire range of activities as they evolved over time could therefore be determined over the course of a single set of experiments. The bilayer clamp assay on the other hand, monitors single transport active species. The result is that, while the cessation of the activity of a particular channel may be observed by this method, the proper assessment of changes to activity over time would require conducting a very large number of trials in order to collect sufficient data to make a definitive correlation.

Common practice in the laboratory is to carry out individual vesicle based HPTS experiments with a duration of ten minutes, and provided the vesicle solution is kept at a low temperature and exposure of the solution to the atmosphere is minimized, the vesicles can maintain their integrity for several hours. Therefore if the HPTS assay was to be used for assessing changes in transport activity, a deactivation process which occurred over the course of an hour or two would be ideal as the entire range of

activities could be monitored with a single sample of vesicles. A process that occurred significantly faster would be difficult to monitor using the HPTS assay since over the course of a single experiment the activity could change dramatically making the analysis of the data more complicated. Conversely, although it would be possible to monitor the changes in activity for a system with a longer deactivation period, due to the somewhat limited lifetime of the vesicles multiple different solutions of these would need to be used. Since even with exceptional care taken in their preparation individual solutions of vesicles tend to show slightly different behavior the data obtained for the changes in activity over time would not be as accurate as if only a single solution of vesicles was used.

The bilayer clamp assay, although not the preferred method for analyzing the changes in activity as discussed previously, has a similar time dependence as the HPTS assay. It has been observed in the laboratory that an individual bilayer membrane once generated can exhibit relatively stable properties for up to about two hours. That being stated the stability of any particular membrane varies considerably, especially with the introduction of transport active compounds, so the two hour time limit should not be relied on too heavily. Due to this time dependence as well as the inability of the assay to detect more than a few transport active species simultaneously, deactivation processes occurring over significantly longer or shorter time periods than approximately an hour would also be more difficult to assess.

Given that the time scales of both assays are on the order of a few hours the deactivation process should also occur over a similar time period. In order to maximize the chances of developing a deactivation reaction that occurs on this time scale it was advantageous to design a system that allowed for varying the rate of the reaction by simple modification of the molecule or the conditions used in the transport assays.

3.3 Design Elements for the Dissipatively Assembling Ion Channel

The lead molecule chosen as the basis for the new ion channel design was the molecule HOOC-Hex-Dip-Hex-Hex-OH (**3-1**) below, previously developed by Moszynski and Fyles [119, 105]. The naming convention used for these oligoesters is to start from the carboxylic acid terminus and name the individual segments based on the number of carbons in the chain, Hex for a six carbon piece for example, or the nature of the substituent, Dip as a short form for the diphenylacetylene containing piece for example, and finally to list the functionality of the other terminus, OH for the hydroxyl in this case. A similar naming system will be used in this document for the dissipative assembly synthetic targets.

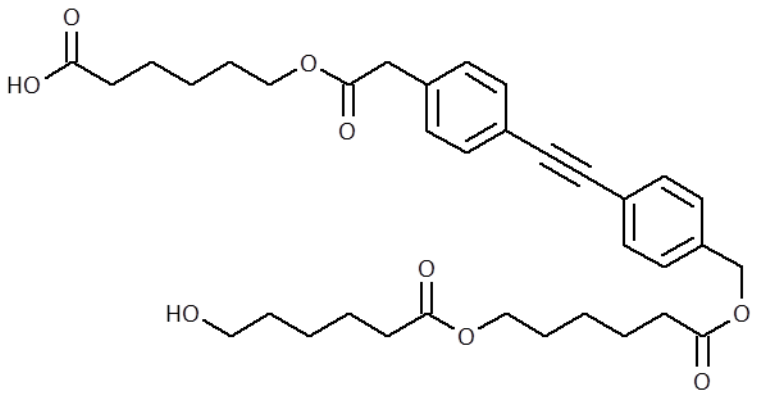

HOOC-Hex-Dip-Hex-Hex-OH (**3-1**)

This molecule was chosen because it has been well studied in the laboratory and was shown to exhibit many properties which were desirable in a new target ion channel. Firstly, the ester coupling reaction conditions and protecting group strategies used for the synthesis of this class of oligoester ion channel have been previously optimized in the lab. The molecule is also structurally simple compared to other transport active molecules from literature so the synthesis was expected to be reasonably facile. Also, this particular molecule showed very high transport activity in both the vesicle based HPTS assay as well as in the bilayer clamp experiment. A molecule of similar length and structural features was therefore expected to show similarly high activity. In addition

the incorporation of the diphenylacetylene chromophore into any design was appealing since this moiety was shown to exhibit environment sensitive fluorescence which allowed for some monitoring of the partitioning behavior of molecules in which it was present.

With the general structure for the synthetic target in mind the next design component to consider was the nature of the deactivated species and the reaction that would result in its generation. Transport studies of HOOC-Hex-Dip-Hex-OH, the truncated version of the lead molecule HOOC-Hex-Dip-Hex-Hex-OH, possessing only one Hex unit at the hydroxyl terminus rather than two, showed a marked decrease in transport activity over the full length molecule. In fact many examples of oligoester ion channels synthesized in the Fyles lab, as well as examples from other labs, have shown that the overall length of the molecule plays a large role in determining the activity [32, 105, 119]; molecules whose length closely matches the thickness of the bilayer membrane are often more reactive than those which are either shorter or longer. These results suggested that a reaction that resulted in a truncated version of the transport active molecule would likely exhibit the desired decrease in transport activity.

In choosing the nature of reaction that would effect this truncation a cue was taken from strategies employed by the pharmaceutical industry for the development of prodrugs; the intramolecular cyclization reaction [121]. This strategy, summarized in Figure 3-2 below, involves a molecule possessing a 'masked' nucleophile at the terminus and an electrophilic carbonyl group at some distance away which is covalently bonded to a heteroatom, which will act as a leaving group, more distal to the terminus. In order to effect the truncation reaction the nucleophile must be 'unmasked' so that it can attack the carbonyl group resulting in the cleavage of the covalent bond to the heteroatom. The overall reaction therefore generates the desired truncated molecule as well as a new cyclic molecule.

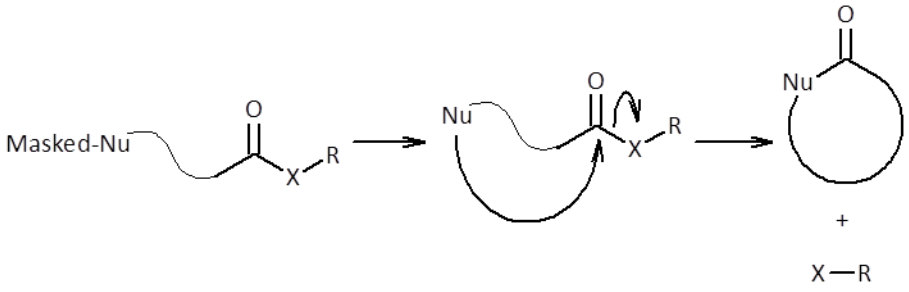

Nu = nucleophile; X = O, N, S; R = remainder of molecule

Figure 3-2: Diagram of the intramolecular cyclization reaction. The masked nucleophile (Nu) of the initial compound is first unmasked; this nucleophile (Nu) is then free to attack the electrophilic carbonyl at some distance away on the same molecule. The covalent bond between the carbonyl and the adjacent heteroatom leaving group (X) is cleaved in the process to afford the final truncated molecule as well as a new cyclic molecule.

This truncation mechanism was also appealing because it is amenable to many different modifications which should allow for the refinement of the reaction kinetics and thermodynamics. For example the nucleophilicity of the nucleophile used can be increased or decreased to modulate the rate of the reaction [122]. In addition the number of atoms between the nucleophile and the carbonyl group can be adjusted; this would result in changes to the size of the final cyclic structure. Since cyclization reactions which result in five or six membered rings are most favored, decreasing or increasing the length of the chain between the carbonyl and the nucleophile should result in a decrease in the rate of the reaction [123, 124, 125]. Finally the heteroatom bonded to the carbonyl can also be changed. Likely candidates for this heteroatom were oxygen, sulfur and nitrogen to produce ester, thioester and amide groups with the carbonyl respectively.

3.4 Dissipative Assembling Ion Channel Synthetic Target

Taking into consideration all of these design considerations a small library of structurally related synthetic targets was conceived; the general structure and sites of modification are shown in Figure 3-3 below.

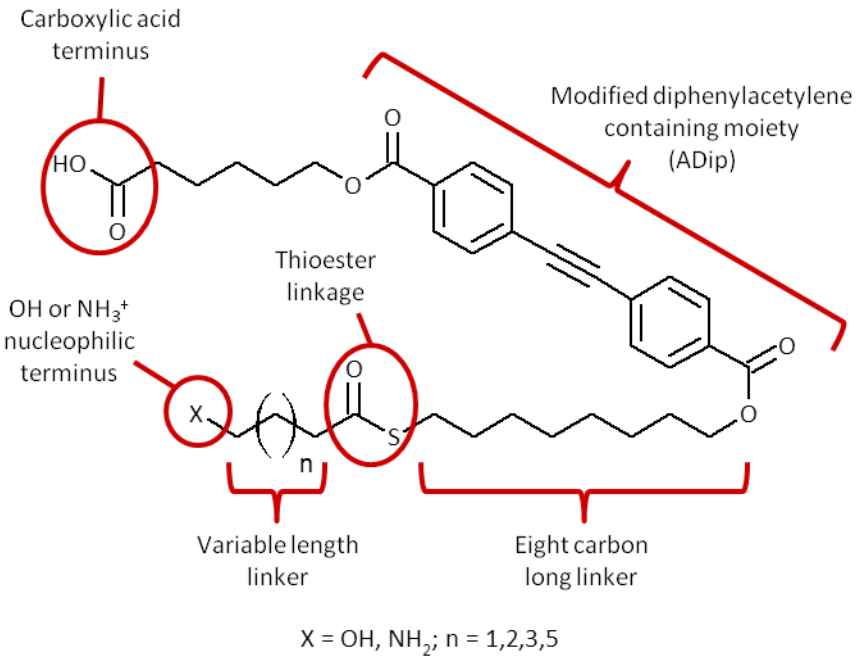

Figure 3-3: Synthetic targets for potential dissipative assembling ion channels with important design features highlighted.

Overall the target molecules retain many similar features to the lead HOOC-Hex-Dip-Hex-Hex-OH that were found to be important such as a carboxylic acid terminus, a fluorescent reporting diphenylacetylene group, a nucleophile at the other terminus as well as retaining roughly the same overall length although with some internal variability in the composition and sequence.

The carboxylic acid terminus was retained in order to provide improved aqueous solubility; previously synthesized compounds lacking this functionality were shown to have poor aqueous solubility resulting in irreversible aggregation and poor transport activity.

The diphenylacetylene group was retained but in a somewhat modified form from the Dip moiety of the lead compound. This modified Dip component was given the short form naming convention, ADip, in order to distinguish it from the previous version. In the lead compound the Dip moiety was intentionally dissymmetric in order to allow for a solid phase synthesis strategy to be employed. Since the synthesis of these targets

was intended to be entirely solution phase, a symmetrical molecule was chosen in order to simplify the synthesis. The modified diphenylacetylene containing component also lacks the methylene units between the diphenylacetylene portion and the functional groups as either end. This has the effect of extending the π system of the chromophore and may result in some improvements in its fluorescent reporting characteristics over the Dip component.

The other terminus of the molecule was designed to be either the nucleophilic hydroxyl or amine functional groups. The variability of the functional group at this position was included in order to provide the ability to adjust the rate of the truncation reaction as discussed previously.

Extending from this nucleophilic terminus was a variable length linker. As previously mentioned using different numbers of methylene units at this position allows for further control of the reaction rate. Although the lengths targeted depended somewhat on the commercial availability of the amino acids to be used as feedstocks, they were also chosen in order to ensure that the products of the cyclization reaction included those with the thermodynamically most stable ring sizes. Particularly desirable were the four and five carbon long pieces which would generate the more stable five and six membered rings respectively. In addition the variability of the length of this component also has an effect on the overall length of the resulting molecule. The effect of these length differences of the full length compound were also expected to be interesting as it has been shown in previous studies of oligoester ion channels that length can play an important role in transport activity, as discussed previously.

The thioester linkage was chosen over the ester and amide options for several reasons. The preference over the amide linkage was due mainly to fears that the relatively stable amide bond would be too difficult to cleave in the cyclization reaction causing the truncation process to be either too slow or to not occur at all. The thioester linkage also has the advantage over the other functional groups because of its unique reactivity with respect to the thiol-thioester exchange reaction [56]. In this reaction a

molecule possessing a nucleophilic thiol functional group can attack the electrophilic carbonyl group of a thioester, resulting in the cleavage of the bond between the carbonyl and the original sulfur atom. The overall effect is that the pendant groups are effectively switched between the original thiol and thioester to form a new thiol and thioester molecules.

The reversible covalent bond forming thioester exchange reaction, unlike the related transesterification reaction, occurs under relatively mild aqueous conditions which can be easily achieved in either of the ion transport assays. The appeal of this reaction is that it could be possible to reactivate the transport activity of the system after the truncation reaction had occurred to deactivate it; see Scheme 3-1. This reactivation could work because the truncated product of the intramolecular cyclization reaction possesses a terminal thiol group. Therefore the addition of a carefully designed thioester containing molecule to the truncated thiol molecule could result in the thioester exchange reaction occurring between these two species resulting in the re-elongation of the inactive truncated molecule to the full length active one. The ability to selectively turn off and on transport function by perturbations to the overall system would bring the model even closer to mimicking the behaviors of natural ion channels.

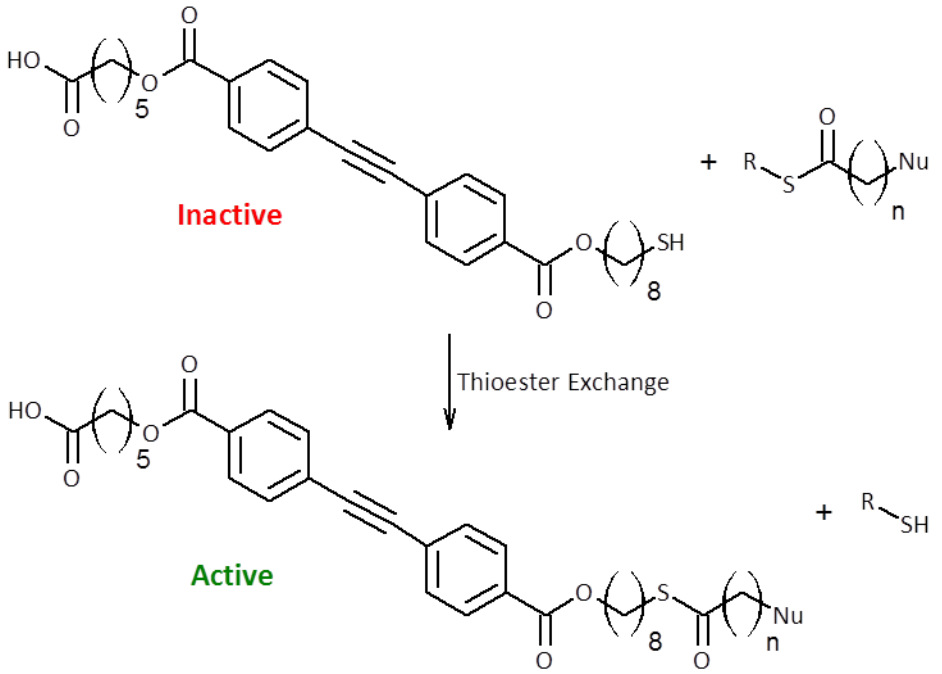

Scheme 3-1: Schematic representation of the thioester exchange reaction between a purportedly inactive, thiol terminated, truncated molecule and a sacrificial thioeser resulting in the regeneration of the purportedly active full length thioester molecule.

The overall cycle of from transport active to transport inactive species via the spontaneous intramolecular cyclization - truncation reaction followed by regeneration of the transport active species by addition of a molecular fuel which undergoes thiol - thioester exchange reaction with the thiol terminated truncated compound is illustrated in Figure 3-4 below.

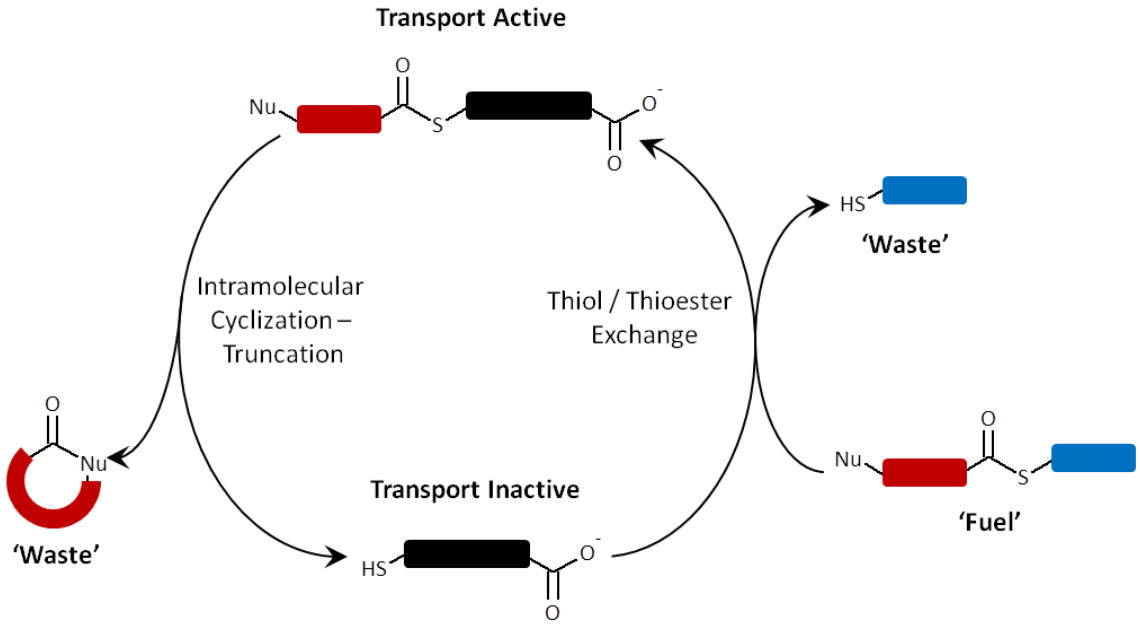

Figure 3-4: Representation of the envisioned deactivation - reactivation cycle for the target compounds. Starting from the top of the figure and working counterclockwise: the full length transport active species undergoes a spontaneous intramolecular cyclyzation - truncation eliminating a cyclic 'waste' molecule while generating the truncated, transport inactive compound possessing a reactive terminal thiol group. By introducing an appropriate molecular 'fuel' possessing a thioester linkage to this truncated compound an intermolecular thioester exchange reaction can occur resulting in the generation of a new 'waste' thiol terminated compound and the regenerating the full length transport active species.

The proposed system therefore falls into the realm of dissipative assembly [126], in particular the topology of the system shares many of the same features as the molecular gelators developed by van Esch [127]. In the van Esch system the modulated function is the physical state of the system between a gel and a solvent phase. The system involves the use of the molecule dibenzoyl-(L)-cysteine (DBC) depicted in Figure 3-5 below.

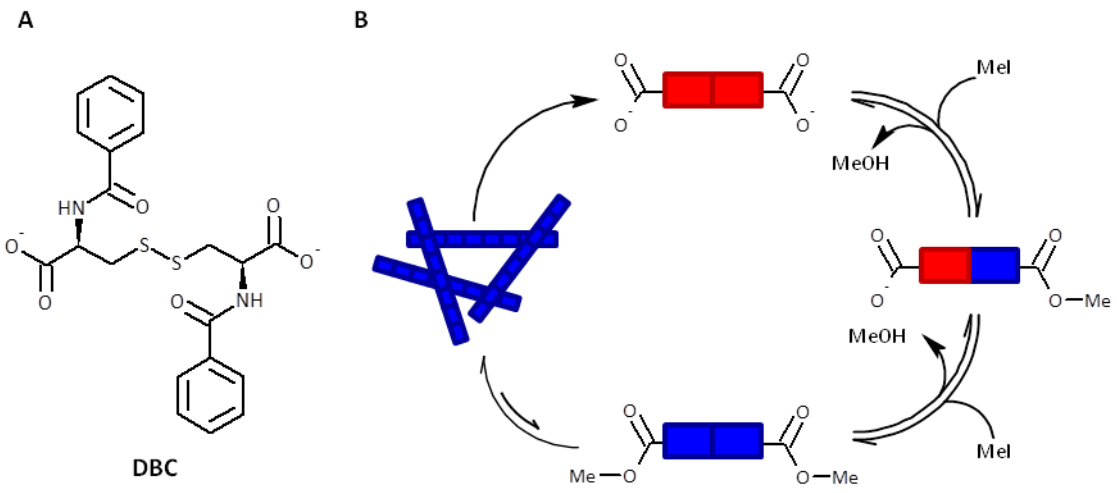

Figure 3-5: A) the structure of dibenzoyl-(L)-cysteine (DBC) and B) a schematic of the dissipative self-assembly cycle used. Red and blue segments represent anionic carboxylate and neutral methyl ester ends of the DBC molecule.

When in its deprotonated form (fully red segments, Figure 3-5) intermolecular repulsion occurs between the carboxylate groups of the DBC molecule causing the molecules to be well solvated in aqueous media. However, if the ionic nature of the carboxylate groups is masked, by protonation in the case of lowered pH for example, the DBC molecules self-assemble into a gel phase via the formation of a network of intermolecular hydrogen bonds. In the van Esch system, rather than using protons as method of neutralizing the charge on the DBC molecules, methyl iodide (MeI) was added to the system as a fuel source at neutral pH in order to spontaneously alkylate the carboxylate groups of the DBC molecule to the corresponding methyl esters (blue segments, Figure 3-5), resulting in conversion to the gel phase. Gradually over time the methyl esters were hydrolyzed to regenerate the di-carboxylate version of the DBC molecule causing a return to the solvent phase of the system. Repeated treatments with MeI could reversibly switch the system back to the gel phase.

The final design component of the envisioned dissipative transport system was the inclusion of an eight carbon chain between the thioester linkage to the nucleophilic terminus and the proximal ester linkage to the ADip component. It was important to ensure that this linkage was of sufficient length. As discussed the intramolecular cyclization reaction occurs when the nucleophilic terminus of the molecule attacks the

internal carbonyl group to generate a cyclic molecule as well as a terminal thiol. This newly generated thiol is itself nucleophilic, therefore the possibility exists of this thiol attacking the next ester over in the molecule as presented in Scheme 3-2 below.

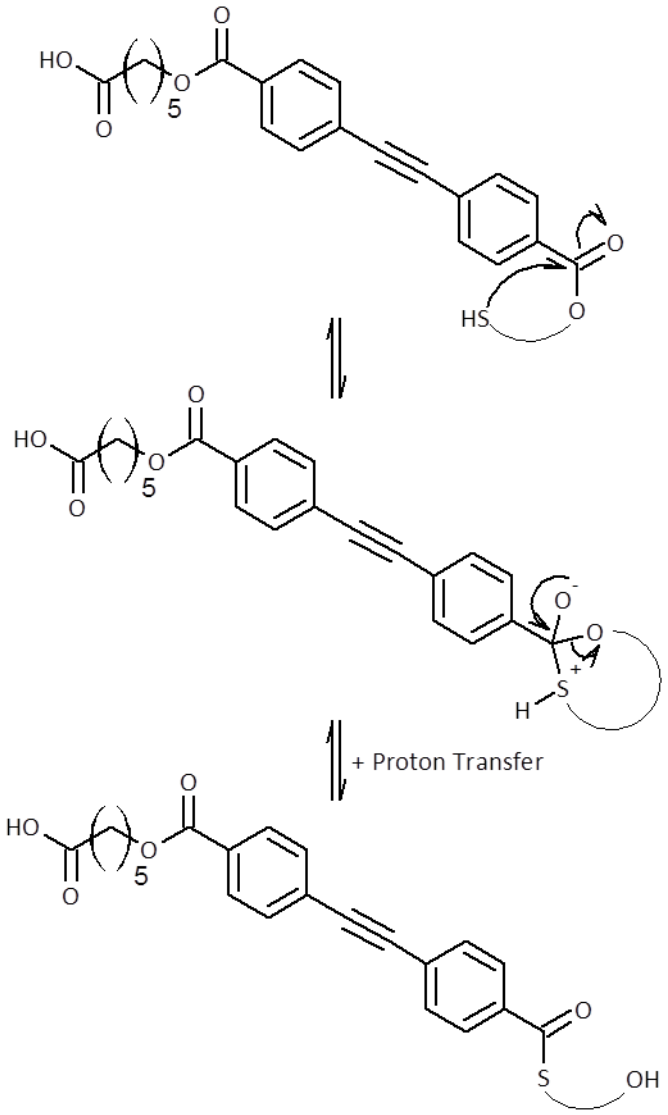

Scheme 3-2: Mechanism of the intramolecular attack of the terminal thiol of the truncated molecule on the adjacent ester to form a new thioester - alcohol containing molecule which would be incompetent in a thioester exchange reaction with another thioester.

This intramolecular reaction would result in the generation of a new thioester bond as well as a terminal alcohol group. If the recovery of transport activity is to be achieved via the thioester exchange reaction with a sacrificial thioester as envisioned, the terminus of the truncated molecule must be a thiol group, not an alcohol. With a

linkage at this position of eight carbons, the nucleophilic attack of the thiol on the adjacent ester would require the formation of an eleven membered ring intermediate, which is entropically disfavoured, and therefore this unwanted side reaction should be slowed down considerably. Although the stability of the oxygen ester is higher than that of the corresponding thioester, the possibility of this undesirable side reaction exists so to be safe this extended linker was an added feature of the design.

3.5 Retrosynthetic Analysis of Target Molecules

A retrosynthetic analysis of the target molecules is presented in Scheme 3-3 below.

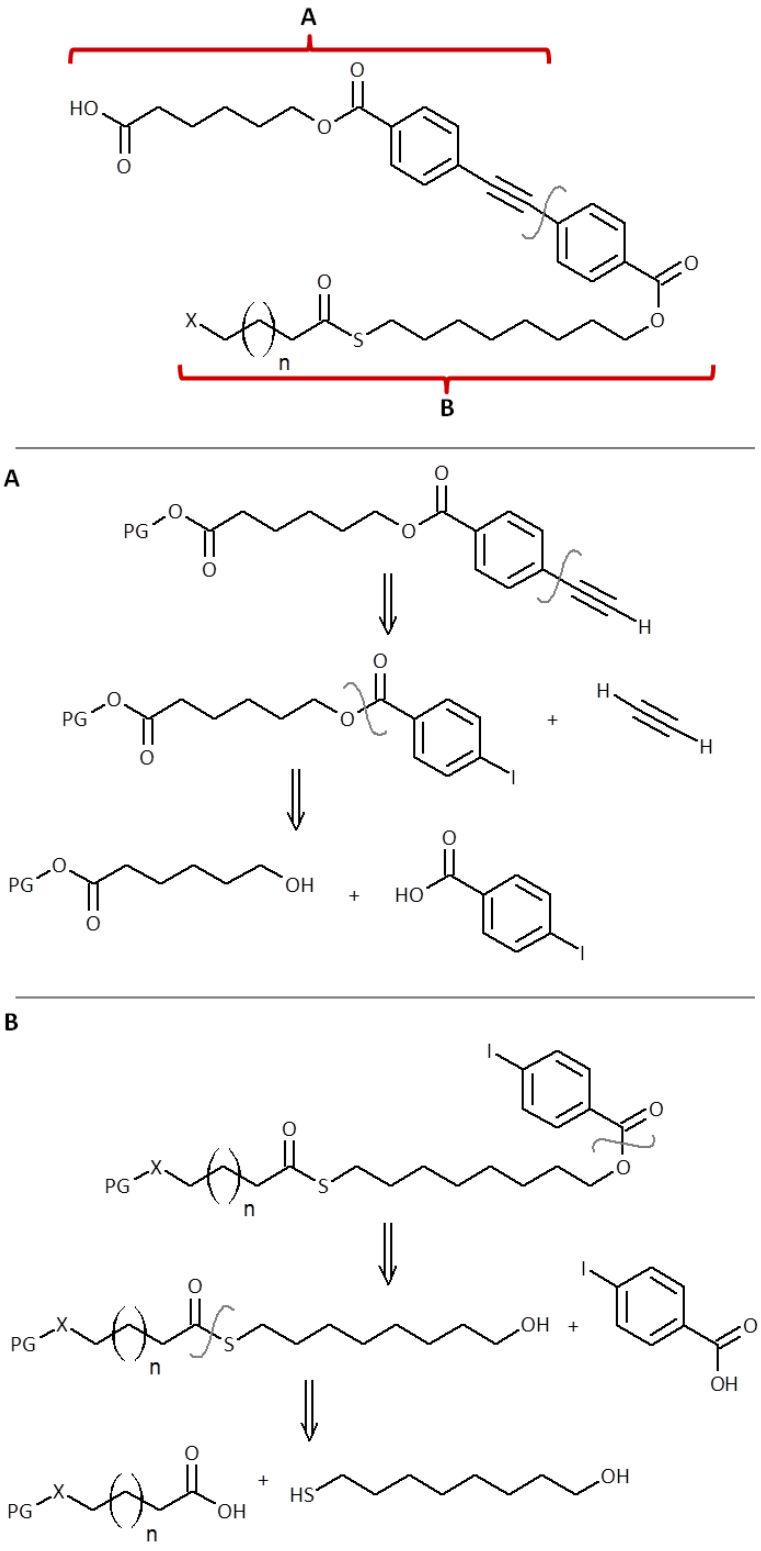

Scheme 3-3: Retrosynthetic analysis of the target dissipative assembling ion channel molecules. The initial disconnection was chosen such that it divided the molecule into two approximately equal halves; one half bearing the carboxylic acid terminus (A) and the other bearing the nucleophilic terminus (B). PG = protecting group, X = O or NH, n = 1,2,3 or 5 methylene units.

From previous solution phase syntheses of the related diphenylacetylene containing oligomers [127], of which the lead compound HOOC-Hex-Dip-Hex-Hex-OH (**3-1**) was one, the target molecules are best considered to be composed of two halves, with the alkyne moiety of the ADip component serving as a logical dividing point between the halves. The first retrosynthetic disconnection was chosen between the alkyne and the aromatic ring on the half of the molecule bearing the nucleophile to provide the two different halves. Following the retrosynthetic course of the carboxylic acid bearing half, the next disconnection was envisioned between the corresponding aryl iodide and the alkyne group. The aryl iodide bearing compound was further disconnected at the ester linkage between the *p*-iodobenzoic acid and the protected carboxylic acid - alcohol portion to provide the two starting materials for this side of the molecule. Turning to the other half of the molecule, the first disconnection of this piece was chosen at the ester linkage between the *p*-iodobenzoic acid and the alcohol end of the fragment bearing the nucleophilic terminus. The final disconnection for this half of the molecule occurs at the thioester linkage between the thiol-alcohol and the protected nucleophile-carboxylic acid portions.

3.6 Synthesis

The synthesis started with the carboxylic acid bearing half of the molecule since this fragment is common to all of the target molecules. The synthesis began with several previously reported [127] synthetic steps leading to the compound **3-7** as shown in Scheme 3-4. First the base catalyzed hydrolysis of ε-caprolactone (**3-2**) was carried out to yield 6-hydroxyhexanoic acid (**3-3**). The alcohol group of this molecule was then protected with the 2-tetrahydropyranyl (THP) protecting group via the *p*-toluenesulfonic acid catalyzed reaction with 3,4-dihydro-2H-pyran to afford compound **3-4**. The next step was the protection of the carboxylic acid functional group of the protected alcohol using the 3-methylbut-2-en-1yl (prenyl) protecting group. The prenyl protecting group was chosen as it has orthogonal deprotection conditions to the already installed THP protecting group; THP is removed using mildly acidic conditions whereas the prenyl

protecting group is commonly removed using trimethylsilyl trifluoromethanesulfonate (TMS-OTf) in dichloromethane [128]. The prenyl protecting group was installed via the active ester intermediate formed from the reaction of diisopropylcarbodiimide (DIC), hydroxybenzotriazole (HOBt) and 3-methyl-2-buten-1-ol (**3-5**) with diisopropylethylamine (DIPEA) as the base. With the THP-prenyl diprotected molecule **3-6** in hand the next step in the synthesis involved the removal of the THP protecting group. This reaction was achieved using *p*-toluenesulfonic acid in a mixture of methanol and dichloromethane as solvent to yield the desired product 3-methylbut-2-en-1-yl-6-hydroxyhexanoate (**3-7**).

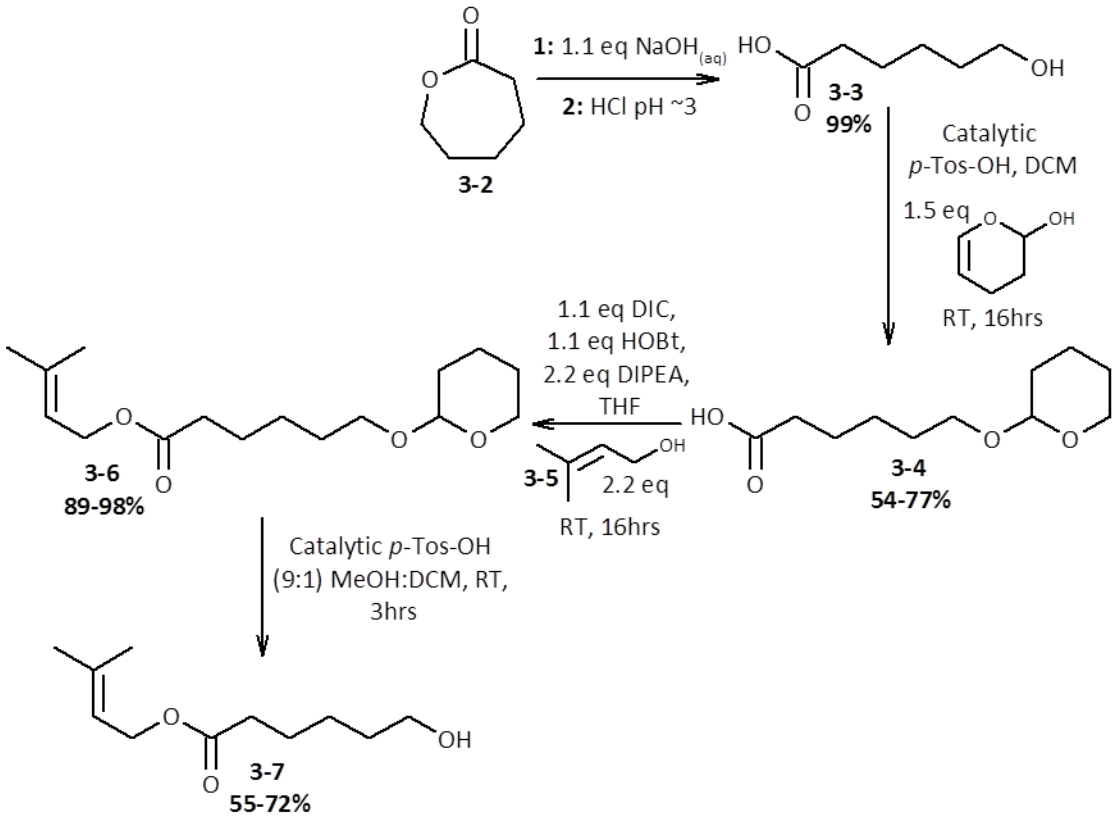

Scheme 3-4: Synthetic scheme carried out for the production of 3-methylbut-2-en-1-yl-6-hydroxyhexanoate (**3-7**) following a previously reported synthetic pathway.

The next step in the synthesis of the carboxylic acid bearing half of the molecule was the formation of the ester between the now liberated hydroxyl group of 3-methylbut-2-en-1-yl-6-hydroxyhexanoate (**3-7**) and *p*-iodobenzoic acid (**3-8**). This ester

coupling was achieved by once again using the DIC, HOBt, DIPEA coupling conditions used for installing the prenyl protecting group to afford 6-[(3-methylbut-2-en-1-yl)oxy]-6-oxohexyl 4-iodobenzoate (**3-9**) as the product, see Scheme 3-5.

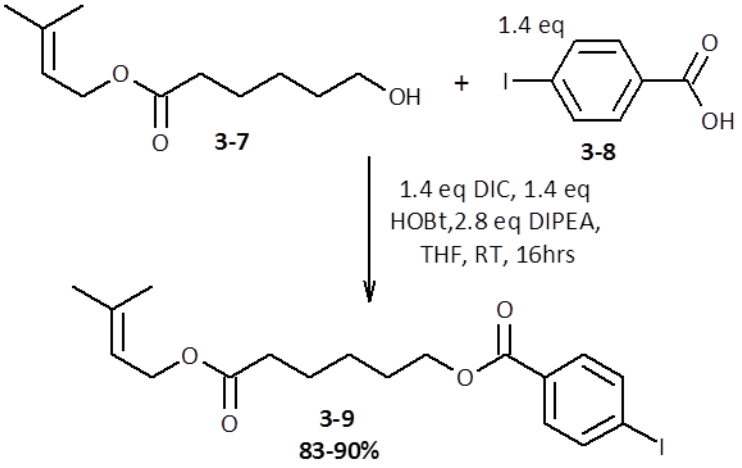

Scheme 3-5: Synthesis of the ester product 6-[(3-methylbut-2-en-1-yl)oxy]-6-oxohexyl 4-iodobenzoate (**3-9**).

The synthesis continued with the palladium catalyzed Sonogashira cross coupling of the aryl iodide (**3-9**) with the protected alkyne, trimethylsilylacetylene (TMS-acetylene); see Scheme 3-6. The reaction was carried out using catalytic amounts of tetrakis(triphenylphospine) palladium(0) and copper iodide with triethylamine acting as the base. The product of this reaction (**3-10**) required the removal of the TMS protecting group from the alkyne in order to generate the terminal alkyne of the final carboxylic acid bearing half of the molecule (**3-11**). This deprotection was achieved by treatment of the compound with tetrabutylammonium fluoride (TBAF) in tetrahydrofuran (THF) as solvent to generate the final prenyl-protected half of the molecule, 6-[(3-methylbut-2-en-1-yl)oxy]-6-oxohexyl 4-ethynylbenzoate (**3-11**).

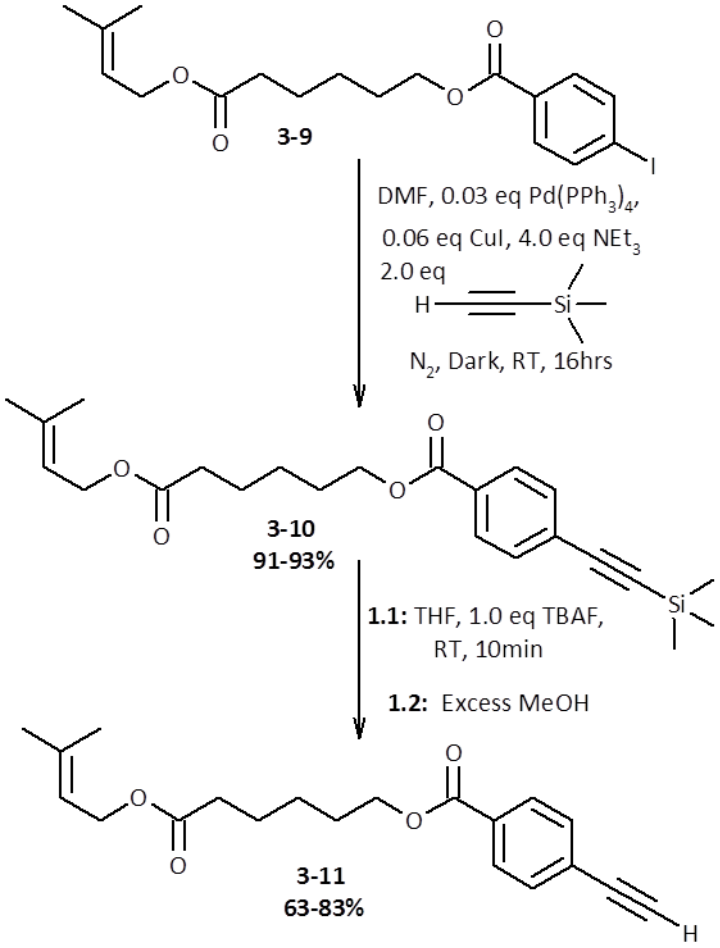

Scheme 3-6: Synthesis of the prenyl protected terminal alkyne 6-[(3-methylbut-2-en-1-yl)oxy]-6-oxohexyl 4-ethynylbenzoate (**3-11**).

With the protected carboxylic acid bearing half of the molecules in hand, the focus now turned to the synthesis of the various other halves of the molecules sporting different nucleophilic termini.

For the amine terminated compounds this first step involved the protection of the amine functional group of amino acids of varying length; see Scheme 3-7. The protecting group of choice in this instance was the N-*tert*-butoxycarbonyl (*t*-BOC) group. This group was chosen as most of the downstream reactions in the synthesis occur under basic conditions, towards which the *t*-BOC group is stable, while the final deprotection of this group occurs after treatment with acid. The *t*-BOC group was installed by reacting the amino acids of varying lengths (4, 5, 6 and 8 carbons long) with

di-*tert*-butyl dicarbonate in a basic solution of tetrahydrofuran and water. Under these conditions all amino acids were efficiently protected providing high yields of the desired compounds (**3-12** - **3-15**) as confirmed by comparison of the NMR spectra to those of the products as previously reported in literature.

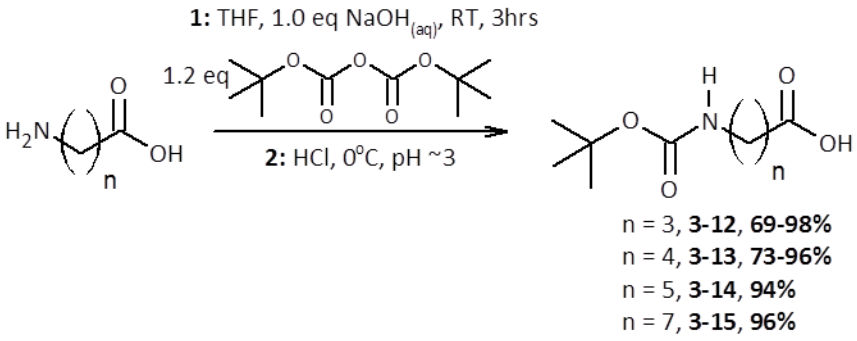

Scheme 3-7: Synthesis of the *t*-Boc protected nucleophiles from amino acids of varying lengths.

For the hydroxyl terminated compounds a different protection strategy was required. Conveniently the required six carbon long appropriately protected alcohol acid had already been prepared in the synthesis of the carboxylic acid bearing half of the molecule; 6-(tetrahydro-2H-pyran-2-yloxy)hexanoic acid (**3-4**, Scheme 3-4). As mentioned previously the THP protecting group present on the alcohol of this molecule is stable to basic conditions and cleaved with an acid treatment.

In order to obtain the four carbon analog of this compound, a similar synthetic strategy starting from γ-butyrolactone (**3-16**) was attempted (Scheme 3-8). Unfortunately the first step of this synthetic pathway, the cleavage of the ester to yield 4-hydroxybutanoic acid failed as only γ-butyrolactone was recovered from the reaction and subsequent neutralization. This was likely due to the equilibrium between the lactone and the alcohol-carboxylic acid molecules lying far towards the lactone form; the five membered ring formed upon cyclization of the lactone being particularly stable.

An alternative pathway to the desired four carbon long compound was carried out as found in literature starting from 1,4-butanediol (**3-17**) and using the fluoride labile *tert*-butyldimethylsilyl (TBDMS) ether protecting group (Scheme 3-8). The switch

to the TBDMS protecting group from the THP protecting group was initiated due to previous experiments in the lab which showed that both the prenyl as well as the TBDMS groups could be deprotected by using TMS-OTf. The deprotections of both the carboxylic acid and the alcohol termini could be carried out at the same time, reducing the number of synthetic and purification steps. The first step involved the installation of the TBDMS group onto only one of the terminal hydroxyl groups. This was achieved by reacting four equivalents of the diol **3-17** with one equivalent of *tert*-butyldimethylsilyl chloride (TBDMSCl) in THF with imidazole as the catalyst in order to minimize the amount of undesired di-protected compound being formed. With the mono protected diol **3-18** in hand the next synthetic step was the oxidation of the unprotected hydroxyl group to the corresponding carboxylic acid. This was achieved in a biphasic reaction of benzene and aqueous potassium permanganate with the phase transfer catalyst tetraoctylammonium bromide (TOAB) to generate the desired product, [(*tert*-butyldimethylsilyl)oxy]butanoic acid (**3-19**) which was confirmed by comparison of the NMR spectra to those from literature.

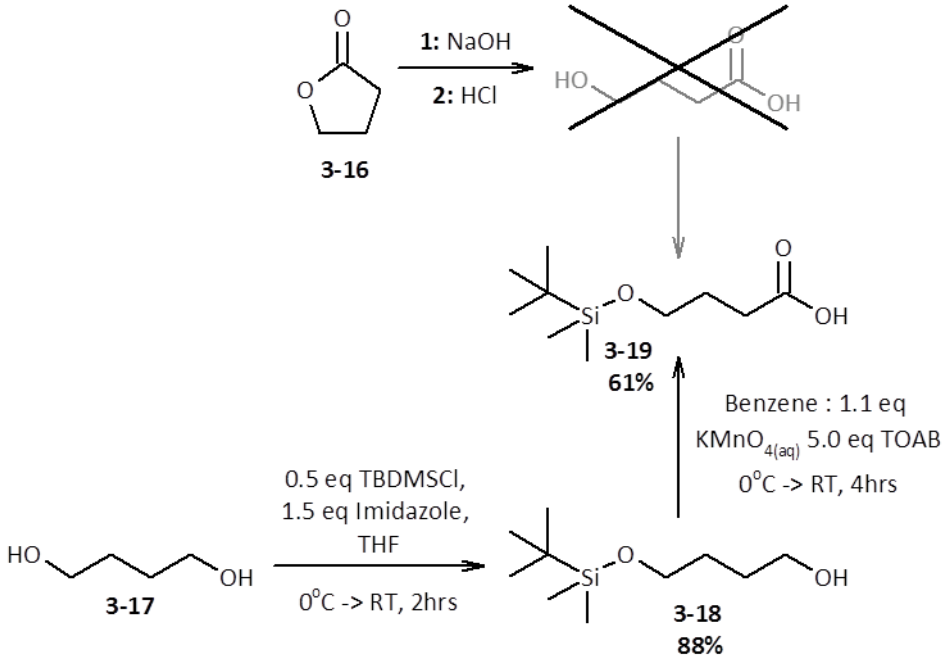

Scheme 3-8: Synthesis of [(tert-butyldimethylsilyl)oxy]butanoic acid (**3-19**).

With the various nucleophilic 'warheads' synthesized (**3-12** - **3-15**, **3-4** and **3-19**), the next synthetic component needed for the nucleophilic half of the molecules was the eight carbon tether, shown in Scheme 3-9. Beginning with 1,8-octanediol (**3-20**) as the starting material, one of the alcohol groups of the molecule was selectively converted to the alkyl bromide by reaction with hydrobromic acid in toluene under refluxing conditions according to a literature procedure to afford the desired 8-bromooctan-1-ol (**3-21**). The structure of the compound was confirmed by comparison of NMR spectra to those from literature. The alkyl bromide group of compound **3-21** was then converted to the terminal thiol **3-22** according to another literature procedure [129]. This transformation was accomplished by reaction of the alkyl bromide **3-21** first with thiourea in ethanol at reflux under an atmosphere of nitrogen and then while still maintaining an inert atmosphere, the treatment of the reaction with ethylenediamine at room temperature. The product of this reaction, 8-sulfanyloctan-1-ol (**3-22**) was of high purity and in high yield and the structure was confirmed by comparison of the NMR spectra to those found in the literature.

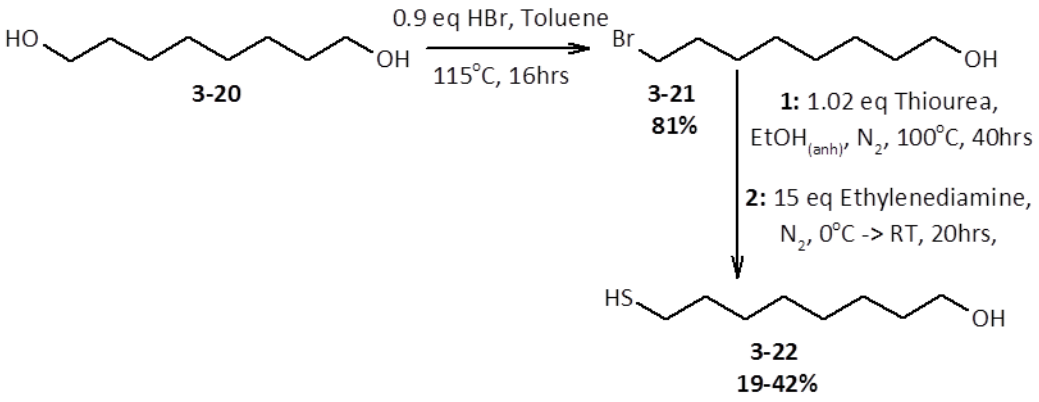

Scheme 3-9: Synthesis of 8-sulfanyloctan-1-ol (**3-22**).

It is worth noting that during this synthesis the option of finding an appropriate protecting group for the alcohol terminus was considered as an alternative in order to allow for cleaner reactions in the following steps. The protection strategy would require two additional steps in the synthesis, one step to install the protecting group and

another further along in the synthesis to remove it. However it was hypothesized at the time that perhaps the small but significant differences in reactivity between the thiol and alcohol functional groups would provide some selectivity in the reactions to follow so in order to shorten the synthesis it was decided to carry on without installing a protecting group onto the hydroxyl moiety.

The next step in the syntheses was the formation of the thioester linkage between the 8-sulfanyloctan-1-ol (**3-22**) and the previously synthesized carboxylic acid bearing compounds with protected nucleophiles (**3-4**, **3-12** - **3-15**, **3-19**). These reactions were carried out using slightly modified active ester coupling conditions to those used previously for the synthesis of the carboxylic acid bearing half of the molecule (Scheme 3-10). While the relative stoichiometries of the DIC and HOBt reagents were kept constant, half of the normal amount of the base DIPEA was used. Due to the lower pK_a of the thiol group relative to its alcohol counterpart, it was believed that by decreasing the stoichiometry of the base relative to 8-sulfanyloctan-1-ol (**3-22**) to a 1:1 ratio the reaction with the thiolate to form the thioesters would be more rapid than that of the alkoxide to form the esters due to the higher relative nucleophilicity of the sulfur to the oxygen at equivalent charge. This assumption proved to be justified as the reactions invariably provided the desired thioester products (**3-23** - **3-28**) in the highest, although still modest, percent yield relative to the other potential products. Somewhat surprisingly the other compounds recovered from the reactions were consistently, in order of percent yield from highest to lowest, the doubly coupled ester-thioester products (**3-29** - **3-34**), the starting 8-sulfanyloctan-1-ol (**3-22**) and finally the ester products (**3-35** - **3-40**), which were always recovered in the lowest yield.

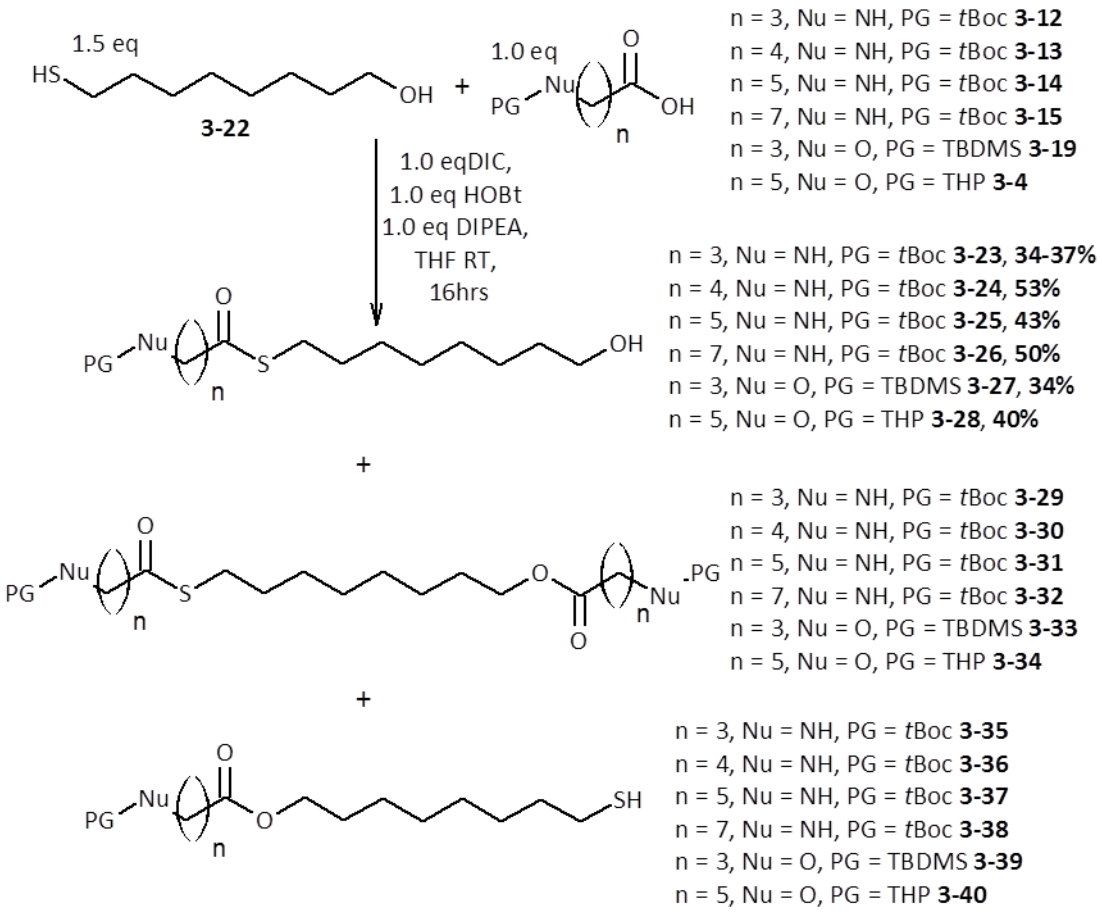

Scheme 3-10: Synthesis of the various protected nucleophile - thioester molecules (**3-23** - **3-28**) and associated ester-thioester (**3-29** - **3-34**) and ester - thiol (**3-35** - **3-40**) side products.

With the successful syntheses of the six thioester containing compounds with protected nucleophilic warheads (**3-23** - **3-28**) the final ester coupling of these compounds to 4-iodobenzoic acid (**3-8**) was all that remained in order to complete the nucleophile bearing halves of the molecules. These coupling reactions were carried out using the same DIC, HOBt and DIPEA catalyzed coupling conditions as used for previous ester couplings to afford the desired protected nucleophile - aryl iodide bearing molecules (**3-41** - **3-46**, Scheme 3-11).

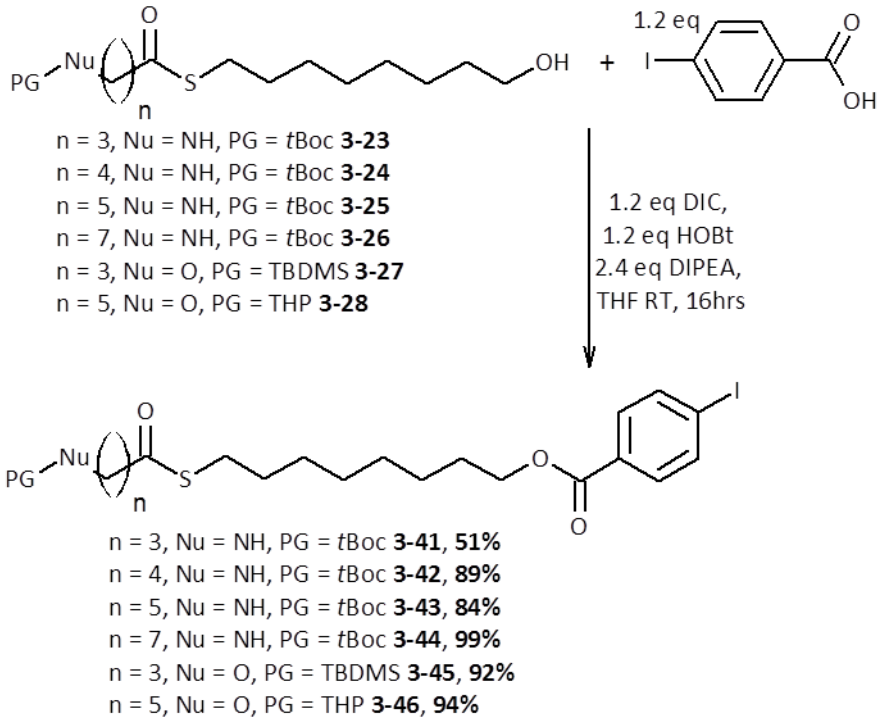

Scheme 3-11: Synthesis of the various protected nucleophile - aryl iodide compounds (**3-41** - **3-46**).

The penultimate step in the syntheses of the target molecules was the Sonogashira cross-coupling between the terminal alkyne of the protected carboxylic acid half of the molecule (**3-11**) and the aryl iodide of the various protected nucleophiles of the other half of the molecule, see Scheme 3-12. These reactions were carried out using the conditions discussed previously for the coupling of TMS-acetylene to 6-[(3-methylbut-2-en-1-yl)oxy]-6-oxohexyl 4-iodobenzoate (Scheme 3-6) to yield the six fully protected full length molecules (**3-47** - **3-52**).

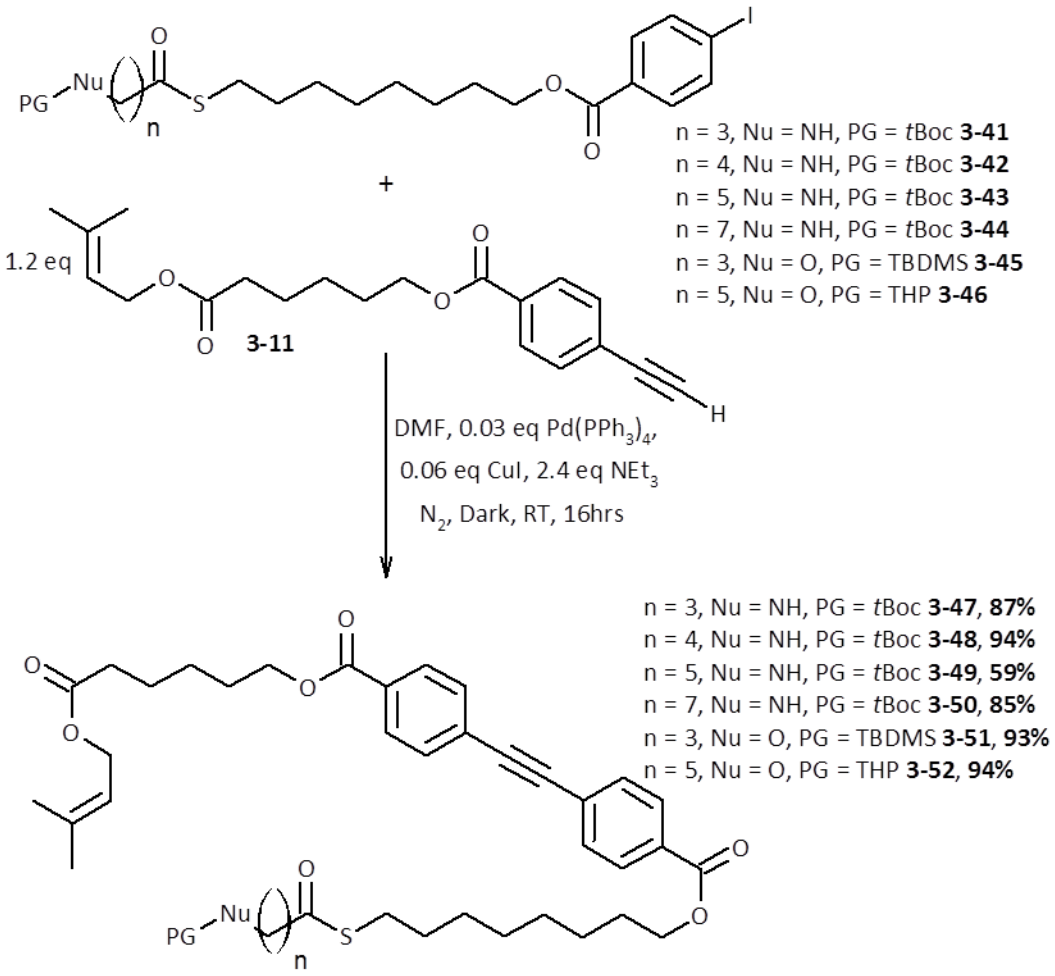

Scheme 3-12: Synthesis of the fully protected full length thioester containing molecules **3-47** - **3-52**.

The final step of the syntheses involved the deprotection of the two termini to yield the final compounds for study. For the *t*-Boc protected amine terminated molecules the initial strategy for the deprotection was to first remove the prenyl group from the carboxylic acid using TMS-OTf and then to deprotect the *t*-Boc protecting group with trifluoroacetic acid in dichloromethane. Fortunately, the TMS-OTf deprotection conditions resulted in both the removal of the prenyl as well as the *t*-Boc protecting groups from the molecule to yield the final amine terminated compounds of varying length (**3-53** - **3-56**, Scheme 3-13).

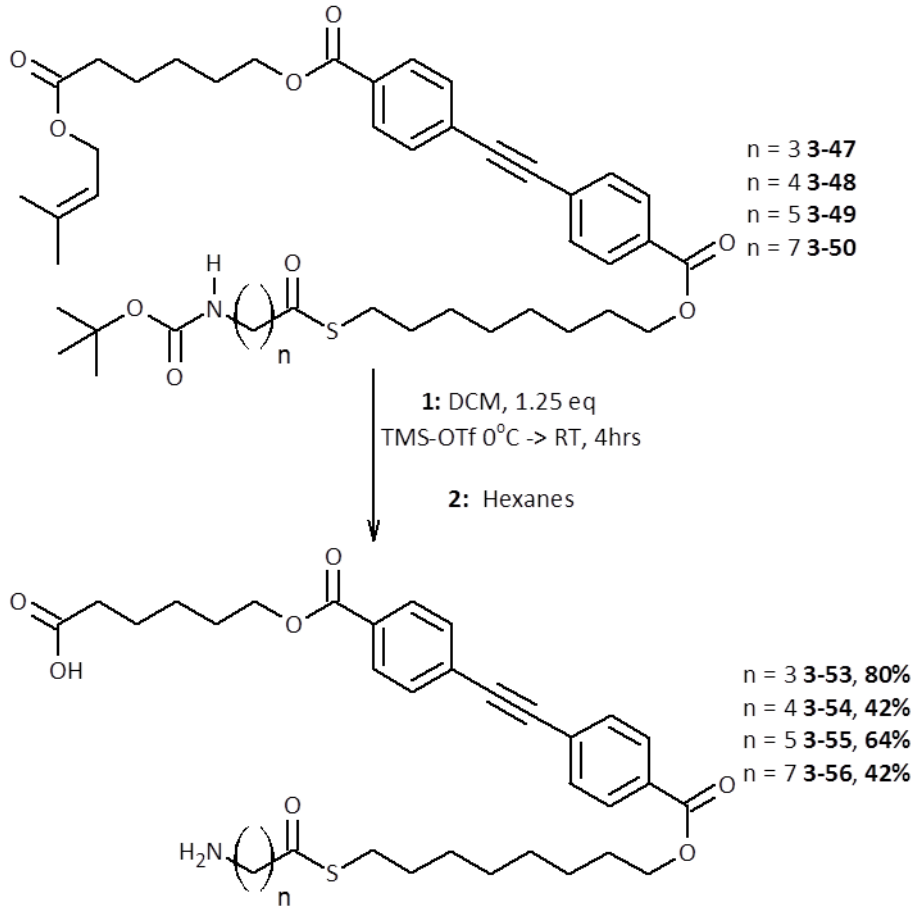

Scheme 3-13: Deprotection reactions for the four *t*-Boc protected amine - prenyl protected carboxylic acid molecules (**3-47** - **3-50**) to afford the final deprotected amine terminated compounds (**3-53** - **3-56**)

The final deprotection conditions attempted for the compound with the TBDMS protected alcohol and four carbon linker to the thioester, **3-51**, were identical to those used for the *t*-Boc protected amine. Unfortunately, although as expected based on previous reactions carried out in the Fyles lab these conditions resulted in the deprotection of both the prenyl as well as the TBDMS protecting groups, the compound isolated from solution was not the carboxylic acid - alcohol, **3-57** but instead the truncated molecule **3-71**; Scheme 3-14.

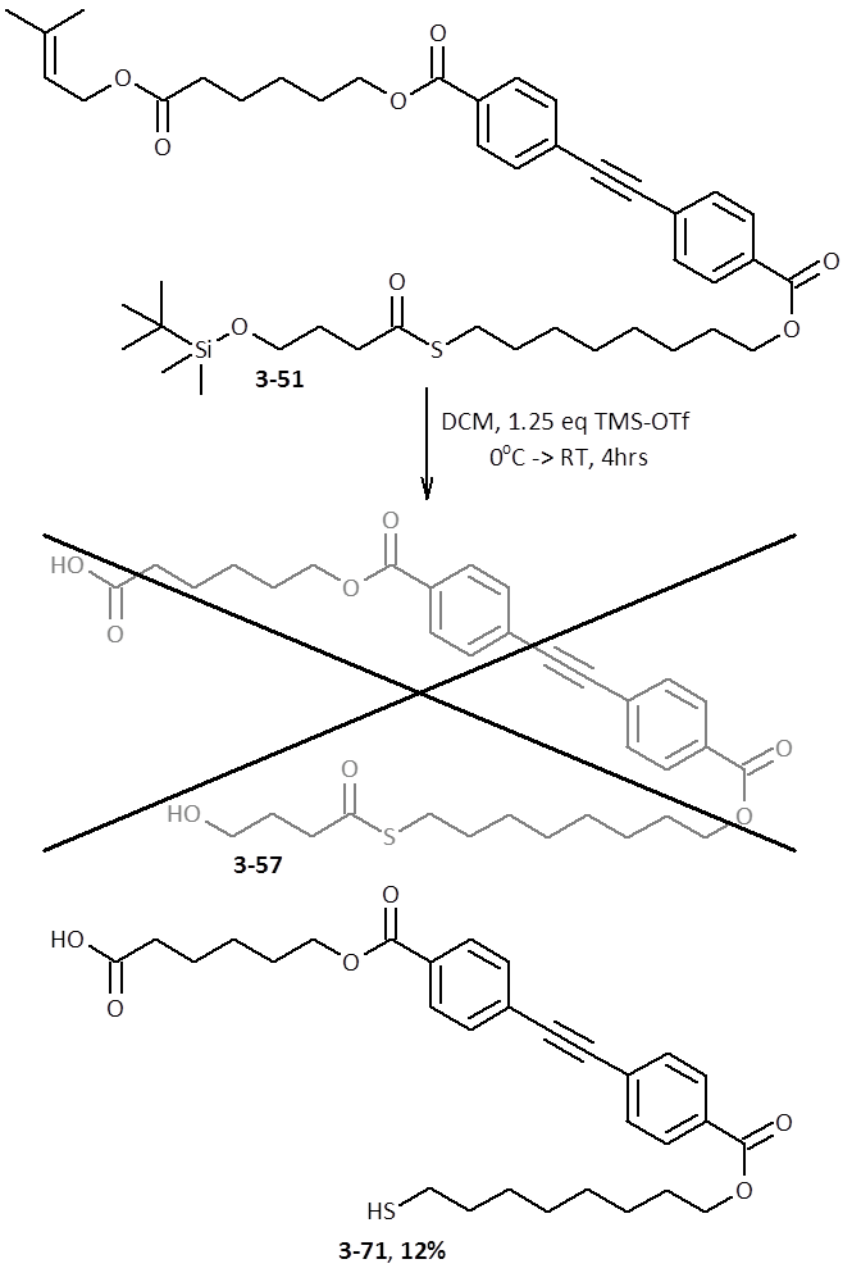

Scheme 3-14: Attempted deprotection of the TBDMS protected alcohol - prenyl protected carboxylic acid **3-51** to afford the final alcohol terminated compound **3-57** instead resulting in the production of the truncated compound **3-71**.

Although a disappointing result in that the desired product was not obtained, it at least indicated that the intramolecular cyclization truncation reaction was an effective mechanism for dissipative assembly.

The THP protected alcohol - prenyl protected carboxylic acid compound **3-52** however required two separate deprotection steps, shown in Scheme 3-15. The first was the deprotection of the THP group using a treatment with *p*-toluenesulfonic acid in a mixed nine to one dichloromethane methanol solvent system to afford the free alcohol **3-58**. The final step was the deprotection of the prenyl protecting group which was once again accomplished using TMS-OTf to afford the final alcohol terminated molecule **3-59**.

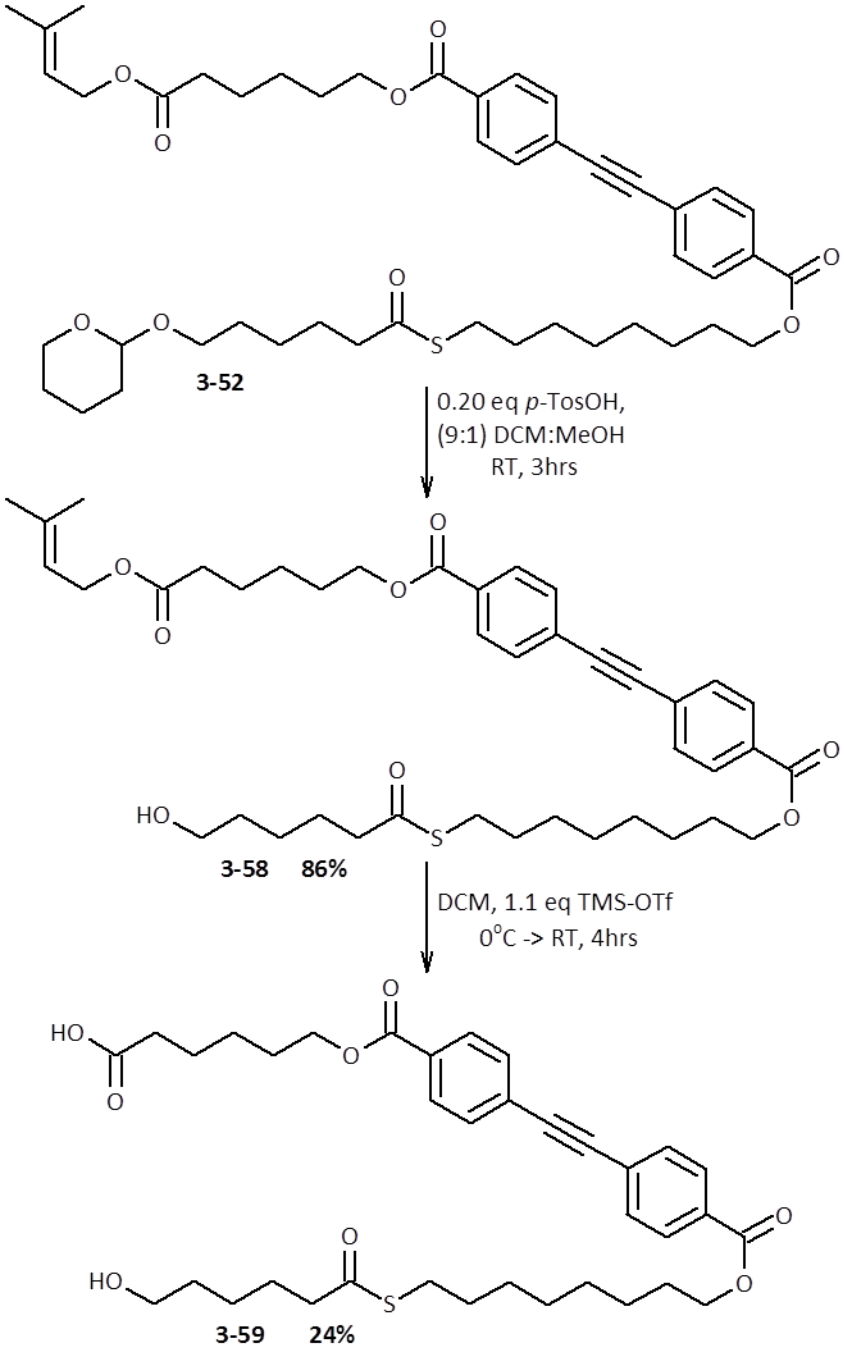

Scheme 3-15: Two step deprotection strategy used to first remove the THP protecting group from compound **3-52** to generate the alcohol - prenyl protected carboxylic acid **3-58** followed by the removal of the prenyl group from this compound to afford the final alcohol - carboxylic acid compound **3-59**.

All compounds were further purified by HPLC as required to ensure only samples of highest purity were used for the various assays.

For convenience a summary table of the full length compounds is provided below with associated compound numbers and naming conventions used in this document.

Table 3-1: Summary of synthesized compounds with associated numbers and naming conventions.

Compound # / Name	Structure
3-53 $^{-}$OOC-Hex-ADip-Oct-S-But-NH_3^+	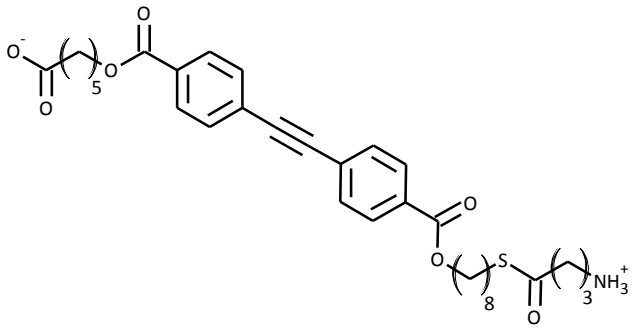
3-54 $^{-}$OOC-Hex-ADip-Oct-S-Pent-NH_3^+	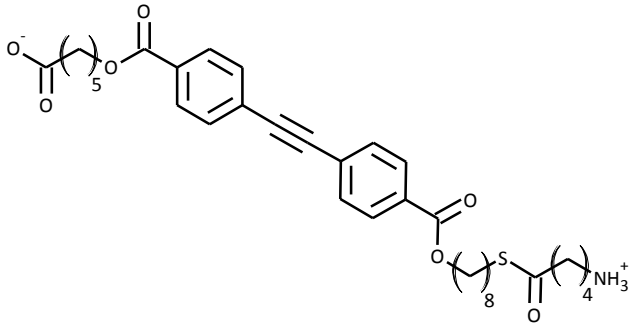
3-55 $^{-}$OOC-Hex-ADip-Oct-S-Hex-NH_3^+	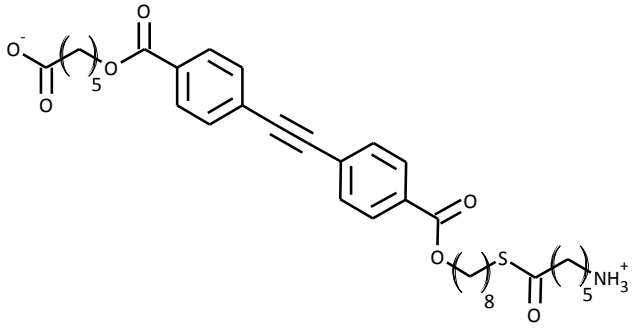

Compound # / Name	Structure
3-56 $^{-}$OOC-Hex-ADip-Oct-S-Oct-NH_3^+	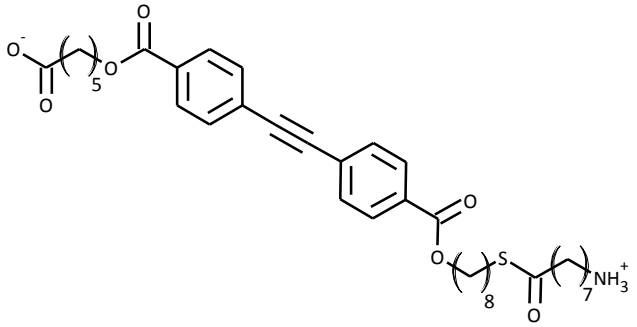
3-57 HOOC-Hex-ADip-Oct-S-But-OH	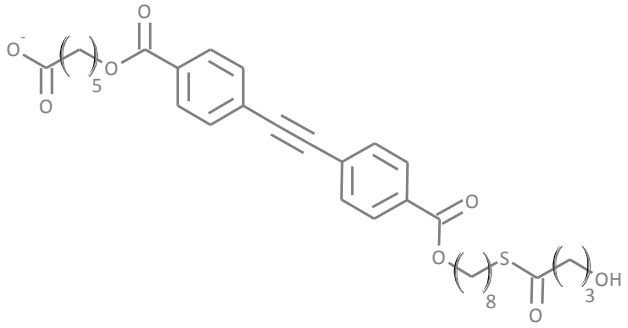
3-59 HOOC-Hex-ADip-Oct-S-Hex-OH	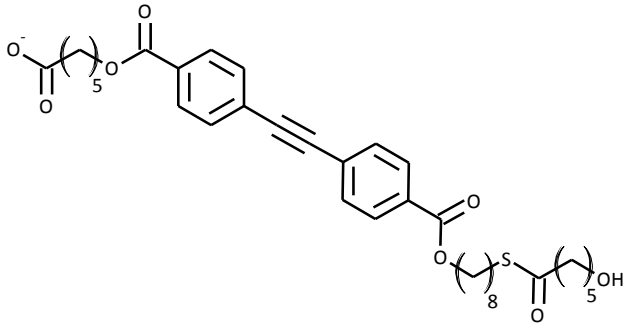

3.7 Vesicle Based HPTS Studies

With the final compounds in hand focus could turn to the analysis of their transport activity. As discussed previously the experiment of choice to study the changes in transport activity of the compounds before and after truncation was the vesicle based HPTS assay. As an experiment that studies the bulk properties of a population of channels, the HPTS assay allows for the rapid determination of effective

transport rates which is not possible with the single channel observations made with the bilayer clamp assay.

The activity assessment of each newly synthesized compound was carried out according to standard Fyles' laboratory procedures (see Experimental) with the maximum concentration of each compound dictated by the highest concentration attainable in the vesicle solution before turbidity was observed indicating that the solubility limit of the compound had been achieved. The observed activities for the compounds are presented in Figure 3-6 below as well as a comparison to the lead compound HOOC-Hex-Dip-Hex-Hex-OH (**3-1**).

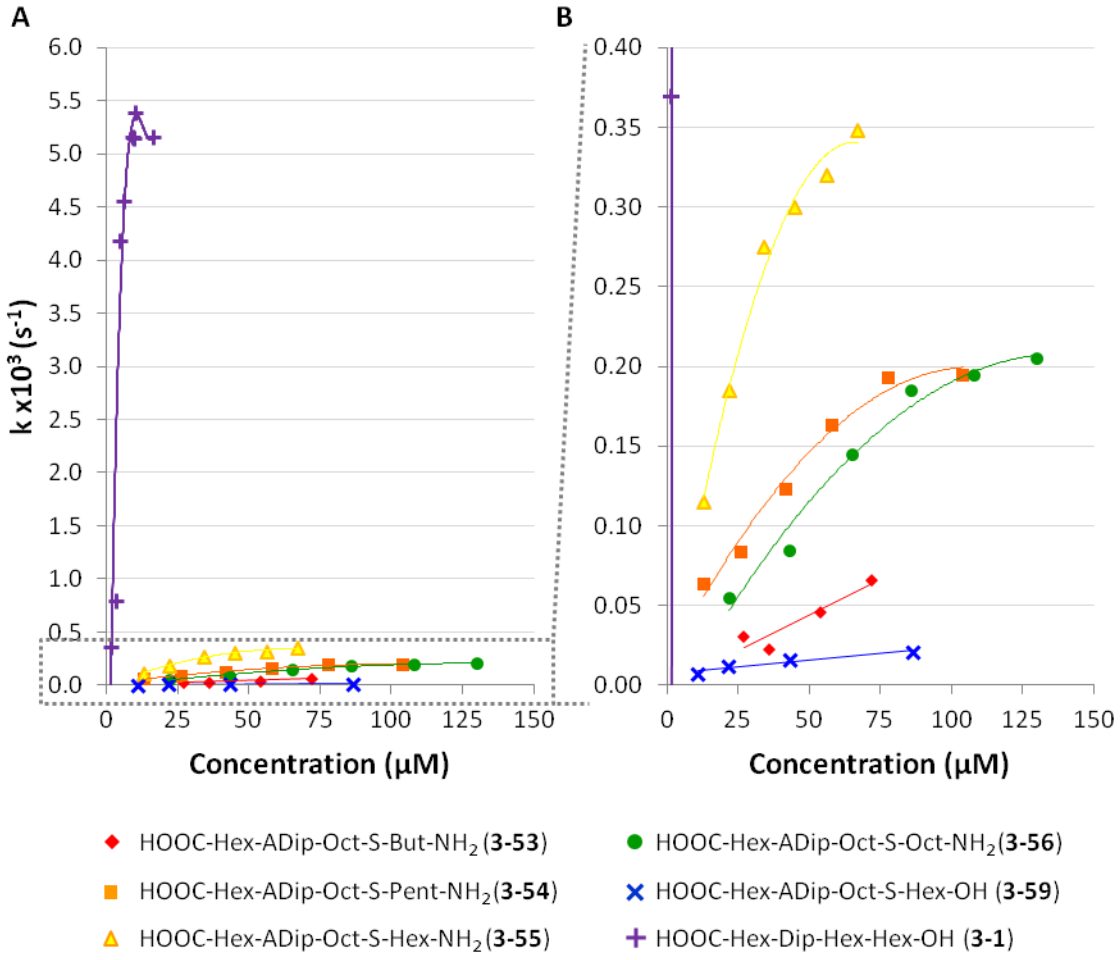

Figure 3-6: Graphs summarizing A) the experimental transport activity observed in the HPTS assay versus concentration for the synthesized compounds tested with the activity of the lead compound included for reference, and B) an expansion of graph A focusing on the activity of the synthesized compounds for clarity.

As can be observed from the data, contrary to predictions, the activity of all synthesized compounds was significantly lower than that observed for the lead compound. For example, the most active of the newly synthesized compounds, $^{-}$OOC-Hex-ADip-Oct-S-Hex-NH_3^+ (**3-55**), is approximately 45 fold less active than the lead compound (**3-1**) at an equivalent concentration of 15 μM. Unfortunately the low activity observed meant that using the HPTS vesicle assay to assess the changes in activity of the compound was not practical. Although many of the overall characteristics of the new molecules were designed to closely mimic those of the lead compound it was clear that one or more of the modifications made had a great impact on the overall transport activity.

3.8 Fluorescence Based Assay of Compound Partitioning

One potential reason for the poor observed transport activity was that the newly synthesized compounds were not effectively partitioning into the bilayer membrane as expected. As previously reported for the lead compound, the diphenylacetylene moiety exhibits environment sensitive fluorescence properties [127, 130, 131]. In aqueous solution the compound existed as an aggregate and exhibited excimer-like emission at approximately 380 nm. In less polar solvents where the compound was well dissolved, the monomer was the dominant emissive species with maximal emission at approximately 320 nm. Therefore it was possible to observe a change from aggregate emission to monomer emission upon partitioning of the compound into the non-polar membrane environment. Furthermore it was shown that after partitioning into the bilayer as a monomer the excimer emission began to increase again over time suggesting the formation of a new membrane bound aggregate. It was for this reason that the diphenylacetylene portion was retained for the newly synthesized compounds, although in a somewhat modified form.

The first step in carrying out the partitioning studies was to determine baseline fluorescence spectra for equimolar solutions of a representative compound in both a relatively non-polar organic solvent and a more polar aqueous solvent so that changes

to the fluorescence spectra of the ADip fluorophore upon addition of the vesicle solution could be properly interpreted. The representative compound chosen was $^{-}$OOC-Hex-ADip-Oct-S-But-NH_3^+ (**3-53**). The organic solvent chosen was acetonitrile while the aqueous solvent was the 0.1M NaCl, 0.01M Na_3PO_4, pH 6.4 external buffer solution used for the HPTS assay. The two spectra obtained showed the same wavelength of maximal excitation at 324 nm but marked differences in both fluorescence intensity as well as the wavelength of maximal emission as presented in Figure 3-7 below. The organic solution showed approximately thirty-fold higher emission intensity with maximal emission at 348 nm as compared to the maximum emission at 402 nm for the compound in aqueous solution.

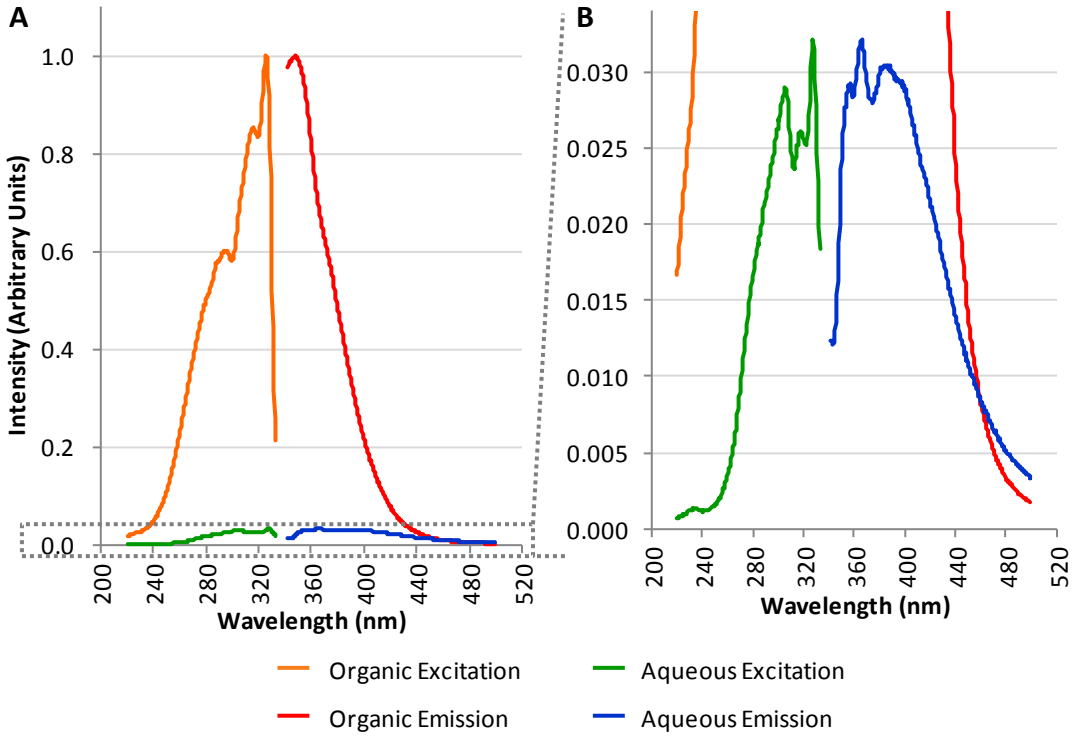

Figure 3-7: A) Excitation and emission spectra of 62 µM solutions of $^{-}$OOC-Hex-ADip-Oct-But-NH_3^+ (**3-53**) in acetonitrile and water and B) a vertical expansion of the first spectra in order to better show the spectra of the aqueous solution.

The observed red shift in the emission spectra is suggestive of excimer like emission which arises from an excited state complex. Excimer emission has been shown to occur for diphenylacetylene and structurally related chromophores such as the Dip

moiety found in the lead compound HOOC-Hex-Dip-Hex-Hex-OH (**3-1**) [130, 127]. The decrease in fluorescence intensity was hypothesized to be due to the formation of aqueous aggregates which eventually precipitated from solution due to the poor solubility of the compound in water. The observed excimer like emission was also indicative of aqueous aggregation as pre-aggregation would enhance the observation of this type of emission.

The next experiment carried out was to observe the evolution of the fluorescence emission spectra of a buffered aqueous solution of the compounds upon the addition of a sample of vesicles containing the same buffered solution. Data for the compounds $^{-}$OOC-Hex-ADip-Oct-S-But-NH_3^+ (**3-53**) and $^{-}$OOC-Hex-ADip-Oct-S-Oct-NH_3^+ (**3-56**) are presented below in Figure 3-8 as representatives of the types of behavior observed in this assay. Other compounds tested showed behaviors intermediate to those of these two compounds.

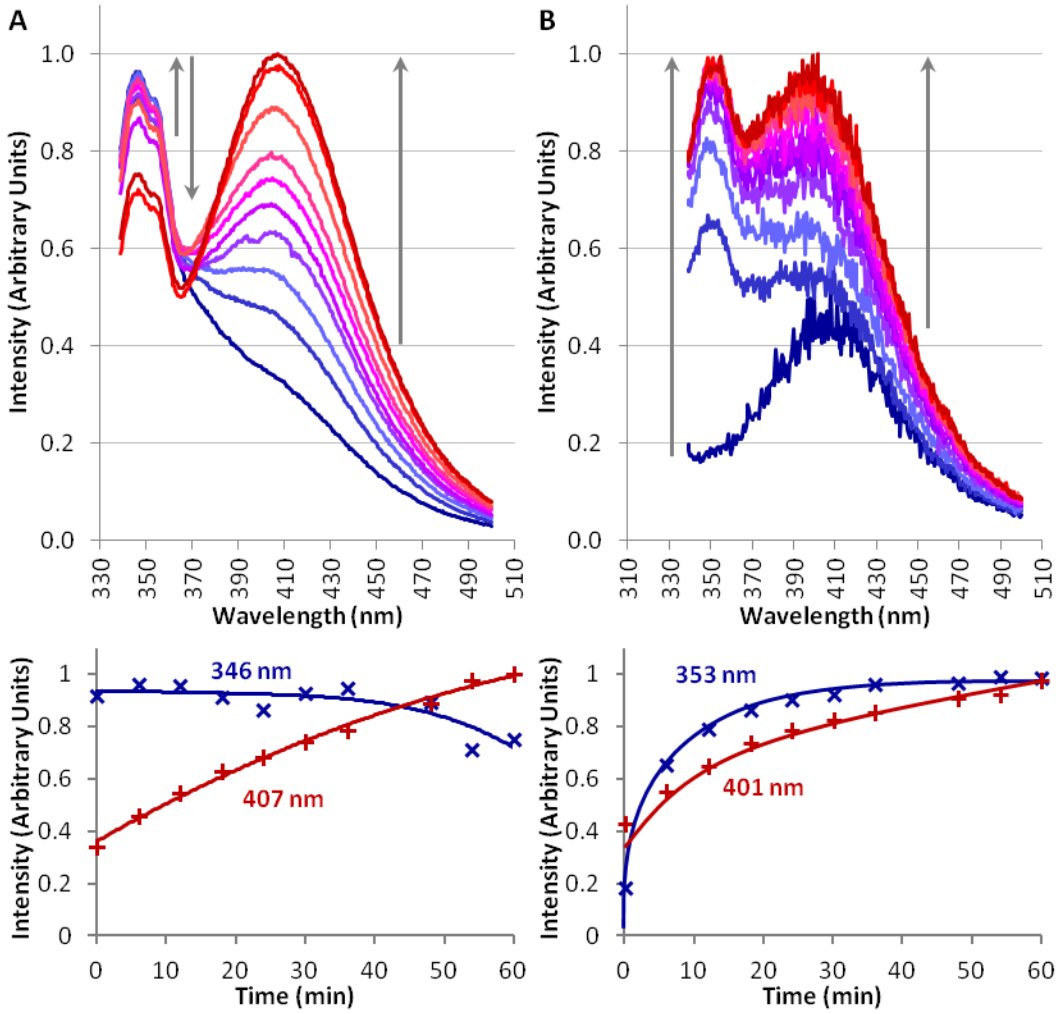

Figure 3-8: Top panel: time lapsed emission spectra spanning a one hour period after introduction of vesicles of 16 µM solutions in aqueous buffer of A) $^{-}$OOC-Hex-ADip-Octi-S-But-NH_3^+ (**3-53**) and B) $^{-}$OOC-Hex-ADip-Oct-S-Oct-NH_3^+ (**3-56**) excited at 324 nm. Spectra are coloured from dark blue (time = 0 min) through intermediate shades to dark red (time = 60 min). Bottom panel: corresponding graphs of the changes in key emission wavelengths for the data presented in the top panel.

As can be seen from both sets of time lapsed spectra there are marked changes in the emission profiles of both compounds upon the addition of the solution of vesicles. The fact that the spectra change is indicative of the environment sensitive ADip fluorophore moving from one environment to another; most likely the partitioning of the compounds into the bilayer membrane. This evidence suggests that the successful partitioning of the compounds into the bilayer has been achieved and is therefore an unlikely reason for the poor activity observed for this series of compounds. More

interesting were the differences in the changes observed for each compound and the interpretations made from these observations.

The $^{-}$OOC-Hex-ADip-Oct-S-But-NH_3^+ (**3-53**) compound initially shows relatively high emission intensity at approximately 350 nm which was attributed to emission from the monomeric form of the compound and very low emission from the approximately 400 nm which was attributed to excimer like emission from an aggregated species. Over time the higher energy emission from the monomer was seen to initially exhibit a very modest increase in intensity before a more marked decrease. On the other hand the lower energy excimer emission was seen to increase steadily before reaching some maximal value at which point no further increase was observed. Together these observations were interpreted as follows; the monomeric form of the compound partitioned rapidly into the bilayer membrane of the vesicles (emission at approximately 340 nm) and once this partitioning had occurred the monomers were then able to diffuse within the bilayer membrane to form membrane bound aggregates (emission at approximately 400 nm), this aggregation resulting in the gradual decrease in membrane associated monomer concentration and therefore the concomitant decrease in fluorescence emission from 340 nm. This type of behavior was similar to that previously observed for the lead compound HOOC-Hex-Dip-Hex-Hex-OH (**3-1**).

The compound $^{-}$OOC-Hex-ADip-Oct-S-Oct-NH_3^+ (**3-56**) showed markedly different behavior in the assay. Initially this compound showed essentially no emission attributable to the monomeric form at approximately 350 nm but relatively high emission at approximately 400 nm which was attributed to excimer like emission from an aggregate form of the compound. Over time both the emission at approximately 350 nm, from the monomeric compound, as well as the emission at approximately 400 nm, due to the aggregate form of the compound, were observed to increase gradually before reaching a maximal emission. These observations were interpreted as the partitioning of the aggregate with poor aqueous solubility from the buffer into the non-polar bilayer environment where the improved solubility of the compound allowed for

the dissociation of the membrane associated aggregate into membrane associated monomers until an equilibrium concentration of each was achieved and the observed emission profile was seen to stabilize. The differences in the observed partitioning behaviours of these two compounds are likely attributable to the differences in their aqueous solubility. The slightly more soluble $^{-}$OOC-Hex-ADip-Oct-S-But-NH_3^+ (**3-53**) was less prone to aggregation and therefore had a non-negligible aqueous monomer concentration so initial partitioning of the compound into the non-polar bilayer environment as individual monomers was possible. The less soluble $^{-}$OOC-Hex-ADip-Oct-S-Oct-NH_3^+ (**3-56**) compound showed no appreciable aqueous monomer concentration and therefore initially partitioned into bilayer membrane as an aggregate. Once in the non-polar environment of the lipid bilayer the loss of the hydrophobic effect holding the aggregates together resulted in the equilibrium between aggregate and monomeric forms of the compound to shift towards the monomer resulting in the observed increase in emission associated with the monomer.

Regardless of the inferred mechanism of partitioning into the bilayer membrane the observed changes to the fluorescence spectra of the compounds upon the introduction of vesicles ruled out a lack of partitioning as the reason for the low transport activity observed. Other possible explanations for the low activity had to be explored.

3.9 HPLC Studies on the Stabilities of the Full Length Compounds

The possibility still remained that the conditions used in the HPTS assay, namely the base pulse used to induce the concentration gradient, were sufficient to effect the truncation reaction to afford the inactive species. Although this was very unlikely since the pH of the solution used in the HPTS experiment only varies between approximately 6.4 before and 7.4 after the addition of the sodium hydroxide, it seemed a worthwhile exercise to explore the truncation and thioester exchange reactions a little further.

One experimental method that allowed for monitoring the changes in concentration of the full length compound over time was quantitative HPLC. In order to perform quantitative HPLC studies an appropriate 'standard' chromophore which was unreactive and possessed similar mobility to the full length compounds under the conditions used for running the samples was required. Rather than trying to find an existing compound that could act as the standard it was decided to synthesize a new small molecule that would also incorporate the ADip moiety. This new standard would also serve the purpose of acting as a UV calibration standard for the ADip chromophore allowing for the determination of its extinction coefficient. The extinction coefficient would in turn allow for the accurate determination of the concentrations of all future solutions of the full length compounds containing the ADip chromophore.

The synthetic target that was decided upon consisted of the ADip chromophore with symmetrical triethylene glycol monomethyl ether tails attached via ester linkages (Compound **3-64**, Scheme 3-16). These groups were chosen as ethylene glycols are relatively polar and are known to enhance the solubility [132] of compounds in polar solvents such as water while also being quite inert. The ethylene group directly between the oxygen of the ester and the oxygen of the nearest ether group of the tail should also serve to shield any effects on the spectroscopic properties that the electronegative oxygen atom of the ether could potentially have on the ADip chromophore. The synthesis of this standard ADip chromophore was carried out according to Scheme 3-16 using analogous conditions to those discussed previously for the synthesis of the various target ADip containing thioester compounds.

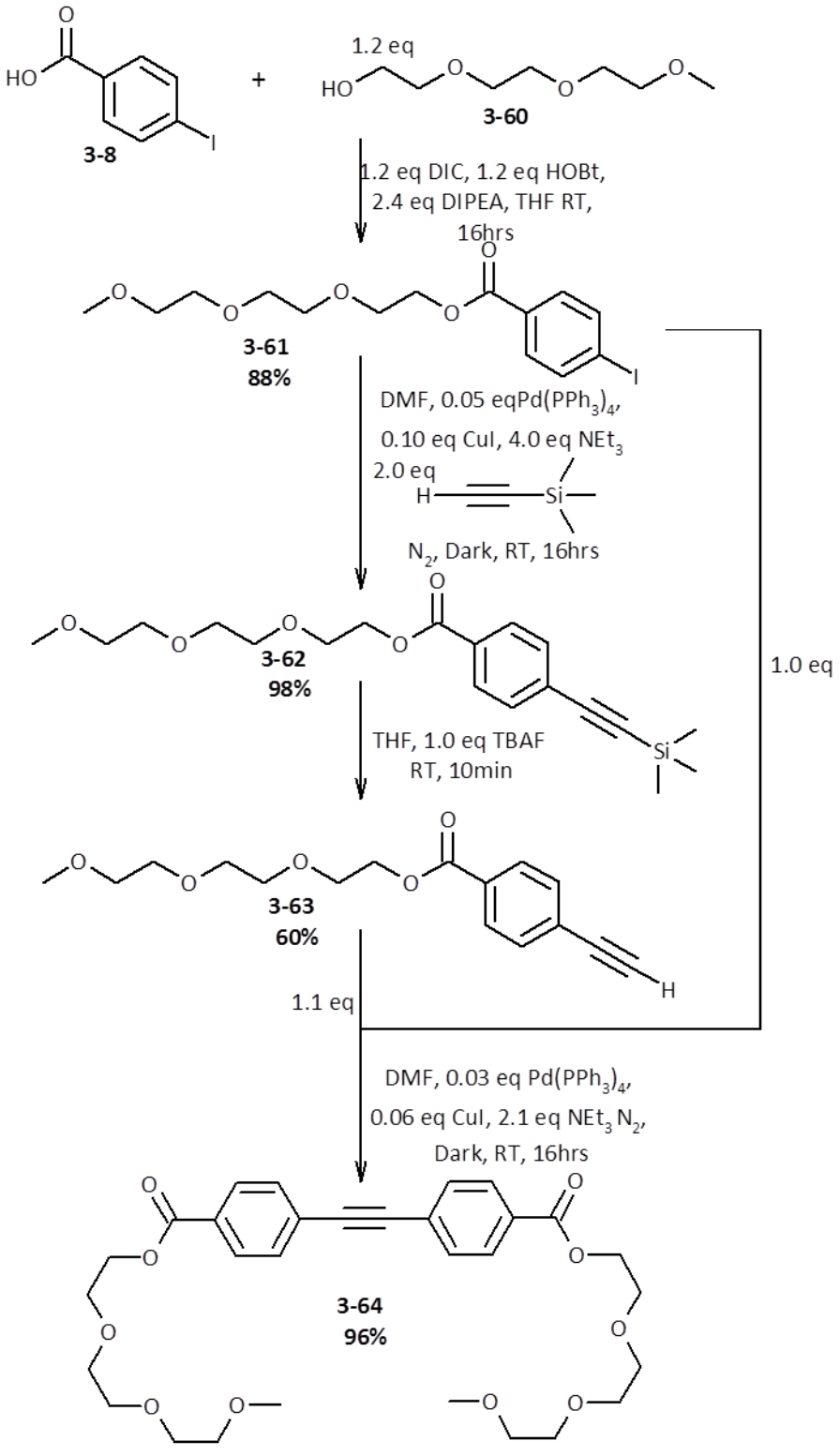

Scheme 3-16: The synthesis of the ADip chromophore standard (**3-64**).

With the purified standard in hand the first task was to determine whether it had similar mobility to the full length oligomers. When running in neat acetonitrile at a flow rate of 1.5 mL per minute through a non-polar C18 semi-preparative column the full length oligomers possessing amine termini (Compounds **3-53** - **3-56**, Table 3-1) were all found to have retention times of approximately four minutes; the synthesized standard (**3-64**) on the other hand was found to have a retention time of approximately 6.7 minutes under these same conditions. The alcohol terminated compounds (Compounds **3-57** and **3-59**, Table 3-1), requiring a slightly faster solvent flow rate of 2.0 mL per minute were found to have retention times of approximately 8.6 minutes while the standard eluted at approximately 4.7 minutes. These observations confirmed that the synthesized compound had appropriate mobility relative to the full length compounds under the conditions used to act as an HPLC calibration standard.

A UV/Visible spectroscopy calibration curve of the standard compound in acetonitrile was also obtained (see Appendix 1: Experimental details for spectra). It was found to have two absorbance maxima at 305 and 323 nm with extinction coefficients of 43500 and 39400 $L \cdot cm^{-1} mol^{-1}$ respectively. These values corresponded closely to literature values reported for structurally related compounds [133].

With the retention times and spectroscopic properties of the standard compound characterized the HPLC based studies of compound stability were carried out. Experiments were carried out by purifying small samples of the respective full length compounds which were then diluted and the concentrations of these determined from the intensity of their UV/Visible absorbance spectra. To these solutions were added a known quantity of the standard compound as well as any additional reagents such as basic catalysts. The mixtures were then analyzed by HPLC at varying time intervals in order to monitor changes in the ratio of the integration of the peaks due to the full length compounds versus the standard compound. Some representative data of the behaviors observed are presented in Figure 3-9 below for the compounds $^{-}$OOC-Hex-ADip-Oct-S-Hex-NH_3^+ (**3-55**) and ^{H}OOC-Hex-ADip-Oct-S-Hex-OH (**3-59**).

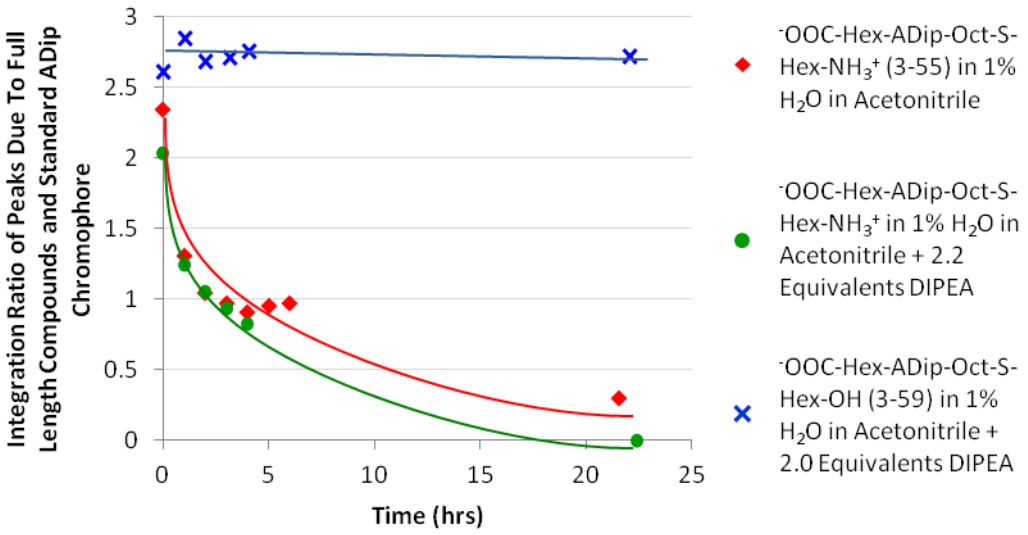

Figure 3-9: Graphs of the ratio of the integration of the signals due to the full length compounds **3-55** and **3-59** and the standard ADip chromophore compound (**3-64**) versus reaction time. The lines are meant to guide the eye and do not represent fits for the data.

From this graph several features of the reactivity of the compounds are apparent. Firstly, the amine terminated compound $^{-}$OOC-Hex-ADip-Oct-S-Hex-NH_3^+ (**3-55**) showed relatively rapid decomposition with a half-life of approximately two hours as can be seen from the decrease in the ratio of the integration of the signals due to this compound and the standard ADip chromophore (**3-64**) over time. This rate was however unaffected by the addition of DIPEA as a base. The likely reason for this lack of rate dependence on base concentration was that the extent of proton transfer from the terminal ammonium group of the compound to the added DIPEA was insufficient to allow for the truncation reaction to occur.

In addition under the conditions used the alcohol terminated compound $^{-}$OOC-Hex-ADip-Oct-S-Hex-OH (**3-59**) showed no truncation reaction occurring even in the presence of base, as can be seen from the relatively stable ratio between the integration of the peaks due to this compound and the standard ADip chromophore (**3-64**). Again, the alcohol terminus is in itself a poor nucleophile and the DIPEA base used was likely too weak to effectively deprotonate it to the alkoxide in order to improve its nucleophilicity.

Although it would have been interesting to subject these compounds to harsher basic treatments in order to observe the effects on the rates of truncation, experimental limitations prevented this. Firstly, since the compounds studied were best solubilized in acetonitrile many of the stronger hydroxide bases available were impractical due to solubility constraints and the potential of clogging the HPLC instrument. In addition the use of a strong base could lead to the hydrolysis of the ester groups in the full length molecules as well as in the standard ADip chromophore which would complicate the HPLC analysis via the generation of other UV absorbing species which would appear in the chromatogram. A further concern was the unknown stability of the column packing towards strongly basic conditions. For these reasons it was decided to err on the side of caution rather than to pursue HPLC based studies using more strongly basic reagents.

Despite the lack of further experimentation the study managed to reinforce the hypothesis that under neutral pH conditions, such as those usually employed in the bilayer clamp experiment, the amine terminated compounds undergo a much more rapid intramolecular cyclization truncation reaction than the corresponding alcohols. Therefore in order for the alcohol terminated compounds to be effectively truncated quite basic conditions would need to be employed which may not be compatible with the lipid vesicles and bilayers commonly used in the Fyles lab. With this information it seems that future efforts to use the intramolecular cyclization reaction to truncate compounds should focus on amine terminated compounds.

3.10 Model NMR Studies of Truncation and Thioester Exchange Reactions

In order to gain a better understanding of the intramolecular cyclization truncation reaction than obtained from the HPLC studies it was decided to try a series of NMR spectroscopy based experiments. These experiments have the advantage of allowing the use of more basic conditions than possible for the HPLC studies but the disadvantage that they require higher quantities of material. In addition to investigating the intramolecular cyclization truncation reaction it was decided that an exploration of

the thioester exchange reaction using NMR spectroscopy techniques was also worthwhile.

Although the full length compounds were already in hand it was decided that it would be best to use shorter analogs of the nucleophilic terminus and thioester linkage for the studies for a few different reasons. Firstly, since the NMR experiments require relatively concentrated solution to obtain quality results it was undesirable to sacrifice any of the full length compounds which required significant synthetic investments. It was also desirable to approximate the aqueous conditions present in the transport assays as closely as possible. Whereas the relatively low aqueous solubilities of the full length compounds were sufficient for the purposes of the transport assays, the concentrations required to obtain a useful NMR spectra are far higher. A compound of significantly lower molecular mass it should be much less prone to aggregation via the hydrophobic effect and therefore possess higher solubility. In addition by reducing the overall number of proton signals from the molecule the analysis of the complex mixture of compounds expected from the reactions was simplified.

To this end a molecular analog consisting of the nucleophilic amine terminus and thioester linkage of the full length molecule was synthesized. Rather than synthesizing analogs for all of the compounds of varying length it was decided to initially focus only on the six carbon long linker between the nucleophilic terminus and the thioester linkage. The justification for this choice was that it was believed that as a starting point the cyclization reaction of the six carbon long linker to form the seven membered ring would be sufficiently slow to allow for the effective monitoring of the process by NMR. The reaction could also be sped up with an appropriate base as catalyst or by increasing the temperature in the event that it proved too slow. With respect to the pendant group on the sulfur side of the thioester linkage the *n*-propyl group was chosen. This group was sufficiently short as to minimize interference with other important proton signals in the NMR spectra and the starting thiol, 1-propanethiol, was a relatively easily

handled, although exceedingly odiferous, liquid unlike the shorter methanethiol or ethanethiol.

The synthesis of the amine terminated model compound (**3-67**), shown in Scheme 3-17, began from the previously prepared 6-[(*tert*-butoxycarbonyl)amino]hexanoic acid (**3-14**). The thioester linkage between this compound and 1-propanethiol was carried out under the previously developed DIC, HOBt, DIPEA conditions to afford S-propyl 6-[(*tert*-butoxycarbonyl)amino]hexanethioate (**3-65**). The final step in the synthesis was the removal of the *t*-Boc protecting group from the amine terminus of the compound. This was achieved by reaction of the compound in a methanolic solution of hydrochloric acid. An initial attempt at the work-up of this reaction involved the careful neutralization of the resulting acidic solution using saturated sodium bicarbonate, unfortunately the product recovered after this step was the cyclized ε-lactam (**3-66**). This result proved a mixed blessing. From a synthetic standpoint it was a clear failure as the desired compound was not obtained, however from the perspective of the viability of the intramolecular cyclization reaction it suggested that using this strategy for the truncation process was sound. This minor setback in the synthesis was easily bypassed by isolating the desired compound as the ammonium chloride salt, 6-oxo-6-(propylsulfanyl)hexan-1-aminium chloride (**3-67**), although this would require the addition of an equivalent of base during any subsequent studies to generate the amine in situ.

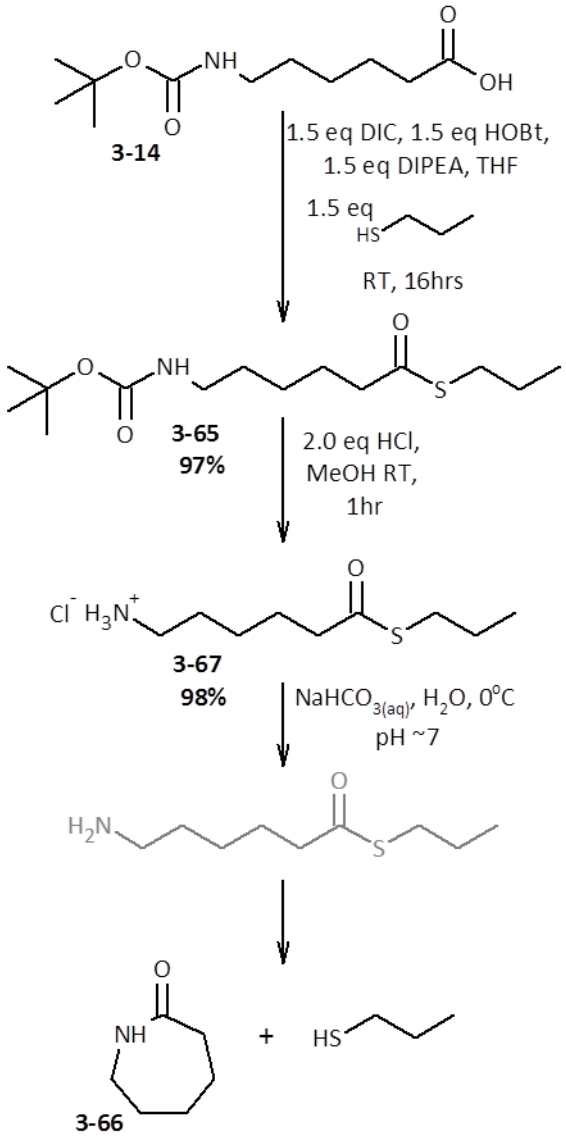

Scheme 3-17: Synthetic scheme for the synthesis of the model compound for NMR based studies, 6-oxo-6-(propylsulfanyl)hexan-1-aminium chloride (**3-67**).

With the model compound in hand focus turned to NMR studies of both the thioester exchange and intramolecular cyclization reactions of this representative amine terminated compound. In order to investigate the thioester exchange reaction an appropriate thiol was required to exchange with the 1-propanethiol. Benzyl thiol was selected as the proton signals from this compound, found primarily in the chemical shift range associated with the aromatic ring, are minimally interfering with the proton signals of the thioester compound (**3-67**). In addition, the chemical shift of the

methylene between the aromatic ring and the thiol at approximately 2.5 ppm should shift considerably downfield if successfully exchanged into the thioester as the electronegative carbonyl will withdraw electron density from the adjacent nuclei.

To perform the experiment equimolar quantities of the ammonium chloride salt of the thioester compound (**3-67**) and benzyl thiol were dissolved into deuterated DMSO. An NMR spectrum of this solution was taken immediately after mixing and then after a period of approximately 120 minutes. Unsurprisingly neither reaction was observed to have occurred under these conditions after this period of time. No intramolecular cyclization reaction was expected since the amine terminus was still protonated as the ammonium ion and was therefore non-nucleophilic. The thioester exchange reaction was expected to be very slow if it occurred at all due to the lack of protic solvent available to aid in solvating the ionic intermediates and facilitating the proton transfer steps in the reaction mechanism.

To this DMSO solution was added two molar equivalents of sodium deuteroxide (NaOD) in deuterium oxide (D_2O). Two equivalents were added rather than one in order to both deprotonate the ammonium ion as well as to provide some catalytic base for the thioester exchange and intramolecular cyclization reactions. NMR experiments were then run at various time intervals after this addition of base starting after approximately 30 minutes in order to monitor the progression of the thioester exchange and intramolecular cyclization reactions. The spectra taken are provided below in a stacked arrangement (Figure 3-10) as well as the integration data for the most important signals summarized in the graph below (Figure 3-11).

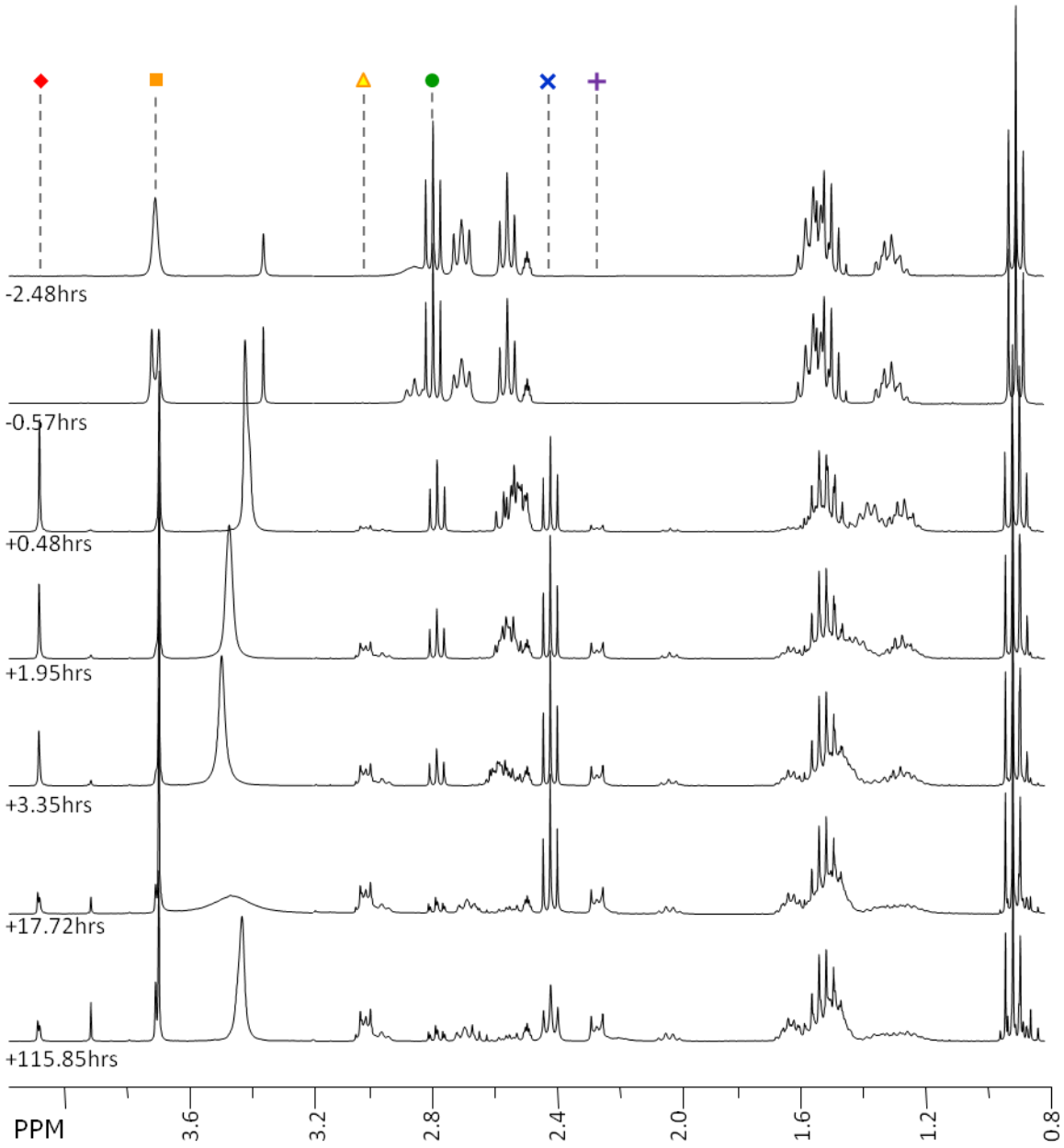

Figure 3-10: Time lapsed proton NMR spectra run on a 1:1 stoichiometric mixture of 6-oxo-6-(propylsulfanyl)hexan-1-aminium chloride (**3-67**) and benzyl thiol, focusing on the region between 4.2 and 0.8ppm. The aromatic region did not show diagnostic changes so was omitted from these spectra for clarity. Times associated with each spectrum are relative to the addition of two equivalents of NaOD to the solution. Symbols at the top of the stacked spectra correspond to those found in the graph below and indicate chemical shifts of peaks to which they are assigned.

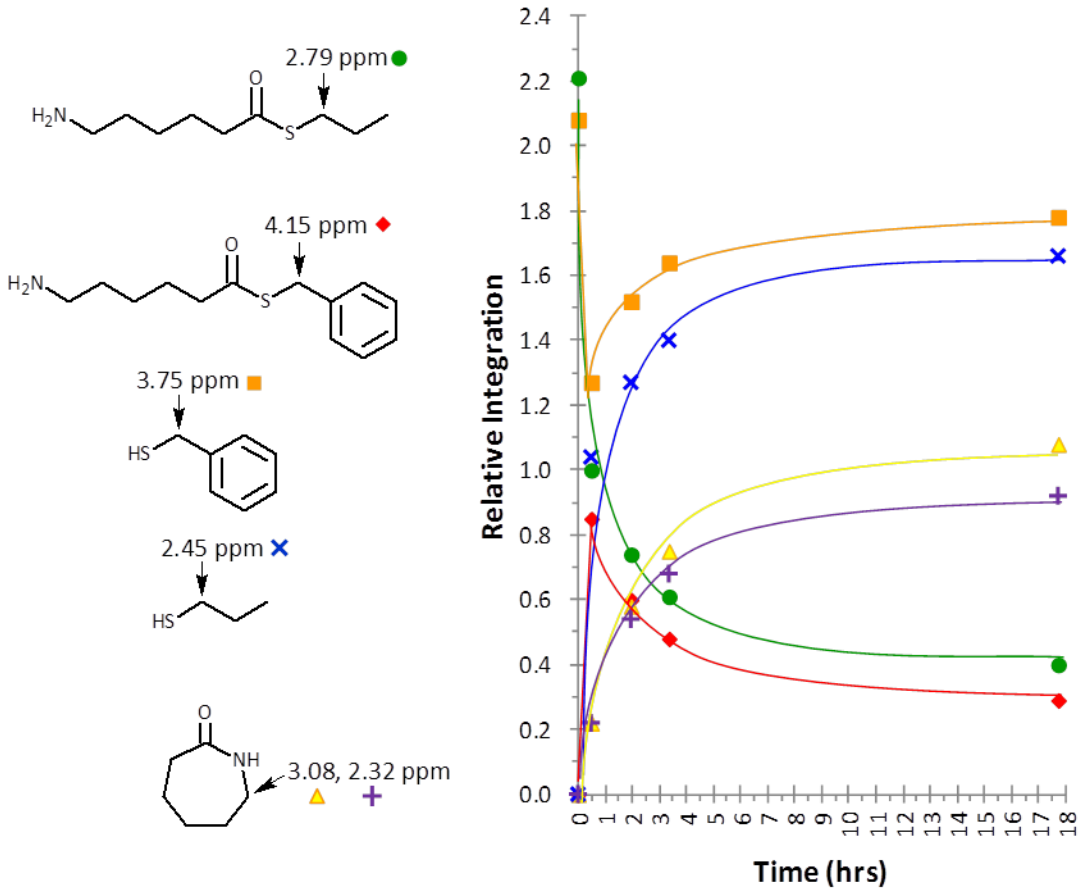

Figure 3-11: Graph of the relative integrations of the important signals from the proton NMR versus time. The structural legend on the left illustrates the protons associated with each chemical shift as well as the associated symbol used in the graph. Lines provided on the graph are not accurate lines of best fit and are only intended to help guide the eye.

Several changes were observed in the proton NMR spectrum taken 30 minutes after the addition of base which indicated that the thioester exchange reaction had taken place. Among these were the appearance of a new singlet at 4.15 ppm and the concomitant decrease of the signal at 3.75 ppm. The new signal at 4.15 ppm was due to the methylene group of the newly formed benzyl thioester while that at 3.75 ppm was due to the methylene group of the starting benzyl thiol; the downfield shift of the signal from the thioester relative to the thiol is due to the electron withdrawing nature of the carbonyl group present in the ester. Other evidence of the successful thioester exchange reaction was the development of a new triplet at 2.45 ppm as well as the concomitant decrease in the integration of the triplet at 2.79 ppm. These two signals

were due to the methylene group α to the sulfur atom in the free propane thiol and the propylthiolate ester respectively. The behavior of the integration of these signals relative to each other was indicative of the disappearance of the propylthiolate ester and the liberation of propanethiol as the thioester exchange reaction replaces the propylthiolate with the benzylthiolate. From this spectrum it was already clear that the thioester exchange reaction was very fast under these conditions as the relative stoichiometry of the two thioester products was near one to one after only thirty minutes; this result was expected once the system had reached equilibrium between the two thioesters provided the two compounds had comparable stability.

Another important observation from these signals was the relative integrations observed between the benzylthiolate ester methylene signal at 4.15 ppm and the propylthiolate ester methylene signal at 2.79 ppm. If only the thioester exchange reaction was occurring in this system it would be expected that the total integration of these two signals should add up to that of the initial integration observed for the propylthioate ester methylene signal since the generation of the benzylthioate ester results in the consumption of the propylthioate ester in a one to one stoichiometry. The sum of the integration of these two signals in the first spectrum taken after the addition of base was found to be 1.84 proton equivalents versus an initial integration of 2.21 proton equivalents for the propylthiolate ester methylene in the solution before reaction; a difference of approximately 0.4 proton equivalents. This disparity in integration can be explained by the occurrence of the other reaction being studied, the intramolecular cyclization reaction. This reaction results in the generation of ε-lactam and either propanethiol or benzylthiol while consuming the propylthiolate ester and benzylthiolate ester respectively. If this reaction was occurring the total concentration of thioesters in the reaction mixture would decrease over time while the concentration of lactam would increase since the intramolecular cyclization reaction is irreversible due to the stability of the amide bond of the lactam under these conditions. Further evidence of the successful intramolecular cyclization reaction is the observation of two new signals in the NMR spectrum at 3.08 and 2.32 ppm. These signals appear as

complex multiplets and are due to the two magnetically inequivalent protons on the methylene α to the nitrogen of the ε-lactam. The integration of these two signals add up to approximately 0.4 proton equivalents in the spectrum taken approximately 30 minutes after the addition of base which accounts for the decrease in the integration observed for the sum of the methylene signals α to the sulfurs in the two thioester molecules. The fact that these signals are relatively small after this time is indicative of the intramolecular cyclization reaction being fairly slow under these conditions in comparison to the thioester exchange reaction which had more or less reached equilibrium in the same time.

Monitoring of the reactions by proton NMR continued over the course of several days. During this time the signals in the proton NMR due to the methylene groups α to the sulfur of the thioester of both thioester compounds were observed to diminish while the signals from the inequivalent protons of the methylene group α to the nitrogen of the lactam as well as the proton signals of the methylenes α to the sulfur of the free thiols increased. Together these changes revealed the progression of the intramolecular cyclization reaction of the thioester compounds over time. There is some error in the relative integration data due to the increasing overlap of many different proton signals in the complex mixture but in general the trends are indicative of the time course of the reactions.

Over the course of the experiment other signals of interest were seen to develop in the proton spectrum. Of particular interest were the small singlets observed between 3.6 and 4.0 ppm. Due to the chemical shifts of these signals they are likely representative of protons on carbons next to electronegative atoms and the fact that they are singlets is indicative that they are not coupling to any adjacent protons. One hypothesis to account for these observed signals is the formation of various disulfide compounds in the reaction mixture. Disulfides are a commonly observed product of the reaction between two thiols in the presence of oxygen as an oxidant [134]. Since no effort was made to conduct the experiment under an inert atmosphere the formation of

disulfide compounds is a possibility. In addition it is known that disulfide formation is catalyzed under basic conditions much like those present in the reaction being studied. Since there are two different thiols present in the reaction, propane thiol and benzyl thiol, it is likely that all three possible disulfide compounds, the two symmetrical disulfides (**3-68** and **3-70**) as well as the dissymmetric one (**3-69**), are being formed in this experiment (Figure 3-12). The singlet nature of the signals suggests that these are due to the benzylic methylenes of the two benzyl containing disulfide products (**3-68** and **3-69**). Fortunately, if these signals are indeed due to the disulfides, the reactions appear to be quite slow relative to the time scale of the transport assays so should have minimal effect on any observed activities.

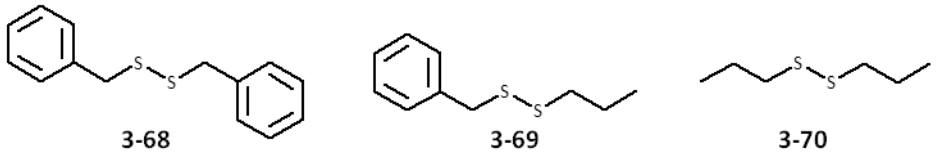

Figure 3-12: Possible disulfide products formed from the reaction of benzylthiol and propylthiol in the NMR study.

Concurrent to the proton NMR spectra, carbon spectra were also obtained. Although the nature of the carbon NMR experiment meant that relative integration data were of little use and that the decreased sensitivity would likely result in the failure to observe all expected signals, some confirmatory observations were still possible. Important regions of the carbon spectra obtained are presented in stacked format in Figure 3-13 below.

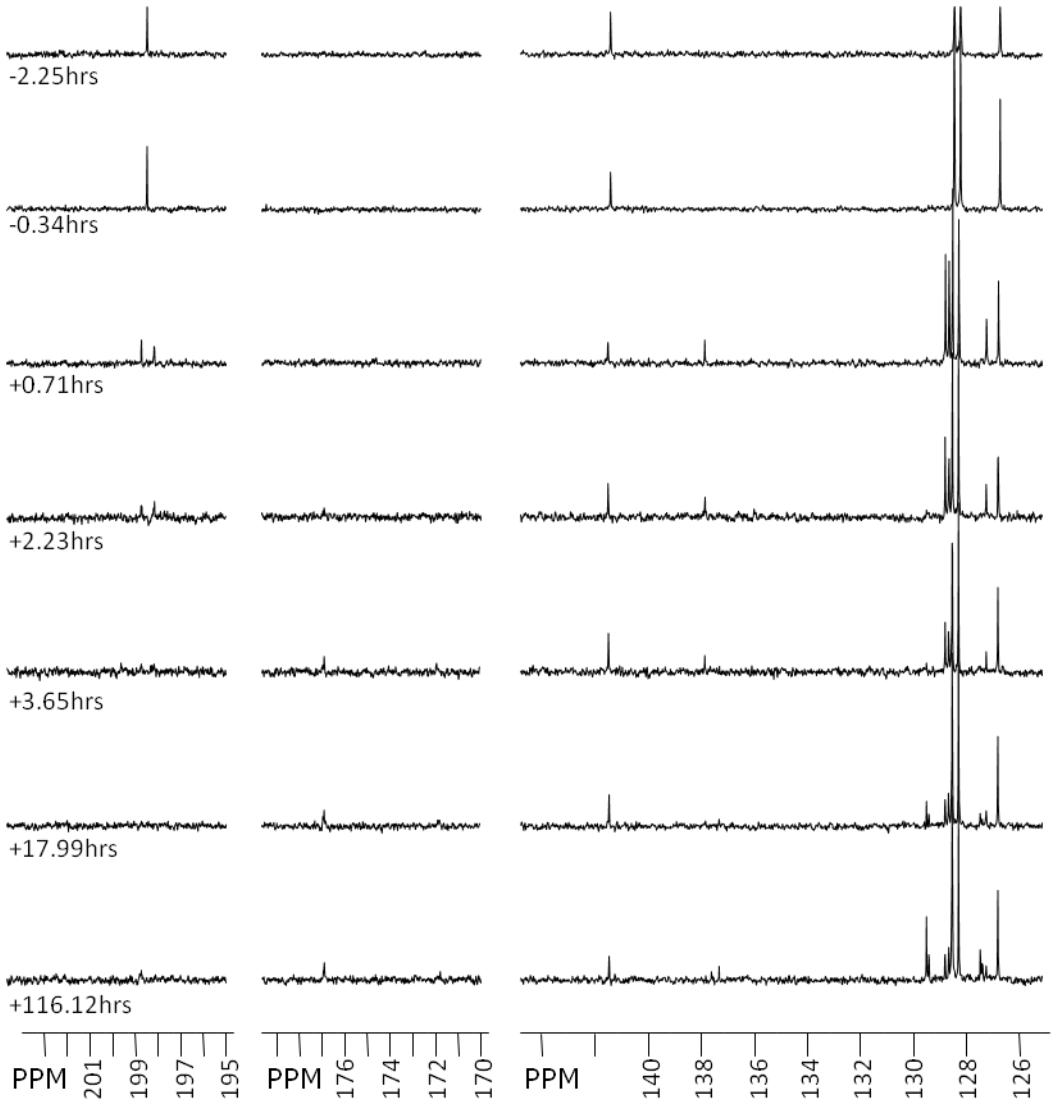

Figure 3-13: Time lapsed carbon NMR spectra run on a 1:1 stoichiometric mixture of 6-oxo-6-(propylsulfanyl)hexan-1-aminium chloride(**3-67**) and benzyl thiol focusing on the downfield regions of the spectra. Data below 125 ppm were omitted due to the complexity of the region and the lack of diagnostic signals.

The first carbon spectrum obtained after the addition of the base at +0.71 hours, although not useful for determining the relative concentrations of species present, did provide additional proof of the successful thioester exchange reaction. For example, as compared to the pre-reaction spectrum where only one signal was present at approximately 198 ppm, there were two signals in this region in the first spectrum taken after the addition of base. Signals found in this region are characteristic of the carbonyls found in thioester groups and the presence of two of them indicated that two unique

thioester containing species were present. In addition, where there were four aromatic signals between 125 and 145 ppm present for the unreacted mixture of benzyl thiol and the model thioester (**3-67**) before the addition of base, after the addition of base there were eight such signals present. This was indicative of two different species containing monosubstituted benzene rings as would be the case if both benzyl thiol and the benzyl thioester compound were both present in solution. There were also many more signals in the alkyl region of the spectrum (not shown), as these are difficult to assign unambiguously they served only to indicate that a more complex mixture than just the benzyl thiol and propylthioate ester was present in solution.

In agreement with the proton NMR spectra, the carbon spectra showed a gradual loss of the signals due to the carbonyls of the two thioester compounds along with the concomitant increase in a signal at approximately 177 ppm which was assigned to the carbonyl of the amide group of the lactam. In addition, by the time the final spectrum was obtained there were at least twelve aromatic carbon signals observed. This indicated that at least three species containing monosubstituted benzene rings were present in solution. This observation provides additional evidence that the disulfide forming reaction involving benzyl thiol was occurring under these reaction conditions.

Regardless of the ambiguities in the NMR study regarding the additional species formed, the principle question of whether the intramolecular cyclization and thioester exchange reactions were viable mechanisms for the truncation and re-elongation processes had been validated. In fact the observation that the thioester exchange reaction was significantly faster than the cyclization reaction raises the possibility of using this model compound itself as the feedstock for reactivating the truncated version of the full length molecule.

In addition the rate of formation for the suspected disulfide products in the model system was also much slower than the thioester exchange reaction. This is important since once the disulfide is formed recovering the terminal thiol group

required for thioester exchange would necessitate the addition of a reducing agent therefore adding unwanted levels of complexity to the system.

A representation of the possible reaction cycles for a system involving the deactivation by the intramolecular truncation reaction, reactivation by thioester exchange with a sacrificial feedstock and disulfide formation into compounds acting as thermodynamic sinks is presented in Figure 3-14 below.

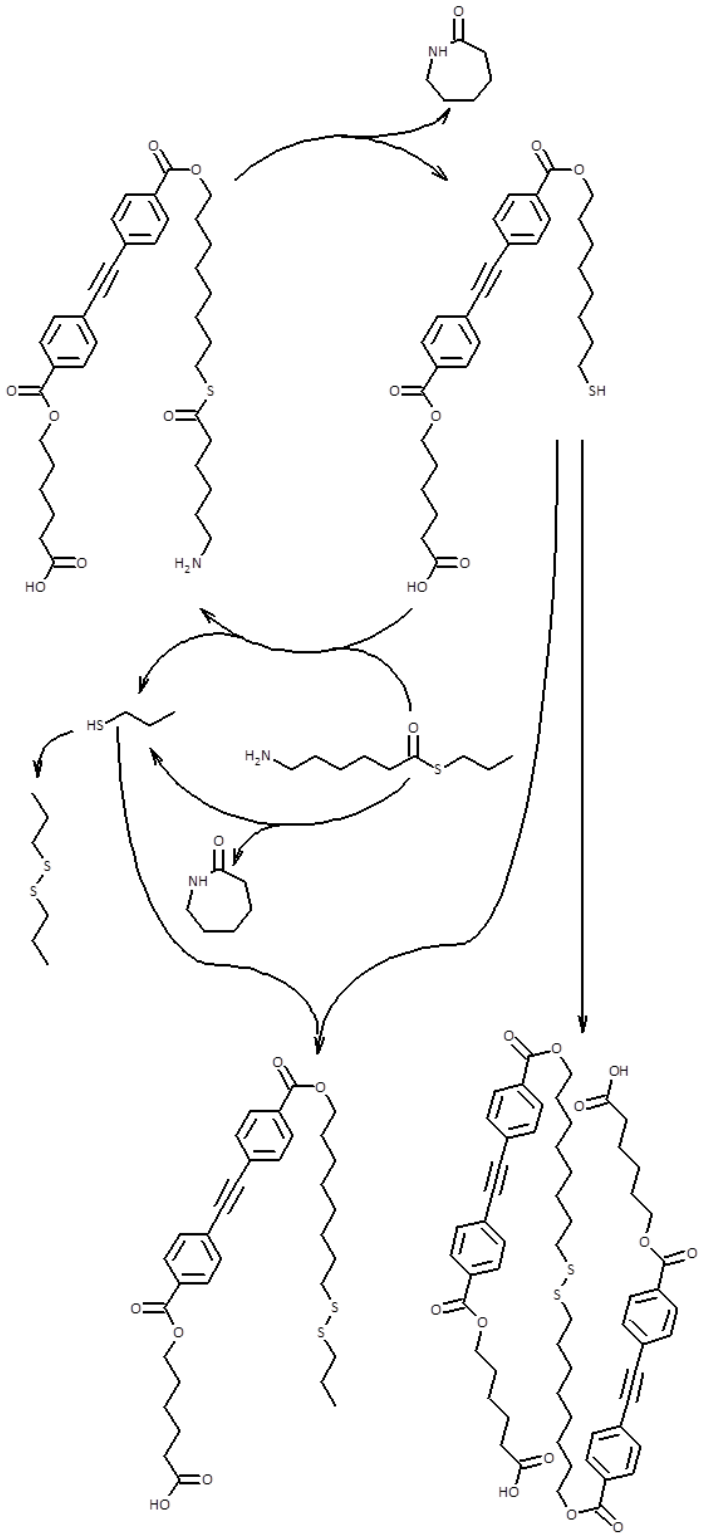

Figure 3-14: Schematic representation of a possible system for the truncation - re-elongation of the synthesized compounds based on observations made during the NMR studies of a compound acting as a model for the nucleophilic terminus and thioester linkage.

Although the study was carried out in a solvent system quite different from that of the transport activity assays due to solubility limitations of the reagents, the relative reactivities observed should translate reasonably well to the aqueous buffers used in the assays; the presence of a higher concentration of water should increase the rate of both reactions by facilitating the proton transfer steps in each mechanism.

Based on the relatively slow reaction rate observed for the intramolecular cyclization reaction even under the more basic conditions used in the NMR study as compared to the conditions present in the HPTS vesicle assay it seems unlikely that the truncation of the compound was responsible for the poor transport activity. This left only some inherent property of the compounds themselves as the culprit for these less than desirable results. Unfortunately this meant that without fundamental structural modifications to the compounds the use of this assay for the assessment of changes in activity between the full length versus truncated molecules was impractical. Despite this setback the compounds were already in hand so it was well worth the effort to assess the system further including activity studies using the bilayer clamp assay to determine if the activity of the compounds could be modulated.

3.11 Bilayer Clamp Based Transport Activity Studies

Given that the vesicle based HPTS assay revealed minimal transport activity for all of the studied compounds the burden fell upon the bilayer clamp assay to either confirm or discount the hypothesized changes in activity upon truncation of the full length compounds. As previously alluded to, it is not uncommon for compounds to show relatively high activity in one assay over the other due to the differences in the experimental set up, primarily the lipid compositions of the bilayers in each study. Although it was less than ideal to rely on single channel observations made with the bilayer clamp experiment over the bulk observations possible using vesicle based assays to observe changes in transport activity over time there remained little choice.

Due to the high sensitivity of the bilayer clamp assay multiple experiments showing similar activity profiles are required in order to confirm that a particular observation of ion transport is due to the added compound rather than any potential contaminant or defect in the bilayer. Conversely it is just as difficult to judge a compound to be completely inactive; as with any method which detects single species the axiom 'the absence of evidence is not evidence of absence' must be taken to heart. It was therefore necessary to undertake many separate bilayer clamp experiments in order to obtain as complete of a picture of the types of activity present for the compounds as possible.

The first compound studied was $^{-}$OOC-Hex-ADip-Oct-S-Hex-NH_3^+ (**3-55**) since its reactivity had been most thoroughly investigated by the NMR and HPLC studies. The initial experiment was set up using conditions that have commonly shown activity for the lead oligoester compound (see experimental for details). Fortunately, unlike for the vesicle based HPTS assay, it was quite common to reliably observe transport activity from the bilayer clamp experiment. Representative traces of the types of activity observed for this compound are presented below in Figure 3-15 to Figure 3-17 along with the summary activity grids in Figure 3-18. Recall that the different classes of potentially observable activity were assigned an associated colour (green for square tops, blue for multi-level, yellow for flickers, red for spikes and purple for erratic) which are then plotted onto a log-log grid of conductance versus open duration with the intensity of coloration indicating the relative abundance of the observed activities. This analysis provides a holistic view of the range of activities observed for a particular channel or group of related channels that is impossible by looking at individual bilayer clamp experiments. Please refer to the introductory Section 1.4.2 for a more thorough discussion of the activity grid analysis.

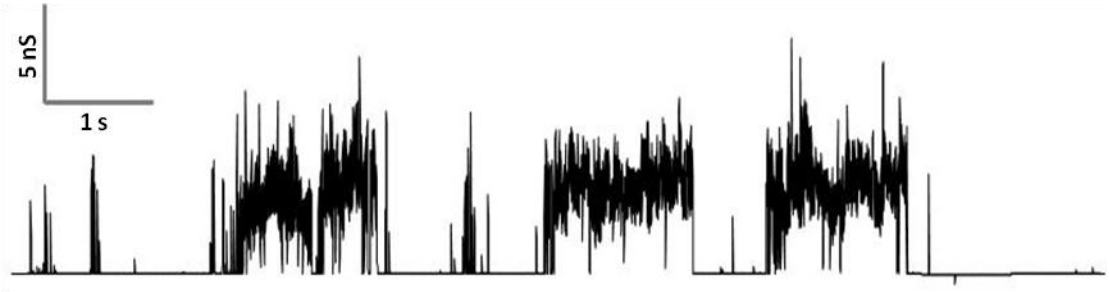

Figure 3-15: Representative trace of multi-level (blue) type activity for the compound $^{-}$OOC-Hex-ADip-Oct-S-Hex-NH_3^+ (**3-55**). Conditions: diPhyPC bilayer, 250 µM diameter aperture, Ag/AgCl electrodes, KCl junction solution and salt bridges, 1M CsCl with 10mM each of TRIS and HEPES as buffer, applied potential +160 mV.

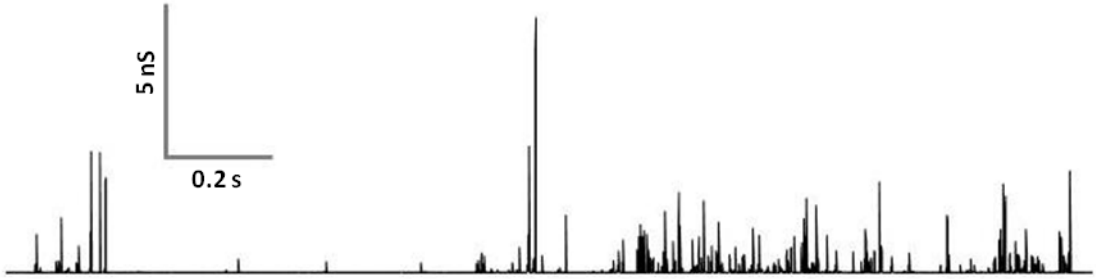

Figure 3-16: Representative trace of spiky (red) type activity for the compound $^{-}$OOC-Hex-ADip-Oct-S-Hex-NH_3^+ (**3-55**). Conditions: diPhyPC bilayer, 250 µM diameter aperture, Ag/AgCl electrodes, KCl junction solution and salt bridges, 1M CsCl with 10mM each of TRIS and HEPES as buffer, applied potential +150 mV.

Figure 3-17: Representative trace of erratic (purple) type activity for the compound $^{-}$OOC-Hex-ADip-Oct-S-Hex-NH_3^+ (**3-55**). Conditions: diPhyPC bilayer, 250 µM diameter aperture, Ag/AgCl electrodes, KCl junction solution and salt bridges, 1M CsCl with 10mM each of TRIS and HEPES as buffer, applied potential +150 mV.

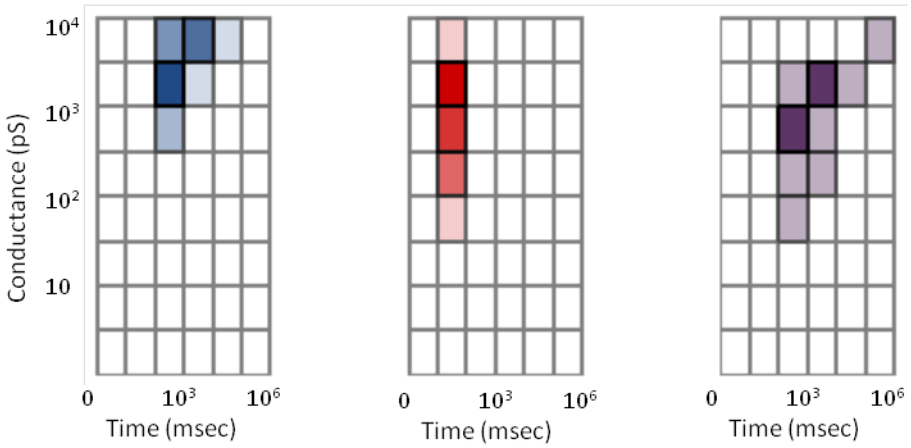

Figure 3-18: Summary activity grids for the compound $^{-}$OOC-Hex-ADip-Oct-S-Hex-NH_3^+ (**3-55**) showing the ranges of conductance and open duration for the observed multi-level (blue), spiky (red) and erratic (purple) transport activities observed.

As can be seen from these traces and activity grids, the compound shows primarily activity of the multi-level (blue), spiky (red) and erratic (purple) varieties. Interestingly, regardless of the type of activity the observed conductances were consistently quite high, in the 300 to 3000 pS range corresponding to single channel diameters of approximately 0.4 to 1.4 nm based on the Hille equation. The opening durations were also of moderately long duration (100 ms to 10 s) for the most part with some longer duration (> several minutes) events also observed. The observation of such large and long lived transport events seemed at odds with the near total lack of activity seen from the vesicle based HPTS assay, but as previously discussed the small differences between the experimental conditions of the two assays can have a marked effect on activity. These highly conducting channels are very interesting however, as they represent activity beyond what is typically observed for synthetic ion channels and further study of this class of molecule could provide some useful findings. Large and long-lived stable pores could have a number of potential applications such as acting as molecular portals for the more effective delivery of drugs [135].

Unfortunately no activity of the most easily understood and quantified square top type was observed; although this type of behavior is by no means the most commonly observed for synthetic ion channels. This lack of more regular square top activity, although unfortunate from an analytical standpoint, is not surprising given the structure

of the compound and by extension the likely nature of the transport active species. Given the large conductances observed it is impossible to conceive a membrane associated structure formed from a single $^{-}$OOC-Hex-ADip-Oct-S-Hex-NH_3^+ (**3-55**) molecule that could generate a sufficiently large pore. The transport active species must therefore be generated via the self-assembly of several molecules in order to afford a structure of sufficient size. In addition the molecule itself possesses no intrinsic features that can be envisioned as leading to a favored geometry for self-assembly, and indeed no attempt was made to introduce any specific interactions for self-assembly into the target molecules. It is therefore likely that the self-assembled superstructure is held together with weaker, non-specific interactions resulting in a transport active structure which is relatively disordered and dynamic. This dynamism is antithetic to the observation of channels with regular square top behavior which require a semi-rigid pore with a well defined internal diameter. These results are in line with the previously observed activity of the Dip containing oligoester ion channels such as the lead compound HOOC-Hex-Dip-Hex-Hex-OH (**3-1**) [105] as well as ones containing an extended version of the Dip chromophore [127].

For comparison of the effects of the two different nucleophilic termini on transport activity, studies were also carried out on the analogous alcohol terminated compound $^{-}$OOC-Hex-ADip-Oct-S-Hex-OH (**3-59**). The experiments were carried out under as similar conditions as possible to those used for the amine terminated compound. Representative traces of the types of activity observed for this compound are presented below in Figure 3-19 to Figure 3-21 along with the summary activity grids in Figure 3-22.

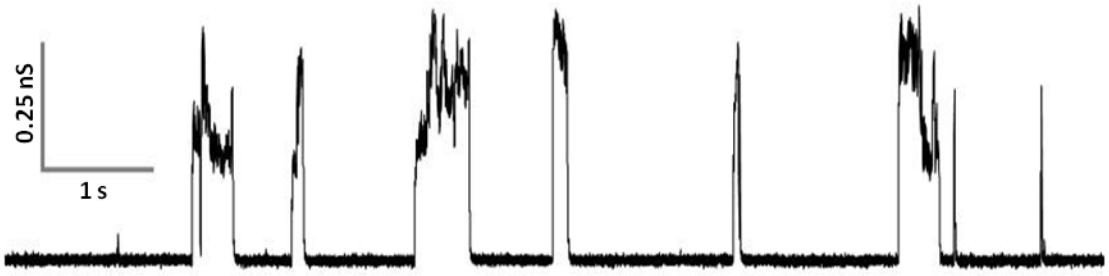

Figure 3-19: Representative trace of multi-level (blue) type activity for the compound ¯OOC-Hex-ADip-Oct-S-Hex-OH (**3-59**). Conditions: diPhyPC bilayer, 250 µM diameter aperture, Ag/AgCl electrodes, KCl junction solution and salt bridges, 1M CsCl with 10mM each of TRIS and HEPES as buffer, applied potential +150 mV.

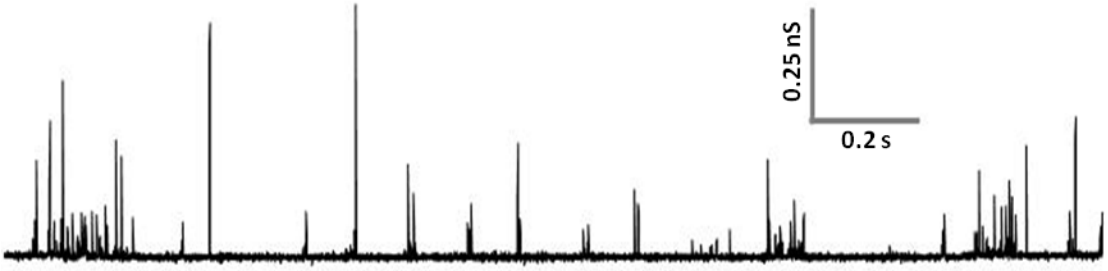

Figure 3-20: Representative trace of spiky (red) type activity for the compound ¯OOC-Hex-ADip-Oct-S-Hex-OH (**3-59**). Conditions: diPhyPC bilayer, 250 µM diameter aperture, Ag/AgCl electrodes, KCl junction solution and salt bridges, 1M CsCl with 10mM each of TRIS and HEPES as buffer, applied potential +140 mV.

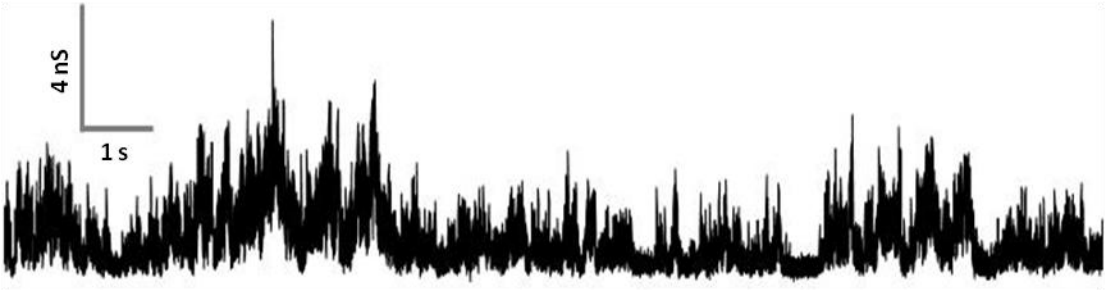

Figure 3-21: Representative trace of erratic (purple) type activity for the compound ¯OOC-Hex-ADip-Oct-S-Hex-OH (**3-59**). Conditions: diPhyPC bilayer, 250 µM diameter aperture, Ag/AgCl electrodes, KCl junction solution and salt bridges, 1M CsCl with 10mM each of TRIS and HEPES as buffer, applied potential +150 mV.

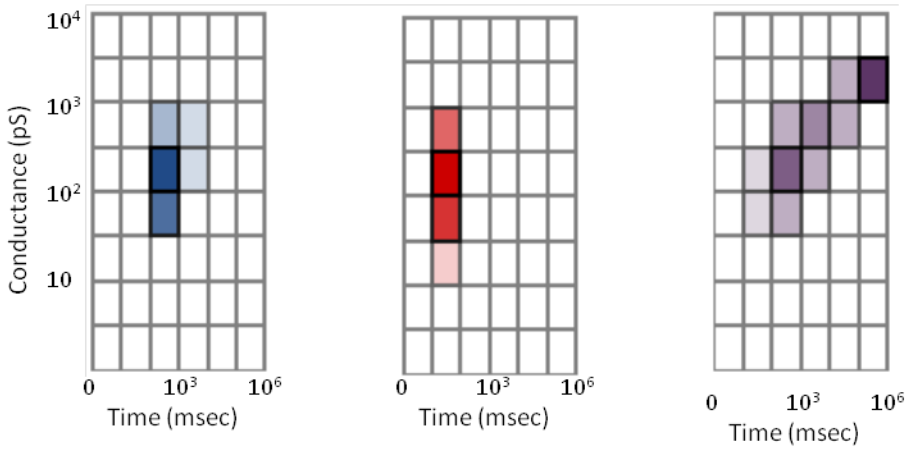

Figure 3-22: Summary activity grids for the compound ¯OOC-Hex-ADip-Oct-S-Hex-OH (**3-59**) showing the ranges of conductance and open duration for the observed multi-level (blue), spiky (red) and erratic (purple) transport activities observed.

At first glance there are many similarities between the activity of this compound and the structurally related amine terminated analog **3-55**. Both exhibit primarily multi-level (blue), spiky (red) and erratic (purple) type activity; however, although the durations of the transport events were only slightly shorter on average, the alcohol terminated compound showed channels which were significantly less conductive, 30 - 300 pS corresponding to pore diameters of approximately 0.1 to 0.4 nm, than the amine terminated analog. One possible explanation for this behavior is that while the alcohol terminated compound is expected to occur in its anionic form under the conditions of the experiments the amine terminated compound likely exists in its zwitterionic form, similar to what is observed for naturally occurring amino acids. Based on the high conductances observed for both compounds it is highly unlikely that the transport active structures are due to single molecules and are much more likely to be some form of self-assembled superstructure. Depending on the nature of this assembly the differences in the ionic properties of the two compounds could have a dramatic effect. For example, the simplified representations of possible arrangements of the two compounds in the bilayer membrane are represented in Figure 3-23 below.

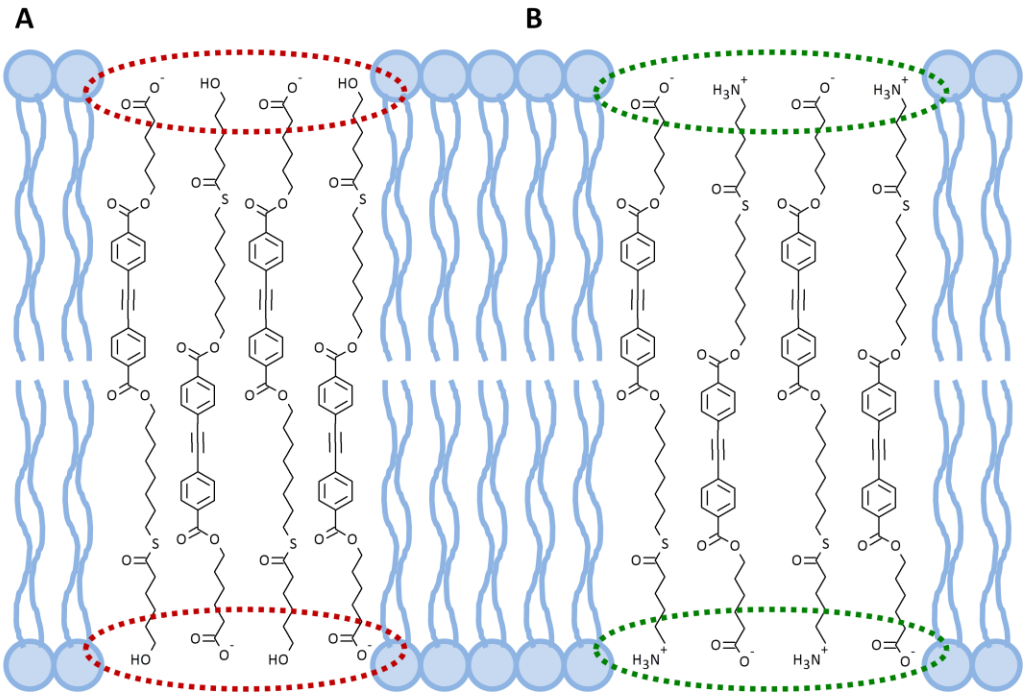

Figure 3-23: Possible arrangements of a small group of molecules of a transport active species; A) the arrangement of the anionic compound $^{-}$OOC-Hex-ADip-Oct-S-Hex-OH (**3-59**) and B) the arrangement of the zwitterionic compound $^{-}$OOC-Hex-ADip-Oct-S-Hex-NH_3^+ (**3-55**). The red dashed ovals highlight the regions of high negative charge density for the grouping of alcohol terminated molecules due to the accumulation of carboxylate groups while the green dashed ovals show the equivalent regions for the grouping of ammonium terminated molecules where there is no net charge density due to the opposing charges of the carboxylate and ammonium groups effectively cancelling each other out.

The Figure above assumes that the transport active structures involve the arrangement of the compounds within the bilayer such that they span the thickness of the bilayer as best they can. Assuming that the compounds arrange themselves so as to minimize repulsive electrostatic interactions between their termini the best arrangement for both compounds would be to have adjacent molecules arranged in a head to tail fashion. For $^{-}$OOC-Hex-ADip-Oct-S-Hex-OH (**3-59**) this arrangement results in the buildup of significant negative charge density as an increasing number of molecules come together to form a larger assembly. This would lead to significant electrostatic repulsion between the individual molecules in a closely packed assembly resulting in the destabilization of the overall supramolecular construct. In the case of $^{-}$OOC-Hex-ADip-Oct-S-Hex-NH_3^+ (**3-55**) however, this arrangement results in the cancellation of opposite charges between the ionic ammonium and carboxylate termini

provided an equal distribution of the two arrangements is achieved. The result is that no additional electrostatic repulsion exists between molecules in a tightly packed assembly that would act to destabilize it.

This destabilization of assemblies of $^{-}$OOC-Hex-ADip-Oct-S-Hex-OH (**3-59**) relative to those composed of $^{-}$OOC-Hex-ADip-Oct-S-Hex-NH_3^+ (**3-55**) would have two effects on the observed activity. Firstly, as an increasing number of molecules came within proximity to each other to form the assembly the net repulsive electrostatic forces between the molecules would increase until the point where they would overwhelm any potential energetic benefit to adding more molecules to the assembly. The effect would be that the potential overall number of molecules, and by extension the size of any resulting channel construct, would be smaller than that possible for the ammonium terminated compound which exhibits significantly less electrostatic repulsion in an analogous conformation. In short it would be expected that the channels formed from $^{-}$OOC-Hex-ADip-Oct-S-Hex-OH (**3-59**) would be significantly smaller, and therefore less conductive, that those formed from $^{-}$OOC-Hex-ADip-Oct-S-Hex-NH_3^+ (**3-55**). The second effect of this decreased stability would be that the overall open duration for the channels formed would be significantly shorter than for the more stable system. Both of these interpretations are in fact borne out in the observed activity grids for the compounds; the alcohol shows both shorter lived as well as lower conductance transport events. Although the proposed active species cannot be directly observed, and therefore the proposed structures remain conjecture, the hypothesis that the activity of the compounds is dependent on their charges seems reasonable. Indeed previous studies of the activity of Dip containing oligoester ion channels have shown that the nature of the termini can have a marked effect on the overall transport activity observed.

Before attempting to effect the in situ intramolecular cyclization reactions that would result in the truncation of the full length compounds bilayer clamp data for a pure sample of the thiol terminated truncated compound was desired for comparison.

Rather than synthesizing the desired thiol terminated compound from scratch it was decided to obtain this compound via truncation of the already synthesized $^{-}$OOC-Hex-ADip-Oct-S-But-NH_3^+ (**3-53**). This shorter compound was chosen as the intramolecular cyclization reaction to form the five membered lactam occurs more readily than for the formation of lactams with larger rings. The reaction, shown in Scheme 3-18, was successfully carried out using a gently heated biphasic system of chloroform and saturated sodium bicarbonate followed by careful neutralization using hydrochloric acid to form the desired truncated compound **3-71**. The five membered lactam side product was not isolated from the reaction.

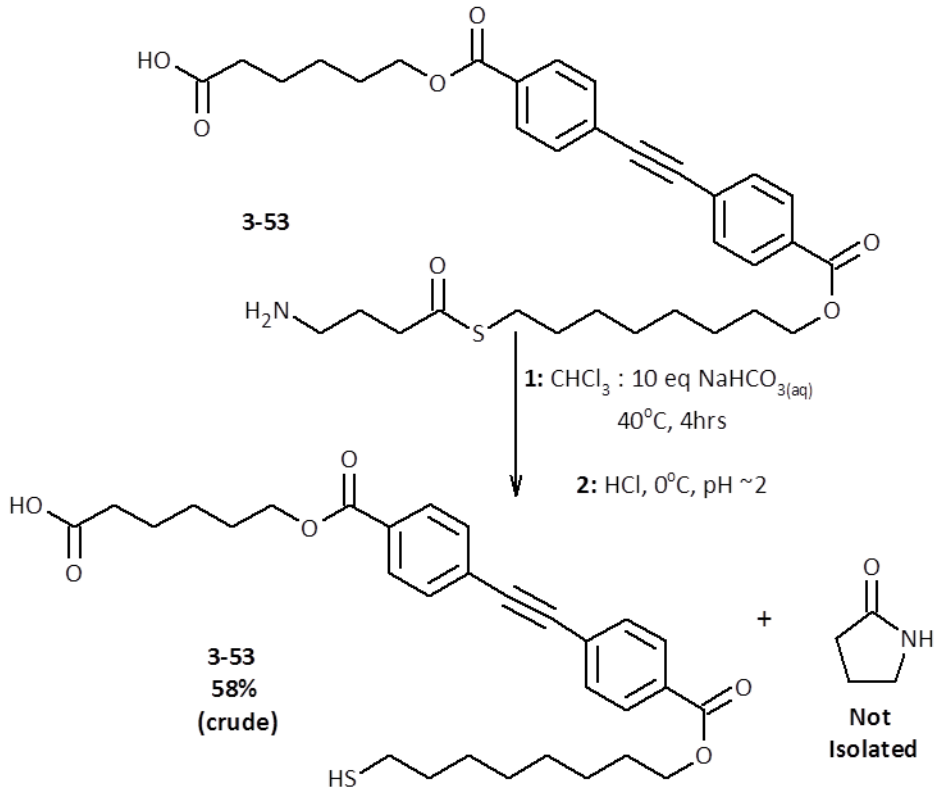

Scheme 3-18: Synthesis of the thiol terminated compound $^{-}$OOC-Hex-ADip-Oct-SH (**3-71**) from $^{-}$OOC-Hex-ADip-Oct-S-But-NH_3^+ (**3-53**).

Bilayer clamp experiments were carried out on the thiol terminated compound $^{-}$OOC-Hex-ADip-Oct-SH (**3-71**) under as similar conditions as possible to those used for the full-length compounds. Representative traces of the types of activity observed for

this compound (**3-71**) are presented in Figure 3-24 to Figure 3-26 below along with the summary activity grids in Figure 3-27.

Figure 3-24: Representative trace of multi-level (blue) type activity for the compound ¯OOC-Hex-ADip-Oct-SH (**3-71**). Conditions: diPhyPC bilayer, 250 µM diameter aperture, Ag/AgCl electrodes, KCl junction solution and salt bridges, 1M CsCl with 10mM each of TRIS and HEPES as buffer, applied potential +150 mV.

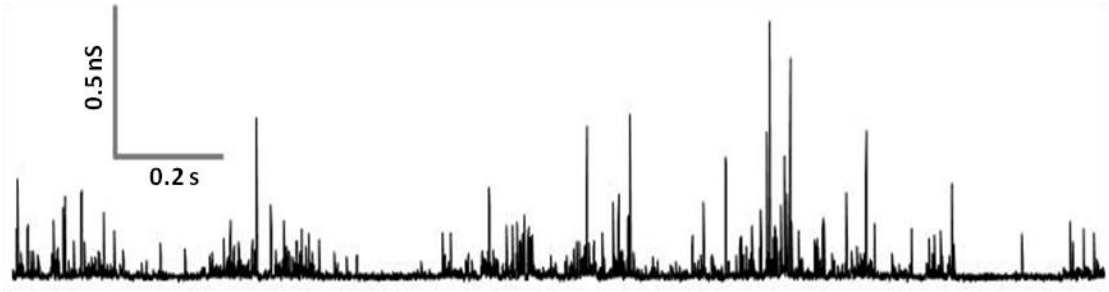

Figure 3-25: Representative trace of spiky (red) type activity for the compound ¯OOC-Hex-ADip-Oct-SH (**3-71**). Conditions: diPhyPC bilayer, 250 µM diameter aperture, Ag/AgCl electrodes, KCl junction solution and salt bridges, 1M CsCl with 10mM each of TRIS and HEPES as buffer, applied potential +100 mV.

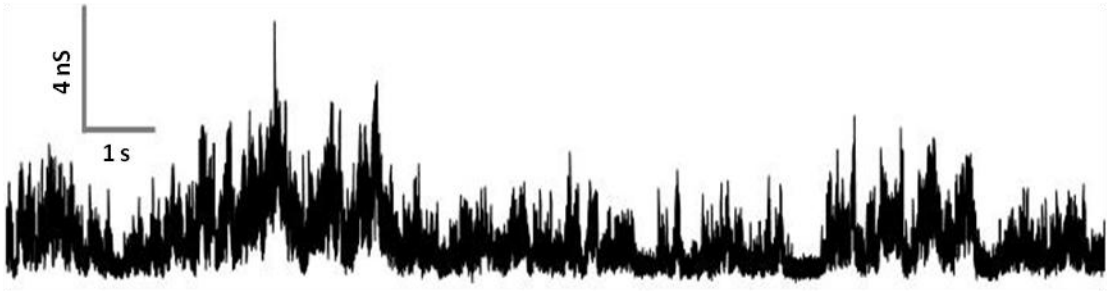

Figure 3-26: Representative trace of erratic (purple) type activity for the compound ¯OOC-Hex-ADip-Oct-SH (**3-71**). Conditions: diPhyPC bilayer, 250 µM diameter aperture, Ag/AgCl electrodes, KCl junction solution and salt bridges, 1M CsCl with 10mM each of TRIS and HEPES as buffer, applied potential +150 mV.

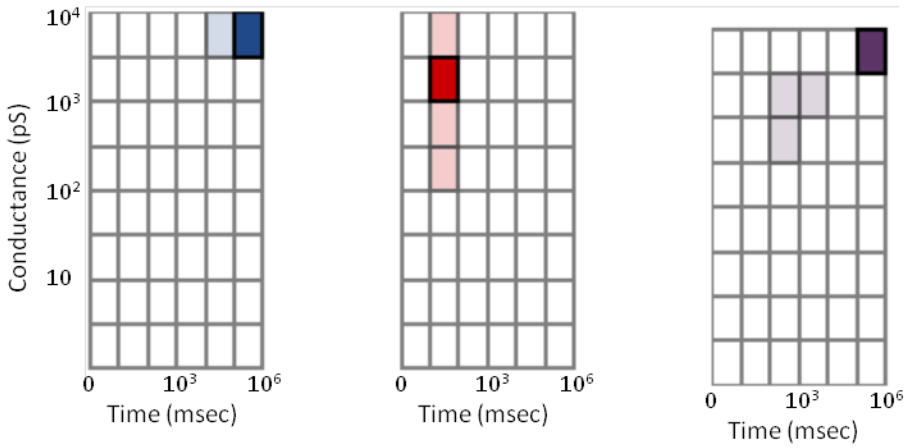

Figure 3-27: Summary activity grids for the compound ¯OOC-Hex-ADip-Oct-SH (**3-71**) showing the ranges of conductance and open duration for the observed multi-level (blue), spiky (red) and erratic (purple) transport activities observed.

As can be seen from the bilayer clamp data, despite expectations of reduced or negligible activity for the truncated compound, much the opposite was observed. Similarly to the two full length compounds studied the primary types of activity observed for the truncated thiol terminated compound were also of the multi-level (blue), spiky (red) and erratic (purple) nature. What was most interesting for this compound was that the observed durations, often several minutes long, and conductances, 1000 to 10000 pS corresponding to pore diameters of 0.8 to 2.8 nm, were longer and larger than those observed for either of the full length compounds (**3-55** and **3-59**). Indeed the transport activity seen for this relatively simple compound was among the highest recorded for any synthetic ion channel. Interestingly the truncated version of the lead compound, HOOC-Hex-Dip-Hex-OH, which is of similar length and structure to the thiol terminated compound was previously shown to be significantly less active than the longer HOOC-Hex-Dip-Hex-Hex-OH (**3-1**) molecule in both the bilayer clamp and HPTS assays. Clearly one or more of the structural differences between the previously reported oligoester ion channels that served as lead compounds and the current molecules had resulted in dramatic differences in activity.

Although the observed activity for this compound was different from that of either of the full length compounds, unfortunately it was not sufficiently so to allow for

the effective monitoring of changes in activity associated with the truncation of the full length compounds. For every intermediate state of the system between totally full length compound and totally truncated compound the range of different transport activities expected was too small to allow for an effective estimate of the relative ratios of the two species. Nevertheless, the observation of such large and stable pores from this relatively structurally simple molecule was quite interesting and likely warrants further examination.

3.12 Conclusions and Future Work: Systems Using Dissipative Assembly

Although the final goal of developing a system for which transport activity could be modulated via a dissipative assembly process remained elusive there were however several worthwhile lessons learned from the studies carried out on the current system.

Firstly, it was discovered that what were believed to be relatively minor changes to the overall structure of the lead compound HOOC-Hex-Dip-Hex-Hex-OH (**3-1**) were in fact significant enough to more or less completely eliminate all transport activity in the vesicle based HPTS assay. As this is the assay of choice for the detection of changes in the activity of reactive compounds over time, the unforeseen impact of these structural modifications proved especially detrimental and disheartening. However, as has been seen previously in the Fyles lab and others seemingly small structural changes can result in drastic changes to activity. As of yet no reliable link has been established between structure and activity for compounds showing transport activity; the compounds synthesized for this body of work have only made the relationship between the two even more opaque.

On the positive side were the experimental results from the trial NMR and HPLC studies on the viability of using both intramolecular cyclization and thioester exchange reactions for the truncation and re-elongation processes for future dissipative assembling systems. Both reactions were seen to be effective at providing the desired products and to occur over time periods appropriate for the investigation of transport

activity using both the vesicle based HPTS assay and the bilayer clamp assay under the conditions studied.

Furthermore, evidence of the disulfide bond forming reaction between thiols may prove to be an interesting avenue to explore as a potential thermodynamic sink for permanently sequestering a compound into an unreactive, transport inactive state.

Finally, even though the bilayer clamp assay failed to be an appropriate method for distinguishing between the activity of full length versus truncated compounds, the discovery that the short thiol terminated compound $^{-}$OOC-Hex-ADip-Oct-SH (**3-71**) generated such long lived and highly conducting events (Figure 3-27) seems to justify the exploration of structurally related compounds.

In addition it cannot be overlooked that the major achievement of realizing transport activity from meta-stable species that exist in the realm beyond the equilibrium state was accomplished, even if the overall goal of having easily differentiated activity between different states still remained elusive. Recall that the approach of obtaining thermodynamically stable transport active structures using metal-ligand self-assembly did not prove to be inherently superior to the dynamic system. Perhaps the movement away from these stable species is the key to obtaining compounds with truly unique and useful properties.

There were many lessons learned from the current research which could be incorporated into the future development of a system showing ion transport activity while incorporating elements of dissipative assembly. The successful implementation of the intramolecular cyclization truncation and thioester exchange re-elongation reactions towards a system incorporating dissipative assembly with differential ion transport activity seems tantalizingly close. Clearly the modifications made to the lead compound for this first run at the system were too drastic since all vesicle transport activity was lost. Promising future synthetic targets are therefore compounds which are structurally much more closely related to the lead compound HOOC-Hex-Dip-Hex-Hex-OH (**3-1**)

which also retain the internal thioester and terminal nucleophilic groups such as those presented in Figure 3-28 below.

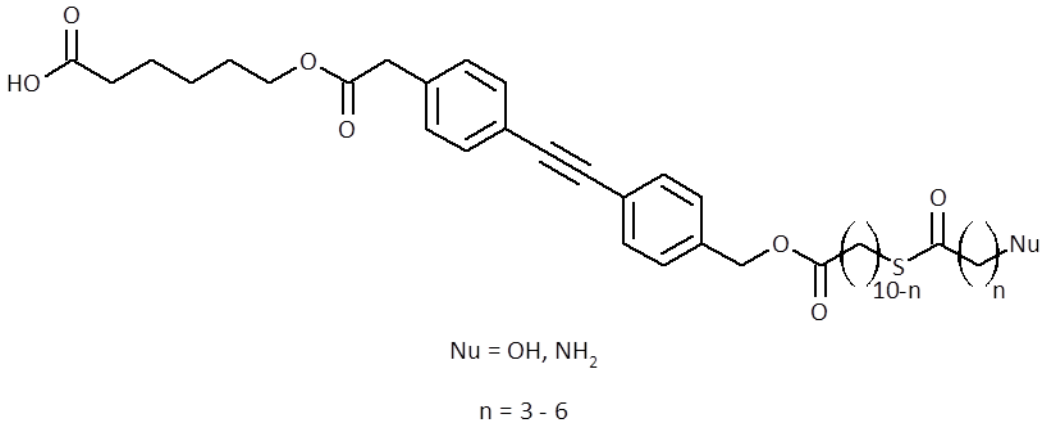

Figure 3-28: Proposed structures for potential future ion channel molecules incorporating a dissipative assembly strategy.

This small library of eight proposed structures are more closely related to the lead compound HOOC-Hex-Dip-Hex-Hex-OH (**3-1**) which showed much higher rates of transport in the vesicle based HPTS assay than any of the current compounds. The carboxylic acid terminus with the six carbon linker remains in place however the symmetrical ADip portion has been removed in favour of the original Dip moiety as the environment sensitive fluorophore. In addition the overall lengths of the newly proposed compounds are all identical and more closely matched to the lead compound HOOC-Hex-Dip-Hex-Hex-OH (**3-1**). This is achieved by synergistically varying the lengths of the two linkers on either side of the thioester group such as to maintain the overall length of this portion at twelve carbons.

This library of compounds allows for a multitude of potentially interesting comparative studies that may provide a better understanding of structure-activity relationships for this class of compounds en route to discovering the best possible structure for an ion channel incorporating dissipative assembly resulting in differential transport activity.

Firstly, the effect of changing the ester of the lead compound HOOC-Hex-Dip-Hex-Hex-OH (**3-1**) to a thioester can be determined by comparing its activity with that of the compound where n = 5 and Nu = OH, HOOC-Hex-Dip-Hex-S-Hex-OH. A complete loss of transport activity in the HPTS assay associated with a change to the thioester alone, although a very interesting result, could unfortunately doom the use of such a modification to an early extinction. If at least some activity was retained a much wider set of comparative studies would become worthwhile pursuits.

For example, comparison of the members of the set of compounds where the nucleophilic terminus was maintained as an alcohol but the two linkers on either side of the thioester varied would provide information on the effect of the relative position of the thioester in the molecule on the overall transport activity. A similar study could be carried out for the analogous set of compounds with an amine as the nucleophilic terminus to see if similar trends in transport activity were observed. The results of such studies would isolate the importance of the position of the thioester on activity.

Another series of comparisons could be made between the transport activities of compounds differing in the nature of their nucleophilic termini, either alcohol or amine, but having the same relative arrangement of linker length on either side of the thioester linkage. If the set of either the alcohol or amine terminated compounds showed consistently higher rates of transport than the other set of compounds then this would provide strong evidence for the importance of the nature of the nucleophilic termini on transport activity.

From this library of compounds it should also be relatively easy to generate the corresponding thiol terminated compounds of varying length. With this set of compounds in hand it would also be possible to compare the relative rates of transport between the members of this set to determine the effect of overall length for the truncated compounds.

Combined all of these studies would provide the full length and associated truncated compounds which exhibited the greatest difference in transport activity and

therefore the system for which monitoring changes in activity over time due to the intramolecular cyclization truncation reaction would prove most facile.

In conclusion, even though the current iteration of compounds failed to provide an easily studied transport active system exhibiting dissipative assembly to afford a transport inactive state, many of the core features built into these compounds are well worth retaining in any future designs.

References

1. Smith, C. A.; Wood, E. J. Biological Membranes. In *Cell Biology,* 2nd ed.; Smith, C. A., Wood, E. J., Eds.; Springer-Verlag USA: New York, 1996; pp 144-183.

2. Luisi, P. L.; Ealde, P.; Oberholzer, T. Lipid vesicles as possible intermediates in the origin of life. *Current Opinion in Colloid & Interface Science* **1999,** No. 4, 33-39.

3. Yeagle, P. L. *The Structure of BIological Membranes,* 2nd ed.; CRC Press: Boca Raton, 2005.

4. Brown, M. F. Curvature forces in membrane lipid-protein interactions. *Biochemistry* **2012,** *51,* 9782-9795.

5. Spector, A. A.; Yorek, M. A. Membrane lipid composition and cellular funciton. *Journal of Lipid Research* **1985,** *26,* 1015-1035.

6. Cooke, I. R.; Deserno, M. Coupling between lipid shape and membrane curvature. *Biophysical Journal* **2006,** *91,* 487-495.

7. Israelachvili, J. N.; Marcelja, S.; Horn, R. G. Physical principles of membrane organization. *Quarterly Reviews of Biophysics* **1980,** *13* (2), 121-200.

8. Finkelstein, A. Water and nonelectrolyte permeability of lipid bilayer membranes. *The Journal of General Physiology* **1976,** *68,* 127-135.

9. Eisenman, G.; Horn, R. Ionic selectivity revisited: the role of kinetic and equilibirum processes in ion permeation through channels. *The Journal of Membrane Biology* **1983,** *76,* 197-225.

10. Andersen, O.; Fuchs, M. Potential energy barrieers to ion transport within lipid bilayers. *Biophysical Journal* **1975,** *15,* 795-830.

11. Saier, M. H.; Yen, M. R.; Noto, K.; Tamang, D. G.; Elkan, C. The transporter classification database: recent advances. *Nucleic Acids Research* **2008,** *37,* 274-278.

12. Bechinger, B. Structure and funciton of membrane-lytic peptides. *Critical Reviews in Plant Sciences* **2004,** *23* (3), 271-292.

13. Riddell, F. G. Structure, conformation, and mechanism in the membrane transport of alkali metal ions by ionophoric antibiotics. *Chirality* **2002,** *14,* 121-125.

14. Vinothkumar, K. R.; Henderson, R. Structures of membrane proteins. *Quarterly Reviews of Biophysics* **2010,** *43* (1), 65-158.

15. Smith, C. A.; Wood, E. J. Mitochondria and chloroplasts. In *Cell Biology,* 2nd ed.; Smith, C. A., Wood, E. J., Eds.; Springer-Verlag USA: New York, 1996; pp 184-213.

16. Lee, A. G.; East, J. M. What the structure of a calcium pump tells us about its mechanism. *Biochemical Journal* **2001,** *356,* 665-683.

17. Gadsby, D. C.; Vergani, P.; Csanady, L. The ABC protein turned chloride channel whose failure causes cystic fibrosis. *Nature* **2006,** *440,* 477-483.

18. Steller, L.; Kreir, M.; Salzer, R. Natural and artificial ion channels for biosensing platforms. *Analytical and Bioanalytical Chemistry* **2012,** *402,* 209-230.

19. Doyle, D. A.; Cabral, J. M.; Pfuetzner, R. A.; Kuo, A.; Gulbis, J. M.; Cohen, S. L.; Chait, B. T.; MacKinnon, R. The structure of the potassium channel: moleular basis of K+ conduction and selectivity. *Science* **1998,** *280,* 69-77.

20. Chang, G.; Spencer, R. H.; Lee, A. T.; Barclay, M. T.; Rees, D. C. Structure of the MscL homolog from mycobacterium tuberculosis: a gated mechanosensitive ion channel. *Science* **1998,** *282,* 2220-2226.

21. Jentsch, T. J.; Stein, V.; Weinreich, F.; Zdebik, A. A. Molecular structure and physiological function of chloride channels. *Physiological Reviews* **2002,** *82* (2), 503-568.

22. Krogh, A.; Larsson, B.; von Heijne, G.; Sonnhammer, E. L. L. Predicting trnasmembrane protein topology with a hidden markov model: application to complete genomes. *Journal of Molecular Biology* **2001,** *305,* 567-580.

23. Tabushi, I.; Kuroda, Y.; Yokota, K. A,B,D,F-tetrasubstituted B-cyclodextrin as artificial channel compound. *Tetrahedron Letters* **1982,** *23* (44), 4601-4604.

24. Gokel, G. W.; Carasel, I. A. Biologically active, synthetic ion transporters. *Chemical Society Reviews* **2007,** No. 36, 378-389.

25. Sakai, N.; Mareda, J.; Matile, S. Ion channels and pores, made from scratch. *Molecular BioSystems* **2007,** *3,* 658-666.

26. Quesada, R. Membrane transport. In *Supramolecular Chemistry: From Molecules to Nanomaterials,* 8th ed.; Steed, J. W., Gale, P. A. G., Eds.; John Wiley & Sons, Ltd., 2012; Vol. 4, pp 1751-1770.

27. Matile, S.; Jentzsch, A. V.; Montenegro, J.; Fin, A. Recent synthetic transport systems. *Chemical Society Reviews* **2011,** *40,* 2453-2474.

28. Sisson, A. L.; Shah, M. R.; Bhosale, S.; Matile, S. Synthetic ion channels and pores (2004-2005). *Chemical Society Reviews* **2006,** *35,* 1269-1286.

29. Fyles, T. M. Synthetic ion channels in bilayer membranes. *Chemical Society Reviews* **2007,** *36,* 335-347.

30. Gokel, G. W. Hydraphiles: design, synthesi and analysis of a family of synthetic cation-conducting channels. *Chemical Communications* **2000,** 1-9.

31. Iqbal, K. S. J.; Cragg, P. J. Transmembrane ion transport by calixarenes and their derivatives. *Dalton Transactions* **2007,** 26-32.

32. Fyles, T. M.; Luong, H. Structure-activity relationships in linear oligoester ion-channels. *Organic & Biomolecular Chemistry* **2009,** *7,* 733-738.

33. Mareda, J.; Matile, S. Anion-pi slides for transmembrane transport. *Chemistry a European Journal* **2009,** No. 15, 28-37.

34. Wang, W.; Li, R.; Gokel, G. W. "Aplosspan:" a bilayer-length, ion-selective ionophore that funcitons in phospholipid bilayers. *Chemical Communications* **2009,** 911-913.

35. Wang, W.; Li, R.; Gokel, G. W. Membrane length amphiphiles exhibiting structural simplicity and ion channel activity. *Chemistry a European Journal* **2009,** *15,* 10543-10553.

36. Eggers, P. K.; Fyles, T. M.; Mitchell, K. D. D.; Sutherland, T. Ion channels from linear and branched bola-amphiphiles. *Journal of Organic Chemistry* **2003,** *68,* 1050-1058.

37. Matile, S.; Sakai, N. The characterization of synthetic ion channels and pores. In *Analytical Methods in Supramolecular Chemistry;* Schalley, C. A., Ed.; WILEY-VCH Verlag GmbH % Co. KGaA: Weinheim, 2007; pp 391-418.

38. Matile, S.; Sakai, N.; Hennig, A. Transport experiments in membranes. In *Supramolecular Chemistry: From Molecules to Nanomaterials,* 8th ed.; Steed, J. W., Gale, P. A., Eds.; John Wiley & Sons, Ltd., 2012; Vol. 2, pp 473-500.

39. Riddell, F. G.; Hayer, M. K. The monensin-mediated transport of sodium ions through phospholipid bilayers studied by 23Na-NMR spectroscopy. *Biochimica et Biophysica Acta* **1985,** *817,* 313-317.

40. Katsu, T.; Nakagawa, H.; Kanamori, T.; Kamo, N.; Tsuchiya, T. Ion-selective electrode for transmembrane pH difference measurements. *Analytical Chemistry*

2001, *73,* 1849-1854.

41. Pajewski, R.; Ferdani, R.; Pajewska, J.; Djedovic, N.; Schlesinger, P. H.; Gokel, G. W. Evidence for dimer formation by an amphiphilic heptapeptide that mediates chloride and carboxyfluorescein release from liposomes. *Organic and Biomolecular Chemistry* **2005,** *3,* 619-625.

42. Kano, K.; Fendler, J. H. Pyranine as a sensitive pH probe for liposome interiors and surfaces - pH gradients across phospholipid vesicles. *Biochimica et Biophysica Acta* **1978,** *509* (3), 289-299.

43. Chui, J. K. W.; Fyles, T. M. ionic conductance of syntehtic channels; analysis, lessons and recommendations. *Chemical Society Reviews* **2012,** *41,* 148-175.

44. Hille, B. *Ion channels of excitable membranes;* Sinaur Associates: Sunderland, MA, 2001.

45. Lehn, J.-M. Supramolecular chemistry. *Science* **1993,** *260,* 1762-1763.

46. Lehn, J.-M. Perspectives in supramolecular chemistry - from molecular recognition towards molecular information processing and self-organization. *Angewandte Chemie International Edition* **1990,** *29,* 1304-1319.

47. Cragg, P. J. An introduction to supramolecular chemistry. In *Supramolecular Chemistry;* Cragg, P. J., Ed.; Springer: New York, 2010; pp 1-44.

48. Chandler, D. Interfaces and the driving force of hydrophobic assembly. *Nature* **2005,** *437,* 640-647.

49. Bagatolli, L. A.; Ipsen, J. H.; Simonsen, A. C.; Mouritsen, O. G. An outlook on organization of lipids in membranes: searching for a realistic connection with the organization of biological membranes. *Progress in Lipid Research* **2010,** *49,* 378-389.

50. Kurth, D. G. Metallo-supramolecular modules as a paradigm for materials science. *Science and Technology of Advanced Materials* **2008,** *9,* 1-26.

51. Irving, H.; Williams, R. J. P. The stability of transition-metal complexes. *Journal of the Chemical Society* **1953,** 3192-3210.

52. Alexeev, Y. E.; Kharisov, B. I.; Garcia, T. C. H.; Garnovskii, A. D. Coordination motifs in modern supramolecular chemistry. *Coordination Chemistry Reviews* **2010,** No. 254, 794-831.

53. Rodgers, M. T.; Armentrout, P. B. Noncovalent metal-ligand bond energies as studied by threshold collision-induced dissociation. *Mass Spectrometry Reviews* **2000,** *19,* 215-247.

54. Pearson, R. G. Hard and soft acids and bases, HSAB, Part II - underlying theories. *Journal of Chemical Education* **1968,** *45* (10), 643-648.

55. Lehn, J.-M. Constittutional dynamic chemistry: bridge from supramolecular chemistry to adaptive chemistry. *Topic in Current Chemistry* **2012,** No. 322, 1-32.

56. Bracher, P. J.; Snyder, P. W.; Bohall, B. R.; Whitesides, G. M. The relative rates of thiol-thioester exchange and hydrolysis fro alkyl and aryl thioalkanoates in water. *Origins of Life and Evolution of the Biosphere* **2011,** *41,* 399-412.

57. Cheng, Y.; Peng, H.; Wang, B. Reversible Covalent Bond Toolbox. In *Supramolecular Chemistry: From Molecules to Nanomaterials;* Steed, J. W., Gale, P. A., Eds.; John Wiley & Sons, Ltd., 2012; Vol. 1, pp 205-216.

58. Maeda, T.; Otsuka, H.; Takahara, A. Dynamic covalent polymers: reorganizable polymers with dynamic covalent bonds. *Progress in Polymer Science* **2009,** No. 34, 581-604.

59. Rowan, S. J.; Cantrill, S. J.; Cousins, G. R. L.; Sanders, J. K. M.; Stoddart, J. F. Dynamic covalent chemistry. *Angewandte Chemie International Edition* **2002,** No. 41, 898-952.

60. Meguellati, K.; Ladame, S. Reversible covalent chemistries compatible with the principles of constitutional dynamic chemistry: new reactions to create more diversity. *Topics in Current Chemistry* **2012,** *322,* 291-314.

61. Hajduk, P. J.; Greer, J. A decade of fragment-based drug desgin: strategic advances and lessons learned. *Nature Reviews. Drug Discovery* **2007,** *6,* 211-219.

62. Wojtecki, R. J.; Meador, M. A.; Rowan, S. J. Using the dynamic bond to access macroscopically responsive structurally dynamic polymers. *Nature Materials* **2011,** *10,* 14-27.

63. Lehn, J.-M. Dynamers: dynamic molecular and supramolecular polymers. *Australian Journal of Chemistry* **2010,** No. 63, 611-623.

64. Cram, D. J.; Cram, J. M. Host-Guest Chemistry. *Science* **1974,** *183,* 803-809.

65. Watson, J. D.; Crick, F. H. Molecular structure of nucleic acids. *Nature* **1953,** 737-738.

66. Kwon, Y.-W.; Lee, C. H.; Choi, D.-H.; Jin, J.-I. Materials science of DNA. *Journal of Materials Chemistry* **2009,** *19,* 1353-1380.

67. Cram, D. J. Preorganization - from solvents to spherands. *Angewwandte Chemie International Edition* **1986,** *25* (12), 1039-1057.

68. Martell, A. E.; Hancock, R. D.; Motekaitis. Factors affecting stabilities of chelate, macrocyclic and macrobicyclic complexes in solution. *Coordination Chemistry Reviews* **1994,** *133,* 39-65.

69. Senge, M. O. Exercises in molecular gymnastics - bending, stretching and twisting porphyrins. *Chemical Communications* **2006,** 243-256.

70. Satake, A.; Yamamura, M.; Oda, M.; Kobuke, Y. Thansmembrane nanopores from porphyrin supramolecules. *Journal of the Amirican Chemical Society* **2008,** *130,* 6314-6315.

71. Boccalon, M.; Iengo, E.; Tecilla, P. Metal-organic transmembrane nanopores. *Journal of the American Chemical Society* **2012,** *134,* 20310-20313.

72. Jung, M.; Kim, H.; Baek, K.; Kim, K. Synthetic ion channel based on metal-organic polyhedra. *Angewandte Cehmie* **2008,** *47,* 5755-5757.

73. Eddaoudi, M.; Kim, J.; Wachter, J. B.; Chae, H. K.; O'Keeffe, M.; Yaghi, O. M. Porous metal-organic polyhedra: 25A cuboctahedron constructed from 12 Cu2(CO2)4 paddle-wheel building blocks. *Journal of the American Chemical Society* **2001,** *123,* 4368-4369.

74. Kulikov, O. V.; Li, R.; Gokel, G. W. A synthetic ion cahnnels derived from a metallogallarene capsule that functions in phospholipid bilayers. *Angewandte Chemie* **2009,** *48,* 375-377.

75. Wilson, C. P.; Webb, S. J. Palladium(II)-gated ion channels. *Chemical Communications* **2008,** 4007-4009.

76. Kobuke, Y.; Nagatani, T. Transmembrane ion channels constructed of cholic acid derivatives. *Journal of Organic Chemistry* **2001,** *66,* 5094-5101.

77. Fujita, M.; Yazaki, J.; Ogura, K. Spectroscopic observation of self-assembly of a macrocyclic tetranuclear complex composed of Pt2+ and 4,4'-bipyridine. *Chemistry Letters* **1991,** 1031-1032.

78. Li, S.; Moorefield, C. N.; Wang, P.; Shreiner, C. D.; Newkome, G. R. Self-assembly of shape-persistent hexagonal macrocycles with trimeric bis(terpyridine)-Fe(II)

connectivity. *European Journal of Organic Chemistry* **2008,** 3328-3334.

79. Fyles, T. M.; Tong, C. C. Long-lived and highly conducting ion channels formed by lipophilic ethylenediamine palladium(II) complexes. *New Journal of Chemistry* **2007,** *31,* 655-661.

80. Fyles, T. M.; Tong, C. C. Predicting speciation in the multi-component equilibrium self-assembly of a metallosupramolecular complex. *New Journal of Chemistry* **2007,** *31,* 296-304.

81. Nagle, J. F.; Tristram-Nagle, S. Structure of lipid bilayers. *BIochimica et Biophysica Acta* **2000,** *1469,* 159-195.

82. Leitgeb, B.; Szekeres, A.; Manczinger, L.; Vagvolgyi, C.; Kredics, L. The history of alamethicin: a review of the most extensively studied peptaibol. *Chamistry & Biodiversity* **2007,** *4,* 1027-1051.

83. Kapinos, L. E.; Sigel, H. Acid-base and metal ion binding properties of pyridine-type ligands in aqueous solution. Effect of ortho substituents and interrelation between complex stability and ligand basicity. *Inorganica Chimica Acta* **2002,** *337,* 131-142.

84. Ruzziconi, R.; Spizzichino, S.; Lunazzi, L.; Mazzanti, A.; Schlosser, M. B values as a sensitive measure of steric effects. *Chemistry a European Journal* **2009,** No. 15, 2645-2652.

85. Miyaura, N.; Suzuki, A. Palladium-catalyzed cross-coupling reactions or organoboron compounds. *Chemical Reviews* **1995,** *95,* 2457-2483.

86. Comins, D. L.; O'Connor, S.; Al-awar, R. S. Pyridines and their benzo derivatives: reactivity at the ring. In *Comprehensive Heterocyclic Chemistry III,* 3rd ed.; Katritzky, A. R., Ramsden, C. A., Scriven, E. F. V., Taylor, R. J. K., Eds.; Elsevier Ltd.: Amsterdam, 2008; Vol. 7, pp 41-99.

87. Youssif, S. Recent trends in the chemistry of pyridine N-oxides. *ARKIVOC* **2001,** 242-268.

88. Bjorsvik, H.-R.; Gambarotti, C.; Jensen, V. R.; Gonzalez, R. R. A novel efficient deoxygenation process for N-heteroarene N-oxides. *Journal of Organic Chemistry* **2005,** *70,* 3218-3224.

89. Marvel, C. S.; Sekera, V. C. n-dodecyl (laryl) p-toluenesulfonate. *Organic Syntheses, Collection* **1955,** *3,* 366.

90. Sniekus, V. Directed ortho metalation. Tertiary amide and o-carbamate directors in synthetic strategies for polysubstituted aromatics. *Chemical Reviews* **1990,** *90*

(6), 879-933.

91. Miller, R. E.; Rantanen, T.; Ogilvie, K. A.; Groth, U.; Sniekus, V. Combined directed ortho metalation-halogen dance (HD) synthetic strategies. HD-anionic ortho Fries rearrangement and double HD sequences. *Organic Letters* **1990,** *12* (10), 2198-2201.

92. Reetz, M. T.; Kesseler, K. Directed ortho metalation of o-pyridyl carbamates. Regiospecific entries into polysubstituted pyridines. *Journal of Organic Chemistry* **1985,** *50,* 5436-5438.

93. Vanderesse, R.; Lourak, M.; Fort, Y.; Caubere, P. Activiation of reducing agents. Sodium hydride containing complex reducing agents 23. symmetrical coupling of nitrogen-containing heterocyclic halides. *Tetrahedron Letters* **1986,** *27* (45), 5483-5486.

94. Bossmann, S. H.; Duerr, H.; Pakhrel, M. R. Synthesis of crown-ester bipyridines and crown-ester-viologens. *Synthesis* **2005,** 907-914.

95. Benniston, A. C.; Harriman, A.; Li, P.; Rostron, J. P.; Harrington, R. W.; Clegg, W. A spectroscopic study of the reduction of geometrically restrained viologens. *Chemistry a European Journal* **2007,** *13,* 7838-7851.

96. Benniston, A. C.; Harriman, A.; Li, P.; Rostron, J. P. Controlling electron delocalization in constrined N,N'-dimethyl-4,4'-bipyridinium dications. *Tetrahedron Letters* **2005,** *46,* 7291-7293.

97. Spivey, A. C.; Shukla, L.; Hayler, J. F. Conjugate addition of 2- and 4-pyridylcuprates: an expeditious asymmetric synthesis of natural (-)-evoninic acid. *Organic Letters* **2007,** *9* (5), 891-894.

98. Diemer, V.; Chaumeil, H.; Defoin, A.; Fort, A.; Boeglin, A.; Carre, C. Syntheses of sterically hindered zwitterionic pyridinium phenolates as model compounds in nonlinear optics. *European Journal of Organic Chemistry* **2008,** 1767-1776.

99. Rebek Jr, J.; Costello, T.; Wattley, R. Binding forces and catalysis. The use of bipyridyl-metal chelation to enhance reaction rates. *Journal of the American Chemical Society* **1985,** *107* (25), 7487-7493.

100. Bunzen, J.; Bruhn, T.; Bringmann, G.; Lutzen, A. Synthesis and helicate formation of a new family of BINOL-based bis(bipyridine) ligands. *Journal of the American Chemical Society* **2009,** *131,* 3621-3630.

101. Fujita, M.; Sasaki, O.; Mitsuhashi, T.; Fujita, T.; Yazaki, J.; Yamaguchi, K.; Ogura, K. On the structure of transition-metal-linked molecular squares. *Chemical*

Communications **1996,** 1535-1536.

102. Fujita, M.; Yazaki, J.; Ogura, K. Preparation of a macrocyclic polynuclear complex, [(en)Pd(4,4'-bpy)]4(NO3)8 which recognizes an organic molecule in aqueous media. *Journal of the American Chemical Society* **1990,** *112,* 5645-5647.

103. Grynkiewicz, G.; Poenie, M.; Tsien, R. Y. A new generation of Ca2+ indicators with greatly improved fluorescence properties. *The Journal of BIological Chemistry* **1985,** *260* (6), 3440-3450.

104. Medvedev, S. S.; Tankelyun, O. V.; Batov, A. Y.; Voronina, O. V.; Martinec, J.; Machackova, I. Ionophorous functions of phospatidic acid in the plant cell. *Russian Journal of Plant Physiology* **2006,** *53* (1), 39-47.

105. Moszynski, J. M.; Fyles, T. M. Synthesis, transport activity, membrane localization, and dynamics of oligoester ion channels containing diphenylacetylene units. *Organic & Biomolecular Chemsitry* **2010,** *8,* 5139-5149.

106. Fyles, T. M.; Knoy, R.; Sieffert, M. Membrane activity of isophthalic acid derivatives: ion channel formation by a low molecular weight compound. *Langmuir* **2001,** *17,* 6669-6674.

107. Arena, G.; Bonomo, R. P.; Musumeci, S.; Rizzarelli, E. Mixed complex formation of copper(II) with 2,2',2''-terpyridine and some tridentate ligands in aqueous solution. *Transition Metal Chemistry* **1982,** No. 7, 29-31.

108. Constable, E. C. Expanded ligands - an assembly principle for supramolecular chemistry. *Coordination Chemistry Reviews* **2008,** *252,* 842-855.

109. Hofmeier, H.; Schubert, U. S. Recent developments in the supramolecular chemistry of terpyridine-metal complexes. *Chemical Society Reviews* **2004,** *33,* 373-399.

110. Du, M.; Cai, H.; Zhao, X.-J. Novel CuII, CoII and PbII supramolecular netowkrs of pyridine-2,6-dicarboxylate (pydc) in coorperation with a bent dipyridyl spacer via coordinative, hydrogen-bonding and aromatic stacking interaction. *Inorganica Chimica Acta* **2006,** *359,* 673-679.

111. Ghosh, S. K.; Ribas, J.; Bharadwaj, P. K. Metal-organic framework structures of Cu(II) with pyridine-2,6-dicarboxylate and different spacers: identification of a metal bound acyclic water tetramer. *CrystEngComm* **2004,** *6* (45), 250-256.

112. Charbonniere, L. J.; Weibel, N.; Ziessel, R. F. Synthesis of mono-, bis- and tris-tridentate ligands based on 5'-substituted-2,2'-bipyridine-6-carboxylic acid.

Tetahedron Letters **2001,** *42,* 659-662.

113. Alderighi, L.; Gans, P.; Ienca, A.; Peters, D.; Sabatini, A.; Vacca, A. Hyperquad simulation and speciation (HySS): a utility program for the investigation of equilibria involving soluble and partially soluble species. *Coordination Chemistry Reviews* **1999,** *184,* 311-318.

114. Kraszkiewicz, L.; Sosnowski, M.; Skulski, L. Oxidative iodination of deactivated arenes in concentrated sufuric acid with I2/NaIO4 iodinating systems. *Synthesis* **2006,** *7,* 1195-1199.

115. Basnet, A.; Thapa, P.; Karki, R.; Na, Y.; Jahng, Y.; Jeong, B.-S.; Jeong, T. C.; Lee, C.-S.; Lee, E.-S. 2,4,6-trisubstituted pyridines: syntehsis, topoisomerase I and II inhibitory activity, cytotoxicity, and structure-activity relationship. *Bioorganic & Medicinal Chemistry* **2007,** *15,* 4351-4359.

116. Constable, E. C.; Redondo, A. H.; Housecraft, C. E.; Neuburger, M.; Schaffner, S. Copper(I) complexes of 6,6'-disubstituted 2,2'-bipyridine dicarboxylic acids: new complexes for incorporation into copper-based fye sensitized solar cells (DSCs). *Dalton Transactions* **2009,** 6634-6644.

117. Wutz, P. G. M.; Greene, T. W. *Greene's protective groups in organic synthesis,* 4th ed.; Wiley Interscience: Hoboken, NJ, 2007.

118. Balzani, V.; Bergamini, G.; Campagna, S.; Puntoriero, F. Photochemistry and photophysics of coordination compounds: overview and general concepts. *Topics in Current Chemistry* **2007,** *280,* 1-36.

119. Moszynski, J. M.; Fyles, T. M. Mechanism of ion transport by fluorescent oligoester channels. *Journal of the American Chemical Society* **2012,** *134,* 15937-15945.

120. Shan, D.; Nicolaou, M. G.; Borchardt, R. T.; Wang, B. Prodrug strategies based on intramolecular cyclizaiton reacitons. *Journal of Pharmaceutical Sciences* **1997,** *86* (7), 765-767.

121. Smith, M. B.; March, J. The effect of the attacking nucleophile. In *March's Advanced Organic Chemistry - Reactions, Mechanisms, and Structure,* 6th ed.; Smith, M. B., March, J., Eds.; Wiley Interscience a John Wiley & Sons, Inc.: Hoboken, NJ, 2007; pp 490-495.

122. Galli, C.; Illuminati, G.; Mandolini, L.; Tamborra, P. Ring-closure reactions. 7. Kinetics and activation parameters of lactone formation in the range of 3 to 22 membered rings. *Journal of the American Chemical Society* **1977,** *99* (8), 2591-2597.

123. Illuminati, G.; Mandolini, L. Ring closure reaction of bifunctional chain molecules. *Accounts of Chemical Research* **1981,** *14* (4), 95-102.

124. Knipe, A. C.; Stirling, J. M. Intramolecular reactions. Part VI. Rates of ring formation in reacitons of w-halogenoalkylmalonic esters with bases. *Journal of the Chemical Society B* **1968,** 67-71.

125. Grzybowski, B. A.; Wilmer, C. E.; Kim, J.; Browne, K. P.; Bishop, K. J. M. Self-assembly: from crystals to cells. *Soft Matter* **2009,** *5,* 1110-1128.

126. Boekhoven, J.; Brizard, A. M.; Kowlgi, K. N. K.; Koper, G. J. M.; Eelkema, R.; van Esch, J. H. Dissipative self-assembly of a molecular gelator by using a chemical fuel. *Angewandte Chemie International Edition* **2010,** *49,* 4825-4828.

127. Moszynski, J. M.; Fyles, T. M. Synthesis and ion transport activity of oligoesters containing an environment-sensitive fluorophore. *Organic & Biomolecular Chemistry* **2010,** *9,* 7468-4775.

128. Nishizawa, M.; Yamamoto, H.; Seo, K.; Imagawa, H.; Sugihara, T. TMS triflate-catalyzed cleavage of prenyl (3-methylbut-2-enyl) ester. *Organic Letters* **2002,** *4* (11), 1947-1949.

129. Iglesias, L. E.; Baldessari, A.; Gros, E. G. Simple procedures for the preparation of a,w-hydroxyalkanethiols. *Organic Preparations and Procedures International* **1996,** *28* (3), 319-324.

130. Letsinger, R. L.; Wu, T. F.; Yang, J. S.; D, L. F. DNA-templated formation and luminescence of diphenylacetylene dimeric and trimeric complexes. *Photochemical & Photobiological Sciences* **2008,** *7,* 854-859.

131. Lakowicz, J. R. *Principles of Fluorescence Spectroscopy,* 3rd ed.; Springer: New York, 2009.

132. Milla, P.; Dosio, F.; Cattel, L. PEGylation of proteins and liposomes: a powerful and flexible strategy to improve the drug delivery. *Current Drug Metabolism* **2012,** *13,* 105-119.

133. Fasina, T. M.; Collings, J. C.; Burke, J. M.; Batsanov, A. S.; Ward, R. M.; Albesa-Jove, D.; Porres, L.; Beeby, A.; Howard, J. A. K.; Scott, A. J.; Clegg, W.; Watt, S. W.; Viney, C.; Marder, T. B. Synthesis, optical properties, crystal structures and phase behavior of symmetric, conjugated ethynylarene-based rigid rods with terminal carboxylate groups. *Journal of Materials Chemistry* **2005,** *15,* 690-697.

134. Witt, D. Recent developments in disulfide bond formation. *Synthesis* **2008,** *16,*

2491-2509.

135. Ma, L.; Harrell, W. A.; Davis, J. T. Stabilizing guanosine-sterol ion channels with a carbamate to urea modification in the linker. *Organic Letters* **2009,** *11* (7), 1599-1602.

Appendix 1: Experimental Details

Most chemicals and solvents were used as received from known suppliers. NMR spectra were recorded on a Bruker AC300 (300 MHz ^{1}H and 75 MHz ^{13}C). Chemical shifts are reported relative to tetramethylsilane in ppm. UV spectra were run on a Cary 5 UV-VIS spectrometer in a 10 x 10 mm quartz cell. ESI Mass spectra were recorded on a Waters MicroMass Q-TOF instrument running in both positive and negative ion mode. HPLC was performed using an HP Series 1100 instrument, with either a Macherey-Nagel "Nucleosil" RP C18 analytical (4 mm x 250 mm) or a Grace Davison "Alltima" RP C18 semi-prep (10 mm x 150 mm) column. Solvents used (Acetonitrile, MeOH; HPLC-grade, H_2O; Milipore) were filtered through a Milipore sub-micrometre filter before use. HPLC elution was monitored at various UV wavelengths (typically 254, 280 and 220 nm) and fluorometrically (λEx = 310, λEm = 330 nm). Fluorescence spectra were run on a PTI QM-2 instrument at T = 20^0C in 10 x 10 mm quartz cells equipped with a micro stir rod.

BILAYER CLAMP ASSAY

A model BC-525A bilayer clamp (Warner Instrument Corp.) was used for planar bilayer experiments, ClampEx 8 and ClampFit 10 (Axon Instruments) were the software used for acquisition and analysis, respectively. Cups used were made of polystyrene and had 250 µm diameter apertures (Warner Instrument Corp). The lipid used in all cases was diphytanoyl phosphatidylcholine (diPhyPC) (Avanti Polar lipids). A stock solution of 25 mg/mL lipid in $CHCl_3$ was dried under N_2 and then re-suspended in 200 µL decane. For compounds that had to be pre-loaded into the lipid, 0.1 – 1 mol% compound in CHCl3 was added to the lipid mix and then dried down. The electrolytes used were 1 M CsCl in 10 mM HEPES, 10 mM TRIS, pH 7 (unadjusted). The aperture was primed with 0.5-1 µL of decane/lipid, excess solvent was removed by blowing N_2 over the aperture. The cup was then placed into the electrolyte-filled holding cell, consisting of 5 mL and 3 mL chambers, and salt bridges (KNO_3 or KCl/Agar) and electrodes (Ag/AgCl) were attached. Bilayers were formed by brushing on 1- 1.5 µL of the decane/lipid mix over the aperture, and were monitored for stability, capacitance and resistance for at least 20 minutes

before test compound was added. Test compounds were added either by injection from an organic solution (typically no more than 1-10 µL of solution) or by breaking the lipid-only bilayer and brushing on the compound-preloaded lipid mix. All data were hardware filtered (8- pole Bessel filter, 1 kHz) and data was collected in a survey mode using the Gap-free protocol. Bilayers were tested repeatedly for capacitance and resistance. Once formed, 'activity' from pristine bilayers was never observed.

HPTS ASSAY

Vesicle preparation: A chloroform solution of 8:1:1 PC:PA:cholesterol (Avanti Polar lipids) was dried in vacuo in a pear-shaped flask and then left on the vacuum line overnight. For compounds that were pre-loaded into the vesicle, a solution of the test compound of interest was added to the initial $CHCl_3$ lipid solution at 0.1 – 1 mol%, and then prepared as described. The 50 mg lipid film was hydrated with 1 mL of internal buffer solution (10 µM HPTS, 10 mM $Na_3PO_4.12H_2O$, 100 mM NaCl in deionized H_2O, pH 6.4, adjusted with conc. H_3PO_4). The suspension was frozen under liquid nitrogen and subsequently thawed at room temperature over ten minutes (3 times). The mixture was then sonicated in an ice bath for 20 seconds with 2 second pulses (at 50% duty cycle and 20% power output) 3 times, with a 30 s rest between cycles. The unilamellar vesicles were then left to anneal overnight. The vesicle solution was then sized 19 times through a 400 nm polycarbonate Nucleopore filter using a LiposoFast membrane extrusion apparatus (Avestin) (0.5 mL x 2) and purified on a PD-10 Sephadex G-25 column (GE Healthsystems) using an external buffer solution (10 mM Na_3PO_4 $.12H_2O$, 100 mM NaCl, pH= 6.4). The first three cloudy drops were discarded but thereafter the cloudy fraction was collected and diluted to 5.00 mL using the external buffer solution. A typical preparation of this vesicle stock solution contained 200 ±20 nm diameter vesicles (determined by dynamic light scattering, Brookhaven Instruments, ZetaPALS particle sizing software) and a lipid concentration of typically 7 mg/mL. The vesicle solution was stored at 50^oC and used within 24 hours of preparation.

Typical experiment: in a typical experiment, 100 µL of the vesicle suspension was added

to the fluorescence cuvette. 2.00 mL of external buffer (10 mM Na_3PO_4 .$12H_2O$, 100 mM NaCl, pH= 6.4) and 25 µL of a solution of the compound being tested, generally in MeOH, was then added. The solution was placed in the fluorimeter and left to equilibrate, generally 10 minutes. An excitation ratio was started (λEx1= 403 nm, λEx2= 460 nm, λEm= 510 nm, excitation and emission monochromator bandwiths = 3 nm, Integration 1s, duration 600 s). At t= 60 s, 50 µL of a 0.5 M aqueous NaOH solution was added through the injection port (continuous monitoring, no pause). At t= 540 s, the experiment was paused and 50 µL of a 0.5% aqueous solution of Triton X-100 was added. The experiment was then restarted after 30 s of stirring time. The data was analysed as reported previously.

Synthesis

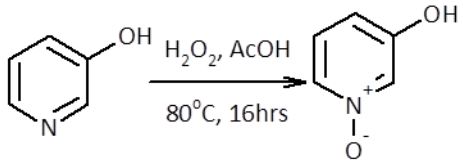

2-7: 3-hydroxypyridine-N-oxide (380 mg, 4.0 mmol scale): 1.0 equivalents of **3-hydroxypyridine** (**2-6**) was dissolved into glacial acetic acid, to this solution was added 8.0 equivalents of H_2O_2 as a 30% solution in water in 8 equal portions over the course of 2 hours. The reaction was then stirred vigorously and heated to 80°C for 16 hours. Over the course of the reaction the solution changed from clear and colourless to a clear pale yellow. The reaction was monitored by TLC (SiO_2, 9:1 EtOAc:MeOH, UV and $KMnO_4$ used for visualization, Rf = 0.17). The reaction was worked up by first removing the solvent under vacuum to afford a pale yellow oil, to this oil was added 2 g of solid Na_2CO_3 and Et_2O and the mixture was sonicated for ~20 minutes. The resulting mixture was then vacuum filtered, the resulting solids were sonicated in methanol and then also vacuum filtered. The filtrate from the second filtration was then dried under vacuum. Yield 60% as a white waxy solid. NMR (CD_3OD): ^{1}**H** = 7.85 (d, 2H, J = 8 Hz), 7.36 (t, 1H, J = 8 Hz), 7.04 (d, 1H, J = 8 Hz). ^{13}**C** = 158.7, 132.1, 129.6, 128.0, 119.4.

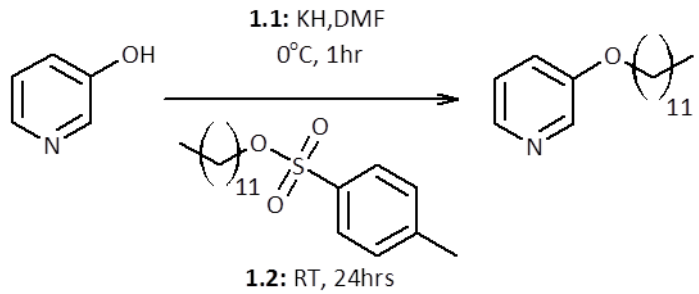

2-11: 3-dodecyloxypyridine (475 - 951 mg, 5.0 - 10.0 mmol scale): 1.1 equivalents of KH were suspended in dry DMF under a stream of N_2 and cooled to 0°C. To this mixture was added 1.0 equivalents of **3-hydroxypyridine** (**2-6**) as a 1M solution in dry DMF and was stirred at 0°C under a stream of N_2 for 1 hour. At this point 1.1 equivalents of ***n*-dodecyl *p*-toluenesulfonate** (**2-14**) were added to the reaction mixture as a 1M solution in dry DMF. The reaction was the stirred under a stream of N_2 for 24 hours while gradually warming to room temperature. The reaction was monitored by TLC (SiO_2, 25:25:1 hexanes:Et_2O:AcOH, UV and $KMnO_4$ used for visualization, Rf = 0.48). The reaction was worked up by first quenching the excess KH by adding 100 mL of H_2O. This mixture was then extracted with Et_2O (3x 50mL). The Et_2O extracts were then combined and washed in order with H_2O and brine before being dried over Na_2SO_4 and filtered. The filtrate was dried under vacuum and then purified by silica gel column chromatography eluting with 0 - 20% Et_2O in hexanes with 3% AcOH. Yields 25 - 89% as a clear colourless oil. NMR ($CDCl_3$): **^{1}H** = 8.24 (s, 1H), 8.05 (s, 1H), 7.10 (s, 2H), 3.86 (t, 2H, *J*= 7Hz), 1.72 (m, 2H), 1.30-1.05 (m, 18H), 0.68 (t, 2H, *J*= 7Hz). **^{13}C** = 155.4, 142.1, 138.3, 123.9, 121.1, 68.5, 32.1, 29.8, 29.7, 29.7, 29.6, 29.4, 26.1, 22.9, 14.3.

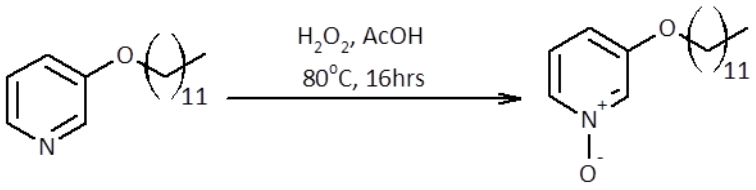

2-12: 3-dodecyloxypyridine-N-oxide (1.0 g, 3.8 mmol scale): 1.0 equivalent of **3-dodecyloxypyridine (2-11)** was dissolved into glacial acetic acid, to this solution was added 3.5 equivalents of H_2O_2 as a 30% solution in water in 8 equal portions over the course of 2 hours. The reaction was then stirred vigorously and heated to 80°C for 16 hours. Over the course of the reaction the solution changed from clear and colourless to a clear pale yellow. The reaction was monitored by TLC (SiO_2, 9:1 Et_2O:MeOH, UV and $KMnO_4$ used for visualization, Rf = 0.43). The reaction was worked up by first evaporating the solvent under vacuum, the resulting yellow oil was then dissolved into $CHCl_3$, sonicated, dried over Na_2SO_4, filtered and then dried under vacuum. Yields 79 - 86% as pale yellow crystals. NMR ($CDCl_3$): **^{1}H** = 7.90 (s, 1H), 7.81 (d, 1H, *J*= 8Hz), 7.15 (t, 1H, *J*= 8Hz), 6.80 (d, 1H, *J*= 8Hz), 3.82 (t, 2H, *J*= 7Hz), 1.85 (m, 2H), 1.40 – 1.10 (m, 18H), 0.78 (t, 2H, *J*= 7Hz). **^{13}C** = 157.8, 132.5, 128.3, 125.5, 113.7, 69.4, 32.1, 29.8, 29.8, 29.7, 29.6, 29.5, 29.1, 26.0, 22.9, 14.3.

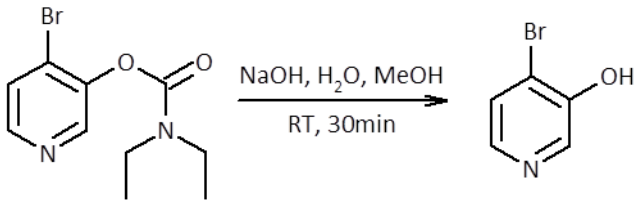

2-20: 4-bromo-3-hydroxypyridine (268 mg, 0.98 mmol scale): 1.0 equivalent of **4-bromopyridin-3-yl diethylcarbamate (2-18)** was dissolved in methanol and to this solution was added 5.0 equivalents of NaOH as a 2M aqueous solution. The reaction was then stirred at room temperature for 30 minutes during which time it was monitored by TLC (SiO_2, EtOAc, UV and $KMnO_4$ used for visualization, Rf = 0.59). The reaction was worked up by first neutralizing the solution with 1M HCl and then diluting the mixture by half with H_2O. This diluted solution was then extracted with Et_2O (x5), the combined organic fractions were then washed with brine, dried over Na_2SO_4, filtered and then dried under vacuum. Yield 84% as pale yellow crystals. NMR (d6-

Acetone): **^{1}H** = 8.12 (d, 1H, *J*= 8Hz), 7.78 (d, 1H, *J*= 8Hz), 7.31 (s, 1H), 3.15 (s, br, 1H). **^{13}C** = 142.4, 139.3, 128.9, 119.7.

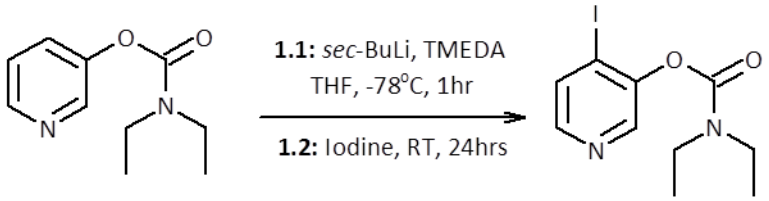

2-24: 4-iodopyridin-3-yl diethylcarbamate (1.94 g, 10.0 mmol scale): 1.0 equivalent of **pyridine-3-yl diethylcarbamate (2-17)** was dissolved into dry THF at -78°C under a stream of N_2. To this solution was added 1.2 equivalents of TMEDA and then 1.2 equivalents of *sec*-BuLi as a 1.4M solution in dry THF dropwise over a period of 90 minutes. At this time 1.2 equivalents of I_2 was added slowly while maintaining the reaction at -78°C under a stream of N_2. The reaction was then allowed to stir vigorously under a stream of N2 while gradually warming to room temperature over a period of 24 hours. The reaction was monitored by TLC (SiO2, 2:3 EtOAc:hexanes, UV and I_2 used for visualization, Rf = 0.45). The reaction was worked up by first adding a saturated solution of NH_4Cl in water and then evaporated under vacuum to remove the THF. This aqueous solution was then extracted with EtOAc (x3) and the combined organic fractions were washed with water (x2) and brine (x2) before being dried over Na_2SO_4, filtered and then dried under vacuum. The resulting crude product was purified by silica gel column chromatography eluting with 0 - 45% EtOAc in hexanes. Yield 84% as a clear colourless oil. NMR ($CDCl_3$): **^{1}H** = 8.21 (s, 1H), 7.88 (s, 1H), 7.60 (s, 1H), 3.42-3.15 (m, 4H), 1.35-1.05 (m, 6H). **^{13}C** = 152.4, 149.5, 146.7, 144.6, 134.0, 102.4, 42.7, 42.4, 14.5, 13.4. *Note* This compound spontaneously and quantitatively decomposed under vacuum in the dark over the period of a few hours to afford the dimer **2-25: AKD2-123-03-08-24-07**as a brick red solid. NMR ($CDCl_3$): **^{1}H** = 8.98 (d, 2H, *J*= 8Hz), 8.62 (m, 4H), 8.21 (d, 2H, *J*= 8Hz), 3.64 – 3.15 (m, 8H), 1.34-0.91 (m, 12H). **^{13}C** = 152.4, 151.6, 150.7, 149.1, 147.1, 141.4, 140.5, 140.4, 139.8, 136.3, 126.6, 120.4, 43.3, 43.2, 42.8, 14.8, 14.3, 13.3, 13.1.

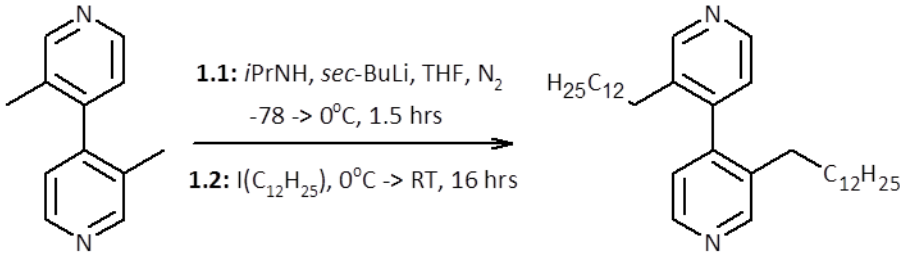

2-34: 3,3'-ditridecyl-4,4'-bipyridine (165 mg, 0.9 mmol scale): To an N_2 purged round bottom flask was added dry THF and 2.1 equivalents of *i*-PrNH2 which was then cooled to -78°C. To this solution was added with constant stirring 2.1 equivalents of *sec*-BuLi as a 2M solution in hexanes dropwise ensuring that the temperature of the reaction did not rise above -78°C. After this addition 1.0 equivalent of **3,3'-dimethyl-4,4'-bipyridine (2-33)** was added to the reaction mixture under a stream of N_2 while maintaining the reaction at -78°C at which point the reaction mixture went from cloudy white to dark inky blue. After 10 minutes 2.1 equivalents of 1-iodododecane was added to the reaction and the temperature was allowed to rise to 0° at which temperature it was stirred in the dark for 90 minutes, after which the reaction was allowed to warm to room temperature and stirred for a further 16 hours. The reaction was monitored by TLC (SiO_2, EtOAc, UV and I_2 used for visualization, Rf = 0.71). The reaction was worked up by first drying the reaction mixture under vacuum and the resulting orangey oil was dissolved into DCM. This organic fraction was then washed with H_2O and then brine before being dried over Na_2SO_4, filtered and then dried under vacuum. The resulting crude material was then purified by silica gel column chromatography eluting with 0 - 90% EtOAc in hexanes. Yield 58% as a waxy white solid. NMR ($CDCl_3$): ^{1}**H** = 8.51 (s, 2H), 8.39 (s, 2H), 6.95 (d, 2H, *J*= 8Hz), 2.34 (m, 4H), 1.42-1.05 (m, 44H), 0.75 (t, 6H, *J*= 7Hz). ^{13}**C** = 151.1, 147.2, 146.1, 135.4, 123.6, 32.1, 30.8, 30.6, 29.8, 29.7, 29.6, 29.6, 29.5, 29.4, 22.9, 14.3.

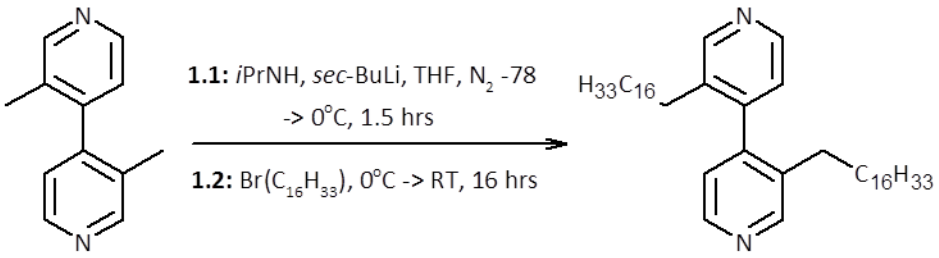

2-35: 3,3'-diheptadecyl-4,4'-bipyridine (165 mg, 0.9 mmol scale): To an N_2 purged round bottom flask was added dry THF and 2.1 equivalents of *i*-PrNH2 which was then cooled to -78°C. To this solution was added with constant stirring 2.1 equivalents of *sec*-BuLi as a 2M solution in hexanes dropwise ensuring that the temperature of the raction did not rise above -78°C. After this addition 1.0 equivalent of **3,3'-dimethyl-4,4'-bipyridine (2-33)** was added to the reaction mixture under a stream of N_2 while maintaining the reaction at -78°C at which point the reaction mixture went from cloudy white to dark inky blue. After 10 minutes 2.1 equivalents of 1-bromohexadecane was added to the reaction and the temperature was allowed to rise to 0° at which temperature it was stirred in the dark for 90 minutes, after which the reaction was allowed to warm to room temperature and stirred for a further 16 hours. The reaction was monitored by TLC (SiO_2, 4:1 hexanes:EtOAc, UV and I_2 used for visualization, Rf = 0.18). The reaction was worked up by first drying the reaction mixture under vacuum and the resulting orangey oil was dissolved into DCM. This organic fraction was then washed with H_2O and then brine before being dried over Na_2SO_4, filtered and then dried under vacuum. The resulting crude material was then purified by silica gel column chromatography eluting with 0 - 35% EtOAc in hexanes. Yield 53% as off-white crystals. NMR ($CDCl_3$): ^{1}**H** = 8.51 (s, 2H), 8.38 (d, 2H, *J*= 8Hz), 6.92 (d, 2H, *J*= 8Hz), 2.35 (m, 2H), 2.15 (m, 2H), 1.35-1.05 (m, 60H), 0.76 (t, 6H, *J*= 7Hz). ^{13}**C** = 151.1, 147.2, 146.1, 135.4, 123.7, 32.1, 30.8, 30.6, 29.9, 29.9, 29.8, 29.6, 29.5, 29.5, 29.4, 22.9, 14.3.

General procedure for the attempted self-assembly of lipophilic ethylenediamine palladium(II) (2-4) with lipophilic 4,4'-bipyridines (2-33, 2-34, 2-35).

The palladium containing lipophilic corner (**2-4**) was dissolved into either DMF, THF or acetonitrile with gentle heating to afford a 1mM solution. The lipophilic 4,4'-bipyridine molecule (**2-33**, **2-34** or **2-35**) was also dissolved into either THF or acetonitrile, also under gentle heating if necessary to provide a 1mM solution. Combinations of these solutions were prepared such that the stoichiometry of the two components was as close to equal as possible. Some common observations upon mixing the two components were a minor change in colour to a slightly yellow-beige solution or the generation of fine gummy precipitates. The resulting mixtures were heated gently in an attempt to dissolve the components and speed up the coordination which was not always possible. The solutions were then allowed to cool to room temperature and then put in area with minimal disturbance in an effort to generate crystals of the product.

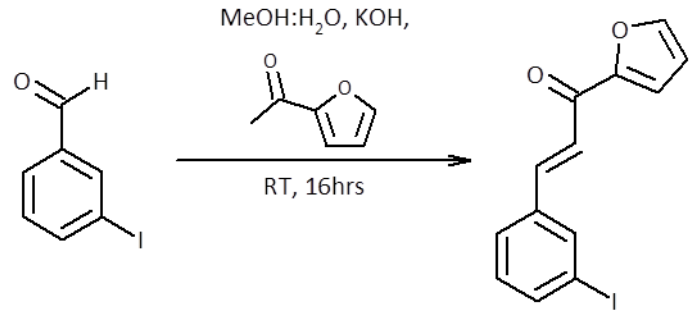

2-49: (2E)-3-(3-iodophenyl)-1-(pyridine-2-yl)prop-2-en-1-one (1.2 - 4.6 g, 5.0 - 20.0 mmol scale): 1.0 equivalent of ***m*-iodobenzaldehyde (2-45)** was finely divided and then suspended in sufficient 0.85M solution of KOH to provide 1.02 equivalents of base under an inert N_2 environment at 0°C. 1.5 equivalents of **2-acetylfuran (2-47)** as a 0.62M solution in anhydrous EtOH was added to the vigorously stirring mixture over a period of ~2 hours while maintaining the temperature at 0°C and under an inert atmosphere. Once the addition was complete the reaction was then allowed to warm to room temperature and stirred vigorously for a further 16 hours. During the reaction the mixture went from a cloudy white suspension to a dark brown solution. The reaction

was monitored by TLC (SiO_2, 3:1 hexanes:EtOAc, UV and vanillin (orange) used for visualization, Rf = 0.51). The reaction was worked up by first neutralizing the solution with 1M HCl resulting in a milky off white suspension. This neutralized mixture was further diluted by a factor of four using H_2O before being extracted several times using Et_2O until further extracts revealed no further product being extracted. The combined organic fractions were then washed with H_2O and brine before being dried over Na_2SO_4, filtered and then dried under vacuum. The resulting crude product was purified by silica gel column chromatography eluting with 0 - 20% EtOAc in hexanes. Yields 31 - 46% as an off white waxy solid. NMR ($CDCl_3$): **^{1}H** = 7.99 (m, 1H), 7.73 (m, 2H), 7.66 (m, 1H), 7.57 (d, 1H, *J*= 8Hz), 7.40 (d, 1H, *J*= 13Hz), 7.34 (d, 1H, *J*= 4Hz), 7.14 (t, 1H, *J*= 8Hz), 6.60 (m, 1H). **^{13}C** = 177.6, 153.7, 146.9, 142.3, 139.4, 136.6, 130.7, 128.1, 122.4, 117.7, 112.9, 94.9.

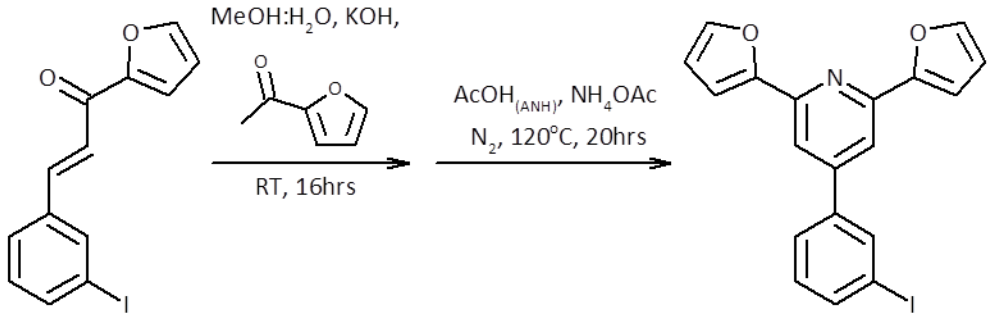

2-54: 2,6-di(furan-2-yl)-4-(3-iodophenyl)pyridine (0.6 - 1.2 g, 1.9 - 3.7 mmol scale): 1.0 equivalent of **(2E)-3-(3-iodophenyl)-1-(pyridine-2-yl)prop-2-en-1-one (2-49)** and 1.5 equivalents of **2-acetylfuran (2-47)** were dissolved in anhydrous ethanol and transferred to an addition funnel. This solution was then added dropwise to 1.5 equivalents of KOH dissolved into enough H_2O to provide a 0.7M solution over the course of ~2 hours at 0°C under a stream of N_2. After the complete addition of the ethanolic solution the reaction was allowed to come to room temperature and stirred vigorously under an inert atmosphere for 16 hours. During the reaction the solution went from a clear and colourless to cloudy white to cloudy yellow and finally to dark brown. The reaction was

monitored by TLC (SiO_2, DCM, UV and vanillin used for visualization) in order to determine when all of the starting **2-49** had been consumed. At this stage the reaction mixture was diluted by a factor of five using H_2O and the resulting gooey brown mixture was extracted with Et_2O several times. The combined organic fractions were then washed with H_2O and brine before being dried over Na_2SO_4, filtered and dried under vacuum to afford a dark brown sticky material. This material was then dissolved into anhydrous AcOH to which 6.0 equivalents of NH_4OAc were added. This mixture was then heated to reflux for 20 hours with vigorous stirring. The reaction was monitored by TLC (Al_2O_3, 22:1:1 hexanes:DCM:EtOAc, UV used for visualization, Rf = 0.59). After this time the reaction was worked up by first drying under vacuum in order to remove as much AcOH as possible. The resulting tar was then treated with Et_2O until no further dissolution of solids was observed before being vacuum filtered. The vacuum filtrate was then washed with saturated $NaHCO_3$ (x2) and brine before being dried over $MgSO_4$, filtered and dried under vacuum to afford a mass of dark orange resinous solid. This crude product was purified by neutral alumina column chromatography eluting with 0 - 5% EtOAc in hexanes. Yields 33 - 63% as a pale yellow waxy solid. NMR ($CDCl_3$): ^{1}**H** = 8.08 (t, 1H, *J*= 1Hz), 7.80 (dq, 1H, *J*= 8, 1Hz), 7.73 (s, 2H), 7.70 (dq, *J*= 8, 1Hz), 7.57 (m, 2H), 7.26 (m, 4H), 6.56 (m, 2H). ^{13}**C** = 153.7, 149.9, 148.4, 143.6, 138.2, 136.1, 130.8, 126.5, 114.9, 112.3, 109.7, 95.3.

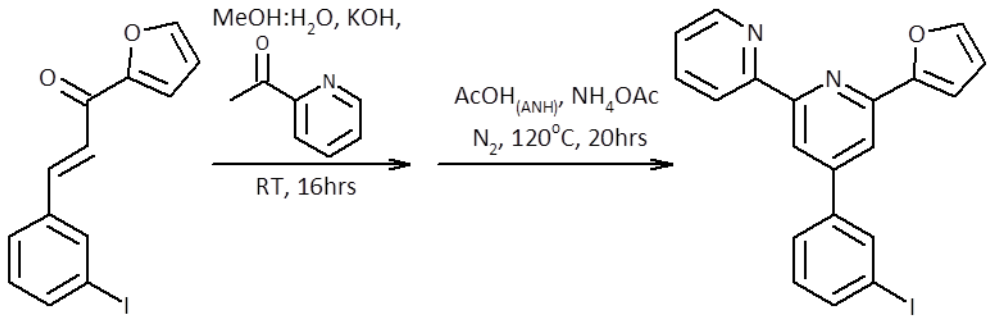

2-55: 6-(furan-2-yl)-4-(3-iodophenyl)-2,2'-bipyridine (0.5 - 1.1 g, 1.5 - 3.4 mmol scale): 1.0 equivalent of **(2E)-3-(3-iodophenyl)-1-(pyridine-2-yl)prop-2-en-1-one (2-49)** and 1.5

equivalents of **2-acetylpyridine (2-46)** were dissolved in anhydrous ethanol and transferred to a pressure equilibrating addition funnel. This solution was then added dropwise to 1.5 equivalents of KOH dissolved into enough H_2O to provide a 0.7M solution over the course of ~2 hours at 0°C under a stream of N_2. After the complete addition of the ethanolic solution the reaction was allowed to come to room temperature and stirred vigorously under an inert atmosphere for 16 hours. During the reaction the solution went from a clear and colourless to cloudy white to cloudy yellow and finally to dark brown. The reaction was monitored by TLC (SiO_2, DCM, UV and vanillin used for visualization) in order to determine when all of the starting **2-49** had been consumed. At this stage the reaction mixture was diluted by a factor of five using H_2O and the resulting gooey brown mixture was extracted with Et_2O several times. The combined organic fractions were then washed with H_2O and brine before being dried over Na_2SO_4, filtered and dried under vacuum to afford a dark brown sticky material. This material was then dissolved into anhydrous AcOH to which 6.0 equivalents of NH_4OAc were added. This mixture was then heated to reflux for 20 hours with vigorous stirring. The reaction was monitored by TLC (Al_2O_3, 22:1:1 hexanes:DCM:EtOAc, UV used for visualization, Rf = 0.47). After this time the reaction was worked up by first drying under vacuum in order to remove as much AcOH as possible. The resulting tar was then treated with Et_2O until no further dissolution of solids was observed before being vacuum filtered. The vacuum filtrate was then washed with saturated $NaHCO_3$ (x2) and brine before being dried over $MgSO_4$, filtered and dried under vacuum to afford a mass of dark orange resinous solid. This crude product was purified by neutral alumina column chromatography eluting with 0 -10% EtOAc in hexanes. Yields 18 - 69% as a pale yellow waxy solid. NMR ($CDCl_3$): ^{1}**H** = 8.61 (dq, 1H, *J*= 4, 1Hz), 8.49 (d, 1H, *J*= 7Hz), 8.40 (s, 1H), 8.05 (t, 1H, *J*= 1Hz), 7.78 (m, 2H), 7.66 (m, 2H), 7.49 (s, 1H), 7.25 (m, 1H), 7.15 (m, 2H), 6.49 (m, 1H). ^{13}**C** = 156.3, 155.7, 153.8, 149.5, 148.9, 148.5, 143.4, 140.6, 138.0, 137.0, 135.9, 30.6, 126.4, 124.0, 121.5, 117.1, 116.1, 112.1, 109.1, 94.8. **DEPT** = 148.9, 143.4, 137.9, 136.9, 135.9, 135.7, 130.6, 126.5, 124.0, 121.5, 117.0, 116.2, 112.2, 109.1.

One pot synthesis of 4'-(3-iodophenyl)-2,2':6',2''-terpyridine (2-51), 2,6-di(furan-2-yl)-4-(3-iodophenyl)pyridine (2-54) and 6-(furan-2-yl)-4-(3-iodophenyl)-2,2'-bipyridine (2-55) (1.2 - 5.8 g, 5.0 - 25.0 mmol scale):

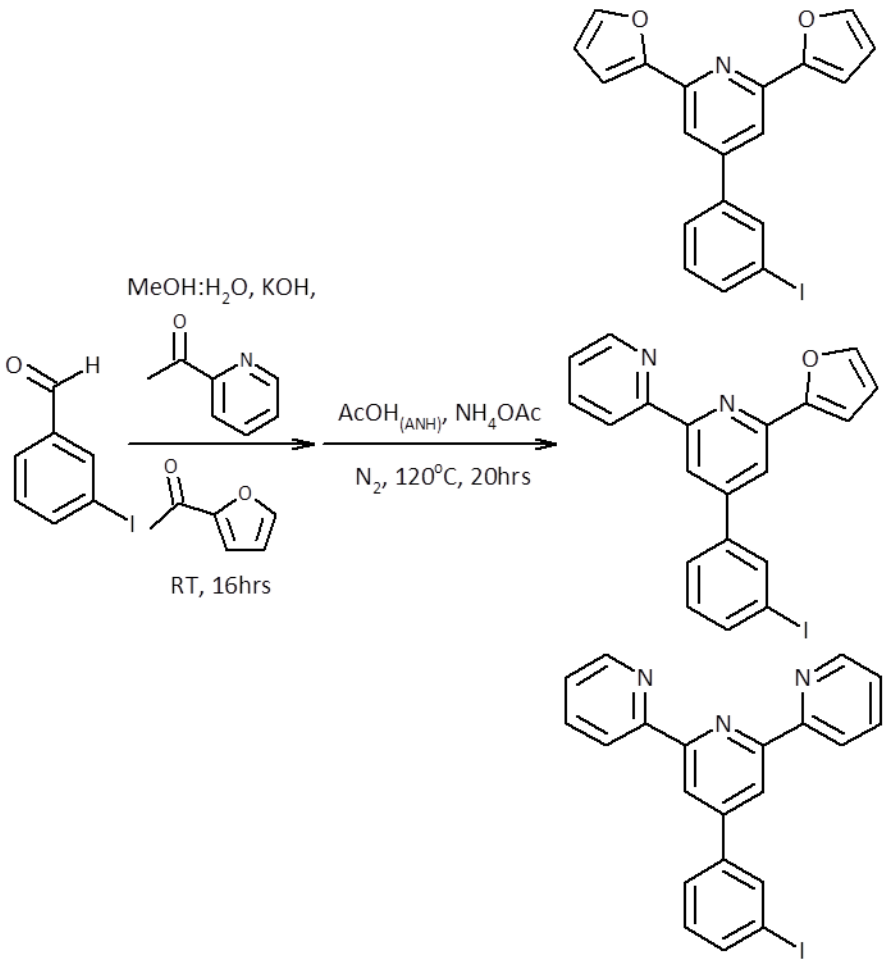

1.0 equivalent of ***m*-iodobenzaldehyde (2-45)**, 1.25 equivalents of **2-acetylfuran (2-47)** 1.1 equivalents of **2-acetylpyridine (2-46)** were dissolved in anhydrous ethanol and transferred to a pressure equilibrating addition funnel purged with N_2. This solution was then added dropwise to 2.5 equivalents of KOH dissolved in water to achieve a 1.0M solution cooled to 0°Cand under a stream of N_2 over a period of ~4 hours. After the addition the reaction was allowed to warm to room temperature and stirred for a further 16 hours. During this time the reaction went from clear and colourless, to

cloudy white, to cloudy yellow and finally to dark brown. The reaction was monitored by TLC (SiO_2, DCM, UV and vanillin used for visualization)and was determined to be complete once the spot due to the ***p*-iodobenzaldehyde (2-45)** had disappeared. At this stage the reaction was diluted by a factor of five using H_2O and the resulting mixture was extracted with Et_2O until the extraction afforded no further material. The combined organic fractions were then washed with H_2O and brine before being dried over $MgSO_4$, filtered and then dried under high vacuum. The resulting dark brown resinous solid was then dissolved in glacial AcOH. To this solution was added 6.0 equivalents of NH_4OAc at which point the reaction mixture was heated to reflux for 20 hours. The reaction was monitored by TLC (Al_2O_3, 22:1:1 hexanes:DCM:EtOAc, UV used for visualization, Rf = 0.59 (**2-54**), 0.47 (**2-55**), 0.35 (**2-51**)). After this time the reaction was worked up by first drying under vacuum in order to remove as much AcOH as possible. The resulting tar was then treated with Et_2O until no further dissolution of solids was observed before being vacuum filtered. The vacuum filtrate was then washed with saturated $NaHCO_3$ (x2) and brine before being dried over $MgSO_4$, filtered and dried under vacuum to afford a mass of dark orange resinous solid. This crude product was purified by neutral alumina column chromatography eluting with 0 -40% (1:1 DCM:EtOAc) in hexanes. Combined overall yields based on ***p*-iodobenzaldehyde (2-45)** 35 - 48% with average product ratios of 1.0:2.1:1.6 **2-54**: **2-55**: **2-51**.

NMR ($CDCl_3$):

2-54: ^{1}**H** = see above. ^{13}**C** = see above.

2-55: ^{1}**H** = see above. ^{13}**C** = see above.

2-51: ^{1}**H** = 8.64-8.74 (m, 6H), 8.21 (s, 1H), 7.82 (m, 4H), 7.35 (tq, 2H, *J*= 7, 1Hz), 7.23(t, 1H, *J*= 8Hz). ^{13}**C** = 155.9, 149.2, 148.7, 140.6, 137.0, 136.8, 136.0, 130.4, 126.9, 124.0, 121.3, 118.7, 94.9.

General procedure for the oxidation of furan containing compounds (2-54, 2-55, 2-58) to the corresponding carboxylic acids (2-56, 2-57, 2-59):

To a round bottom flask was added 1.0 equivalent of **furan containing compound (2-54, 2-55, 2-58)**, 6.5 equivalents of $KMnO_4$ per furan moiety and 5:1 *t*-BuOH:H_2O as solvent. The reaction was then heated to reflux for 16 hours. During this time the reaction went from a deep purple to a thick brown mixture. The reaction was worked up by first hot vacuum filtering through a bed of celite, rinsing the dark brown solids several times with hot 1:4 *t*-BuOH:H_2O. The filtrate was then treated with a sodium bisulfate solution until clear and colourless and then reduced in volume by ¾ under vacuum. The concentrated solution was then cooled to 4°C for several hours during which time an opalescent while precipitate formed. This precipitate was isolated by vacuum filtration and then dried further under high vacuum to afford the final desired compounds. Attempts at characterizing these products by NMR spectroscopy resulted in poor quality spectra with very broad signals, these materials were carried through to the TMSE ester forming reactions without further purification.

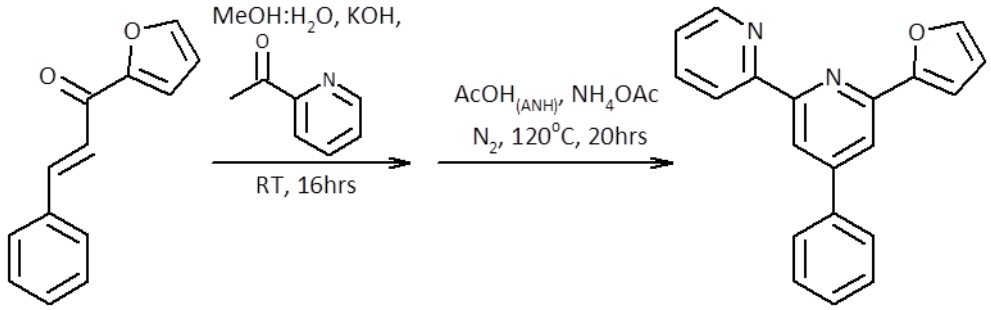

2-58: 6-(furan-2-yl)-4-phenyl-2,2'-bipyridine (1.4 g, 7.0 mmol scale): 1.0 equivalent of **(2E)-1-(furan-2-yl)-3-phenylprop-2-en-1-one (2-76)** and 1.5 equivalents of **2-acetylpyridine (2-46)** were dissolved in anhydrous ethanol and transferred to a pressure equilibrating addition funnel. This solution was then added dropwise to 1.5 equivalents of KOH dissolved into enough H_2O to provide a 1.0M solution over the course of ~2 hours at 0°C under a stream of N_2. After the complete addition of the ethanolic solution the reaction was allowed to come to room temperature and stirred vigorously under an inert atmosphere for 16 hours. During the reaction the solution went from a clear and

colourless to cloudy white to cloudy yellow and finally to dark brown. The reaction was monitored by TLC (SiO_2, DCM, UV and vanillin used for visualization) in order to determine when all of the starting **2-76** had been consumed. At this stage the reaction mixture was diluted by a factor of five using H_2O and the resulting gooey brown mixture was extracted with Et_2O several times. The combined organic fractions were then washed with H_2O and brine before being dried over Na_2SO_4, filtered and dried under vacuum to afford a dark brown sticky material. This material was then dissolved into anhydrous AcOH to which 6.0 equivalents of NH_4OAc were added. This mixture was then heated to reflux for 20 hours with vigorous stirring. The reaction was monitored by TLC (SiO_2, 5:1 hexanes:acetonex, UV used for visualization, Rf = 0.54). After this time the reaction was worked up by first drying under vacuum in order to remove as much AcOH as possible. The resulting tar was then treated with Et_2O until no further dissolution of solids was observed before being vacuum filtered. The vacuum filtrate was then washed with saturated $NaHCO_3$ (x2) and brine before being dried over $MgSO_4$, filtered and dried under vacuum to afford a mass of dark orange resinous solid. This crude product was purified by neutral alumina column chromatography eluting with 0 - 50% acetone in hexanes. Yield 64% as an off-white waxy solid. NMR ($CDCl_3$): ^{1}**H** = 8.71 (dq, 1H, *J*= 6, 1Hz), 8.59 (m, 2H), 7.97 (m, 1H), 7.85 (m, 3H), 7.58 (m, 1H), 7.34 (tq, 1H, *J*= 6, 1Hz), 7.25 (d, 1H, *J*= 6Hz), 6.59 (m, 1H). ^{13}**C** = 156.3, 156.2, 150.3, 149.6, 149.1, 143.4, 138.5, 137.2, 129.2, 127.3, 124.1, 121.7, 117.5, 116.5, 112.2, 108.9.

General procedure for the TMSE protection of the carboxylic acid bearing molecules (2-56, 2-57, 2-59):

To a round bottom flask set up for reflux under a N_2 atmosphere was added the **carboxylic acid bearing molecule (2-56, 2-57 or 2-59)**. To this vessel was added 3 mL of $SOCl_2$ and 2 drops of dry DMF. The reaction was then heated to reflux under a stream of N_2 and stirred vigorously for 4 hours. During this time the reaction mixture went from an off-white solid suspension in a clear colourless solution to a pale yellow solution. After this time the $SOCl_2$ was removed under a stream of N_2 to afford a pale yellow waxy

solid. This solid was then dissolved in dry DCM while maintaining an inert atmosphere and to the resulting solution was added 2.0 equivalents of trimethylsilylethanol and 2.2 equivalents of dry pyridine per carboxylic acid group of the starting material. The reaction was then heated to reflux under a stream of N_2 and stirred vigorously for 16 hours. The reaction was monitored by TLC and upon completion the reaction was worked up by first diluting the solution with DCM until doubled in volume. This solution was then filtered and the filtrate washed in order with saturated $NaHCO_3$ and then brine before being dried over Na_2SO_4, filtered and dried under vacuum. The crude product was then purified by silica gel column chromatography.

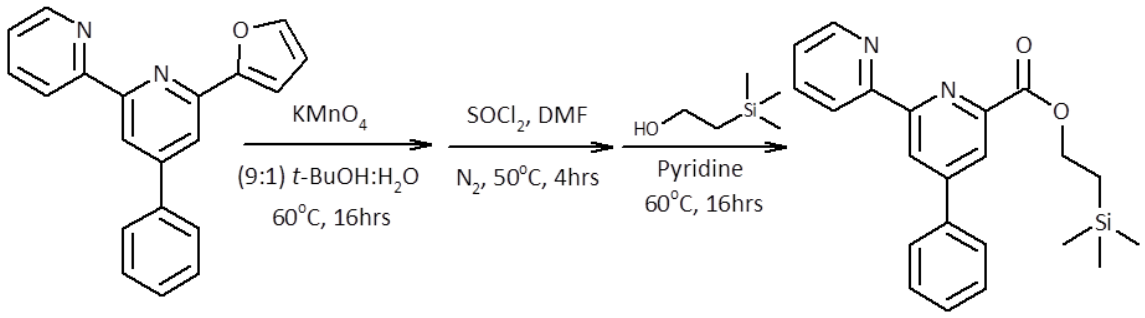

2-63: trimethylsilylethyl 4-phenyl-2,2'-bipyridine carboxylate (250 - 410 mg, 0.84 - 1.37 mmol scale): TLC conditions - SiO_2, 5:1 hexanes:acetone, UV used for visualization, Rf = 0.42. Silica gel column chromatography carried out using 0 - 8% acetone in hexanes. Yields 50 - 79% of waxy off-white solid. NMR ($CDCl_3$): ^{1}**H** = 8.57 (d, 1H, *J*= 2Hz), 8.70 (dq, 1H, *J*= 5, 1Hz), 8.62 (dq, 1H, *J*= 8, 1Hz), 7.84 (m, 3H), 7.49 (m, 3H), 7.35 (m, 1H), 4.57 (m, 2H), 1.25 (m, 2H), 0.14 (s, 9H). ^{13}**C** = 165.7, 156.9, 155.4, 150.4, 149.3, 148.8, 137.6, 137.3, 129.6, 129.5, 129.2, 124.3, 123.1, 122.2, 122.0, 64.4, 17.6, -1.2.

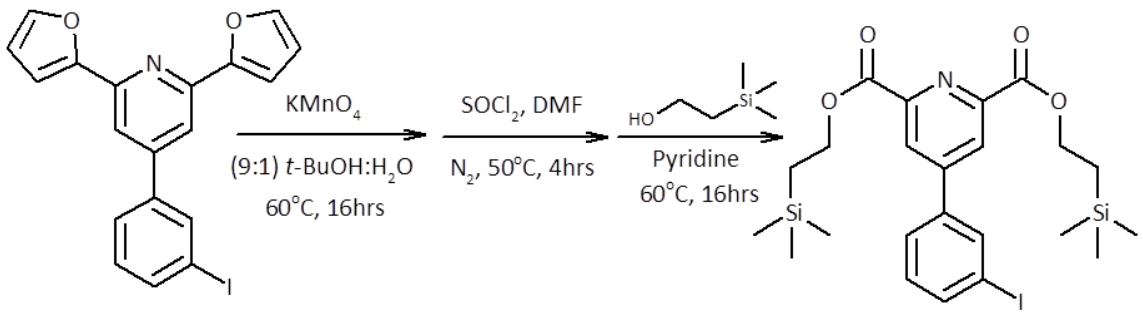

2-67: di-trimethylsilylethyl 4-(3-iodophenyl)pyridine-2,6-dicarboxylate (150 - 545 mg, 0.36 - 1.32 mmol scale): TLC conditions - SiO_2, 9:1 hexanes:acetone, UV used for visualization, Rf = 0.36. Silica gel column chromatography carried out using 0 - 10% acetone in hexanes. Yields 12 - 99% of fan like white crystals. NMR ($CDCl_3$): ^{1}**H** = 8.43 (s, 2H), 8.07 (t, 1H, *J*= 1Hz), 7.82 (dq, 1H, *J*= 8, 1Hz), 7.69 (dq, *J*= 8, 1Hz), 7.27 (m, 1H), 4.54 (m, 4H), 1.24 (m, 4H), 0.10 (s, 18H). ^{13}**C** = 164.9, 149.7, 149.2, 138.6, 136.4, 131.0, 126.3, 125.6, 95.4, 65.1, 17.8, -1.3.

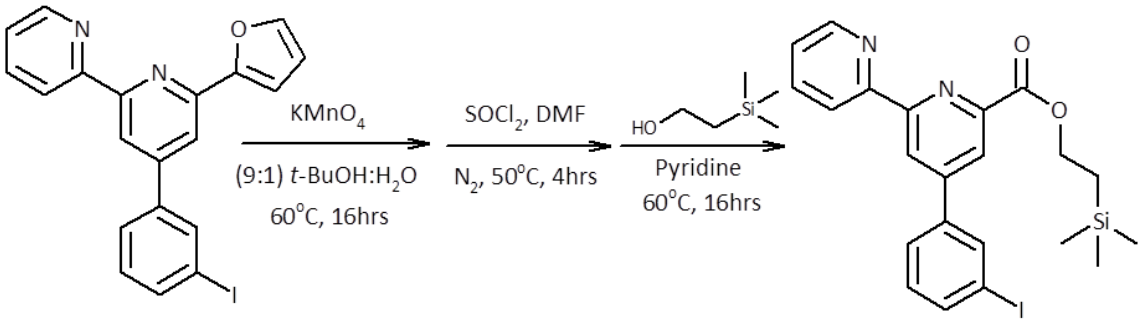

2-71: trimethylsilylethyl 4-(3-iodophenyl)-2,2'-bipyridine carboxylate (240 - 650 mg, 0.57 - 1.5 mmol scale): TLC conditions - Al_2O_3, 3:1 hexanes:EtOAc, UV used for visualization, Rf = 0.79. Neutral alumina column chromatography carried out using 0 - 10% EtOAc in hexanes. Yields 43 - 99% of pale yellow oil. NMR ($CDCl_3$): ^{1}**H** = 8.82 (d, 1H, *J*= 1Hz), 8.71 (d, 1H, *J*= 1Hz), 8.62 (d, 1H, *J*= 8Hz), 8.30 (d, 1H, *J*= 1Hz), 8.15 (t, 1H, *J*= 1Hz), 8.56 (td, 1H, *J*= 8, 1Hz), 7.79 (m, 2H), 7.37 (m, 1H), 7.25 (t, 1H, *J*= 8Hz), 4.57 (m, 2H), 1.25 (m, 2H), 0.13 (s, 9H). ^{13}**C** = 165.5, 157.5, 155.3, 149.2, 148.9, 139.8, 138.4, 137.2, 136.4, 130.9, 126.5, 124.6, 122.8, 122.3, 121.7, 95.4, 64.2, 18.0, -1.3.

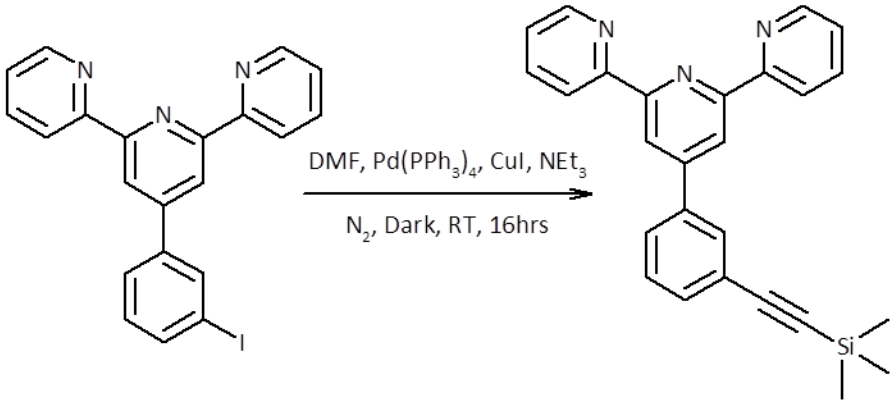

2-65 (155 - 715 mg, 0.36 - 1.64 mmol scale): 1.0 equivalent of **4'-(3-iodophenyl)-2,2':6',2''-terpyridine (2-51)** was dissolved in dry THF. This solution was then purged with N_2 and to it was added in order 2.0 equivalents of DIPEA, 0.03 equivalents of $Pd(PPh_3)_4$, 0.06 equivalents of CuI and 2.0 equivalents of trimethylsilyl acetylene. The reaction was then stirred vigorously at room temperature under and inert atmosphere in the dark for 16 hours. The reaction was monitored by TLC (Al_2O_3, 22:1:1 hexanes:DCM:EtOAc, UV and vanillin (blue) used for visualization, Rf = 0.37) and determined to be complete with the disappearance of a spot due to starting material (**2-51**). The reaction was worked up by first drying the product under vacuum and then dissolving the resulting sticky orange solid in Et2O. This solution was vacuum filtered and the filtrate was then washed in order with an aqueous solution of disodium EDTA, saturated $NaHCO_3$ and brine before being dried over Na_2SO_4, filtered and then dried under vacuum. The crude material was then purified using neutral alumina column chromatography eluting with 0 - 15% (DCM:EtOAc) in hexanes. Yield 82 % as an off white solid. NMR ($CDCl_3$): ^{1}**H** = 8.71 (dq, 1H, *J*= 4,1Hz), 8.69 (s, 2H), 8.63 (d, 2H, *J*= 8Hz), 8.01 (t, 1H, *J*= 1Hz), 7.83 (m, 2H), 7.54 (dt, 1H, *J*= 8, 1Hz), 7.43 (t, 1H, *J*= 8Hz), 7.32 (m, 2H), 0.29 (s, 9H). ^{13}**C** = 156.4, 149.7, 149.1, 139.1, 137.1, 132.4, 130.8, 129.9, 123.9, 121.7, 119.1, 105.0, 95.1, 0.6.

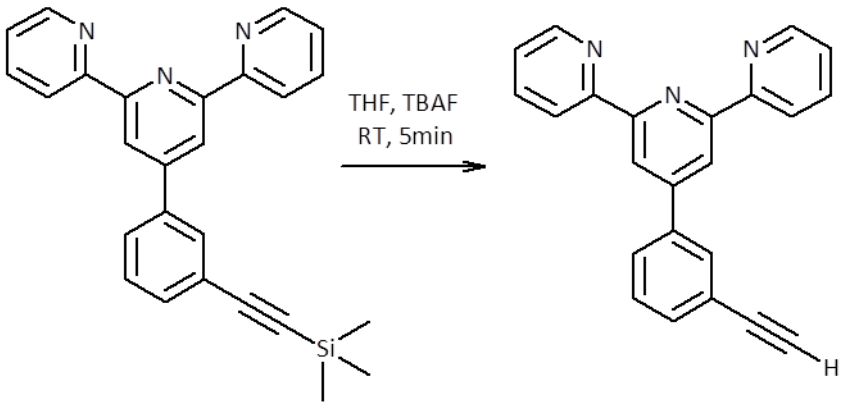

2-66 (202 - 405 mg, 0.5 - 1.0 mmol scale): 1.0 equivalents of **2-65** was dissolved into dry THF and to this solution was added 1.0 equivalents of TBAF as a 1M solution in THF. Upon the addition of TBAF the reaction went instantaneously inky blue. The reaction was monitored by TLC (Al_2O_3, 18:1:1 hexanes:DCM:EtOAc, UV used for visualization, Rf = 0.30) and determined to be complete after 5 minutes. The reaction was worked up by first treating the reaction with 1 mL of MeOH before being dried under high vacuum. The resulting pale yellow solution was dried under vacuum and the resulting orange oil dissolved in DCM. This solution was then washed with H2O and brine before being dried over Na_2SO_4, filtered and dried under vacuum. The crude material was purified by neutral alumina column chromatography eluting with 0 - 25% (DCM:EtOAc) in hexanes. Yields 65 - 90% as an off white waxy solid. NMR ($CDCl_3$): ^{1}**H** = 8.73 (m, 4H), 8.67 (d, 2H, *J*= 8Hz), 8.04 (t, 1H, *J*= 1Hz), 7.88 (m, 3H), 7.58 (dt, 1H, *J*= 8, 1Hz), 7.47 (t, 1H, *J*= 8Hz), 7.35 (m, 2H), 3.15 (s, 1H). ^{13}**C** = 155.9, 149.5, 149.3, 138.9, 137.2, 132.8, 131.1, 129.1, 127.9, 124.1, 132.0, 121.4, 119.1, 83.6.

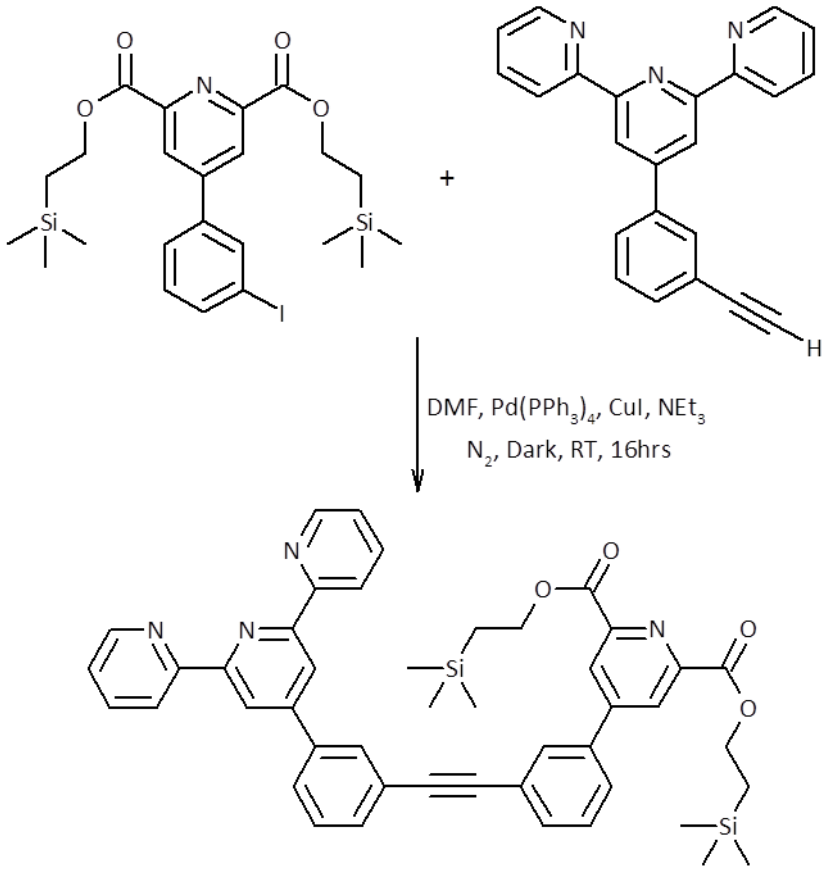

2-68: di-TMSE protected TERPY-DPA bis ligand (146 - 228 mg, 0.26 - 0.4 mmol scale): 1.0 equivalent of **di-trimethylsilylethyl 4-(3-iodophenyl)pyridine-2,6-dicarboxylate (2-67)** was dissolved in dry THF. This solution was then purged with N_2 and to it was added in order 2.2 equivalents of DIPEA, 0.03 equivalents of $Pd(PPh_3)_4$, 0.06 equivalents of CuI and 1.1 equivalents of **4'-(3-ethynylphenyl)-2,2':6',2''-terpyridine (2-66)**. The reaction was then stirred vigorously at room temperature under and inert atmosphere in the dark for 16 hours. The reaction was monitored by TLC (Al_2O_3, 3:1 hexanes: EtOAc, UV used for visualization, Rf = 0.29) and determined to be complete with the disappearance of a spot due to the aryl iodide starting material (**2-67**). The reaction was worked up by first drying the product under vacuum and then dissolving the resulting sticky orange solid in EtOAc. This solution was vacuum filtered and the filtrate was then washed in order with an aqueous solution of disodium EDTA, saturated $NaHCO_3$ and brine before being dried over $MgSO_4$, filtered and then dried under vacuum. The crude material was then purified using neutral alumina column chromatography eluting with 0 - 20%

acetone in hexanes. Yields 19 - 39 % as pale orange solid. NMR ($CDCl_3$): **^{1}H** = 8.77 (s, 2H), 8.75 (d, 2H, *J*= 2Hz), 8.68 (d, 2H, *J*= 8Hz), 8.53 (s, 2H), 8.13 (s, 1H), 7.97 (s, 1H), 7.89 (m, 3H), 7.69 (m, 3H), 7.54 (m, 2H), 7.37 (m, 2H), 4.54 (m, 4H), 1.25 (m, 4H), 0.10 (s, 18H). **^{13}C** = 165.2, 156.1, 150.2, 149.6, 149.1, 139.0, 137.2, 133.1, 132.2, 130.8, 129.7, 129.3, 127.8, 127.3, 125.3, 124.8, 124.6, 123.7, 121.7, 119.1, 90.4, 89.2, 64.6, 60.7, 17.5, 14.4, -1.3.

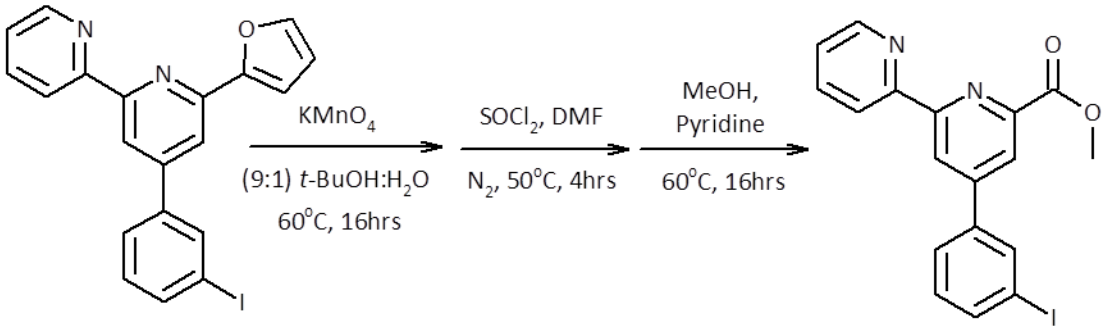

2-69: methyl 4-(3-iodophenyl)-2,2'-bipyridine-6-carboxylate (400 mg, 0.94 mmol scale): To a round bottom flask set up for reflux under a N_2 atmosphere was added the **4-(3-iodophenyl)-2,2'-bipyridine-6-carboxylic acid (2-57)**. To this vessel was added 5 mL of $SOCl_2$ and 3 drops of dry DMF. The reaction was then heated to reflux under a stream of N_2 and stirred vigorously for 4 hours. During this time the reaction mixture went from an off-white solid suspension in a clear colourless solution to a pale orange solution. After this time the $SOCl_2$ was removed under a stream of N_2 to afford a pale yellow waxy solid. This solid was then dissolved in dry MeOH and 2.2 equivalents of dry pyridine were added. The reaction was then heated to reflux under a stream of N_2 and stirred vigorously for 16 hours. The reaction was monitored by TLC (Al_2O_3, 10:1:1 hexanes:DCM:EtOAc, UV used for visualization, Rf = 0.37) and upon completion the reaction was worked up by first removing the MeOH solvent under vacuum. The resulting waxy yellow solids were dissolved in DCM and washed with saturated $NaHCO_3$ and brine before being dried over Na_2SO_4, filtered and dried under vacuum. The crude product was then purified by neutral alumina column chromatography eluting with 0 - 25% (DCM:EtOAc) in hexanes. Yield 88% as a white crystalline solid. NMR ($CDCl_3$): **^{1}H** =

8.79 (d, 1H, J= 2Hz), 8.70 (ddq, 1H, *J*= 2Hz, 2Hz, 5Hz), 8.57 (dt, 1H, *J*= 2Hz, 8Hz), 8.30 (d, 1H, J= 2Hz), 8.13 (t, 1H, J=2Hz), 7.85 (dt, 1H, J= 2Hz, 8Hz), 7.79 (ddq, 1H, J= 2Hz, 2Hz, 8Hz), 7.75 (ddq, 1H, J= 2Hz, 2Hz, 8Hz), 7.35 (ddd, 1H, J= 2Hz, 5Hz, 8Hz), 7.24 (t, 1H, J= 8Hz), 4.06 (s, 3H). **^{13}C** =165.9, 157.3, 155.1, 149.3, 149.0, 148.4, 139.7, 138.5, 137.2, 136.2, 130.9, 126.6, 124.5, 122.9, 122.0, 121.9, 95.1, 53.1.

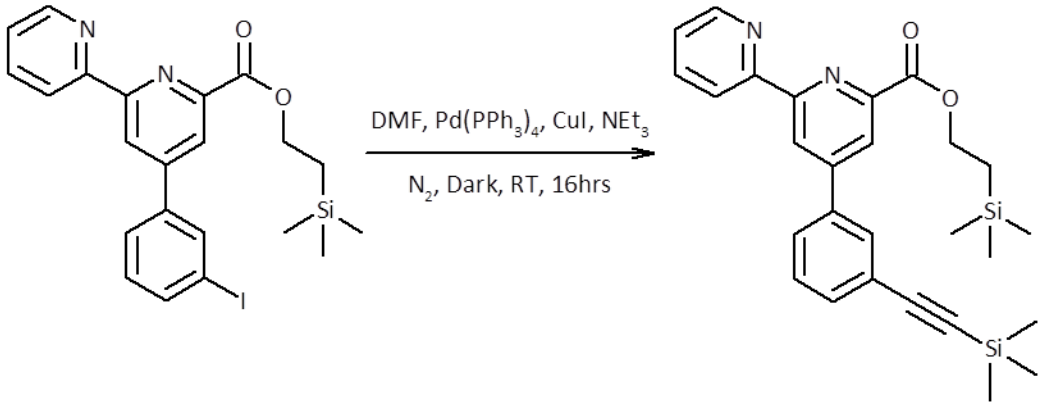

2-72 (450 mg, 0.90 mmol scale): 1.0 equivalent of **trimethylsilylethyl 4-(3-iodophenyl)-2,2'-bipyridine carboxylate (2-71)** was dissolved in dry THF. This solution was then purged with N_2 and to it was added in order 3.0 equivalents of DIPEA, 0.05 equivalents of $Pd(PPh_3)_4$, 0.10 equivalents of CuI and 3.0 equivalents of trimethylsilyl acetylene. The reaction was then stirred vigorously at room temperature under and inert atmosphere in the dark for 16 hours. The reaction was monitored by TLC (SiO_2, 9:1 hexanes:acetone, UV and vanillin (green) used for visualization, Rf = 0.43) and determined to be complete with the disappearance of a spot due to starting material (**2-71**). The reaction was worked up by first drying the product under vacuum and then dissolving the resulting sticky orange solid in Et_2O. This solution was washed in order with 0.1M citrate buffer pH~3, saturated $NaHCO_3$, an aqueous solution of disodium EDTA and brine before being dried over Na_2SO_4, filtered and then dried under vacuum. The crude material was then purified using silica gel column chromatography eluting with 0 - 8% acetone in hexanes. Yield 85 % as an off white waxy solid. NMR ($CDCl_3$): **^{1}H** = 8.84 (d, 1H, *J*= 2Hz), 8.71 (dq, 1H, *J*= 4, 1Hz), 8.62 (d, 1H, *J*= 8Hz), 8.34 (d, 1H, *J*= 2Hz), 7.92 (t, 1H, *J*= 1Hz), 7.84 (td, 1H, *J*= 8, 1Hz), 7.75 (dq, 1H, *J*= 8, 1Hz), 7.56 (dq, 1H, *J*= 8, 1Hz), 7.45 (t, 1H, *J*= 8Hz), 7.36 (m,

1H), 4.56 (m, 2H), 1.26 (m, 2H), 0.28 (s, 9H), 0.12 (s, 9H). **^{13}C** = 165.6, 157.0, 155.4, 149.7, 149.3, 148.6, 137.7, 137.1, 132.9, 131.0, 129.4, 127.3, 124.3, 122.8, 122.3, 121.9, 104.9, 95.4, 64.6, 17.6, 0.1, -1.1.

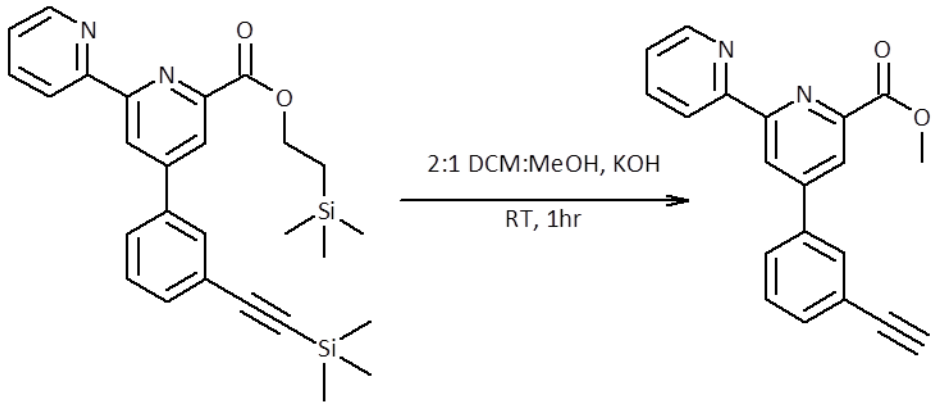

2-73: methyl 4-(3-ethynylphenyl)-2,2'-bipyridine-6-carboxylate (320 mg, 0.68 mmol scale): 1.0 equivalent of **2-72** was dissolved into a 2:1 mixture of dry DCM:MeOH to which was added 1.0 equivalent of solid KOH. The reaction was stirred vigorously at room temperature while monitoring by TLC (SiO_2, 2:1 hexanes:acetone, UV and vanillin (teal) used for visualization, Rf = 0.46) by which it was observed that the reaction was complete after 1 hour with the clear spot to spot conversion of starting material to product. The reaction was worked up by first neutralizing the reaction by adding 1.0 equivalents of concentrated HCl and then removing the solvent under vacuum. The resulting solid was then treated with DCM and filtered to remove the precipitated salts. The filtrate was then dried under vacuum. Yield 98% as a white solid. NMR ($CDCl_3$): **^{1}H** = 8.86 (d, 1H, *J*= 2Hz), 8.71 (dq, 1H, *J*= 4, 1Hz), 8.59 (d, 1H, *J*= 8Hz), 8.36 (d, 1H, *J*= 2Hz), 7.95 (t, 1H, *J*= 1Hz), 7.84 (td, 1H, *J*= 8, 1Hz), 7.75 (dq, 1H, *J*= 8, 1Hz), 7.56 (dq, 1H, *J*= 8, 1Hz), 7.45 (t, 1H, *J*= 8Hz), 7.36 (m, 1H), 4.56 (m, 2H), 4.06 (s, 3H), 3.15 (s, 1H). **^{13}C** = 155.3, 149.7, 149.2, 148.6, 137.9, 137.2, 133.2, 130.8, 129.4, 124.6, 123.4, 123.0, 122.1, 83.3, 78.3, 53.3.

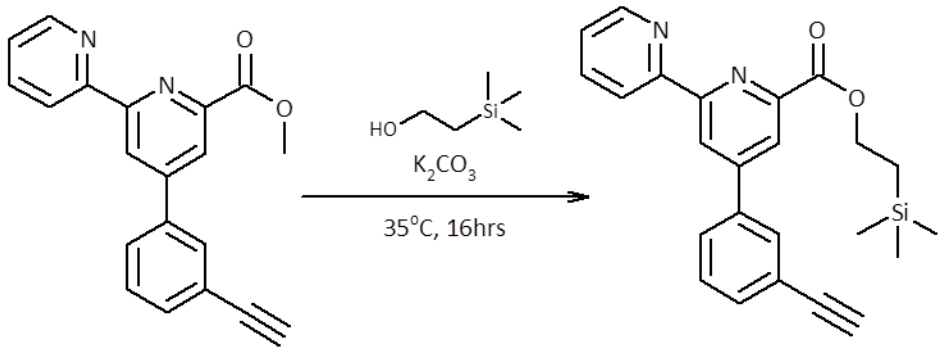

2-74 (190 mg, 0.60 mmol scale): 1.0 equivalent of **methyl 4-(3-ethynylphenyl)-2,2'-bipyridine-6-carboxylate (2-73)** was suspended in 3 mL of trimethylsilylethanol and to this mixture was added 2.0 equivalents of finely powdered K_2CO_3. The reaction mixture was then stirred at 35°C for 16 hours while monitoring by TLC (SiO_2, 4:1 hexanes:acetone, UV and vanillin (teal) used for visualization, Rf = 0.32). The reaction was worked up by first diluting the reaction x10 using Et_2O. This solution was then washed with H_2O and then brine followed by drying over Na_2SO_4, filtering and drying under vacuum. The crude product was purified by silica gel column chromatography eluted with 0 - 10% acetone in hexanes. Yield 79% as a white waxy solid. NMR ($CDCl_3$): **^{1}H** = 8.87 (s, 1H), 8.71 (s, 1H), 8.62 (d, 1H, *J*= 8Hz), 8.34 (s, 1H), 7.95 (s, 1H), 7.87 (t, 1H, *J*= 8Hz), 7.79 (dt, 1H, *J*= 8, 1Hz), 7.59 (dt, 1H, *J*= 8, 1Hz), 7.47 (t, 1H, *J*= 8Hz), 7.36 (m, 1H), 4.57 (m, 2H), 3.16 (s, 1H), 1.05 (m, 2H), 0.07 (s, 9H). **^{13}C** = 157.0, 155.3, 149.6, 149.1, 148.8, 138.1, 137.4, 133.3, 133.0, 130.8, 129.3, 127.7, 124.4, 123.3, 83.3, 78.2, 64.5, 17.8, 0.9.

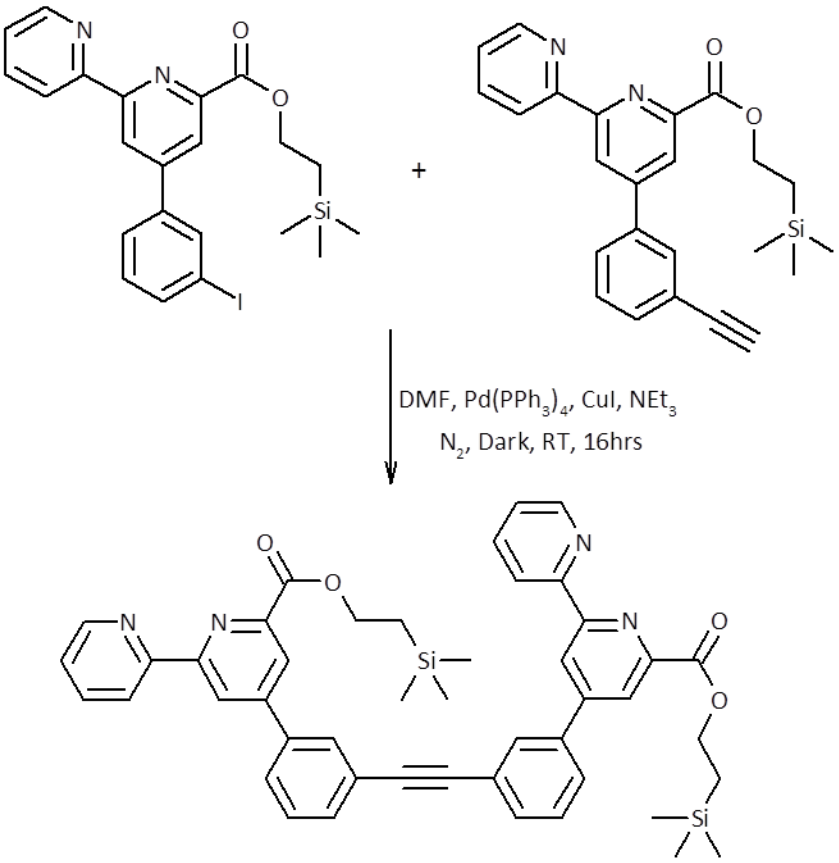

2-75: di-TMSE protected BIPYA-BIPYA bis ligand (200 mg, 0.50 mmol scale): 1.1 equivalent of **trimethylsilylethyl 4-(3-iodophenyl)-2,2'-bipyridine carboxylate (2-71)** was dissolved in dry THF. This solution was then purged with N_2 and to it was added in order 2.2 equivalents of DIPEA, 0.05 equivalents of $Pd(PPh_3)_4$, 0.10 equivalents of CuI and 1.0 equivalents of **(2-74)**. The reaction was then stirred vigorously at room temperature under and inert atmosphere in the dark for 16 hours. The reaction was monitored by TLC (Al_2O_3, 3:1 hexanes: EtOAc, UV used for visualization, Rf = 0.31) and determined to be complete with the disappearance of a spot due to the aryl iodide starting material (**2-71**). The reaction was worked up by first drying the product under vacuum and then dissolving the resulting sticky orange solid in EtOAc. This solution was vacuum filtered and the filtrate was then washed in order with an aqueous solution of disodium EDTA, saturated $NaHCO_3$ and brine before being dried over $MgSO_4$, filtered and then dried under vacuum. The crude material was then purified using neutral alumina column chromatography eluting with 0 - 15% acetone in hexanes. Yield 24 % as

pale yellow solid. NMR ($CDCl_3$): **^{1}H** =8.73 (s, 2H), 8.63 (d, 2H, J= 8Hz), 8.37 (s, 2H), 7.95 (s, 2H), 7.86 (t, 2H, J= 8Hz), 7.79 (td, 2H, J= 8, 2Hz), 7.60 (td, 2H, J= 8, 1Hz), 7.44 (t, 2H, J= 8Hz), 7.36 (m, 2H), 4.57 (m, 4H), 1.25 (m, 4H), 0.09 (s, 9H). **^{13}C** = 157.3, 155.3, 149.7, 149.0, 148.7, 138.2, 137.4, 133.4, 133.1, 130.8, 129.1, 127.7, 124.5, 123.1, 89.1, 64.4, 17.9, -0.4.

General procedure for the attempted one pot deprotection self-assembly of the di-TMSE protected bis-tridentate ligands (2-68, 2-71) with transition metal fluoride salts in the +2 oxidaiton state.

1mM solutions of the bis-tridentate ligands were prepared in a variety of solvents (DMSO, DMF, THF, acetonitrile) as well as 1mM solutions of the fluoride salts CoF_2, NiF_2 and ZnF_2 in deionized water. Trials were carried out using equal volumes of the equimolar solutions of ligand and metal salt by first mixing the solutions while agitating and gently warming (40°C) in an ultrasonic bath. Upon mixing many of the mixtures resulted in visible colour changes and in some instances the evolution of turbidity in the system. The solutions were then heated to reflux for a period of 1 to 48 hours at which time they were allowed to cool. Any solids formed upon cooling were removed by vacuum filtration and the filtrates analyzed by ESI-MS. Attempts were made at resuspending the solids into various solvents with and without heating, those producing solutions were also analyzed be ESI-MS.

General procedure for the attempted two step deprotection and self-assembly of the di-TMSE protected bis-tridentate ligands (2-68, 2-71) with non-fluoride containing transition metal salts in the +2 oxidaiton state.

1mM solutions of the bis-tridentate ligands were prepared in THF and to these were added 2.0 equivalents of TBAF in THF. The resulting deeply coloured solutions were treated with 2.0 equivalents of AcOH resulting in return in the colour of the solutions to a pale yellow. In addition 1mM solutions of the transition metal salts $FeCl_2$, $CuNO_2$, $MnCl_2$ and $CdCl_2$ were prepared in deionized water. Trials were carried out using equal

volumes of the equimolar solutions of ligand and metal salt by first mixing the solutions while agitating and gently warming (40°C) in an ultrasonic bath. Upon mixing many of the mixtures resulted in visible colour changes and in some instances the evolution of turbidity in the system. The solutions were then heated to reflux for a period of 1 to 48 hours at which time they were allowed to cool. Any solids formed upon cooling were removed by vacuum filtration and the filtrates analyzed by ESI-MS. Attempts were made at resuspending the solids into various solvents with and without heating, those producing solutions were also analyzed be ESI-MS.

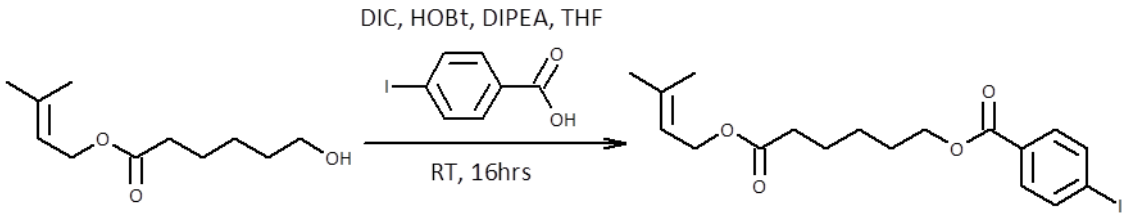

3-9: 6-[(3-methylbut-2-en-1-yl)oxy]-6-oxohexyl 4-iodobenzoate (1.0 -2.0 g, 5.0 - 10.0 mmol scale): 1.4 equivalents of **4-iodobenzoic acid (3-8)**, 1.4 equivalents of HOBt was dissolved into dry THF to which was added in order 1.4 equivalents of HOBt, 1.4 equivalents of DIC, 1.0 equivalent of **3-methylbut-2-en-1-yl 6-hydroxyhexanoate (3-7)** and 2.8 equivalents of DIPEA. The reaction was then stirred vigorously at room temperature for 16 hours monitoring by TLC (SiO_2, 2:1 hexanes:Et_2O, UV and vanillin (blue) used for visualization, R_f = 0.54). In the beginning the reaction mixture was clear and colourless but over time a white precipitate was observed to form in the now pale yellow solution. The reaction was worked up by first filtering the reaction mixture through celite and then evaporating the filtrate under vacuum. The resulting light brown oil was dissolved into Et_2O and this resulting solution was washed in order with water, saturated bicarb solution and brine. The organic fraction was dried over Na_2SO_4, filtered and then dried under vacuum. The resulting oil was purified by silica gel column chromatography eluting with 0 - 10% Et_2O in hexanes. Yields 83 - 90% as a pale yellow

oil. NMR ($CDCl_3$): **^{1}H** = 7.76 (m, 4H), 5.32 (m, 1H), 4.56 (d, 2H, J= 6Hz), 4.29 (t, 2H, J= 7Hz), 2.32 (t, 2H, J= 7Hz), 1.79-1.65 (m, 11H), 1.42 (m, 2H). **^{13}C** = 173.6, 166.2, 139.2, 137.8, 131.1, 129.9, 118.7, 100.7, 65.2, 61.4, 34.3, 28.5, 25.9, 25.7, 24.8, 18.1.

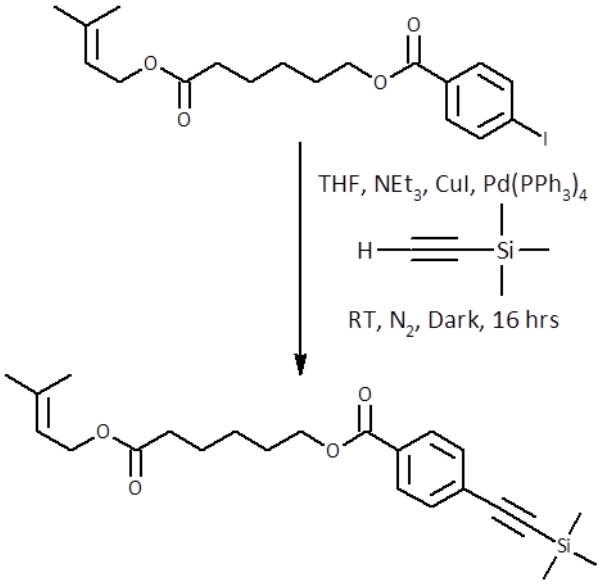

3-10: 6-[(3-methylbut-2-en-1-yl)oxy]-6-oxohexyl 4-(trimethylsilylethynyl)benzoate (1.0 - 2.3 g, 2.15 - 5.0 mmol scale): 1.0 equivalent of **6-[(3-methylbut-2-en-1-yl)oxy]-6-oxohexyl 4-iodobenzoate (3-9)** was dissolved into dry THF, this solution was then degassed and purged with N_2. To this solution was added in order 4.0 equivalents of NEt_3, 0.06 equivalents of CuI, 0.03 equivalents of $Pd(PPh_3)_4$ and 2.0 equivalents of TMS-acetylene. The reaction mixture, a pale yellow solution, was stirred for 16 hours under an atmosphere of N_2 in the dark, monitoring by TLC (SiO_2, 5:1 hexanes:Et_2O, UV and vanillin (teal) used for visualization, R_f = 0.38). Upon completion the reaction mixture appeared as a dark yellow solution with dark orange precipitate. The reaction was worked up by first filtering the reaction mixture through celite and then evaporating the filtrate under vacuum. The resulting yellow semi-solid was then dissolved into Et_2O. This solution was then washed in order with disodium EDTA solution, water, 1M sodium phosphate buffer pH 3 and brine. The organic fraction was dried over Na_2SO_4, filtered and then dried under vacuum. The resulting yellow oil was purified by silica gel column

chromatography eluting with 0 - 10% Et_2O in hexanes. Yields 91 - 93% as a yellow oil. NMR ($CDCl_3$): **^{1}H** = 7.94 (d, 2H, J= 8Hz), 7.50 (d, 2H, J= 8Hz), 5.32 (m, 1H), 4.55 (d, 2H, J= 6Hz), 4.29 (t, 2H, J= 7Hz), 2.33 (t, 2H, J= 7Hz), 1.74 (m, 10H), 1.45 (m, 2H), 0.25 (s, 9H). **^{13}C** = 173.6, 166.2, 139.1, 131.9, 130.1, 129.5, 127.8, 118.9, 97.7, 65.1, 61.5, 34.3, 28.6, 25.9, 25.7, 24.8, 18.1, 0.03.

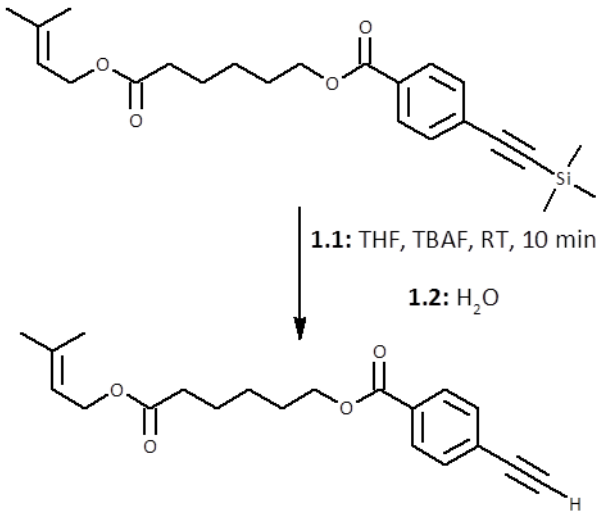

3-11: 6-[(3-methylbut-2-en-1-yl)oxy]-6-oxohexyl 4-ethynylbenzoate (1.2 g, 3.0 mmol scale): 1.0 equivalents of **6-[(3-methylbut-2-en-1-yl)oxy]-6-oxohexyl 4-(trimethylsilylethynyl)benzoate (3-10)** was dissolved into a minimum amount of dry THF. To this solution was added 1.0 equivalents of a 1.0M solution of TBAF in THF with vigorous stirring. Upon addition of the TBAF the solution went instantly from a pale yellow colour to a dark olive brown. The reaction was monitored by TLC (SiO_2, 2:1 hexanes:Et_2O, UV and vanillin (blue) used for visualization, R_f = 0.53) and found to be complete after 10 minutes. The reaction was worked up by first treating it with a few mL of H_2O during which time the solution turned cloudy pale yellow. The THF was removed from this solution under vacuum to afford a goopy yellow clod in an aqueous solution which was treated with sufficient Et_2O to dissolve the semi-solid resulting in a two phase mixture. The organic fraction was isolated and the aqueous fraction extracted with another portion of Et_2O which was combined with the first organic fraction. The combined organic fraction was then washed with H_2O and then brine after

which time it was dried over Na_2SO4, filtered and then dried under vacuum. The resulting yellow oil was then purified using silica gel column chromatography eluting with 0 - 20% Et_2O in hexanes. Yields 63 - 83% as a pale yellow oil. NMR ($CDCl_3$): **^{1}H** = 7.95 (d, 2H, J= 8Hz), 7.52 (d, 2H, J=8Hz), 5.31 (m, 1H), 4.55 (d, 2H, J= 6Hz), 4.28 (t, 2H, J= 7Hz), 3.22 (s, 1H), 2.32 (t, 2H, J= 7Hz), 1.70 (m, 11H), 1.51 (m, 2H). **^{13}C** = 173.5, 166.0, 139.2, 132.2, 130.5, 129.5, 126.8, 118.8, 82.9, 80.1, 65.1, 61.4, 34.3, 28.5, 25.9, 25.7, 24.7, 18.1.

General procedure for the thioester coupling of 8-sulfanyloctan-1-ol (3-22) with carboxylic acids with protected nucleophiles (3-12 - 3-15, 3-19 and 3-4):

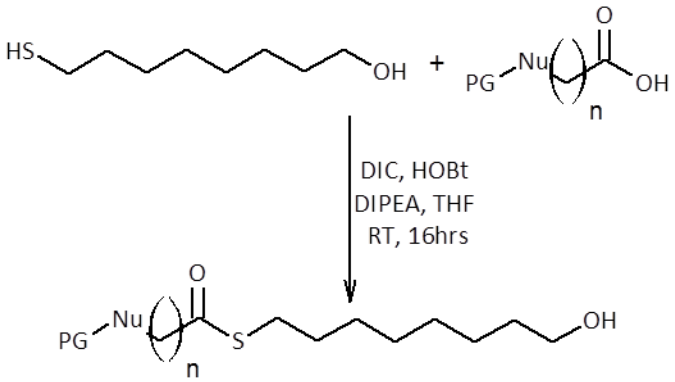

1.0 equivalent of the **carboxylic acid with protected nucleophile (3-12 - 3-15, 3-19 or 3-4)** was dissolved into dry THF and to this solution was added in order 1.0 equivalents of HOBt, 1.0 equivalent DIC, 1.5 equivalents of **8-sulfanyloctan-1-ol (3-22)** and 1.0 equivalents of DIPEA. The solution was stirred vigorously at room temperature and after ~15 minutes the formation of DIU was observed as an opalescent white precipitate. The reactions were monitored by TLC chromatography and after 16 hours the reactions were determined to be complete. The reactions were worked up by first vacuum filtering to remove the DIU side product. The filtrates were then evaporated under vacuum to remove the THF and the resulting oils were re-dissolved into Et_2O. The organic solutions were then washed in order with H_2O, 1M sodium phosphate buffer pH~3 and then brine before being dried over Na_2SO_4, filtered and then evaporated

under vacuum to remove the organic solvent. The resulting crude oils were then purified using silica gel column chromatography using appropriate conditions.

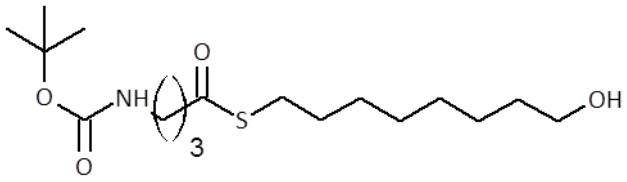

3-23: *t*BocHN-4-S-8-OH (813 mg, 4.0 mmol scale): TLC conditions - SiO_2, 2:1 hexanes:EtOAc, Hanessian's stain (dark blue) used for visualization, Rf = 0.19. Silica gel column chromatography carried out using 0 - 45% EtOAc in hexanes. Yields 34 - 37% of pale yellow oil. NMR ($CDCl_3$): **^{1}H** = 4.65 (s, br, 1H), 4.06 (m, 2H), 3.59 (m, 2H), 3.45 (m, 2H), 3.11 (m, 2H), 2.82 (t, 2H, J= 7Hz), 2.55 (t, 2H, J= 7Hz), 1.81 (m, 3H), 1.53 (m, 4H), 1.41 (s, br, 9H), 1.26 (m, 9H). **^{13}C** = 199.3, 171.3, 156.0, 79.9, 66.3, 62.9, 60.5, 41.3, 39.7, 32.7, 29.6, 29.4, 29.1, 28.9, 28.8, 28.5, 26.1, 25.8, 21.2, 15.5, 14.4.

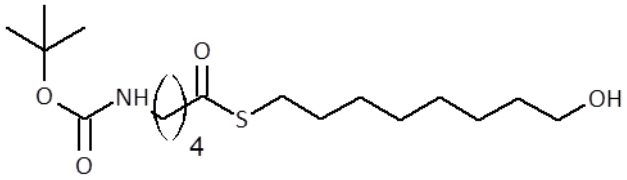

3-24: *t*BocNH-5-S-8-OH (869 mg, 4.0 mmol scale): TLC conditions - SiO_2, 1:1 hexanes:EtOAc, Hanessian's stain (dark blue) used for visualization, Rf = 0.43. Silica gel column chromatography carried out using 0 - 40% EtOAc in hexanes. Yield 53% of a white waxy solid. NMR ($CDCl_3$): **^{1}H** = 4.62 (s, br, 1H), 3.59 (t, 2H, J= 7Hz), 3.08 (m, 2H), 2.80 (t, 2H, J= 7Hz), 2.54 (t, 2H, J= 7Hz), 1.74-1.41 (m, 19H), 1.29 (s, br, 8H). **^{13}C** = 199.4, 156.3, 79.3, 62.9, 43.6, 32.7, 29.5, 29.4, 29.3, 29.1, 28.9, 28.8, 28.5, 25.8, 22.8.

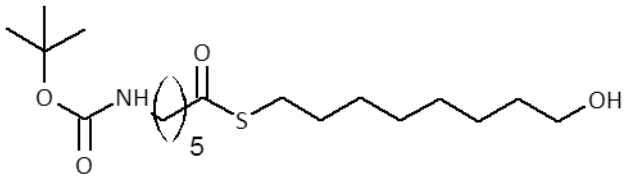

3-25: *t*BocNH-6-S-8-OH (925 mg, 4.0 mmol scale): TLC conditions - SiO_2, 2:1 hexanes:EtOAc, Hanessian's stain (dark blue) used for visualization, Rf = 0.23. Silica gel column chromatography carried out using 0 - 40% EtOAc in hexanes. Yield 43% of a clear colourless oil. NMR ($CDCl_3$): **^{1}H** = 4.56 (s, br, 1H), 3.61 (t, 2H, J= 7Hz), 3.08 (m, 2H), 2.84 (t, 2H, J= 7Hz), 2.52 (t, 2H, J= 7Hz), 1.65-1.24 (m, 30H). **^{13}C** = 200.0, 156.3, 79.9, 63.0, 44.1, 40.5, 32.9, 29.9, 29.6, 29.3, 29.1, 28.9, 28.8, 28.5, 26.2, 25.8, 25.4, 14.3.

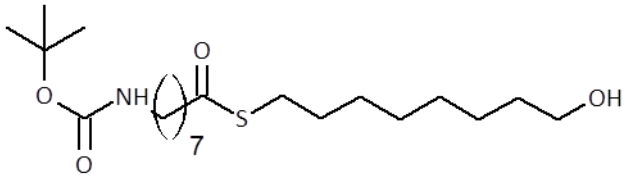

3-26: *t*BocNH-8-S-8-OH (778 mg, 3.0 mmol scale): TLC conditions - SiO_2, 2:1 hexanes:EtOAc, Hanessian's stain (dark blue) used for visualization, Rf = 0.29. Silica gel column chromatography carried out using 0 - 40% EtOAc in hexanes. Yield 50% of a white waxy solid. NMR ($CDCl_3$): **^{1}H** = 4.55 (s, br, 1H), 3.59 (t, 2H, J= 7Hz), 3.05 (m, 2H), 2.82 (t, 2H, J= 7Hz), 2.49 (t, 2H, J= 7Hz), 1.84 (s, br, 1H), 1.61-1.28 (m, 32H). **^{13}C** = 200.2, 156.1, 79.1, 63.0, 44.2, 40.6, 32.8, 30.1, 29.6, 29.3, 29.1, 28.9, 28.8, 28.7, 28.5, 26.7, 25.7, 25.7.

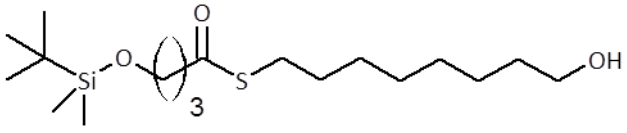

3-27: TBDMSO-4-S-8-OH (865 mg, 4.0 mmol scale): TLC conditions - SiO_2, 2:1 hexanes:EtOAc, Hanessian's stain (dark blue) used for visualization, Rf = 0.36. Silica gel

column chromatography carried out using 0 - 25% EtOAc in hexanes. Yield 34% of a clear colourless oil. NMR ($CDCl_3$): **^{1}H** = 3.61 (m, 4H), 2.86 (q, 2H, J= 7Hz), 2.62 (t, 2H, J= 7Hz), 1.86 (p, 2H, J= 7Hz), 1.54 (m, 5H), 1.30 (m, 8H), 0.87 (s, 9H), 0.03 (s, 6H). **^{13}C** = 199.7, 63.1, 61.9, 40.7, 32.8, 29.7, 29.3, 29.2, 28.9, 28.8, 28.7, 26.0, 25.8, 18.5, -5.2.

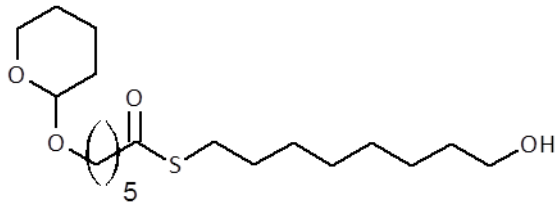

3-28: THPO-6-S-8-OH (875 mg, 4.0 mmol scale): TLC conditions - SiO_2, 2:1 Et_2O:hexanes, Hanessian's stain (dark blue) used for visualization, Rf = 0.30. Silica gel column chromatography carried out using 0 - 60% Et_2O in hexanes. Yield 40% of a white waxy solid. NMR ($CDCl_3$): **^{1}H** = 4.54 (m, 1H), 3.82 (m, 1H), 3.69 (m, 1H), 3.61 (m, 1H), 3.59 (t, 2H, J= 7Hz), 3.46 (m, 1H), 3.34 (m, 1H), 2.85 (t, 2H, J= 7Hz), 2.52 (t, 2H, J= 7Hz), 1.66 (m, 16H), 1.29 (m, 10H). **^{13}C** = 199.8, 99.1, 67.4, 62.8, 62.3, 44.1, 32.8, 30.9, 30.8, 29.7, 29.6, 29.5, 29.4, 29.3, 29.1, 28.8, 28.7, 25.9, 25.6, 25.5.

General procedure for the ester coupling of alcohol terminated thioester with protected nucleophile (3-23 - 3-28) with *p*-iodobenzoic acid:

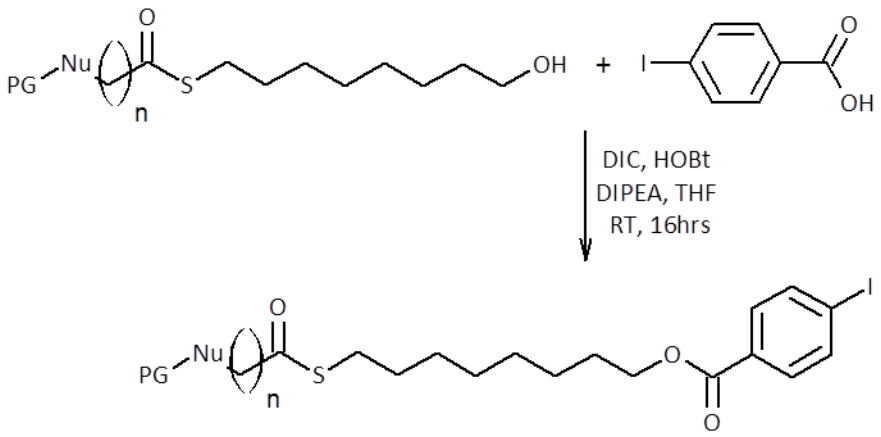

1.2 equivalents of ***p*-iodobenzoic acid (3-8)** was dissolved into dry THF and to this solution was added in order 1.2 eqiuvalents of HOBt, 1.2 equivalents of DIC, 1.0 equivalent of the **alcohol terminated thioester with protected nucleophile (3-23 - 3-28)** and 2.4 equivalents of DIPEA. The reaction was stirred at room temperature and after ~15 minutes the formation of DIU was observed as an opalescent white precipitate. The reactions were monitored by TLC and after 16 hours the reactions were determined to be complete. The reactions were worked up by first vacuum filtering to remove the DIU side product. The filtrates were then evaporated under vacuum to remove the THF and the resulting oils were re-dissolved into Et_2O. The organic solutions were then washed with H_2O, 0.1M sodium phosphate buffer pH~3 and then brine before being dried over Na_2SO_4, filtered and then evaporated under vacuum to remove the organic solvent. The resulting crude oils were then purified using silica gel column chromatography using appropriate conditions.

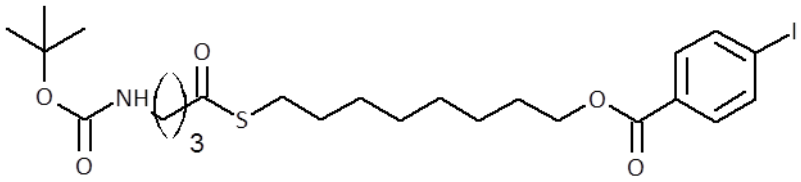

3-41: *t*BocHN-4-S-8-OBzI (348 mg, 1.0 mmol scale): TLC conditions - SiO_2, 2:1 hexanes:EtOAc, UV and Hanessian's stain (dark blue) used for visualization, Rf = 0.69.

Silica gel column chromatography carried out using 0 - 50% EtOAc in hexanes. Yield 51% of pale yellow oil. NMR ($CDCl_3$): **^{1}H** = 7.74 (m, 4H), 4.64 (s, br, 1H), 4.28 (t, 2H, J= 7Hz), 3.13 (m, 2H), 2.84 (t, 2H, J= 7Hz), 2.59 (t, 2H, J= 7Hz), 1.77 (m, 4H), 1.53 (m, 2H), 1.42-1.31 (m, 18H). **^{13}C** = 199.3, 166.3, 155.9, 137.8, 131.0, 130.2, 100.8, 79.3, 65.4, 41.4, 39.7, 29.6, 29.2, 29.0, 28.9, 28.8, 28.7, 28.5, 26.0.

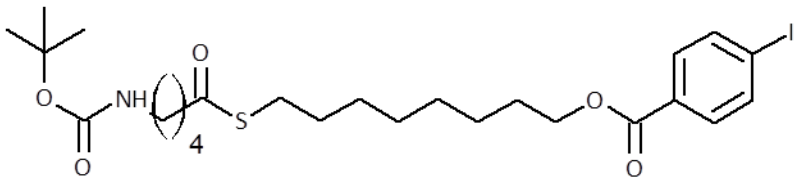

3-42: *t*BocHN-5-S-8-OBzl (362 mg, 1.0 mmol scale): TLC conditions - SiO_2, 5:1 hexanes:EtOAc, UV and Hanessian's stain (dark blue) used for visualization, Rf = 0.27. Silica gel column chromatography carried out using 0 - 15% EtOAc in hexanes. Yield 89% of pale yellow waxy solid. NMR ($CDCl_3$): **^{1}H** = 7.74 (m, 4H), 4.58 (s, br, 1H), 4.28 (t, 2H, J= 7Hz), 3.09 (m, 2H), 2.87 (p, 2H, J= 7Hz), 2.55 (t, 2H, J= 7Hz), 1.73-1.33 (m, 26H). **^{13}C** = 199.7, 166.1, 156.1, 137.7, 130.9, 129.8, 100.5, 79.1, 65.5, 43.7, 39.9, 29.6, 29.4, 29.2, 29.0, 28.9, 28.7, 28.6, 28.5, 26.1, 22.9.

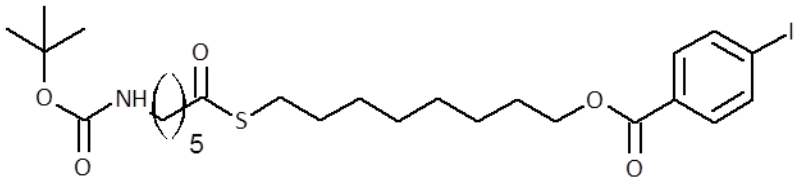

3-43: *t*BocHN-6-S-8-OBzl (376 mg, 1.0 mmol scale): TLC conditions - SiO_2, 2:1 hexanes:Et_2O, UV and Hanessian's stain (dark blue) used for visualization, Rf = 0.30. Silica gel column chromatography carried out using 0 - 40% Et_2O in hexanes. Yield 84% of pale yellow waxy solid. NMR ($CDCl_3$): **^{1}H** = 7.74 (m, 4H), 4.53 (s, br, 1H), 4.28 (t, 2H, J= 7Hz), 2.09 (m, 2H), 2.84 (t, 2H, J= 7Hz), 2.52 (t, 2H, J= 7Hz), 1.76-1.32 (m, 28H). **^{13}C** = 199.7, 166.3, 156.3, 137.9, 131.1, 130.1, 100.6, 65.4, 44.0, 40.3, 29.9, 29.7, 29.6, 29.2, 29.1, 28.8, 28.7, 28.6, 26.2, 26.1, 25.4, 15.3.

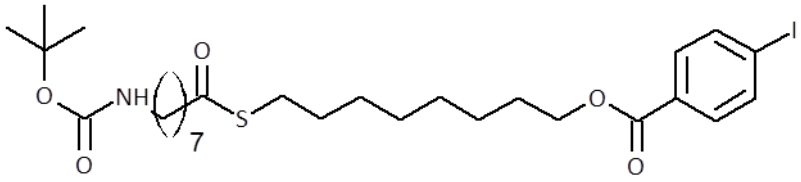

3-44: *t*BocHN-8-S-8-OBzI (130 mg, 0.50 mmol scale): TLC conditions - SiO_2, 5:1 hexanes:EtOAc, UV and Hanessian's stain (dark blue) used for visualization, Rf = 0.35. Silica gel column chromatography carried out using 0 - 15% EtOAc in hexanes. Yield 99% of pale yellow waxy solid. NMR ($CDCl_3$): **^{1}H** = 7.75 (m, 4H), 4.52 (s, br, 1H), 4.29 (t, 2H, J= 7Hz), 3.09 (m, 2H), 2.85 (t, 2H, J= 7Hz), 2.52 (t, 2H, J= 7Hz), 1.75 – 1.31 (m, 31H). **^{13}C** = 200.3, 166.1, 156.1, 137.7, 132.0, 121.3, 129.8, 125.0, 120.8, 108.3, 100.8, 65.4, 44.1, 40.9, 30.1, 29.7, 29.2, 29.1, 29.0, 28.9, 28.8, 28.7, 28.6, 26.7, 26.0, 25.8.

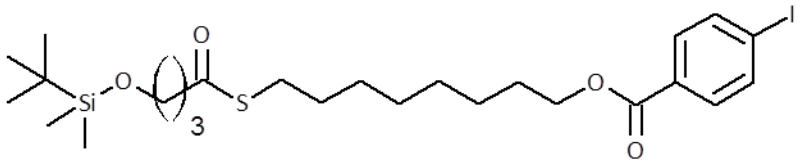

3-45: TBDMSO-4-S-8-OBzI (127 mg, 0.35 mmol scale): TLC conditions - SiO_2, 11:1 hexanes:acetone, UV and Hanessian's stain (dark blue) used for visualization, Rf = 0.62. Silica gel column chromatography carried out using 0 - 5% Et_2O in hexanes. Yield 92% of clear colourless oil. NMR ($CDCl_3$): **^{1}H** = 7.75 (m, 4H), 4.29 (t, 2H, J= 7Hz), 3.62 (t, 2H, J= 7Hz), 2.86 (t, 2H, J= 7Hz), 2.63 (t, 2H, J= 7Hz),1.85 (p, 2H, J= 7Hz), 1.75 (m, 2H), 1.56 (m, 2H), 1.33 (m, 8H), 0.89 (s, 9H), 0.04 (s, 6H). **^{13}C** = 199.6, 166.2, 137.7, 131.2, 130.2, 100.9, 65.4, 62.0, 40.7, 29.8, 29.3, 29.1, 28.9, 28.7, 28.7, 26.0, 18.6, -5.2.

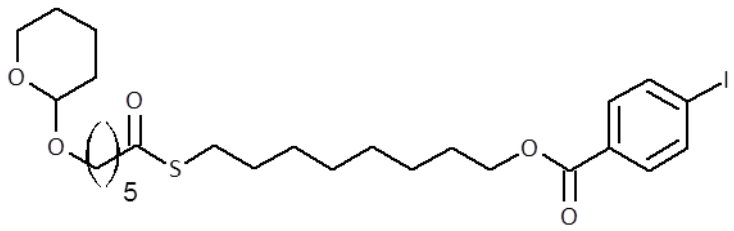

3-46: THPO-6-S-8-OBzI (252 mg, 0.70 mmol scale): TLC conditions - SiO_2, 11:1 hexanes:acetone, UV and Hanessian's stain (dark blue) used for visualization, Rf = 0.33. Silica gel column chromatography carried out using 0 - 8% acetone in hexanes. Yield 94% of white waxy solid. NMR ($CDCl_3$): ^{1}**H** = 7.74 (m, 4H), 4.52 (m, 1H), 4.29 (t, 2H, J= 7Hz), 3.83 (m, 1H), 3.70 (m, 1H), 3.47 (m, 1H), 3.36 (m, 1H), 2.81 (t, 2H, J= 7Hz), 2.53 (t, 2H, J= 7Hz), 1.75- 1.32 (m, 25H). ^{13}**C** = 199.6, 266.2, 137.8, 131.2, 130.1, 100.5, 99.1, 67.3, 65.4, 62.4, 44.2, 30.7, 29.6, 29.5, 29.1, 29.0, 28.8, 28.7, 28.6, 25.9, 25.8, 25.6, 25.5, 19.7.

General procedure for the Sonogashira cross-coupling of aryliodide terminated thioester with protected nucleophile (3-41 - 3-46) with 6-[(3-methylbut-2-en-1-yl)oxy]-6-oxohexyl 4-ethynylbenzoate (3-11):

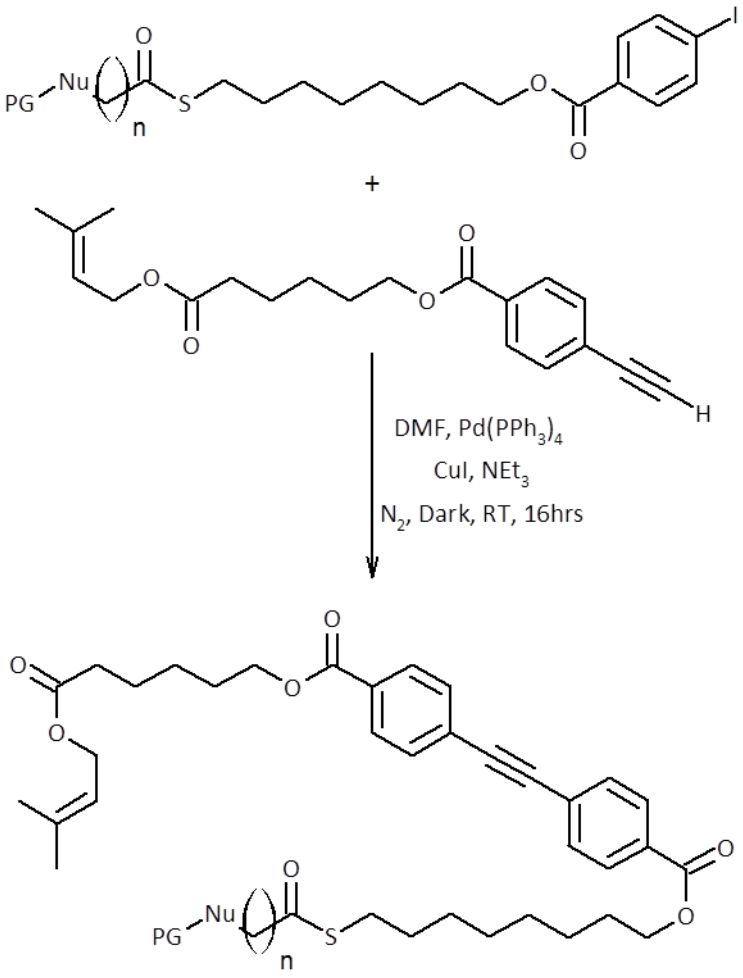

1.0 equivalents of **aryliodide terminated thioester with protected nucleophile (3-41 - 3-46)** was dissolved in dry THF and the solution was degassed and then purged with N_2. To his solution under a constants stream of N_2 was added in order 2.4 equivalents of NEt_3, 0.06 equivalents of CuI, 0.03 equivalents of $Pd(PPh_3)_4$ and 1.2 equivalents of **6-[(3-methylbut-2-en-1-yl)oxy]-6-oxohexyl 4-ethynylbenzoate (3-11)**. The reaction was then stirred vigorously at room temperature under and inert N_2 atmosphere shielded from light. The reaction was monitored by TLC and after ~16 - 24 hrs was determined to be complete as indicated by complete consumption of the aryl iodide. During the reaction the solutions generally went from clear yellow solutions to orange solutions with visible dark orange precipitates. The reaction was worked up by first vacuum filtering the mixture to remove the dark orange precipitates and the filtrate was then evaporated under vacuum. The resulting sticky solids were then dissolved in Et_2O and the resulting

solution washed in order with a solution of disodium EDTA, saturated sodium bicarbonate, H_2O, 0.1M sodium phosphate buffer pH~3 and then brine. The organic fraction was then dried over Na_2SO_4, filtered, evaporated under vacuum and then purified by silica gel column chromatography using conditions appropriate for the compound.

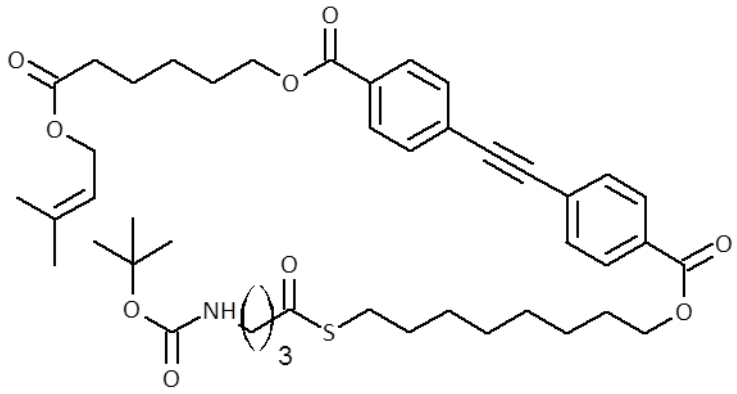

3-47: PreOOC-6-ADIP-8-S-4-NH*t*Boc (230 mg, 0.40 mmol scale): TLC conditions - SiO_2, 1:1 hexanes:Et_2O, UV and vanillin stain (green) used for visualization, Rf = 0.33. Silica gel column chromatography carried out using 0 - 50% Et_2O in hexanes. Yield 87% of a waxy pale yellow solid. NMR ($CDCl_3$): **^{1}H** = 8.02 (dd, 4H, J= 8Hz), 7.59 (d, 4H, J= 8Hz), 5.30 (m, 1H), 4.57 (s, br, 1H), 4.56 (d, 2H, J= 6H), 4.31 (m, 4H), 3.14 (m, 2H), 2.86 (t, 2H, J= 7Hz), 2.58 (t, 2H, J= 7Hz), 2.34 (t, 2H, J= 7Hz), 1.86-1.69 (m, 15H), 1.56-1.34 (m, 21H). **^{13}C** = 199.3, 173.7, 165.9, 155.9, 139.2, 131.8, 130.4, 129.6, 127.4, 118.7, 91.4, 65.5, 65.3, 61.5, 41.4, 39.8, 34.3, 29.6, 29.2, 29.1, 28.9, 28.8, 28.8, 28.6, 26.1, 25.9, 25.8, 24.8.

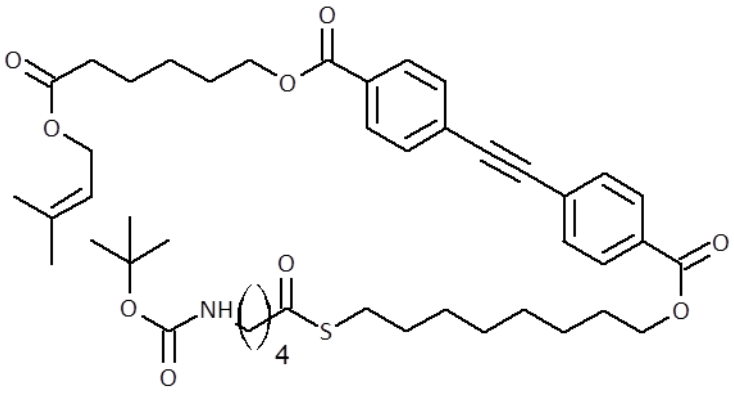

3-48: PreOOC-6-ADIP-8-S-5-NH*t*Boc (237 mg, 0.40 mmol scale): TLC conditions - SiO_2, 1:1 hexanes:Et_2O, UV and vanillin stain (green) used for visualization, Rf = 0.29. Silica gel column chromatography carried out using 0 - 50% Et_2O in hexanes. Yield 94% of a waxy pale yellow solid. NMR ($CDCl_3$): **^{1}H** = 8.01 (dd, 4H, J= 8, 1Hz), 7.58 (d, 4H, J= 8Hz), 5.32 (m, 1H), 4.55 (d, 3H, J= 6Hz), 3.11 (m, 2H), 2.84 (t, 2H, J= 7Hz), 2.55 (t, 2H, J= 7Hz), 2.33 (t, 2H, J= 7Hz), 1.74 (m, 14H), 1.54-1.33 (m, 24H). **^{13}C** = 199.6, 173.6, 166.1, 156.0, 139.1, 131.7, 130.4, 129.8, 127.5, 118.7, 91.4, 65.1, 61.4, 43.5, 40.4, 34.2, 29.7, 29.4, 29.3, 29., 28.9, 28.8, 28.7, 28.5, 26.0, 25.9, 25.7, 25.0, 18.1, 15.4.

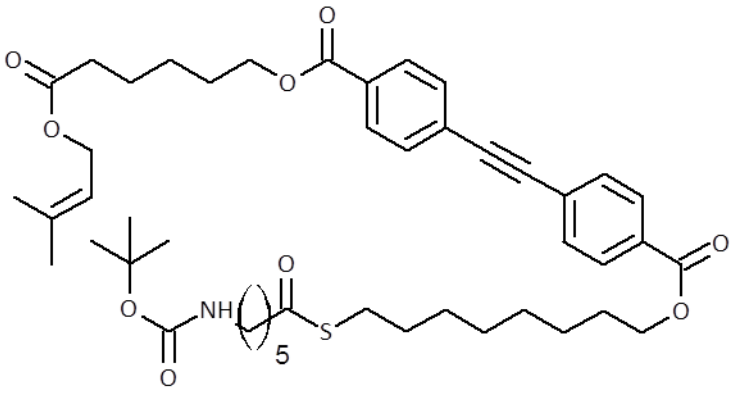

3-49: PreOOC-6-ADIP-8-S-6-NH*t*Boc (425 mg, 0.70 mmol scale): TLC conditions - SiO_2, 1:1 hexanes:Et_2O, UV and vanillin stain (green) used for visualization, Rf = 0.39. Silica gel column chromatography carried out using 0 - 40% Et_2O in hexanes. Yield 59% of a waxy pale yellow solid. NMR ($CDCl_3$): **^{1}H** = 8.01 (dd, 4H, J= 8, 1Hz), 7.58 (d, 4H), 5.32 (m, 1H),

4.55 (d, 3H, J= 6Hz), 4.29 (m, 4H), 3.08 (m, 2H), 2.84 (t, 2H, J= 7Hz), 2.52 (t, 2H, J= 7Hz), 2.33 (t, 2H, J= 7Hz), 1.74 (m, 14H), 1.42 (m, 26H). ^{13}**C** = 199.6, 173.7, 166.1, 155.9, 139.1, 131.7, 130.4, 130.3, 129.6, 127.4, 118.7, 91.5, 65.4, 65.1, 61.4, 44.0, 40.5, 34.3, 29.9, 29.6, 29.2, 29.0, 28.8, 28.7, 28.7, 28.5, 26.0, 25.9, 25.7, 25.4, 24.7, 18.5.

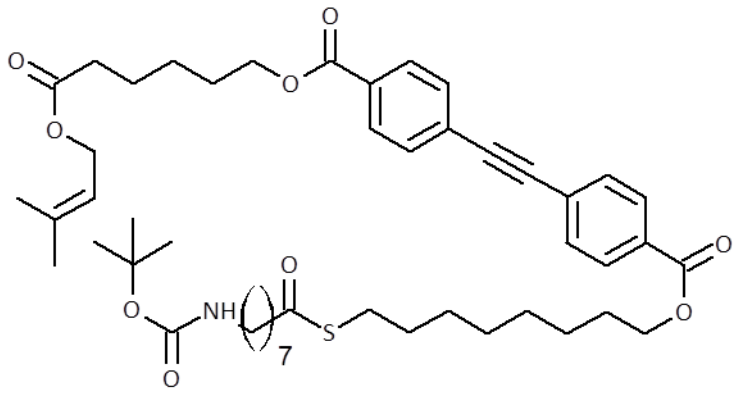

3-50: PreOOC-6-ADIP-8-S-8-NH*t*Boc (190 mg, 0.30 mmol scale): TLC conditions - SiO_2, 1:1 hexanes:Et_2O, UV and vanillin stain (green) used for visualization, Rf = 0.28. Silica gel column chromatography carried out using 0 - 50% Et_2O in hexanes. Yield 85% of a waxy pale yellow solid. NMR ($CDCl_3$): ^{1}**H** = 8.01 (d, 4H, J= 8Hz), 7.58 (d, 4H, J= 8Hz), 5.32 (m, 1H), 4.55 (d, 3H, J= 7Hz), 4.31 (m, 4H), 3.06 (m, 2H), 2.84 (t, 2H, J= 7Hz), 2.51 (t, 2H, J= 7Hz), 2.33 (t, 2H, J= 7Hz), 1.70 (m, 14H), 1.67-1.28 (m, 29H). ^{13}**C** = 199.9, 173.6, 165.8, 156.5, 138.9, 131.7, 130.4, 129.7, 127.3, 118.5, 91.6, 65.2, 65.1, 61.3, 44.2, 40.6, 34.2, 30.0, 29.7, 29.2, 29.1, 29.0, 28.9, 28.8, 28.7, 28.5, 26.7, 26.0, 25.9, 25.7, 25.7, 17.9.

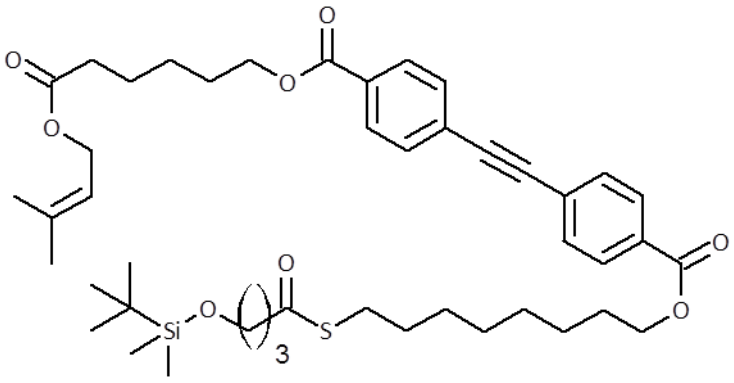

3-51: PreOOC-6-ADIP-8-S-4-OTBDMS (150 mg, 0.25 mmol scale): TLC conditions - SiO_2, 9:1 hexanes:acetone, UV and vanillin stain (green) used for visualization, Rf = 0.23. Silica gel column chromatography carried out using 0 - 50% Et_2O in hexanes. Yield 93% of a waxy pale yellow solid. NMR ($CDCl_3$): **^{1}H** = 8.02 (dd, 4H, *J*= 8, 2Hz), 7.59 (d, 4H, *J*= 8Hz), 5.33 (m, 1H), 4.57 (d, 2H, *J*= 6Hz), 4.32 (m, 4H), 3.62 (t, 2H, *J*= 7Hz), 2.86 (t, 2H, *J*= 7Hz), 2.63 (t, 2H, *J*= 7Hz), 2.35 (t, 2H, *J*= 7Hz), 1.88-1.60 (m, 14H), 1.35 (m, 13H). **^{13}C** = 199.2, 173.7, 166.1, 139.7, 131.7, 130.5, 118.8, 91.6, 65.4, 61.9, 61.5, 40.6, 34.4, 29.7, 29.3, 29.1, 28.9, 28.8, 28.8, 28.7, 28.6, 26.1, 25.9, 25.8, 24.9, 18.5, -5.2.

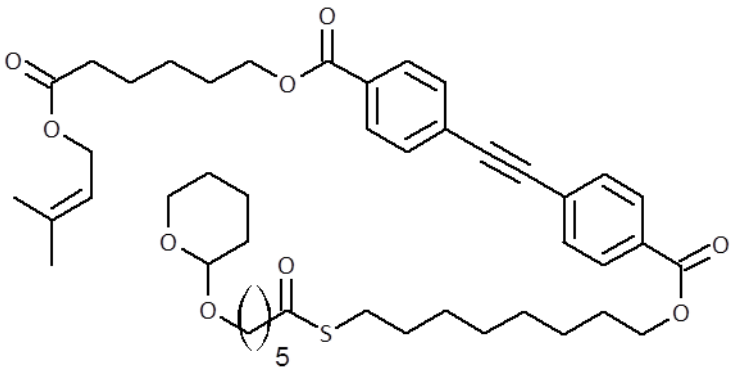

3-52: PreOOC-6-ADIP-8-S-6-OTHP (300 mg, 0.5 mmol scale): TLC conditions - SiO_2, 1:1 hexanes:Et_2O, UV and vanillin stain (green) used for visualization, Rf = 0.29. Silica gel column chromatography carried out using 0 - 50% Et_2O in hexanes. Yield 94% of a waxy pale yellow solid. NMR ($CDCl_3$): **^{1}H** = 8.01 (dd, 4H, *J*= 8Hz), 7.58 (d, 2H, *J*= 8Hz), 5.32 (m, 1H), 4.55 (m, 3H), 4.29 (m, 4H), 3.82 (m, 1H), 3.71 (m, 1H), 3.46 (m, 1H), 3.36 (m, 1H),

2.84 (t, 2H, *J*= 7Hz), 2.51 (t, 2H, *J*= 7Hz), 2.33 (t, 2H, *J*= 7Hz), 1.69 (m, 18H), 1.34 (m, 21H). **^{13}C** = 199.7, 172.9, 166.3, 138.9, 132.1, 130.4, 130.0, 127.5, 118.7, 99.0, 91.4, 67.3, 65.4, 65.0, 62.4, 61.0, 44.1, 34.3, 30.8, 29.5, 29.4, 29.2, 29.0, 28.8, 28.5, 26.0, 25.9, 25.8, 25.7, 25.6, 25.5, 24.7.

General procedure for the *t*-Boc and Pre deprotection of the doubly protected amine terminated full length compounds (3-47 - 3-50):

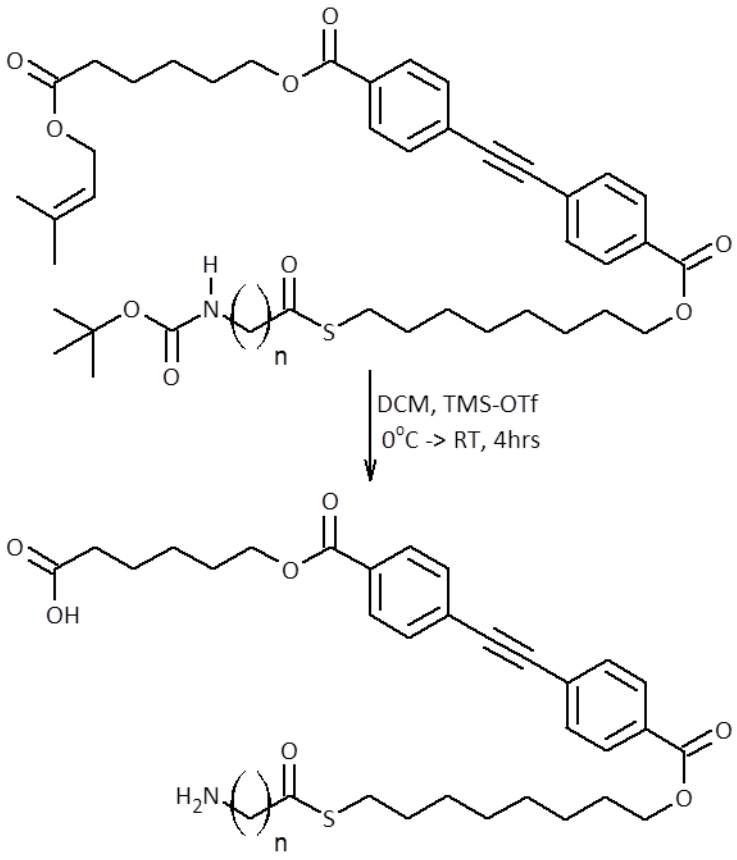

1.0 equivalent of **doubly protected amine terminated full length compound (3-47 - 4-50)** was dissolved in DCM and cooled to 0°C. To this solution was added 1.25 equivalents of TMSOTf and the reaction was allowed to warm to room temperature over the course of 4 hours. The reaction was monitored by TLC (SiO_2, 2:1 hexanes:EtOAc, UV used for visualization) to determine completion by disappearance of

the spot due to starting material. Note that the products were all of insufficient mobility to be resolved from the baseline. Upon completion the reaction was worked up by first reducing the volume by half using a stream of N_2 after which the mixture was slowly diluted by a factor a five using hexanes. This diluted solution was then cooled in the freezer for a few hours to facilitate the precipitation of the final deprotected products. All products were purified via preparatory HPLC using a C18 column and eluting with 0 - 5% MeOH in acetonitrile.

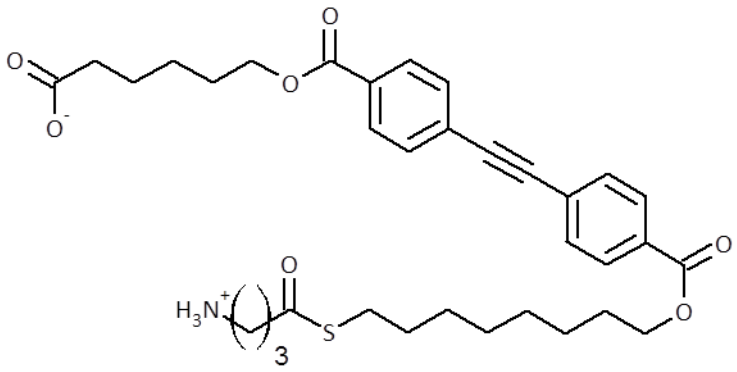

3-53: $^{-}$OOC-6-ADip-8-S-4- NH_3^+ (150 mg, 0.26 mmol scale): Yield 80% of a waxy pale yellow solid. NMR (CD_3CN): **^{1}H** = 8.06 (dd, 4H, *J*= 8, 2Hz), 7.70 (d, 4H, *J*= 8Hz), 6.39 (t, 3H, *J*= 9H), 4.34 (m, 4H), 3.06 (m, 2H), 3.00 (t, 2H, *J*= 7Hz), 2.73 (t, 2H, *J*= 7Hz), 2.35 (t, 2H, *J*= 7Hz), 1.98 (m, 4H), 1.79-1.39 (m, 19H). **^{13}C** = 199.5, 175.2, 166.5, 132.6, 131.5, 130.4, 127.9, 91.9, 65.9, 65.1, 41.0, 40.5, 34.1, 30.2, 29.7, 29.3, 29.0, 26.6, 26.2, 25.1, 23.4.

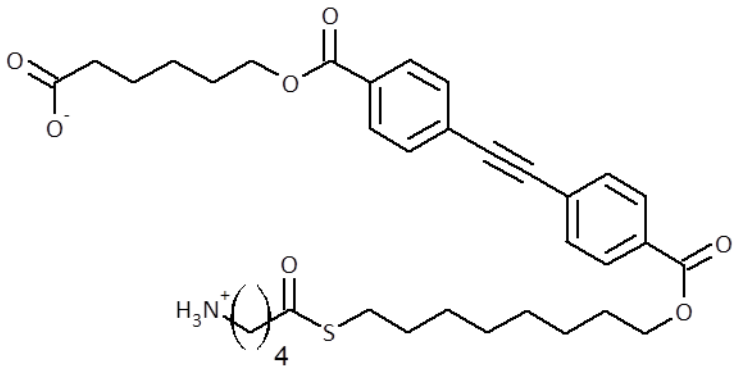

3-54: $^{-}$OOC-6-ADip-8-S-5-NH_3^+ (111 mg, 0.19 mmol scale): Yield 42% of an off white waxy solid. NMR (d6-acetone): **^{1}H** = 8.06 (d, 4H, J= 8Hz), 7.71 (d, 4H, J= 8Hz), 7.63 (br s, 3H), 4.33 (q, 4H, J= 7Hz), 3.27 (m, 2H), 2.87 (t, 2H, J= 7Hz), 2.66 (t, 2H, J= 7Hz), 2.34 (t, 2H, J= 7Hz), 1.98-1.25 (m, 22H). **^{13}C** = 198.9, 174.6, 166.1, 132.6, 131.5, 130.4, 127.9, 91.9, 65.9, 65.7, 43.7, 41.1, 34.1, 30.5, 29.7, 29.2, 27.3, 26.7, 26.3, 25.3, 22.9.

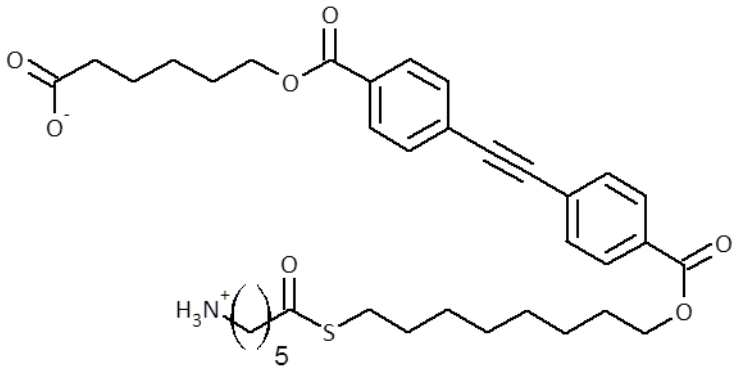

3-55: $^{-}$OOC-6-ADip-8-S-6- NH_3^+ (230 mg, 0.38 mmol scale): Yield 64% of an off white waxy solid. NMR (d6-DMSO): **^{1}H** = 7.98 (d, 4H, *J*= 8Hz), 7.72 (d, 4H, *J*= 8Hz), 7.57 (s, br, 3H), 4.27 (s, 4H), 2.79 (m, 3H), 2.50 (m, 3H), 2.23 (m, 2H), 1.79-1.28 (m, 27H). **^{13}C** = 198.6, 17.5, 165.1, 131.8, 129.9, 129.4, 126.3, 91.2, 64.9, 43.1, 33.6, 29.2, 28.5, 28.3, 28.1, 27.9, 26.7, 26.6, 25.1, 24.5, 24.2, 23.9.

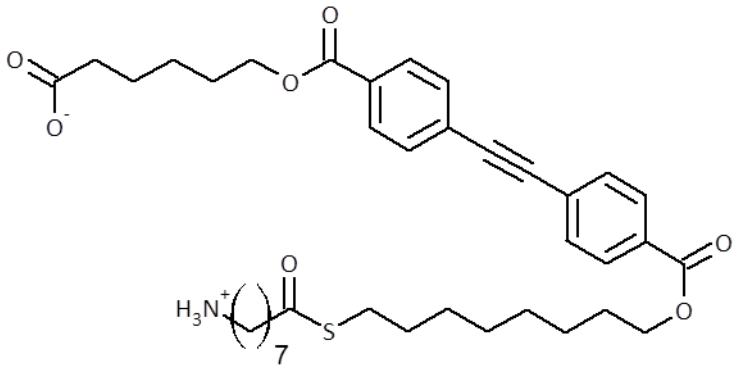

3-56: $^{-}$OOC-6-ADip-8-S-8- NH_3^+ (120 mg, 0.14 mmol scale): Yield 42% of an off white glassy solid. NMR (d6-acetone): **^{1}H** = 8.05 (d, 2H, *J*= 8Hz), 7.70 (d, 2H, *J*= 8Hz), 7.55 (s, br, 2H), 4.32 (m, 4H), 3.24 (m, 2H), 2.86 (t, 2H, *J*= 7Hz), 2.57 (t, 2H, *J*= 7Hz), 2.36 (t, 2H, *J*= 7Hz), 1.80-1.36 (m, 27H). **^{13}C** = 199.2, 174.6, 166.0, 132.5, 131.4, 130.3, 127.8, 91.9, 65.5, 44.3, 41.4, 34.0, 30.4, 29.0, 27.9, 26.7, 26.2, 25.2.

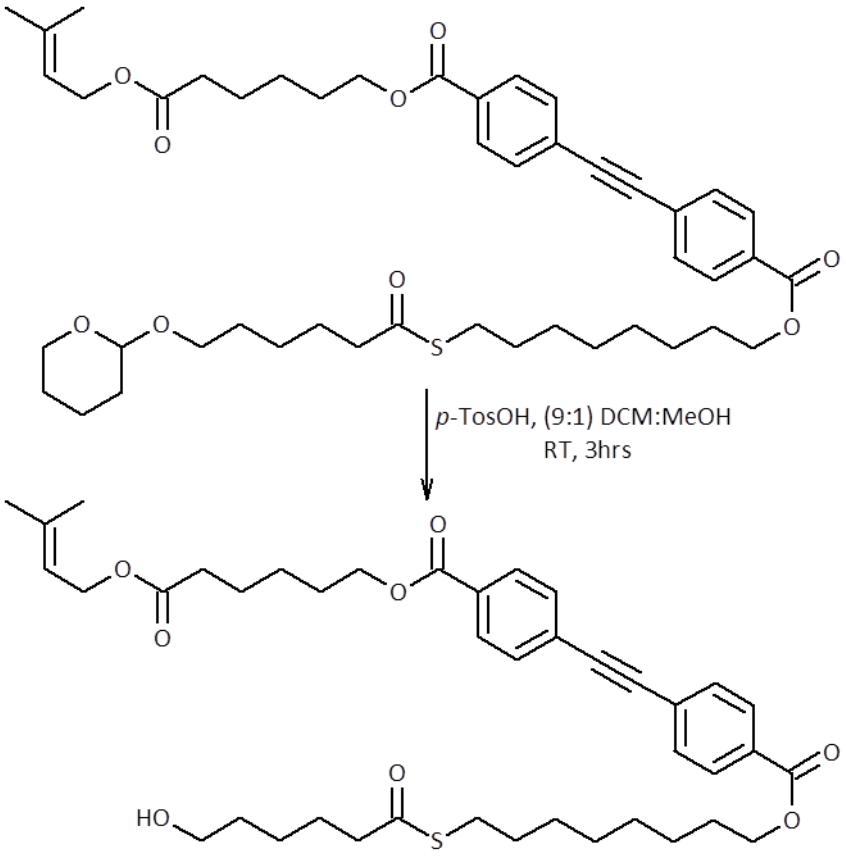

3-58: PreOOC-6-ADip-8-S-6-OH (316 mg, 0.4 mmol scale): 1.0 equivalent of **PreOOC-6-ADIP-8-S-6-OTHP (3-52)** was dissolved in 9:1 DCM: MeOH and to the resulting solution was added 0.20 equivalents of *p*-TosOH. The reaction was stirred vigorously for 3 hours while monitoring by TLC (SiO_2, 2:1 hexanes:acetone, UV and vanillin (purple) used for visualization, Rf = 0.38). The reaction was worked up by diluting by a factor of 5 using DCM. This solution was then washed with H_2O and brine before being dried over $MgSO_4$, filtered and then dried under vacuum. The crude material was purified by silica

gel column chromatography eluting with 0 - 25% acetone in hexhanes. Yield 86% of a pale yellow waxy solid. NMR ($CDCl_3$): **^{1}H** = 8.01 (dd,4H, *J*= 8, 2Hz), 7.58 (d, 4H, *J*= 8Hz), 5.32 (m, 1H), 4.56 (d, 2H, *J*= 7Hz), 4.31 (m, 4H), 3.62 (m, 2H), 2.84 (t, 2H, *J*= 7Hz), 2.54 (t, 2H, *J*= 7Hz), 2.36 (t, 2H, *J*= 7Hz), 1.74 (m, 14H), 1.45 (m, 18H). **^{13}C** = 199.5, 173.4, 165.9, 139.2, 131.8, 130.3, 129.7, 127.4, 118.7, 91.4, 65.2, 65.4, 62.7, 61.4, 44.1, 34.2, 32.2, 29.7, 29.2, 29.0, 28.9, 28.7, 28.5, 26.0, 25.8, 25.7, 25.5, 25.2, 24.7, 18.0.

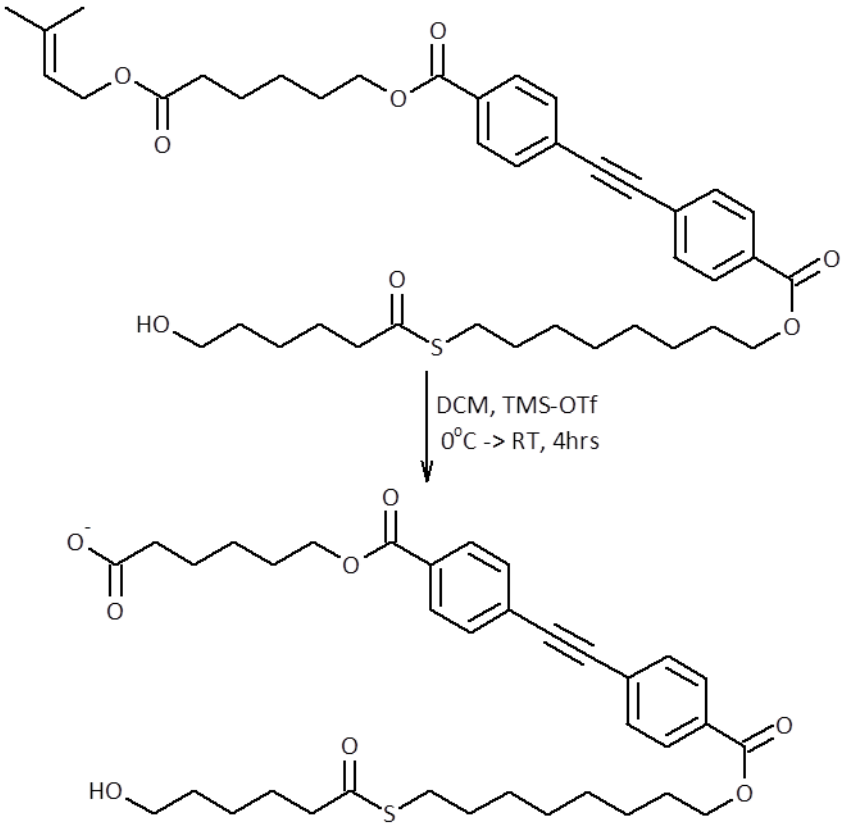

3-59: $^-$OOC-6-ADip-8-S-6-OH (180 mg, 0.28 mmol scale): 1.0 equivalent of **PreOOC-6-ADip-8-S-6-OH (3-58)** was dissolved in dry DCM and cooled to 0°C to which was added 1.1 equivalents of TMSOTf. The reaction was then allowed to stir for 4 hours while gradually warming to room temperature. The reaction was monitored by TLC (SiO_2, 2:1 hexanes:acetone, UV used to visualize, Rf = 0.27). The reaction was worked up by first adding several drops of glacial acetic acid and then diluting the reaction by a factor of 10 using dry DCM. The resulting solution was then washed with H_2O and brine before

being dried over $MgSO_4$, filtered and dried under vacuum. The resulting brown solid was dissolved in a minimum amount of DCM to which was added Et2O until the formation of a fine white precipitate was observed at which point the solution was put in the freezer for a few hours. This precipitate was then filtered off and then dried under vacuum to afford the final product. Yield 24% of an off-white waxy solid. The product was further purified via preparatory HPLC using a C18 column and eluting with 0 - 5% MeOH in acetonitrile as required for studies. NMR ($CDCl_3$): **^{1}H** = 8.01 (dd,4H, *J*= 8, 2Hz), 7.58 (d, 4H, *J*= 8Hz), 5.32 (m, 1H), 4.56 (d, 2H, *J*= 7Hz), 4.31 (m, 4H), 3.62 (m, 2H), 2.84 (t, 2H, *J*= 7Hz), 2.54 (t, 2H, *J*= 7Hz), 2.36 (t, 2H, *J*= 7Hz), 1.74 (m, 14H), 1.45 (m, 18H). **^{13}C** = 199.5, 173.4, 165.9, 139.2, 131.8, 130.3, 129.7, 127.4, 118.7, 91.4, 65.2, 65.4, 62.7, 61.4, 44.1, 34.2, 32.2, 29.7, 29.2, 29.0, 28.9, 28.7, 28.5, 26.0, 25.8, 25.7, 25.5, 25.2, 24.7, 18.0.

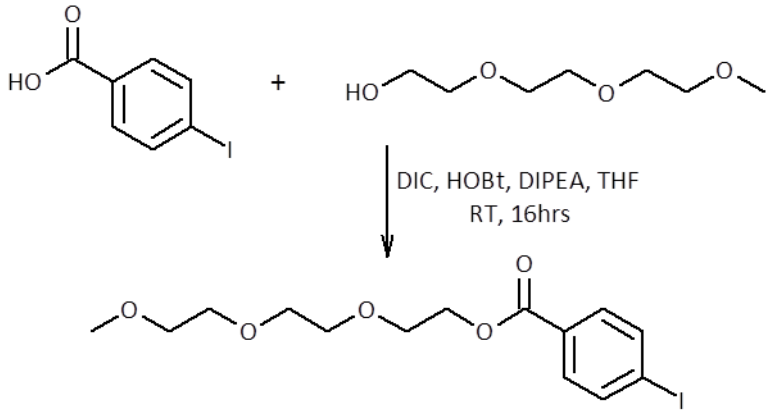

3-61: 2-[2-(2-methoxyethoxy)ethoxy]ethyl 4-iodobenzoate (5.0 g, 20 mmol scale): 1.0 equivalent of ***p*-iodobenzoic acid (3-8)** was dissolved into dry THF. To this solution was added in order 1.2 equivalents of HOBt, 1.2 equivalents of DIC, 1.2 equivalents of **triethylene glycol monomethyl ether (3-60)** and 2.4 equivalents of DIPEA. The reaction was then stirred vigorously for 16 hours while being monitored by TLC (SiO_2, 1:1 hexanes:EtOAc, UV used for visualization, Rf = 0.41). Upon completion of the reaction as indicated by the loss of the spot due to the starting material (**3-8**) on the TLC plate,

the reaction was worked up by first vacuum filtering to remove the solid diisopropyl urea (DIU) side product. The filtrate was then dried under high vacuum before being dissolved into Et_2O. This Et_2O was washed with H_2O and brine before being dried over Na_2SO_4, filtered and then dried under high vacuum. The resulting crude material was purified by silica gel column chromatography eluting with 0 - 50% EtOAc in hexanes. Yield 88% as a white waxy low melting solid. NMR ($CDCl_3$): **^{1}H** = 7.72 (m, 4H), 4.42 (m, 2H), 3.77 (m, 2H), 3.61 (m, 6H), 3.48 (m, 2H), 3.31 (s, 3H). **^{13}C** = 165.9, 137.7, 131.1, 129.5, 100.7, 71.8, 70.6, 69.1, 64.4, 59.1.

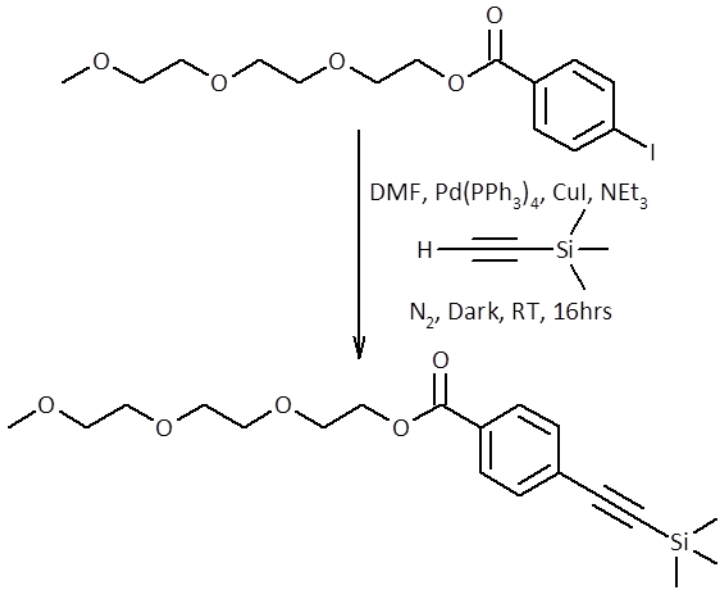

3-62: 2-[2-(2-methoxyethoxy)ethoxy]ethyl 4-trimethylsilyl-ethynylbenzoate (2.4 g, 6.0 mmol scale): 1.0 equivalents of **2-[2-(2-methoxyethoxy)ethoxy]ethyl 4-iodobenzoate (3-61)** was dissolved into dry THF and the resulting solution was purged under N_2. To this solution was added in order under a stream of nitrogen 4.0 equivalents of NEt_3, 0.05 equivalents of $Pd(PPh_3)_4$, 0.10 equivalents of CuI and 2.0 equivalents of TMS-acetylene. The reaction was allowed to stir at room temperature, in the dark and under a stream of N_2 for 16 hours. The reaction was monitored by TLC (SiO2, 1:1 hexanes:EtOAc, UV used for visualization, Rf = 0.52). The reaction was worked up by first removing the solvent

under vacuum to afford dark yellow sticky solid which was treated with Et_2O. The resulting cloudy mixture was vacuum filtered and the filtrate washed with a solution of disodium EDTA, H_2O and brine before being dried over Na_2SO_4, filtered and then dried under vacuum. This crude product was purified by silica gel column chromatography eluting with 0 - 80% Et_2O in hexanes. Yield 98% as a pale orange oil. NMR ($CDCl_3$): **^{1}H** = 7.96 (d, 2H, *J*= 8Hz), 7.49 (d, 2H, *J*= 8Hz), 4.45 (t, 2H, *J*= 6Hz), 3.81 (t, 2H, *J*= 6Hz), 3.65 (m, 6H), 3.51 (m, 2H), 3.35 (s, 3H), 0.24. **^{13}C** = 166.0, 132.3, 129.5, 127.9, 103.8, 97.3, 72.1, 70.6, 69.3, 64.4, 59.1, -0.1.

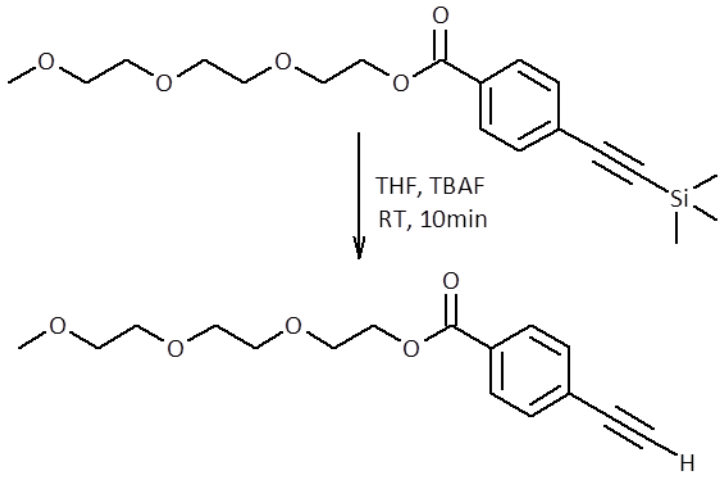

3-63: 2-[2-(2-methoxyethoxy)ethoxy]ethyl 4- ethynylbenzoate (2.0 g, 5.5 mmol scale): 1.0 equivalent of **2-[2-(2-methoxyethoxy)ethoxy]ethyl 4-trimethylsilyl-ethynylbenzoate (3-62)** was dissolved in dry THF and then cooled to 0°C. To this solution was added 1.0 equivalent of TBAF as a 1M solution in THF with vigorous stirring. The reaction immediately went inky black blue. The reaction was monitored by TLC (SiO_2, 1:2 hexanes:Et_2O, UV used for visualization, Rf = 0.29). After ~5 minutes the reaction was complete and worked up by first adding a drop of AcOH causing the colour to fade slightly. The reaction was diluted by a factor of 5 using Et_2O and the resulting solution was washed with H_2O and brine before being dried over Na_2SO_4, filtered and then dried under vacuum. The crude material was purified using silica gel column

chromatography eluting with 0 - 75% EtOAc. Yield 60% as a pale yellow oil. NMR ($CDCl_3$): **^{1}H** = 7.97 (dd, 2H, *J*= 8, 2H), 7.50 (d, 2H, *J*= 8Hz), 4.45 (t, 2H, *J*= 7Hz), 3.80 (t, 2H, *J*= 7Hz), 3.59 (m, 6H), 3.49 (m, 2H), 3.33 (s, 3H), 3.23 (s, 1H). **^{13}C** = 166.3, 132.2, 130.2, 129.6, 126.9, 82.8, 80.2, 72.1, 70.5, 69.2, 64.5, 59.1.

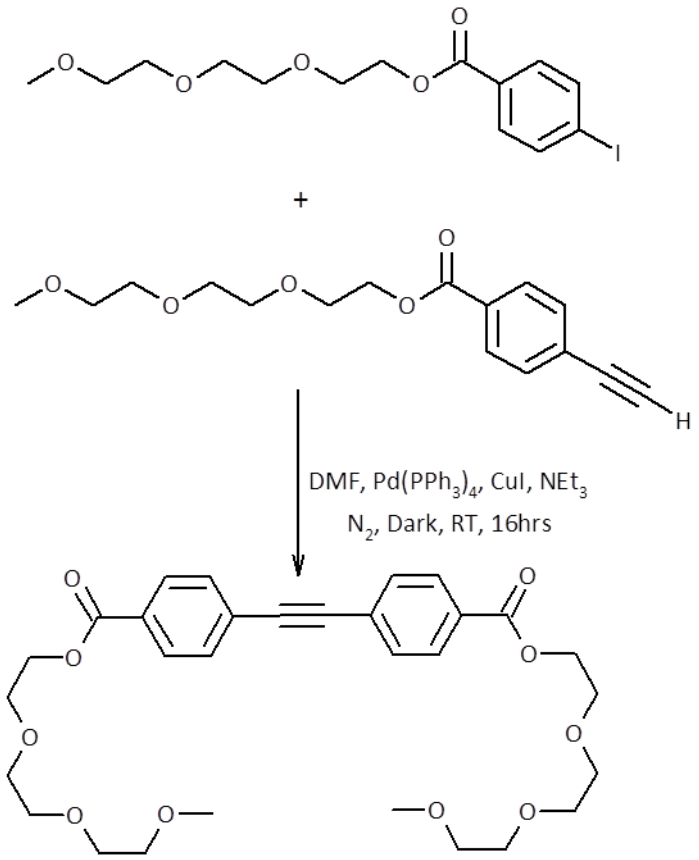

3-64: Adip chromophore standard (1.0 g, 2.5 mmol scale): 1.0 equivalent of **2-[2-(2-methoxyethoxy)ethoxy]ethyl 4-iodobenzoate (3-61)** was dissolved in dry THF and the resulting solution purged with N_2. To this solution was added in order 2.1 equivalents of NEt_3, 0.03 equivalents of $Pd(PPh_3)_4$, 0.06 equivalents of CuI, and 1.1 equivalents of **2-[2-(2-methoxyethoxy)ethoxy]ethyl 4- ethynylbenzoate (3-63)**. The reaction was allowed to stir vigorously in the dark under N_2 for 16 hours. The reaction was monitored by TLC (SiO_2, 2:1 hexanes:acetone, UV used for visualization, Rf = 0.23). Upon completion the reaction was worked up by first removing the solvent under vacuum to afford a mass of

sticky orange solid. This solid was treated with Et_2O resulting in a cloudy orange solution which was vacuum filtered. The filtrate was then washed with a solution of disodium EDTA, H_2O and then brine before being dried over Na_2SO_4, filtered and then dried under vacuum. The resulting orange oil was purified by silica gel column chromatography eluting with 0 - 30% acetone in hexanes. Yield 96% as a pale orange oil. NMR ($CDCl_3$): ^{1}**H** = 8.01 (d, 4H, *J*= 8Hz), 7.56 (d, 4H, *J*= 8Hz), 4.45 (m, 4H), 3.81 (m, 4H), 3.69 (m, 4H), 3.59 (m, 12H), 3.48 (m, 4H), 3.30 (m, 6H). ^{13}**C** = 166.1, 131.7, 129.9, 129.7, 127.4, 91.4, 71.9, 70.7, 70.6, 69.1, 64.4, 59.1.

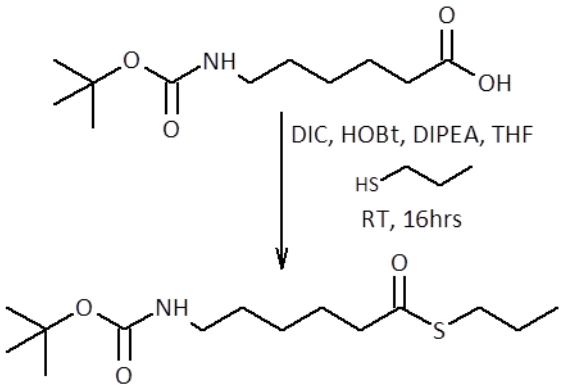

3-65: S-propyl 6-[(tert-butoxycarbonyl)amino]hexanethioate (1.0 g, 4.3 mmol scale): 1.0 equivalent of **6-[(tert-butoxycarbonyl)amino]hexanoic acid (3-14)** was dissolved into dry THF and to this solution was added in order 1.5 equivalents of HOBt, 1.5 equivalents of DIC, 1.5 equivalents of propanethiol and 1.5 equivalents of DIPEA. The reaction was stirred vigorously for 16 hours while monitoring by TLC (SiO_2, 2:1 hexanes:Et2O, Hanessian's stain (blue) used for visualization, Rf = 0.46). The reaction was worked up by first vacuum filtering to remove the DIU side product. The filtrate was then dried under vacuum and the resulting oil was dissolved in Et_2O. This solution was washed with H_2O and brine before being dired over Na_2SO_4, filtered and dried under vacuum. The resulting crude product was purified by silica gel column chromatography eluting with 0 - 30% Et_2O in hexanes. Yield 97% as a pale yellow oil. NMR ($CDCl_3$): ^{1}**H** = 4.56 (s, br, 1H), 3.02 (s, br, 2H), 2.84 (td, 2H, *J*= 7, 1Hz), 2.52 (td, 2H,

J= 7, 1Hz), 1.62-1.30 (m, 18H), 0.90 (td, 3H, *J*= 6, 1Hz). **^{13}C** = 199.4, 155.9, 79.0, 44.0, 40.4, 30.8, 29.9, 28.6, 26.2, 25.5, 22.9, 13.5.

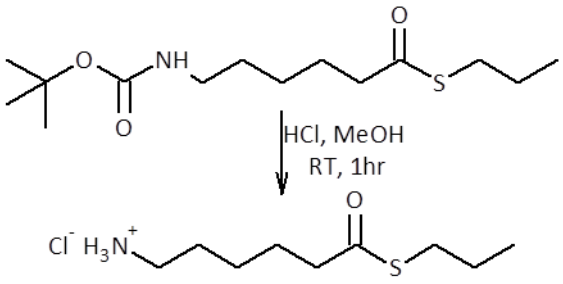

3-67: 6-oxo-6-(propylsulfanyl)hexan-1-amonium chloride (600 mg, 2.0 mmol scale) : 1.0 equivalents of **S-propyl 6-[(tert-butoxycarbonyl)amino]hexanethioate (3-65)** was dissolved in MeOH and to this solution was added 2.0 equivalents of HCl as a 2M aqueous solution. The reaction was stirred vigorously for 1 hour at room temperature. The reaction was worked up by evaporating the solvent under vacuum to afford a waxy off white solid. This solid was triturated with 1:1 hexane:Et_2O before being vacuum filtered. The resulting solids were dried further under vacuum. Yield 98% as a white crystalline solid. NMR ($CDCl_3$): **^{1}H** = 8.14 (br, s, 3H), 2.9 (br, s, 2H), 2.78 (t, 2H, *J*= 7Hz), 2.52 (t, 2H, *J*= 7Hz), 1.76 (m, 2H), 1.64 (m, 2H), 1.52 (p, 2H, *J*= 7Hz), 1.39 (m, 2H), 0.90 (t, 3H, *J*= 7Hz). **^{13}C** = 199.3, 43.7, 39.8, 30.7, 33.0, 27.0, 25.8, 25.0, 13.4.

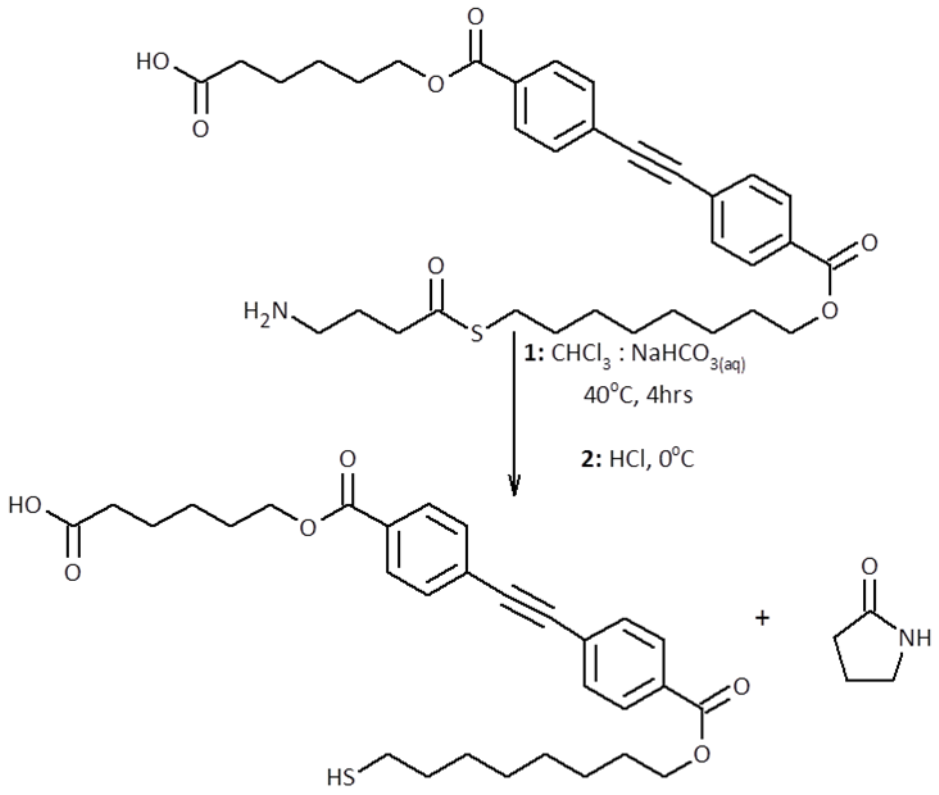

3-71: HOOC-6-ADip-8-SH (25 mg, 0.041 mmol scale): 1.0 equivalent of **$^-$OOC-6-ADip-8-S-4- NH_3^+(3-53)** was dissolved in DCM and to this was added 10.0 equivalents of $NaHCO_3$ as a saturated aqueous solution. The reaction was stirred vigorously while gently heating for 4 hours. The reaction was then cooled in an ice bath and the carefully acidified to pH ~2 with vigorous stirring. The aqueous and organic phases were allowed to separate, retaining the organic phase which was washed with brine and then dried over Na_2SO_4, filtered and then dried under high vacuum to afford the final compound which was purified by HPLC as needed. Crude yield 58% as a waxy off-white solid. NMR (d6-acetone): **^{1}H** = 8.06 (d, 4H, J= 8Hz), 7.71 (d, 4H, J= 8Hz), 7.63 (br s, 3H), 4.33 (q, 4H, J= 7Hz), 3.27 (m, 2H), 2.87 (t, 2H, J= 7Hz), 2.66 (t, 2H, J= 7Hz), 2.34 (t, 2H, J= 7Hz), 1.98-1.25 (m, 22H). **^{13}C** = 198.9, 174.6, 166.1, 132.6, 131.5, 130.4, 127.9, 91.9, 65.9, 65.7, 43.7, 41.1, 34.1, 30.5, 29.7, 29.2, 27.3, 26.7, 26.3, 25.3, 22.9.

Appendix 2: Crystallographic Data

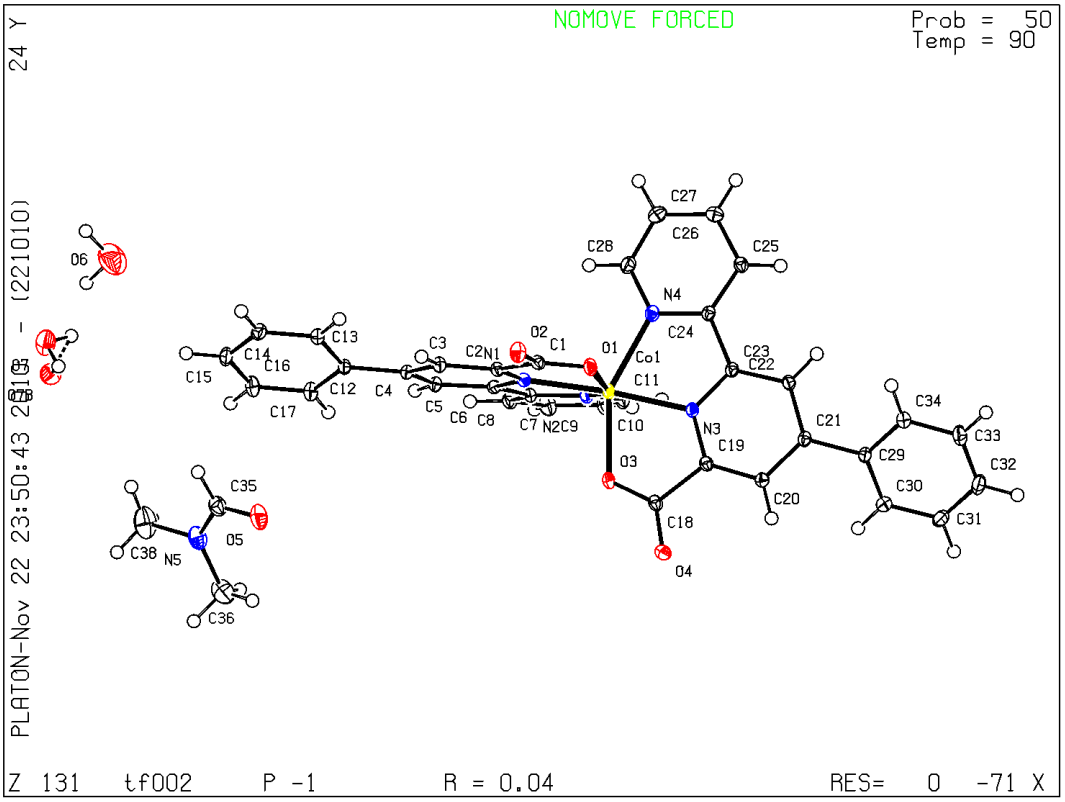

Data Collection

An orange blade crystal of $C_{34}H_{22}N_4O_4Co.DMF.2H_2O$ having approximate dimensions of 0.04 x 0.12 x 0.50 mm was mounted on a glass fiber. All measurements were made on a Bruker APEX DUO diffractometer with graphite monochromated Mo-Kα radiation..

The data were collected at a temperature of -183.0 ± 0.1°C to a maximum 2θ value of 60.2°. Data were collected in a series of ϕ and ω scans in 0.5° oscillations using 3.0-second exposures. The crystal-to-detector distance was 40.05 mm.

Data Reduction

Of the 41458 reflections that were collected, 9598 were unique (R_{int} = 0.039); equivalent reflections were merged. Data were collected and integrated using the

Bruker SAINT[1] software package. The linear absorption coefficient, μ, for Mo-Kα radiation is 5.87 cm^{-1}. Data were corrected for absorption effects using the multi-scan technique (SADABS[2]), with minimum and maximum transmission coefficients of 0.905 and 0.977, respectively. The data were corrected for Lorentz and polarization effects.

Crystal Data

Empirical Formula	$C_{37}H_{33}N_5O_7Co$
Formula Weight	718.61
Crystal Colour, Habit	orange, blade
Crystal Dimensions	0.04 X 0.12 X 0.50 mm
Crystal System	triclinic
Lattice Type	Primitive
Lattice Parameters	a = 12.2490(5) Å
	b = 12.6130(4) Å
	c = 13.1171(5) Å
	α = 66.283(2)°
	β = 62.476(2)°
	γ = 72.627(2)°
	V = 1629.5(1) $Å^3$
Space Group	*P* -1 (#2)
Z value	2
D_{calc}	1.465 g/cm^3

F_{000}	746.00
μ(Mo-Kα)	5.87 cm^{-1}

Intensity Measurements

Diffractometer	Bruker APEX DUO
Radiation	Mo-Kα (λ = 0.71073 Å)
Data Images	2573 exposures @ 3 seconds
Detector Position	40.05 mm
$2\theta_{max}$	60.2^{o}
No. of Reflections Measured	Total: 41458
	Unique: 9598 (R_{int} = 0.039)
Corrections	Absorption (T_{min} = 0.905, T_{max}= 0.977)
	Lorentz-polarization

Structure Solution and Refinement

Structure Solution	Direct Methods (SIR97)
Refinement	Full-matrix least-squares on F^2
Function Minimized	Σ w $(Fo^2 - Fc^2)^2$
Least Squares Weights	$w=1/(\sigma^2(Fo^2)+(0.0421P)^2+ 1.1133P)$
Anomalous Dispersion	All non-hydrogen atoms
No. Observations (I>0.00σ(I))	9598
No. Variables	473
Reflection/Parameter Ratio	20.29

Residuals (refined on F^2, all data): R1; wR2	0.052; 0.097
Goodness of Fit Indicator	1.04
No. Observations ($I>2.00\sigma(I)$)	7728
Residuals (refined on F): R1; wR2	0.038; 0.090
Max Shift/Error in Final Cycle	0.00
Maximum peak in Final Diff. Map	0.47 $e^-/Å^3$
Minimum peak in Final Diff. Map	-0.74 $e^-/Å^3$

Atomic coordinates (x 10^4) and equivalent isotropic displacement parameters (A^2 x 10^3) for tf002

U(eq) is defined as one third of the trace of the orthogonalized Uij tensor.

	x	y	z	U(eq)
C(1)	2608(1)	7949(1)	2120(1)	13(1)
C(2)	3123(1)	6663(1)	2232(1)	11(1)
C(3)	3566(1)	5892(1)	3103(1)	13(1)
C(4)	4020(1)	4727(1)	3101(1)	12(1)
C(5)	4004(1)	4408(1)	2201(1)	12(1)
C(6)	3518(1)	5227(1)	1375(1)	11(1)
C(7)	3355(1)	5000(1)	434(1)	11(1)
C(8)	3664(2)	3911(1)	266(1)	14(1)
C(9)	3414(2)	3788(1)	-608(2)	18(1)
C(10)	2862(2)	4750(2)	-1290(2)	19(1)
C(11)	2600(2)	5809(1)	-1081(2)	16(1)
C(12)	4486(1)	3864(1)	4027(1)	12(1)
C(13)	4126(2)	4033(1)	5133(1)	14(1)
C(14)	4569(2)	3220(1)	5997(2)	16(1)
C(15)	5373(2)	2221(1)	5783(2)	17(1)
C(16)	5728(2)	2041(1)	4690(2)	19(1)
C(17)	5296(2)	2846(1)	3819(2)	16(1)
C(18)	4340(1)	8925(1)	-2104(1)	13(1)
C(19)	3086(1)	9454(1)	-2200(1)	12(1)
C(20)	2898(1)	10369(1)	-3158(1)	13(1)
C(21)	1686(1)	10753(1)	-3125(1)	12(1)

C(22)	709(1)	10204(1)	-2114(1)	12(1)
C(23)	976(1)	9280(1)	-1193(1)	11(1)
C(24)	65(1)	8558(1)	-103(1)	11(1)
C(25)	-1204(1)	8788(1)	183(1)	13(1)
C(26)	-1966(2)	8031(1)	1210(2)	16(1)
C(27)	-1429(2)	7058(1)	1894(2)	18(1)
C(28)	-155(2)	6889(1)	1542(2)	16(1)
C(29)	1448(1)	11695(1)	-4154(1)	13(1)
C(30)	2261(2)	11737(1)	-5338(2)	16(1)
C(31)	2022(2)	12603(2)	-6304(2)	18(1)
C(32)	993(2)	13457(2)	-6098(2)	20(1)
C(33)	182(2)	13424(1)	-4924(2)	19(1)
C(34)	390(2)	12538(1)	-3954(2)	15(1)
C(35)	8432(2)	3247(2)	3881(2)	21(1)
C(36)	10097(2)	2760(2)	2129(2)	32(1)
C(38)	9436(2)	1243(2)	4139(2)	38(1)
N(1)	3096(1)	6331(1)	1398(1)	11(1)
N(2)	2839(1)	5946(1)	-249(1)	13(1)
N(3)	2145(1)	8924(1)	-1253(1)	11(1)
N(4)	588(1)	7627(1)	581(1)	13(1)
N(5)	9255(2)	2440(1)	3384(2)	23(1)
O(1)	2217(1)	8496(1)	1266(1)	14(1)
O(2)	2582(1)	8345(1)	2853(1)	17(1)
O(3)	4323(1)	7980(1)	-1229(1)	15(1)
O(4)	5257(1)	9414(1)	-2865(1)	17(1)
O(5)	8267(1)	4290(1)	3347(1)	27(1)

O(6)	4467(2)	1198(2)	9185(2)	53(1)
O(7)	6758(2)	-620(1)	8287(2)	30(1)
O(7B)	7340(30)	-670(20)	7640(30)	26(8)
Co(1)	2547(1)	7569(1)	91(1)	11(1)

Bond lengths [A] and angles [deg] for tf002

C(1)-O(2)	1.2338(19)
C(1)-O(1)	1.2789(19)
C(1)-C(2)	1.528(2)
C(2)-N(1)	1.335(2)
C(2)-C(3)	1.382(2)
C(3)-C(4)	1.407(2)
C(3)-H(3)	0.9500
C(4)-C(5)	1.402(2)
C(4)-C(12)	1.481(2)
C(5)-C(6)	1.387(2)
C(5)-H(5)	0.9500
C(6)-N(1)	1.3411(18)
C(6)-C(7)	1.480(2)
C(7)-N(2)	1.3555(19)
C(7)-C(8)	1.391(2)
C(8)-C(9)	1.389(2)
C(8)-H(8)	0.9500
C(9)-C(10)	1.386(2)
C(9)-H(9)	0.9500
C(10)-C(11)	1.385(2)
C(10)-H(10)	0.9500
C(11)-N(2)	1.336(2)
C(11)-H(11)	0.9500
C(12)-C(13)	1.394(2)
C(12)-C(17)	1.406(2)

C(13)-C(14)	1.391(2)
C(13)-H(13)	0.9500
C(14)-C(15)	1.387(2)
C(14)-H(14)	0.9500
C(15)-C(16)	1.386(2)
C(15)-H(15)	0.9500
C(16)-C(17)	1.386(2)
C(16)-H(16)	0.9500
C(17)-H(17)	0.9500
C(18)-O(4)	1.2330(19)
C(18)-O(3)	1.2769(18)
C(18)-C(19)	1.524(2)
C(19)-N(3)	1.3365(19)
C(19)-C(20)	1.380(2)
C(20)-C(21)	1.404(2)
C(20)-H(20)	0.9500
C(21)-C(22)	1.400(2)
C(21)-C(29)	1.478(2)
C(22)-C(23)	1.390(2)
C(22)-H(22)	0.9500
C(23)-N(3)	1.3411(19)
C(23)-C(24)	1.484(2)
C(24)-N(4)	1.3529(19)
C(24)-C(25)	1.386(2)
C(25)-C(26)	1.390(2)
C(25)-H(25)	0.9500

C(26)-C(27)	1.385(2)
C(26)-H(26)	0.9500
C(27)-C(28)	1.381(2)
C(27)-H(27)	0.9500
C(28)-N(4)	1.336(2)
C(28)-H(28)	0.9500
C(29)-C(30)	1.394(2)
C(29)-C(34)	1.402(2)
C(30)-C(31)	1.387(2)
C(30)-H(30)	0.9500
C(31)-C(32)	1.389(2)
C(31)-H(31)	0.9500
C(32)-C(33)	1.386(3)
C(32)-H(32)	0.9500
C(33)-C(34)	1.386(2)
C(33)-H(33)	0.9500
C(34)-H(34)	0.9500
C(35)-O(5)	1.222(2)
C(35)-N(5)	1.338(2)
C(35)-H(35)	0.9500
C(36)-N(5)	1.443(3)
C(36)-H(36A)	0.9800
C(36)-H(36B)	0.9800
C(36)-H(36C)	0.9800
C(38)-N(5)	1.452(2)
C(38)-H(38A)	0.9800

C(38)-H(38B)	0.9800
C(38)-H(38C)	0.9800
N(1)-Co(1)	2.0288(13)
N(2)-Co(1)	2.1607(13)
N(3)-Co(1)	2.0362(13)
N(4)-Co(1)	2.1639(14)
O(1)-Co(1)	2.1204(11)
O(3)-Co(1)	2.1135(12)
O(6)-H(6A)	1.031(12)
O(6)-H(6B)	1.019(9)
O(7)-O(7B)	0.83(3)
O(7)-H(7A)	0.88(3)
O(7)-H(7B)	0.86(4)
O(7B)-H(7A)	1.06(4)
O(7B)-H(7B)	0.96(4)

O(2)-C(1)-O(1)	126.98(14)
O(2)-C(1)-C(2)	118.47(13)
O(1)-C(1)-C(2)	114.53(13)
N(1)-C(2)-C(3)	121.94(13)
N(1)-C(2)-C(1)	113.12(13)
C(3)-C(2)-C(1)	124.94(14)
C(2)-C(3)-C(4)	119.12(14)
C(2)-C(3)-H(3)	120.4
C(4)-C(3)-H(3)	120.4
C(5)-C(4)-C(3)	117.79(13)

C(5)-C(4)-C(12)	121.06(13)
C(3)-C(4)-C(12)	121.14(14)
C(6)-C(5)-C(4)	119.62(14)
C(6)-C(5)-H(5)	120.2
C(4)-C(5)-H(5)	120.2
N(1)-C(6)-C(5)	121.12(14)
N(1)-C(6)-C(7)	113.00(13)
C(5)-C(6)-C(7)	125.83(13)
N(2)-C(7)-C(8)	121.67(14)
N(2)-C(7)-C(6)	114.32(13)
C(8)-C(7)-C(6)	123.99(13)
C(9)-C(8)-C(7)	118.95(14)
C(9)-C(8)-H(8)	120.5
C(7)-C(8)-H(8)	120.5
C(10)-C(9)-C(8)	119.42(15)
C(10)-C(9)-H(9)	120.3
C(8)-C(9)-H(9)	120.3
C(11)-C(10)-C(9)	118.18(15)
C(11)-C(10)-H(10)	120.9
C(9)-C(10)-H(10)	120.9
N(2)-C(11)-C(10)	123.30(15)
N(2)-C(11)-H(11)	118.4
C(10)-C(11)-H(11)	118.4
C(13)-C(12)-C(17)	118.21(14)
C(13)-C(12)-C(4)	120.90(13)
C(17)-C(12)-C(4)	120.88(14)

C(14)-C(13)-C(12)	120.64(15)
C(14)-C(13)-H(13)	119.7
C(12)-C(13)-H(13)	119.7
C(15)-C(14)-C(13)	120.79(15)
C(15)-C(14)-H(14)	119.6
C(13)-C(14)-H(14)	119.6
C(16)-C(15)-C(14)	118.95(15)
C(16)-C(15)-H(15)	120.5
C(14)-C(15)-H(15)	120.5
C(17)-C(16)-C(15)	120.82(15)
C(17)-C(16)-H(16)	119.6
C(15)-C(16)-H(16)	119.6
C(16)-C(17)-C(12)	120.58(15)
C(16)-C(17)-H(17)	119.7
C(12)-C(17)-H(17)	119.7
O(4)-C(18)-O(3)	126.66(14)
O(4)-C(18)-C(19)	118.75(13)
O(3)-C(18)-C(19)	114.57(13)
N(3)-C(19)-C(20)	121.59(14)
N(3)-C(19)-C(18)	113.09(13)
C(20)-C(19)-C(18)	125.31(14)
C(19)-C(20)-C(21)	118.85(14)
C(19)-C(20)-H(20)	120.6
C(21)-C(20)-H(20)	120.6
C(22)-C(21)-C(20)	118.74(14)
C(22)-C(21)-C(29)	120.52(14)

C(20)-C(21)-C(29)	120.72(14)
C(23)-C(22)-C(21)	118.92(14)
C(23)-C(22)-H(22)	120.5
C(21)-C(22)-H(22)	120.5
N(3)-C(23)-C(22)	121.04(14)
N(3)-C(23)-C(24)	113.20(13)
C(22)-C(23)-C(24)	125.70(14)
N(4)-C(24)-C(25)	122.47(14)
N(4)-C(24)-C(23)	113.82(13)
C(25)-C(24)-C(23)	123.70(13)
C(24)-C(25)-C(26)	118.65(14)
C(24)-C(25)-H(25)	120.7
C(26)-C(25)-H(25)	120.7
C(27)-C(26)-C(25)	119.02(15)
C(27)-C(26)-H(26)	120.5
C(25)-C(26)-H(26)	120.5
C(28)-C(27)-C(26)	118.65(15)
C(28)-C(27)-H(27)	120.7
C(26)-C(27)-H(27)	120.7
N(4)-C(28)-C(27)	123.27(15)
N(4)-C(28)-H(28)	118.4
C(27)-C(28)-H(28)	118.4
C(30)-C(29)-C(34)	119.25(14)
C(30)-C(29)-C(21)	120.13(14)
C(34)-C(29)-C(21)	120.60(14)
C(31)-C(30)-C(29)	120.21(15)

C(31)-C(30)-H(30)	119.9
C(29)-C(30)-H(30)	119.9
C(30)-C(31)-C(32)	120.18(16)
C(30)-C(31)-H(31)	119.9
C(32)-C(31)-H(31)	119.9
C(33)-C(32)-C(31)	119.97(15)
C(33)-C(32)-H(32)	120.0
C(31)-C(32)-H(32)	120.0
C(34)-C(33)-C(32)	120.16(16)
C(34)-C(33)-H(33)	119.9
C(32)-C(33)-H(33)	119.9
C(33)-C(34)-C(29)	120.16(15)
C(33)-C(34)-H(34)	119.9
C(29)-C(34)-H(34)	119.9
O(5)-C(35)-N(5)	125.63(18)
O(5)-C(35)-H(35)	117.2
N(5)-C(35)-H(35)	117.2
N(5)-C(36)-H(36A)	109.5
N(5)-C(36)-H(36B)	109.5
H(36A)-C(36)-H(36B)	109.5
N(5)-C(36)-H(36C)	109.5
H(36A)-C(36)-H(36C)	109.5
H(36B)-C(36)-H(36C)	109.5
N(5)-C(38)-H(38A)	109.5
N(5)-C(38)-H(38B)	109.5
H(38A)-C(38)-H(38B)	109.5

N(5)-C(38)-H(38C)	109.5
H(38A)-C(38)-H(38C)	109.5
H(38B)-C(38)-H(38C)	109.5
C(2)-N(1)-C(6)	120.37(13)
C(2)-N(1)-Co(1)	118.26(10)
C(6)-N(1)-Co(1)	121.15(10)
C(11)-N(2)-C(7)	118.45(13)
C(11)-N(2)-Co(1)	126.23(11)
C(7)-N(2)-Co(1)	115.28(10)
C(19)-N(3)-C(23)	120.84(13)
C(19)-N(3)-Co(1)	117.80(10)
C(23)-N(3)-Co(1)	121.36(10)
C(28)-N(4)-C(24)	117.88(14)
C(28)-N(4)-Co(1)	126.10(11)
C(24)-N(4)-Co(1)	115.78(10)
C(35)-N(5)-C(36)	121.21(16)
C(35)-N(5)-C(38)	120.21(18)
C(36)-N(5)-C(38)	118.06(17)
C(1)-O(1)-Co(1)	116.47(9)
C(18)-O(3)-Co(1)	116.13(10)
H(6A)-O(6)-H(6B)	104.1(18)
O(7B)-O(7)-H(7A)	76(2)
O(7B)-O(7)-H(7B)	69(3)
H(7A)-O(7)-H(7B)	109(3)
O(7)-O(7B)-H(7A)	54(2)
O(7)-O(7B)-H(7B)	56(3)

H(7A)-O(7B)-H(7B)	89(3)
N(1)-Co(1)-N(3)	173.17(5)
N(1)-Co(1)-O(3)	97.96(5)
N(3)-Co(1)-O(3)	77.06(5)
N(1)-Co(1)-O(1)	77.00(5)
N(3)-Co(1)-O(1)	99.21(5)
O(3)-Co(1)-O(1)	101.13(5)
N(1)-Co(1)-N(2)	75.35(5)
N(3)-Co(1)-N(2)	109.25(5)
O(3)-Co(1)-N(2)	92.34(5)
O(1)-Co(1)-N(2)	150.63(5)
N(1)-Co(1)-N(4)	110.63(5)
N(3)-Co(1)-N(4)	75.06(5)
O(3)-Co(1)-N(4)	150.20(5)
O(1)-Co(1)-N(4)	93.55(5)
N(2)-Co(1)-N(4)	87.07(5)

Anisotropic displacement parameters (A^2 x 10^3) for tf002

The anisotropic displacement factor exponent takes the form:

-2 pi^2 [h^2 a*^2 U11 + ... + 2 h k a* b* U12]

	U11	U22	U33	U23	U13	U12
C(1)	11(1)	11(1)	14(1)	-4(1)	-5(1)	0(1)
C(2)	11(1)	11(1)	12(1)	-4(1)	-5(1)	0(1)
C(3)	14(1)	13(1)	13(1)	-4(1)	-7(1)	0(1)
C(4)	12(1)	11(1)	11(1)	-1(1)	-5(1)	-1(1)
C(5)	13(1)	10(1)	12(1)	-2(1)	-6(1)	-1(1)
C(6)	11(1)	10(1)	11(1)	-3(1)	-4(1)	-1(1)
C(7)	10(1)	12(1)	11(1)	-2(1)	-5(1)	0(1)
C(8)	13(1)	13(1)	15(1)	-5(1)	-7(1)	1(1)
C(9)	20(1)	17(1)	22(1)	-10(1)	-11(1)	2(1)
C(10)	22(1)	21(1)	19(1)	-10(1)	-13(1)	1(1)
C(11)	17(1)	19(1)	14(1)	-5(1)	-10(1)	1(1)
C(12)	13(1)	11(1)	13(1)	-1(1)	-7(1)	-1(1)
C(13)	14(1)	15(1)	13(1)	-3(1)	-6(1)	0(1)
C(14)	17(1)	18(1)	13(1)	-2(1)	-7(1)	-5(1)
C(15)	19(1)	16(1)	17(1)	2(1)	-12(1)	-4(1)
C(16)	22(1)	13(1)	22(1)	-3(1)	-14(1)	2(1)
C(17)	19(1)	13(1)	16(1)	-4(1)	-10(1)	1(1)
C(18)	12(1)	12(1)	14(1)	-6(1)	-6(1)	2(1)
C(19)	11(1)	11(1)	13(1)	-5(1)	-5(1)	1(1)
C(20)	12(1)	12(1)	12(1)	-3(1)	-5(1)	-1(1)
C(21)	14(1)	10(1)	11(1)	-3(1)	-6(1)	0(1)

C(22)	11(1)	12(1)	12(1)	-4(1)	-6(1)	1(1)
C(23)	13(1)	11(1)	10(1)	-4(1)	-5(1)	1(1)
C(24)	13(1)	11(1)	10(1)	-4(1)	-5(1)	0(1)
C(25)	13(1)	12(1)	14(1)	-5(1)	-6(1)	0(1)
C(26)	14(1)	17(1)	17(1)	-6(1)	-5(1)	-3(1)
C(27)	20(1)	16(1)	16(1)	-2(1)	-5(1)	-7(1)
C(28)	18(1)	13(1)	14(1)	-2(1)	-6(1)	-2(1)
C(29)	13(1)	13(1)	12(1)	-1(1)	-7(1)	-2(1)
C(30)	14(1)	17(1)	14(1)	-2(1)	-5(1)	-3(1)
C(31)	19(1)	21(1)	12(1)	1(1)	-6(1)	-7(1)
C(32)	25(1)	17(1)	18(1)	3(1)	-14(1)	-6(1)
C(33)	20(1)	14(1)	23(1)	-2(1)	-14(1)	0(1)
C(34)	15(1)	15(1)	15(1)	-3(1)	-7(1)	-1(1)
C(35)	20(1)	24(1)	21(1)	-10(1)	-11(1)	0(1)
C(36)	29(1)	46(1)	29(1)	-24(1)	-14(1)	6(1)
C(38)	52(1)	18(1)	56(2)	-11(1)	-35(1)	1(1)
N(1)	10(1)	11(1)	12(1)	-3(1)	-5(1)	-1(1)
N(2)	13(1)	13(1)	13(1)	-3(1)	-7(1)	1(1)
N(3)	11(1)	10(1)	11(1)	-3(1)	-5(1)	1(1)
N(4)	15(1)	10(1)	13(1)	-3(1)	-6(1)	0(1)
N(5)	26(1)	19(1)	29(1)	-11(1)	-16(1)	3(1)
O(1)	15(1)	12(1)	15(1)	-3(1)	-8(1)	2(1)
O(2)	23(1)	14(1)	19(1)	-7(1)	-12(1)	1(1)
O(3)	13(1)	12(1)	16(1)	-2(1)	-8(1)	2(1)
O(4)	12(1)	17(1)	18(1)	-3(1)	-5(1)	-1(1)
O(5)	31(1)	22(1)	31(1)	-10(1)	-20(1)	8(1)

O(6)	45(1)	50(1)	61(1)	-27(1)	-24(1)	14(1)
O(7)	37(1)	25(1)	34(1)	0(1)	-23(1)	-11(1)
Co(1)	12(1)	10(1)	11(1)	-2(1)	-6(1)	1(1)

Hydrogen coordinates (x 10^4) and isotropic displacement parameters (A^2 x 10^3) for tf002

	x	y	z	U(eq)
H(3)	3565	6145	3695	15
H(5)	4324	3636	2157	15
H(8)	4040	3261	742	17
H(9)	3618	3052	-738	22
H(10)	2670	4684	-1884	23
H(11)	2230	6471	-1553	20
H(13)	3572	4709	5297	17
H(14)	4319	3351	6744	19
H(15)	5676	1670	6375	21
H(16)	6273	1357	4536	22
H(17)	5550	2710	3074	19
H(20)	3578	10732	-3827	15
H(22)	-124	10459	-2059	14
H(25)	-1547	9450	-313	15
H(26)	-2841	8178	1440	19
H(27)	-1927	6519	2590	21
H(28)	210	6215	2006	19
H(30)	2981	11170	-5483	19
H(31)	2563	12612	-7109	22
H(32)	846	14063	-6762	24
H(33)	-519	14011	-4784	22
H(34)	-185	12501	-3150	18

H(35)	7932	2986	4721	25
H(36A)	10004	3613	1778	48
H(36B)	9904	2421	1687	48
H(36C)	10954	2463	2068	48
H(38A)	8847	1163	4977	57
H(38B)	10287	1047	4103	57
H(38C)	9296	713	3847	57
H(6A)	5185(15)	532(14)	9000(18)	17
H(6B)	4150(20)	1020(20)	10097(9)	42(7)
H(7A)	6390(30)	-670(20)	7880(30)	51(8)
H(7B)	7110(30)	0(30)	7910(30)	66(10)

Torsion angles [deg] for tf002

O(2)-C(1)-C(2)-N(1)	179.47(14)
O(1)-C(1)-C(2)-N(1)	1.10(19)
O(2)-C(1)-C(2)-C(3)	0.2(2)
O(1)-C(1)-C(2)-C(3)	-178.20(15)
N(1)-C(2)-C(3)-C(4)	1.0(2)
C(1)-C(2)-C(3)-C(4)	-179.79(14)
C(2)-C(3)-C(4)-C(5)	0.3(2)
C(2)-C(3)-C(4)-C(12)	-179.05(14)
C(3)-C(4)-C(5)-C(6)	-1.8(2)
C(12)-C(4)-C(5)-C(6)	177.61(14)
C(4)-C(5)-C(6)-N(1)	2.0(2)
C(4)-C(5)-C(6)-C(7)	-175.32(14)
N(1)-C(6)-C(7)-N(2)	1.43(19)
C(5)-C(6)-C(7)-N(2)	178.95(15)
N(1)-C(6)-C(7)-C(8)	-176.85(14)
C(5)-C(6)-C(7)-C(8)	0.7(2)
N(2)-C(7)-C(8)-C(9)	-1.3(2)
C(6)-C(7)-C(8)-C(9)	176.88(15)
C(7)-C(8)-C(9)-C(10)	-0.1(2)
C(8)-C(9)-C(10)-C(11)	1.0(3)
C(9)-C(10)-C(11)-N(2)	-0.7(3)
C(5)-C(4)-C(12)-C(13)	-157.58(15)
C(3)-C(4)-C(12)-C(13)	21.8(2)
C(5)-C(4)-C(12)-C(17)	21.9(2)
C(3)-C(4)-C(12)-C(17)	-158.77(15)

C(17)-C(12)-C(13)-C(14)	0.7(2)
C(4)-C(12)-C(13)-C(14)	-179.83(14)
C(12)-C(13)-C(14)-C(15)	-0.4(2)
C(13)-C(14)-C(15)-C(16)	-0.2(2)
C(14)-C(15)-C(16)-C(17)	0.4(3)
C(15)-C(16)-C(17)-C(12)	-0.1(3)
C(13)-C(12)-C(17)-C(16)	-0.4(2)
C(4)-C(12)-C(17)-C(16)	-179.91(15)
O(4)-C(18)-C(19)-N(3)	-172.91(14)
O(3)-C(18)-C(19)-N(3)	8.58(19)
O(4)-C(18)-C(19)-C(20)	8.3(2)
O(3)-C(18)-C(19)-C(20)	-170.21(15)
N(3)-C(19)-C(20)-C(21)	0.5(2)
C(18)-C(19)-C(20)-C(21)	179.17(14)
C(19)-C(20)-C(21)-C(22)	0.9(2)
C(19)-C(20)-C(21)-C(29)	-177.33(14)
C(20)-C(21)-C(22)-C(23)	-1.6(2)
C(29)-C(21)-C(22)-C(23)	176.61(14)
C(21)-C(22)-C(23)-N(3)	1.0(2)
C(21)-C(22)-C(23)-C(24)	-175.82(14)
N(3)-C(23)-C(24)-N(4)	-4.55(19)
C(22)-C(23)-C(24)-N(4)	172.51(14)
N(3)-C(23)-C(24)-C(25)	177.00(14)
C(22)-C(23)-C(24)-C(25)	-5.9(2)
N(4)-C(24)-C(25)-C(26)	-0.2(2)
C(23)-C(24)-C(25)-C(26)	178.15(14)

C(24)-C(25)-C(26)-C(27)	-1.7(2)
C(25)-C(26)-C(27)-C(28)	1.3(2)
C(26)-C(27)-C(28)-N(4)	0.9(3)
C(22)-C(21)-C(29)-C(30)	-138.28(16)
C(20)-C(21)-C(29)-C(30)	39.9(2)
C(22)-C(21)-C(29)-C(34)	40.1(2)
C(20)-C(21)-C(29)-C(34)	-141.75(16)
C(34)-C(29)-C(30)-C(31)	-0.1(2)
C(21)-C(29)-C(30)-C(31)	178.31(15)
C(29)-C(30)-C(31)-C(32)	2.2(3)
C(30)-C(31)-C(32)-C(33)	-2.0(3)
C(31)-C(32)-C(33)-C(34)	-0.3(3)
C(32)-C(33)-C(34)-C(29)	2.4(2)
C(30)-C(29)-C(34)-C(33)	-2.2(2)
C(21)-C(29)-C(34)-C(33)	179.40(15)
C(3)-C(2)-N(1)-C(6)	-0.8(2)
C(1)-C(2)-N(1)-C(6)	179.89(13)
C(3)-C(2)-N(1)-Co(1)	-175.47(12)
C(1)-C(2)-N(1)-Co(1)	5.21(17)
C(5)-C(6)-N(1)-C(2)	-0.7(2)
C(7)-C(6)-N(1)-C(2)	176.93(13)
C(5)-C(6)-N(1)-Co(1)	173.80(11)
C(7)-C(6)-N(1)-Co(1)	-8.55(17)
C(10)-C(11)-N(2)-C(7)	-0.6(2)
C(10)-C(11)-N(2)-Co(1)	176.93(13)
C(8)-C(7)-N(2)-C(11)	1.6(2)

C(6)-C(7)-N(2)-C(11)	-176.70(14)
C(8)-C(7)-N(2)-Co(1)	-176.20(12)
C(6)-C(7)-N(2)-Co(1)	5.48(17)
C(20)-C(19)-N(3)-C(23)	-1.1(2)
C(18)-C(19)-N(3)-C(23)	-179.95(13)
C(20)-C(19)-N(3)-Co(1)	179.13(11)
C(18)-C(19)-N(3)-Co(1)	0.28(16)
C(22)-C(23)-N(3)-C(19)	0.3(2)
C(24)-C(23)-N(3)-C(19)	177.55(13)
C(22)-C(23)-N(3)-Co(1)	-179.91(11)
C(24)-C(23)-N(3)-Co(1)	-2.69(17)
C(27)-C(28)-N(4)-C(24)	-2.7(2)
C(27)-C(28)-N(4)-Co(1)	171.34(12)
C(25)-C(24)-N(4)-C(28)	2.3(2)
C(23)-C(24)-N(4)-C(28)	-176.16(13)
C(25)-C(24)-N(4)-Co(1)	-172.36(11)
C(23)-C(24)-N(4)-Co(1)	9.17(16)
O(5)-C(35)-N(5)-C(36)	3.0(3)
O(5)-C(35)-N(5)-C(38)	174.63(19)
O(2)-C(1)-O(1)-Co(1)	175.25(13)
C(2)-C(1)-O(1)-Co(1)	-6.54(17)
O(4)-C(18)-O(3)-Co(1)	168.60(13)
C(19)-C(18)-O(3)-Co(1)	-13.04(16)
C(2)-N(1)-Co(1)-N(3)	50.3(5)
C(6)-N(1)-Co(1)-N(3)	-124.3(4)
C(2)-N(1)-Co(1)-O(3)	93.10(12)

C(6)-N(1)-Co(1)-O(3)	-81.53(12)
C(2)-N(1)-Co(1)-O(1)	-6.55(11)
C(6)-N(1)-Co(1)-O(1)	178.81(12)
C(2)-N(1)-Co(1)-N(2)	-176.55(12)
C(6)-N(1)-Co(1)-N(2)	8.81(11)
C(2)-N(1)-Co(1)-N(4)	-95.46(12)
C(6)-N(1)-Co(1)-N(4)	89.91(12)
C(19)-N(3)-Co(1)-N(1)	38.5(5)
C(23)-N(3)-Co(1)-N(1)	-141.3(4)
C(19)-N(3)-Co(1)-O(3)	-5.15(11)
C(23)-N(3)-Co(1)-O(3)	175.09(12)
C(19)-N(3)-Co(1)-O(1)	94.25(11)
C(23)-N(3)-Co(1)-O(1)	-85.51(12)
C(19)-N(3)-Co(1)-N(2)	-93.10(12)
C(23)-N(3)-Co(1)-N(2)	87.14(12)
C(19)-N(3)-Co(1)-N(4)	-174.51(12)
C(23)-N(3)-Co(1)-N(4)	5.73(11)
C(18)-O(3)-Co(1)-N(1)	-164.93(11)
C(18)-O(3)-Co(1)-N(3)	10.32(11)
C(18)-O(3)-Co(1)-O(1)	-86.70(11)
C(18)-O(3)-Co(1)-N(2)	119.54(11)
C(18)-O(3)-Co(1)-N(4)	31.35(16)
C(1)-O(1)-Co(1)-N(1)	7.19(11)
C(1)-O(1)-Co(1)-N(3)	-167.03(11)
C(1)-O(1)-Co(1)-O(3)	-88.52(11)
C(1)-O(1)-Co(1)-N(2)	27.22(17)

C(1)-O(1)-Co(1)-N(4)	117.55(11)
C(11)-N(2)-Co(1)-N(1)	174.96(14)
C(7)-N(2)-Co(1)-N(1)	-7.42(11)
C(11)-N(2)-Co(1)-N(3)	-10.31(15)
C(7)-N(2)-Co(1)-N(3)	167.31(10)
C(11)-N(2)-Co(1)-O(3)	-87.42(14)
C(7)-N(2)-Co(1)-O(3)	90.20(11)
C(11)-N(2)-Co(1)-O(1)	154.77(12)
C(7)-N(2)-Co(1)-O(1)	-27.61(17)
C(11)-N(2)-Co(1)-N(4)	62.75(14)
C(7)-N(2)-Co(1)-N(4)	-119.63(11)
C(28)-N(4)-Co(1)-N(1)	-6.21(14)
C(24)-N(4)-Co(1)-N(1)	167.96(10)
C(28)-N(4)-Co(1)-N(3)	177.76(14)
C(24)-N(4)-Co(1)-N(3)	-8.07(10)
C(28)-N(4)-Co(1)-O(3)	156.54(12)
C(24)-N(4)-Co(1)-O(3)	-29.29(16)
C(28)-N(4)-Co(1)-O(1)	-83.64(13)
C(24)-N(4)-Co(1)-O(1)	90.53(11)
C(28)-N(4)-Co(1)-N(2)	66.95(13)
C(24)-N(4)-Co(1)-N(2)	-118.88(11)

Hydrogen bonds

Donor - H....Acceptor	[ARU]	D - H	H...A	D...A	D - H...A
O(6) --H(6A) ..O(7)	[ ]	1.031(19)	2.11(2)	3.130(3)	169.3(16)
O(6) --H(6B) ..O(7)	[2657.03]	1.019(11)	1.811(11)	2.808(3)	165(2)
O(7) --H(7A) ..O(4)	[1546.01]	0.87(4)	1.99(4)	2.852(3)	168(3)
O(7) --H(7B) ..O(2)	[2666.01]	0.85(4)	1.99(4)	2.818(2)	164(4)

Appendix 3: NMR Spectra

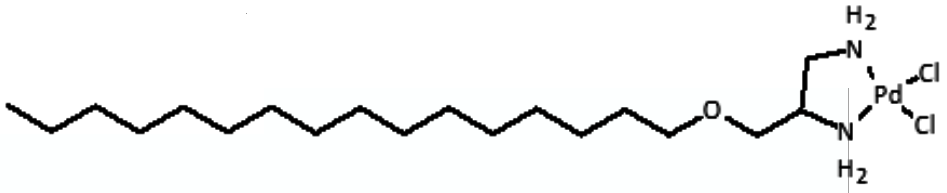

2-4

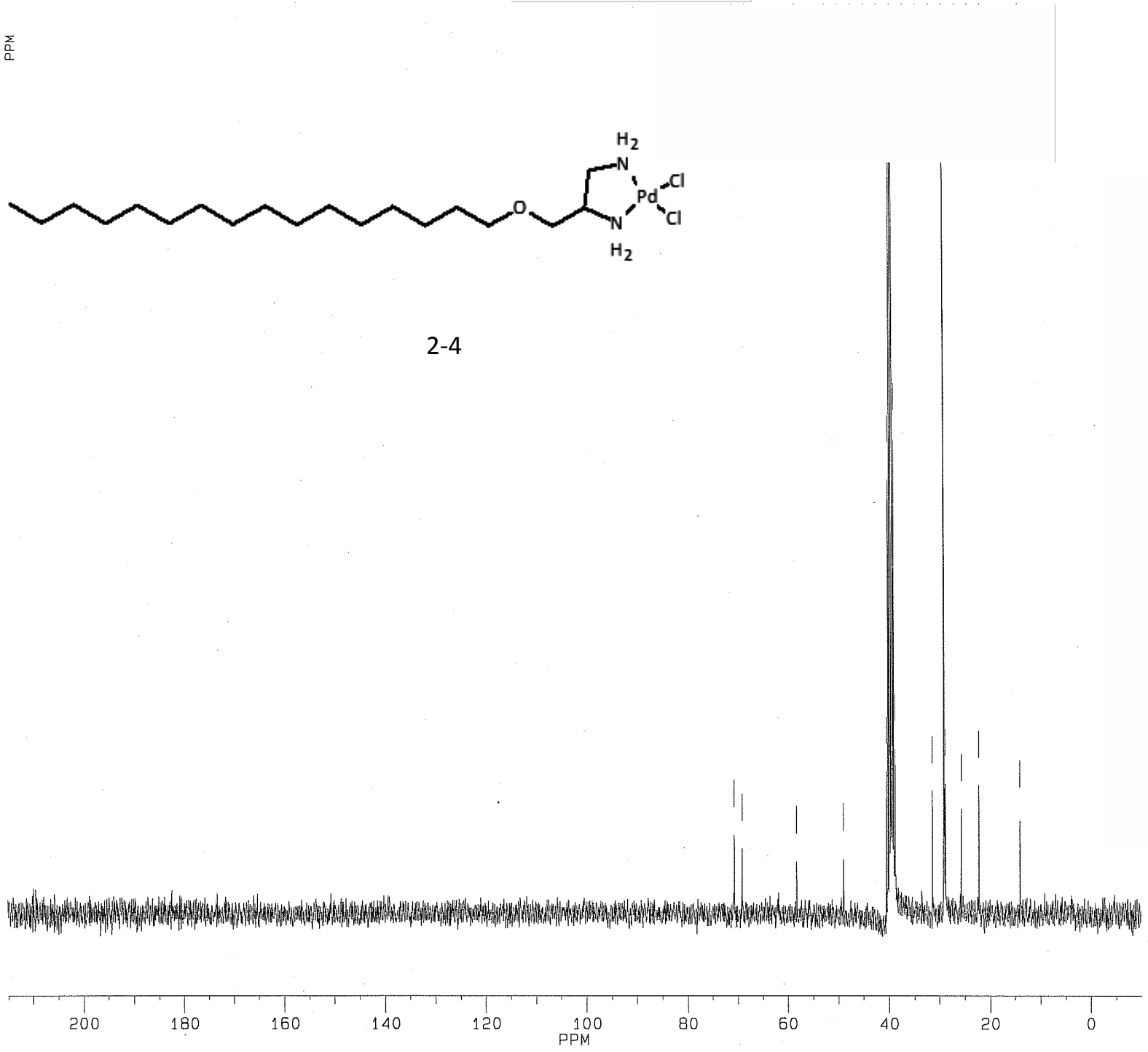

2-4

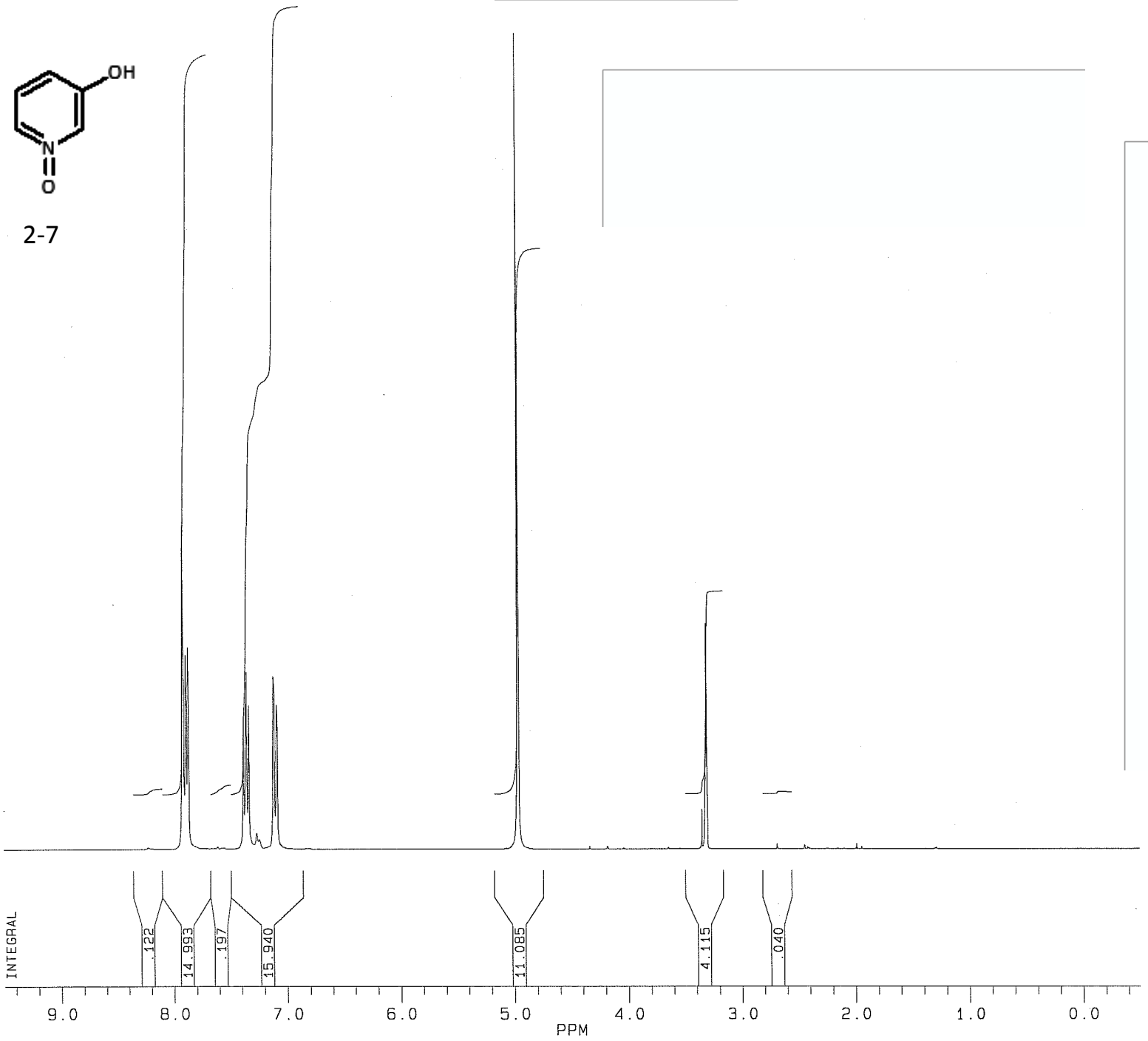
OH
N
O
2-7
INTEGRAL
.122
14.993
.197
15.940
11.085
4.115
.040
9.0
8.0
7.0
6.0
5.0
4.0
3.0
2.0
1.0
0.0
PPM

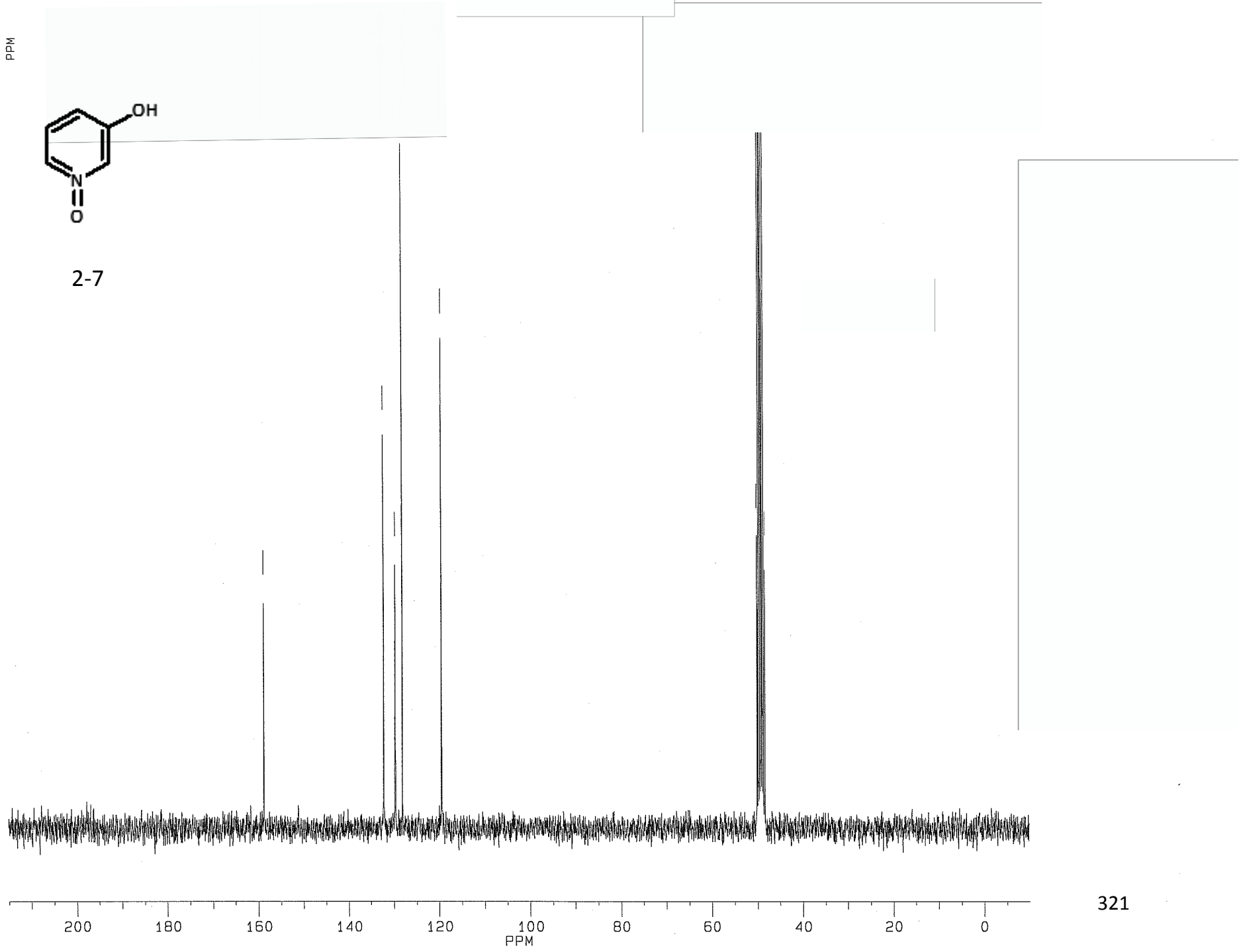
PPM
OH
N
O
2-7
200
180
160
140
120
100
80
60
40
20
0
PPM

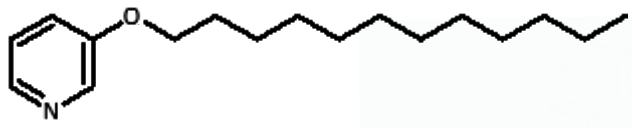
O
N

2-11

INTEGRAL
6.105
6.036
6.153
72.643
9.0
8.0
7.0
6.0
5.0
4.0
3.0
2.0
1.0
0.0
PPM

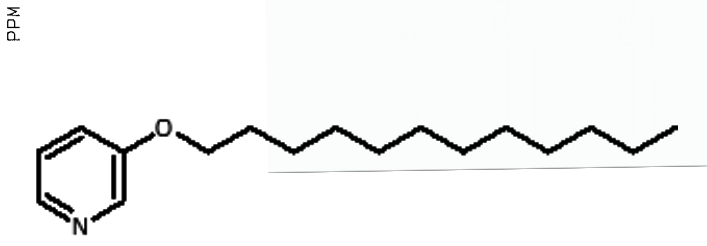

2-11

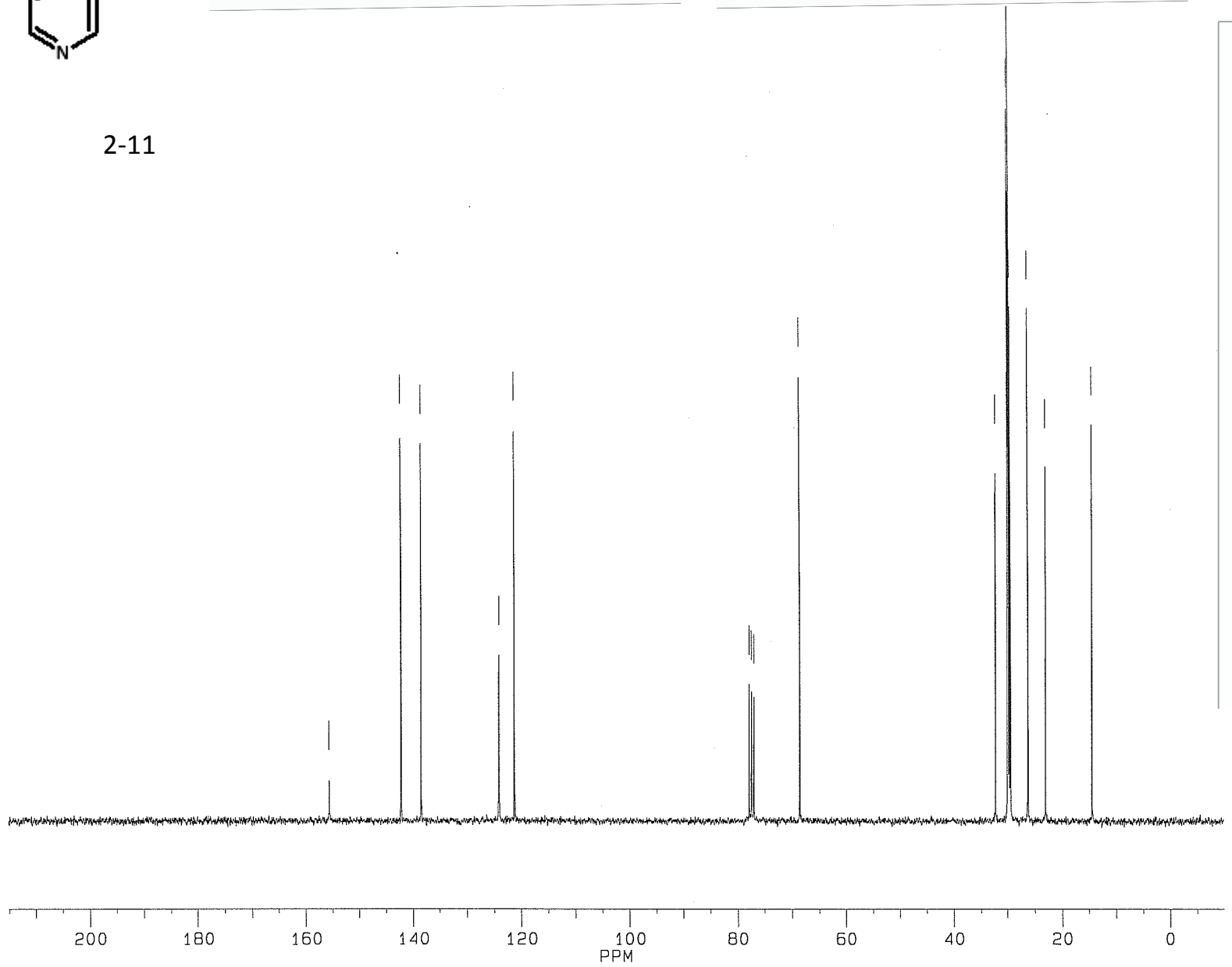

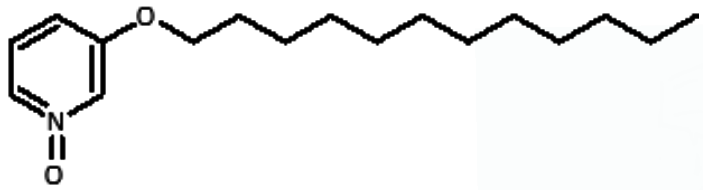

2-12

INTEGRAL
7.676
4.934
3.916
8.243
84.178
11.968
1.135
9.0
8.0
7.0
6.0
5.0
4.0
3.0
2.0
1.0
0.0
PPM

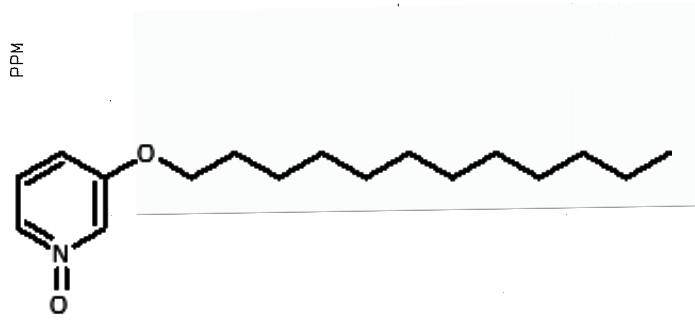

2-12

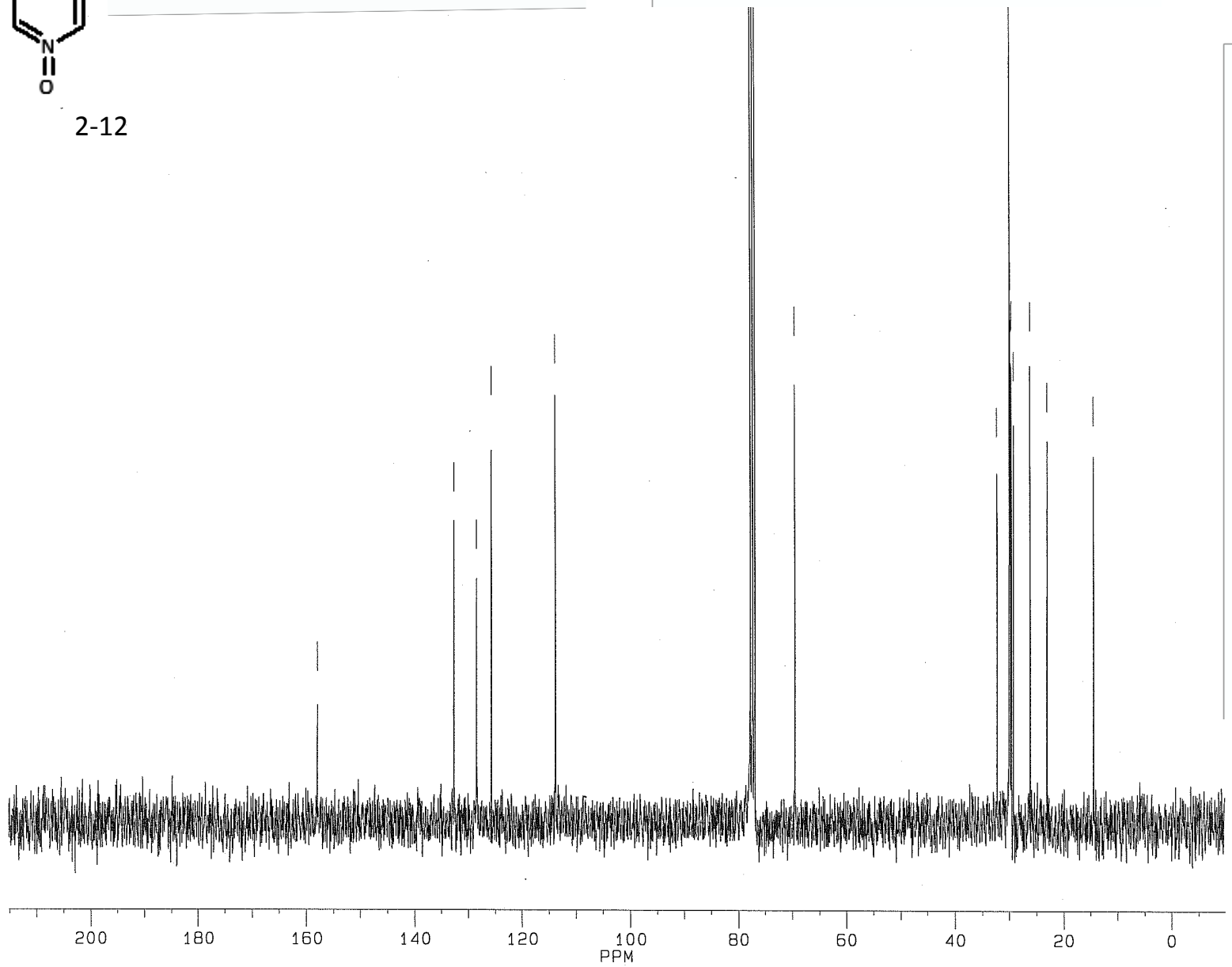

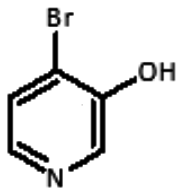
Br
OH
N

2-20

INTEGRAL
51.606
52.812
47.304
.587
39.679
.730
36.769
3.576
1.293
9.0
8.0
7.0
6.0
5.0
4.0
3.0
2.0
1.0
0.0
PPM

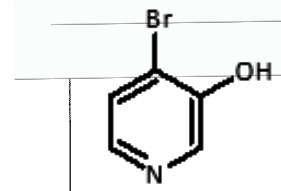

2-20

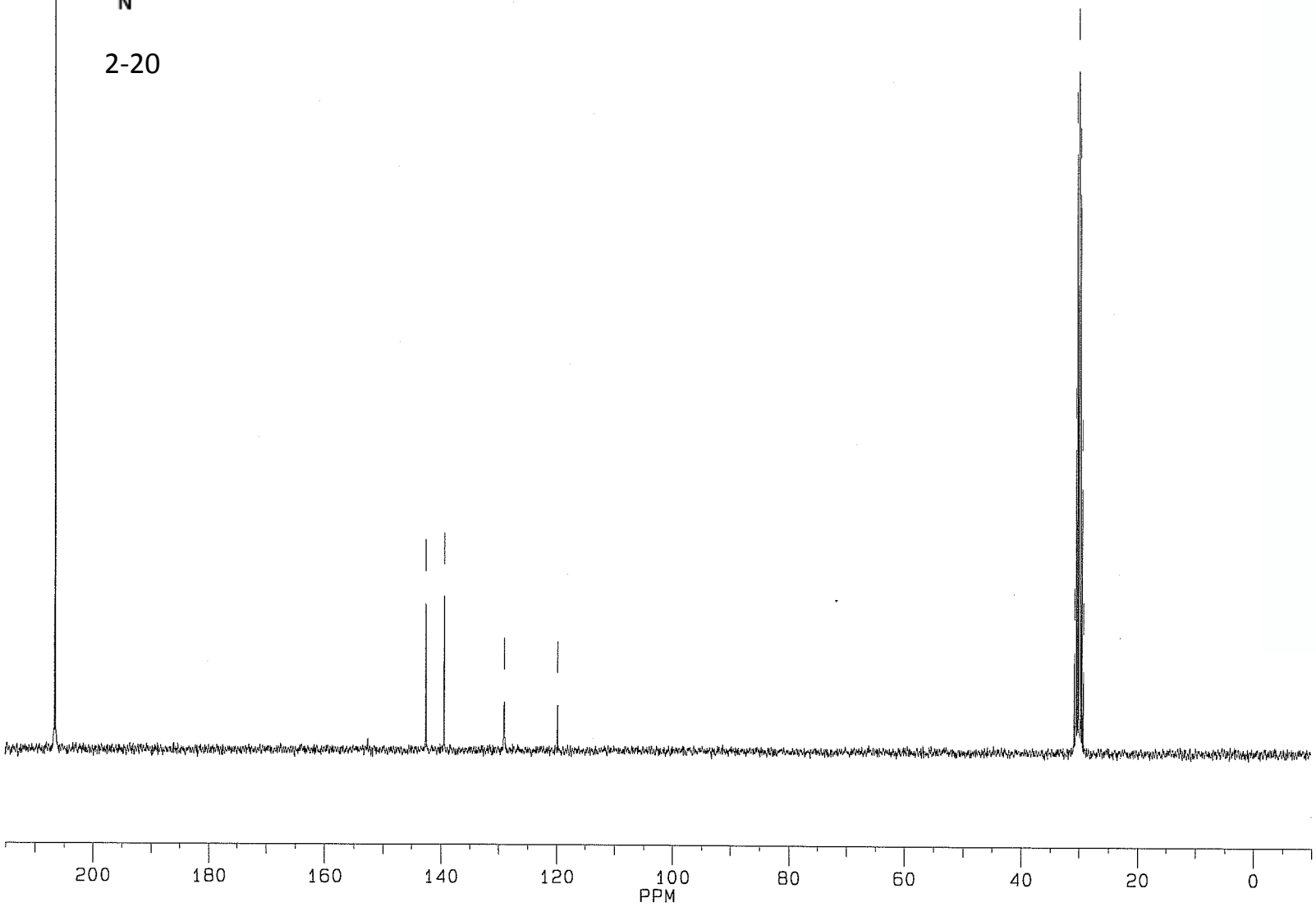

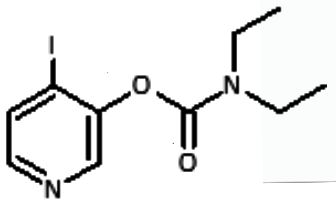
I
O
N
O
N

2-24

INTEGRAL
17.91
19.29
19.25
9.70
86.22
14.59
147.53
9.0
8.0
7.0
6.0
5.0
4.0
3.0
2.0
1.0
0.0
PPM

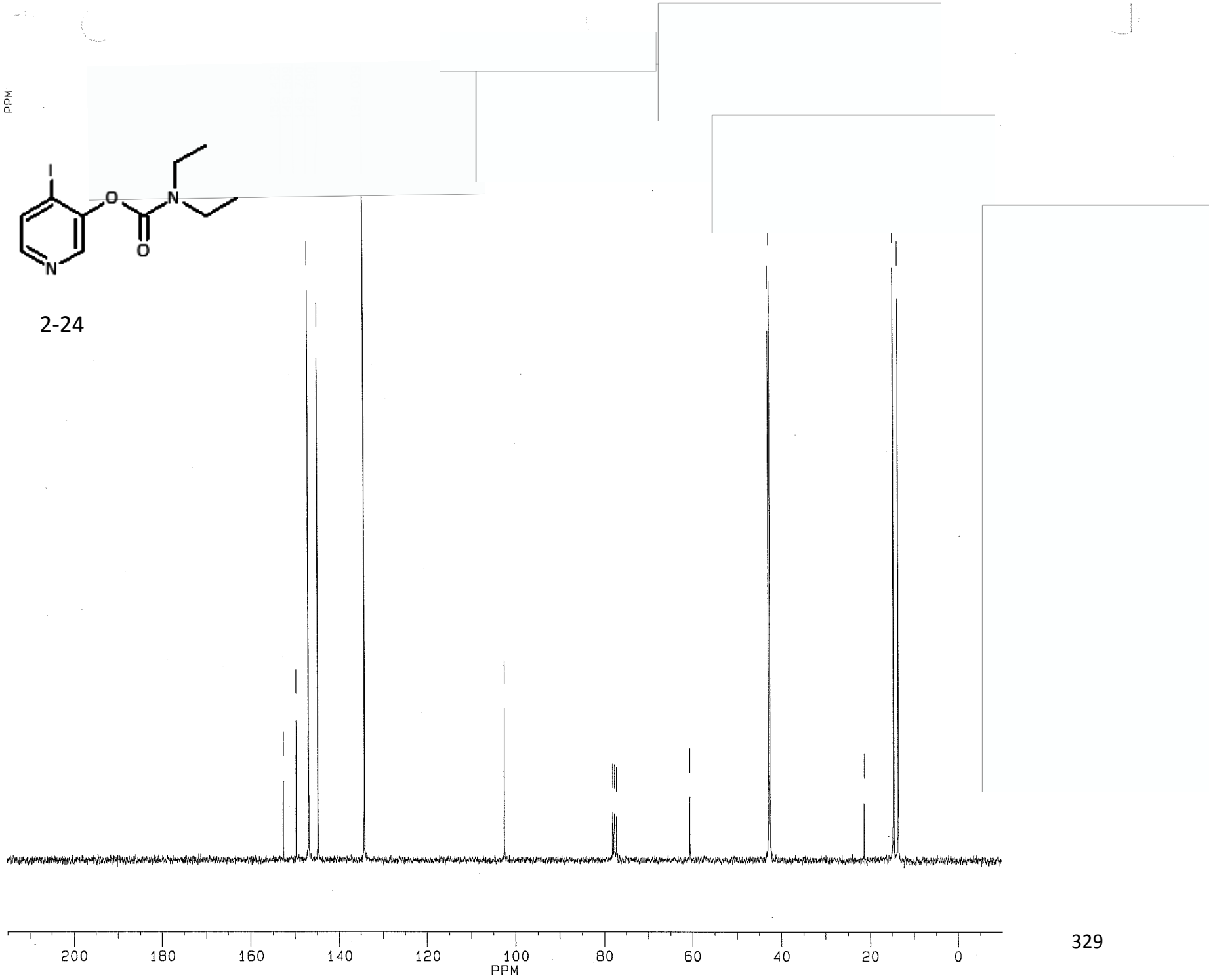
PPM
I
O
N
O
N
2-24
200
180
160
140
120
100
80
60
40
20
0
PPM

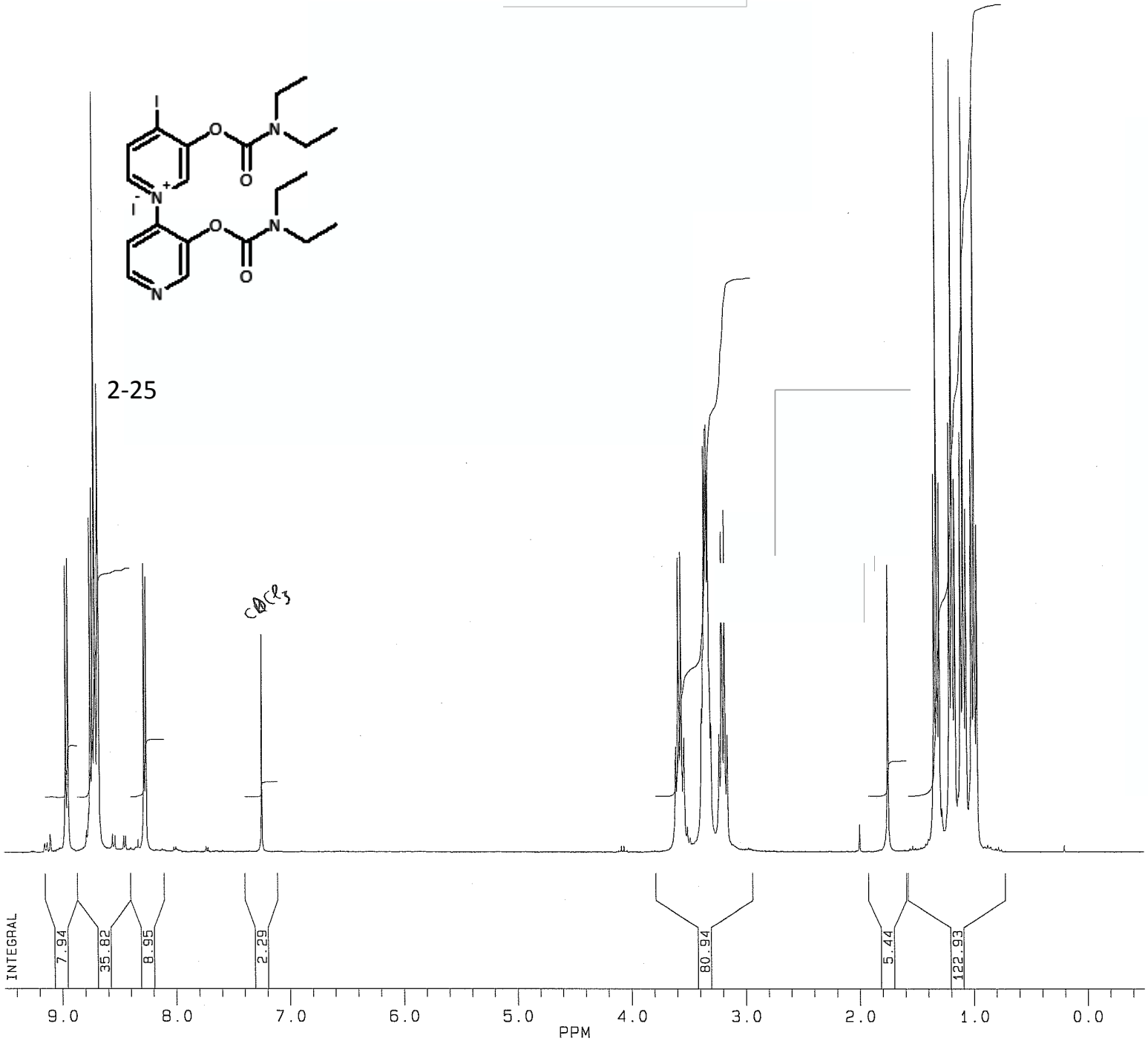
2-25
INTEGRAL
7.94
35.82
8.95
2.29
80.94
5.44
122.93
9.0
8.0
7.0
6.0
5.0
4.0
3.0
2.0
1.0
0.0
PPM

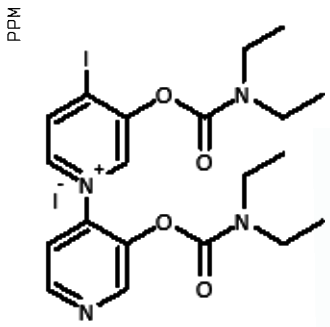

2-25

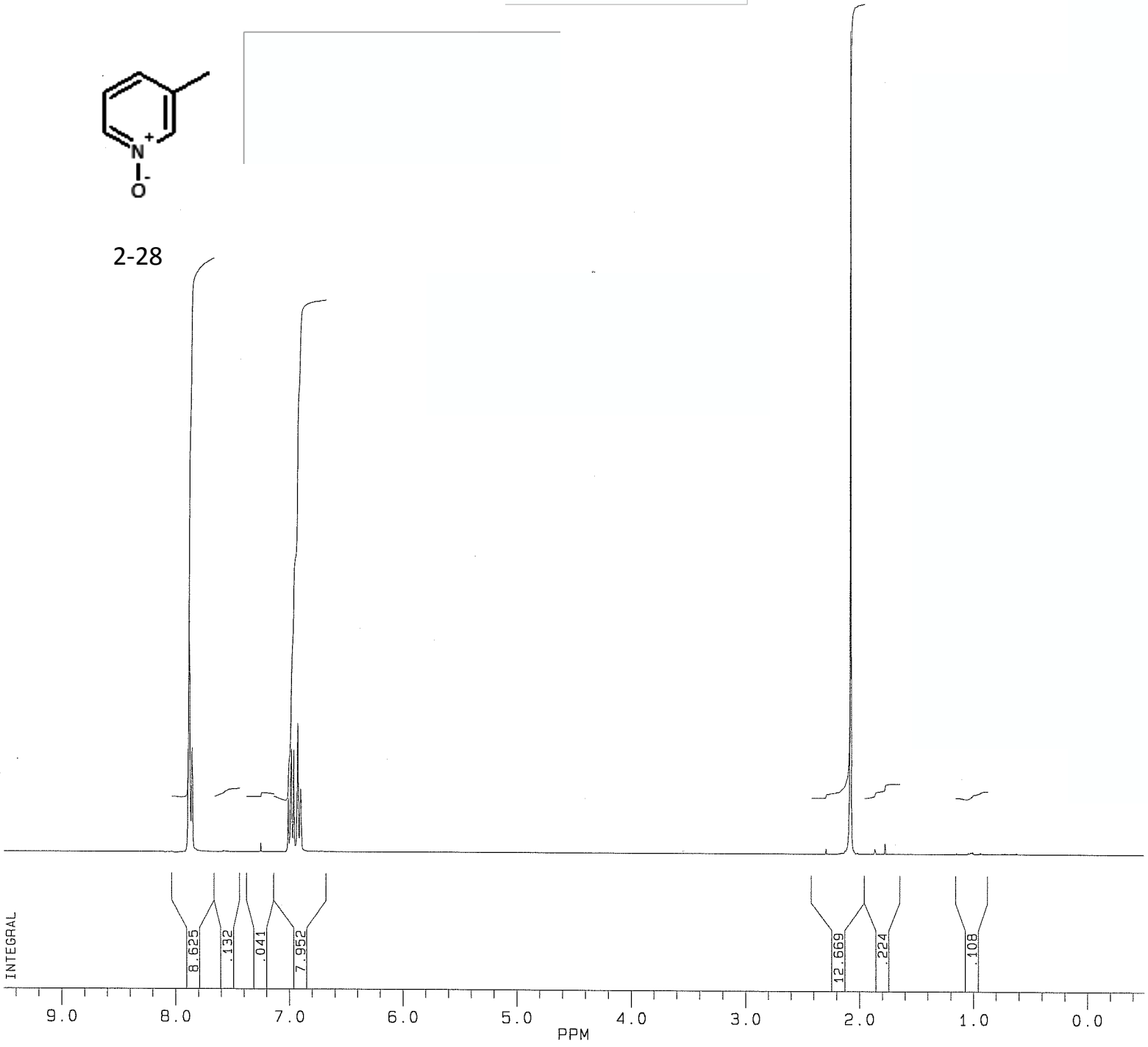
2-28
INTEGRAL
8.625
.132
.041
7.952
12.669
.224
.108
9.0
8.0
7.0
6.0
5.0
4.0
3.0
2.0
1.0
0.0
PPM

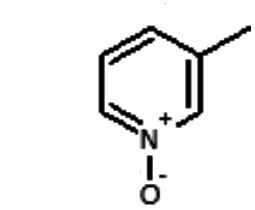

2-28

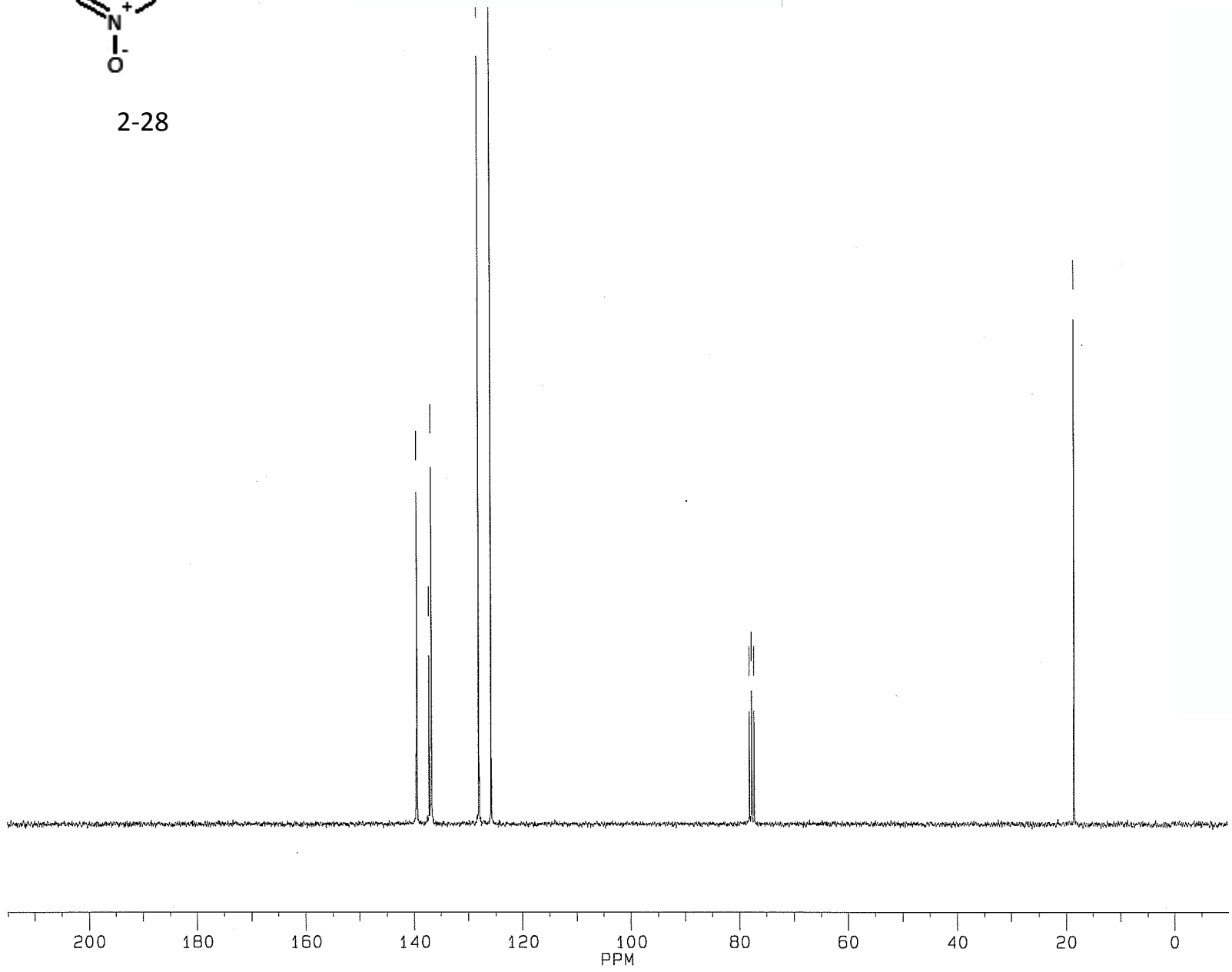

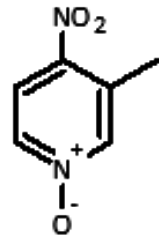
NO2
N+
O-

2-29

INTEGRAL
11.234
.423
12.026
.492
.047
9.0
8.0
7.0
6.0
5.0
4.0
3.0
2.0
1.0
0.0
PPM

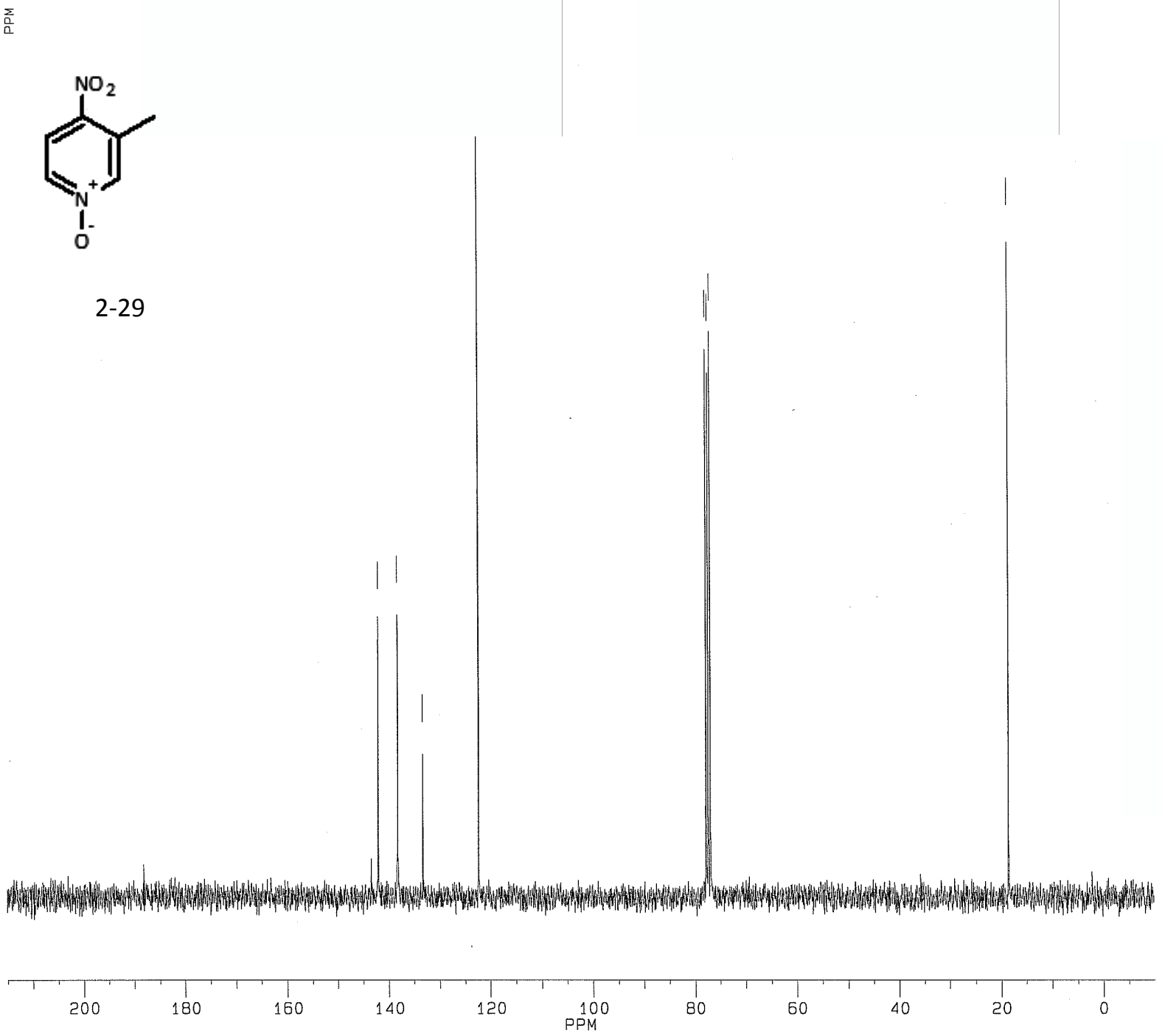

2-29

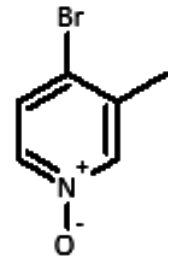
Br
N
+
O
-

2-30

INTEGRAL
.096
20.731
10.079
.052
.972
.212
.455
30.411
.160
9.0
8.0
7.0
6.0
5.0
4.0
3.0
2.0
1.0
0.0
PPM

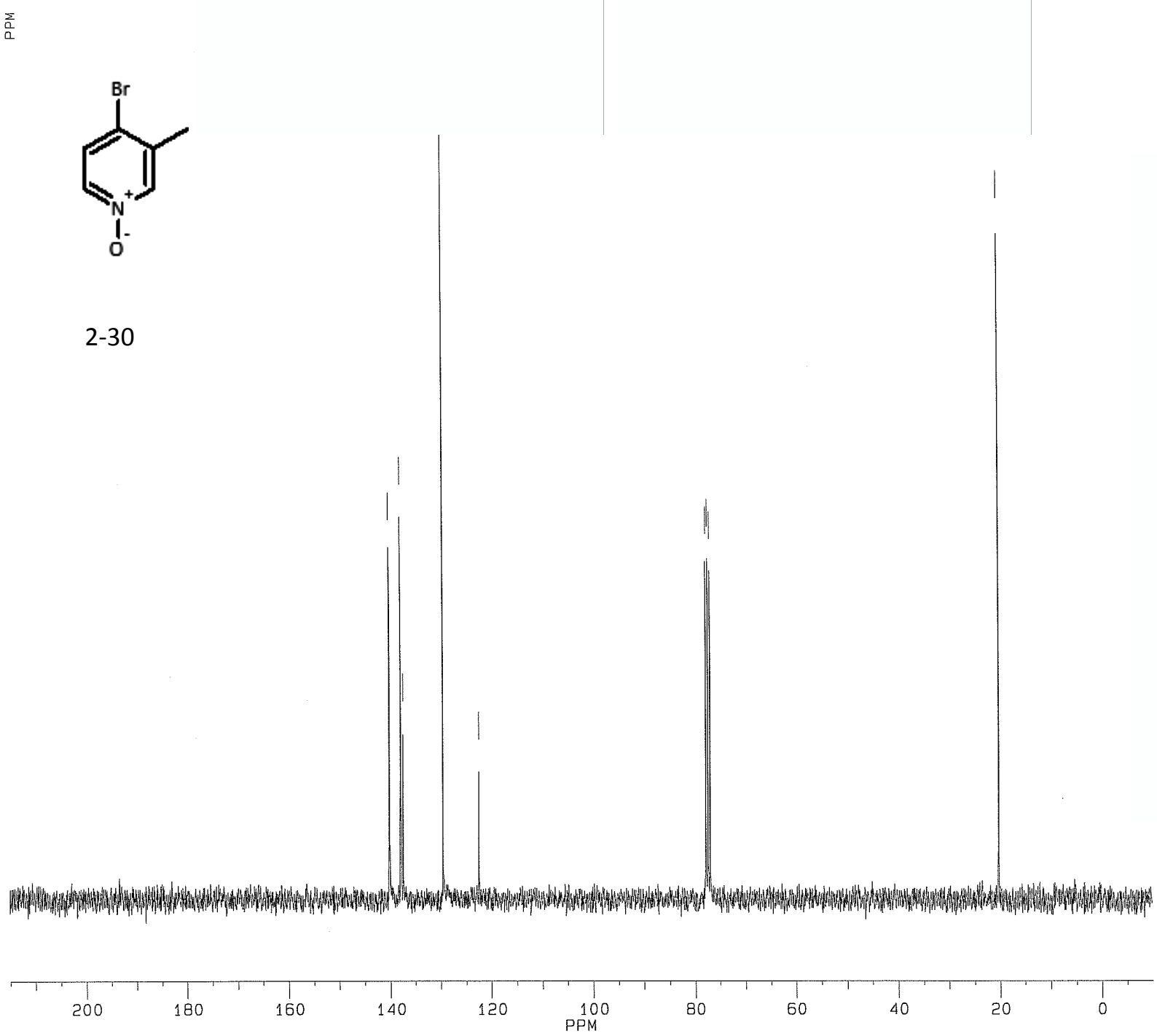

2-30

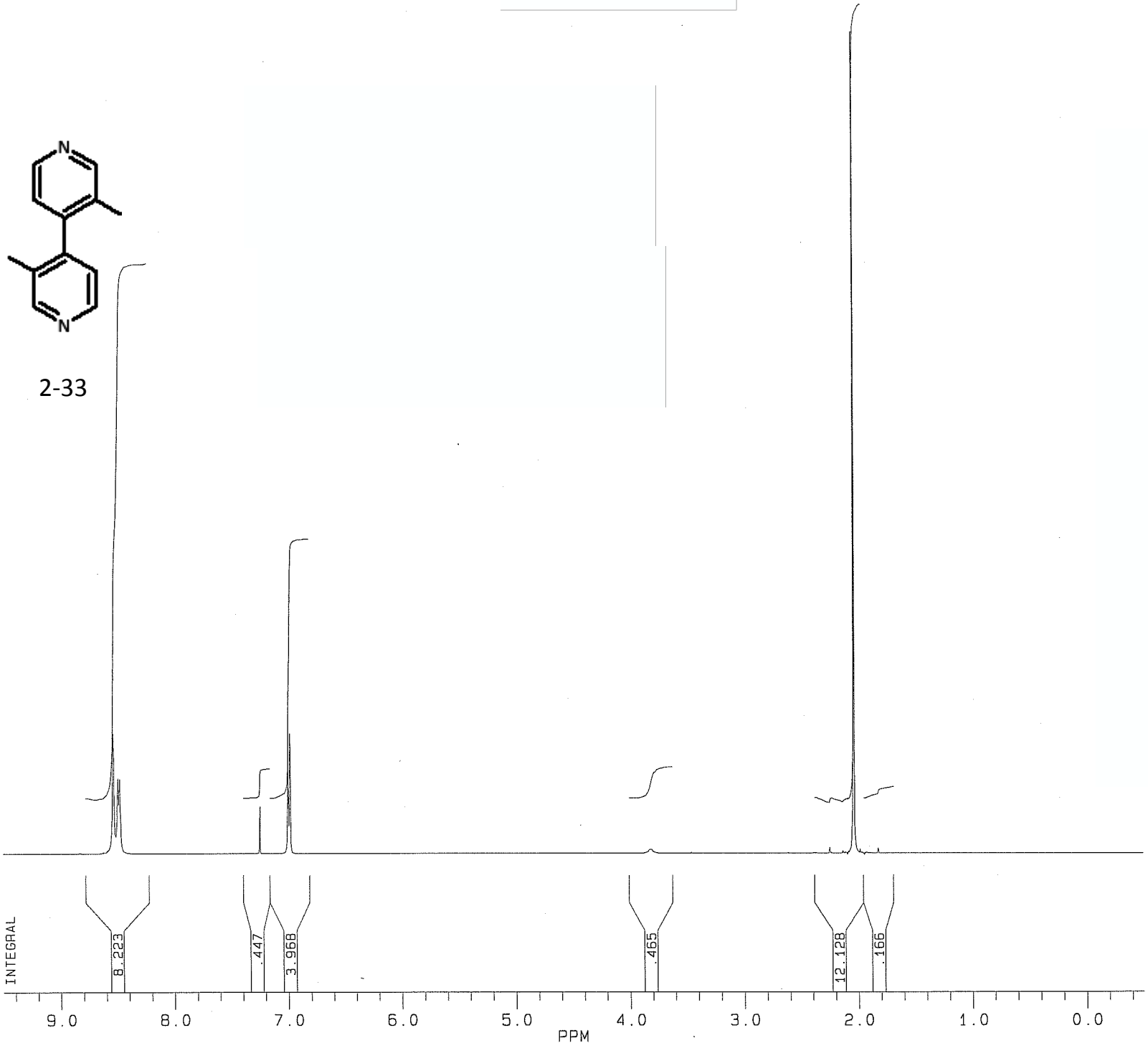
N
N
2-33
INTEGRAL
8.223
.447
3.968
.465
12.128
.166
9.0
8.0
7.0
6.0
5.0
4.0
3.0
2.0
1.0
0.0
PPM

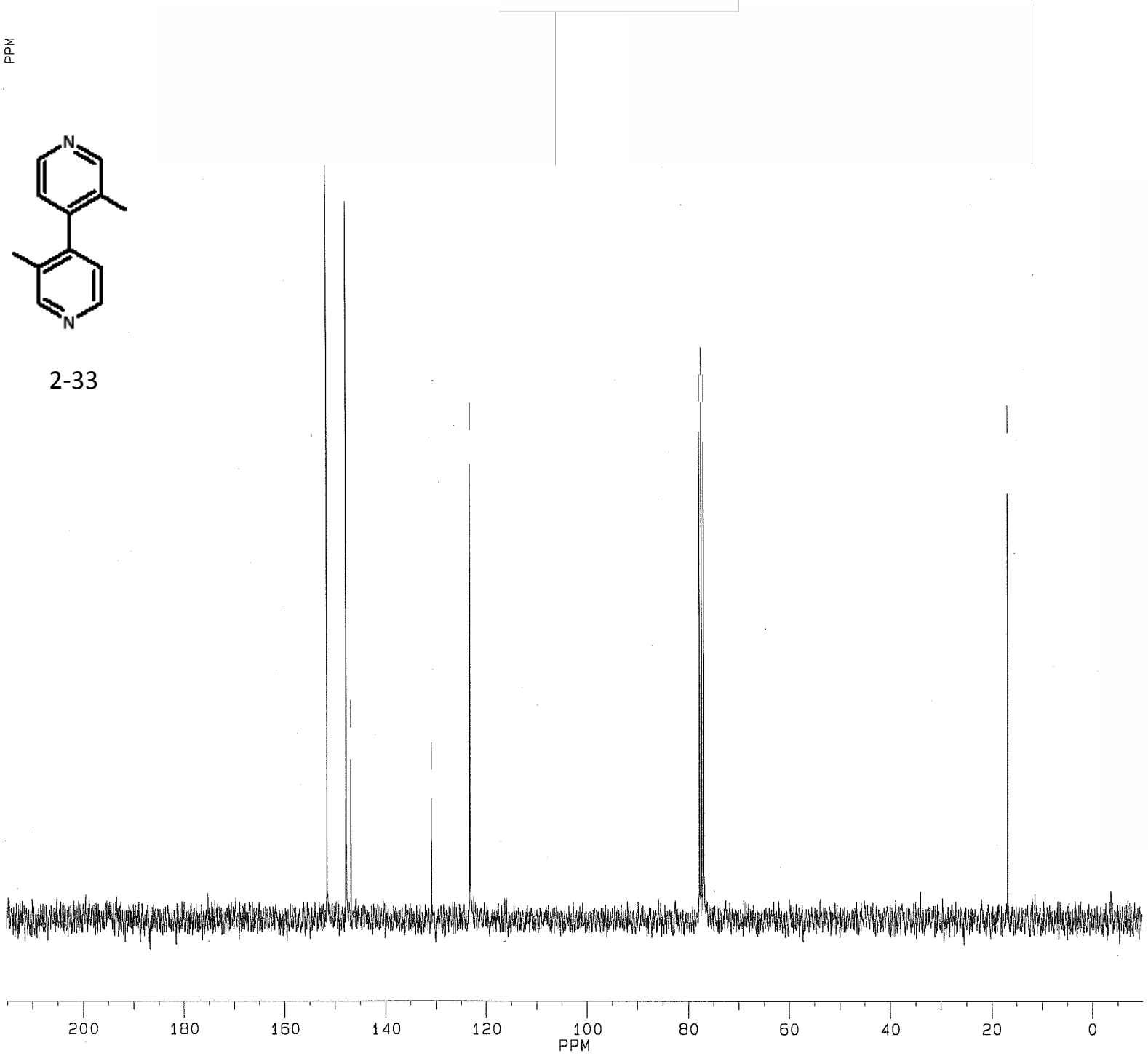
PPM
N
N
2-33
200
180
160
140
120
100
80
60
40
20
0
PPM

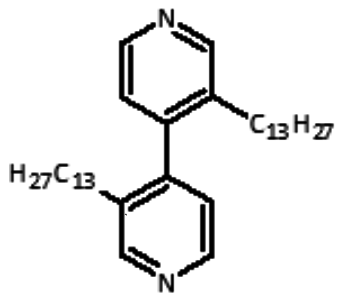
N
$C_{13}H_{27}$
$H_{27}C_{13}$
N

2-34

INTEGRAL
5.680
.319
2.871
6.110
.795
72.301
5.336
9.0
8.0
7.0
6.0
5.0
4.0
3.0
2.0
1.0
0.0
PPM

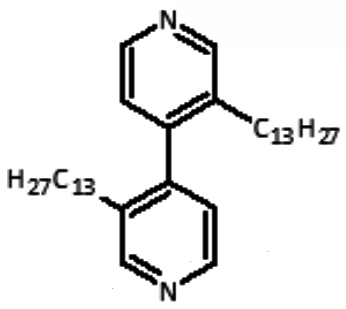

2-34

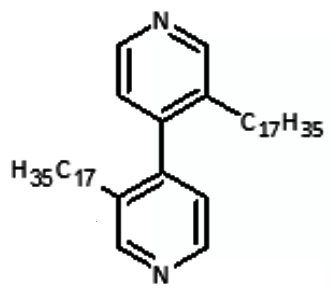
N
$C_{17}H_{35}$
$H_{35}C_{17}$
N

2-35

INTEGRAL
3.085
.498
1.533
3.433
53.642
4.391
9.0
8.0
7.0
6.0
5.0
4.0
3.0
2.0
1.0
0.0
PPM

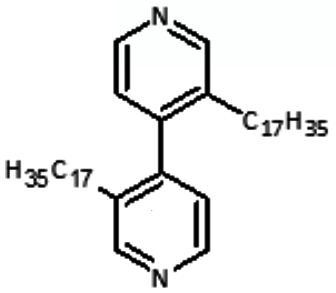

2-35

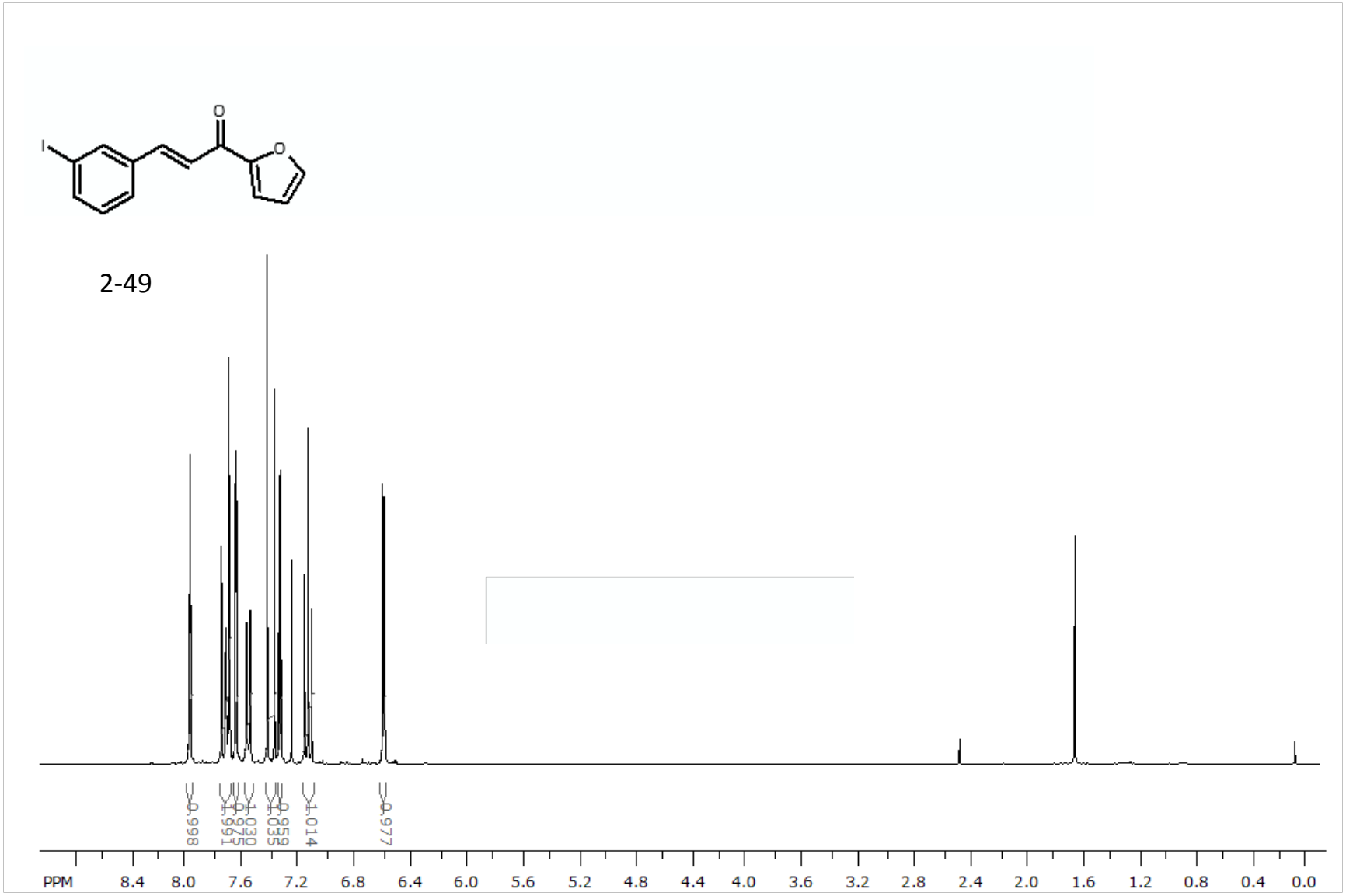
O
I
O
2-49
0.998
1.991
1.030
1.035
0.959
1.014
0.977
PPM
8.4
8.0
7.6
7.2
6.8
6.4
6.0
5.6
5.2
4.8
4.4
4.0
3.6
3.2
2.8
2.4
2.0
1.6
1.2
0.8
0.4
0.0

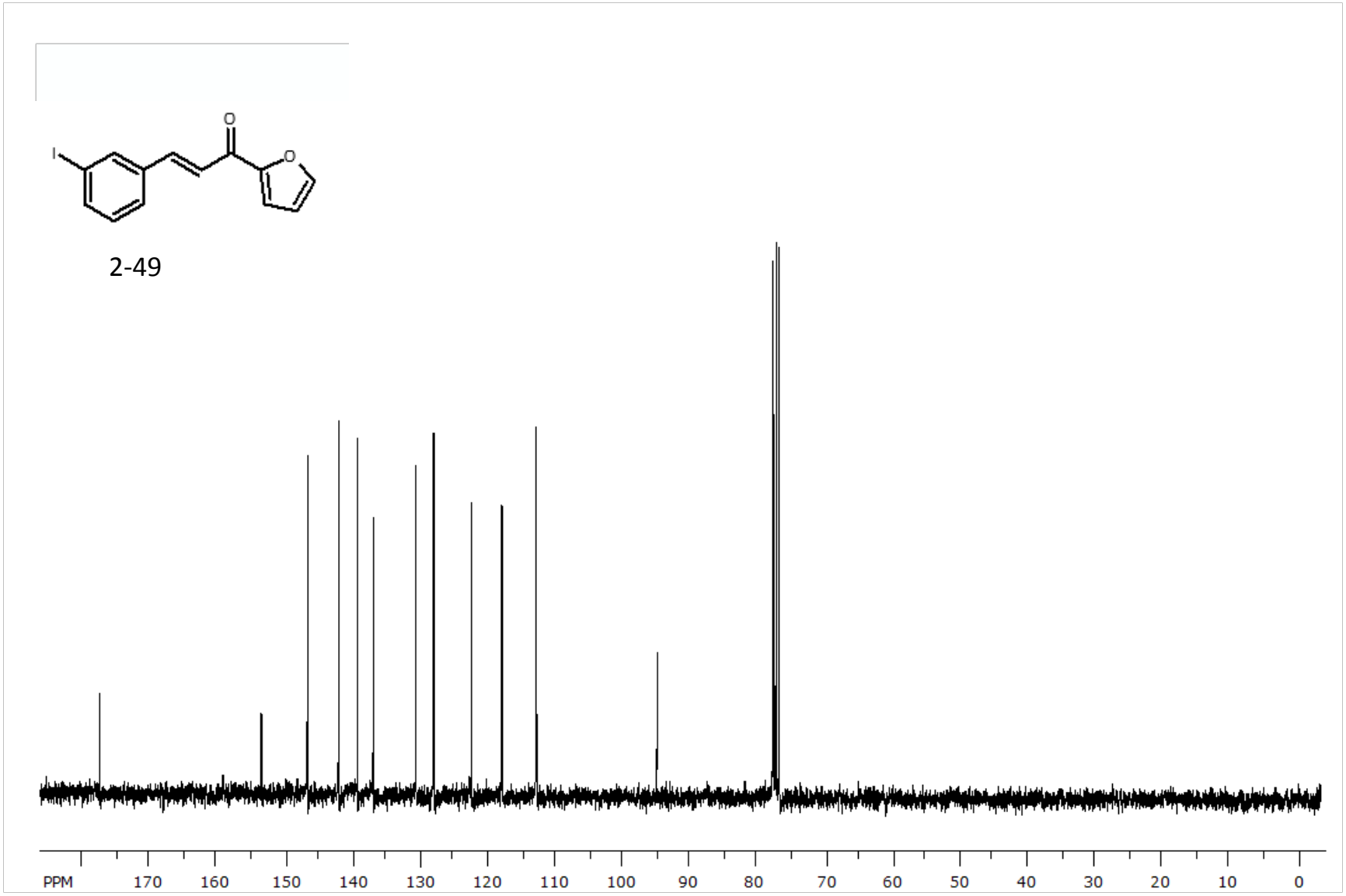
O
I
O
2-49
PPM
170
160
150
140
130
120
110
100
90
80
70
60
50
40
30
20
10
0

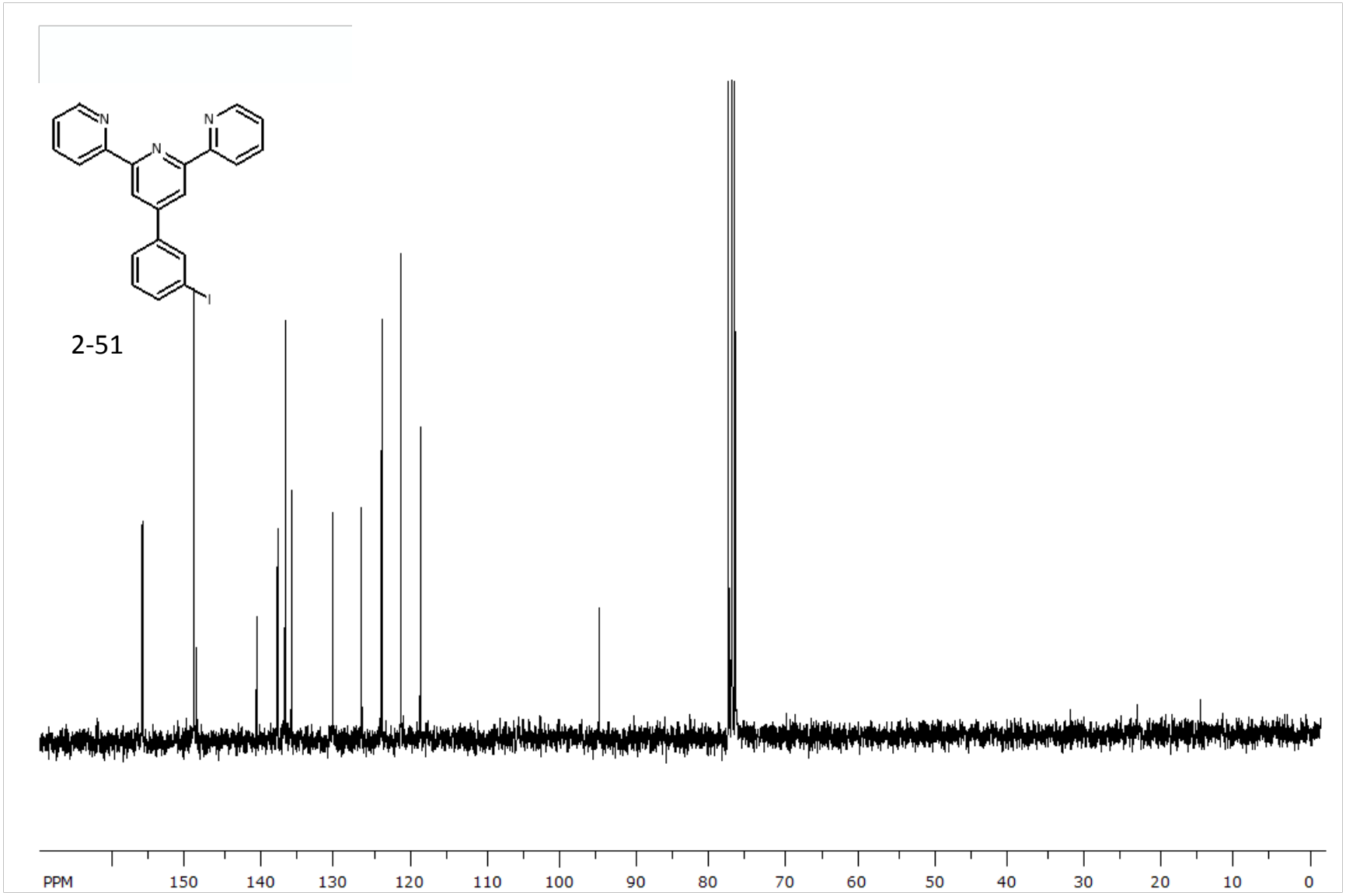
N
N
N
I
2-51
PPM
150
140
130
120
110
100
90
80
70
60
50
40
30
20
10
0

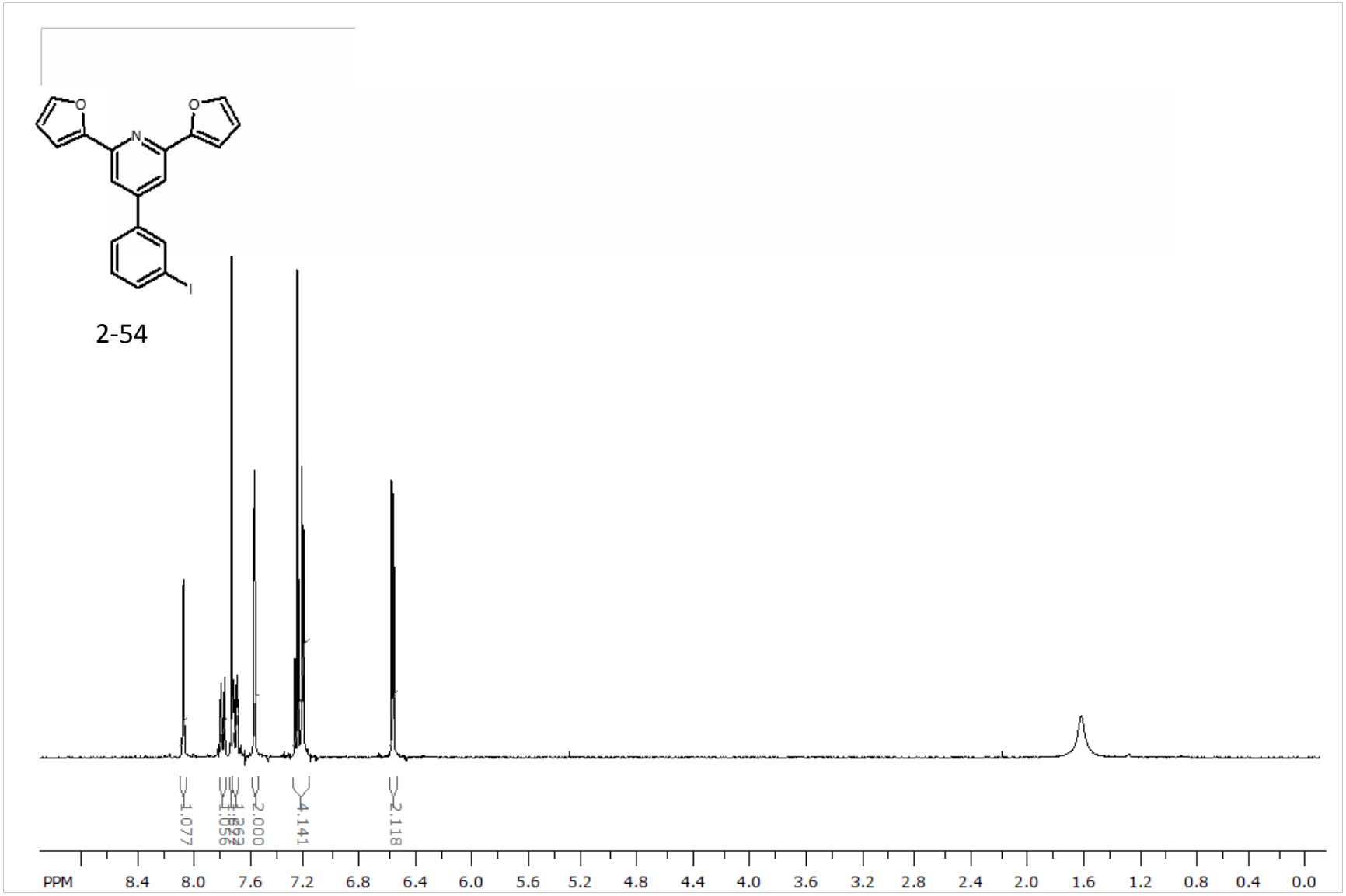
O
O
N
I
2-54
1.077
2.000
4.141
2.118
PPM
8.4
8.0
7.6
7.2
6.8
6.4
6.0
5.6
5.2
4.8
4.4
4.0
3.6
3.2
2.8
2.4
2.0
1.6
1.2
0.8
0.4
0.0

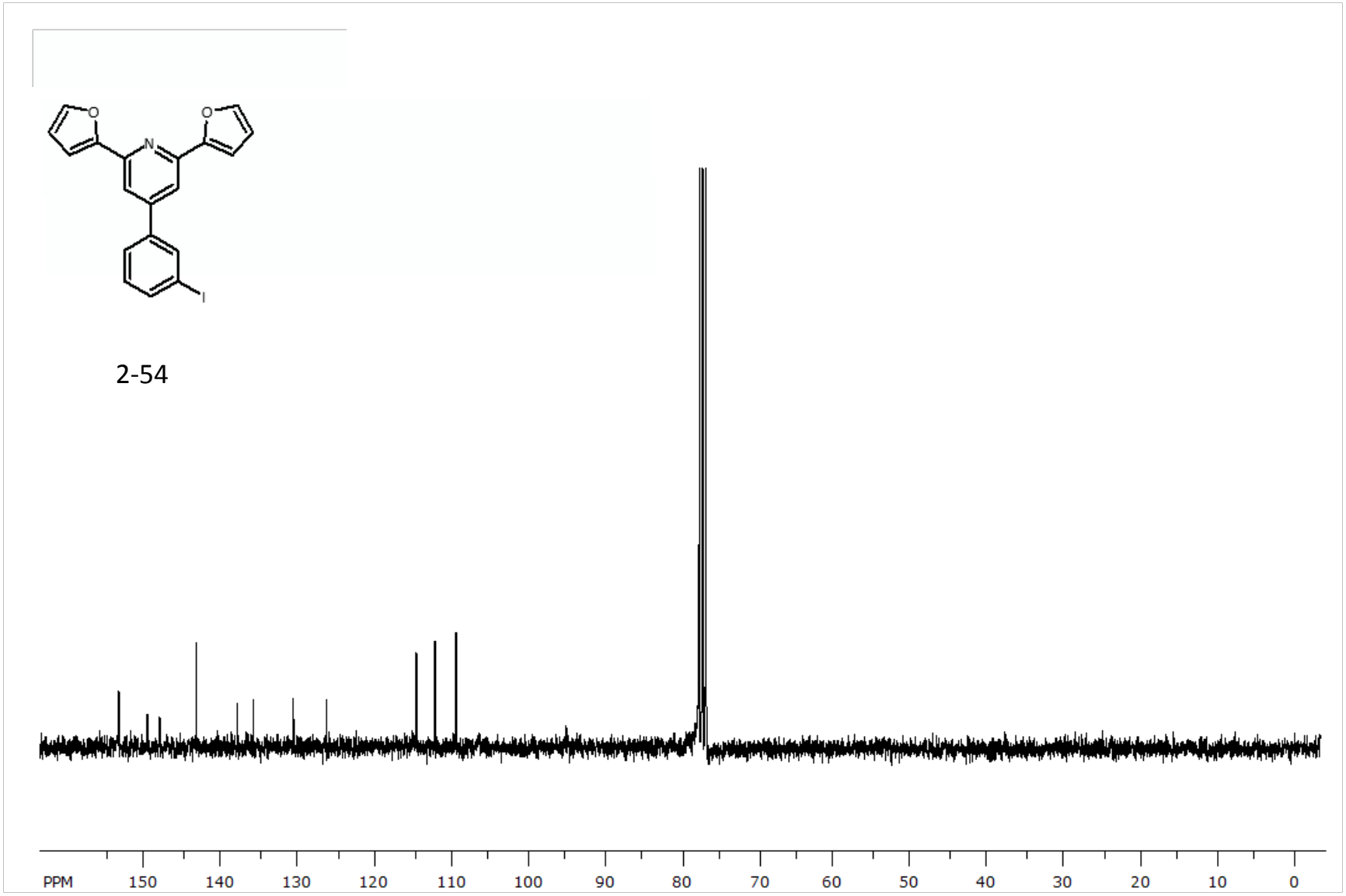
O
N
O
I
2-54
PPM
150
140
130
120
110
100
90
80
70
60
50
40
30
20
10
0

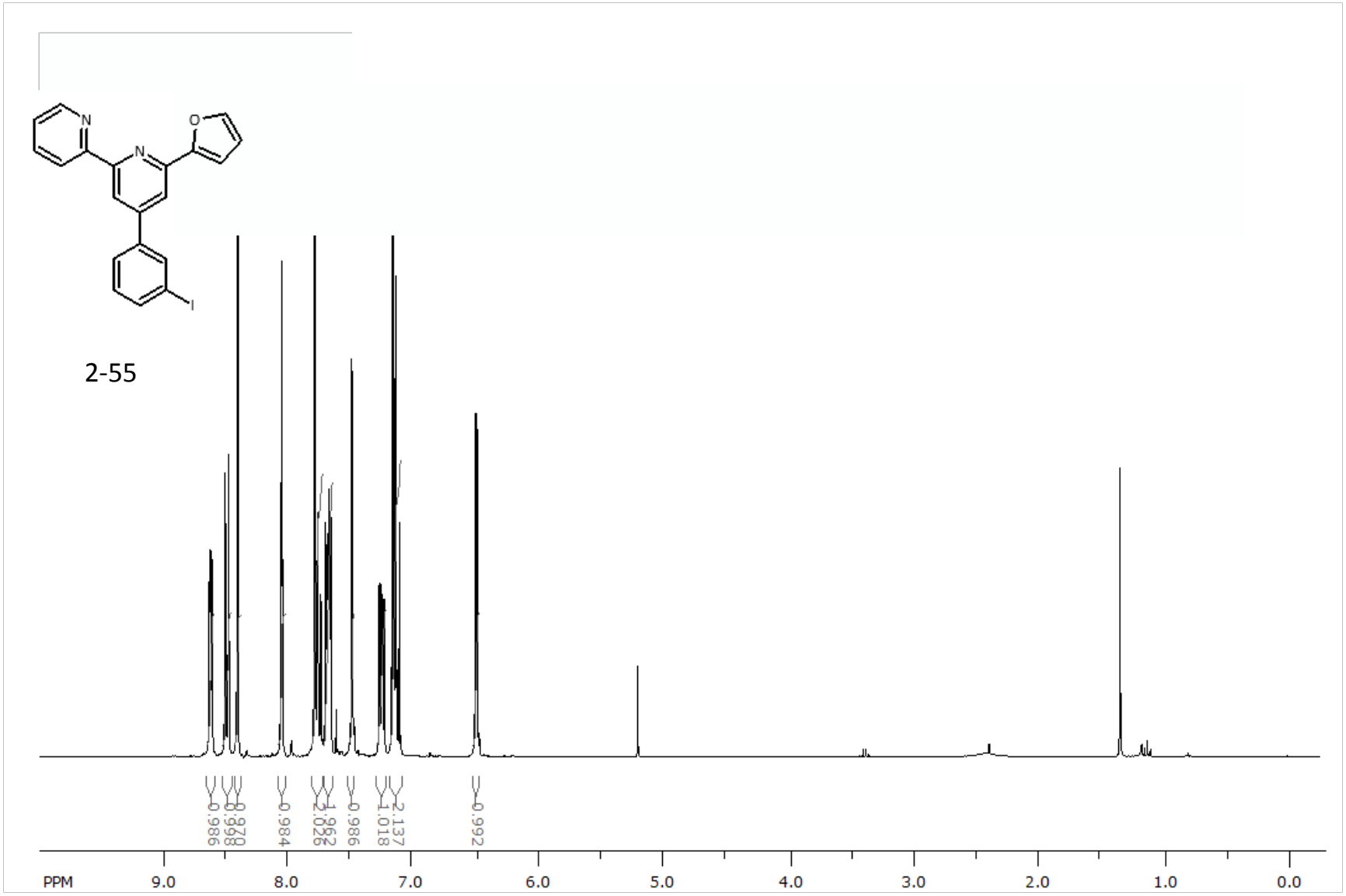
N
N
O
I
2-55
0.986
0.998
0.970
0.984
2.026
1.962
0.986
1.018
2.137
0.992
PPM
9.0
8.0
7.0
6.0
5.0
4.0
3.0
2.0
1.0
0.0

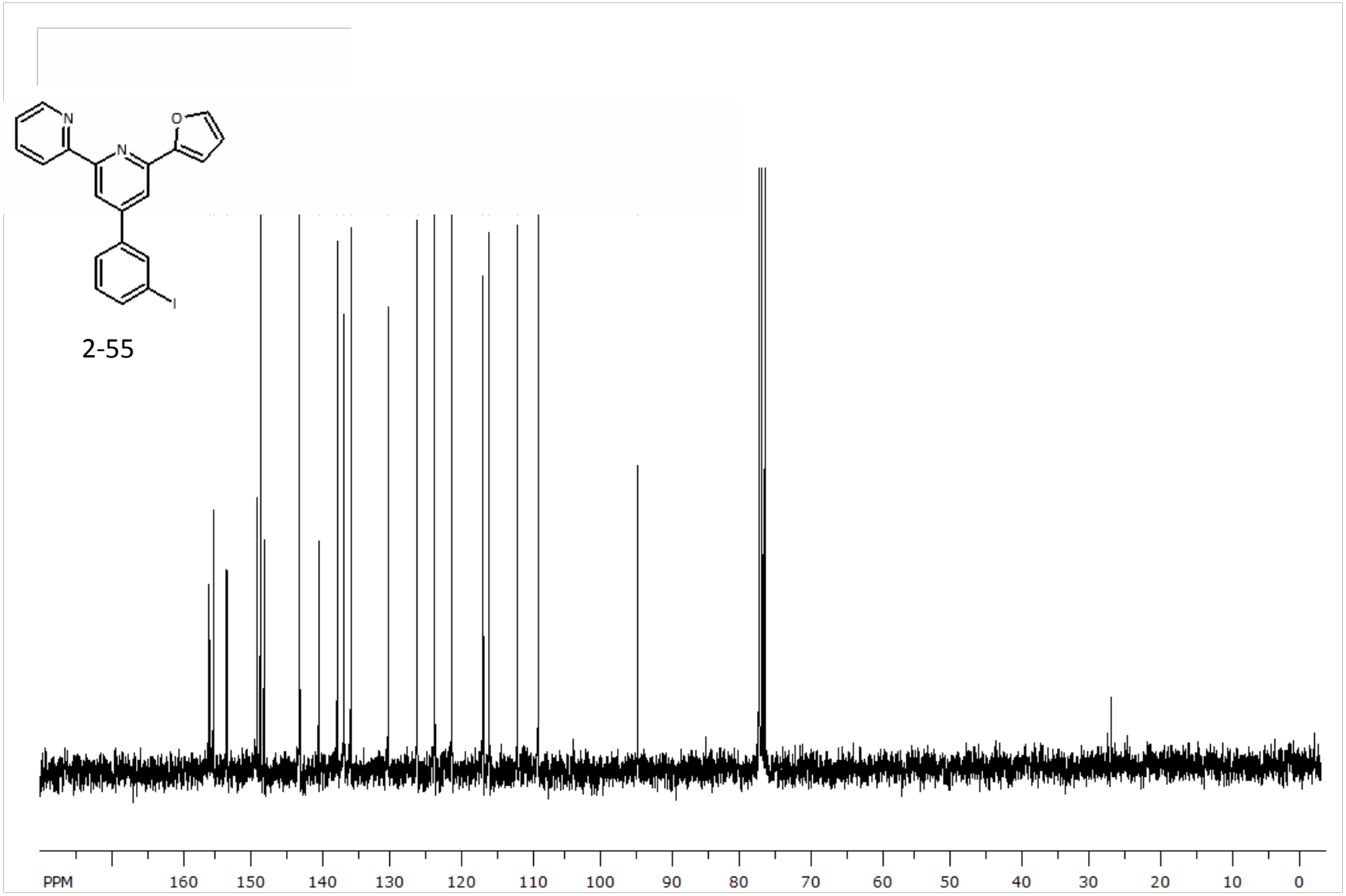
N
N
O
I
2-55
PPM
160
150
140
130
120
110
100
90
80
70
60
50
40
30
20
10
0

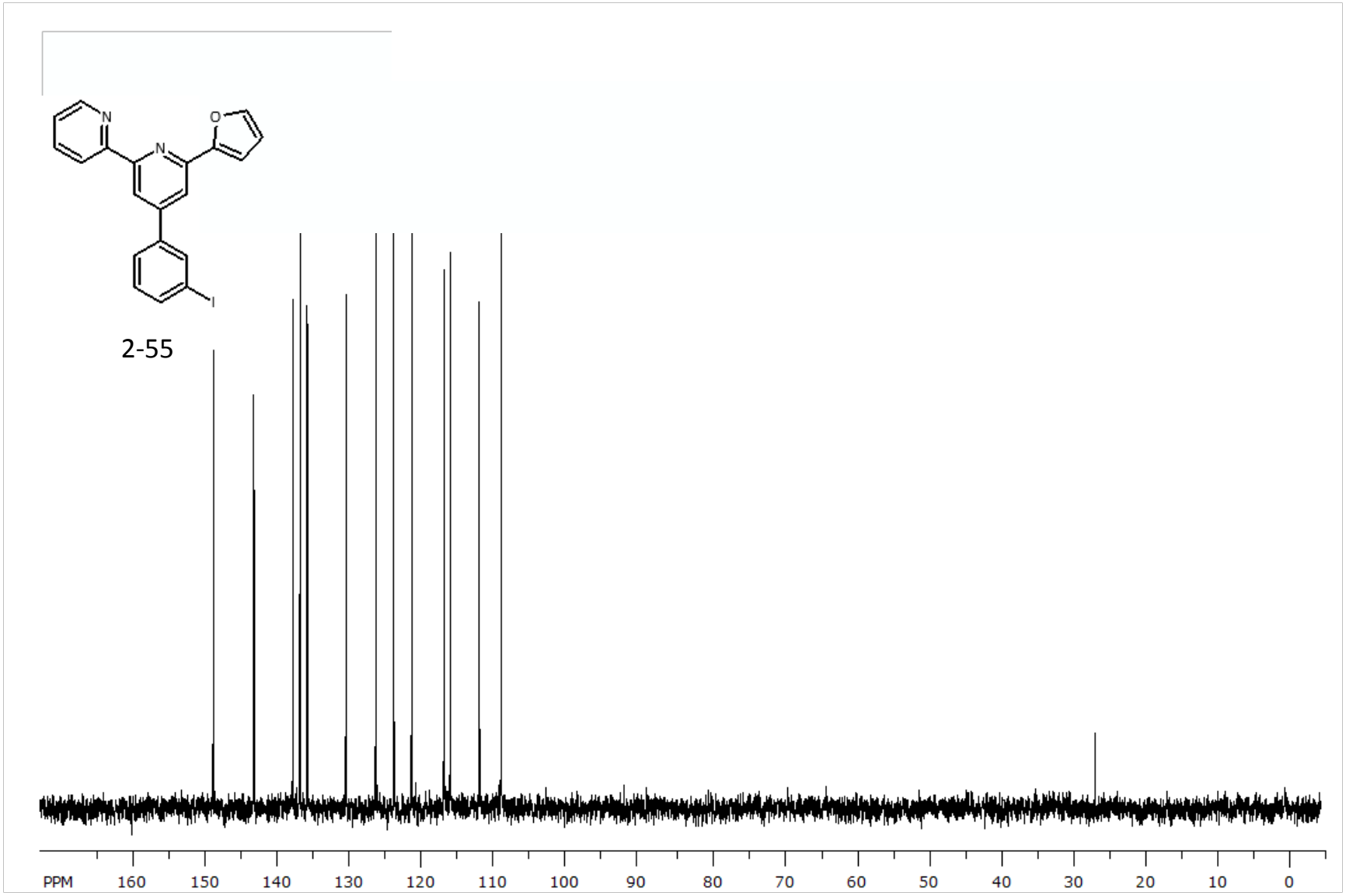
N
N
O
I
2-55
PPM
160
150
140
130
120
110
100
90
80
70
60
50
40
30
20
10
0

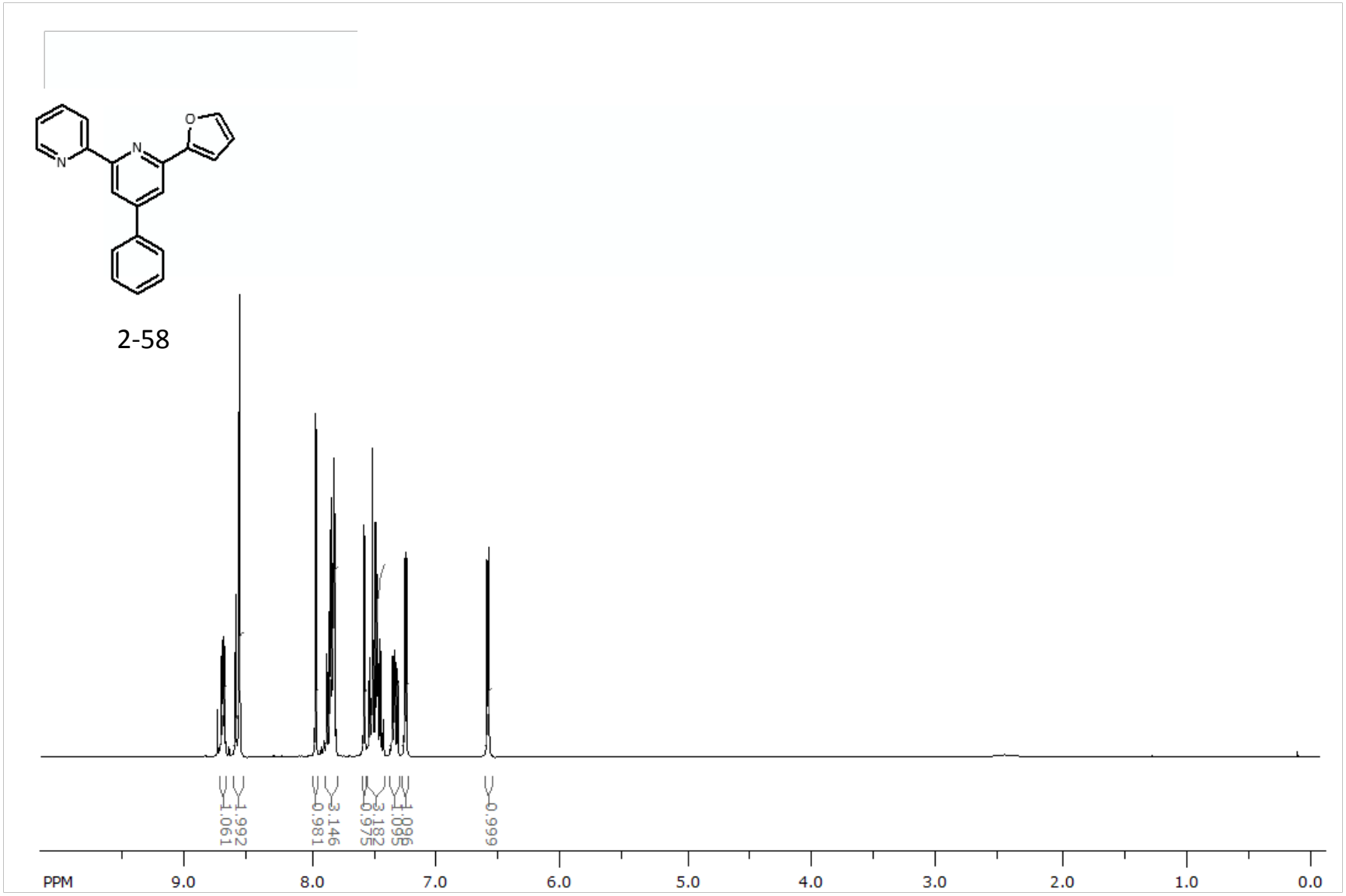
2-58
1.061
1.992
0.981
3.146
0.975
3.182
1.095
1.096
0.999
PPM
9.0
8.0
7.0
6.0
5.0
4.0
3.0
2.0
1.0
0.0

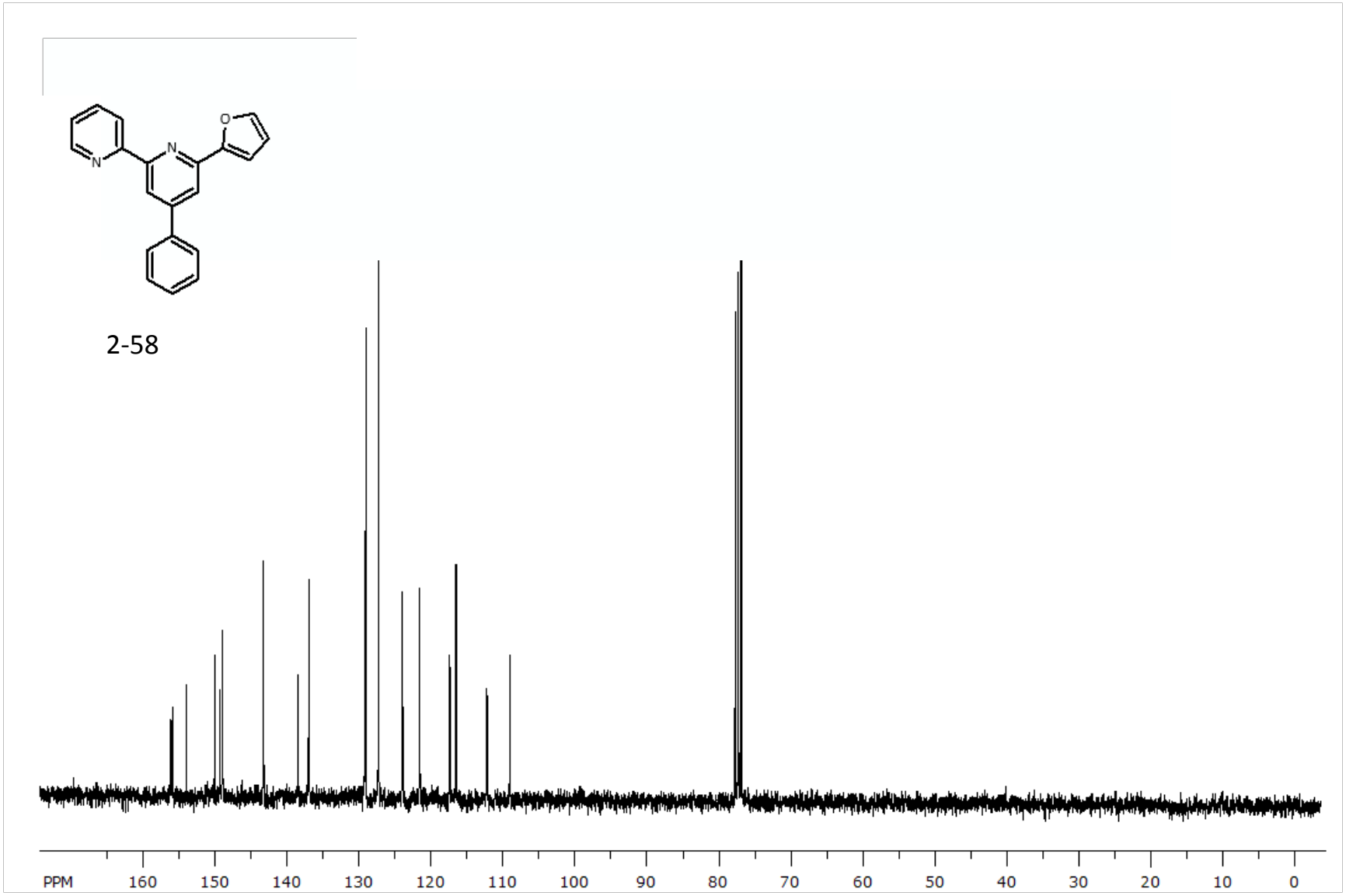
N
N
O
2-58
PPM
160
150
140
130
120
110
100
90
80
70
60
50
40
30
20
10
0

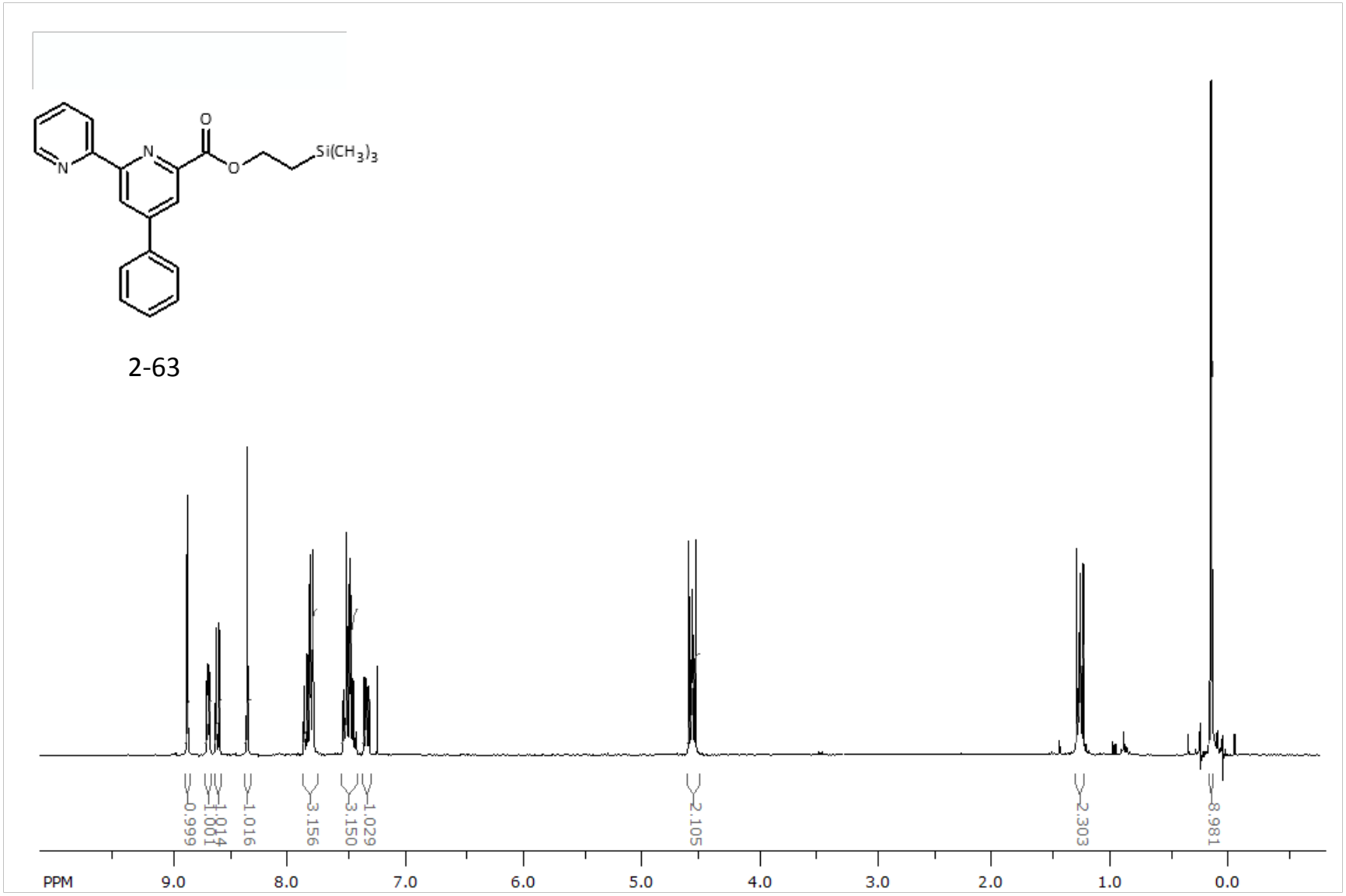
O
N
N
O
Si(CH3)3
2-63
0.999
1.001
1.014
1.016
3.156
3.150
1.029
2.105
2.303
8.981
PPM
9.0
8.0
7.0
6.0
5.0
4.0
3.0
2.0
1.0
0.0

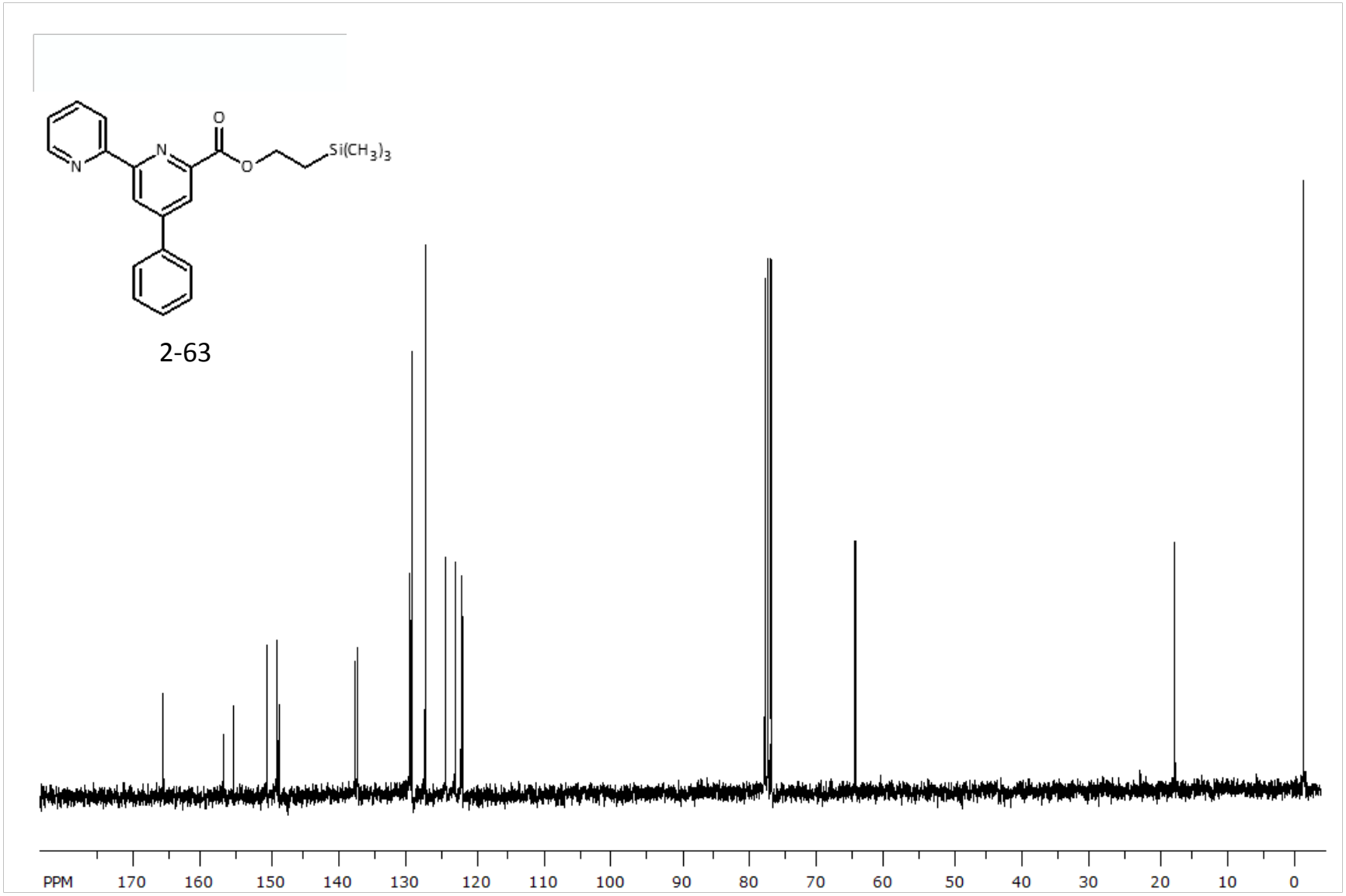
O
N
N
O
Si(CH3)3
PPM
170
160
150
140
130
120
110
100
90
80
70
60
50
40
30
20
10
0

2-63

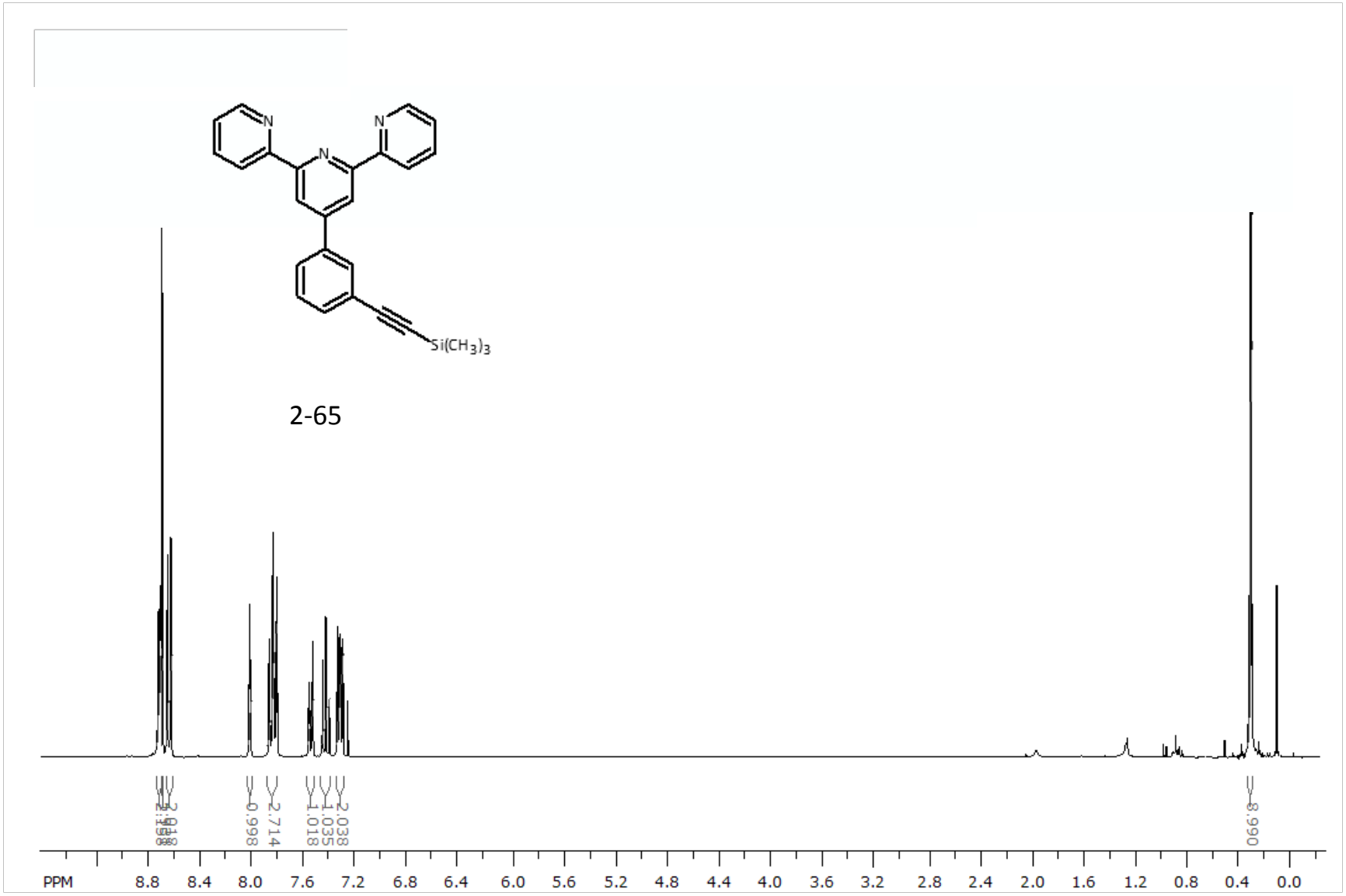
N
N
N
Si(CH3)3
2-65
2.013
0.998
2.714
1.018
1.035
2.038
8.990
PPM
8.8
8.4
8.0
7.6
7.2
6.8
6.4
6.0
5.6
5.2
4.8
4.4
4.0
3.6
3.2
2.8
2.4
2.0
1.6
1.2
0.8
0.4
0.0

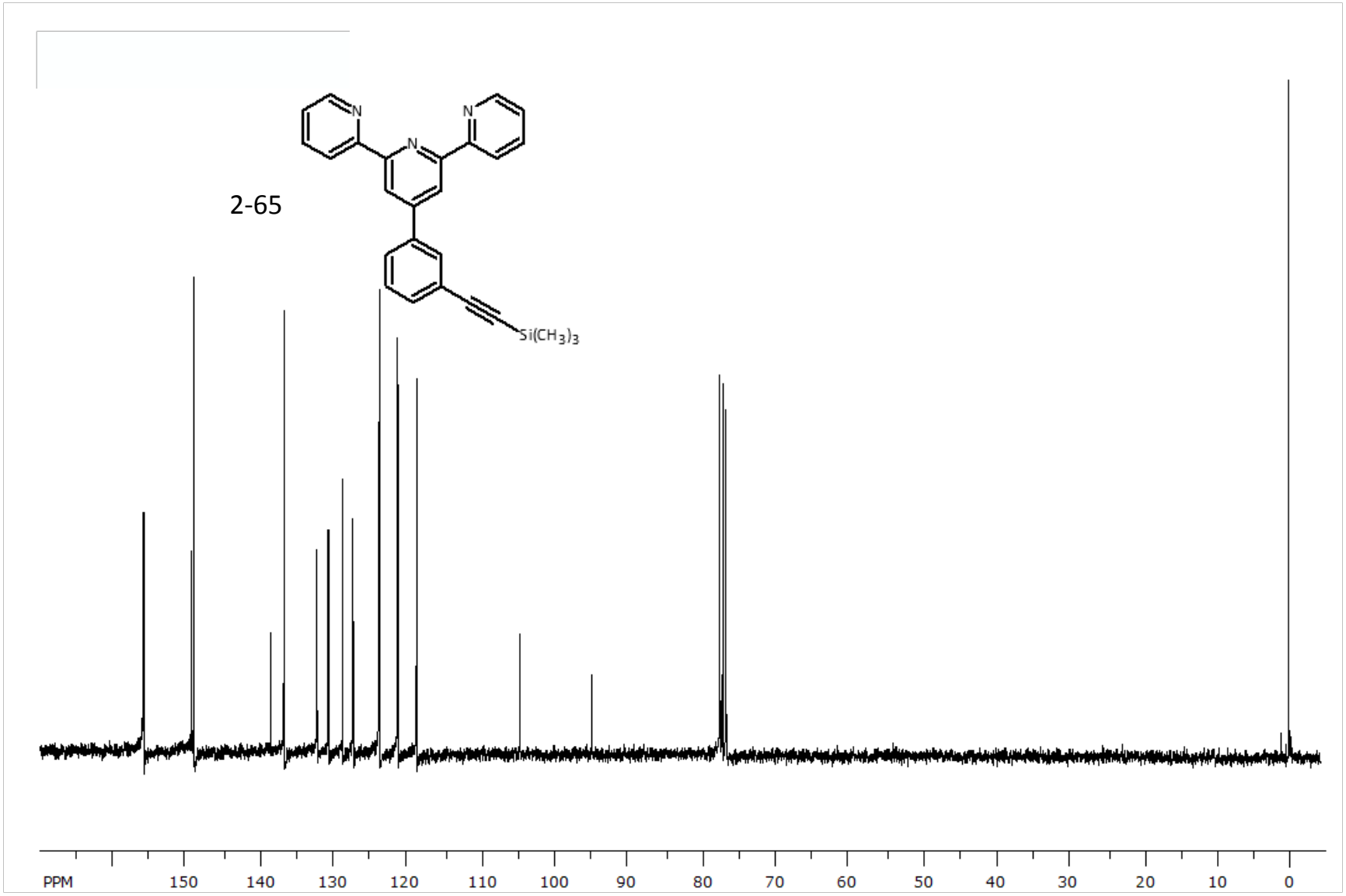
2-65
N
N
N
Si(CH3)3
PPM
150
140
130
120
110
100
90
80
70
60
50
40
30
20
10
0

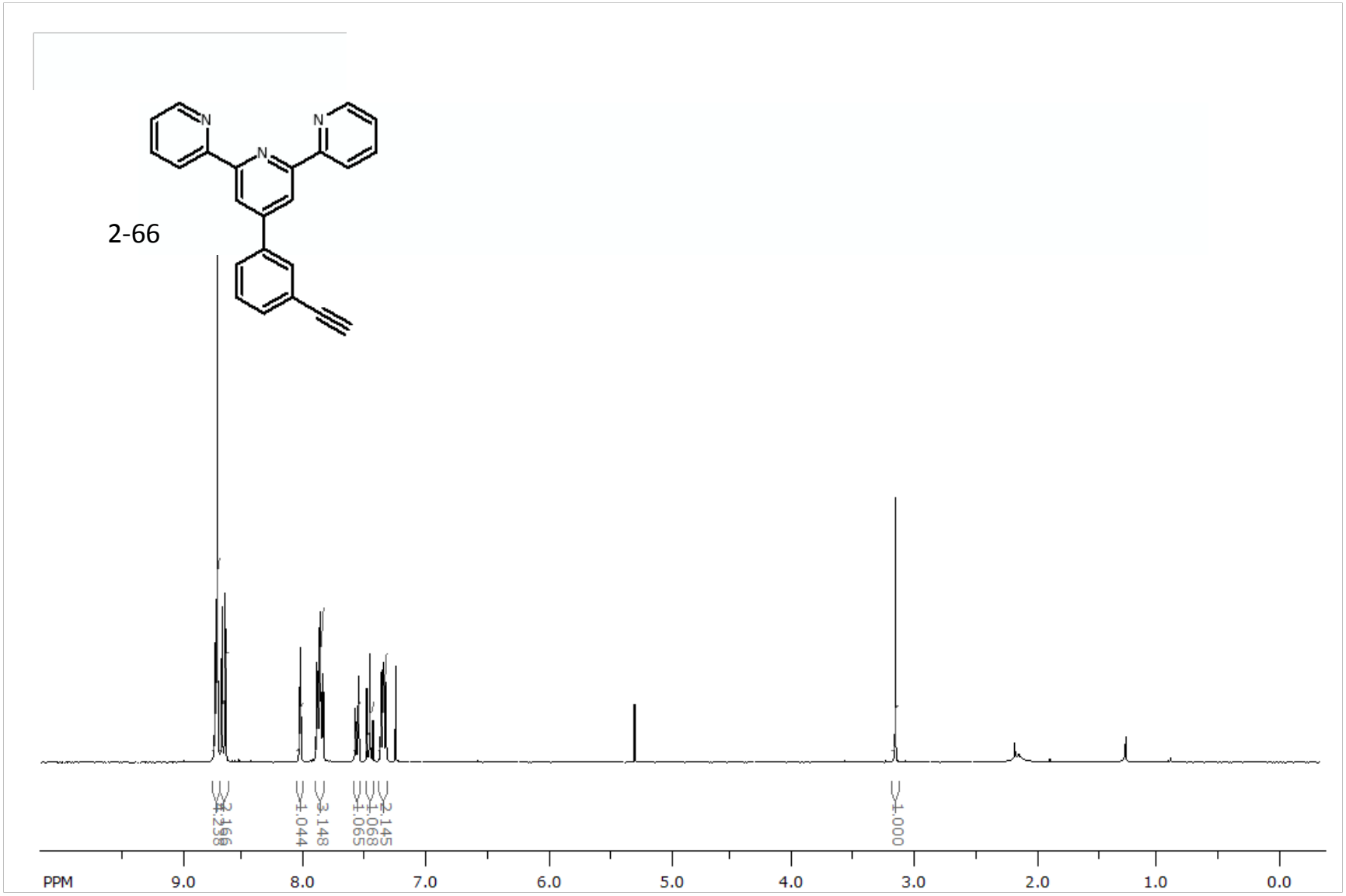
2-66
N
N
N
4.238
2.166
1.044
3.148
1.065
1.068
2.145
1.000
PPM
9.0
8.0
7.0
6.0
5.0
4.0
3.0
2.0
1.0
0.0

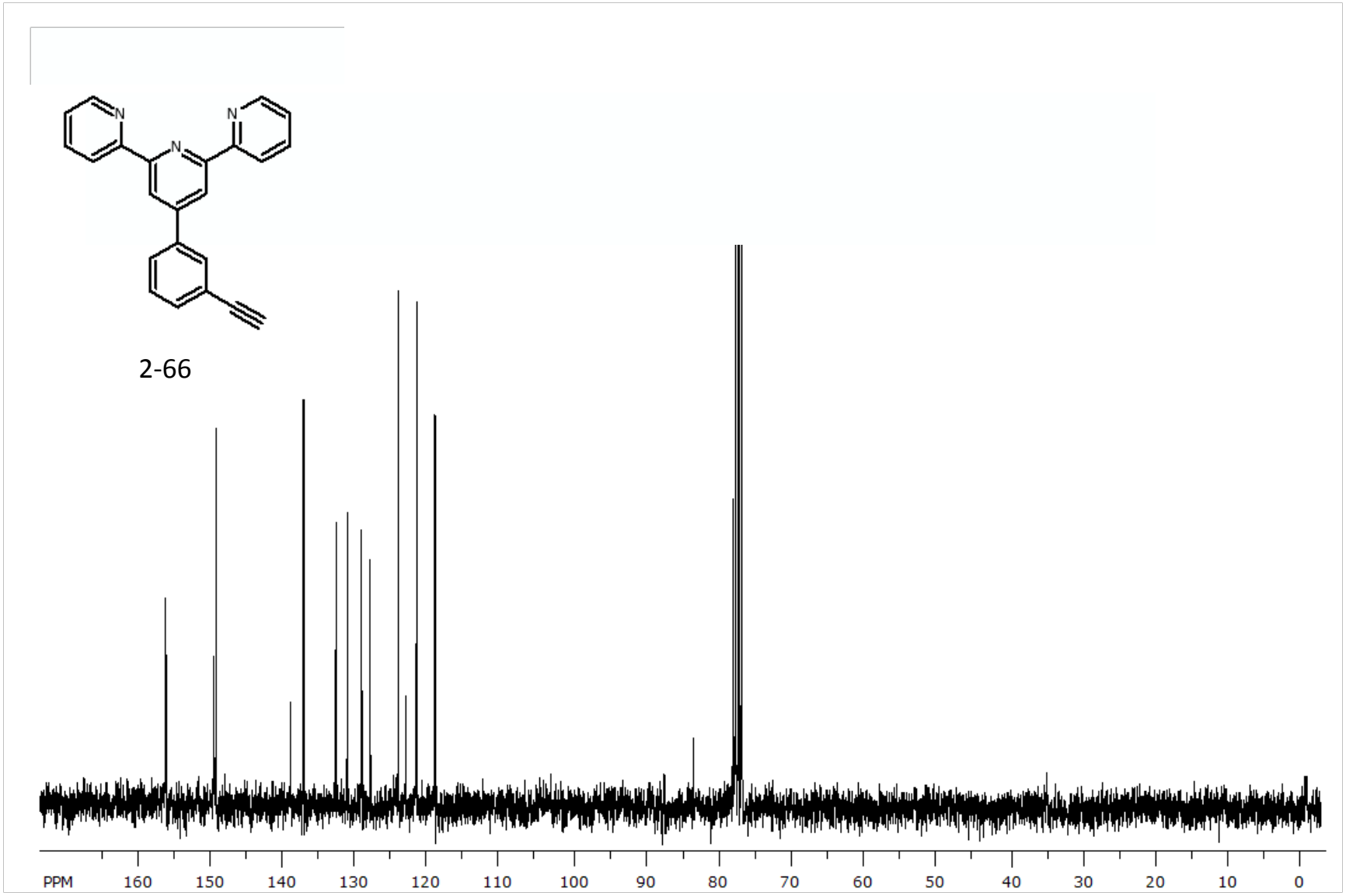
N
N
N
2-66
PPM
160
150
140
130
120
110
100
90
80
70
60
50
40
30
20
10
0

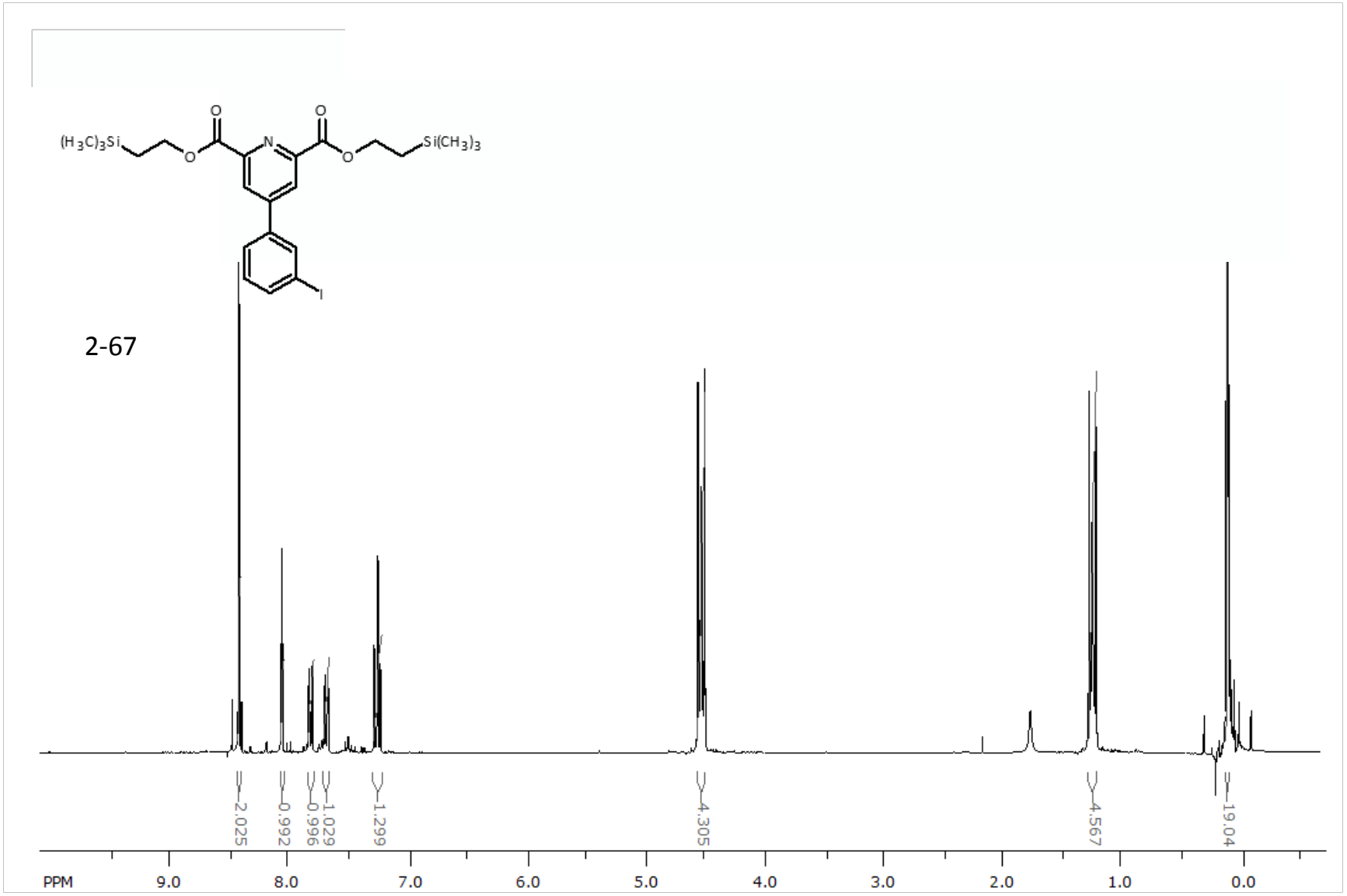
(H3C)3Si
O
O
N
O
O
Si(CH3)3
I
2-67
2.025
0.992
0.996
1.029
1.299
4.305
4.567
19.04
PPM
9.0
8.0
7.0
6.0
5.0
4.0
3.0
2.0
1.0
0.0

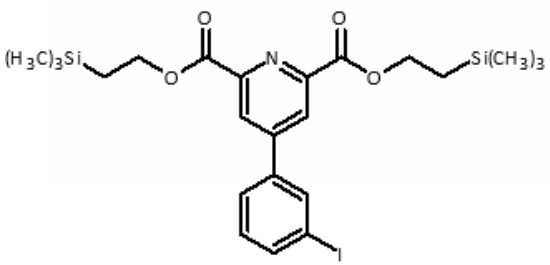
(H3C)3Si
O
O
N
O
O
Si(CH3)3
I

2-67

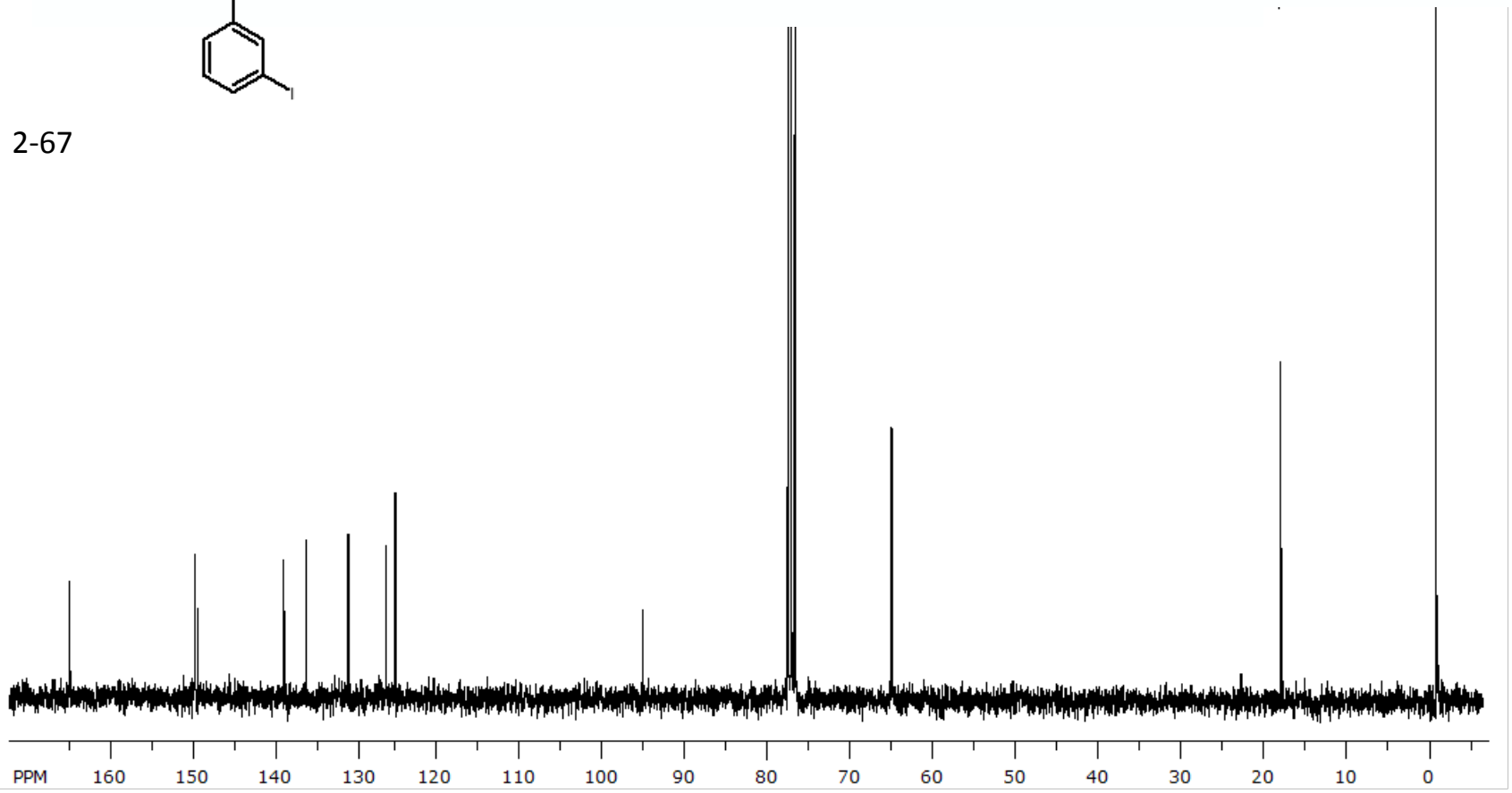
PPM
160
150
140
130
120
110
100
90
80
70
60
50
40
30
20
10
0

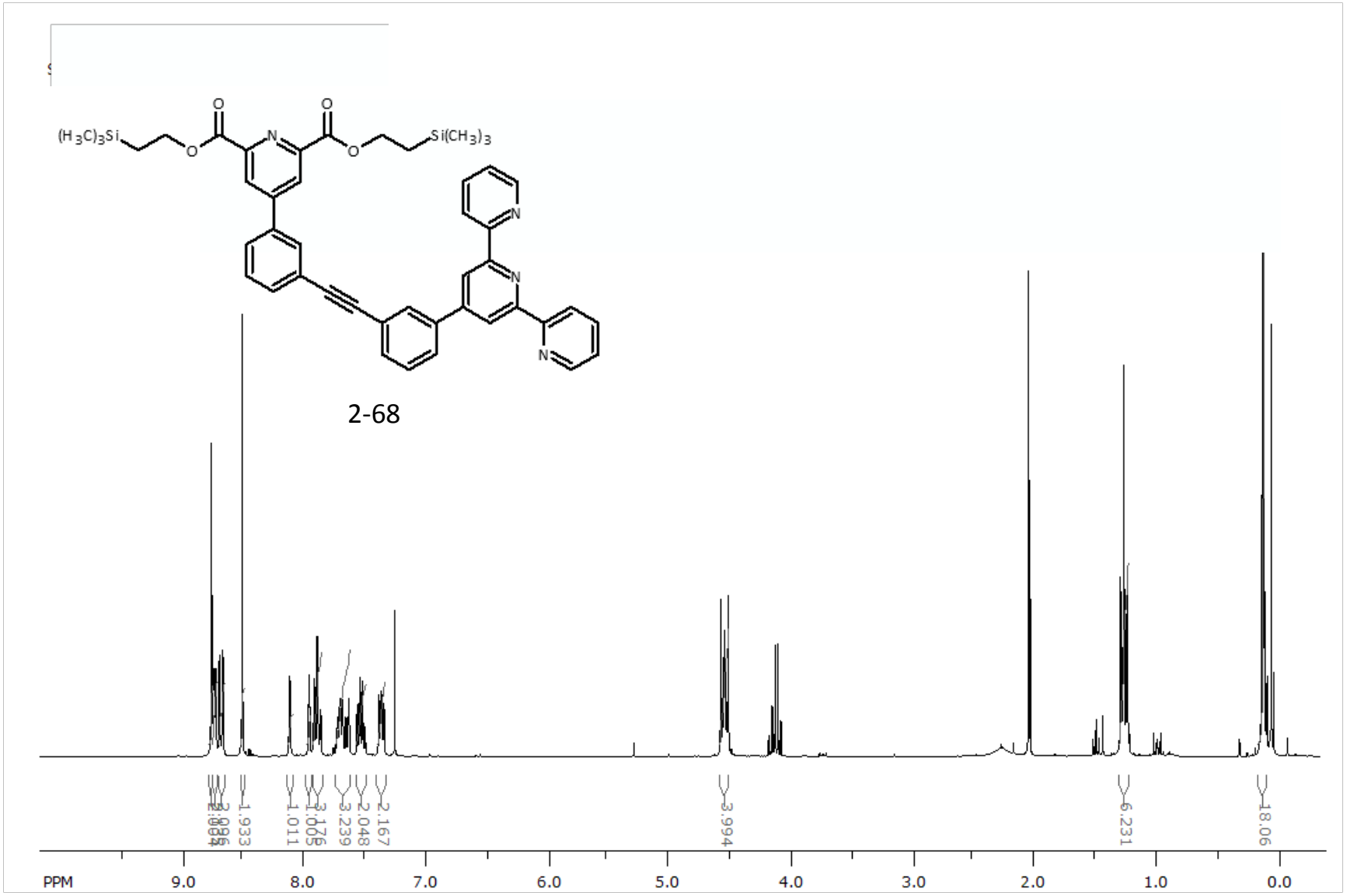
(H3C)3Si
O
O
N
O
O
Si(CH3)3
N
N
N
1.933
1.011
3.239
2.048
2.167
3.994
6.231
18.06
PPM
9.0
8.0
7.0
6.0
5.0
4.0
3.0
2.0
1.0
0.0

2-68

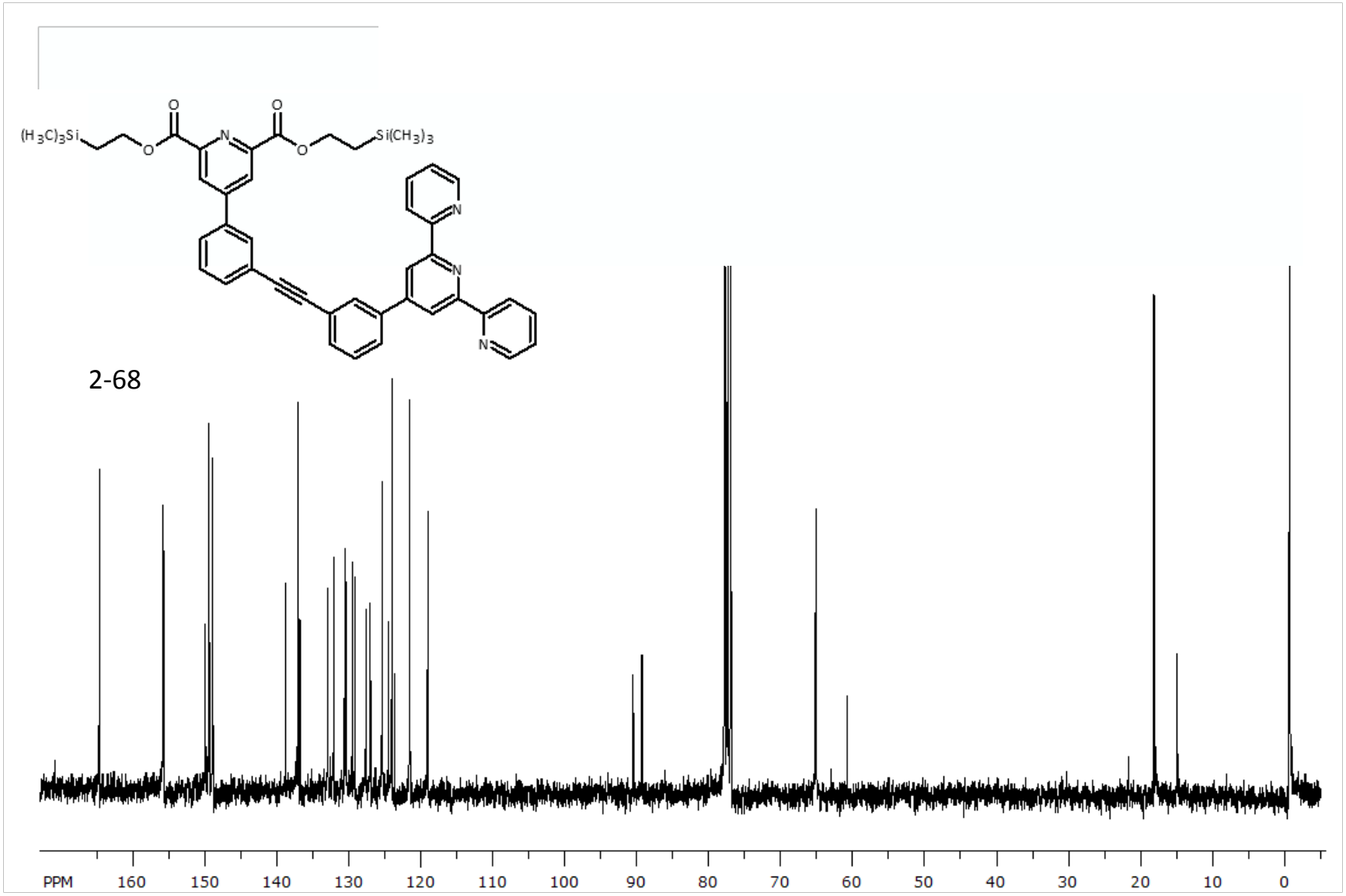
2-68
PPM
160
150
140
130
120
110
100
90
80
70
60
50
40
30
20
10
0

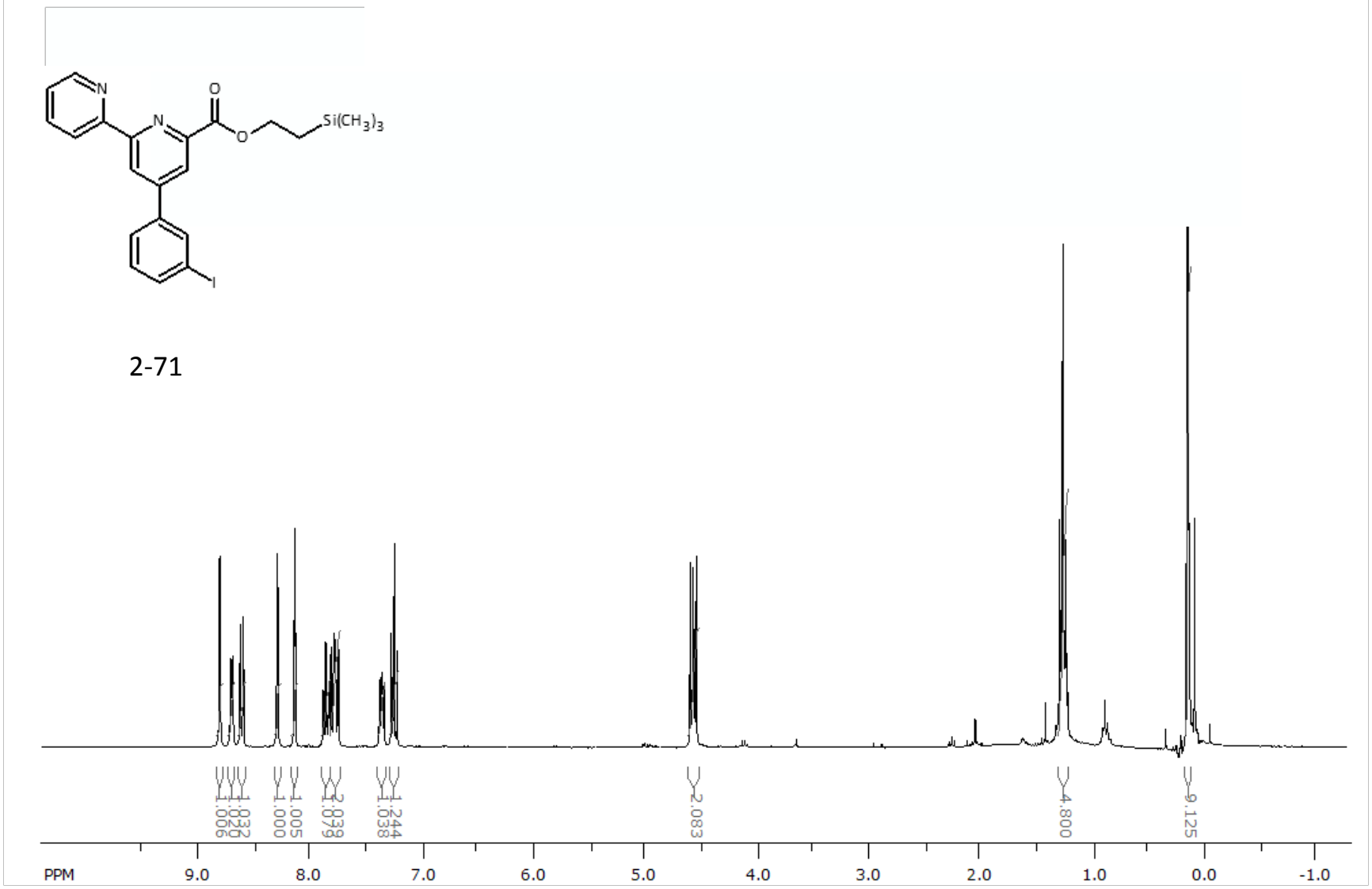
N
O
N
O
Si(CH3)3
I
2-71
1.006
1.032
1.000
1.005
2.039
1.038
1.244
2.083
4.800
9.125
PPM
9.0
8.0
7.0
6.0
5.0
4.0
3.0
2.0
1.0
0.0
-1.0

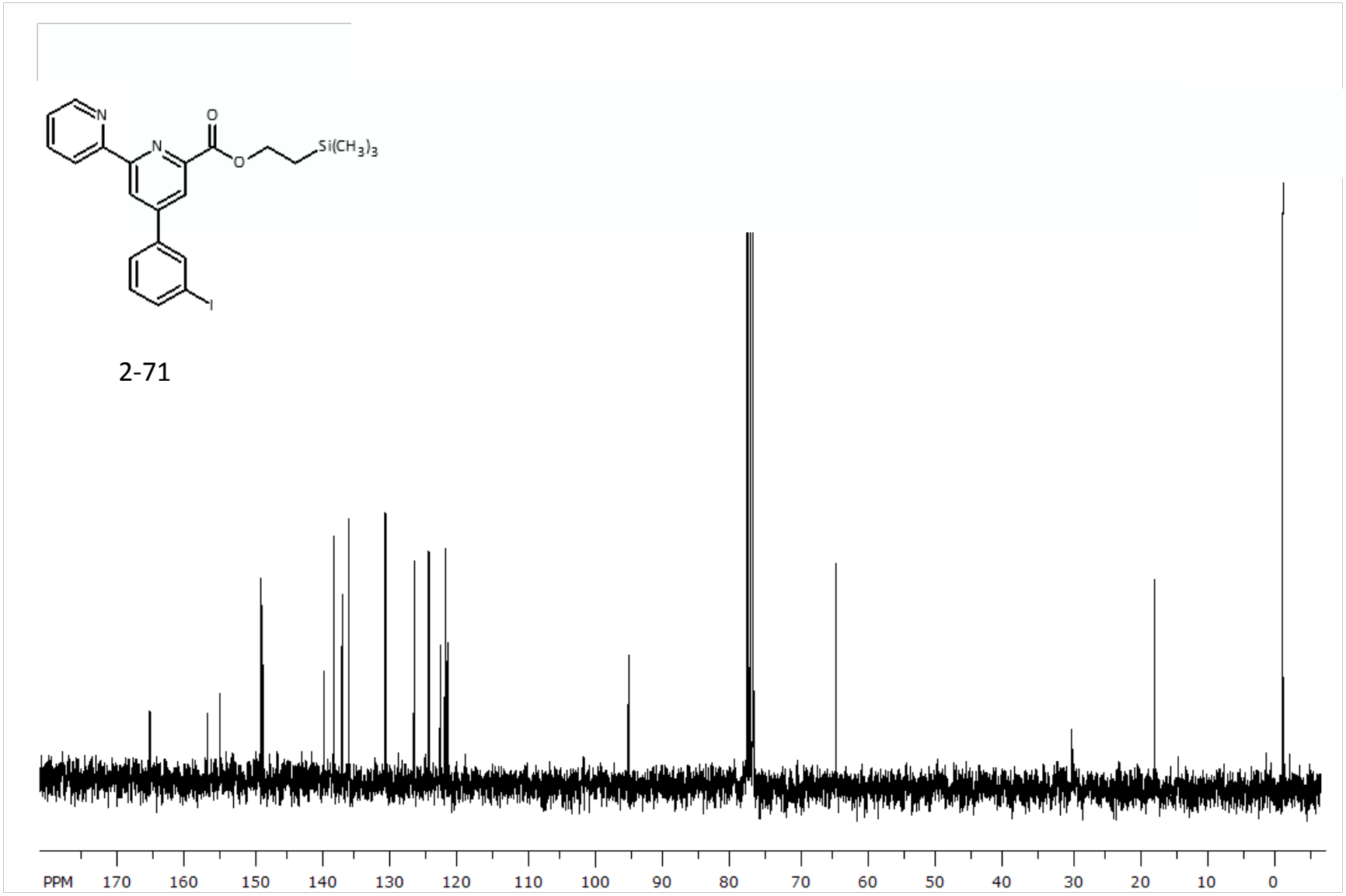
N
O
N
O
Si(CH3)3
I
PPM
170
160
150
140
130
120
110
100
90
80
70
60
50
40
30
20
10
0

2-71

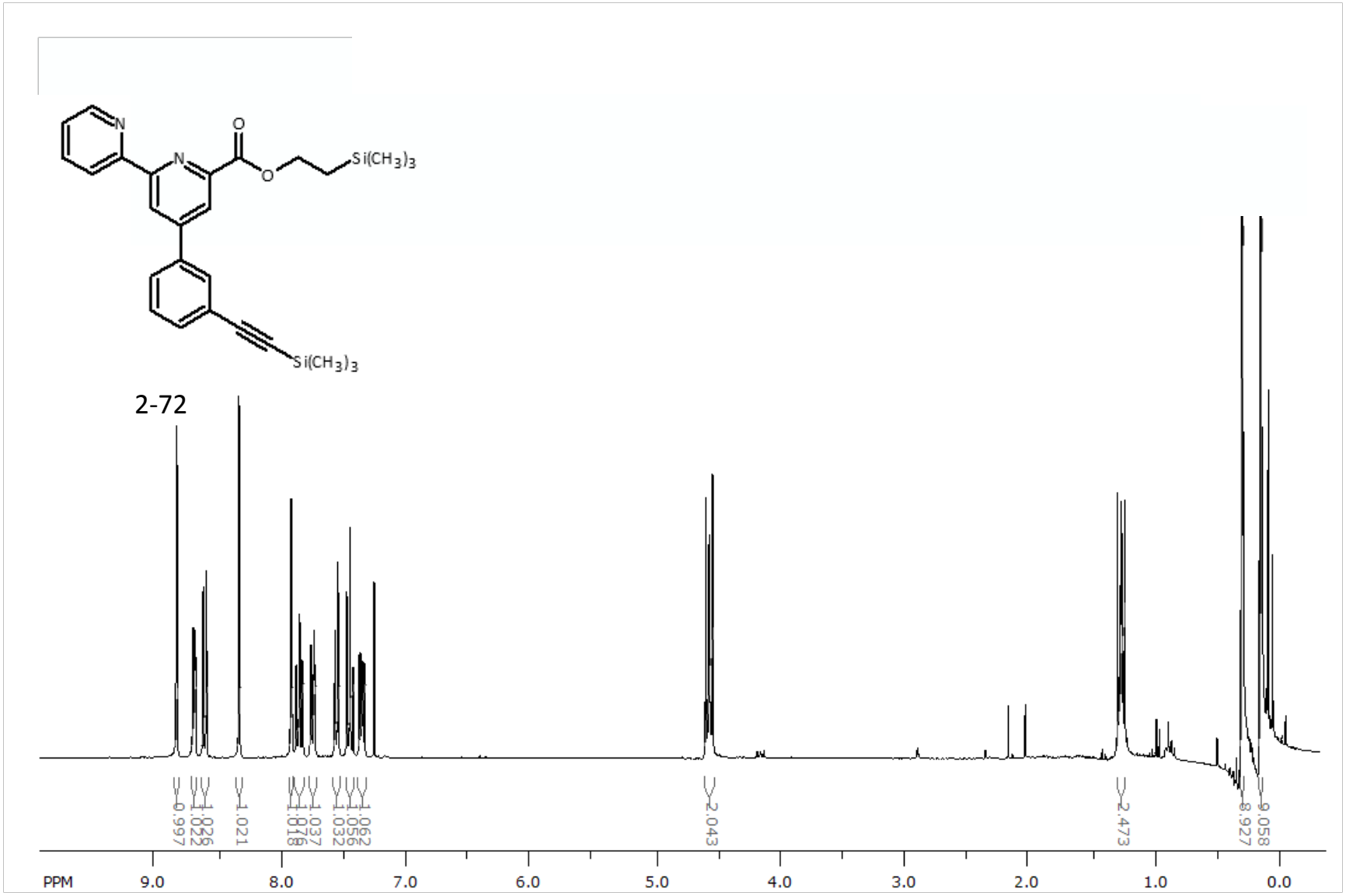
N
O
N
O
Si(CH3)3
Si(CH3)3
2-72
0.997
1.022
1.026
1.021
1.037
1.032
1.056
1.062
2.043
2.473
8.927
9.058
PPM
9.0
8.0
7.0
6.0
5.0
4.0
3.0
2.0
1.0
0.0

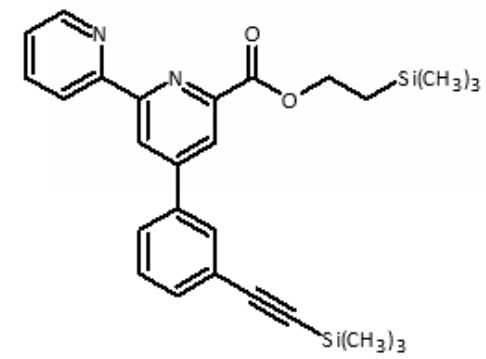
N
O
N
O
Si(CH3)3
Si(CH3)3

2-72

PPM
160
150
140
130
120
110
100
90
80
70
60
50
40
30
20
10
0

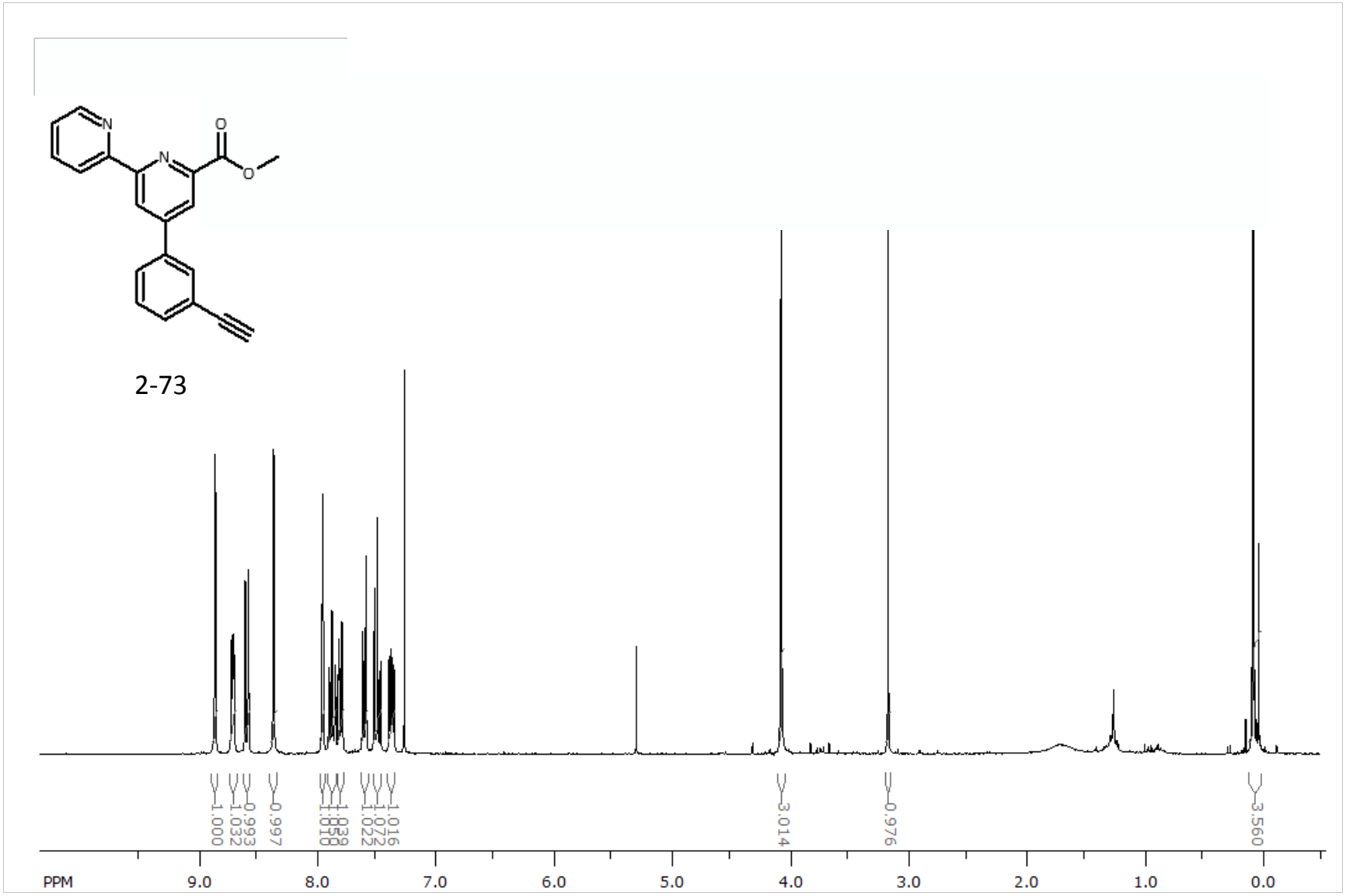
N
N
O
O
2-73
1.000
1.032
0.993
0.997
1.016
1.022
3.014
0.976
3.560
PPM
9.0
8.0
7.0
6.0
5.0
4.0
3.0
2.0
1.0
0.0

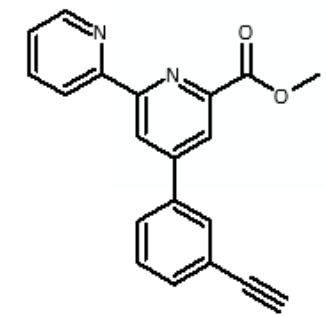

2-73

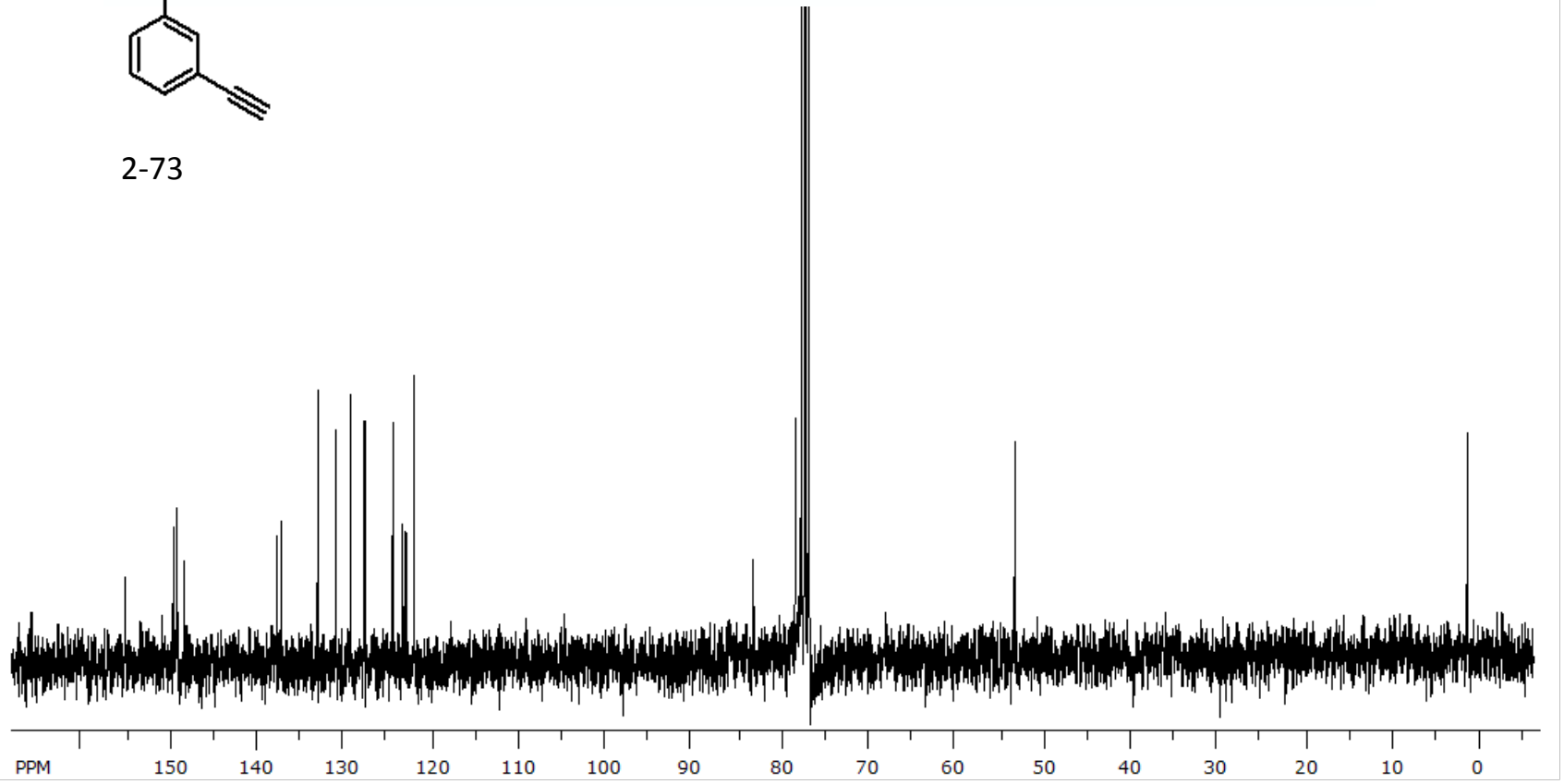

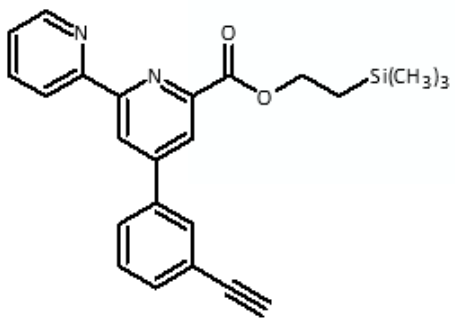
N
O
N
O
Si(CH3)3

2-74

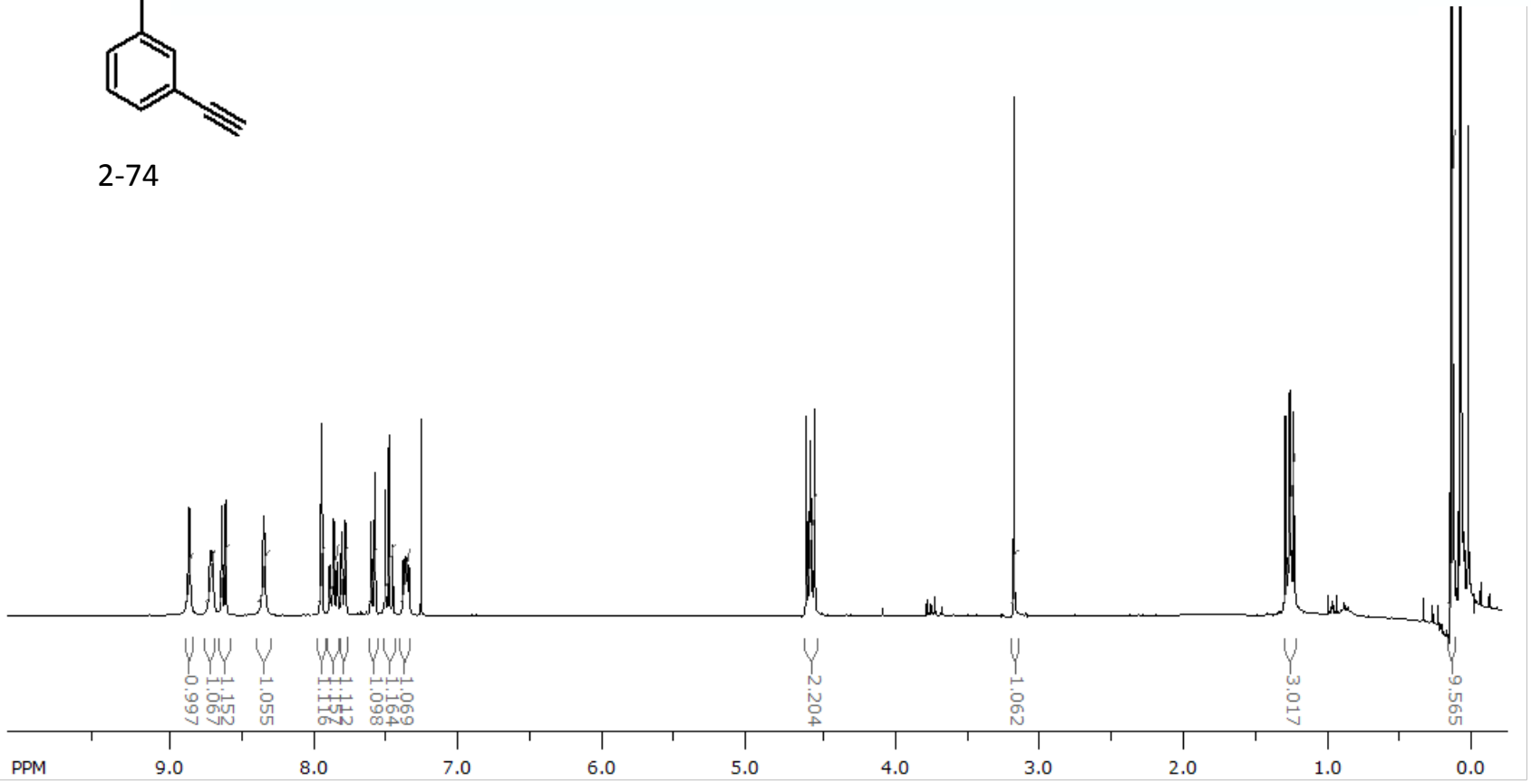
0.997
1.067
1.152
1.055
1.116
1.098
1.164
1.069
2.204
1.062
3.017
9.565
PPM
9.0
8.0
7.0
6.0
5.0
4.0
3.0
2.0
1.0
0.0

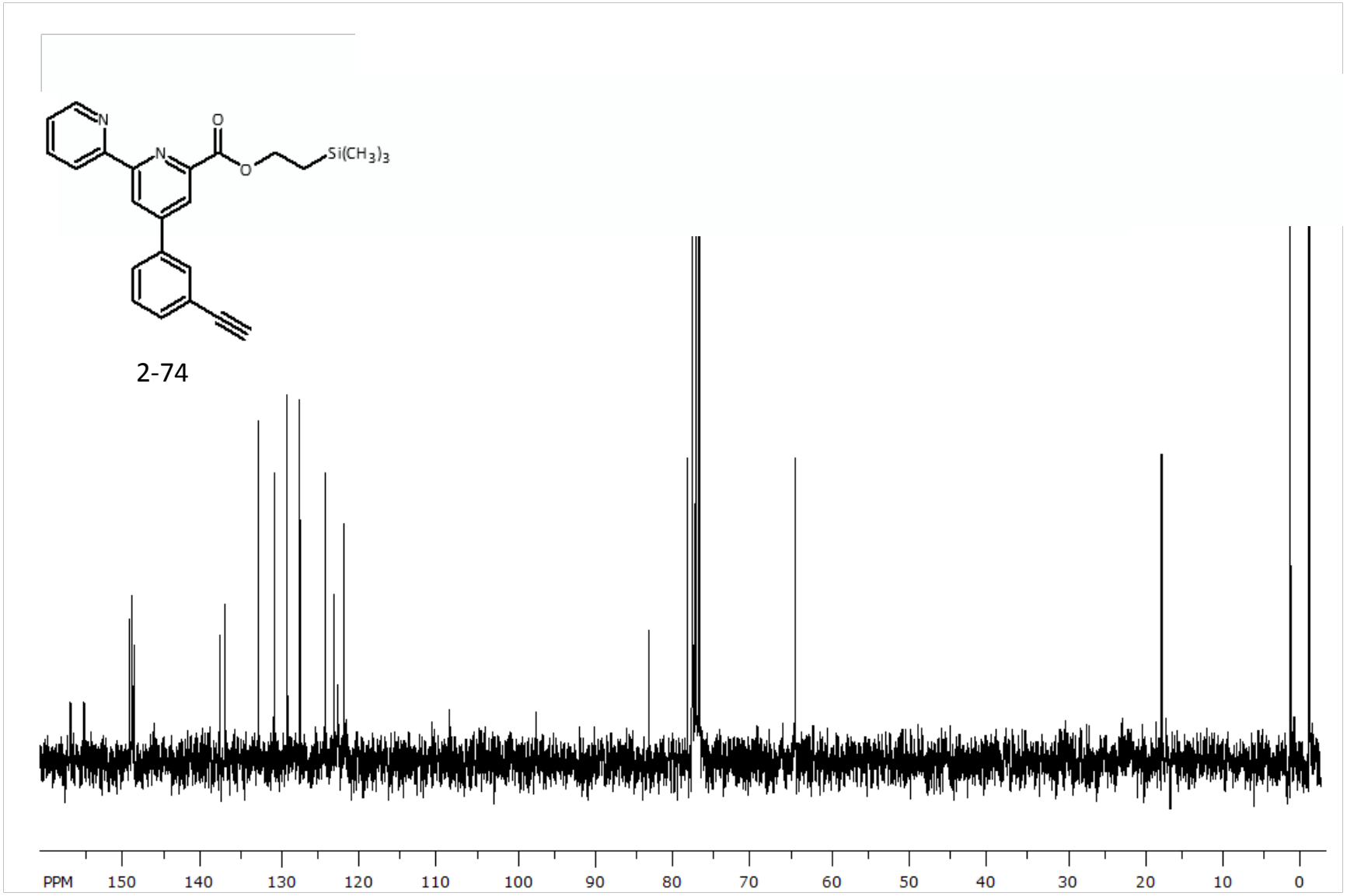
N
O
N
O
Si(CH3)3
PPM
150
140
130
120
110
100
90
80
70
60
50
40
30
20
10
0

2-74

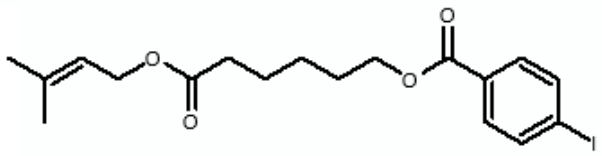

3-9

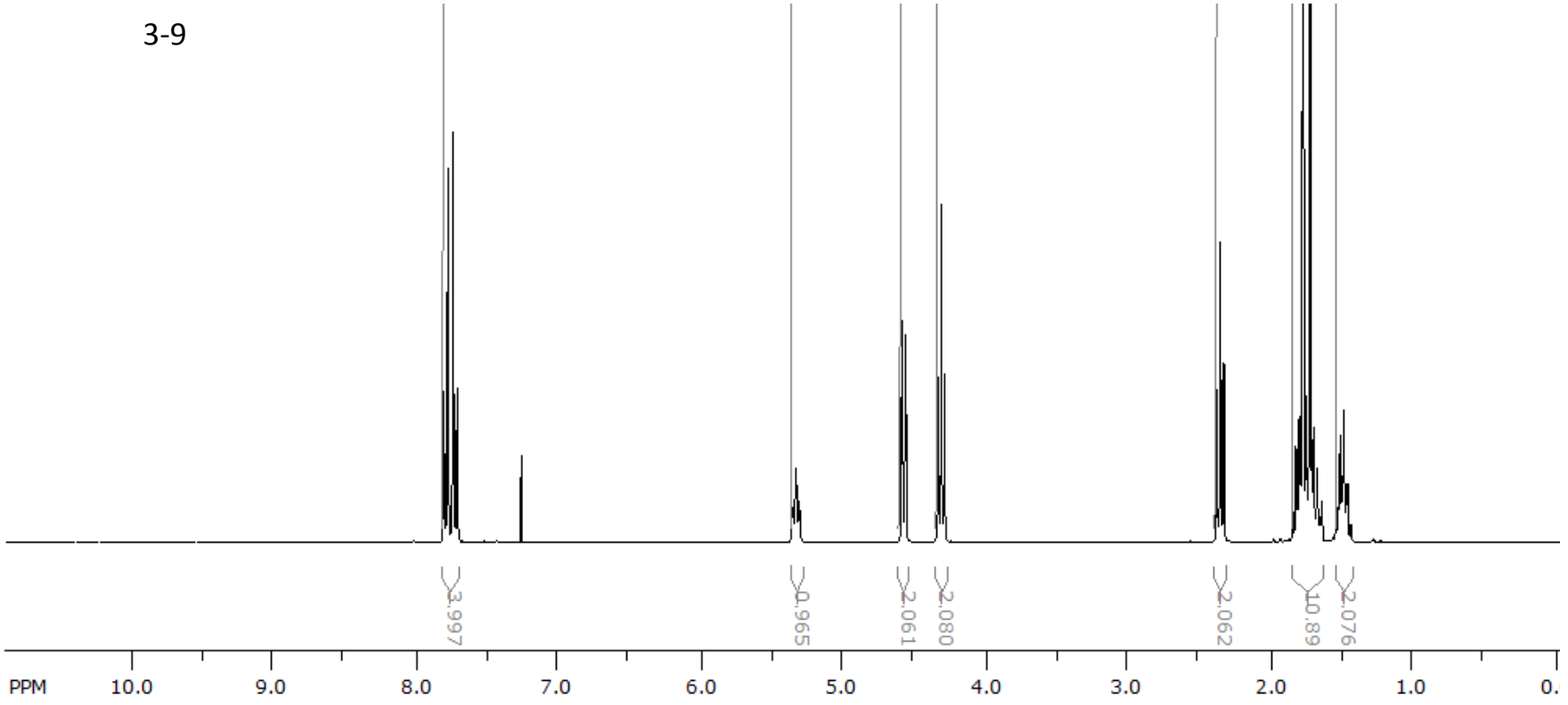
3.997
0.965
2.061
2.080
2.062
10.89
2.076
PPM
10.0
9.0
8.0
7.0
6.0
5.0
4.0
3.0
2.0
1.0
0.

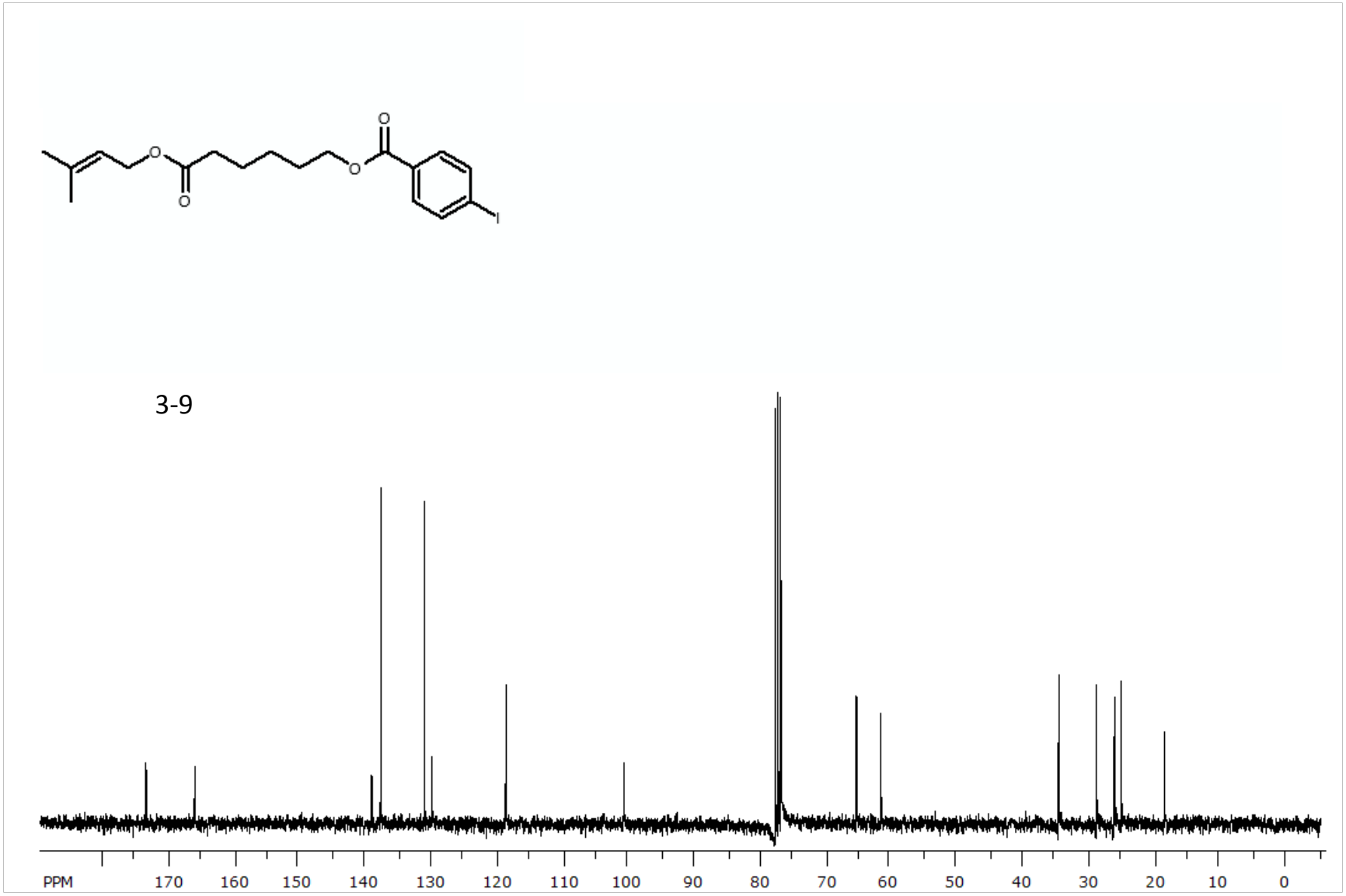
3-9
PPM
170
160
150
140
130
120
110
100
90
80
70
60
50
40
30
20
10
0

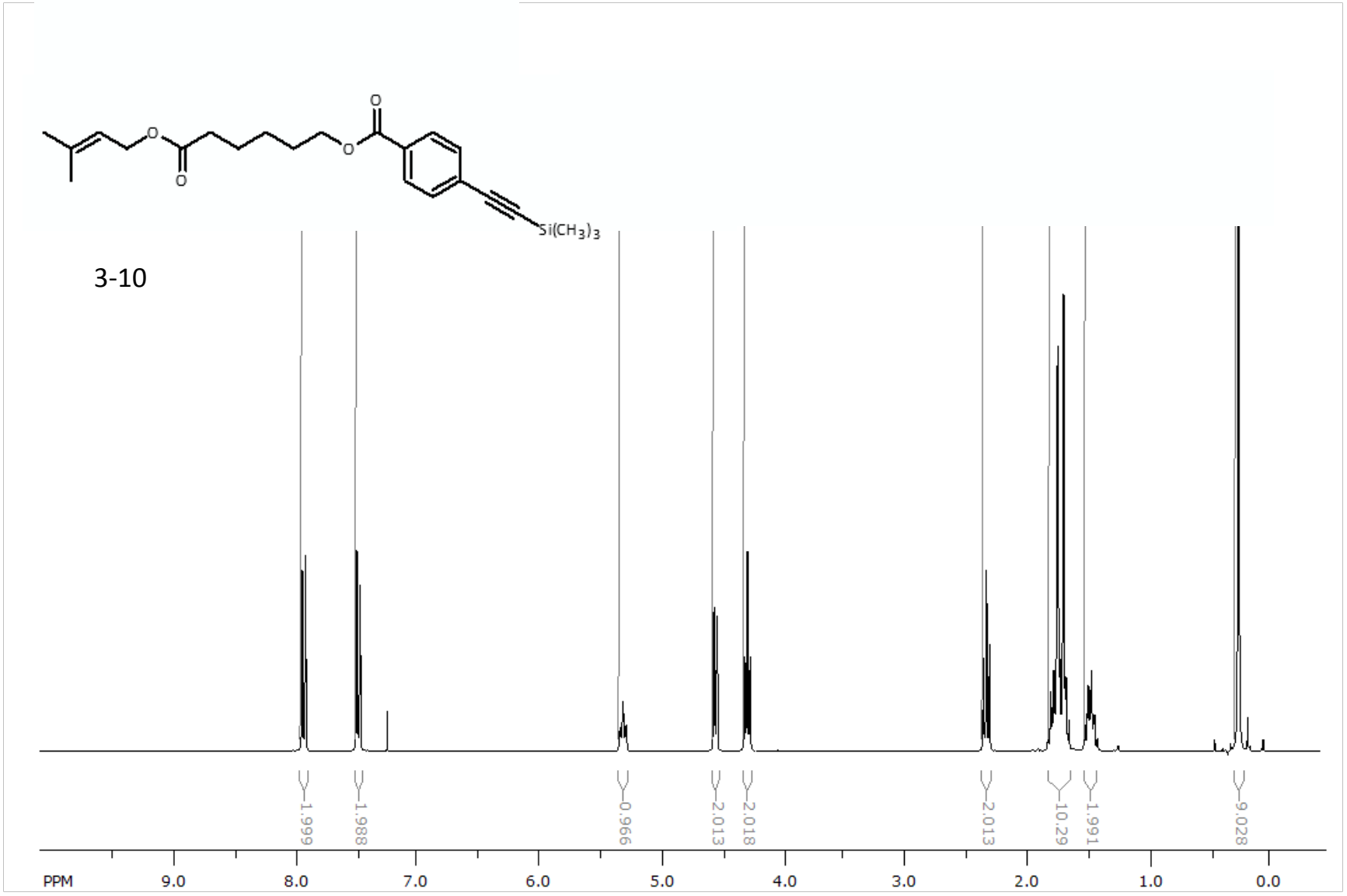
3-10
Si(CH3)3
1.999
1.988
0.966
2.013
2.018
2.013
10.29
1.991
9.028
PPM
9.0
8.0
7.0
6.0
5.0
4.0
3.0
2.0
1.0
0.0

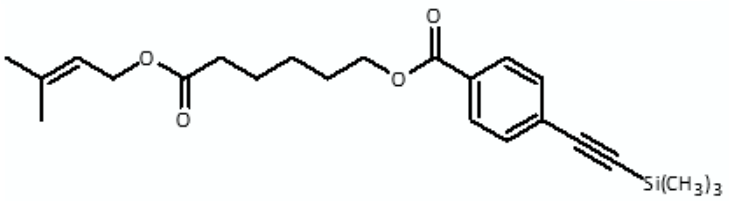
O
O
O
O
Si(CH3)3

3-10

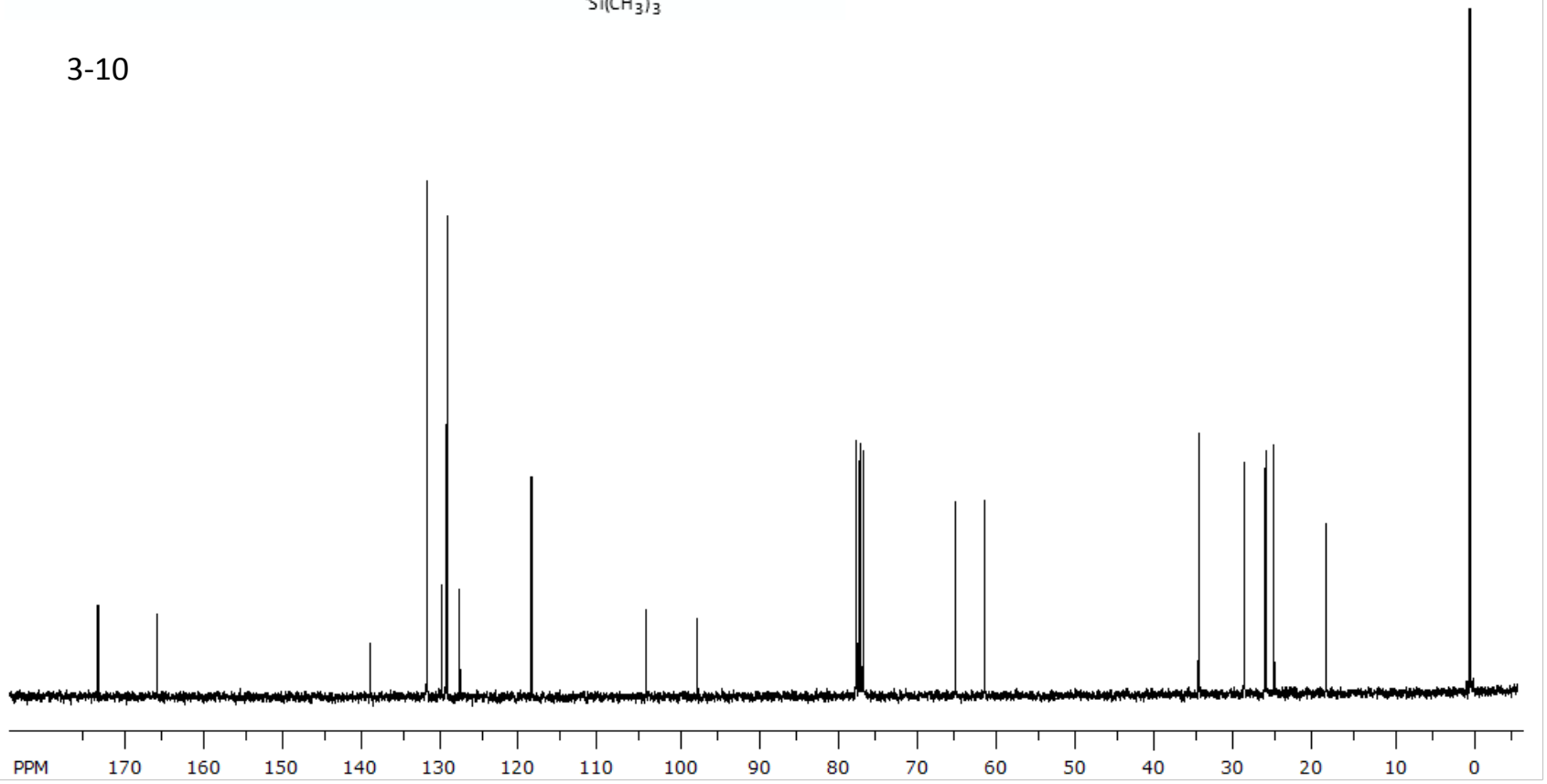
PPM
170
160
150
140
130
120
110
100
90
80
70
60
50
40
30
20
10
0

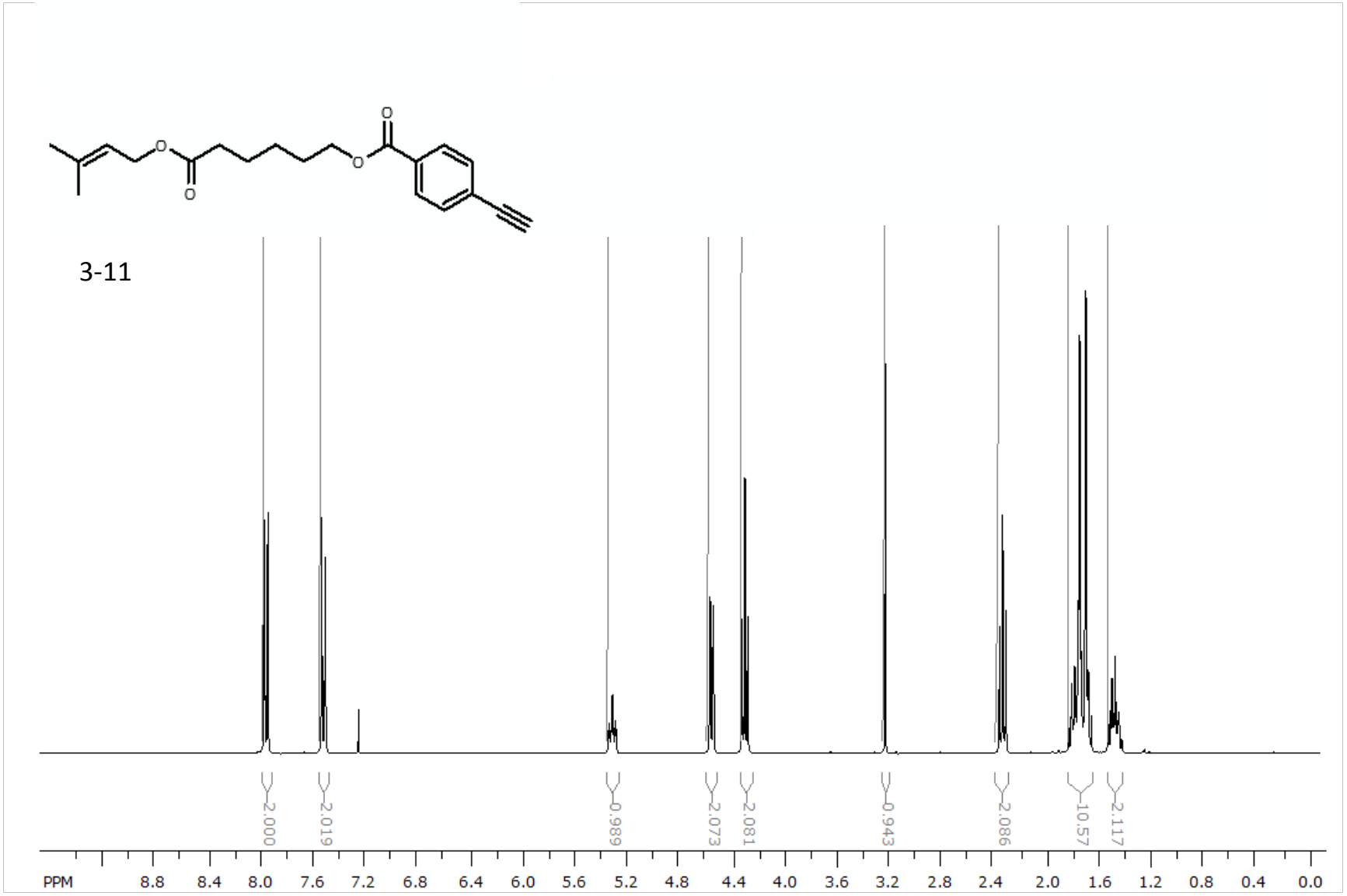
3-11
2.000
2.019
0.989
2.073
2.081
0.943
2.086
10.57
2.117
PPM
8.8
8.4
8.0
7.6
7.2
6.8
6.4
6.0
5.6
5.2
4.8
4.4
4.0
3.6
3.2
2.8
2.4
2.0
1.6
1.2
0.8
0.4
0.0

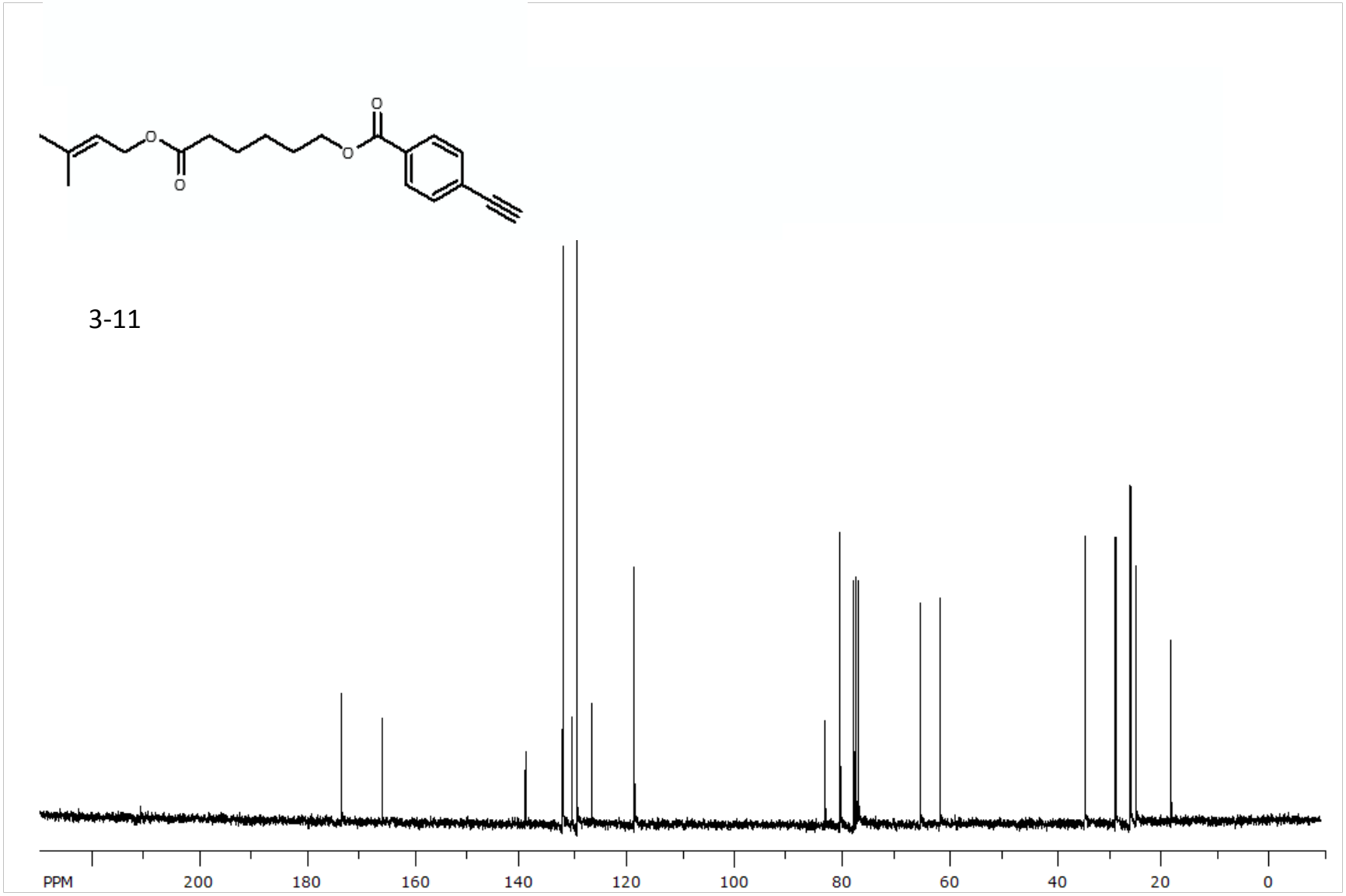
3-11
PPM
200
180
160
140
120
100
80
60
40
20
0

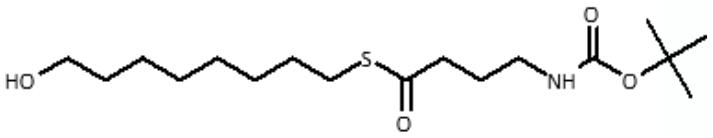
HO
S
O
NH
O
O

3-23

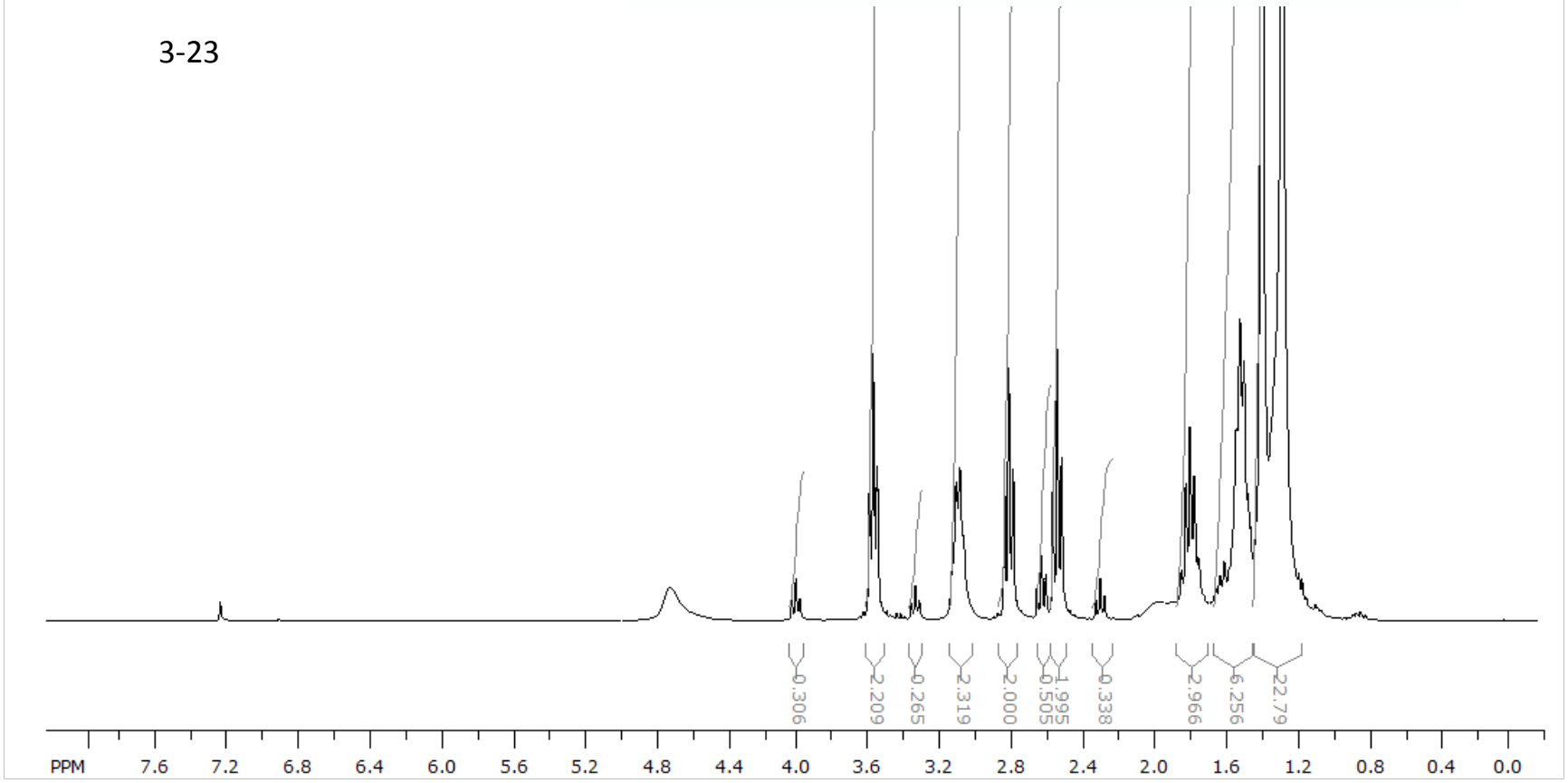
0.306
2.209
0.265
2.319
2.000
0.505
1.995
0.338
2.966
6.256
22.79
PPM
7.6
7.2
6.8
6.4
6.0
5.6
5.2
4.8
4.4
4.0
3.6
3.2
2.8
2.4
2.0
1.6
1.2
0.8
0.4
0.0

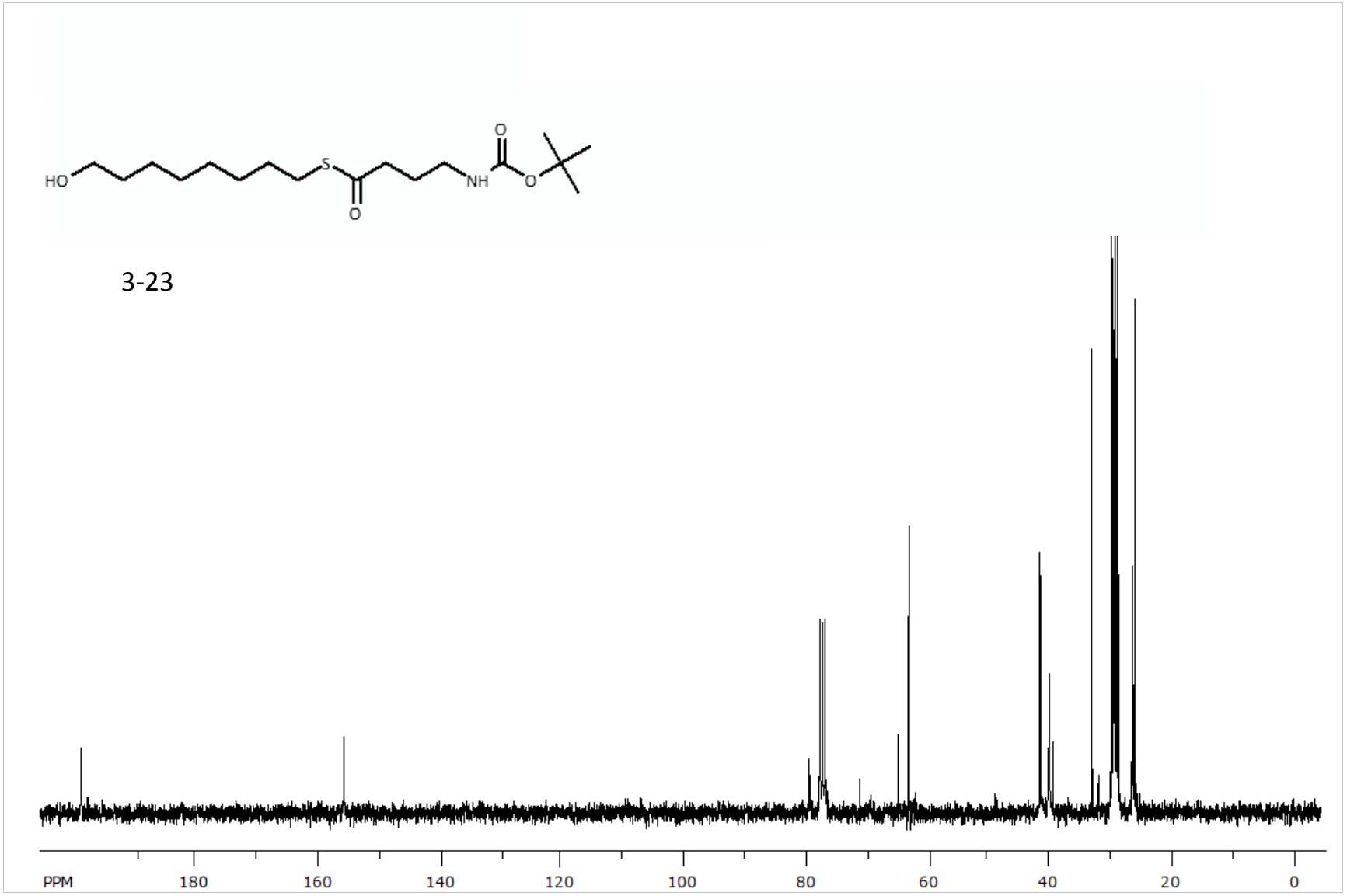
HO
S
O
NH
O
O
O
3-23
PPM
180
160
140
120
100
80
60
40
20
0

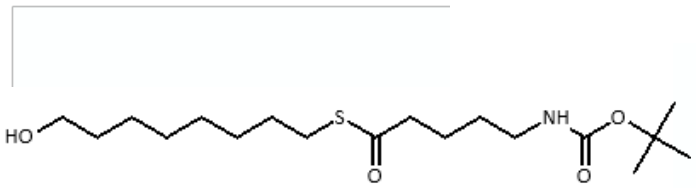
HO
S
O
NH
O
O

3-24

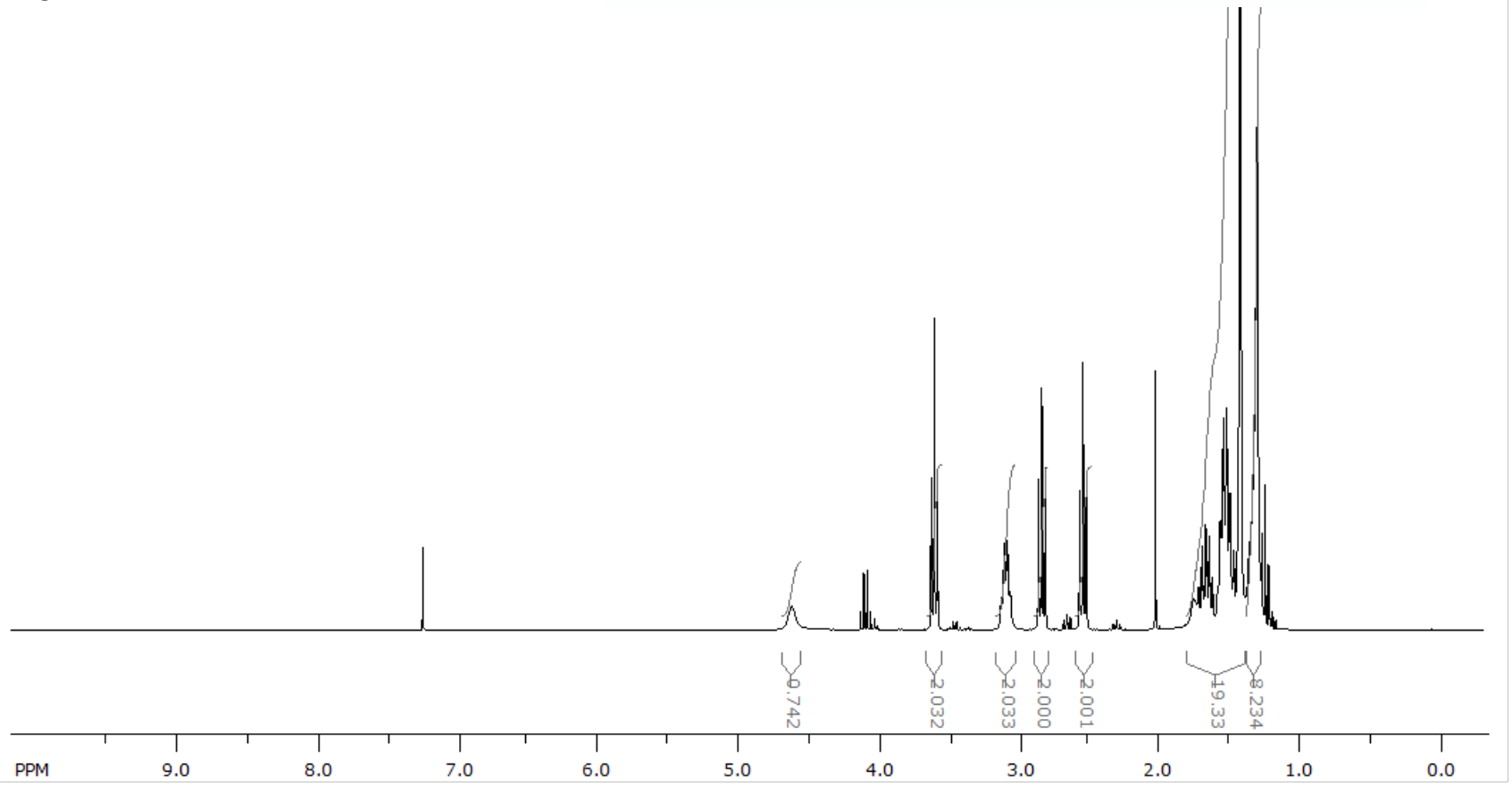
0.742
2.032
2.033
2.000
2.001
19.33
8.234
PPM
9.0
8.0
7.0
6.0
5.0
4.0
3.0
2.0
1.0
0.0

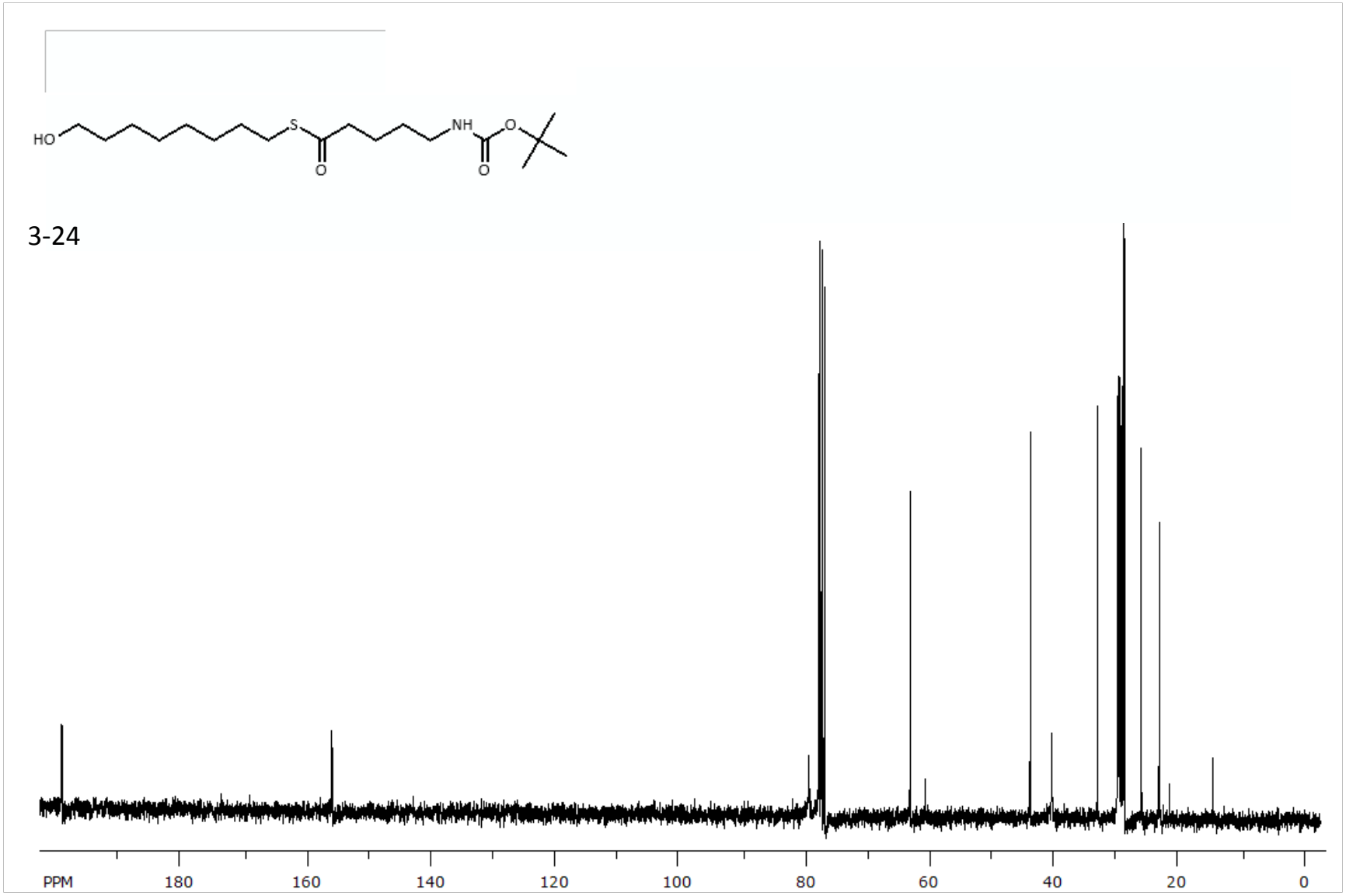
HO
S
O
NH
O
O
3-24
PPM
180
160
140
120
100
80
60
40
20
0

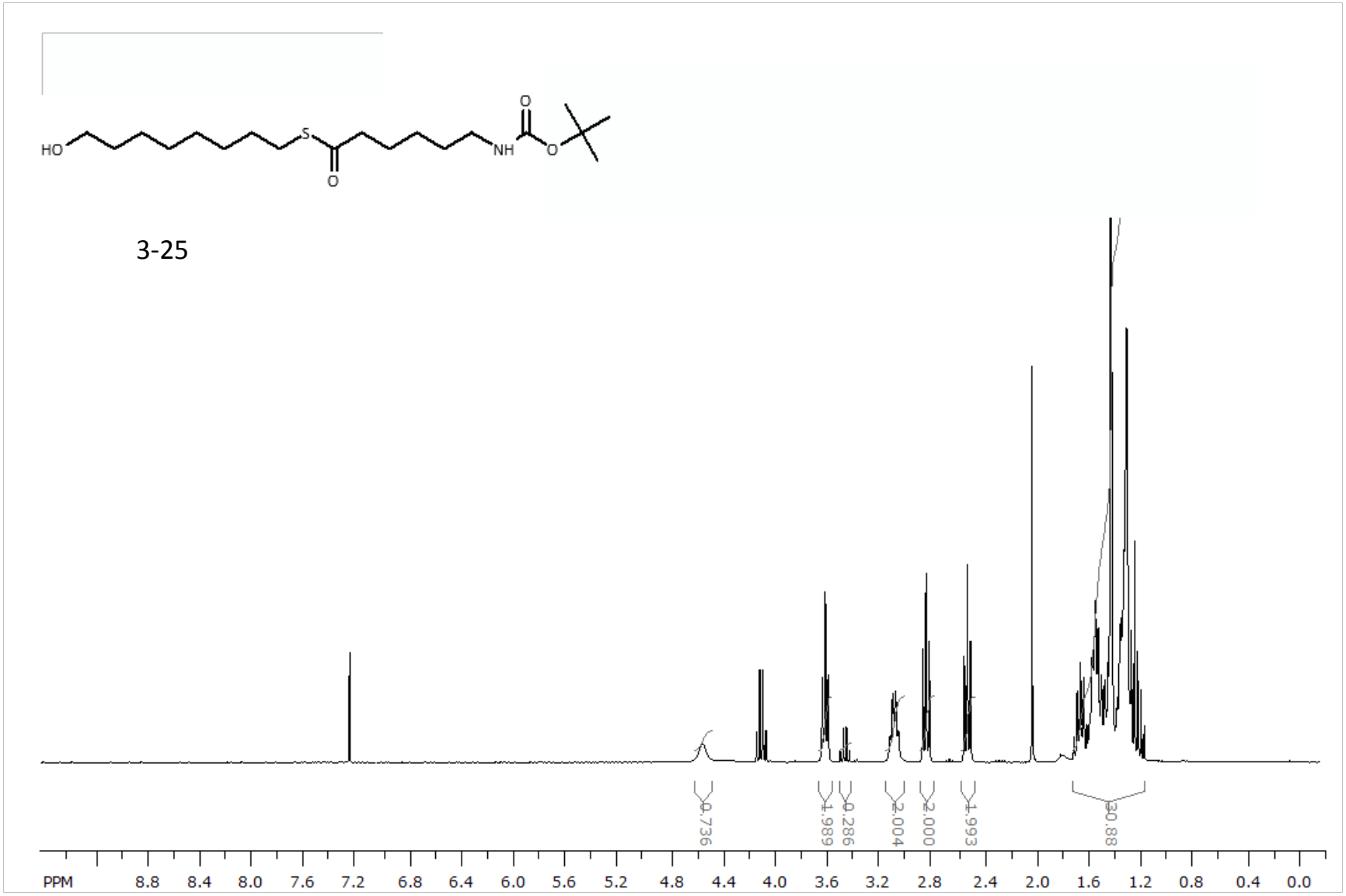
HO
S
O
NH
O
O
3-25
0.736
1.989
0.286
2.004
2.000
1.993
30.88
PPM
8.8
8.4
8.0
7.6
7.2
6.8
6.4
6.0
5.6
5.2
4.8
4.4
4.0
3.6
3.2
2.8
2.4
2.0
1.6
1.2
0.8
0.4
0.0

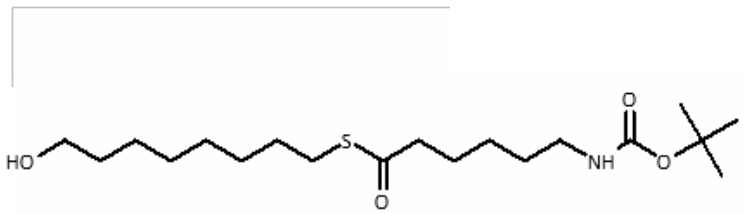

3-25

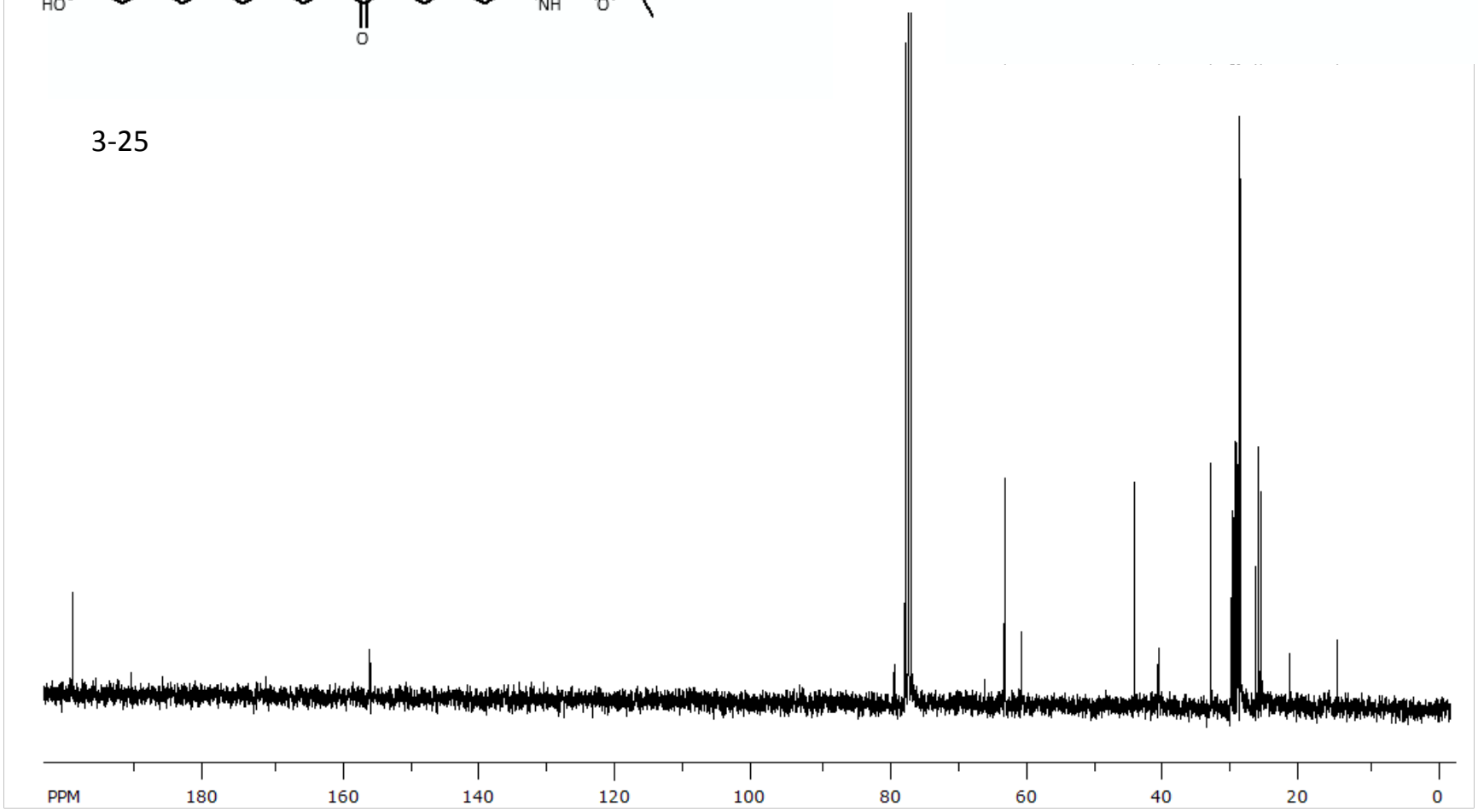

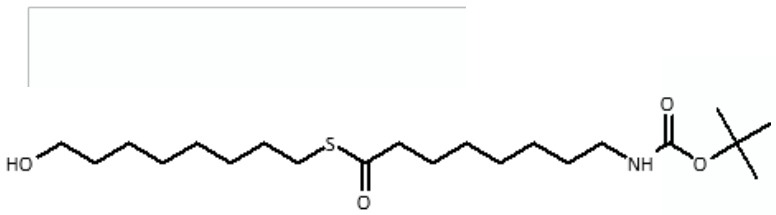
HO
S
O
NH
O
O

3-26

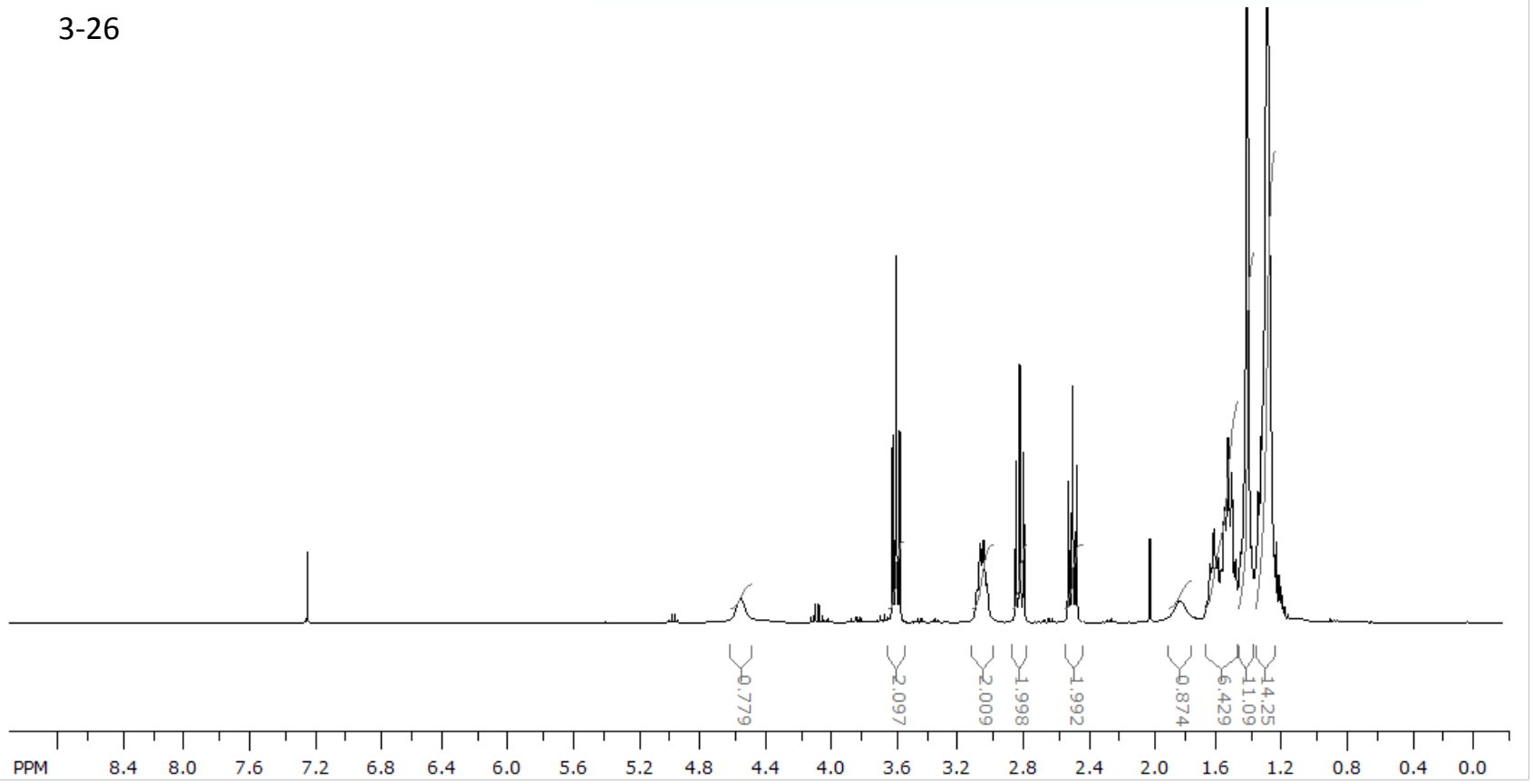
0.779
2.097
2.009
1.998
1.992
0.874
6.429
11.09
14.25
PPM
8.4
8.0
7.6
7.2
6.8
6.4
6.0
5.6
5.2
4.8
4.4
4.0
3.6
3.2
2.8
2.4
2.0
1.6
1.2
0.8
0.4
0.0

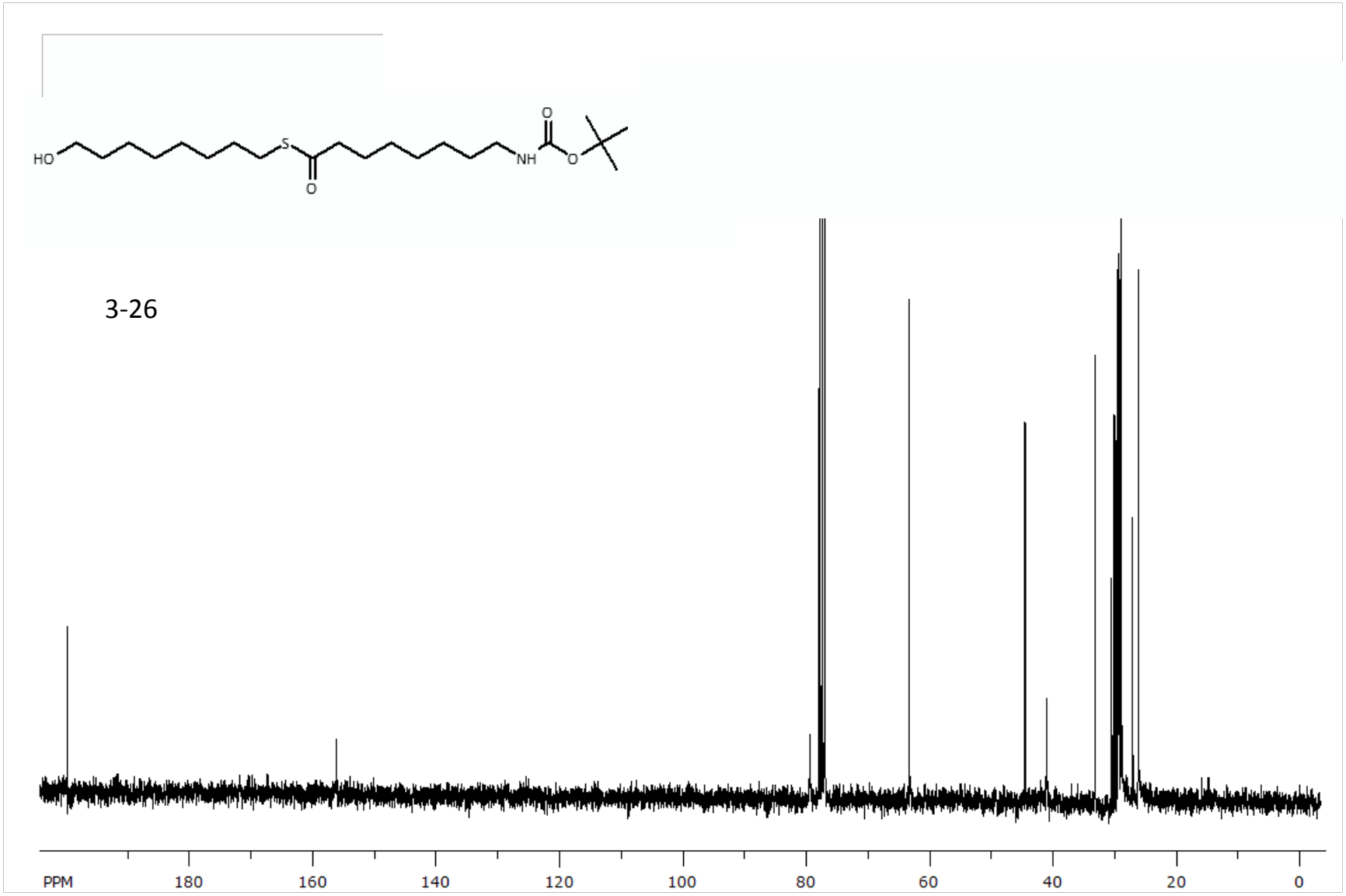
HO
S
O
NH
O
O
3-26
PPM
180
160
140
120
100
80
60
40
20
0

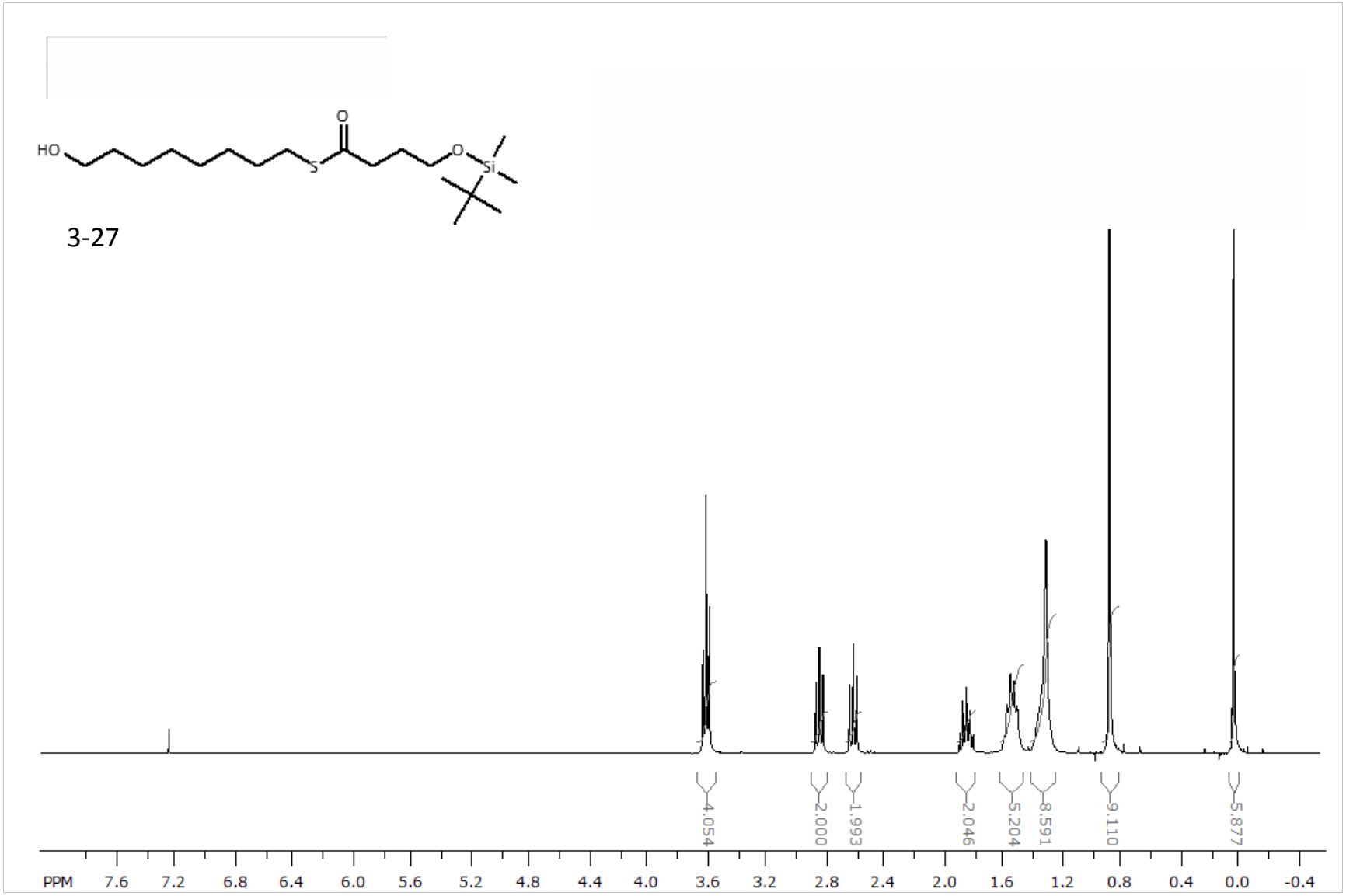
HO
O
S
O
Si
3-27
4.054
2.000
1.993
2.046
5.204
8.591
9.110
5.877
PPM
7.6
7.2
6.8
6.4
6.0
5.6
5.2
4.8
4.4
4.0
3.6
3.2
2.8
2.4
2.0
1.6
1.2
0.8
0.4
0.0
-0.4

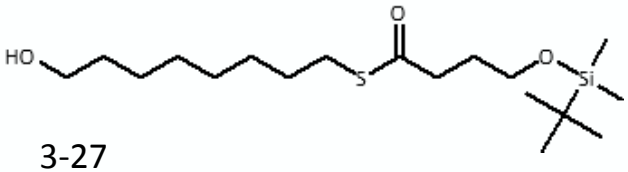

3-27

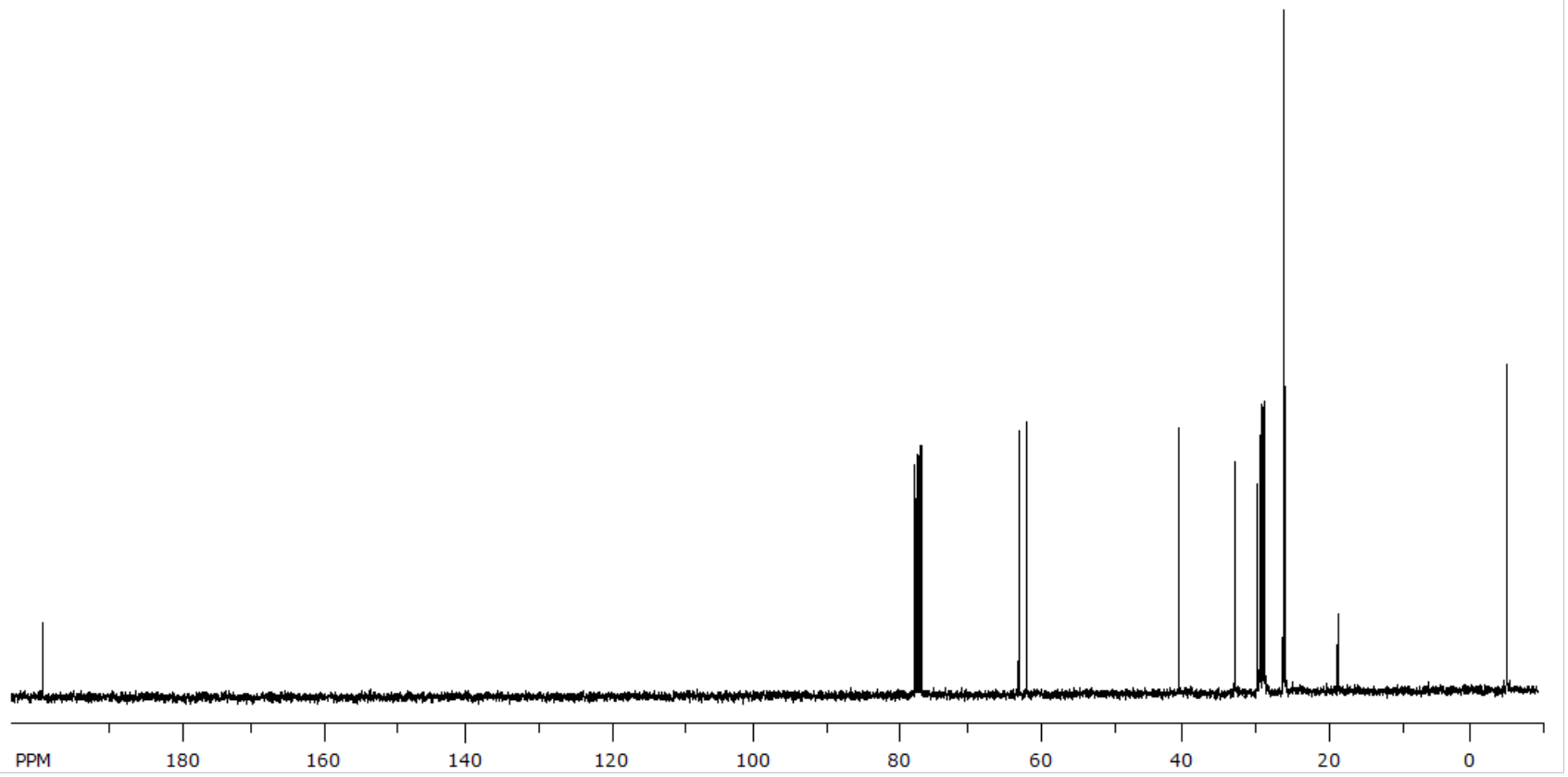

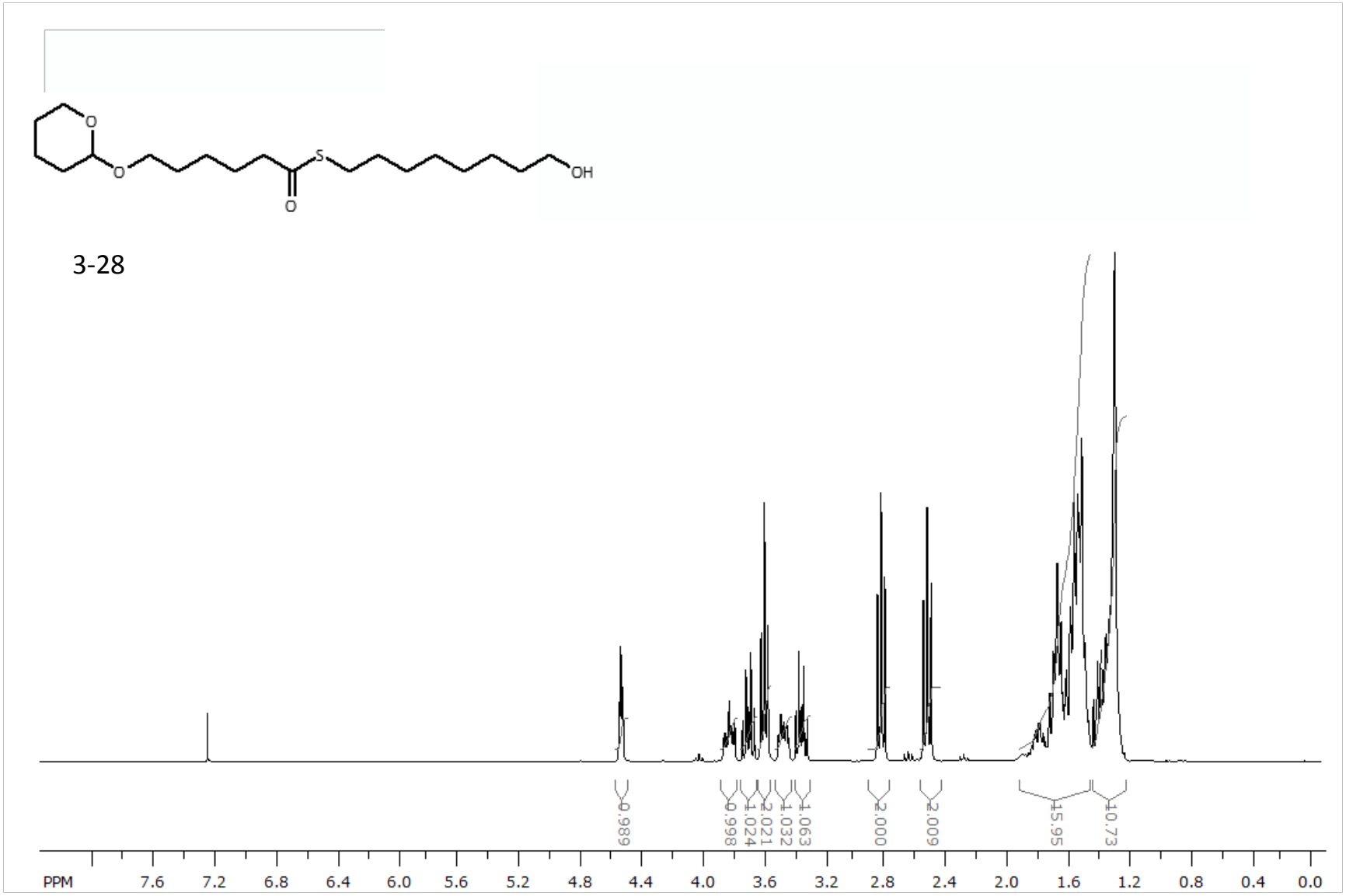
O
O
S
OH
O
3-28
0.989
0.998
1.024
2.021
1.032
1.063
2.000
2.009
15.95
10.73
PPM
7.6
7.2
6.8
6.4
6.0
5.6
5.2
4.8
4.4
4.0
3.6
3.2
2.8
2.4
2.0
1.6
1.2
0.8
0.4
0.0

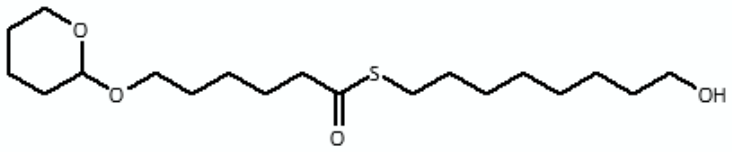

3-28

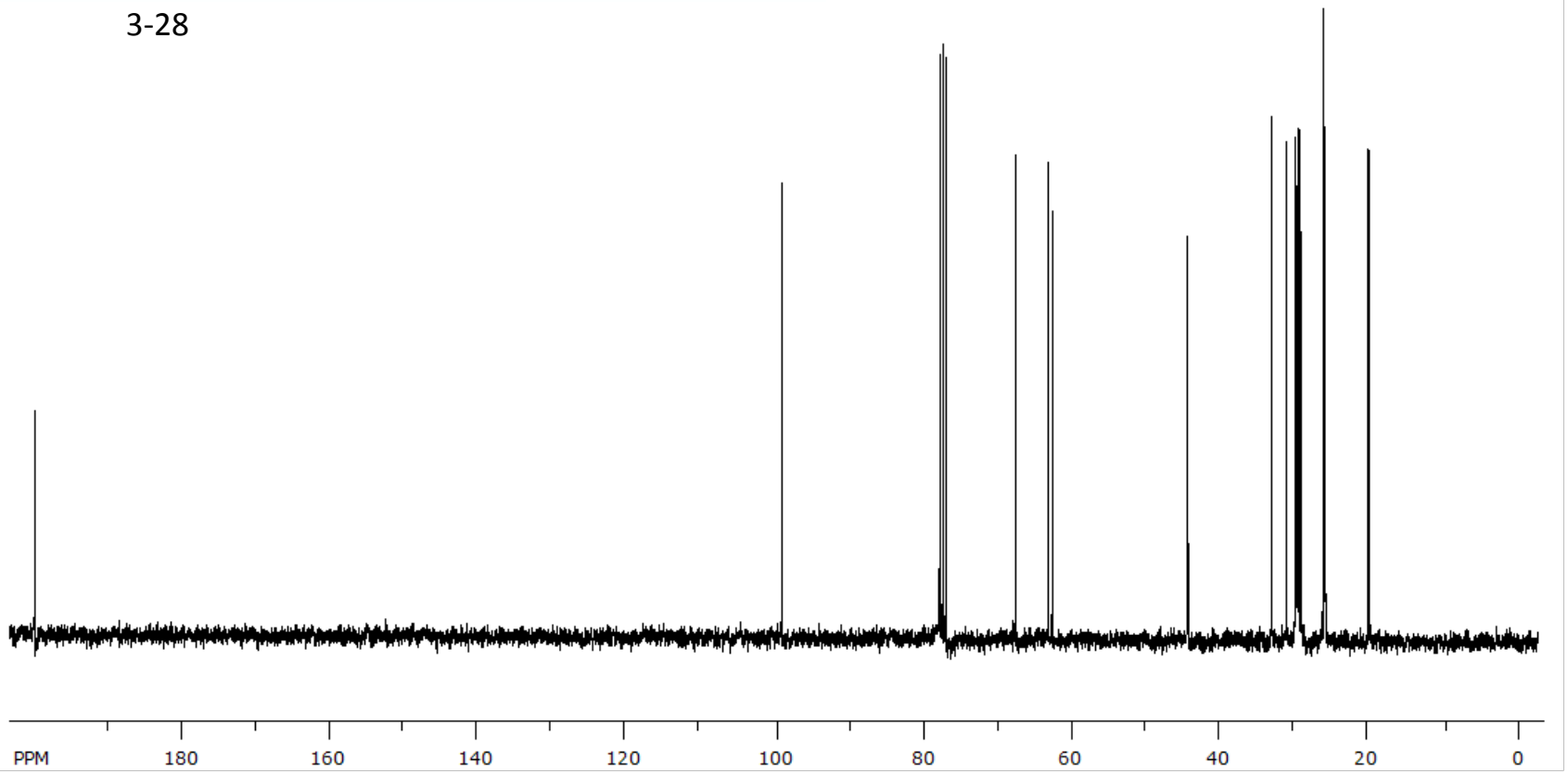

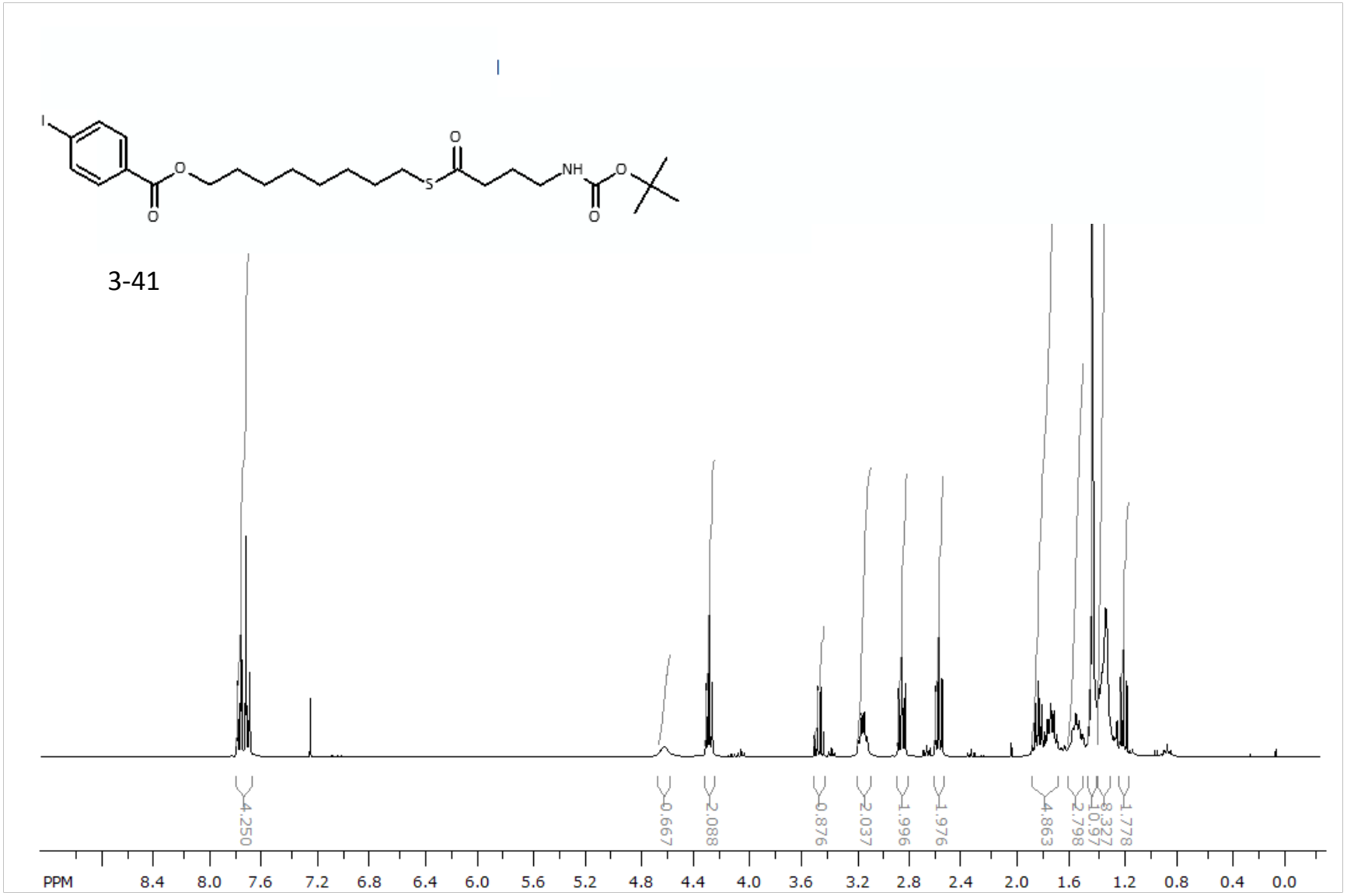
I
O
O
S
O
NH
O
O
3-41
4.250
0.667
2.088
0.876
2.037
1.996
1.976
4.863
2.798
10.97
8.327
1.778
PPM
8.4
8.0
7.6
7.2
6.8
6.4
6.0
5.6
5.2
4.8
4.4
4.0
3.6
3.2
2.8
2.4
2.0
1.6
1.2
0.8
0.4
0.0

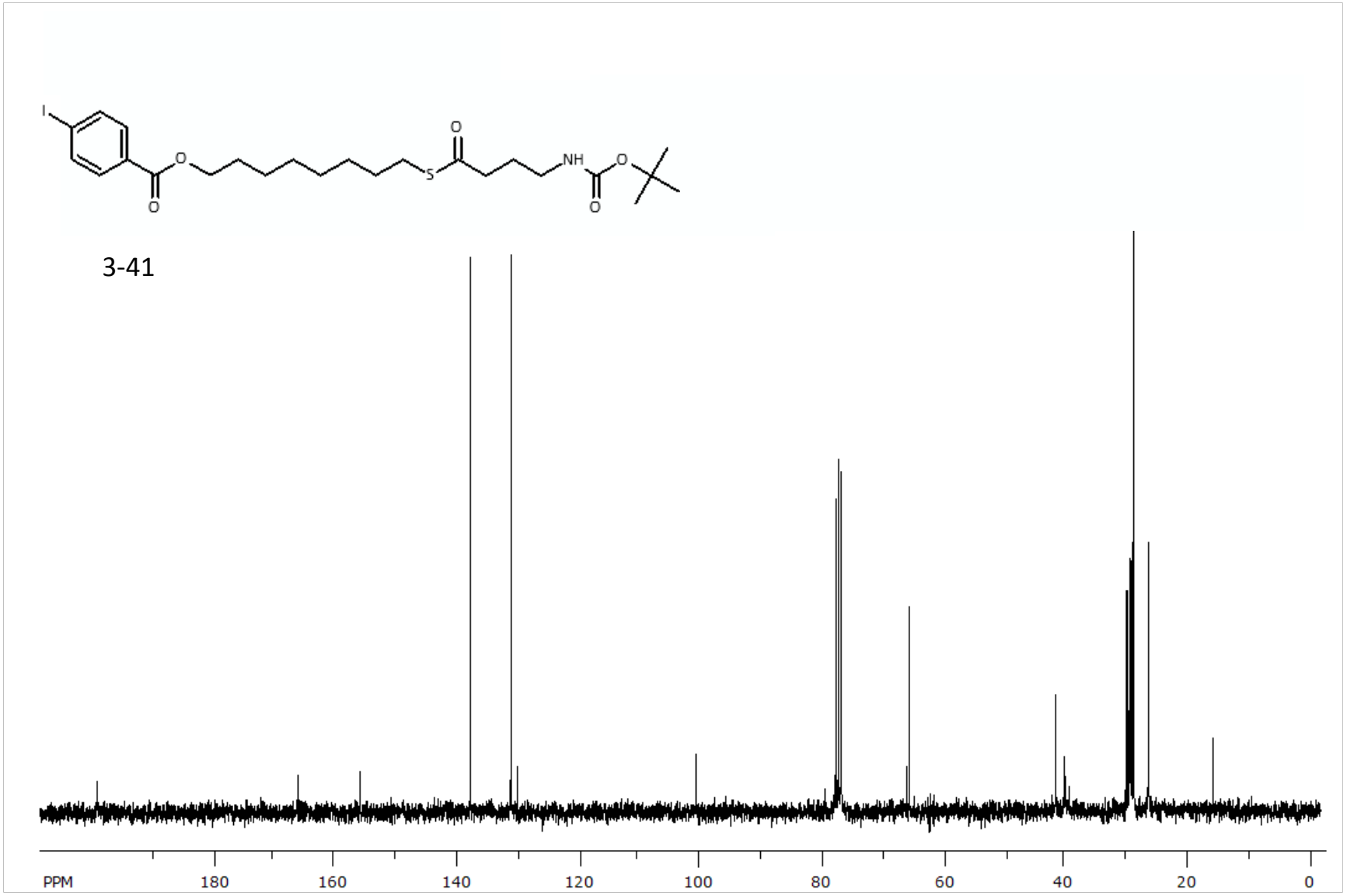
I
O
O
O
S
NH
O
O
O
3-41
PPM
180
160
140
120
100
80
60
40
20
0

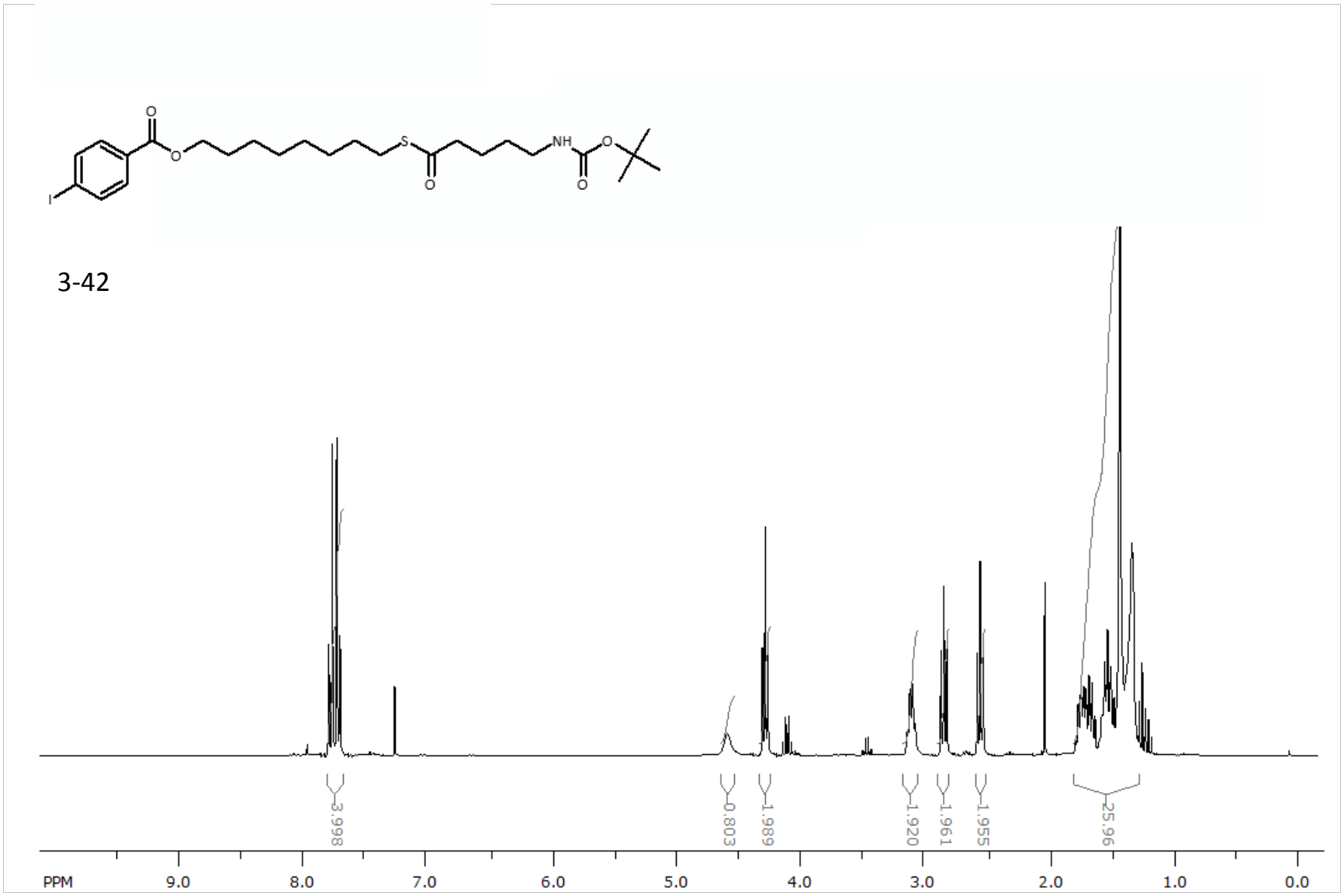
3-42
3.998
0.803
1.989
1.920
1.961
1.955
25.96
PPM
9.0
8.0
7.0
6.0
5.0
4.0
3.0
2.0
1.0
0.0

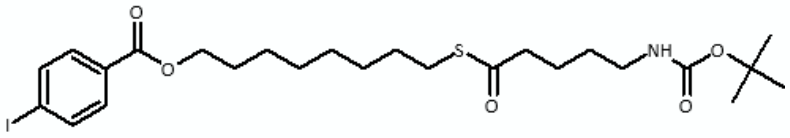

3-42

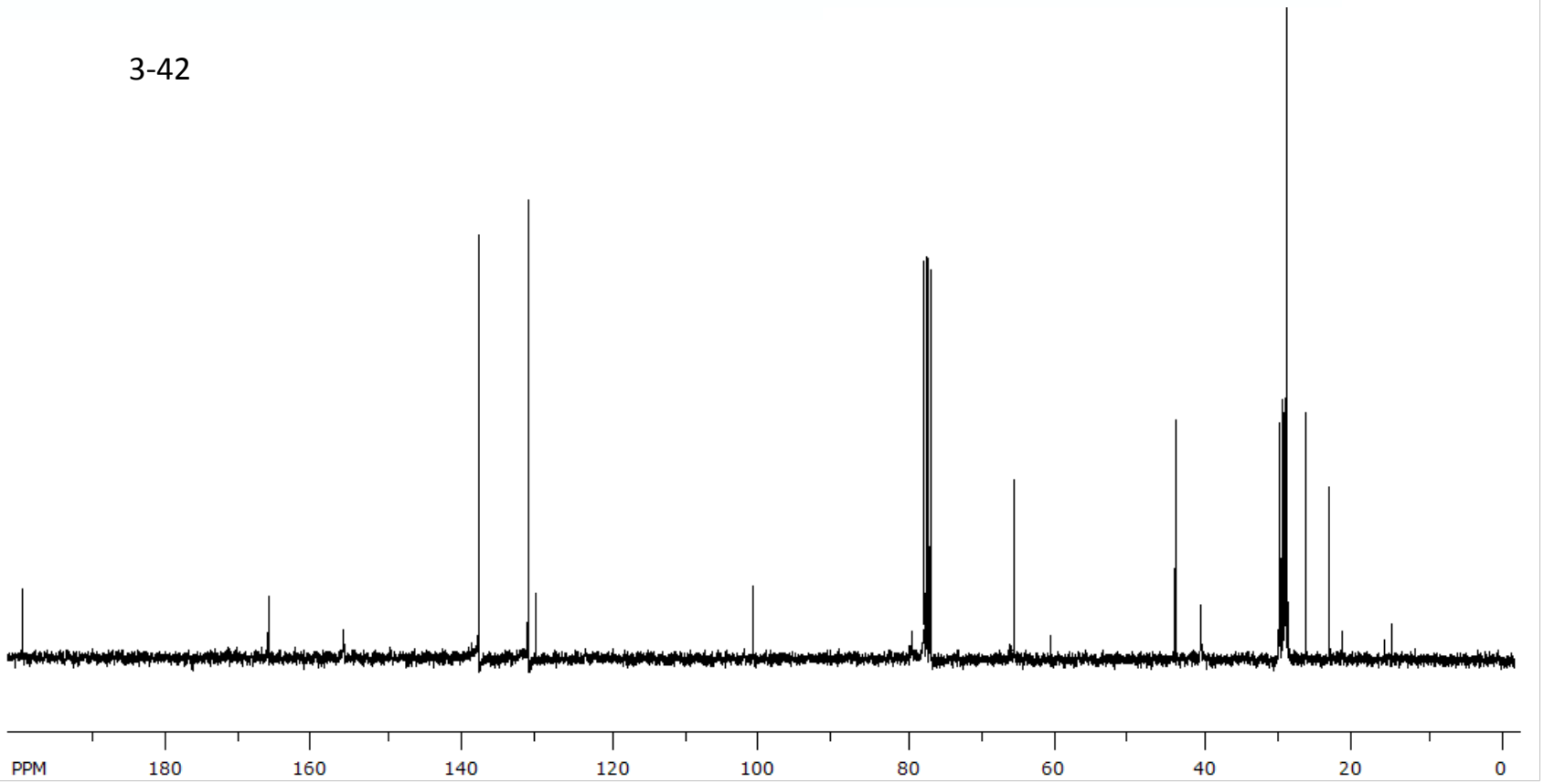

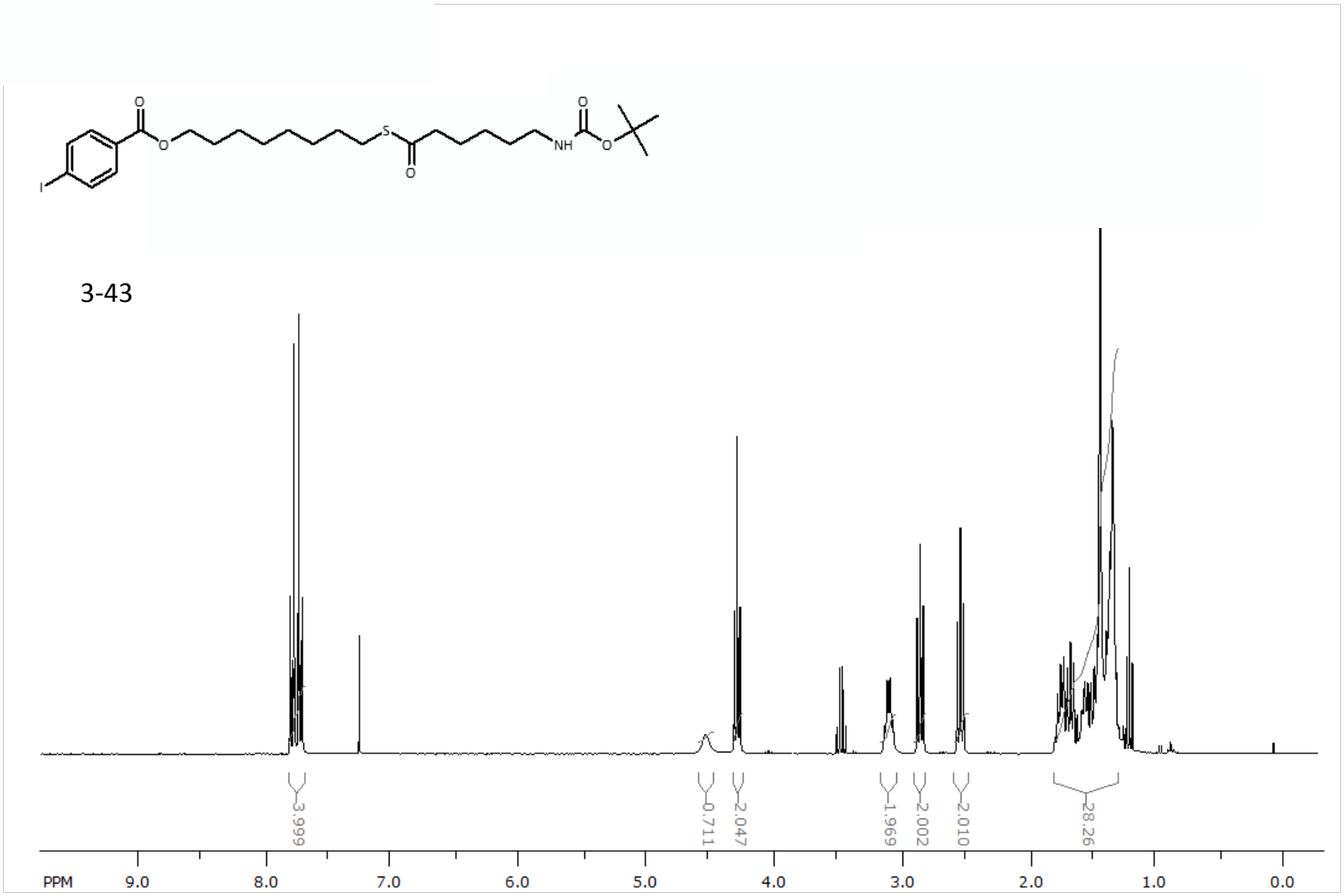
3-43
3.999
0.711
2.047
1.969
2.002
2.010
28.26
PPM
9.0
8.0
7.0
6.0
5.0
4.0
3.0
2.0
1.0
0.0

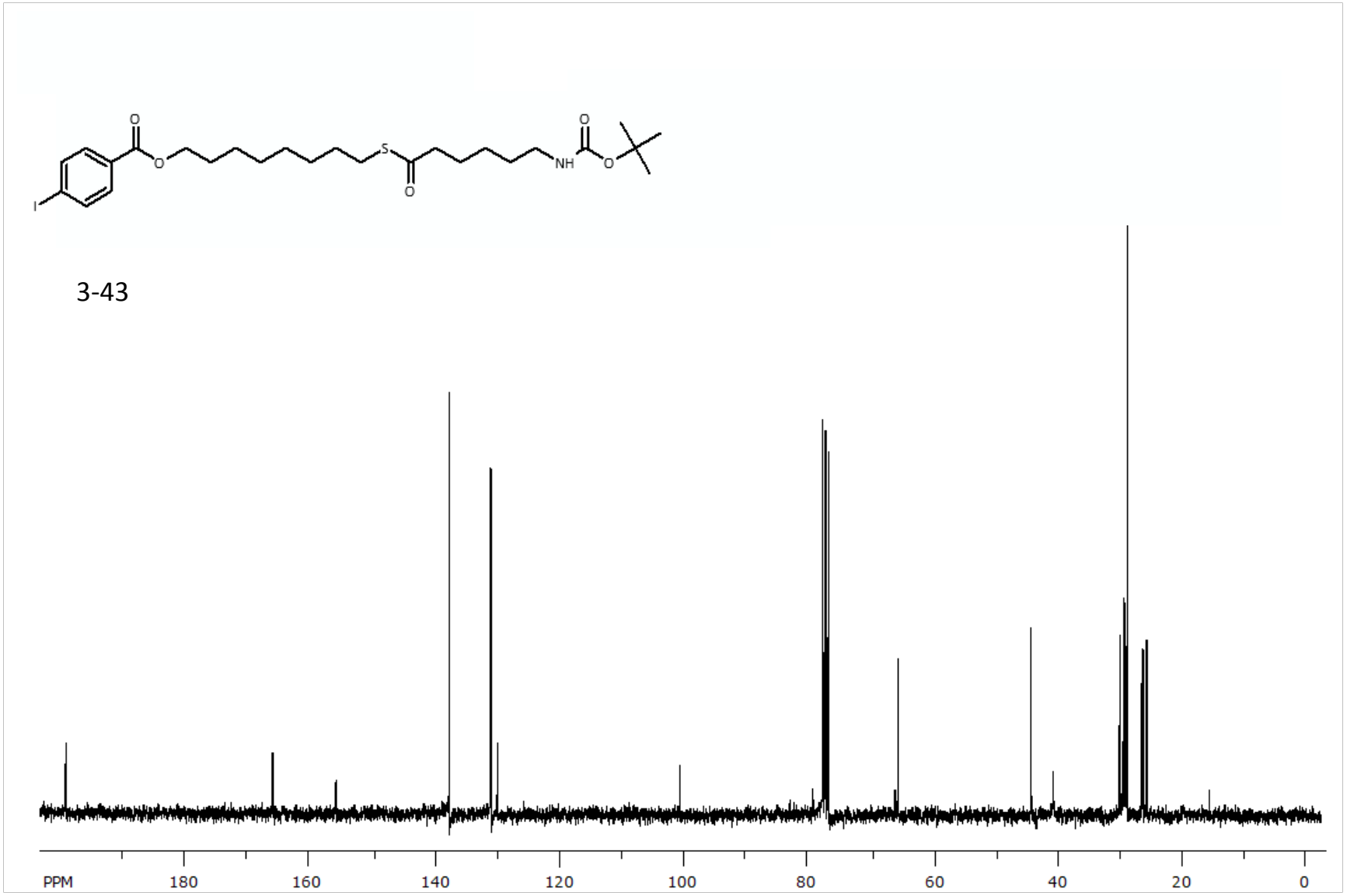
3-43
PPM
180
160
140
120
100
80
60
40
20
0

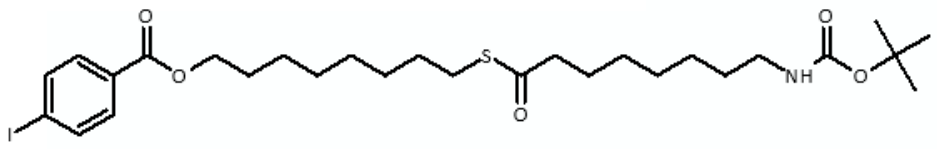
O
O
S
O
NH
O
O
I

3-44

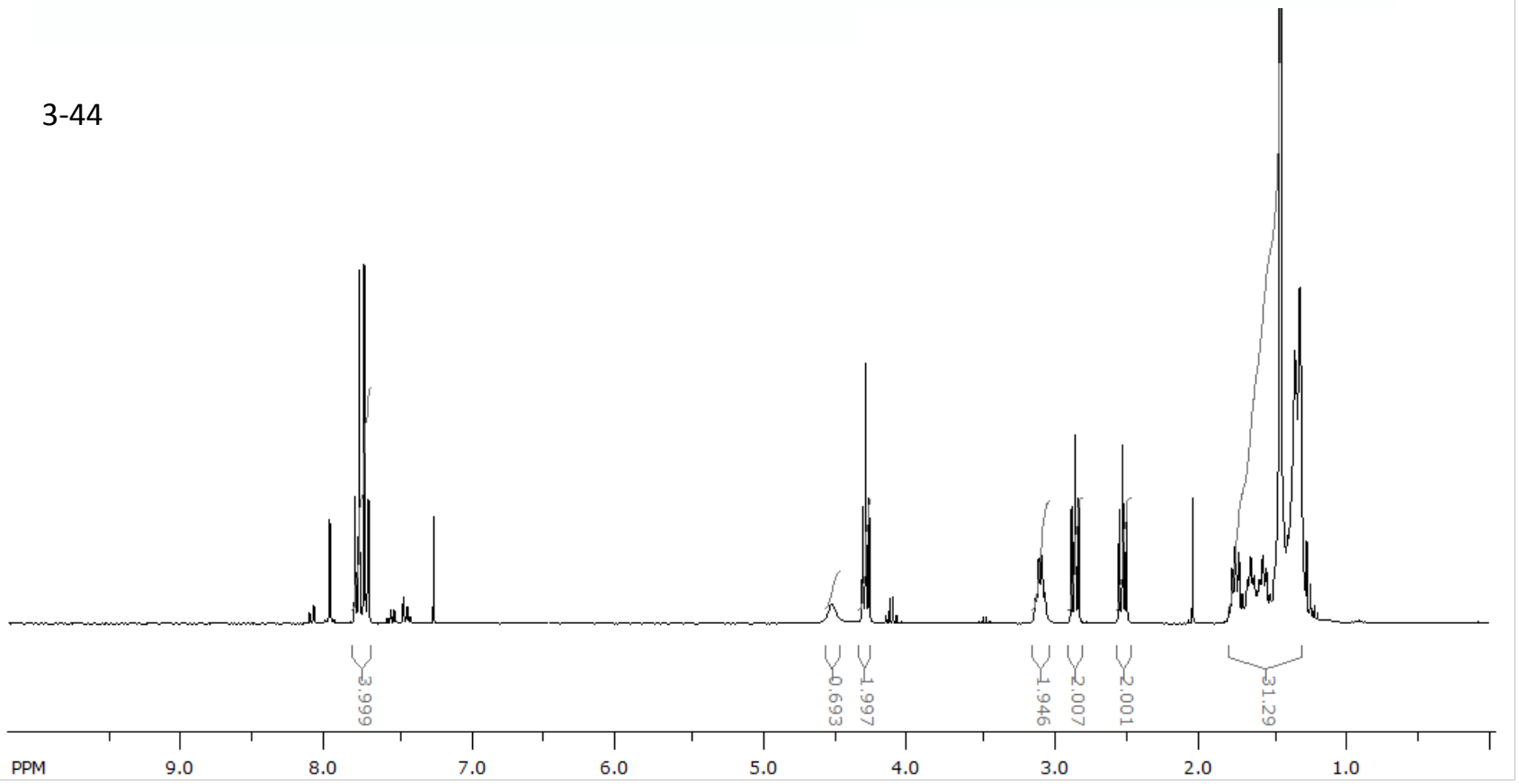
3.999
0.693
1.997
1.946
2.007
2.001
31.29
PPM
9.0
8.0
7.0
6.0
5.0
4.0
3.0
2.0
1.0

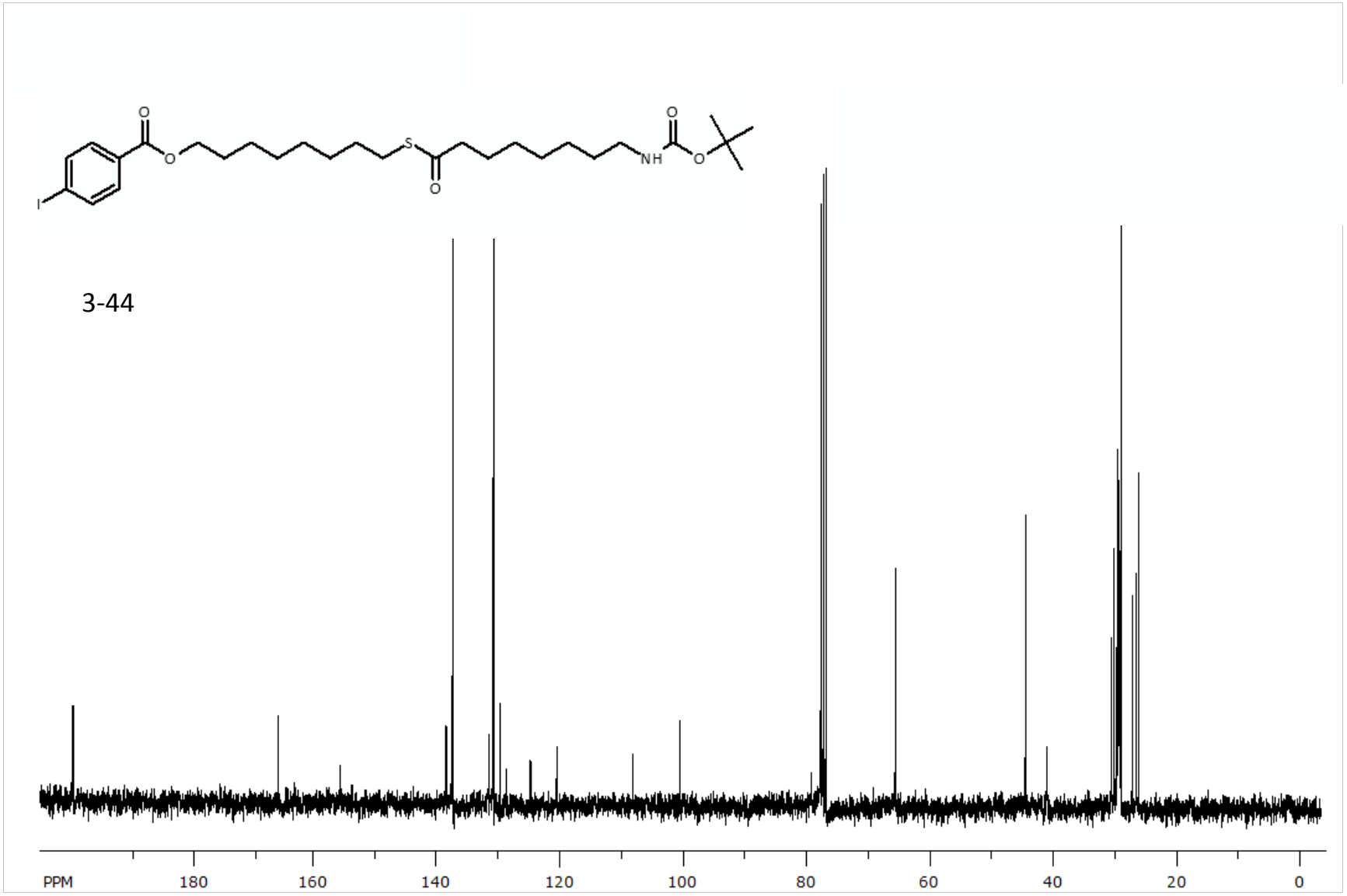
3-44
PPM
180
160
140
120
100
80
60
40
20
0

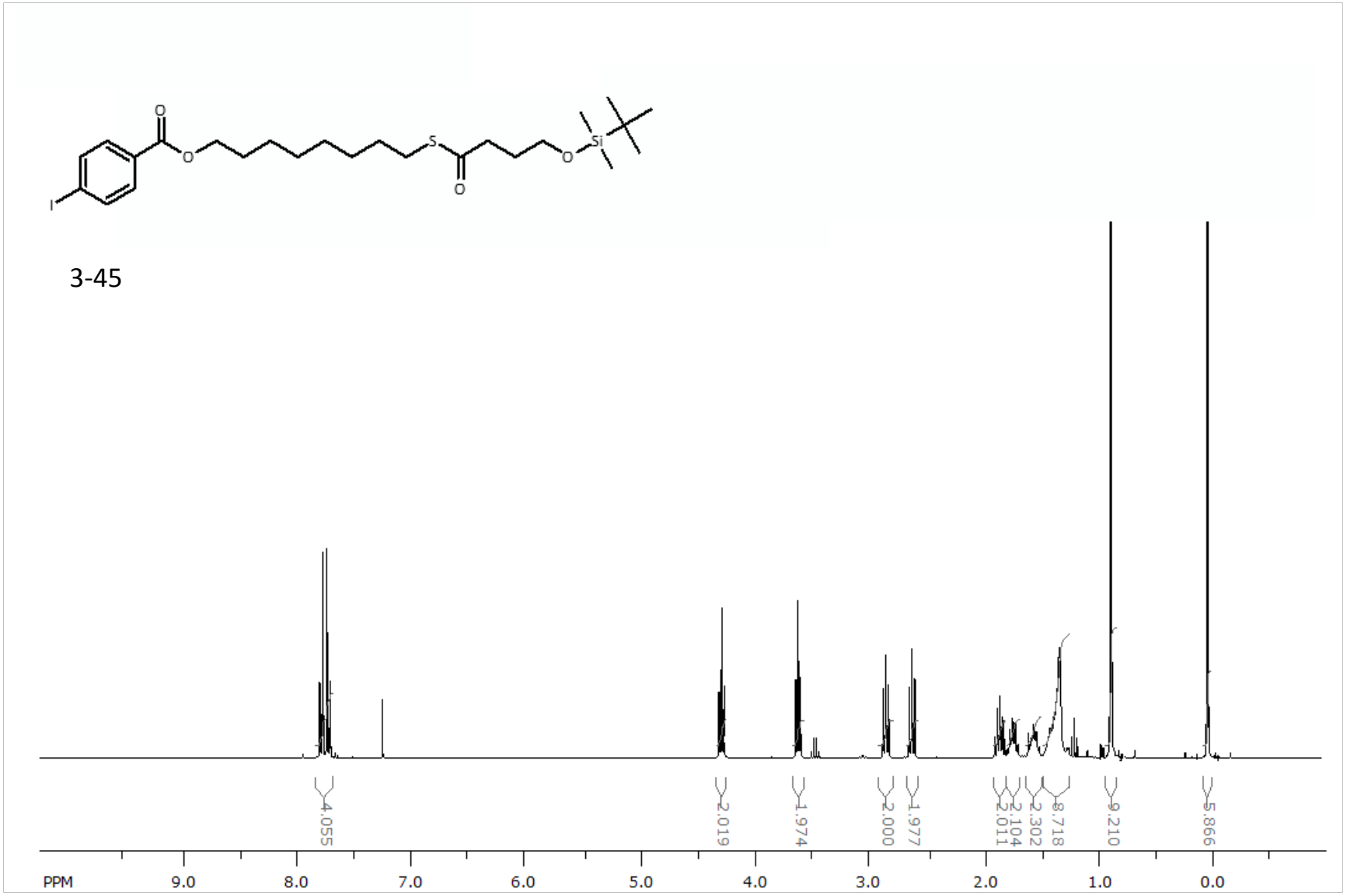
3-45
PPM
9.0
8.0
7.0
6.0
5.0
4.0
3.0
2.0
1.0
0.0
4.055
2.019
1.974
2.000
1.977
2.011
2.104
2.302
8.718
9.210
5.866

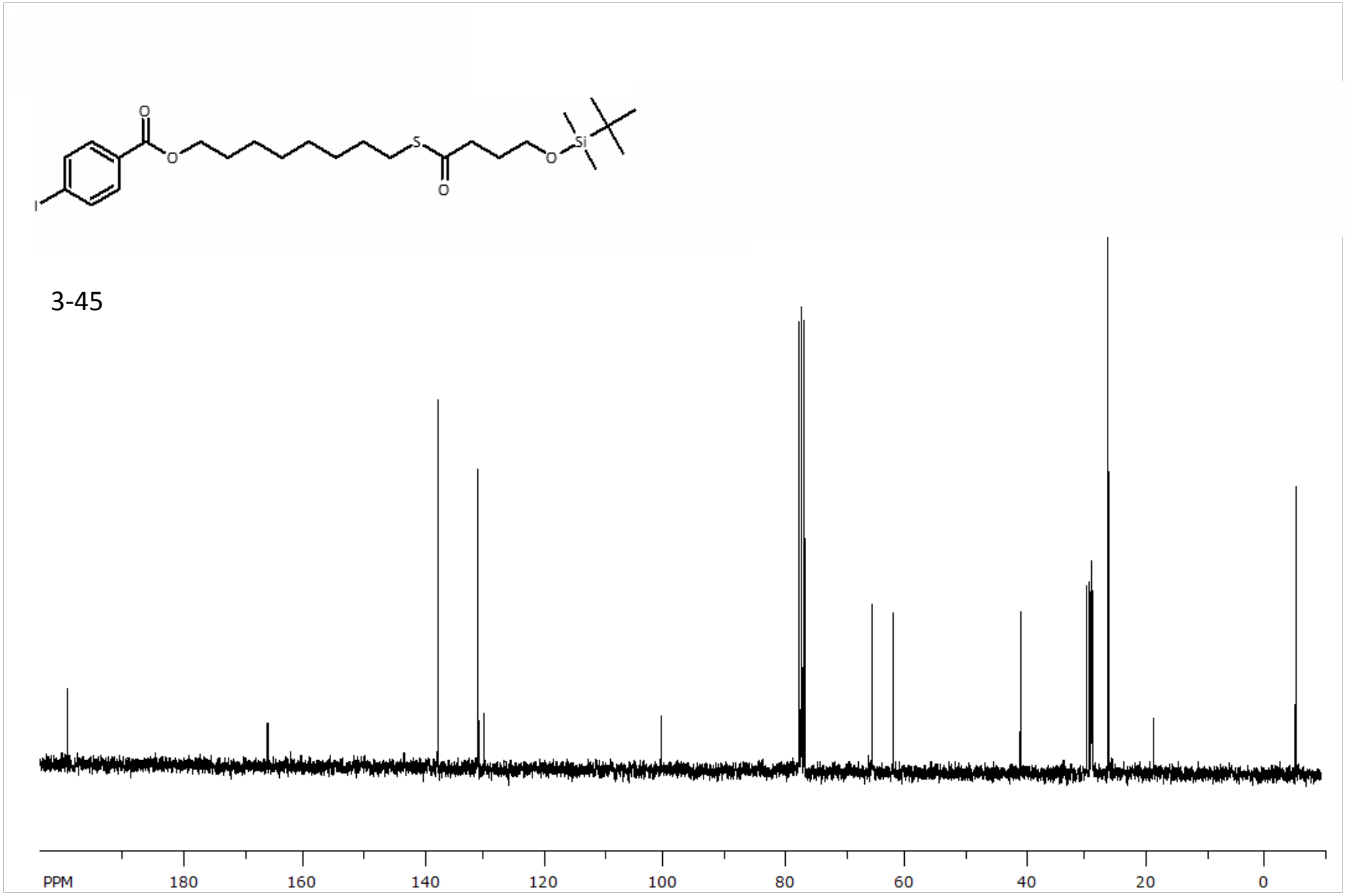
3-45
PPM
180
160
140
120
100
80
60
40
20
0

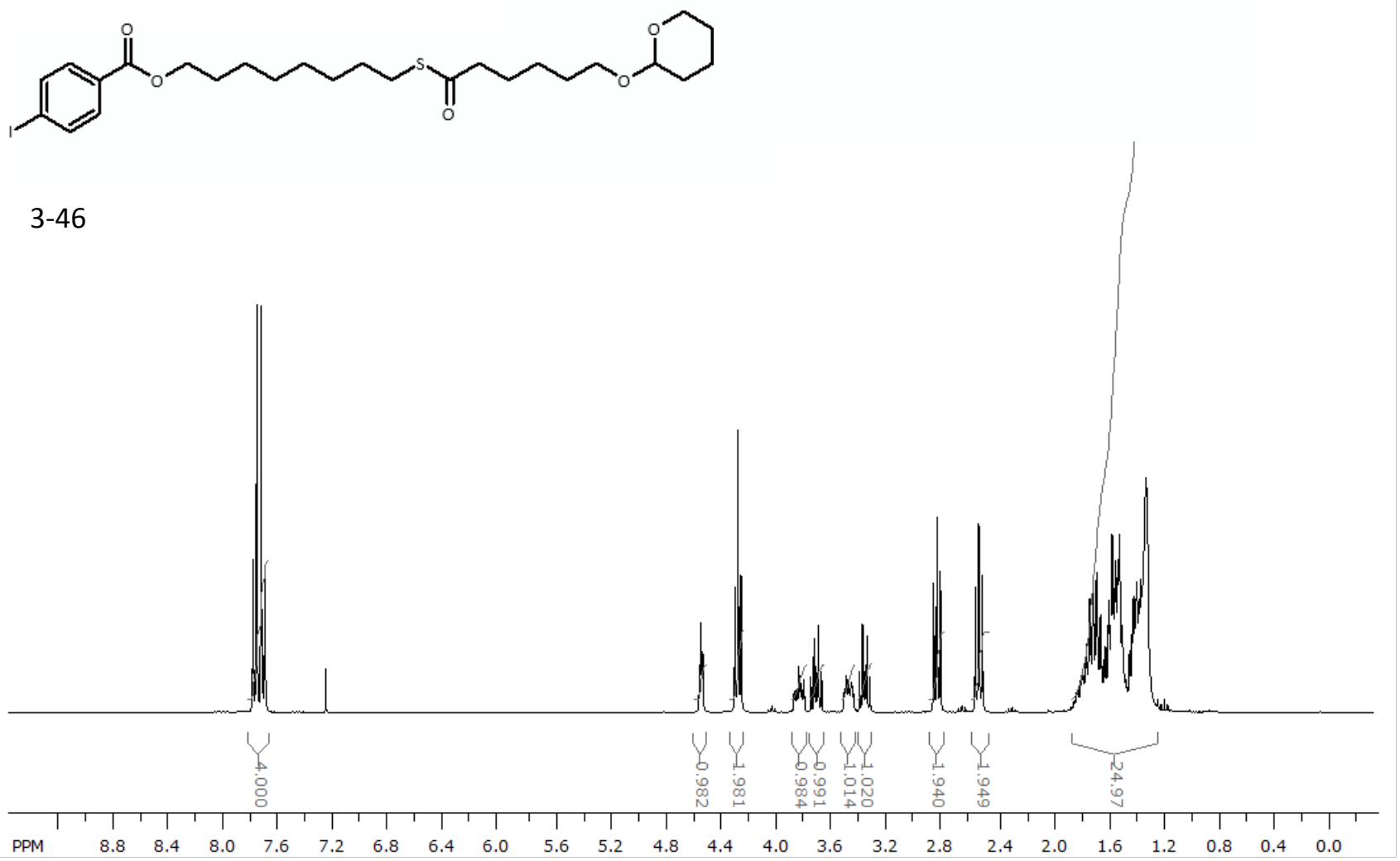
3-46
4.000
0.982
1.981
0.984
0.991
1.014
1.020
1.940
1.949
24.97
PPM
8.8
8.4
8.0
7.6
7.2
6.8
6.4
6.0
5.6
5.2
4.8
4.4
4.0
3.6
3.2
2.8
2.4
2.0
1.6
1.2
0.8
0.4
0.0

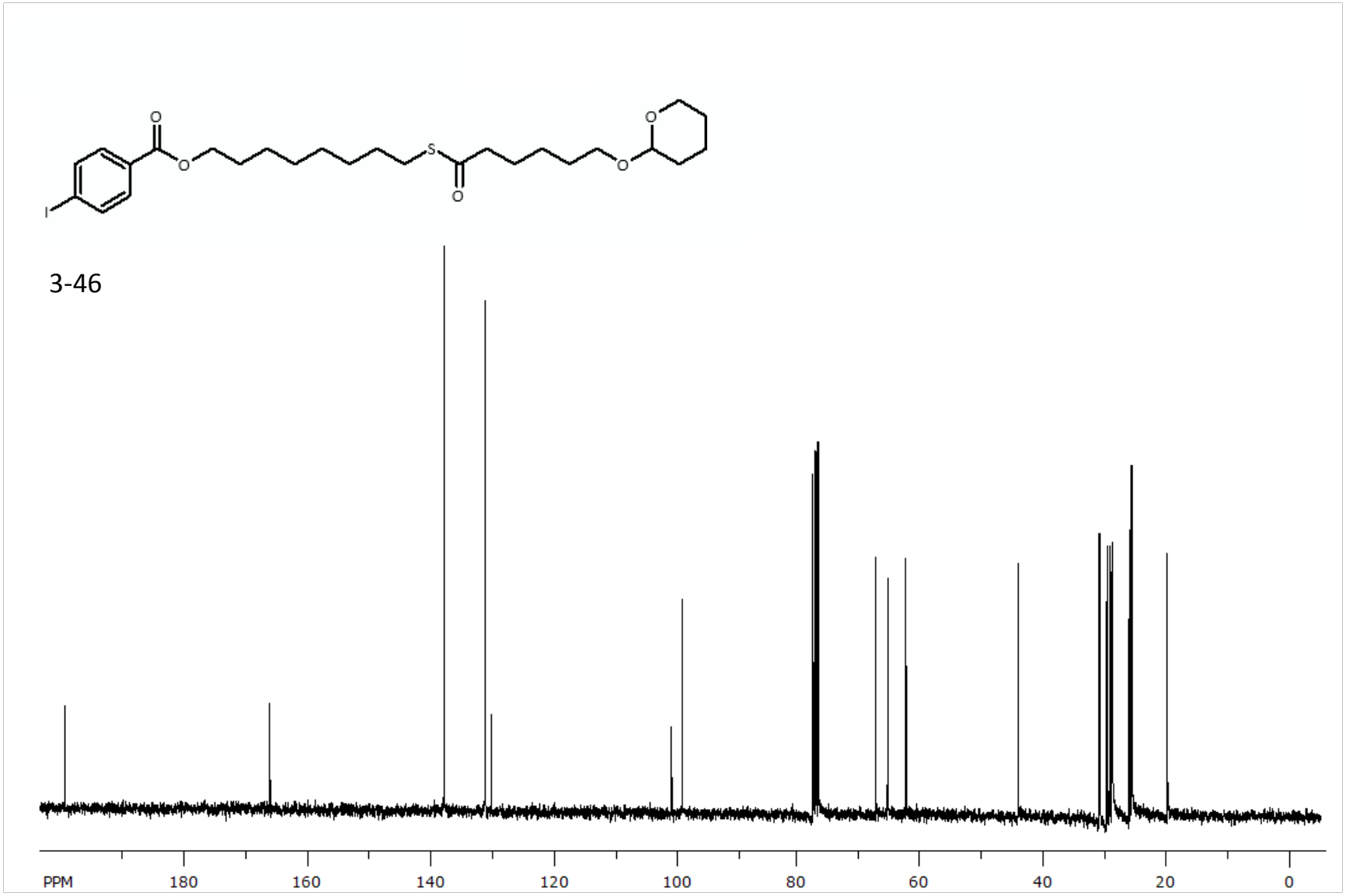
3-46
PPM
180
160
140
120
100
80
60
40
20
0

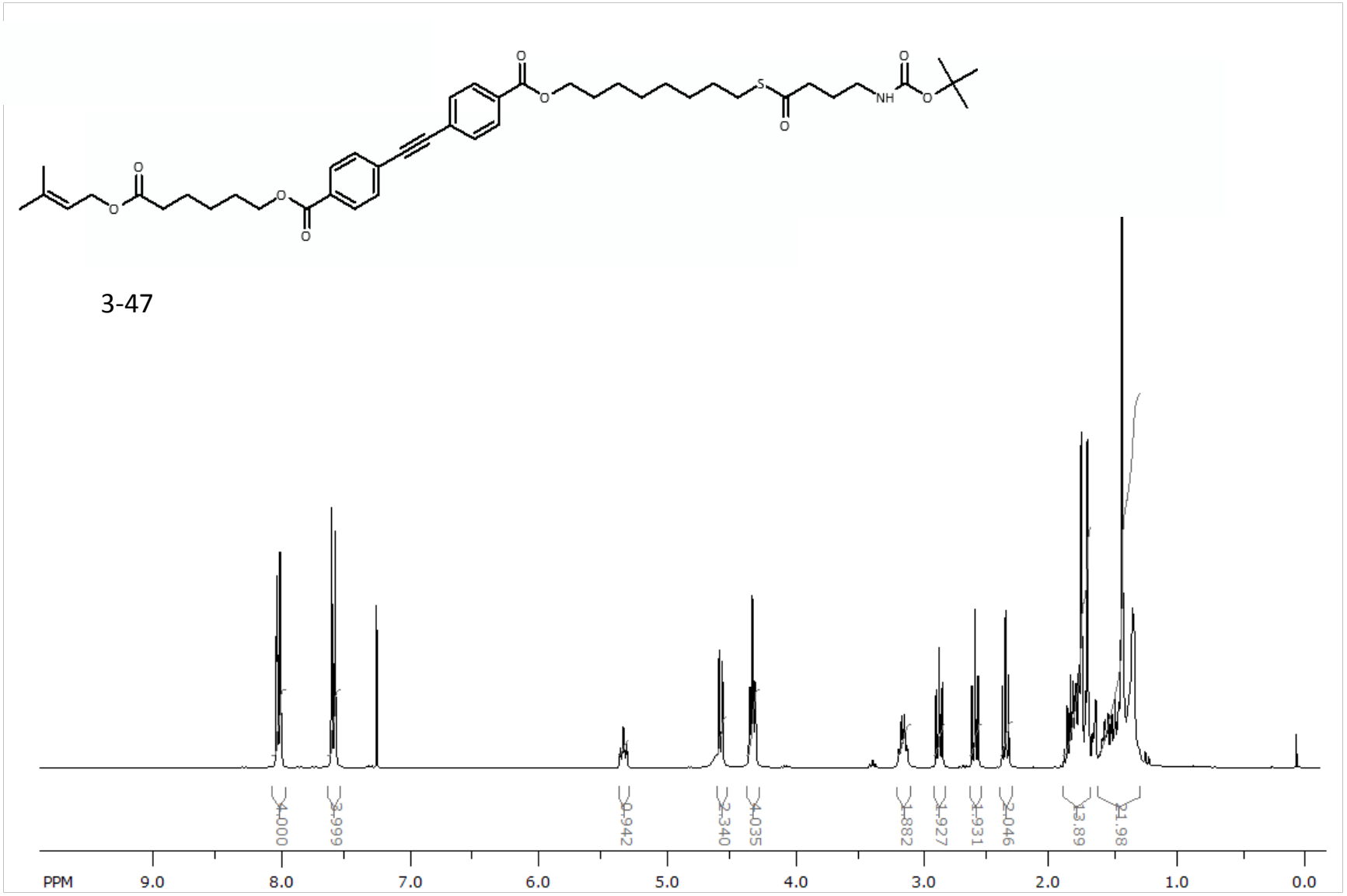
O
O
S
NH
O
O
O
O
O
O
3-47
4.000
3.999
0.942
2.340
4.035
1.882
1.927
1.931
2.046
3.89
1.98
PPM
9.0
8.0
7.0
6.0
5.0
4.0
3.0
2.0
1.0
0.0

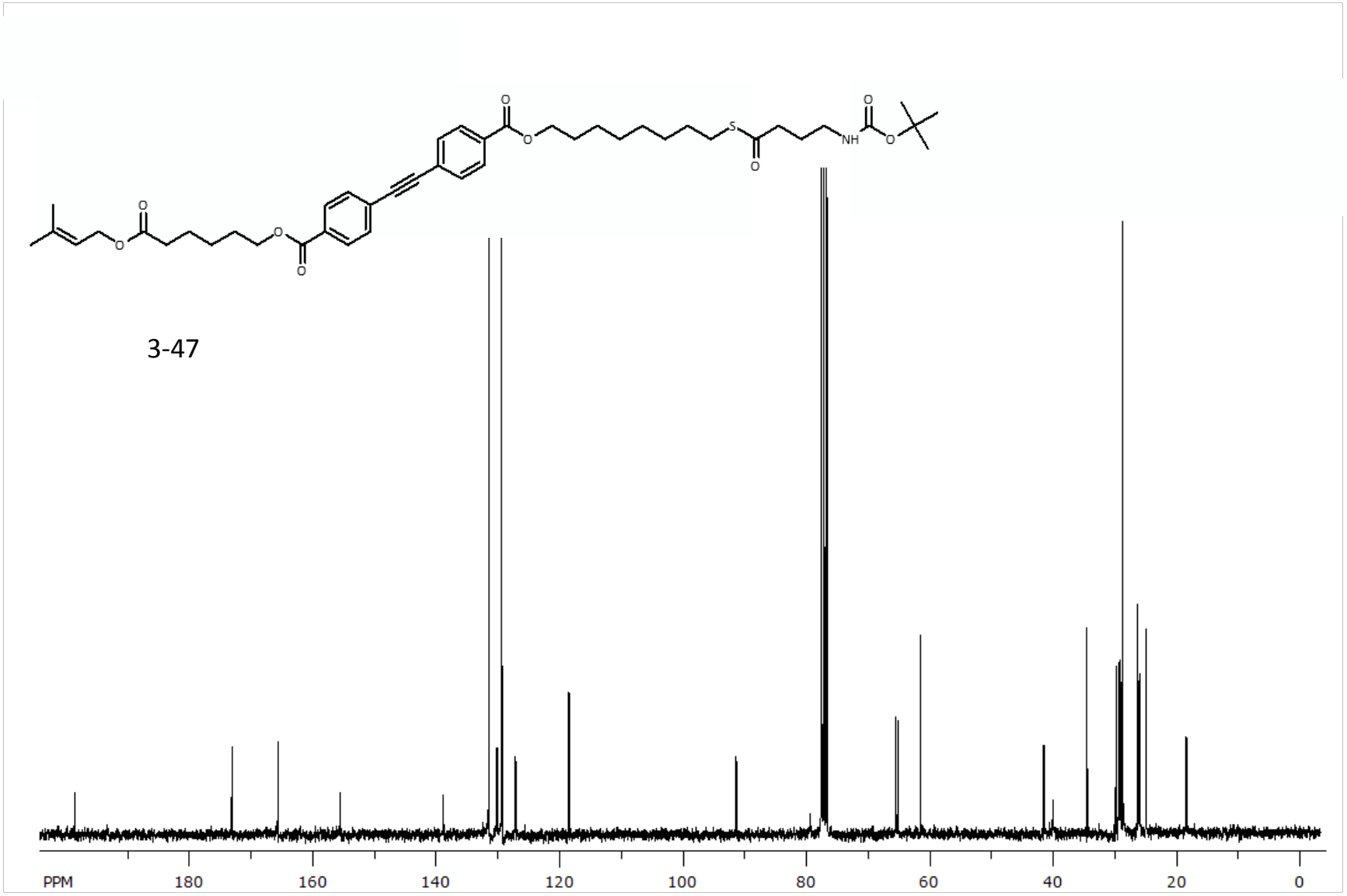
3-47
PPM
180
160
140
120
100
80
60
40
20
0

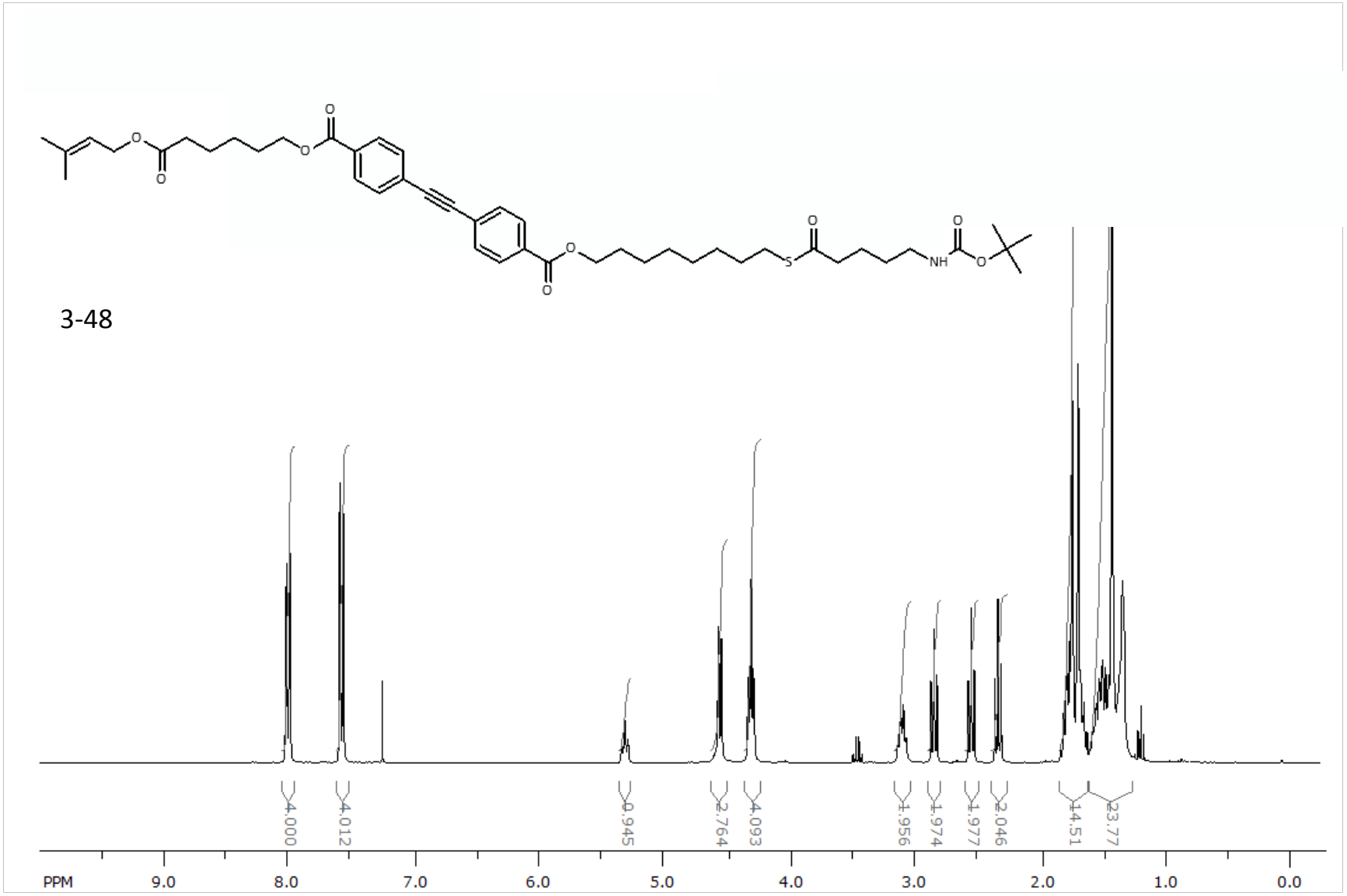
3-48
4.000
4.012
0.945
2.764
4.093
1.956
1.974
1.977
2.046
14.51
23.77
PPM
9.0
8.0
7.0
6.0
5.0
4.0
3.0
2.0
1.0
0.0

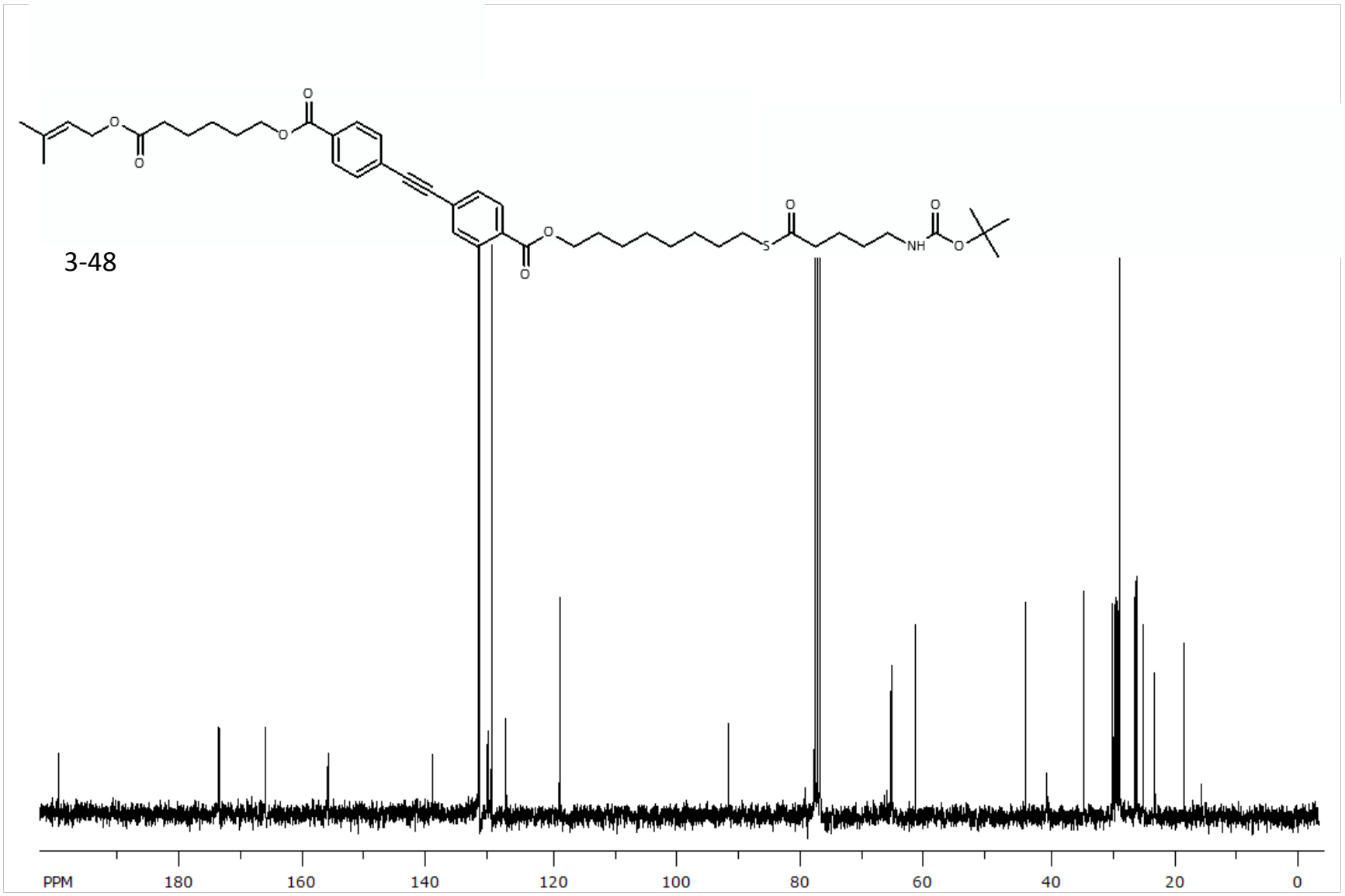
3-48
PPM
180
160
140
120
100
80
60
40
20
0

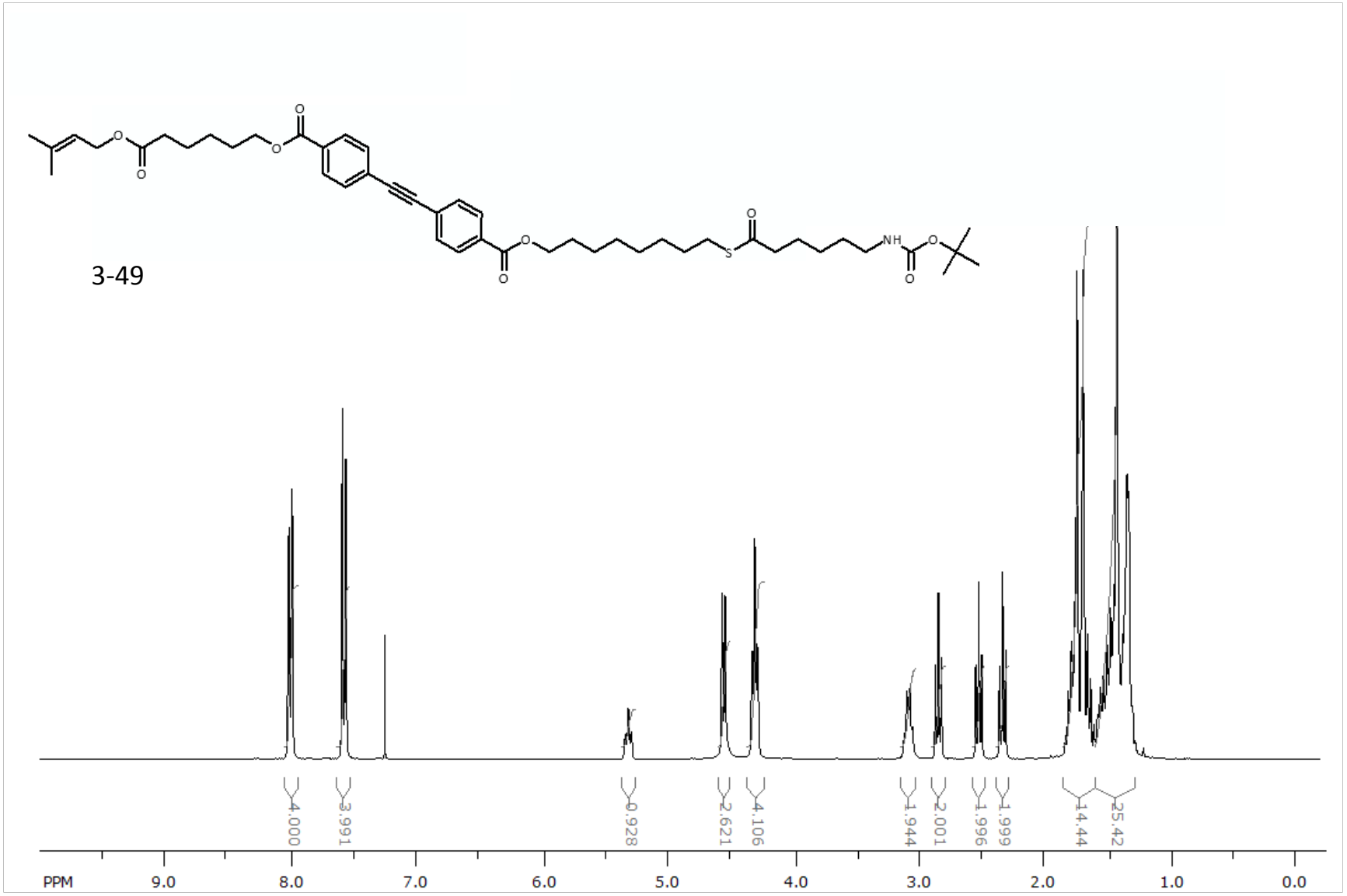
3-49
4.000
3.991
0.928
2.621
4.106
1.944
2.001
1.996
1.999
14.44
25.42
PPM
9.0
8.0
7.0
6.0
5.0
4.0
3.0
2.0
1.0
0.0

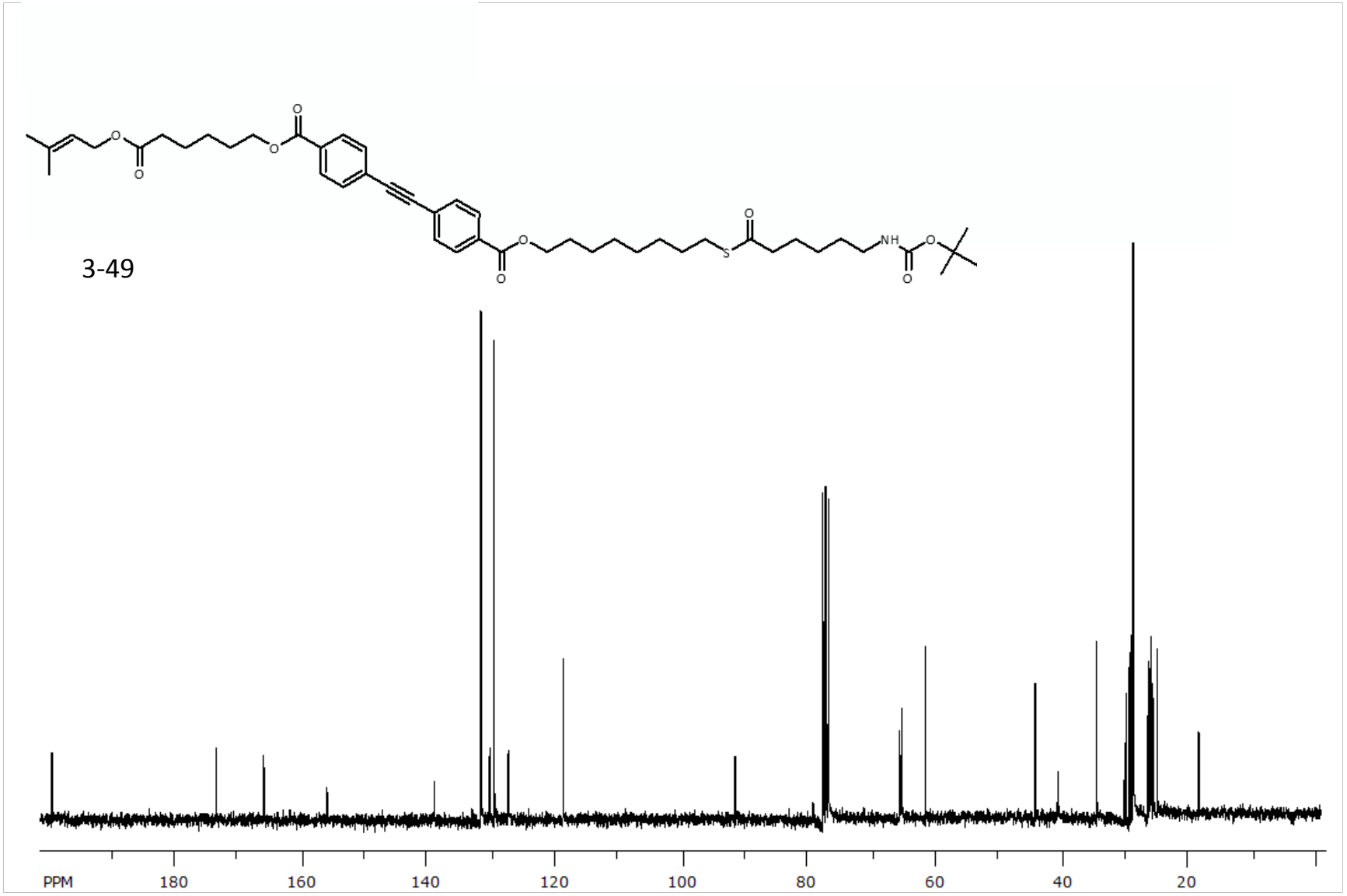
3-49
PPM
180
160
140
120
100
80
60
40
20

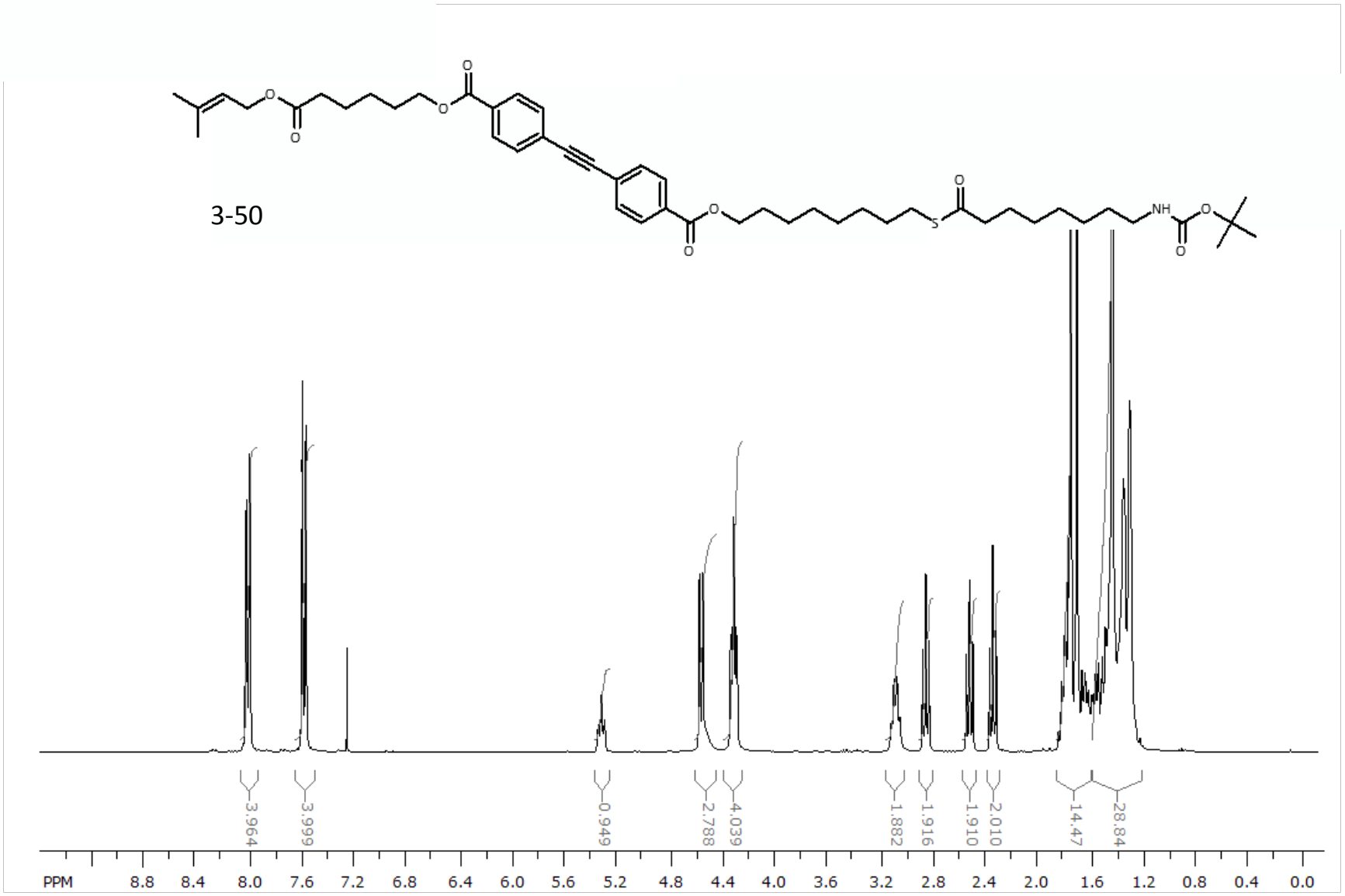
3-50
O
O
O
O
O
O
O
O
S
NH
O
O
3.964
3.999
0.949
2.788
4.039
1.882
1.916
1.910
2.010
14.47
28.84
PPM
8.8
8.4
8.0
7.6
7.2
6.8
6.4
6.0
5.6
5.2
4.8
4.4
4.0
3.6
3.2
2.8
2.4
2.0
1.6
1.2
0.8
0.4
0.0

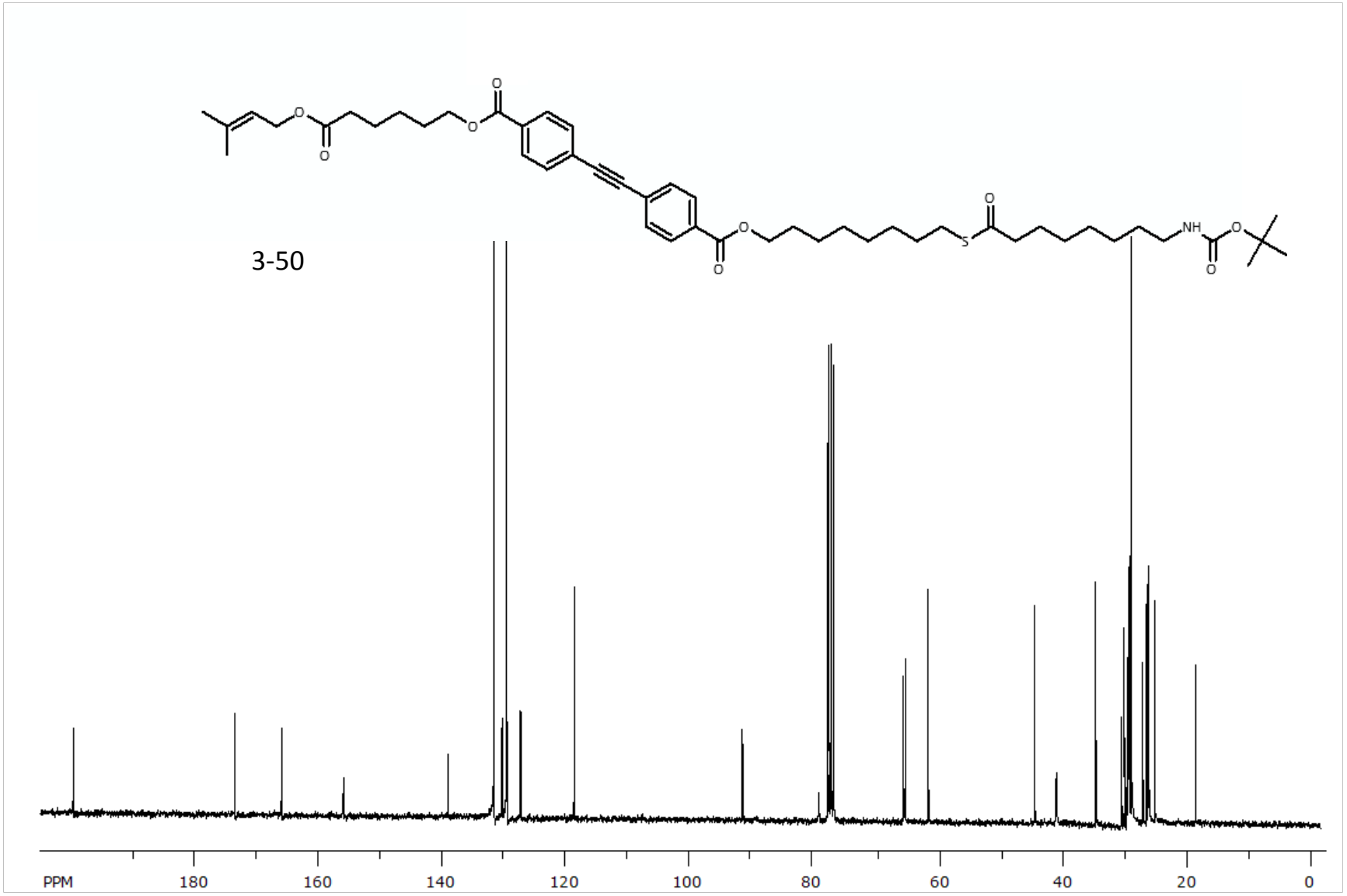
3-50
PPM
180
160
140
120
100
80
60
40
20
0

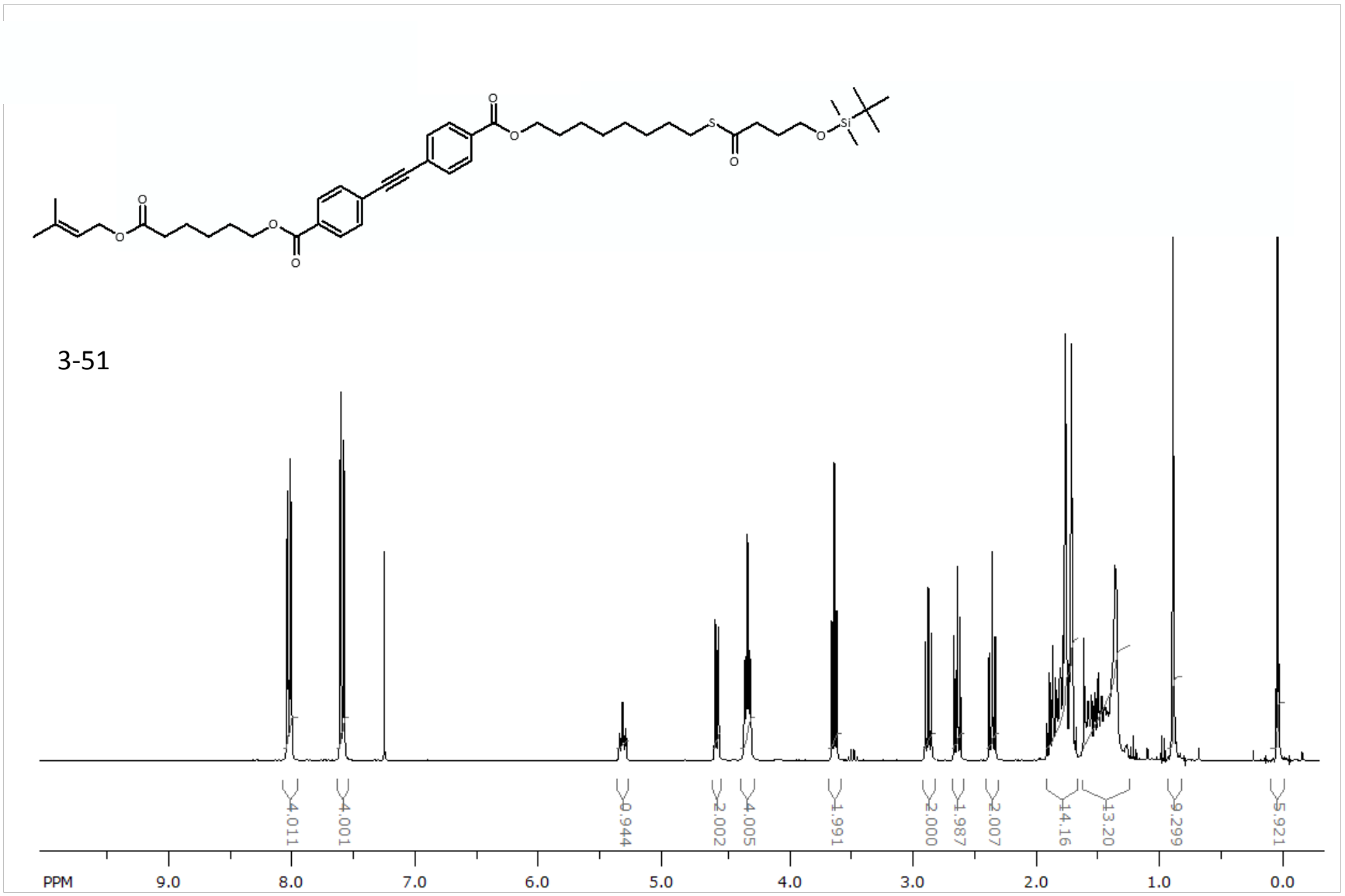
3-51
4.011
4.001
0.944
2.002
4.005
1.991
2.000
1.987
2.007
14.16
13.20
9.299
5.921
PPM
9.0
8.0
7.0
6.0
5.0
4.0
3.0
2.0
1.0
0.0

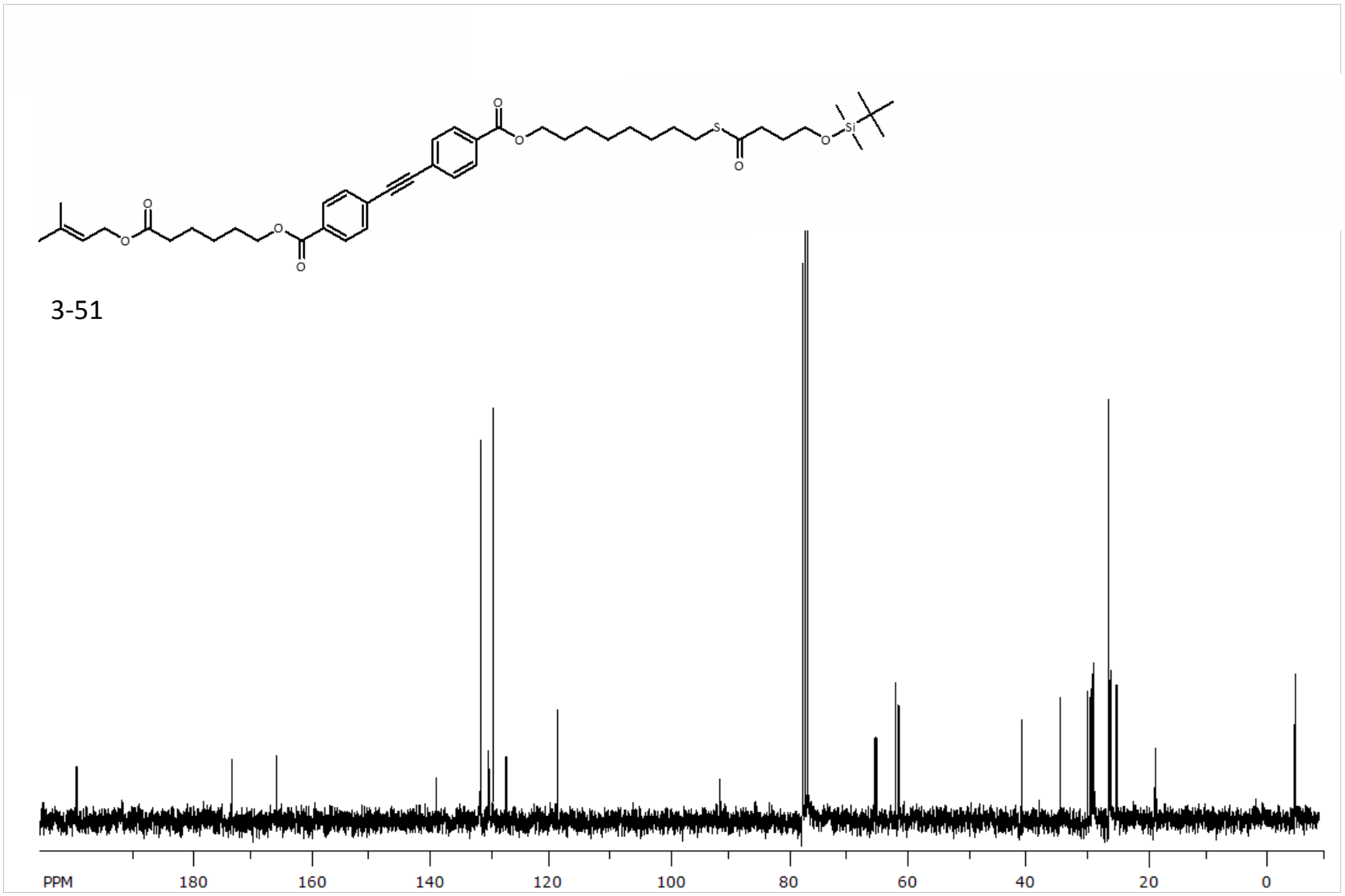
3-51
PPM
180
160
140
120
100
80
60
40
20
0

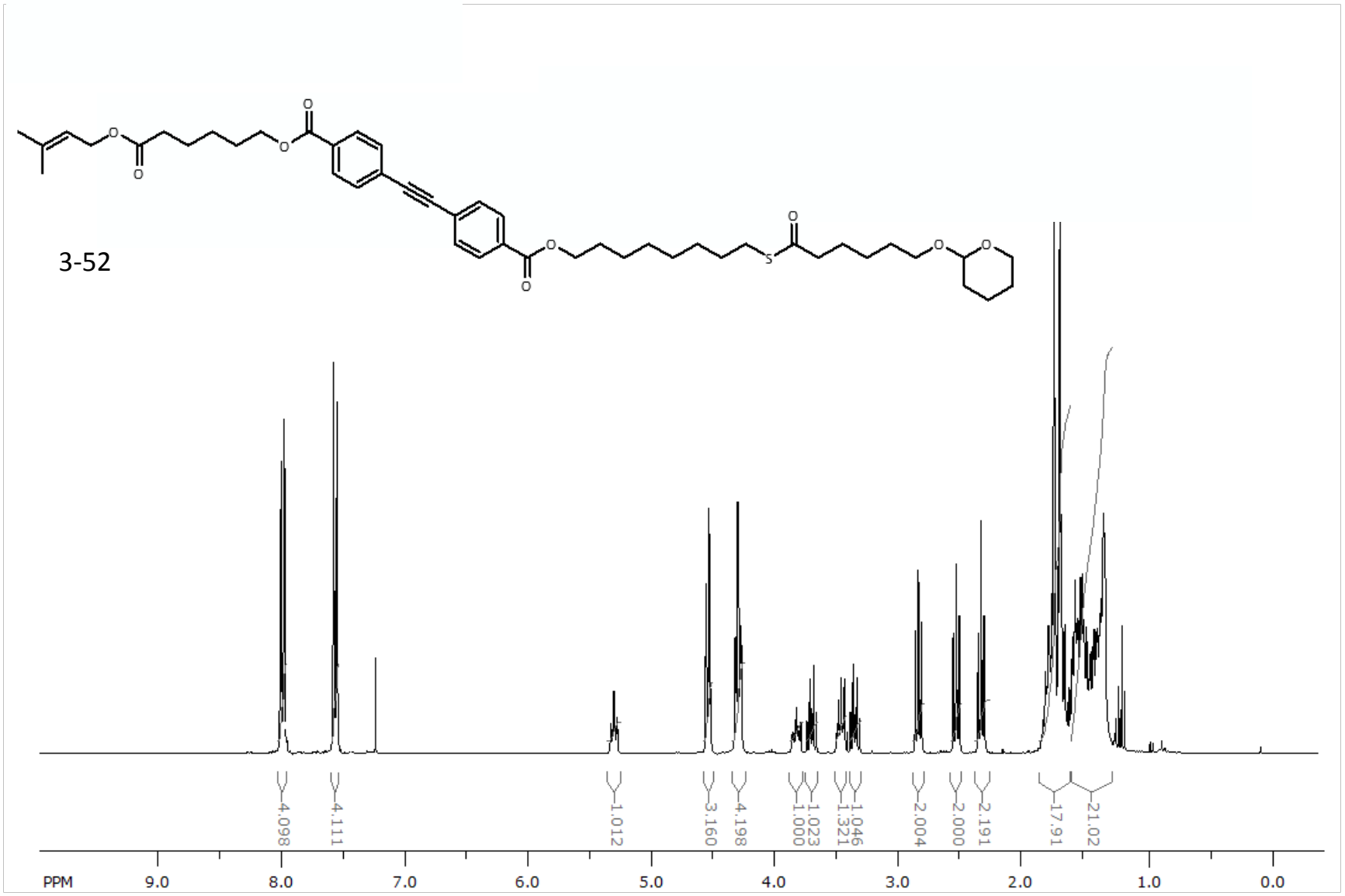
3-52
4.098
4.111
1.012
3.160
4.198
1.000
1.023
1.321
1.046
2.004
2.000
2.191
17.91
21.02
PPM
9.0
8.0
7.0
6.0
5.0
4.0
3.0
2.0
1.0
0.0

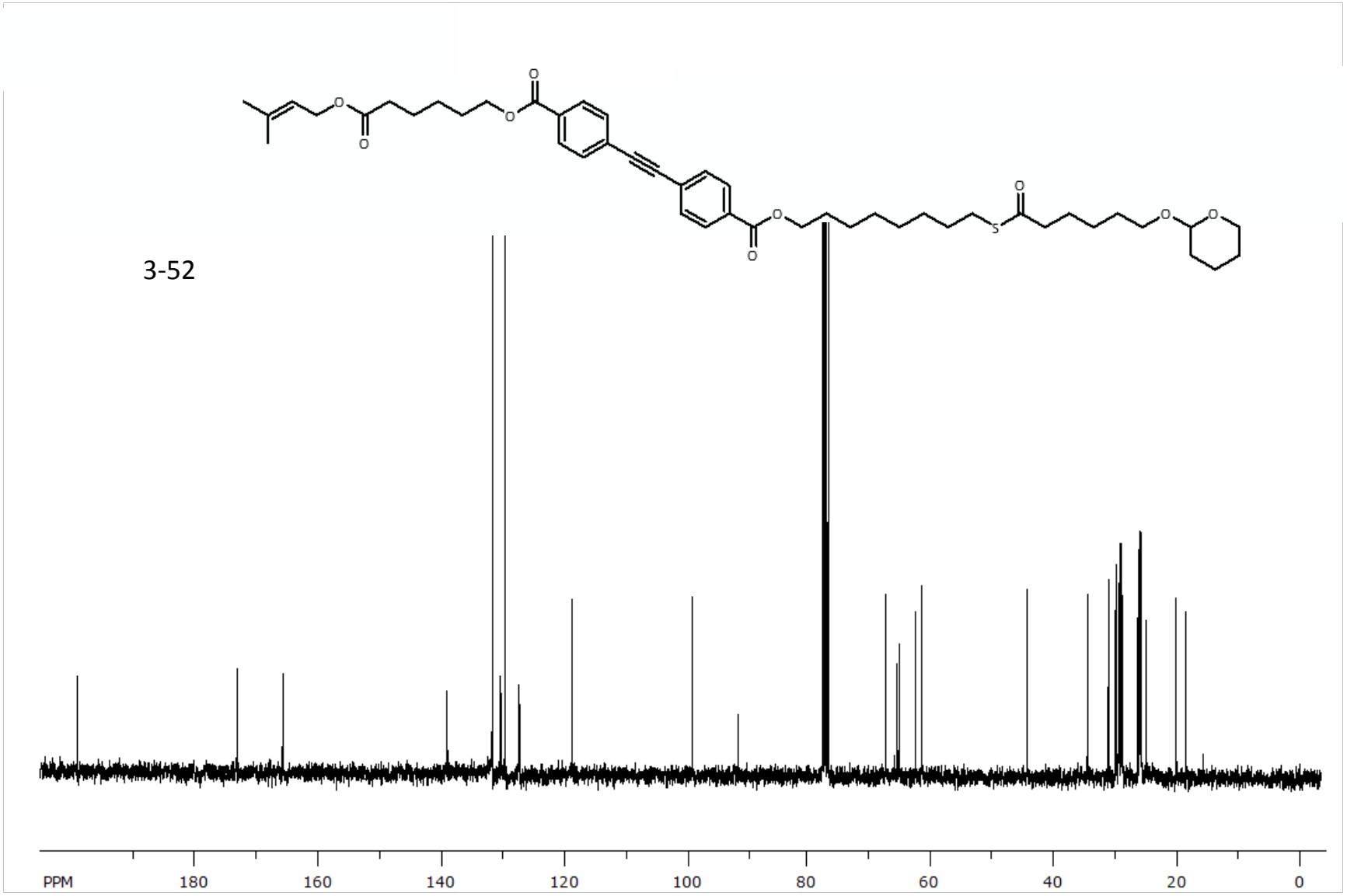
3-52
PPM
180
160
140
120
100
80
60
40
20
0

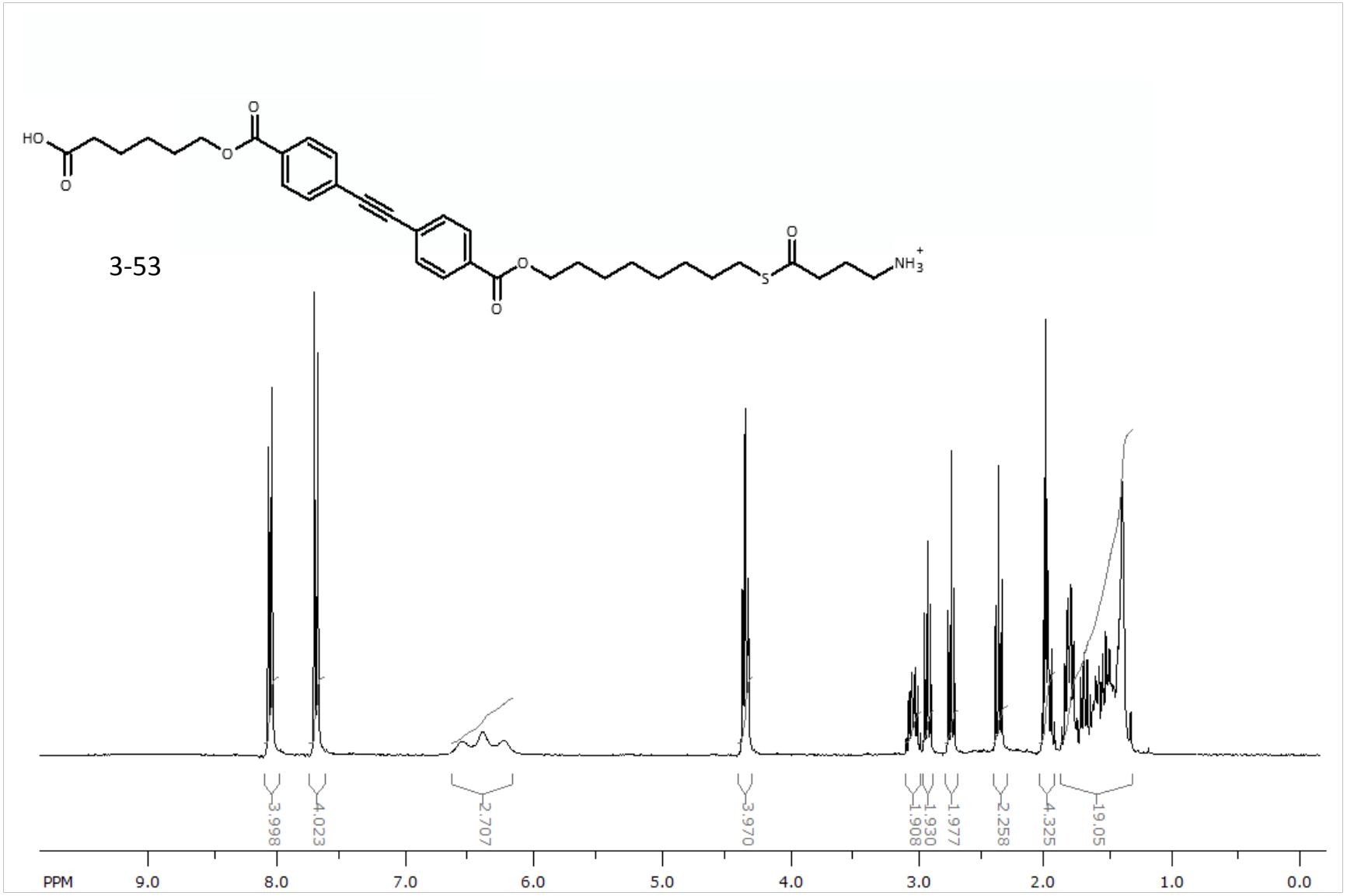
3-53
HO
O
O
O
O
O
O
O
S
NH3+
3.998
4.023
2.707
3.970
1.908
1.930
1.977
2.258
4.325
19.05
PPM
9.0
8.0
7.0
6.0
5.0
4.0
3.0
2.0
1.0
0.0

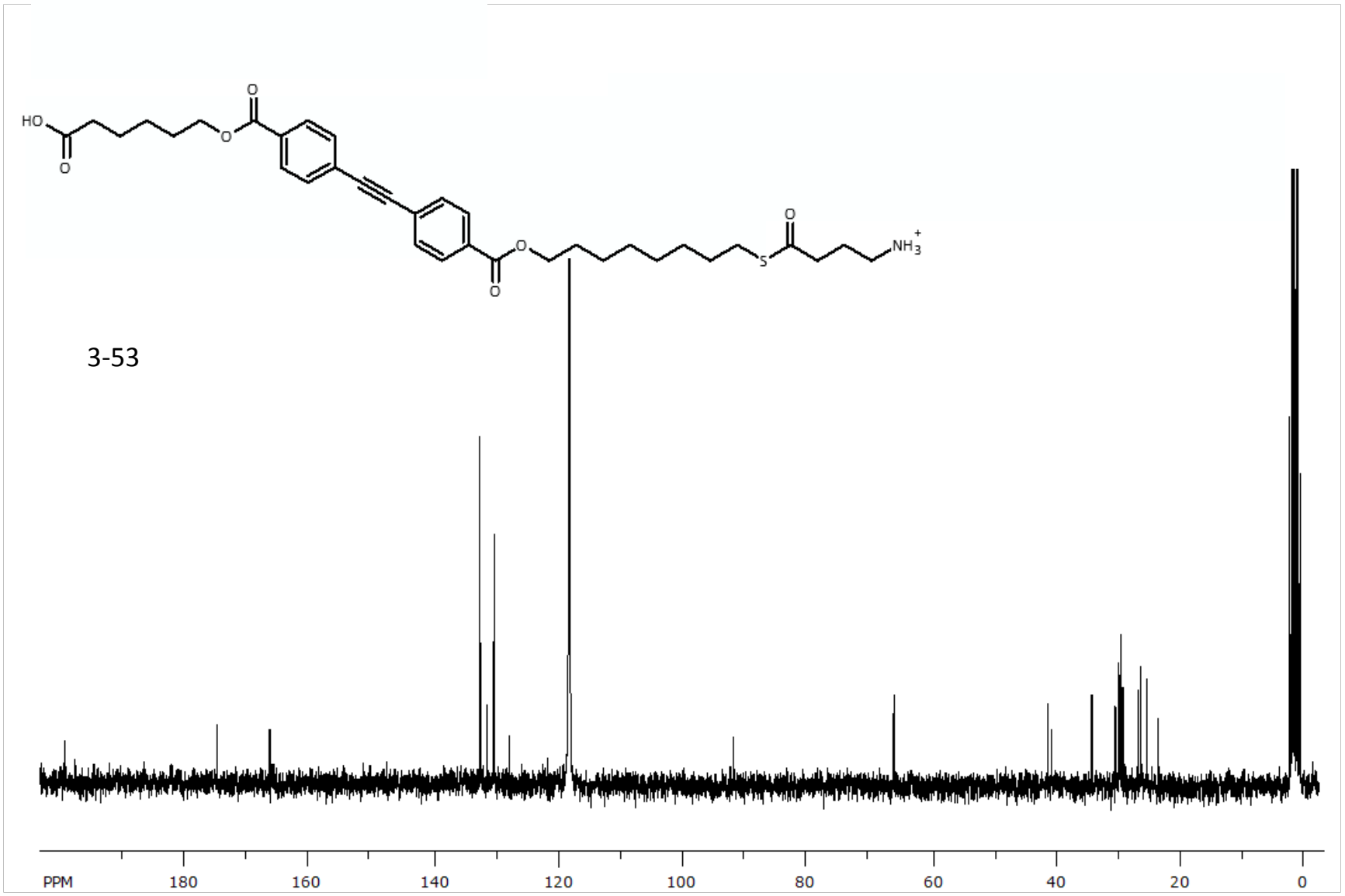
HO
O
O
O
O
O
O
O
S
NH3+
3-53
PPM
180
160
140
120
100
80
60
40
20
0

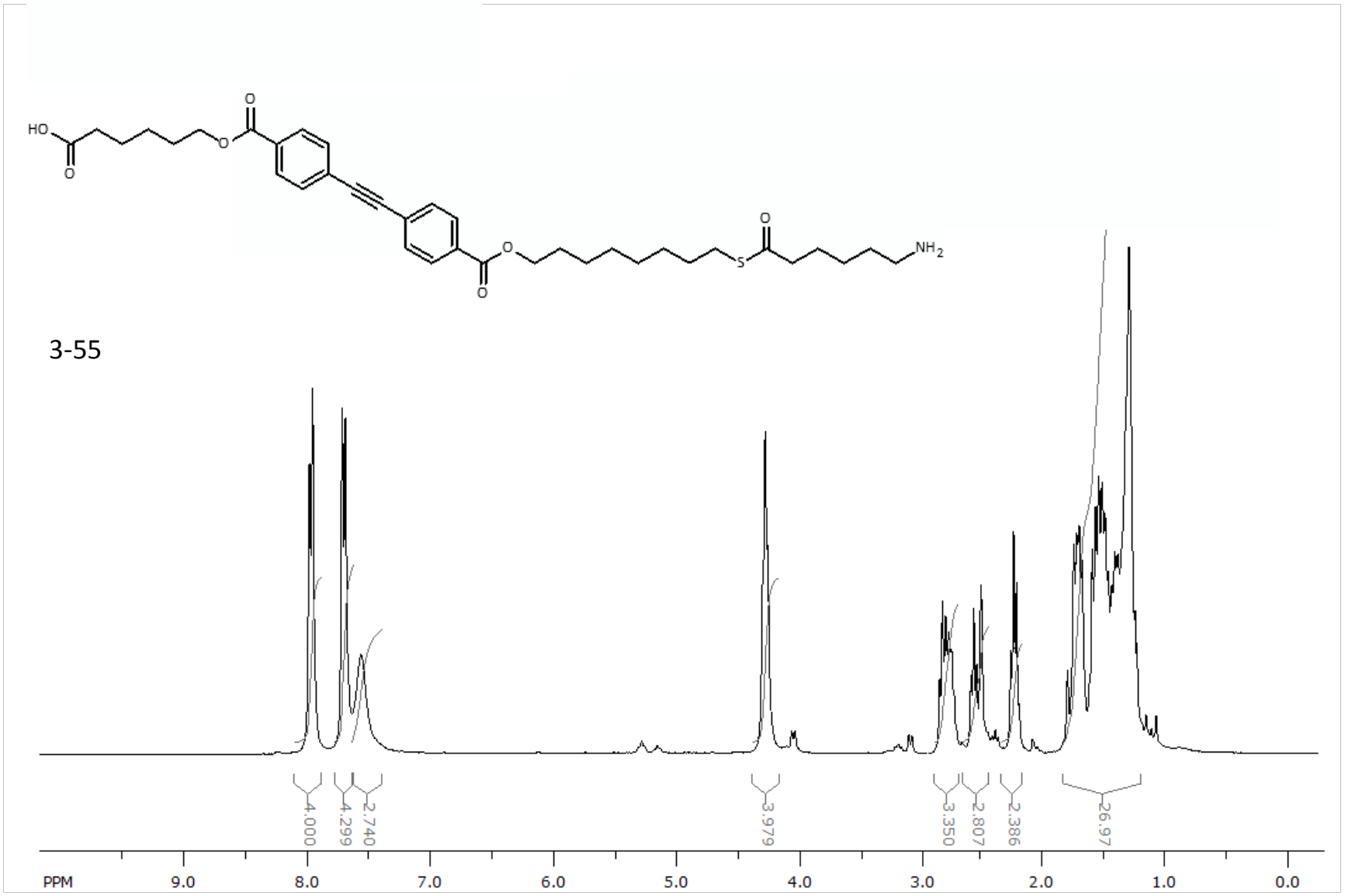
HO
O
O
O
O
O
O
O
S
NH2
3-55
4.000
4.299
2.740
3.979
3.350
2.807
2.386
26.97
PPM
9.0
8.0
7.0
6.0
5.0
4.0
3.0
2.0
1.0
0.0

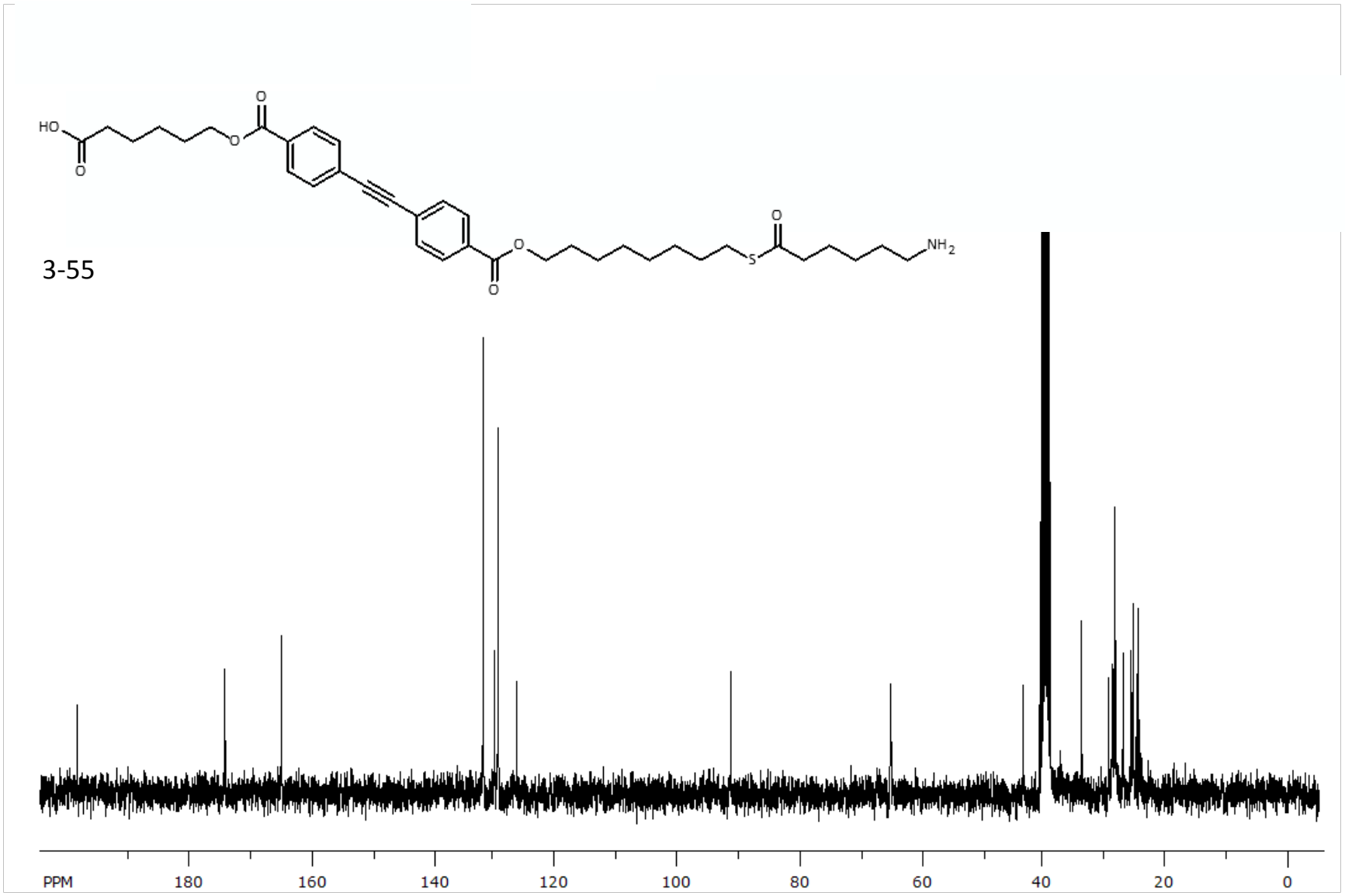
HO
O
O
O
O
O
O
O
S
NH2
3-55
PPM
180
160
140
120
100
80
60
40
20
0

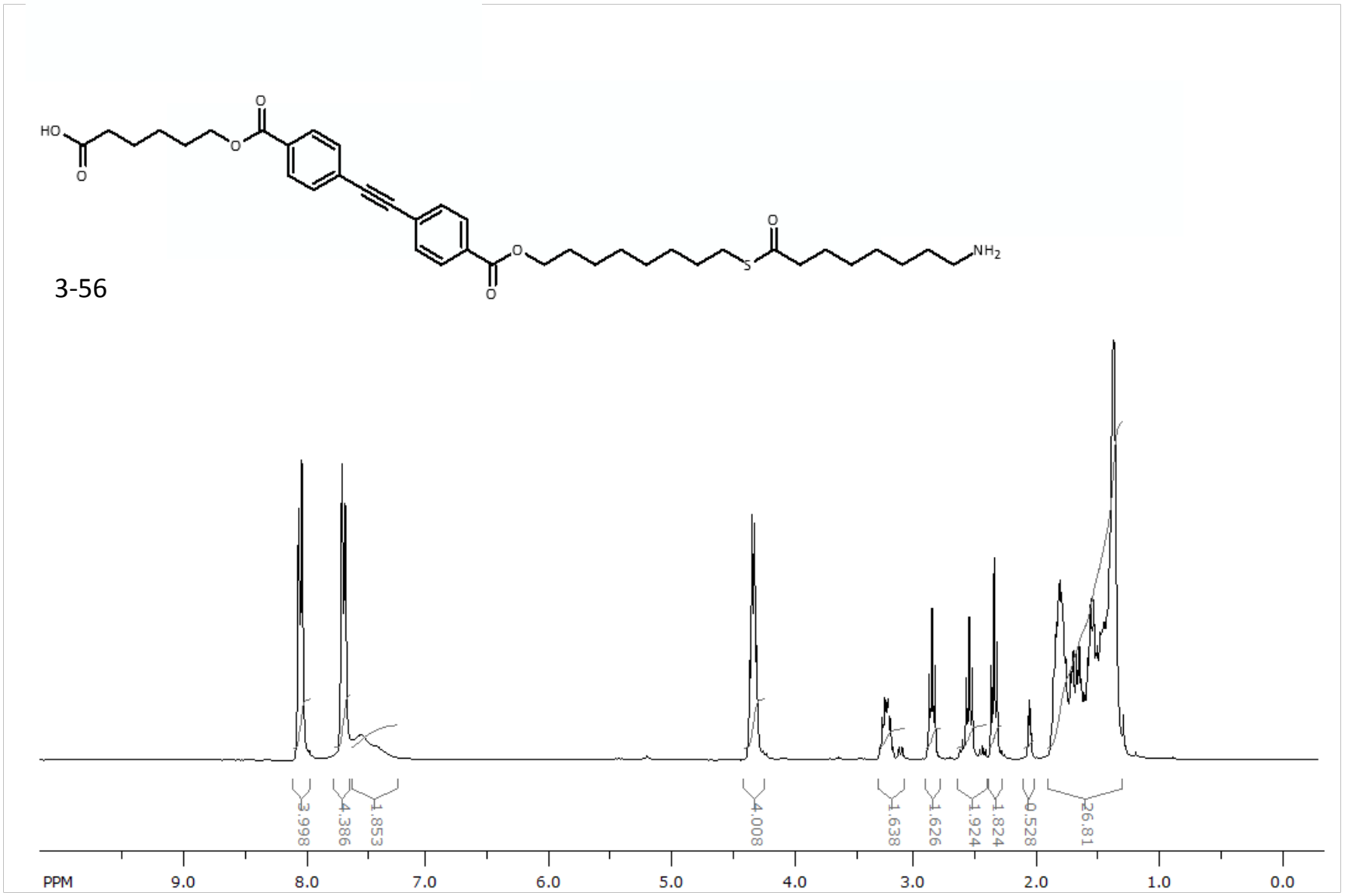
HO
O
O
O
O
O
O
S
NH2
3-56
3.998
4.386
1.853
4.008
1.638
1.626
1.924
1.824
0.528
26.81
PPM
9.0
8.0
7.0
6.0
5.0
4.0
3.0
2.0
1.0
0.0

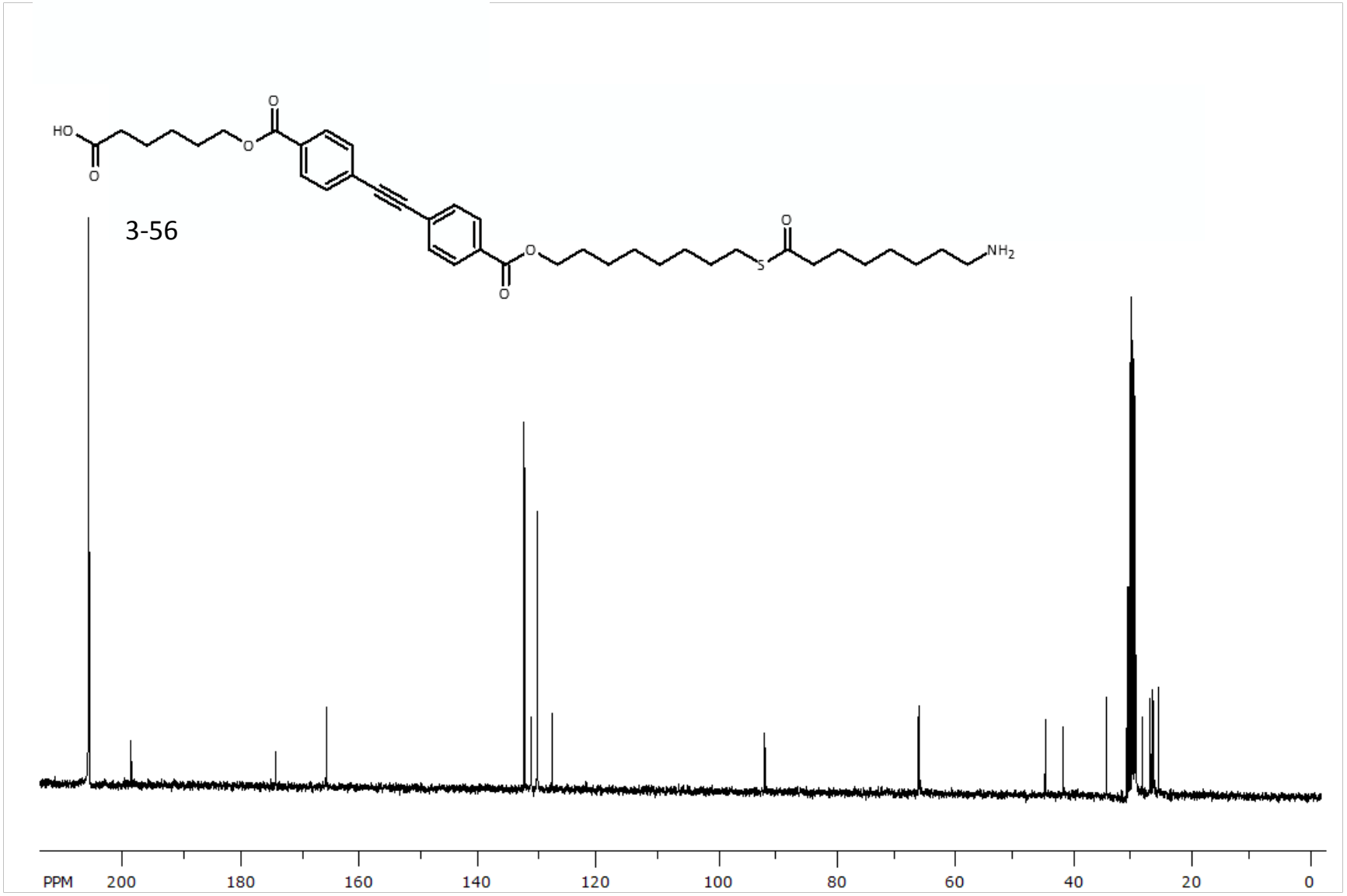
3-56
HO
O
O
O
O
O
O
O
S
NH2
PPM
200
180
160
140
120
100
80
60
40
20
0

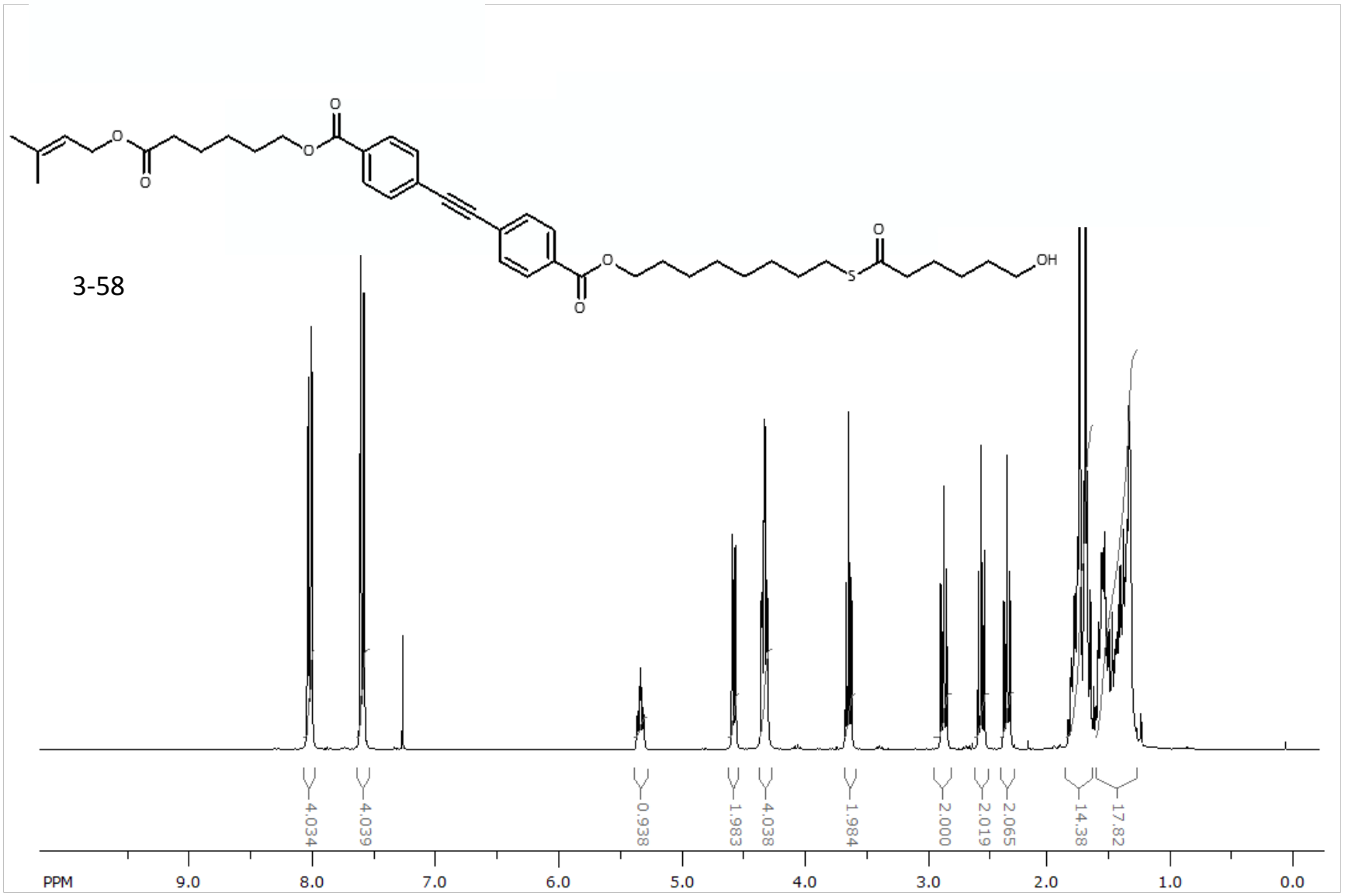
3-58
O
O
O
O
O
O
O
O
S
OH
4.034
4.039
0.938
1.983
4.038
1.984
2.000
2.019
2.065
14.38
17.82
PPM
9.0
8.0
7.0
6.0
5.0
4.0
3.0
2.0
1.0
0.0

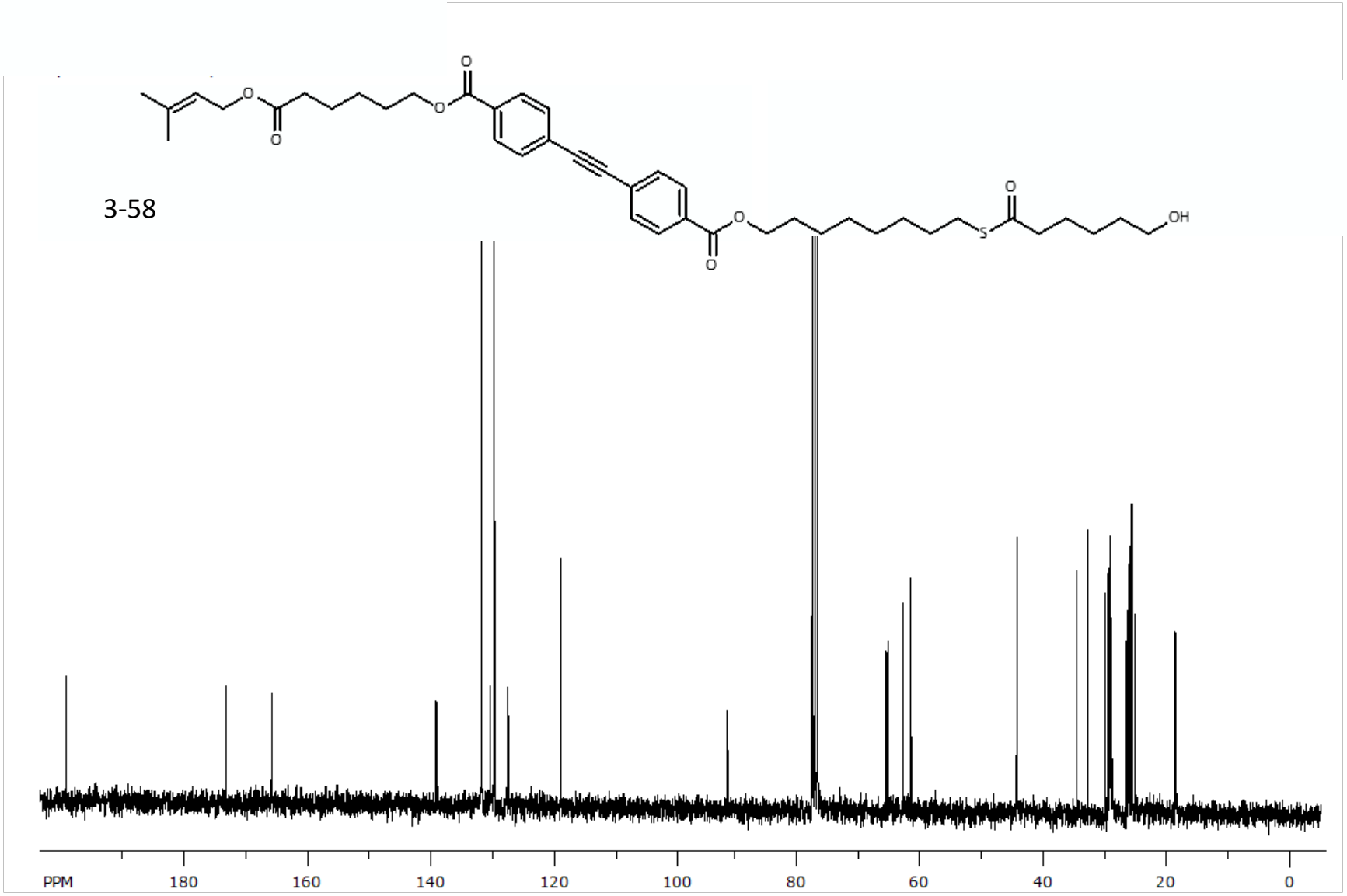
3-58
O
O
O
O
O
O
O
S
OH
PPM
180
160
140
120
100
80
60
40
20
0

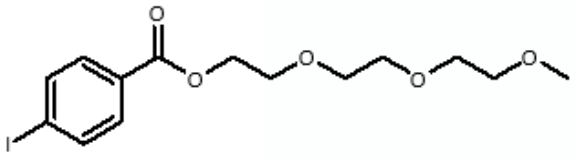

3-61

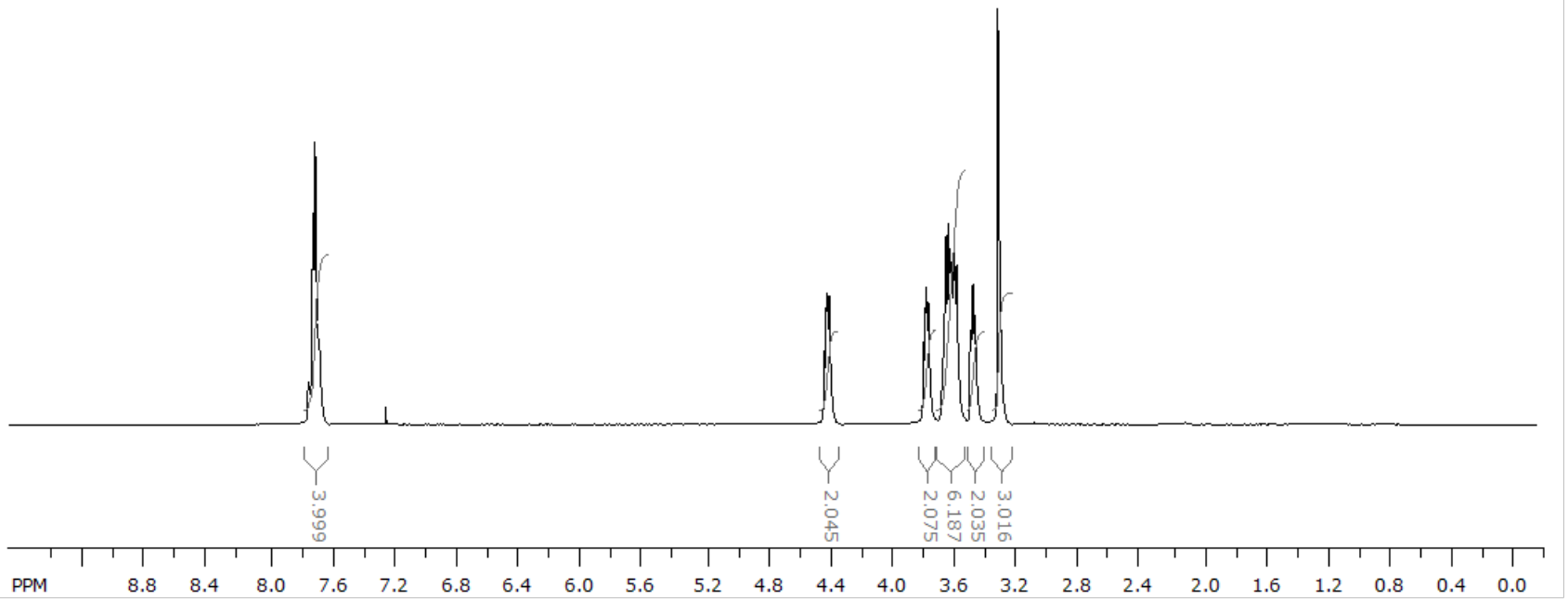
3.999
2.045
2.075
6.187
2.035
3.016
PPM
8.8
8.4
8.0
7.6
7.2
6.8
6.4
6.0
5.6
5.2
4.8
4.4
4.0
3.6
3.2
2.8
2.4
2.0
1.6
1.2
0.8
0.4
0.0

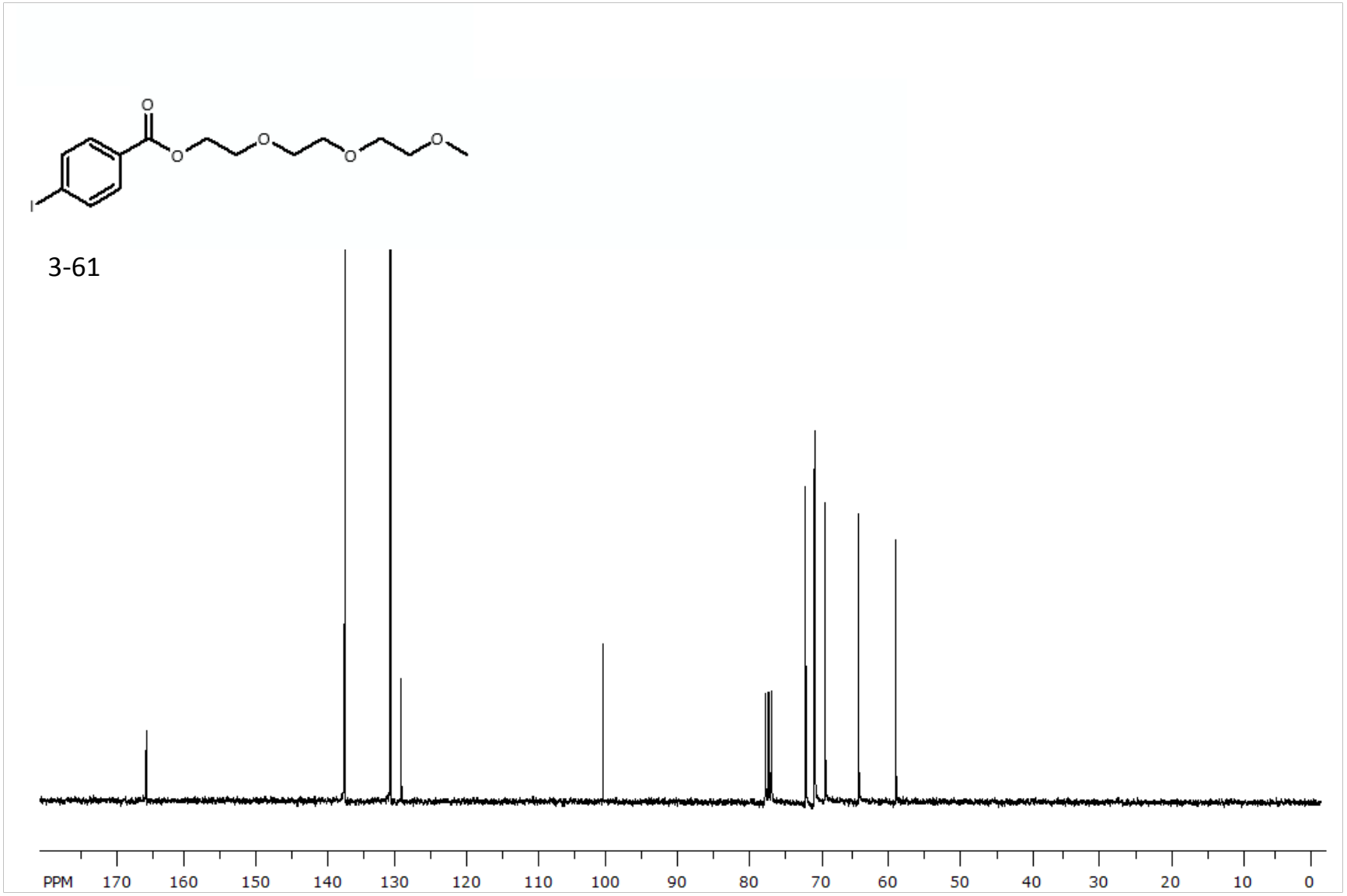
3-61
PPM
170
160
150
140
130
120
110
100
90
80
70
60
50
40
30
20
10
0

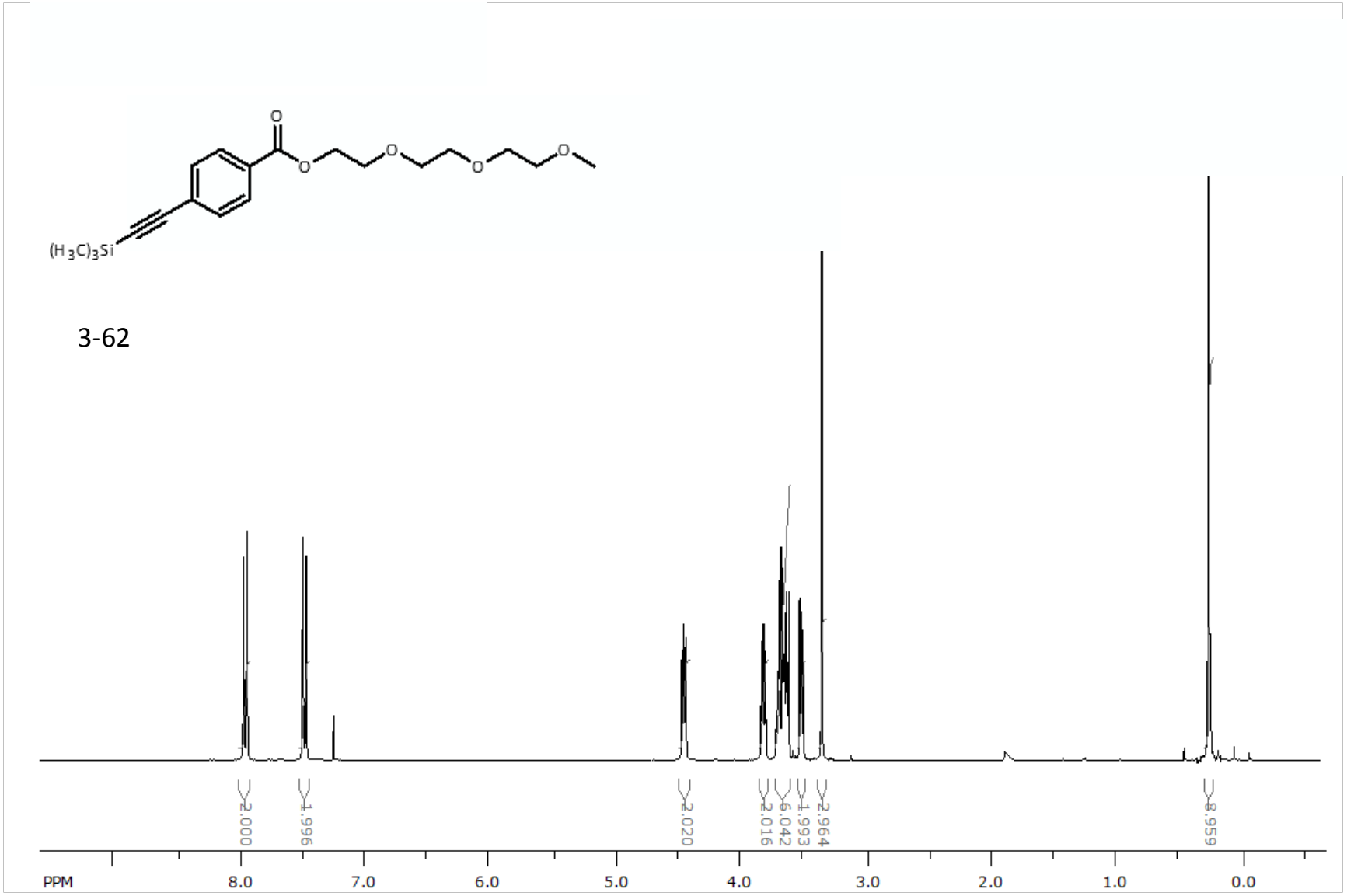
O
O
O
O
O
O
(H3C)3Si
3-62
2.000
1.996
2.020
2.016
6.042
1.993
2.964
8.959
PPM
8.0
7.0
6.0
5.0
4.0
3.0
2.0
1.0
0.0

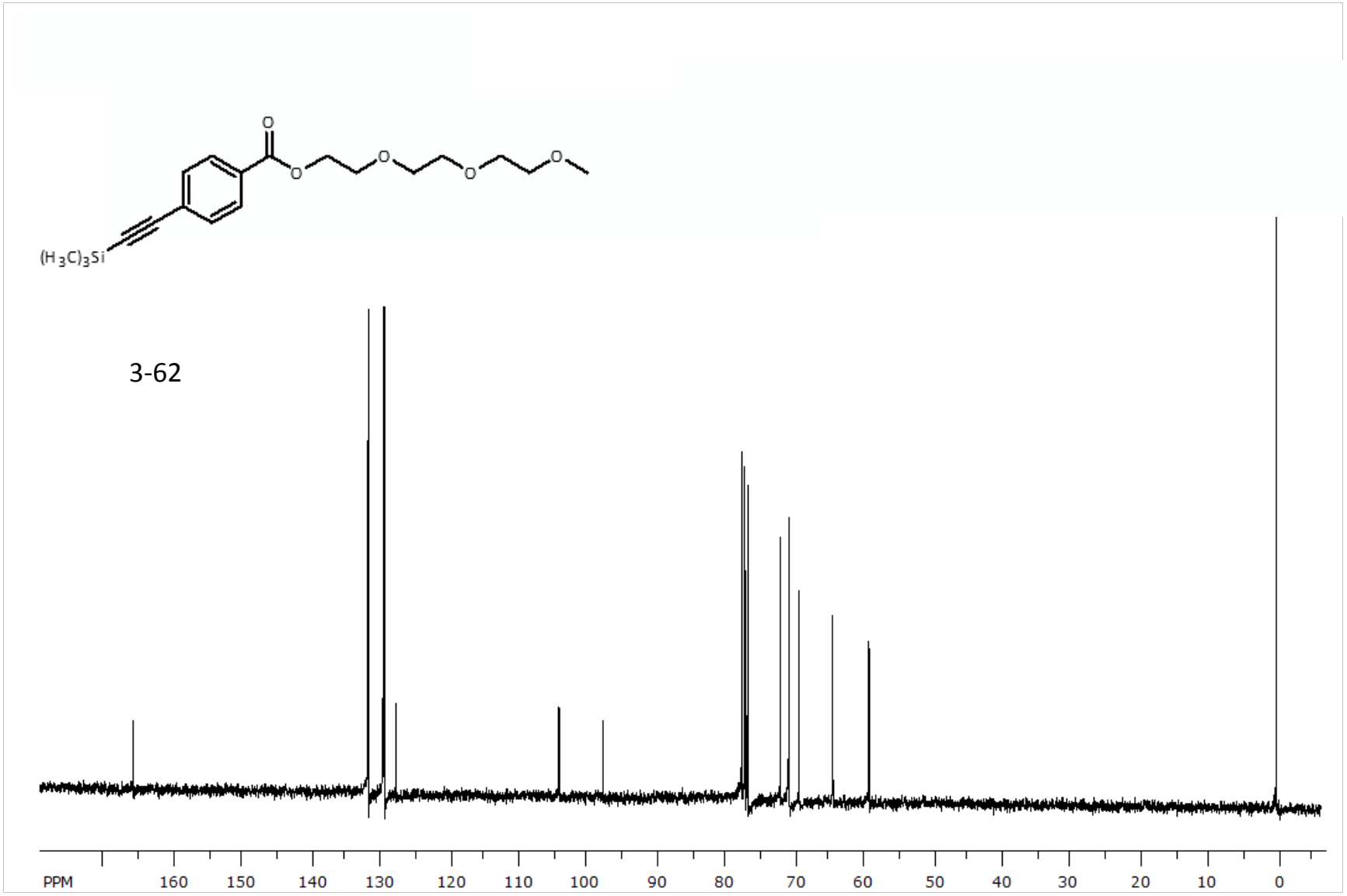
O
O
O
O
O
(H3C)3Si
3-62
PPM
160
150
140
130
120
110
100
90
80
70
60
50
40
30
20
10
0

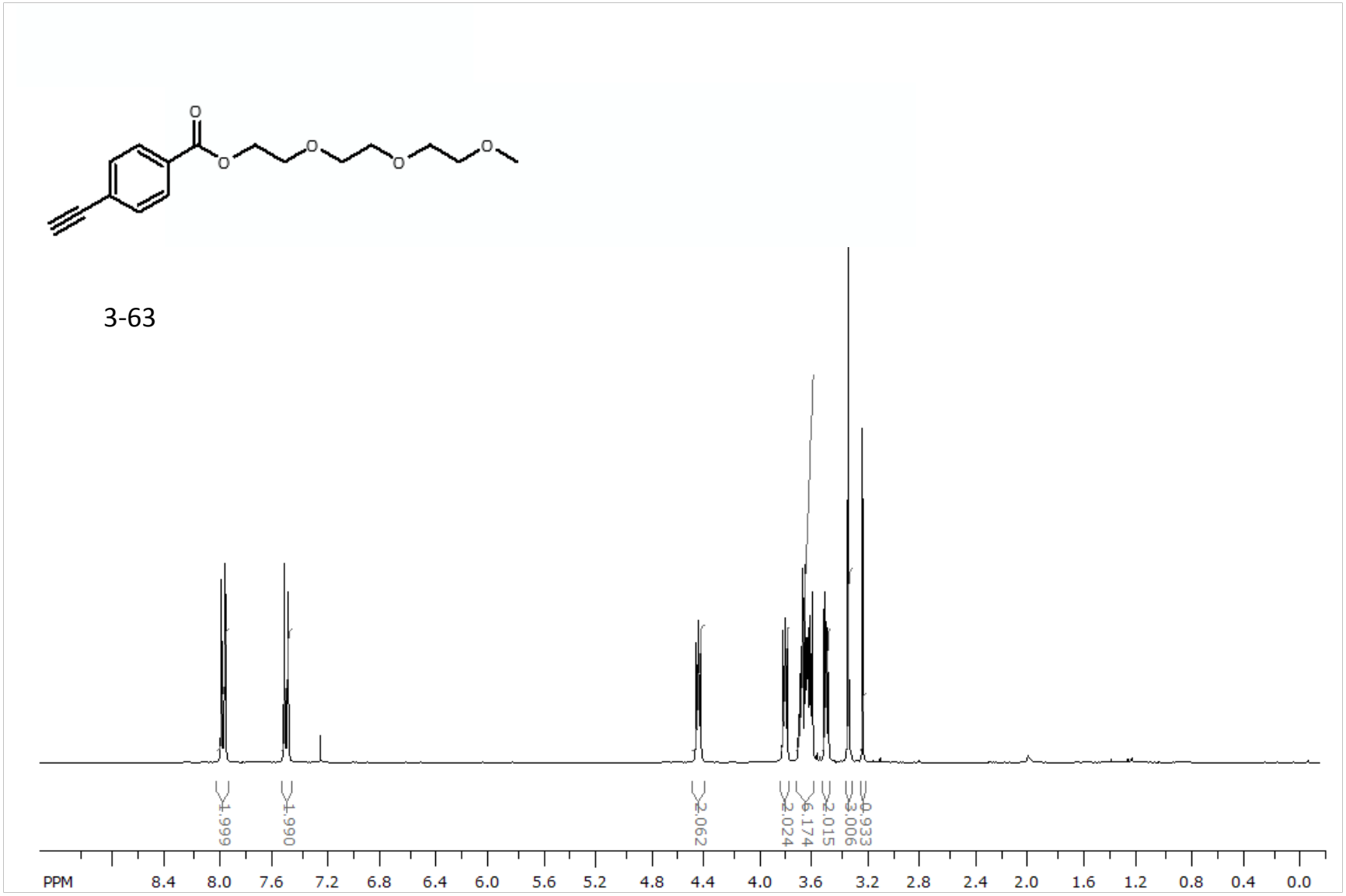
3-63
1.999
1.990
2.062
2.024
6.174
2.015
3.006
0.933
PPM
8.4
8.0
7.6
7.2
6.8
6.4
6.0
5.6
5.2
4.8
4.4
4.0
3.6
3.2
2.8
2.4
2.0
1.6
1.2
0.8
0.4
0.0

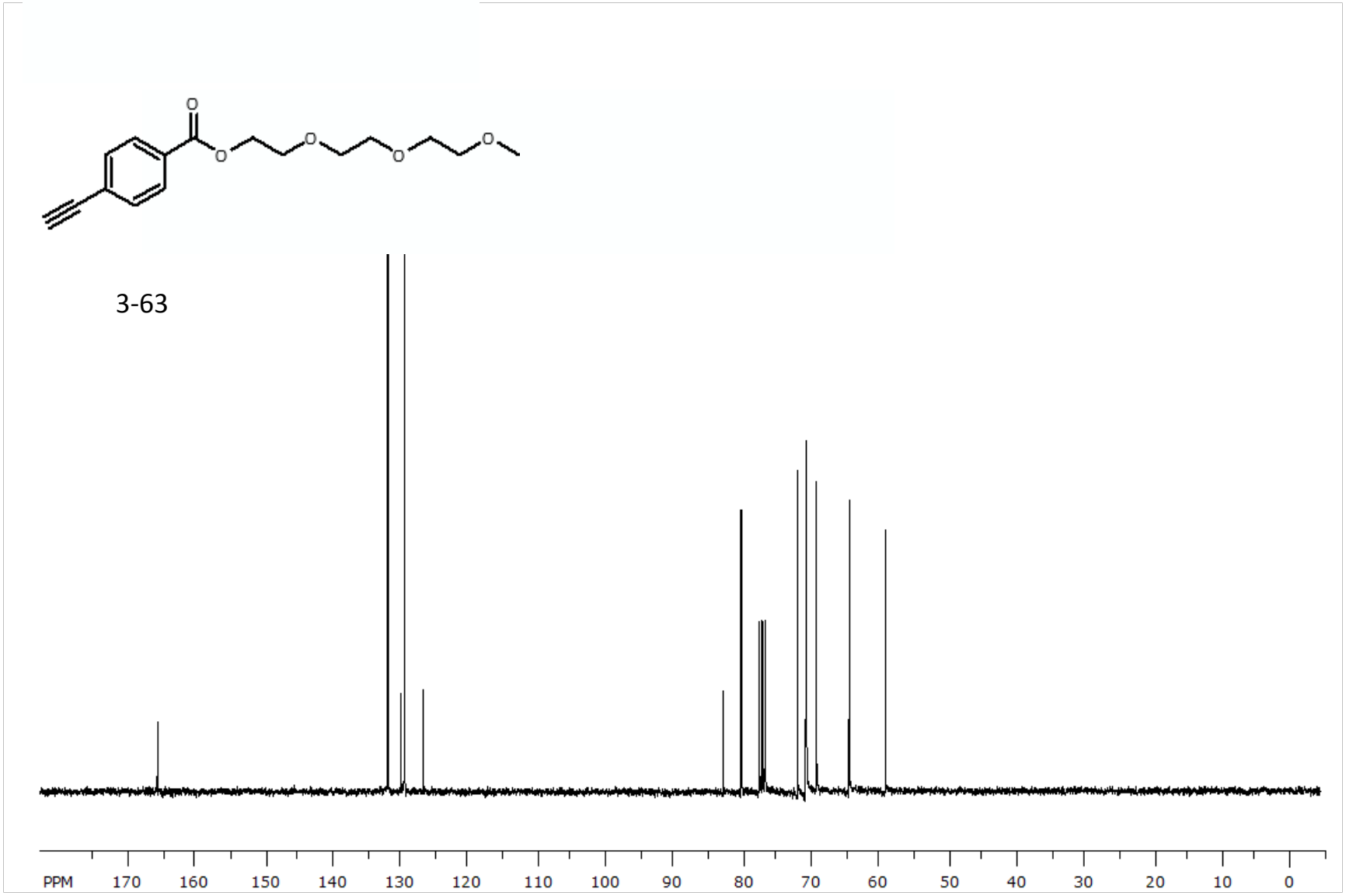
O
O
O
O
O
3-63
PPM
170
160
150
140
130
120
110
100
90
80
70
60
50
40
30
20
10
0

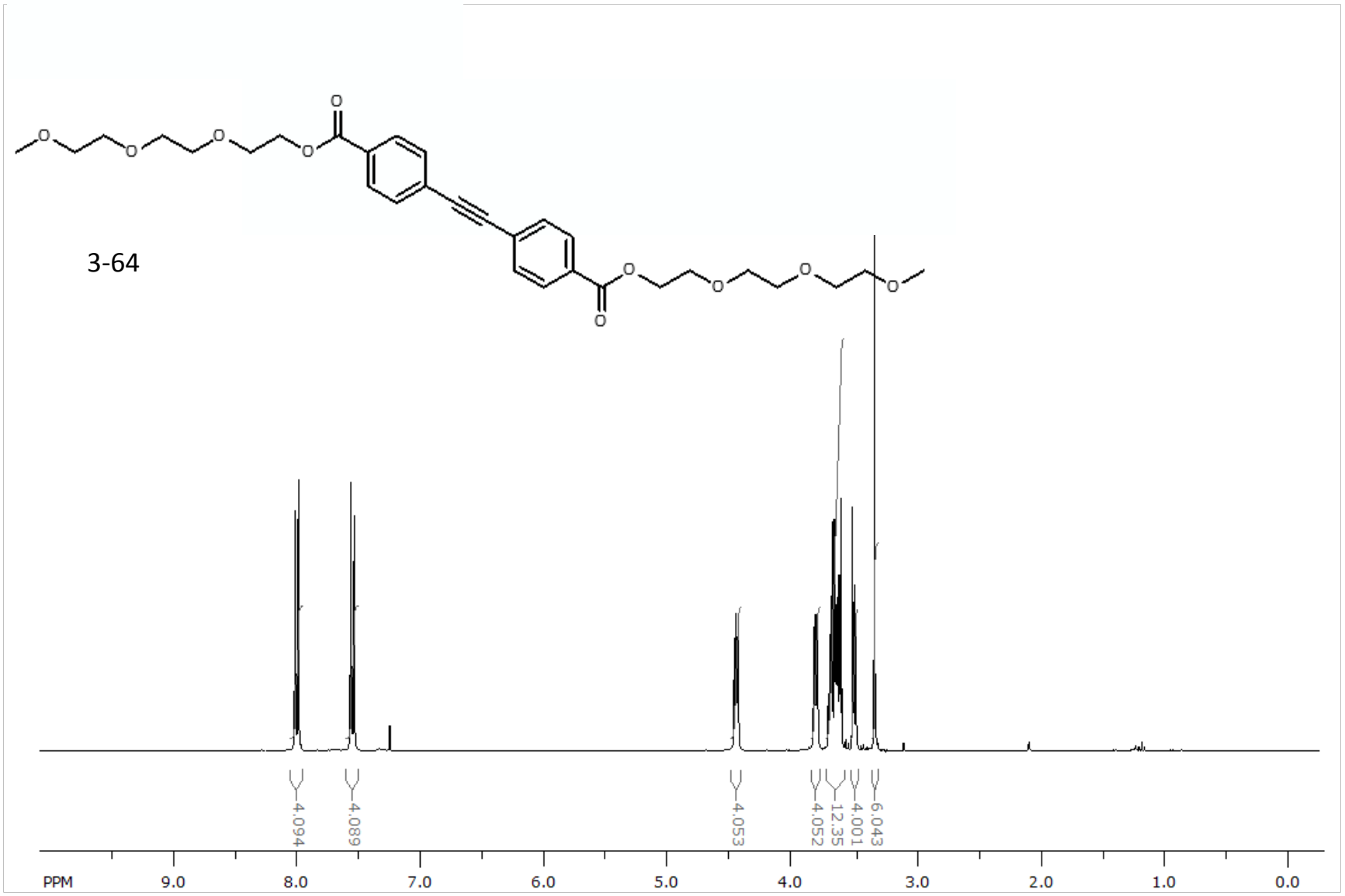
3-64
4.094
4.089
4.053
4.052
12.35
4.001
6.043
PPM
9.0
8.0
7.0
6.0
5.0
4.0
3.0
2.0
1.0
0.0

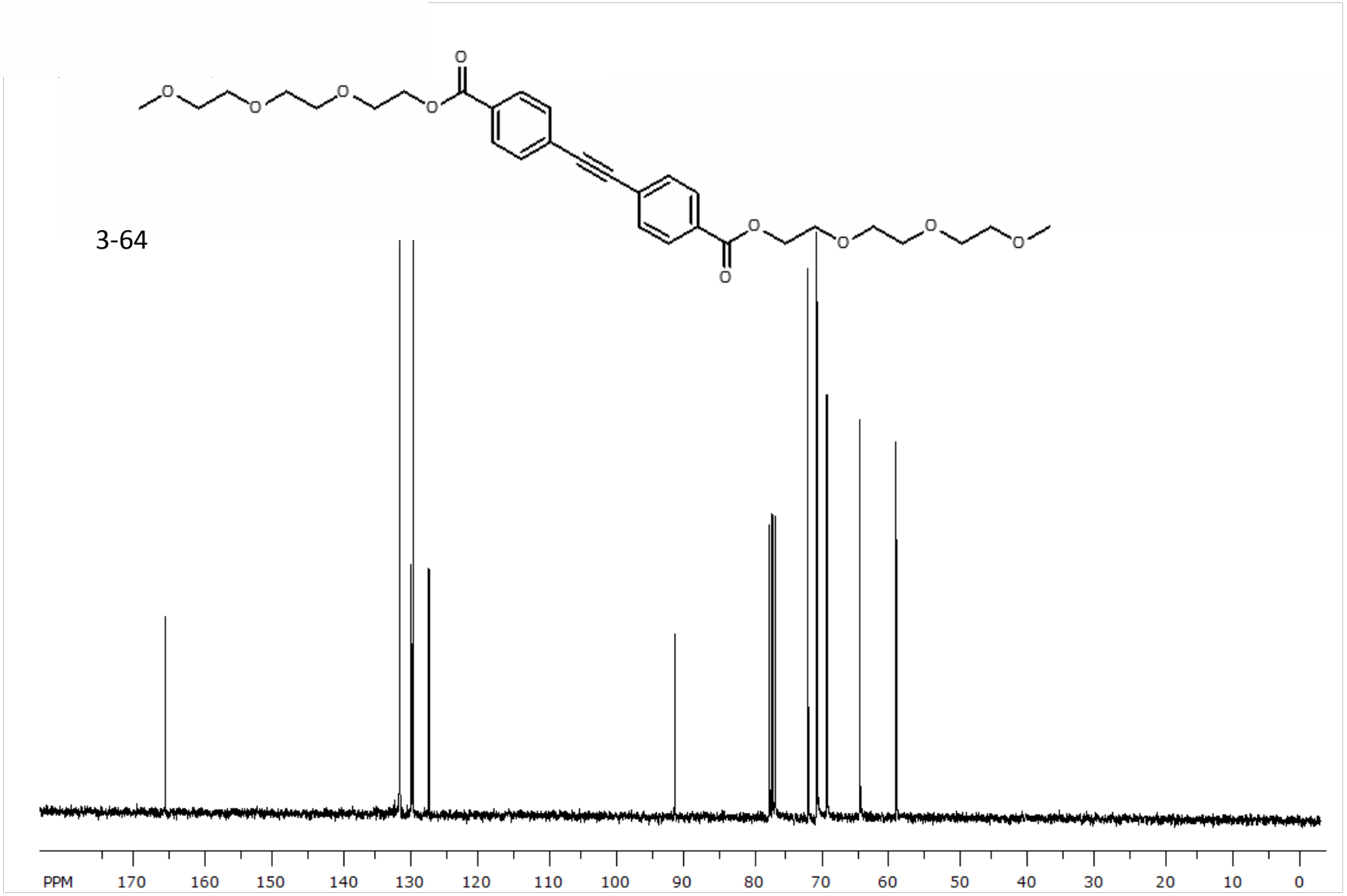
3-64
PPM
170
160
150
140
130
120
110
100
90
80
70
60
50
40
30
20
10
0

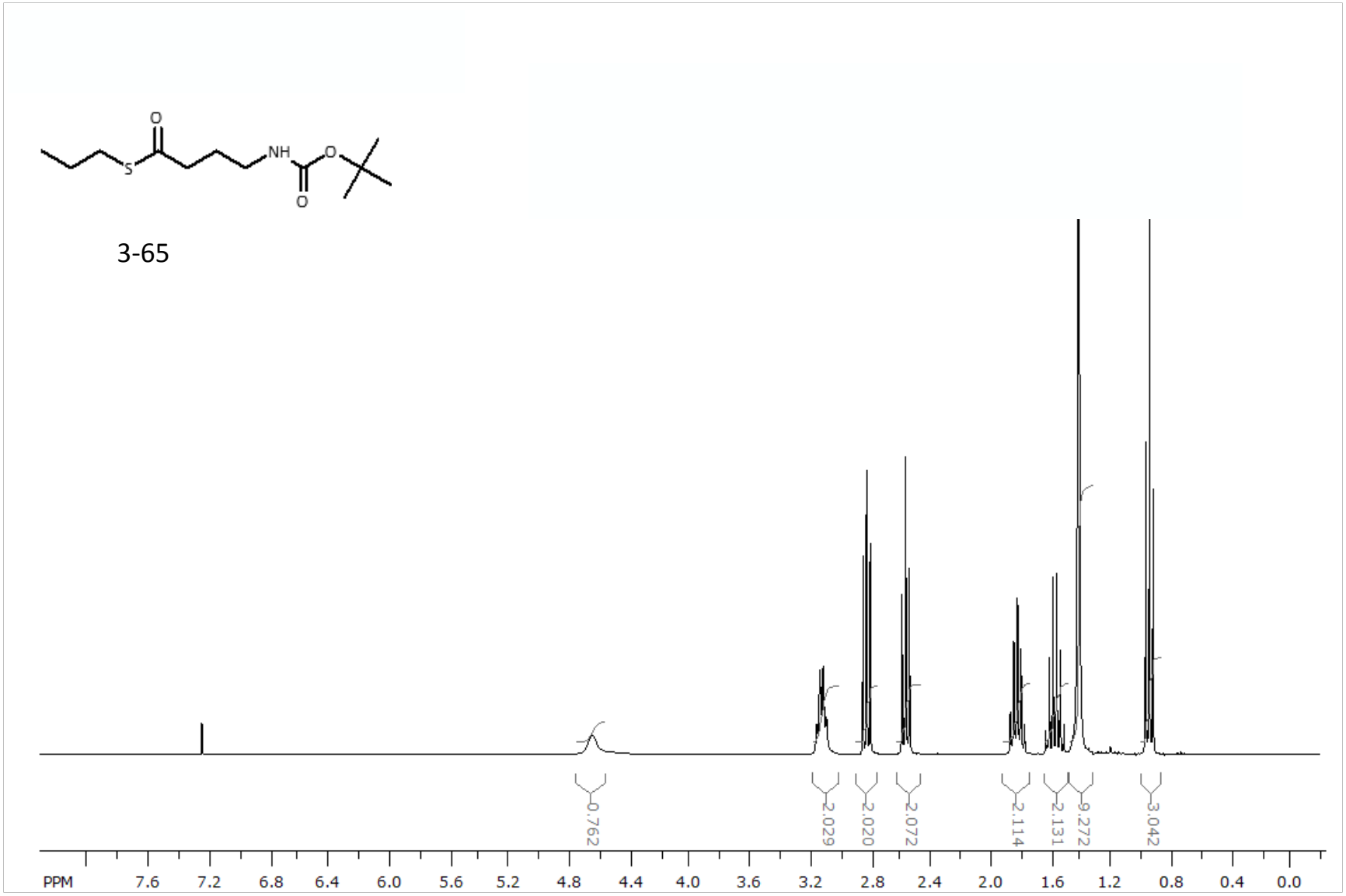
O
S
NH
O
O
3-65
0.762
2.029
2.020
2.072
2.114
2.131
9.272
3.042
PPM
7.6
7.2
6.8
6.4
6.0
5.6
5.2
4.8
4.4
4.0
3.6
3.2
2.8
2.4
2.0
1.6
1.2
0.8
0.4
0.0

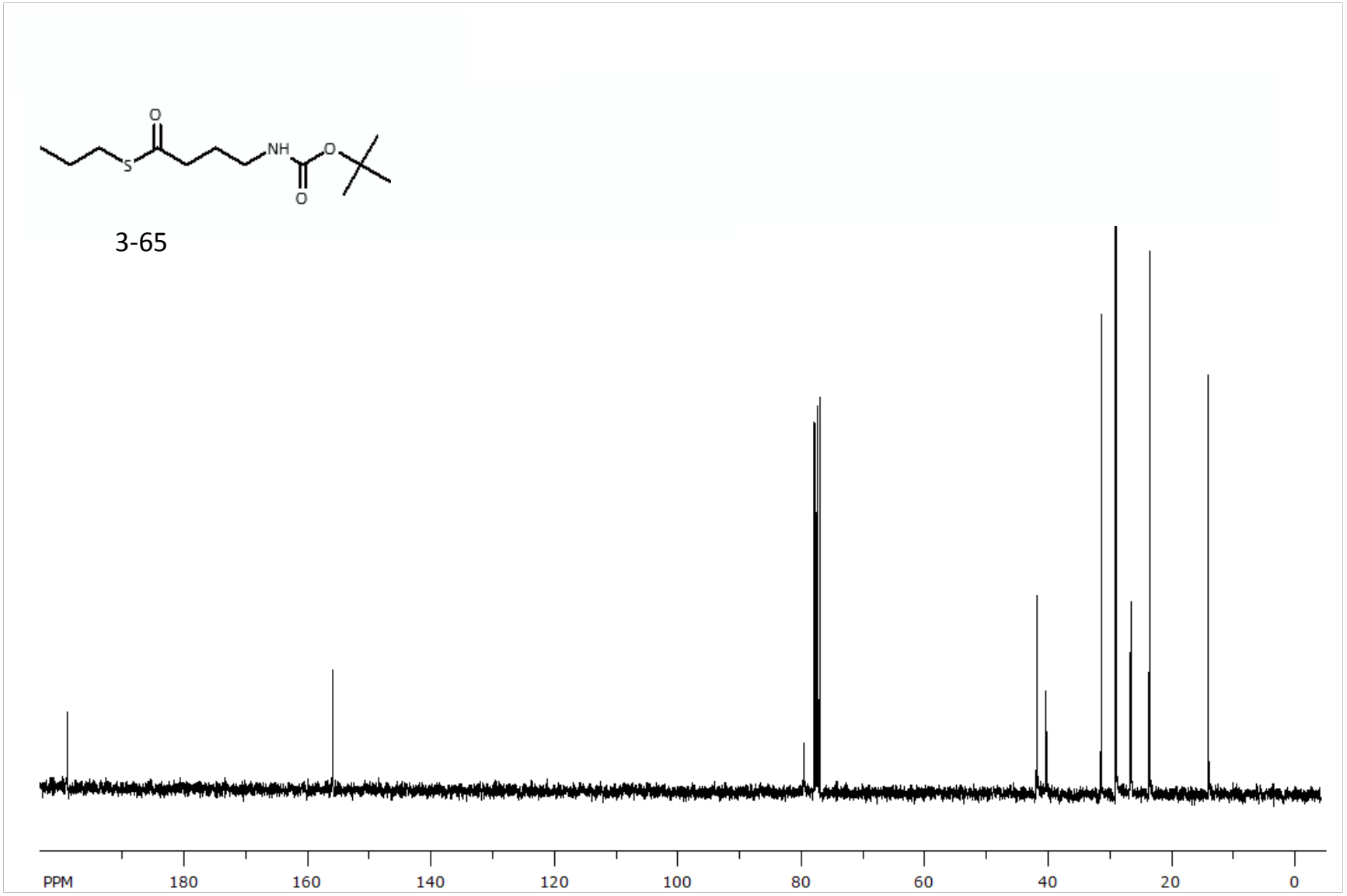
O
S
NH
O
O
3-65
PPM
180
160
140
120
100
80
60
40
20
0

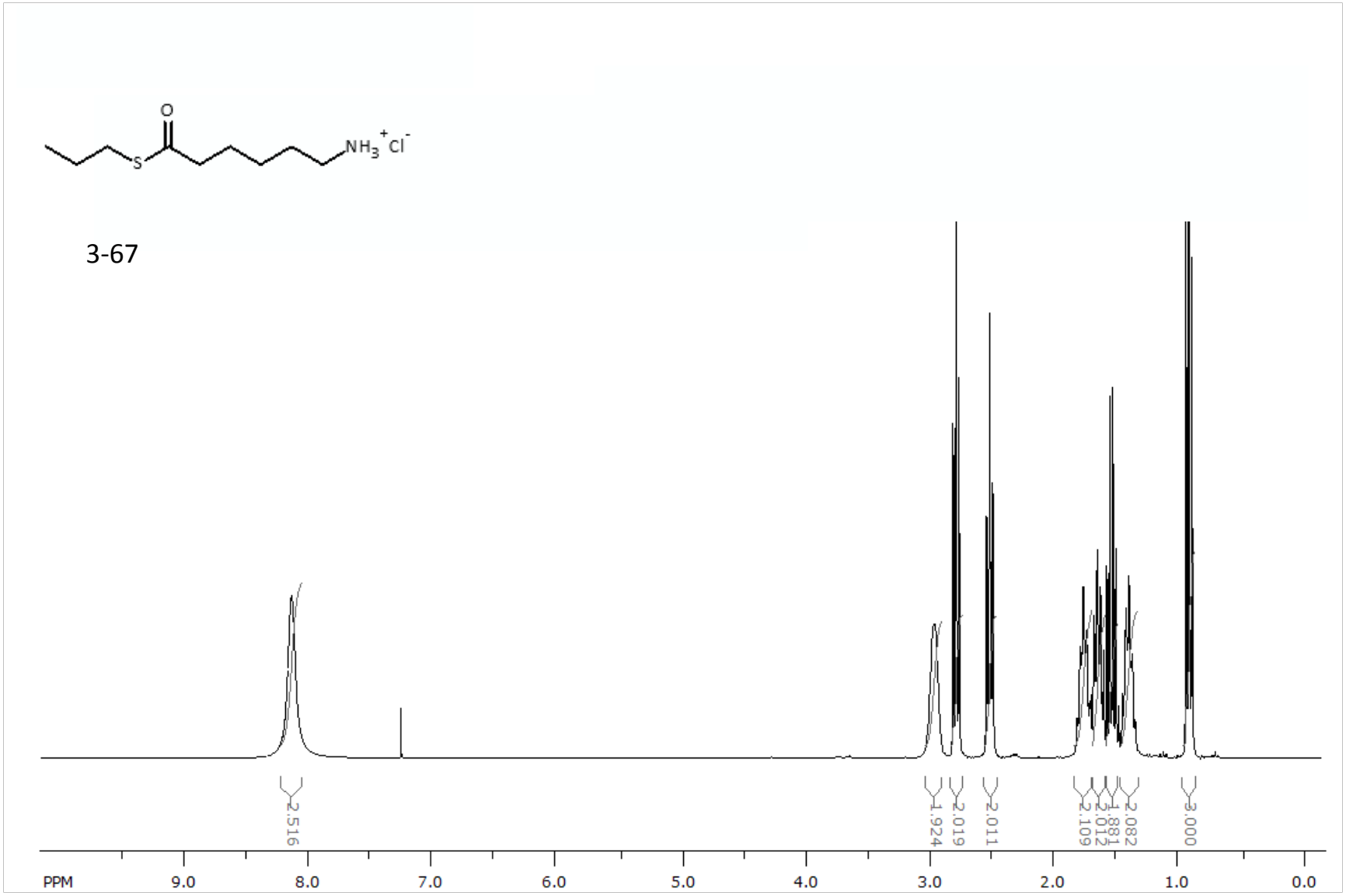
O
S
NH3+ Cl-
3-67
2.516
1.924
2.019
2.011
2.109
2.012
1.881
2.082
3.000
PPM
9.0
8.0
7.0
6.0
5.0
4.0
3.0
2.0
1.0
0.0

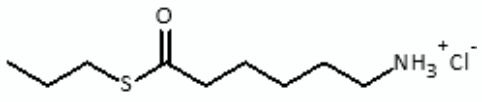

3-67